UNIVERSITAT POLITÈCNICA DE CATALUNYA
BARCELONATECH

Department of Material Science and Metallurgical Engineering (CMEM)
Technical Superior School of Industrial Engineering of Barcelona (ETSEIB)
Polytechnic University of Catalonia (UPC)

PhD program in Biomedical Engineering
2010-2014

PhD Thesis

LACTATE-RELEASING PLA SCAFFOLDS FOR BRAIN REGENERATION

Author: Zaida Álvarez Pinto

Director: Dr. Elisabeth Engel (UPC)
Co-director: Dr. Soledad Alcántara (UB)

Barcelona, July 2014

This dissertation is submitted to Polytechnic University of Catalonia
for the degree of Doctor of Biomedical Engineering

A mis padres y
a mis hermanos, Raquel y Carlos

"Si buscas resultados distintos, no hagas siempre lo mismo".

Albert Einstein (1879-1955)

Agradecimientos

Después de 5 años, ha llegado el momento de agradecer a todas aquellas personas que durante el transcurso de esta tesis han estado a mi lado. Primero de todo, tengo que dar las gracias a mis dos jefas; Elisabeth y Soledad. Gracias a las dos por darme la oportunidad de hacer en vuestros respectivos laboratorios la tesina de master y la tesis doctoral. Eli, si no fuera porque el día que fui a hablar contigo me diste la oportunidad de realizar la tesis de máster no hubiéramos acabado aquí. Gracias por todos los votos de confianza durante todos estos años, nuestras charlas en tu despacho, por estar a mi lado en momentos duros y estresantes y por confiar en que podía hacerlo. Sole, a ti darte las gracias por el día a día en el laboratorio, por enseñarme a pensar más allá de lo que me obcecaba en aquel momento, a ser crítica con los experimentos y con mi trabajo, a ser perseverante y hacer el trabajo lo más impecable posible, y por nuestras charlas en el laboratorio a las tantas de la noche. Y a las dos, mil y una gracias por estar allí como personas y no como jefas en más de un momento en estos 5 años.

Quisiera dar las gracias a Josep A. Planell por todos estos años animándome para que tirara hacia adelante esta tesis. Gracias por ayudarme a ser crítica con mi trabajo, por valorar tan bien siempre mis resultados y por ayudarme siempre en todo lo que he necesitado.

Para empezar desde el principio, agradecer a la gente del laboratorio de la UB con los que día a día hemos estado codo con codo trabajando. Primero tengo que dar las gracias a Marta Mattotti (Martoti), con quien tuve la suerte de empezar a trabajar en el lab. Gracias Marta por haberme enseñado tantas cosas durante mi primera etapa en el laboratorio de Bellvitge, por nuestros experimentos diseñados y empezados un viernes por la tarde, o por los momentos de risas y rabiadas en todo este tiempo. A Alberto Ortega, o como yo le llamo a Albert (ya sé que te cabrea…). Muchísimas gracias por todos estos años como compañero de batallas en el laboratorio y sobretodo como amigo. Sé que te quedará marcado que no trajera una libreta conmigo el día que me enseñaste a hacer Western Blot, pero que sepas que al final el alumno supera al maestro, y puedes estar orgulloso de mis Westerns. Quisiera darte las gracias por el apoyo que he recibido y sigo recibiendo de ti, aunque ya no estés por aquí. Gracias por enseñarme un montón de técnicas y a trabajar fino, por hacerme los esquemas del capítulo 3 y el súper esquema de la discusión, por poder discutir de ciencia contigo, por valorar siempre tan

bien mi trabajo y finalmente por confiar tanto en mí. En fin, gracias por creer que esta tesis iba a tirar hacia adelante y por estar a mi lado en este proceso. No quisiera olvidarme de todos los buenos momentos que vivimos los tres juntos en congresos, calçotadas y fiestas en las que nuestro lema eran las rabiadas a diario con la ciencia y nuestro futuro en ella.

Como no, Nuno (Elaaaaaa!), por fin llegó el momento. Junto con Marta y Alberto, la primera etapa en el laboratorio, la recuerdo muy divertida también gracias a ti. Gracias por estar en todos aquellos momentos en que todo lo veía gris, por todos aquellos momentos que hemos podido charlar de todo dándonos ánimos y escuchándonos mutuamente. Sabes que en este grupo tu yo éramos los positivos! Así que nunca podíamos estar los dos de bajón sino esto podía ser un desastre. Gracias por esas caipiriñas party que montábamos y la liábamos tanto. Simplemente gracias por ser un amigo en el que he podido contar cada vez que te he necesitado. A Greti Espona, que aunque no fuera de nuestro grupo, siempre la adoptamos con mucho cariño. Aun me acuerdo el primer verano solas las dos con Nuno, que cruzaste las primeras palabras con nosotros. Greti, a ti y a Marta quiero daros las gracias por los buenos momentos vividos las tres por Málaga y Sevilla…por reírnos, beber y comer hasta no poder más….por compartir conmigo momentos muy buenos en el lab y fuera de él. En fin que hasta tus silencios me gustaban!. Gracias también por animarme en momentos que parecía que esta tesis podía encallarse y por confiar en que podía ser una muy buena tesis. Gracias.

Acabados una etapa en el laboratorio, quisiera empezar esta segunda dando las gracias a la persona en la que creía al principio que seríamos dos compañeras más de laboratorio pero se convirtió en una gran amiga en estos años. Aina, a tu donar-te les gracies per aquests anys tan durs en el laboratori. Sé que quan es va marxar l'Alberto ens vam quedar les dues soles, però sempre he cregut que es quan tu i jo vam començar a estar agust l'una amb l'altre. Gràcies por estar aquí ens els mals moments de papers que ens van rebutjar o de d'experiments que ni tan sols volia mirar…. Gracies per confiar en que les coses sortirien bé quan una semblava que havia tocat fons i per donar-me ànims creient sempre en el meu treball. La veritat, es que t'haig de donar les gràcies perquè en part tu ets la que has viscut més a prop els moments finals d'aquesta tesis, i això ha comportat molts bons moments però també algun una mica desastrós. Fora de l' àmbit professional, gracies també per totes les tardes de shopping, birres i xerrades fins no poder més, sempre ens hem fet costat i això en part ha estat un punt per portar aquesta

tesis endavant. Finalment a Rafel (Rafa!!!), l'últim en entrar a aquest grup i al que per sort o per desgracia li ha tocat viure la meva ultima etapa. Rafa, gracies pels ànims en els moments que m'has vist baixa o solament per estar escoltant. Espero que hagis après alguna cosa en aquest any i mig que hem estat junts i que et serveixi per el temps que et queda aquí. Gracies junt amb l'Aina per les festes del campus, o els "dinars" dels migdies que ens servien a tots per poder acabar de portar millor el dia o fins i tot la setmana. Cuida a l'Aina i aquí et quedes amb dos dones al grup!!.

Como no, tengo que dar las gracias a toda la gente de la Unidad de Biología Celular de Bellvitge. Primeramente a Jordi Domingo por darme su apoyo en esta etapa y por estar allí para lo que he necesitado. Gracias por revisarme la tesis y más de un artículo y darme tu opinión sobre el trabajo. Gracias al grupo de cáncer de Ricardo Pérez. Hemos compartido laboratorio durante todo este tiempo y aunque ha habido tiempos de más o menos bonanza siempre nos hemos ayudado mutuamente. Gracias a Vanessa, Celia, Pili, Ananda, y Korrodi por estar para cualquier cosa que he necesitado. Sobretodo daros las gracias por la paciencia que habéis tenido en estos últimos meses al compartir despacho conmigo y lo que eso ha supuesto. Gracias a Miquel Viñas, Teresa Vinuesa, Ana Méndez, Natalia, Santiago y Mercè por estar allí en los momentos en los que he necesitado su ayuda. Gracias a Eva, por si no fuera por ella muchos cerebros de esta tesis aun estarían por cortar en el -80ºC.También dar las gracias a los búlgaros, Dencho y Joro. Gracias sobre todo a Dencho por ayudarme siempre con experimentos en los que he necesitado de sus habilidades y su microscopio.

Quisiera dar las gracias a todos mis compañeros del grupo de "Bio/non-Bio o Biomaterials for regenerative therapies"…… Sobre todo a Tiziano, Ricardo, Xavi, Aitor Sánchez y Arlyng con los que me lo he pasado en grande en congresos compartiendo habitación, comidas, charlas y cervezas. Gracias chicos porque aunque no haya estado el día a día con vosotros en el laboratorio en el IBEC, siempre me habéis hecho sentir parte del grupo. No olvidarme de los post-docs, Oscar y Miguel Ángel, muchísimas gracias por haberme ayudado tanto con la parte de caracterización y diseño de los materiales durante esta tesis doctoral. Sin vuestra ayuda y paciencia no hubiera sido posible hacer esta tesis.

Tampoco me puedo olvidar de la gente de la 4º planta de Bellvitge con los que he compartido buenos momentos. A Edy, que aunque ya no esté por aquí nos hemos reído

mucho juntos. Gracias por ayudarnos en cualquier cosa que hemos necesitado. A Petra y José Carlos, sin vosotros parte de esta tesis no hubiese salido. Petra, muchas gracias por ayudarme con las cuantificaciones de glucosa y lactato y por todos aquellos experimentos que hemos tenido que hacer juntas para tirar algún artículo hacia adelante.

Gracias al SCT-Bellvitge y en particular a Benja. Benja, que por fin se acabó!!. Gracias por toda la ayuda que me has dado con todos los microscopios que he toqueteado en estos 5 años. A pesar de haberte traído muestras raras y difíciles de ver en el confocal, al final hemos salido muy airosos. Siempre he dicho que este confocal y este técnico le dan veinte mil vueltas a más de un two-photon y a más de un súper guays del campo!. Gracias por las charlas que hemos tenido delante del microscopio los dos, y por escucharme y aconsejarme en muchos momentos.

Para terminar con la gente de Bellvitge, dar las gracias a la gente del estabulario que siempre nos han tratado muy bien. En especial quiero agradecer a Marta por cuidar de nuestro box y por estar tan atenta con mis animales operados. Gracias.

Dar las gracias a mis amigas de la uni que han estado aguantando todos estos años tantos momentos vividos. Gracias a Aida, Gema y Rita. Vosotras también habéis hecho posible que esta tesis saliera hacia adelante. Gracias a las tres por todas esas cenas escuchando mis problemas y compartiendo mis alegrías. Solo quisiera dar en particular las gracias a Rita por esas tardes de biblioteca escribiendo la tesis las dos juntas o por esos momentos en los que las dos ya no podíamos con nuestra alma y nos íbamos de cena o de birras. Gracias chicas.

Finalmente, y no menos importante por ello, quisiera dar las gracias a mi Familia. Sin ellos esta tesis seguro que no hubiese sido posible. Quiero dedicarles esta tesis a mis padres, mis dos grandes pilares en esta vida, y a mis hermanos Raquel y Carlos. Ellos siempre han estado a mi lado apoyándome durante todos estos años de estudio. Gracias por estar simplemente ahí, para lo bueno y lo malo, en los momentos de decepción y de alegría. Siempre he pensado que las fuerzas que he tenido para sacar esta tesis adelante han sido porque vosotros habéis estado día a día a mi lado. Simplemente Gracias.

UNIVERSITAT POLITÈCNICA DE CATALUNYA
BARCELONATECH
Escola de Doctorat

Acta de calificación de tesis doctoral

Curso académico:

Nombre y apellidos

Programa de doctorado

Unidad estructural responsable del programa

Resolución del Tribunal

Reunido el Tribunal designado a tal efecto, el doctorando / la doctoranda expone el tema de la su tesis doctoral titulada _____

_____.

Acabada la lectura y después de dar respuesta a las cuestiones formuladas por los miembros titulares del tribunal, éste otorga la calificación:

☐ NO APTO ☐ APROBADO ☐ NOTABLE ☐ SOBRESALIENTE

(Nombre, apellidos y firma) Presidente/a	(Nombre, apellidos y firma) Secretario/a

(Nombre, apellidos y firma) Vocal	(Nombre, apellidos y firma) Vocal	(Nombre, apellidos y firma) Vocal

_____, _____ de _____ de _____

El resultado del escrutinio de los votos emitidos por los miembros titulares del tribunal, efectuado por la Escuela de Doctorado, a instancia de la Comisión de Doctorado de la UPC, otorga la MENCIÓN CUM LAUDE:

☐ SÍ ☐ NO

(Nombre, apellidos y firma) Presidente de la Comisión Permanente de la Escuela de Doctorado	(Nombre, apellidos y firma) Secretaria de la Comisión Permanente de la Escuela de Doctorado

Barcelona a _____ de _____ de _____

ABSTRACT

Physical brain injuries involving extensive tissue loss are common causes of disability. Regenerative medicine strategies to promote recovery following traumatic brain injuries are currently focused on the use of biomaterials as delivery systems for cells or bioactive molecules. An ideal therapy needs to support neuronal and vascular growth and to activate endogenous progenitors and appropriate brain developmental programs. In this thesis we tested two types of poly L/DL lactic acid (PLA95/5 and PLA70/30), a biodegradable material permissive for neural cell adhesion and growth, as materials for nerve regeneration. PLA95/5 films were highly crystalline, stiff (GPa), and did not degrade significantly in the one-month period analyzed in culture. In contrast, PLA70/30 films were more amorphous, softer (MPa) and degraded faster, releasing significant amounts of lactate into the culture medium. PLA70/30 performed better than PLA95/5 for primary cortical neural cell adhesion, proliferation and differentiation, maintaining the pools of neuronal and glial progenitor cells *in vitro*. L-lactate in the medium recapitulated PLA70/30's maintenance of neuronal restricted progenitors but did not sustain bipotential or glial restricted progenitors in the cultures, as occurred when neural cells were grown on PLA70/30. L-lactate was intake through MCT2 transporter and its subsequent oxidative metabolism direct progenitor commitment to a neuronal progenitor fate. The consequence of lactate metabolism was a dependence on cataplerosis through the mitochondrial phosphoenolpyruvate carboxykinase (PEPCK-M) pathway.

On the other hand, in the embryonic brain, radial glia serve as neural stem cells and as substrate for neuronal migration and are retained in the adult brain of species that regenerate. For *in vivo* studies, we designed 3D cell-free biomimetic scaffolds consisting of electrospun PLA70/30 nanofibers. Radially aligned PLA70/30 nanofibers released L-lactate and reproduced the 3D organization and supportive function of radial glia embryonic neural stem cells. These scaffolds implanted into cavities made in mouse brain, fostered complete implant vascularization, sustained neurogenesis, and allowed the long-term survival and integration of the newly generated neurons. Our results suggest that PLA70/30 scaffolds mimic some of the physical and biochemical characteristics of the NSC niche. The topology of PLA nanofibers supports neuronal migration while L-lactate released during PLA degradation acts as an alternative fuel for neurons and is required for progenitor maintenance. Overall, our results show that the endogenous central nervous system is capable of regeneration through the *in vivo* dedifferentiation induced by biophysical and metabolic cues, with no need for exogenous cells, growth factors, or genetic manipulation.

FIGURES AND TABLES INDEX

FIGURES:

INTRODUCTION (I)

DISCUSSION (D)

TABLES:

DISCUSSION (D)

ABBREVIATIONS

AF-CBT: alexa fluor conjugates of cholera toxin subunit B

APCs: astrocyte precursor cells

BBB: blood brain barrier

BLBP: brain lipid-binding protein

BrdU: bromodeoxy Uridine

BSCB: blood spinal cord barrier

CBT: cell-based therapy

CD31: also known as endothelial cell adhesion molecule-1 (PECAM-1)

CNS: central nervous system

CRT: cell replacement therapy

CXCR3: chemokine receptor 3

DCX: doublecortin

DIC: differential interface contrast

DiI: indocarbocyanine dye

Div: days *in vitro*

E: embryonic day

EC: endothelial cell

ECM: extracellular matrix

ESC: embryonic stem cell

GABA: gamma amino butiric acid

GFAP: glial fibrillary acidic protein

GLAST: astrocyte-specific glutamate transporter

GPR81: G protein-coupled receptor 81

GRP: glial restricted precursor

HA: hyaluronic acid

Iba-1: ionized calcium binding adaptor molecule 1

ICC: immunocitochemistry

IHC: immunohistochemistry

IPC: intermediate progenitor cells

iPCS: induced-pluripotent stem cell

IZ: intermediate zone

3-MPA: 3-mercaptopicolinic acid

MAP-2: microtubule-associated protein 2

MCT2: monocarboxylate transporter 2

MRI: magnetic resonance imaging

NeuN: neuronal nuclei

NG2: neural/glial antigen 2

NSC: neural stem cells

OB: olfactory bulb

Olig-2: oligodendrocyte transcription factor-2

OPCs: oligodendrocyte progenitor's cells

Pax6: paired box protein 6

PDGFRα: platelet-derived growth factor receptor alpha

PDMS-TEOS: polydimethylsiloxane–tetraethoxysilane

PEPCK-M: phosphoenolpyruvate carboxykinase- Mithocondrial

PLA: poly (lactic) acid or polylactide

PLGA: poly (lactic-co-glycolic) acid

PMMA: poly (methyl methacrylate)

PNS: peripherial nervous system

PV: parvalbumin

RGC: radial glial cells

RMS: rostral migratory stream

ROS: reactive oxygen species

SC: stem cell

SCI: spinal cord injury

SGZ: subgranular zone

Sox-2: sex determining region Y (SRY)-box 2

SVZ: subventricular zone

TBI: traumatic brain injury

TCP: tissue culture plate

Tuj-1: β- tubulin III

Tbr1: T-box-brain-1

Tbr2: T-box-brain-2

VEGF: vascular endothelial growth factor

VZ: ventricular zone

INTRODUCTION

1. Traumatic injury in the central nervous system (CNS): brain and spinal cord

The central nervous system (CNS) is a network of more than 100 billion individual nerve cells that control our actions, sense our surroundings and define who we are. The brain and spinal cord make up the CNS (Fig. I-1); the brain coordinates higher-level functions and the spinal cord transmits information from the brain to the peripheral nervous system and back (Shoichet et al., 2008).

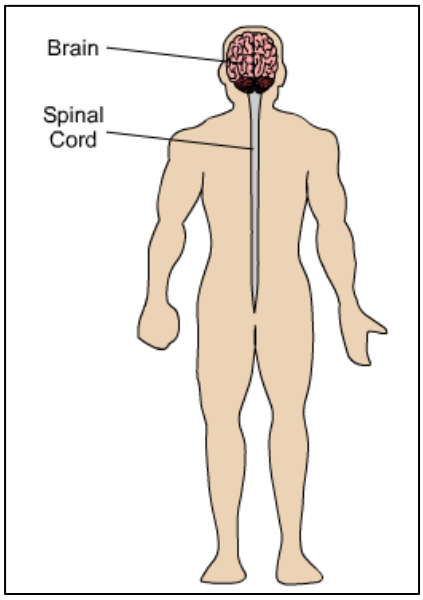

Figure I-1. The central nervous system consisting of the brain and spinal cord. Adapted from Sherwood, 2001.

There are two main cell types in CNS; neurons and glial cells (Fig. I-2). The functional units of the CNS are neurons, which are unique in their ability to transmit rapid electrical signals in the form of action potential (Allen and Barres, 2009), yet they are vulnerable to injury. Most mature neurons are post-mitotic cells incapable of cell division, so their destruction can leave severe functional deficit. In mammals, glial cells are classified as oligodendrocytes, microglia and astrocytes (Fig. I-2). However, this classification is very simplistic because many intermediate glial cell forms have been described between oligodendrocytes and astrocytes. Oligodendrocytes provide a lipid-rich membrane called myelin, which enwraps axons, thereby speeding up the conduction of electrical impulses (Allen and Barres, 2005), and they or/and their progenitors can remyelinate under certain injury circumstances (Chang et al., 2000; Nishiyama, 2007; Trotter, 2005). Microglial cells are resident immune system phagocytic cells within the brain and spinal cord (Kim and de Vellis, 2005). They respond rapidly for neuronal protection or healing after an injury (Davalos et al., 2005; Wu et al., 2007) and have also been implicated in synaptic remodeling during the development of the nervous system, when they are proposed to remove inappropriate synaptic connections through the process of phagocytosis (Allen and Barres, 2009). Finally, astrocytes are the predominant glial cell types in the adult mammalian CNS, comprising the majority of glial cells, which outnumber neurons ten to one (O'Kusky and Colonnier, 1982; White and Jakeman, 2008). Traditionally, they were associated with providing only structural support. However, in the last decades different studies conclude that astrocytes also regulate brain homeostasis and maintain the blood brain barrier (Abbott et al., 2006), contribute in the formation of synapses and in modulating synaptic functions

(Anderson and Swanson, 2000; Tanaka, 2007). They act as physical barriers between the synaptic connections of neighboring neurons and remove excess neurotransmitter molecules from the extracellular space allowing discrete and precise encoding of synaptic signals and neurotransmission. Astrocytes also play a key role in ATP production and metabolism (Jakovcevic and Harder, 2007), in extracellular matrix molecules production destined for basal lamina and perineuronal net (Massey et al., 2006; Tom et al., 2004) and play an important function limiting CNS injury. While most research is focused on the direct protection of neuronal cells, non-neuronal cells, such astrocytes, may exert an active role in the pathogenesis of CNS injury.

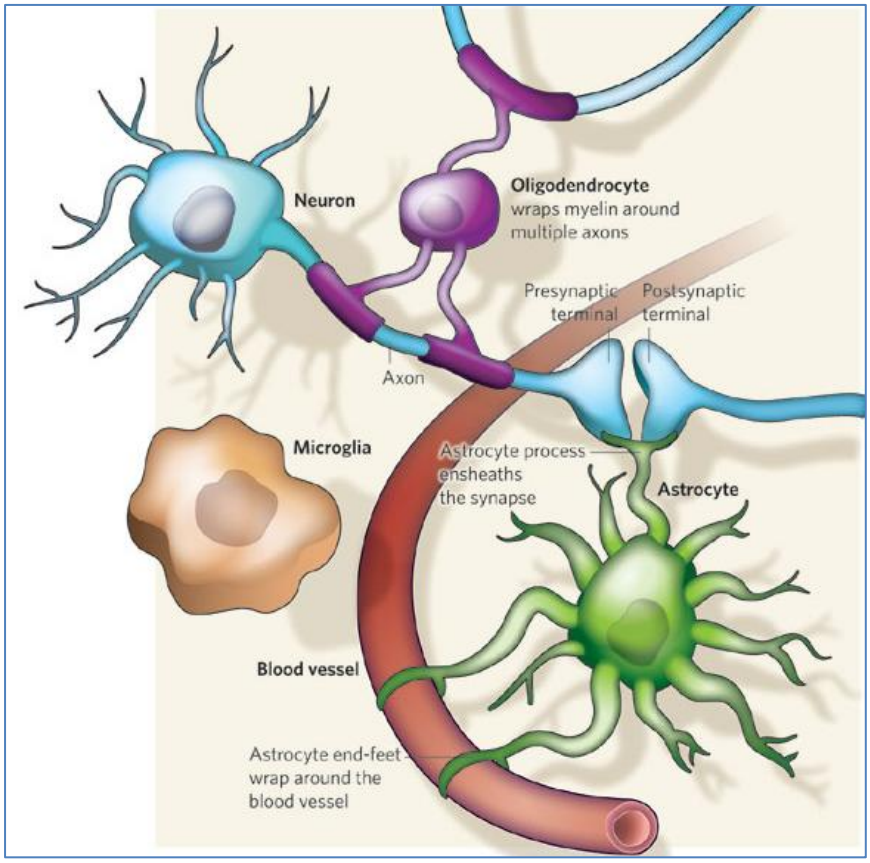

Figure I-2. Glia–neuron interactions. Different types of glia interact with neurons and the surrounding blood vessels. Oligodendrocytes wrap myelin around axons to speed up neuronal transmission. Astrocytes extend processes that ensheath blood vessels and synapses. Microglia keeps the brain under surveillance for damage or infection. Adapted from Allen and Barres, 2009.

The CNS has several anatomical and physiological characteristics: it is enclosed in bone structures making it difficult to access; it has a special vascular system that serves as barrier for drug delivery and it has limited capacity for repair. Injury in the CNS includes stroke, traumatic brain and spinal cord injury and degenerations (Kim et al., 2012). These conditions affect millions worldwide, and cover the entire age spectrum. CNS in the pediatric population includes predominantly traumatic or congenital defects, while in adult population the injuries are

traumatic or degenerative (Lo et al., 2003).Regardless of the initial location of the insult to the CNS, injury is an ongoing process, with primary damage leading to a cascade of deleterious events that can affect cell body and axonal function, resulting in continued dysfunction and prolonged degeneration.

1.1. Environment of the injured CNS; challenges and opportunities

The evolution of CNS injury response involves a dynamic interplay between events promoting repair and regeneration and those of damage and inhibition. Physical insults to brain or spinal cord tissue imitates a series of cellular and molecular events that progress over several days with a final structure called reactive gliosis or glial scarring (Buffo et al., 2008; Shoichet et al., 2008). The glial scar is an evolving structure, with different cells arriving and participating at different times (Fig. I-3).

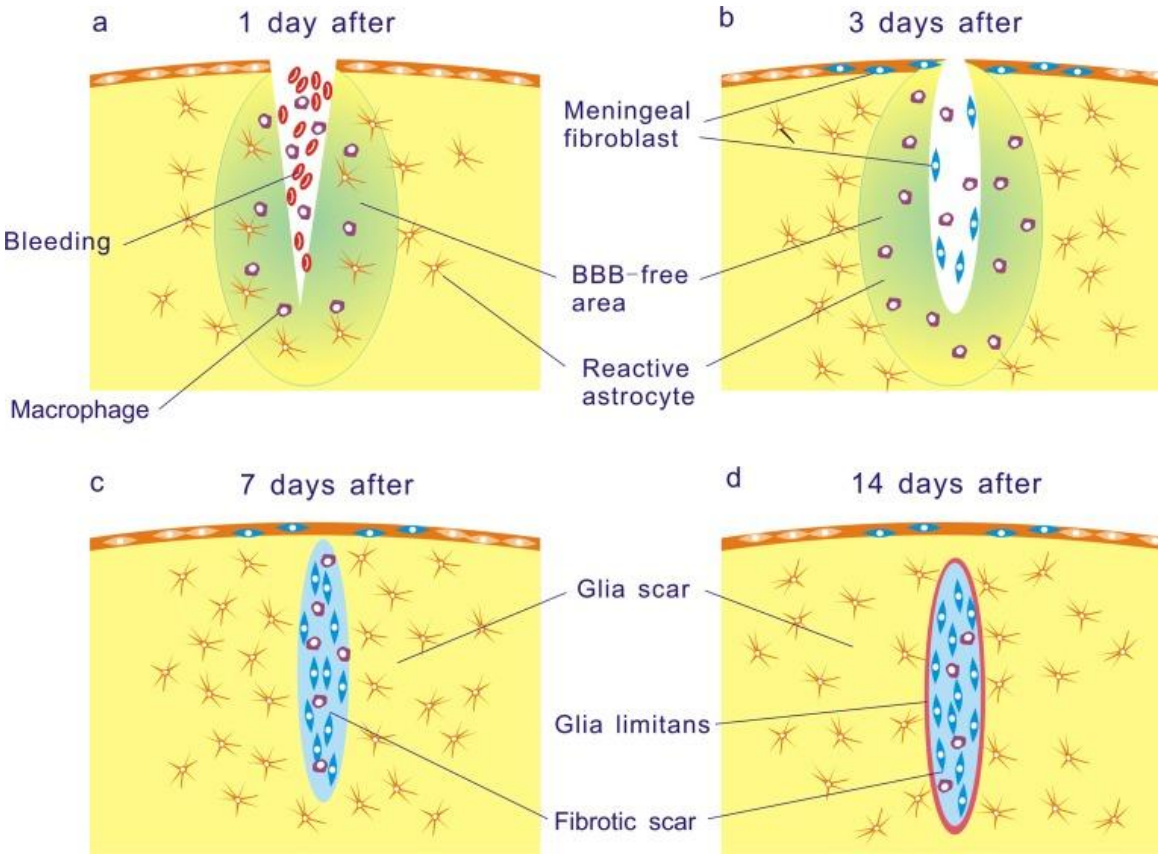

Figure I-3. Schematic drawings represent the process of the lesion scar formation in the mouse brain. **a**. One day after traumatic CNS injury, the BBB is disrupted and macrophages infiltrate the BBB-free area. Up regulation of GFAP immunoreactivity in reactive astrocytes is already observed. **b**. Three days after the injury, reactive astrocytes significantly increase around the lesion site but they are absent from the lesion center where the BBB is destroyed. Fibroblasts intrude from the damaged meninges to the lesion site. **c.** By 1 week after injury, fibroblasts actively proliferate and secrete ECMs to form the fibrotic scar. Reactive astrocytes re-occupy the surrounding area of the lesion site and the BBB-free area around the lesion site is eliminated. **d**. At 2 weeks after, processes of reactive astrocytes seal the lesion site to form a glia limitans. Adapted from Kawano et al., 2012.

The main cell types involved in these changes are astrocytes, microglia and oligodendrocyte precursors, with some involvement of meningeal cells and stem cells (Fawcett and Asher, 1999). The first cells to arrive in a CNS injury are macrophages from the bloodstream and microglia migrating in from the surrounding tissue, which initially causes necrotic cell death, damage and inflammation in the underlying tissue, and these, are seen within hours of injury (Fig. I-3a) (Kreutzberg, 1996). After 3-5 days, large numbers of oligodendrocyte precursors are recruited from the surrounding tissue and if the injury penetrates the meninges, meningeal cells will migrate to cover the exposed CNS surface (Fig. I-3b) (Fawcett and Asher, 1999; Kruger et al., 1986). The multiple subsequent cascades of secondary events such as opening of the blood–brain (BBB) or blood–spinal cord barrier (BSCB), inflammation, edema, ischemia, excitotoxicity, increase in free radicals, cell signaling and gene expression variation (Gaetz, 2004; Verma, 2000) leads to additional cell death, demyelination and axonal degeneration. The environmental cues associated with cell damage and neuroinflamation lead astrocytes to undergo hypertrophy, proliferate, migrate and differentiate forming a dense network bordering the lesion site (Fig. I-3, I-4). Astrocytes that undergo these changes at the lesion site are considered to be "reactive" astrocytes (White and Jakeman, 2008). In addition to changing morphology after injury, reactive astrocytes also alter their protein expression (Fig. I-4). They increase expression of the typical astrocyte marker glial fibrillary acidic protein, GFAP (Vijayan et al., 1990), the Ca^{2+} related protein S100β (Corvino et al., 2003; do Carmo Cunha et al., 2007), the glutamate transporter GLAST (EAAT1) (Beschorner et al., 2007), and re-express markers found during their development such as the intermediate filament protein Vimentin (Miyake et al., 1988). The final structure of glial scar is predominantly astrocytic and traditionally was viewed as both physical and chemical barrier to regeneration (Rudge and Silver, 1990; White and Jakeman, 2008).

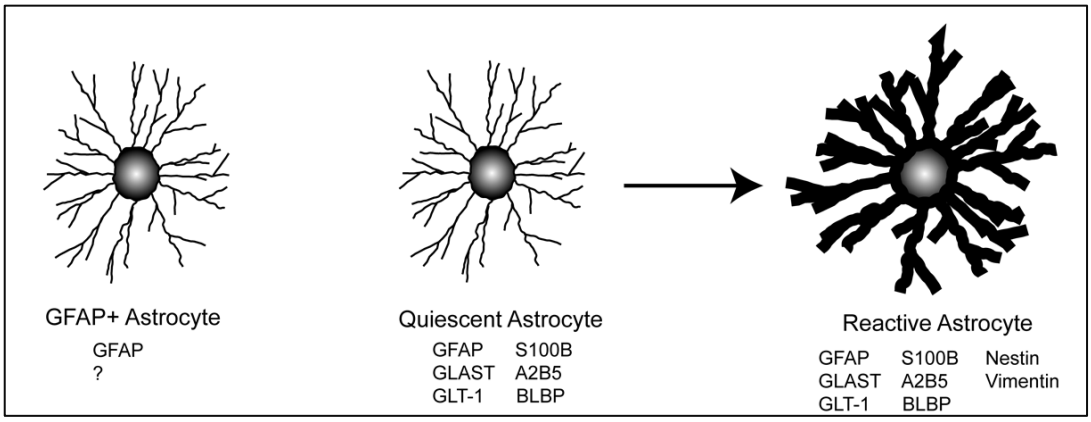

Figure I-4. Astrocyte differentiation after CNS injury. After CNS injury quiescent astrocytes will exhibit hypertrophied processes and increase expression of cytoskeletal proteins, becoming reactive astrocytes. Adapted from White and Jakeman, 2008.

1.1.1 The double-edged sword: beneficial role of astrocytes vs. limitations of glial scar

Since damage to CNS will always produce a reactive gliosis, the place where regeneration fails inevitably contains a developing or established glial scar. All the cell types; astrocytes, oligodendrocyte precursors, meningeal cells, and microglia that make up this scar have inhibitory properties, and inhibition mediated by any one of these cell types, is probably sufficient to block CNS regeneration. However, not all of the cells are inhibitory all of the time (White and Jakeman, 2008).

Scarring astrocytes have long been considered as a major impediment to regeneration of damaged axons (Cajal, 1928) and consequently a detrimental to nervous tissue repair and functional restoration. Because of this response, astrocytes have historically had a stigma that has led many researchers to target them as cells that should be depleted after injury in order to attenuate their presence at the lesion site (Davies et al., 1997). However, astrocytes are enormously plastic, and can display growth-promoting or growth-inhibiting properties under different circumstances and in response to different stimuli.

The concept of a protective role for astroglial reactivity has only recently been established, emerging from the ability of reactive astrocytes to isolate the damaged core of vascular and traumatic lesions from the surrounding healthy tissue, thus reducing the spreading of toxic substances and metabolites released from dead cells and limiting the development of secondary damage (Rolls et al., 2009). These beneficial effects are related to the capability of astrocytes to produce supportive signals for neuronal and oligodendroglial survival, to preserve and restore altered homeostatic conditions (Hamill et al., 2005; Sofroniew, 2005), to generate an adaptative inflammatory response to aid in the removal of damaged and dead tissue from the site of injury, creating an improved niche for a subsequent reparative response and, when lost, to re-establish the anatomical barriers (glia limitans and BBB) (Eddleston and Mucke, 1993) necessary for the correct CNS functioning. However, glial cells that persist at the injury site produce inhibitory factors that manifest within hours of the original insult and severely inhibit growth into the lesion, including myelin-associated glycoprotein (McKerracher et al., 1994; Mukhopadhyay et al., 1994), chemokines that attract macrophages from the periphery to the site of injury (Otto et al., 2002; Strack et al., 2002), inhibitory extracellular matrix molecules such as ephrins (Fitch and Silver, 2008; Morgenstern et al., 2002; Zuo et al., 1998), Nogo (Bandtlow and Schwab, 2000), and chondroitin sulfate proteoglycans (CSPGs) (Lin et al., 2008) inducing new growth cones that extend very short distances because of the inhibitory chemical environment (Schwab and Bartholdi, 1996) forming at the end dystrophic cones (“abortive sprouting”) (Silver and Miller, 2004).

To achieve axonal regeneration, which is particularly crucial following injury, the physical and chemical inhibitory environment of the glial scar must be overcome. For example, Fawcett and colleagues have investigated the use of the enzyme chondroitinase ABC to degrade significant amounts of chondroitin sulphate proteoglycans contained by the glial scar and thereby provide a pathway for regeneration with some success (Crespo et al., 2007; Rhodes and Fawcett, 2004). Others have found that the inhibitory environment presented by astrocytes following injury can be neutralized by targeting the Rho-kinase receptor (Fournier et al., 2003; McKerracher and Higuchi, 2006). The complex environment of injured CNS exhibits aspects of inhibition and ongoing cell death with endogenous attempts to repair and regeneration. Some studies demonstrated (Tate et al., 2007) that endogenous reparative matrix proteins such as fibronectin and laminin could play and important role after CNS injury. Both of these extracellular matrix proteins are elevated following traumatic brain and spinal cord injury (TBI and SCI) and colocalize with macrophages, activated microglia (fibronectin) and brain microvasculature (laminin), suggesting that these proteins may play a function in repairing CNS damaged tissue.

Based on the dual role of astrogliosis (i.e., beneficial/detrimental with respect to tissue preservation/neuroprotection, tissue repair and functional recovery), ideal approaches try to inhibit the deleterious effects associated with neuroinflammation while preserving the inflammatory pathways that lead to neuroprotection and sustain regenerative responses in terms of circuit reorganization and cells replacement (Buffo et al., 2010) (Fig. I-5).

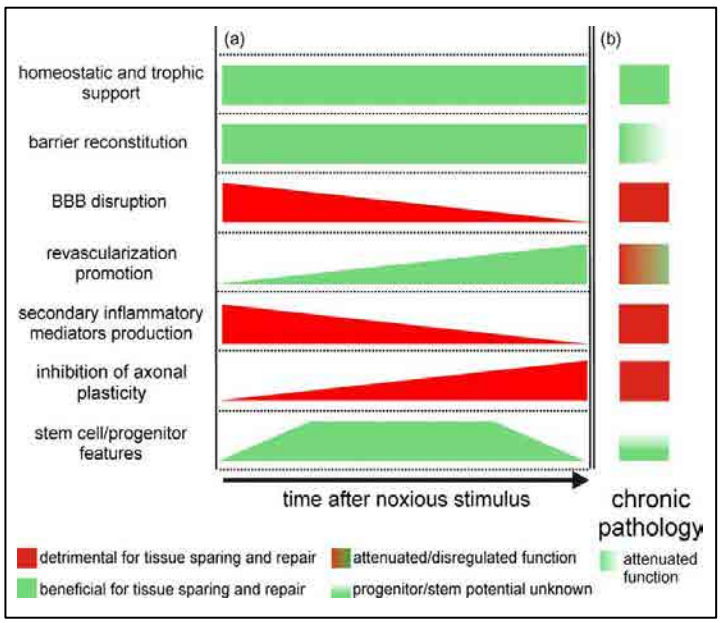

Figure I-5. Astrocyte functions in acute and chronic lesions. Panel (a). illustrates the evolution of detrimental and beneficial effects of astrocytic functions over time after injury. Increases or decreases over time as variation in the thickness of the horizontal bars. (b). Summarizes the outcomes of the same functions in chronic lesions. Adapted from Buffo et al., 2010.

Unfortunately, this strategy finds its limits suggesting that any attempt to interfere with negative traits will also affect reparative functions. However, the actual dynamic view of gliosis reveals that distinct detrimental effects are occurring at specific time points during the response to acute lesions or are specifically harmful when persisting chronically (Fig. I-5). On the basis of this knowledge, therapeutic approaches might be designed to inhibit deleterious effects during well-defined time windows or in specific types of injury (Buffo et al., 2010).

1.1.2 Blood–Brain Barrier (BBB) and Blood–Spinal Cord Barrier (BSCB)

The BBB or BSCB is a multicellular vascular structure that separates the CNS from the peripheral blood circulation. Beyond barrier function, influx and efflux are actively regulated at the blood-brain or spinal cord interface. By tightly controlling the passage of molecules and ions, instantaneously delivering nutrients and oxygen according to current neuronal needs and protecting the CNS from toxins and pathogens, the BBB or BSCB maintains an environment that allows neurons to function properly (Obermeier et al., 2013). The development and maintenance of the BBB-BSCB are governed by cellular and non-cellular elements that interact with the endothelial cells (ECs). Astrocytes, pericytes and extracellular matrix (ECM) components provide both structural and functional support to the BBB-BSCB. The term 'neurovascular unit' (NVU) additionally refers to neurons, microglial cells and, optionally, peripheral immune cells as they interact with core elements of the BBB-BSCB and influence barrier function (Abbott et al., 2006; Neuwelt et al., 2011) (Fig. I-6).

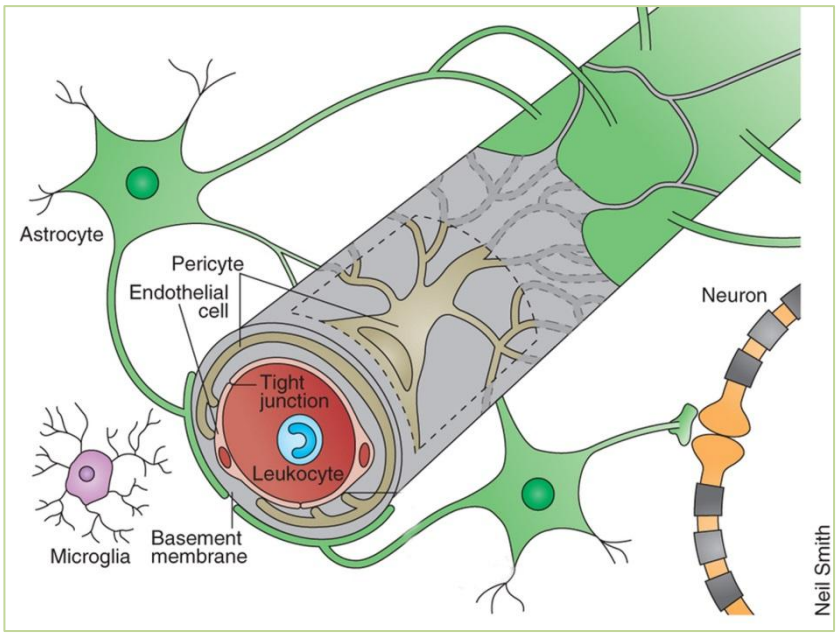

Figure I-6. Cellular interplay at neurovascular unit (NVU) in BBB. Adapted from Obermeier et al., 2013.

The BBB and the BSCB are similar and play an important role in the normal and pathologic injury response. A breach in the BBB or BSCB permits infiltration of macrophages, fibroblasts and other cell types, and inflammatory molecules into the site of injury. The opening of damage to the BBB and BSCB is a hallmark of CNS injury and disease, and while it can expose neural tissue to harmful blood-borne components, this symptom can also be exploited for neuroprotective and reparative molecules (Shoichet et al., 2008).

1.1.3. Dual role of inflammation in traumatic CNS injury

The inflammatory response is a subject of active debate within the neuroscience community. While some inflammation is clearly needed to limit degeneration and address the cellular debris resulting from CNS injury, there is active discussion on whether the inflammatory response should be further enhanced (Correale and Villa, 2004; Schwartz, 2000). Pro-inflammatory cytokines are released by microglia within minutes following traumatic injury, with acutely destructive effects (e.g., BBB and BSCB dysfunction, promotion of neuronal death) but are beneficial at later time points (e.g., inducing synthesis of antiinflammatory cytokines, inducing neurotrophic factor secretion, and promoting proliferation of oligodendrocyte precursor cells that may help in remyelination) (Morganti-Kossmann et al., 2002). With respect to the cellular aspect of the inflammatory response, microglia are the first to respond (minutes to hours) by proliferating, activating, and migrating to the area of injury, where they essentially function as macrophages (Kato and Walz, 2000; Ladeby et al., 2005). Increased BBB and BSCB permeability contributes to leukocyte infiltration from the blood to the injury site, a process that is mediated by cytokines, chemokines, and complement proteins (Schmidt et al., 2005). Neutrophils infiltrate (hours to days), followed by monocytes (days) (Kato and Walz, 2000). Again, these immune cells have dual roles. The oxidative burst of neutrophils and macrophages is harmful because of the release of oxygen free radicals and neurotoxic enzymes (Schmidt et al., 2005); however, both activated microglia and monocyte-derived macrophages aid in clearing debris from dead and damaged cells via phagocytosis (Ladeby et al., 2005).

Schwartz and collaborators have found that infiltrating monocyte-derive macrophages, expressing markers as CX3CR-1, act as resolving macrophages needed for terminating the local inflammatory phase that occurs as part of an ongoing process of healing (Shechter et al., 2009; Shechter et al., 2011). These cells were further shown to secrete the matrix degrading enzyme metalloproteinase (MMP-13) needed for resolving the glial scar tissue. Moreover, they also found that *ex-vivo* transplantation of macrophages stimulated to an “alternatively” activated phenotype are pivotal for recovery spinal cord injury if they are introduced to the margins of the lesion site at the precise time and at specific concentrations after the injury; however, clinical

trials have been stopped (Schwartz and Yoles, 2005).

Efforts are ongoing to further elucidate the critical components of CNS injury responses that prevent meaningful regeneration. While these recent advances offer promises in restoring function, a number of challenges remain unclear because of the complex and dynamic environment of the injured CNS.

Due to the complexity of CNS, in this thesis we will focus on the evolution of the brain injury response, which involves a dynamic interplay between events promoting repair and regeneration and those of damage and inhibition. However, in spinal cord the majority of the events are similar.

2. Regeneration is possible following CNS injury?

‘‘In the adult centers the nerve paths are something fixed, ended and immutable. Everything may die, nothing may be regenerated.’’ Ramon y Cajal’s *Degeneration and Regeneration of the Nervous System (1928) (Cajal, 1928).*

The above statement formed the basis for the scientific dogma ‘‘adult neurogenesis does not happen’’ that dominated neuroscience for more than 30 years. A consequence to this is that for those who have sustained CNS damage, there is no hope of recovery. However, in contrast to the historical belief of the missing capability of the CNS to regenerate it was demonstrated that in special CNS areas, new neurons are constantly generated from progenitor cells (Altman and Das, 1964). Many studies now confirm that new neurons are continuously formed in adult brains in diverse species including primates and humans (Eriksson et al., 1998; Gould et al., 1999b). Furthermore, studies have shown that traumatic and ischemic injuries to adult brain stimulate the formation of new neurons, glial cells, and the migration of neural progenitors to the sites of injury thought to be an attempt to self-repair increasing optimism for functional recovery after a CNS insult (Gould et al., 1999a; Kernie et al., 2001; Ramaswamy et al., 2005; Rola et al., 2006).

2.1 Aspects of evolution and development in CNS

For many years the mammalian CNS has been seen as an organ that is unable to regenerate. However, it was also long known that lower vertebrate species are capable of notable regeneration of CNS structures. How did this situation arise through evolution? It has long been argued whether the ability to regenerate was present in the ancestral species and was lost during evolution (Tanaka and Ferretti, 2009) (Fig. I-7). Caution must be taken when comparing regeneration between species based on the accumulated experiments from many researchers because regeneration is a complex trait that can vary according to location and damage. Another important question of regeneration is its life-stage dependence. In response to injury, primitive animals regenerate complex structures (including brain and spinal cord) from remnants of themselves, whereas higher vertebrates as frogs, birds and in particular mammals, lose regeneration capacity over the course of maturation in various regeneration contexts such as brain lesion and non-CNS structures as the limbs, healing or 'wall-off' their injuries by fibrosis and scarring (Fig.I-7) (Beattie et al., 1990; Gallien and Beetschen, 1951; Nicholls and Saunders, 1996; Tanaka and Ferretti, 2009). Why would evolution select for scarring?, which is a less structurally and functionally refined mechanism of tissue repair?

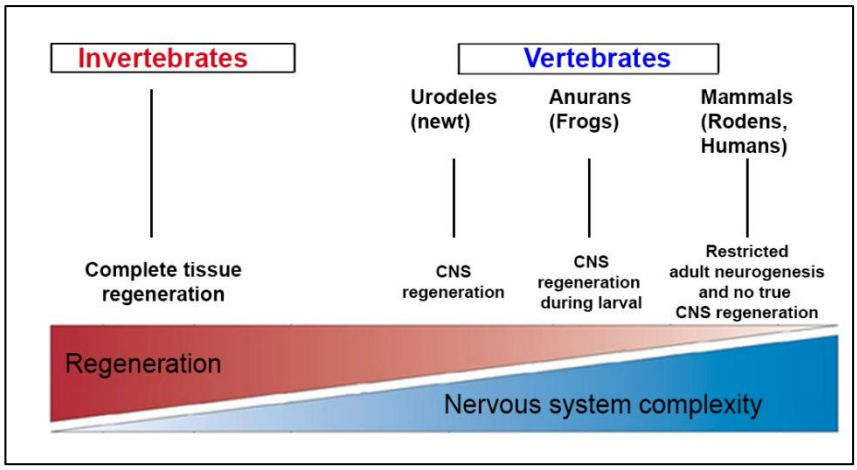

Figure I-7. Schematic overview of CNS regeneration ability in invertebrates and vertebrates. Adapted from Popovich and Longbrake, 2008.

2.2 Radial glia; the neural stem cell

The key point in CNS regeneration that differs among vertebrates is the response of glial cells to injury. Organisms with capacity to regenerate, such as newt or salamander, can successfully resolve a lesion recapitulating the steps carried out during early embryonic development to establish CNS in the first place. A common feature of these species that regenerate the CNS is that they retain a type of embryonic glia during the adult called radial glia (Tanaka and Ferretti, 2009).

During embryonic brain development (also in mammals) radial glia cells (RGC) were first identified to serve as scaffold for radial migrating neurons (Hatten, 2002; Levitt and Rakic, 1980; Rakic, 1988). Recently, RGC have acquired further interest due to their crucial role in a variety of developmental processes including their role as a principal neural stem cell (NSC-RGC) (Campbell and Gotz, 2002; Kriegstein and Gotz, 2003) and maintaining their self-renewal capacity giving rise to multiple cell types such as neurons, astrocytes and oligodendrocytes (Fig. I-8).

Radial glial cells are well defined by their characteristic bipolar/radial morphology and their glial properties. The soma of a radial glial cell lies in the ventricular zone (VZ) of the brain and a long radial process extends from its cell-body throughout the neural wall to the basement membrane (BM) at the pial surface (Bentivoglio and Mazzarello, 1999; Cameron and Rakic, 1991) (Fig. I-8). They express a specific pattern of cellular markers as they proceed in development (Malatesta et al., 2000). A variety of proteins like the intermediate filaments Vimentin (Barry and McDermott, 2005; Dahl, 1981) and Nestin (Barry and McDermott, 2005; Gilyarov, 2008), the brain lipid binding protein BLbP (Barry and McDermott, 2005), the

transcription factors Pax6, and the intracellular protein Sox2 (Wen et al., 2008) can be used as markers to identify the NSC-RGC.

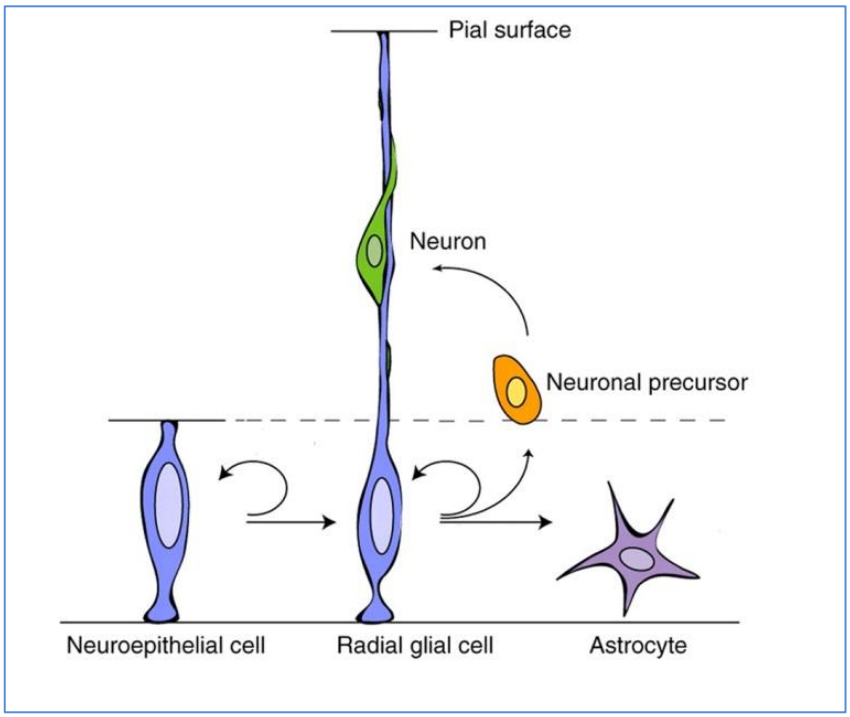

Figure I-8. Radial glial evolution during development. Radial glia derives from neuroepithelial cells. Radial glia can divide symmetrically and asymmetrically to produce neurons and glia. In mammals, radial cells disappear perinatally, when they are thought to transform into astrocytes. Adapted from Kageyama et al., 2007.

Furthermore, taking advantage of the proliferative nature of RGC, S-phase markers such as Bromodeoxyuridine (BrdU, a timidine analogous), and different proteins present in particular phases of the cell cycle as Ki67 (G1, S, G2, and mitosis phase marker) and phosphorylated histone H3 (mitosis phase marker), also allow to identify these progenitor cells. In non-regenerating vertebrates including humans, in postnatal stages of development, radial glia that are used as scaffold to neuronal migration into their final destination, transform into astrocytes at the end of neurogenesis (Ponti et al., 2013).

Therefore the composition of glial cell population and its response to injury is the major difference among regenerative and non-regenerative vertebrates; regenerative species have retained radial glia cells which serve as a neurogenic and gliogenic stem cell whereas glial cells in non-regenerative vertebrates lose their radial character and transform to mature neurons and astrocytes (see 2.3). After an injury astrocytes do not have the capacity to be reprogramed to radial glia cells and they change to reactive astrocytes ultimately generating a glial scar as we described before. However, several studies demonstrated that neural stem cell niches remain in in the adult brain and can be active after injury (see chapter 3) (Tanaka and Ferretti, 2009; Weissman et al., 2003).

2.3 Neurogenesis – Gliogenesis and their cellular lineages

2.3.1 Neurogenesis

Neurogenesis is a process, in which the principal neural stem cells; *radial glia (NSC-RGC)* lead to all neurons that will form the mature brain. Generally, NSC-RGC first generate neurons, and later produce glia, and the switch from neurogenesis to gliogenesis is the result of changes in stem-cell properties that are controlled by both extrinsic and intrinsic cues (Bertrand et al., 2002).

During embryonic development there are two main neurogenic regions in the brain: the ventricular zone (VZ) and the subventricular zone (SVZ). The ventricular zone (VZ) is a pseudo-stratified epithelium containing NSC-RGC (Bonfanti and Peretto, 2007; Brazel et al., 2003). Neurogenic niches have similar cellular components at all life stages: neural stem cells (Doetsch et al., 1999; Quinones-Hinojosa et al., 2006); blood vessels (Doetsch, 2003; Shen et al., 2004); extrinsic factors released by supporting cells within the niche (EGF, VEGF, BDNF, Sonic hedgehog or BMP) (Jiao and Chen, 2008); and extracellular matrix (basal lamina collagens and laminin) (Fuchs et al., 2004; Kazanis et al., 2010).

These populations physically reside within instructive local niches that maintain and regulate stem cells fate. These neurogenic zones are intimately associated with their local microvasculature beds. At the time of early neurogenesis, sprouts of preexisting blood vessels enter the neural tube from outside and are distributed radially. Once in the CNS, blood vessels and neural tissue develop in parallel, influencing each other, giving rise to the neurovascular niche at the subventricular zone (SVZ) (Fig. I-9) (Stubbs et al., 2009; Tam and Watts, 2010).

Fig. 1 .Schematic of the neurovas
niche. Distinct neurogenic re
including the SVZ (illustrated
and the subgranular zone (SGZ)
have been shown to res
differentially to injuries and sti
The vasculature is an int
component of these neurogenic
and angio- and neuro-genesis in
areas appears to be co-regulated
reciprocally signaled (7). Sign
among the cell types present is th
occur *via* soluble and solid
factors and their cognate recepto

Figure I-9. Schematic of the neurovascular niche. The neurovascular niche located in the SVZ and the co-regulation mechanisms between endothelial and neural stem cells. Adapted from Madri, 2009.

During neurogenesis, NSC-RGC generate post-mitotic neurons and intermediate or basal progenitors. This multipotency gives the capacity to exhibit different types of division (Anthony

et al., 2004; Tanaka and Ferretti, 2009; Weissman et al., 2003); namely symmetric divisions that increase the NSC-RGC population; asymmetric divisions that produce another NSC-RGC and a daughter cell that is more restricted in its differentiation ability (an intermediate progenitor cell); and terminal symmetric divisions, which generate two differentiated daughter cells (post-mitotic neurons) (Alvarez-Buylla and Garcia-Verdugo, 2002; Morshead and van der Kooy, 2004; Weiss et al., 1996) (Fig. I-10). Post-mitotic newborn neurons originated from NSC-RGC migrate to reach their corresponding position in the developing brain, while intermediate progenitors (IPC) appear at the onset of neurogenesis and also migrate away from the ventricular surface where they establish in a second proliferative layer at the basal side of the VZ generating the SVZ (Fig. I-10). As development proceeds, the VZ diminishes in size and the subventricular zone (SVZ) grows. The VZ reaches its maximal size during midstage neurogenesis and after this phase begins to shrink while the SVZ begins to expand and takes on the responsibility of cell genesis, including astroglial and oligodendroglial cells (Bonfanti and Peretto, 2007; Brazel et al., 2003; Skihar et al., 2009).

The populations of ventricular and subventricular progenitors share common markers like Ki67 and phosphorylated histone H3 (PH3) demonstrating their proliferative nature. Derived from RGC, IPC, which divide in basal positions in the VZ, are the first cell types to initially seed the SVZ (Tabata et al., 2012). While some observations describe the distribution of IPC throughout the upper VZ and lower intermediate zones (Noctor et al., 2004; Tarabykin et al., 2001) they are predominantly concentrated in the SVZ, where they almost exclusively divide symmetrically producing two IPCs or two neurons in one or two mitotic cycles (Englund et al., 2005b; Noctor et al., 2004; Pontious et al., 2008) (Fig. I-10). Additionally, *IPC (also called neuronal restricted progenitors)* have been proposed as a neurogenic transit amplifying progenitors, which would exponentially increase the neuronal pool (Reillo et al., 2010). Some studies have pointed out that the early loss of IPC produces a dramatic decrease in cortical surface expansion and thickness along the cortical wall demonstrating the importance of this progenitor population (Reillo et al., 2010; Sessa et al., 2008).

IPCs (or neuronal restricted progenitors) populations can be distinguished from NSC-RGC, by the expression of characteristic transcription factors. Englund and collaborators clearly described the sequential expression pattern of Pax6→Tbr2→Tbr1→NeuN during the differentiation of RGC ($Pax6^+$) to IPC ($Tbr2^+$) and the resulting *newborn neurons* ($Tbr1^+$) (Englund, Fink et al. 2005) that give rise to the *post-mitotic neurons*; $NeuN^+$ (Englund et al., 2005a) and β-Tubulin III^+. Tbr2 gene encodes a member of the T-box family of transcription factors that are characterized by the common feature of the evolutionary highly conserved T-box DNA-binding domain and is widely used as IPC marker. Other transcription factors allow to distinguish RGC from IPC too: Emx2 and Sox2 are expressed exclusively in RGC, while Cux1-2, Lmo4 and Svet are exclusive to IPC (Gotz and Huttner, 2005; Nieto et al., 2004;

Tarabykin et al., 2001) (Fig. I-10). During postnatal period, this secondary proliferative region (SVZ) will aid to increase the neuronal pool whereas RGC lose their ventricular attachment and they transform into astrocytes. Consequently, proliferative IPC become the predominant component of the cortical neuronal progenitor pool, and eventually comprise the majority of mitotic progenitors as embryonic neurogenesis nears completion.

Once the neurogenesis ends, the *post-mitotic neuronal cells* are identified by the expression of specific markers such as β-III-tubulin (Tuj-1) or Neuron-specific nuclear (NeuN) protein. The corresponding antibody of NeuN, developed by Mullen in 1992 (Mullen et al., 1992) primarily stains the neuronal nucleus, but the cytoplasm and dendrites are also immunoreactive, though to a lesser extent (Lavezzi et al., 2013). Noteworthy NeuN does not stain the immature neuronal cells until they exit from the cell cycle and achieve a stage of development that at least approaches mature function. However, *newborn neuronal cells* could be discerned to post-mitotic neurons by the aid of immature neuronal markers such as the transcription factor Tbr1 mentioned before, or the microtubule binding protein doublecortin (DCX) (Brown et al., 2003b; Rousselot et al., 1995). This marker apart to be associated to newly born neurons is used to determine the levels of neurogenesis in the adult brain and could be related to neurite and axon elongation, and synaptogenesis (Deuel et al., 2006; Plumpe et al., 2006; Ribak et al., 2004).

2.3.2 Gliogenesis

The gliogenesis starts during the perinatal period, at the end of neurogenesis, when the radial scaffold is no longer required for neuronal migration because they reach their final position (Rakic, 1971; Rakic, 1972). RGC from the VZ lose their bipolar morphology and transform into astrocytes. They gradually down-regulate expression of Nestin (Barry and McDermott, 2005) and Pax6 (Pinto et al., 2007), become morphologically more complex and start to express typical astrocyte markers as GFAP (Bullon et al., 1984); BLbP (Eng et al., 1971) and maintaining the glutamate transporters GLAST (EEAT-1) and GLT-1 (EEAT-2) (Sims and Robinson, 1999) (Fig. I-10). The inner accumulation of GFAP in transforming cells is strong evidence that support this developmental transition. Immunostaining assays for different antigens expressed by RGC and immature astrocytes, precisely describe how during neurogenesis the expression of the radial precursors markers change, increasing the expression of more astrocytic related proteins (Hartfuss et al., 2001).

During the initial postnatal period, *astrocytes* and *oligodendrocytes* are generated in the highly proliferative SVZ. There are precursors in the SVZ that are restricted to generate glial cells, such in case of neurons (Pinto et al., 2007). The SVZ precursors can be rather easily distinguished from RGC, because most of the more characteristic radial markers, such as Nestin, Vimentin, BLBP, GLAST, are absent in subventricular progenitors. In contrast, two-thirds of SVZ cells that will generate astrocytes and oligodendrocytes express markers such as

polysialic acid neural cell adhesion molecule (PSA-NCAM) (Bonfanti and Theodosis, 1994), which is not expressed by RGC (Fig. I-10) (Rowitch and Kriegstein, 2010).

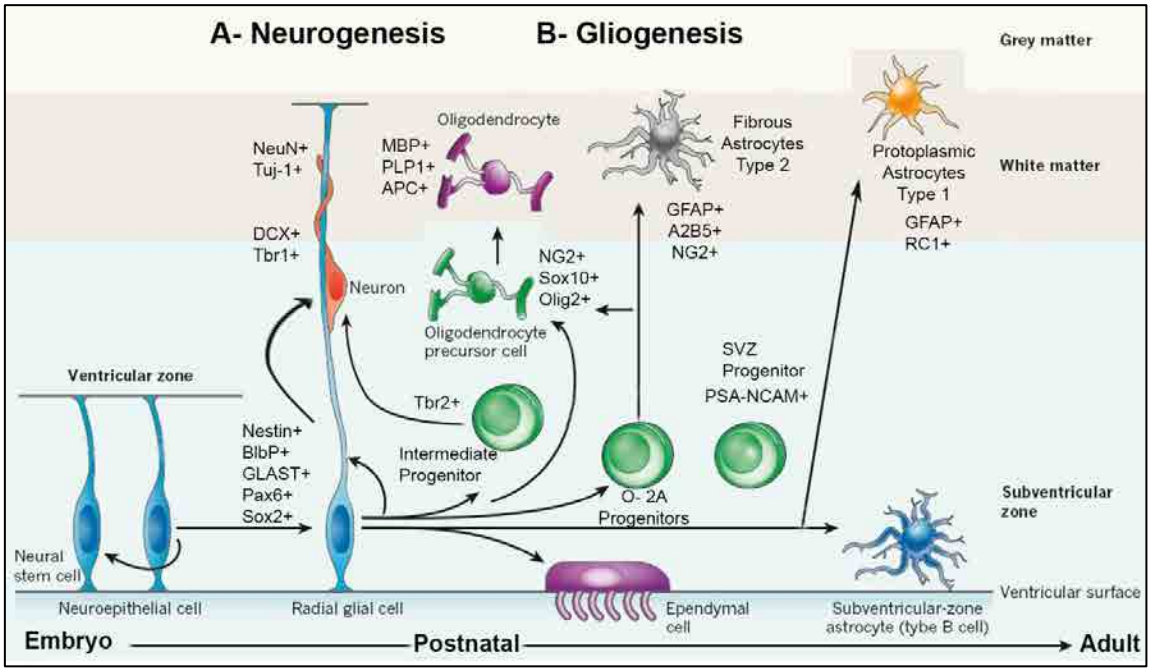

Figure I-10. Schematic patterns of gliogenesis and neurogenesis in embryonic and postnatal progenitor zones. Black arrows indicate self-renewal or differentiation from one cell type to another. Markers of macroglia and their precursors are listed. Radial glia produce intermediate progenitor cells and oligodendrocyte precursor cells (OPCs), which in turn produce neurons and oligodendrocytes, respectively. Radial glia can also produce neurons and become astrocytes, as well as producing intermediate progenitors that expand in number before producing astrocytes. Protoplasmic astrocytes and fibrous astrocytes might arise from independent progenitors. Radial glia also produce ependymal cells. Adapted from Rowitch and Kriegstein, 2010.

Mature astrocytes constitute a heterogeneous group of cells, which show different morphology and molecular patterns, including levels of intermediate filaments (mainly GFAP), growth factors, ions channels and neurotransmitter transporters. It is still unknown if these differences are determined by their origin (RGC or SVZ progenitors) or by local environmental factors (Eng et al., 1976; Vives et al., 2003). However, mature astrocytes are subclassified by their morphology, location (Rowitch and Kriegstein, 2010) and depending on their lineage and antigenic features (Raff et al., 1983) (Fig. I-10) as either.

Protoplasmic or type 1 astrocytes are found in the grey matter, have more irregular, 'bushy' processes and typically have few glial filaments. They are GFAP positive cells and come into contact with and ensheath synapses by extending thousands of thin processes, some of which also contact blood vessels (Rowitch and Kriegstein, 2010). It has been suggested that Type 1 astrocytes are generated from RGC because it is known that they develop early during

gliogenesis and they initially express RC1 marker. In fact, there is clear evidence that RGC would generate a subset of astrocyte-restricted precursors with radial-shape that initially retain RC1 epitope and posteriorly express GFAP and acquire stellate-shape typical of astrocytes (Culican et al., 1990).

Fibrous or type 2 astrocytes populate the white matter and typically have a 'star-like' appearance with dense thinner, and longer glial filaments that can be stained with the intermediate filament marker GFAP. Type 2 astrocytes appear during postnatal period and come from a bipotential O-2A progenitor (able to give rise to type 2 astrocytes and oligodendrocytes). Ganglioside A2B5, proteoglycan NG2, growth associated protein GAP-43 among others, are specific markers for type 2 astrocyte and O-2A progenitors (Scolding et al., 1999).

Oligodendrocyte precursors cells (OPCs) also derive from radial glial cells, but whether intermediate progenitors are involved is uncertain. OPCs express platelet-derived growth-factor receptor-α (PDGFR-α), transcription factor Olig-2 and the proteoglycan NG2 (also known as CSPG4). These cells maintain proliferative and migratory competence during development, in the adult, and are early responders to injury. *Mature oligodendrocytes* by contrast, express a variety of myelin markers, including myelin basic protein (MBP), proteolipid protein 1 (PLP1) and adenomatous polyposis coli (APC) protein (Fig. I-10) (Rowitch and Kriegstein, 2010).

2.4 The adult stem cell niche

Although the idea that the nervous system contains stem cells was viewed as a radical one in the not so distant past, recent studies show that the adult brain contains NSCs that can and do generate neurons and glial cells on an ongoing basis. These adult NSCs, which are generated from the precursors that build the nervous system during development (Kokovay et al., 2008), are maintained into adulthood in at least two niches; the subventricular zone (SVZ) (Gage, 2000; Lois and Alvarez-Buylla, 1994; Luskin, 1993) of the lateral ventricles and the dentate gyrus (DG) in the hippocampus (Eriksson et al., 1998; Knoth et al., 2010). From the SVZ, the newly generated neurons reach their final destination in the olfactory bulb (OB) after long-distance migration through a well-defined path called the rostral migratory stream (RMS) or pathway (RMP) while what guides this migration is not well understood (Fig. I-11) (Alvarez-Buylla et al., 2001; Lois and Alvarez-Buylla, 1994; Luskin, 1993). The major function of the neurogenesis in adult brain seems to be replacing the neurons that die regularly in certain brain areas (Wiltrout et al., 2007). Although there is lively discussion concerning the possibility that NSCs are more widely scattered throughout the adult brain (Gould, 2007) the composition of neurogenic niches have been well characterized in adult mammals (Doetsch and Scharff, 2001).

In the adult brain, three populations of precursors in the SVZ, including adult NSCs, lie adjacent to a layer of ependymal cells lining the lateral ventricle wall (Fig. I-11, I-12); The B cells are astrocytes and are considered as the "stem cells". They are relatively quiescent cells that express markers reminiscent of embryonic radial precursors, as well as the typical astrocyte protein GFAP.

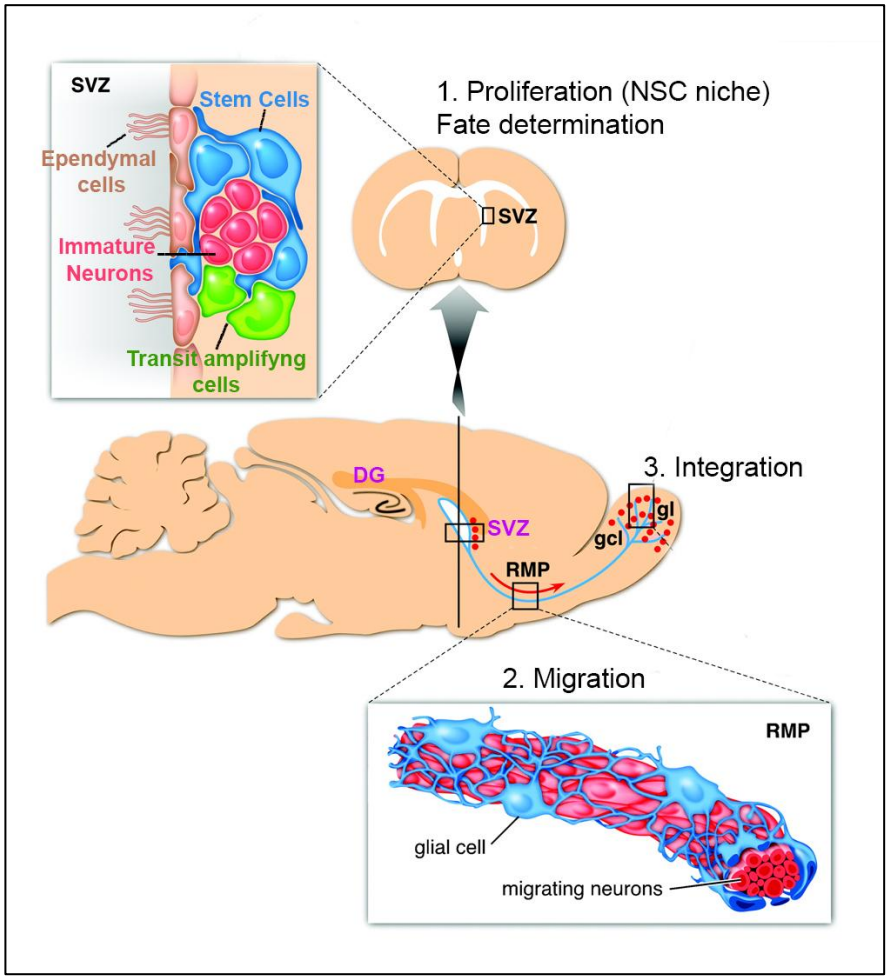

Figure I-11. Neurogenic zones of the adult mammalian CNS. The dentate gyrus (DG) and the Subventricular zone (SVZ) are the two niches in adult brain. 1. Proliferation and fate determination: Stem cells in the SVZ of the lateral ventricle (blue) give rise to transit amplifying cells (green) that differentiate into immature neurons (red). Adjacent ependymal cells (brown) of the lateral ventricle are essential for the neuronal fate determination by providing inhibitors of glial differentiation. 2. Migration: Immature neurons (red) migrate along each other in chains through the rostral migratory pathway (RMP). The migrating neurons are ensheathed by astrocytes (blue). 3. Integration: Immature neurons differentiate local interneurons (red) in the granule cell layer and the periglomerular layer. Adapted from Lie et al., 2004.

B cells give rise to transit-amplifying cells, called C cells, which in turn generate neuroblasts. C cells are more rapidly dividing population and are GFAP negative but positive for EGF receptor and the transcription factor Dlx2. The third population is the neuroblasts, called A cells, that express markers of newborn neurons such as doublecortin and PSA-NCAM. (Miller and

Gauthier-Fisher. 2009) (Fig. I-11 and I-12). The neuroblasts migrate along the RMS to the olfactory bulb (OB) and generate neurons that integrate into the neural circuitry (Doetsch et al., 1997) (Fig. I-11 and I-12).

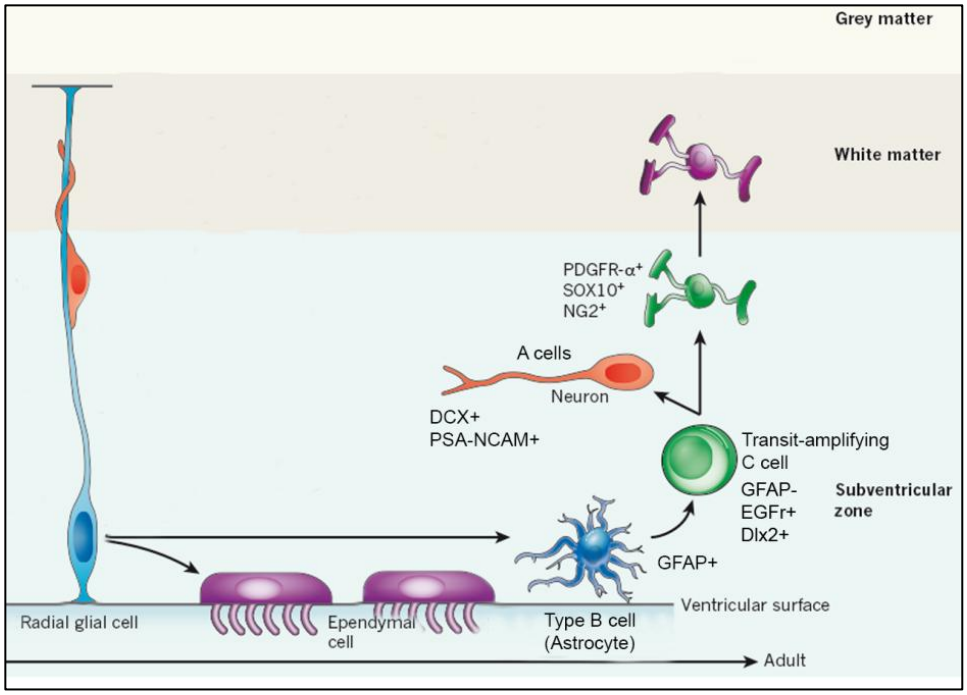

Figure I-12. Schematic patterns of neurogenic niche in adult progenitor zones. Black arrows indicate self-renewal or differentiation from one cell type to another. Type B cells in the cortical subventricular zone produce transit-amplifying cells (known as type C cells), which in turn produce neurons as well as some OPCs. Adapted from Rowitch and Kriegstein, 2010.

The main function of a niche is to maintain a constant number of stem cells. When challenged by damage or injury, stem cells leave their niche and proliferate or differentiate to try to regenerate lost tissue (Lander et al., 2012).

The maintenance of any tissue stem cell population is the result of a complex interplay between intrinsic mechanisms and extrinsic cues derived from the stem cell niche. Emerging evidences indicate that the NSC niche also provides an environment that ensures maintenance of NSCs for the lifetime of the animal. The NSC niche, like all tissues, is a constantly changing microenvironment with many factors at play. Soluble factors including cytokines, neurotrophic or growth factors, and differentiation cues are constantly synthesized, secreted, transported, and depleted. Apart from the relevance of the soluble factors which play an important role in maintaining stemness and directing stem cell fates *in vivo* (Fig. I-13) (Kokovay et al., 2008; Zhao et al., 2008) distinct aspects of two particularly interesting components of the niche will be considered.

The first highlights the importance of the interaction between NSCs and *the vasculature* (Fig. I-13). Interestingly, the SVZ vasculature is somewhat unique. Differences in permeability, stability, and perivascular cell coverage are thought to account for these differences (Goldberg and Hirschi, 2009). NSC and transit-amplifying cells both display an intimate relationship with SVZ blood vessels, as three-dimensional niche modeling indicates closer proximity and increased vascular contact relative to other SVZ cells (Javaherian and Kriegstein, 2009). It has been suggested that the developing vasculature within the SVZ promotes neuronal restricted progenitors/IPC (see chapter 2.3) expansion during neurogenesis by providing a suitable microenvironment (Javaherian and Kriegstein, 2009). It is noteworthy that SVZ endothelial cells (EC) share similar molecular profiles with their neighboring NSC. For example, ventral and dorsal EC, as well as NSC, express Dlx1/5 and Nkx2.1, and Pax6, respectively, while pial EC are negative for all three (Vasudevan and Bhide, 2008). This strongly suggests that mechanisms of patterning during early angiogenesis and neurogenesis in the brain are shared. Moreover, increasing evidences suggest that neuronal restricted progenitors Tbr2, are temporally and spatially correlated with the appearance of cortical vasculature, and even follow and mimic the pattern of nascent blood vessels. Similarly, the positions of neuronal restricted progenitors/IPC during mitosis, migration and differentiation are all correlated with EC development in the SVZ (Javaherian and Kriegstein, 2009). These data collectively suggest that the SVZ vasculature serves as a niche for mitotic neuronal restricted progenitors/IPC (Javaherian and Kriegstein, 2009), and provides instructive and permissive cues for stem and progenitor cell expansion and tissue invasion (Goldman and Chen, 2011).

Interestingly, these neurovascular associations are further exaggerated in niche regeneration models (Shen et al., 2008; Tavazoie et al., 2008). Additionally, NSC extends a long basal process that terminates on blood vessels in the form of specialized endfeet, potentially serving to integrate vascular cues (Fig. I-13) (Mirzadeh et al., 2008; Shen et al., 2008). Moreover, blood vessels not only serve as signaling conduits, facilitating local and long-distance systemic transmission of molecules; they are also used as migratory scaffolds for neural progenitor cells (Palmer et al., 2000), and the intimate association between stem cells and endothelial cells has been reported to regulate stem cell self-renewal and differentiation (Riquelme et al., 2008; Shen et al., 2004). Multiple co-culture experiments demonstrate that endothelial cells significantly affect the composition of embryonic NSC cultures. For example, the presence of endothelial cells in NSC co-cultures seems to increase stem cell self-renewal through the Notch1 effector Hes1 (Goldberg and Hirschi, 2009; Shen et al., 2004).

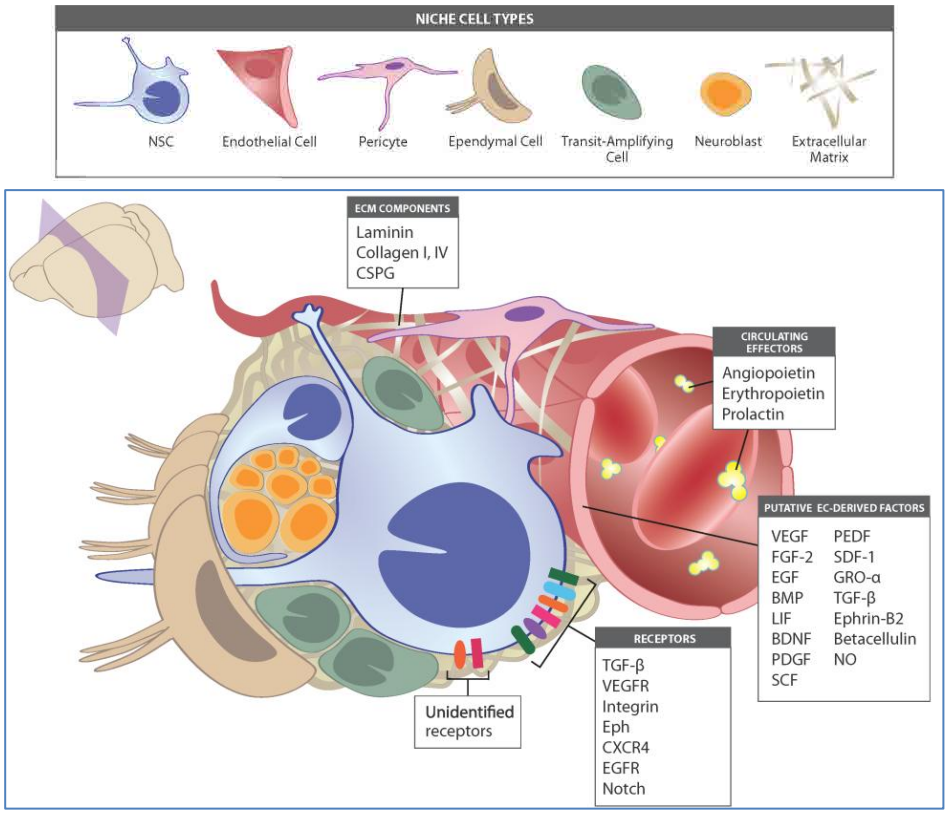

Figure I-13. Vascular – derived regulators of the neural stem cell niche. Sources of vascular –adult NSC niche effectors originate from the endothelium, circulation, ECM deposition, and perivascular cell types. Adapted from Goldberg and Hirschi, 2009.

The second component involves *the extracellular matrix (ECM) proteins*. The ECM is an integral component of the NSC niche, regulating signaling by providing, storing, and compartmentalizing growth factors and cytokines indispensable for the activation, proliferation and differentiation of NSCs (Fig. I-13). Within the SVZ, a unique basal lamina, rich in laminins, collagen I and collagen IV, extends from perivascular cells as 'fractones' (Kerever et al., 2007). Each fractone consists of a base, attached to the perivascular cell, a stem that crosses the SVZ, and terminate just underneath the ependymal layer (Mercier et al., 2003). The branched configuration of fractones has been suggested to enable sequestration and subsequent presentation of growth factors and other signaling molecules to stem cells and progenitors to regulate their activation and proliferation, within the niche (Mercier et al., 2002).

ECM molecules secreted by niche cells like laminin and fibronectin have been implicated in neural stem cell growth, differentiation, and migration. Shen and coworkers (Shen et al., 2008) have proposed that NSC contacts with vasculature occur primarily through integrins that bind the laminin present in blood vessels. Landmark studies by Mercier and coworkers (Mercier et al., 2002) have served to describe the most neurogenic regions of the SVZ in the adult brain as

dense laminin-rich extravascular basal lamina structures, which further signify the importance of integrin ligands in the NSC niche.

Moreover, Campos and colleagues showed the activity of the laminin receptor integrin β1 in neurogenesis (Campos et al., 2004) and the important role of laminin–integrin interactions within the SVZ in migration, spreading and proliferation of NSC (Shen et al., 2004).

Other studies *in vitro* have highlighted a critical role for β1-integrin in mediating multiple effects of ECM on NSC in a temporally and spatially controlled manner. For example, genetic ablation of β1-integrin results in reduced neural progenitor proliferation, increased cell death, and impairment of cell migration on different ECM substrates (Tsang et al., 2010). In β1-integrin-deficient neurospheres, β1-integrin signaling is not required for NSC maintenance, and instead seems to cooperate with growth factor signaling to regulate progenitor number (Leone et al., 2005). Studies *in vivo* demonstrated that the role of laminins in migration and recruitment are critical, as injection of intact laminin and peptide infusion mimicking the E8 domain of the laminin α chain dramatically redirects neuroblast migration towards the site of administration. Interestingly, adult neural stem cells interact with the endothelial cells of blood vessels in their vicinity via the laminin receptor, α6β1 integrin (Shen et al., 2008). Inhibiting the α6 or β1 subunits with antibodies also recapitulates the migratory defect without causing neuroblast death (Emsley and Hagg, 2003). It also has been demonstrated that β-integrins might indirectly activate other cell surface receptors that transduce information to NSCs (Campos et al., 2004; Mobley et al., 2009) which indicate that integrin ligands serve as key signals in regulating the NSCs environment (Goetz et al., 2006).

3. Remodeling the neurovascular niche after brain injury

3.1 Angiogenesis and neurogenesis after traumatic brain Injury (TBI)

Following CNS injury the repair/recovery process is thought to involve both angiogenesis and neurogenesis. The discovery of neural stem cell niches in the adult brain has raised the possibility of endogenous neuronal replacement after injury or disease. It is now established that following CNS injury several changes in the brain take place at the proliferative niche, the SVZ and also near the damaged area (Mirzadeh et al., 2008; Shen et al., 2008). Different classes of molecules such as trophic factors, morphogens, cytokines, and other cell signaling molecules have been identified as key players regulating this process. Neural repair involves remodeling the boundaries of the lesion, forming new blood vessels, elaborating new neuronal connections and generating new populations of neurons and glia. Notably, recent studies have shown that the vasculature in the SVZ is an important component of stem-cell niches (Mirzadeh et al., 2008; Shen et al., 2008), suggesting that the formation of new blood vessels through sprouting from preexisting vessels (Quaegebeur et al., 2010), a phenomenon called angiogenesis, occurs after stroke or/and traumatic brain injury processes (Ergul et al., 2012).

Szele and Chesselet reported that aspiration lesions of the cerebral cortex resulted in increased cell number in the SVZ (Szele and Chesselet, 1996). Saha et al. reported that many studies showed that blood vessels can act as a scaffold for cortical brain lesion (Saha et al., 2013); Some examples are showed by Gotts and Chesselet, where thermocoagulation lesion of the cortex induced an increase in the endothelial cell proliferation followed by expansion of vascular tree at the level of the SVZ after 7 days of injury (Gotts and Chesselet, 2005). Others corroborated that vasculature and neuroblast migration patterns go hand-in-gloves after brain injury. In cerebral ischemia, neuroblasts DCX^+ are shown to migrate from the SVZ to the areas of infarct (Fig. I-14a). These new neuronal cells frequently forming chain-like structures similar to those observed in the RMS, are in close association with blood vessels and astrocytic processes (Figure I-14b-d) (Kojima et al., 2010; Ohab et al., 2006; Thored et al., 2007; Yamashita et al., 2006).

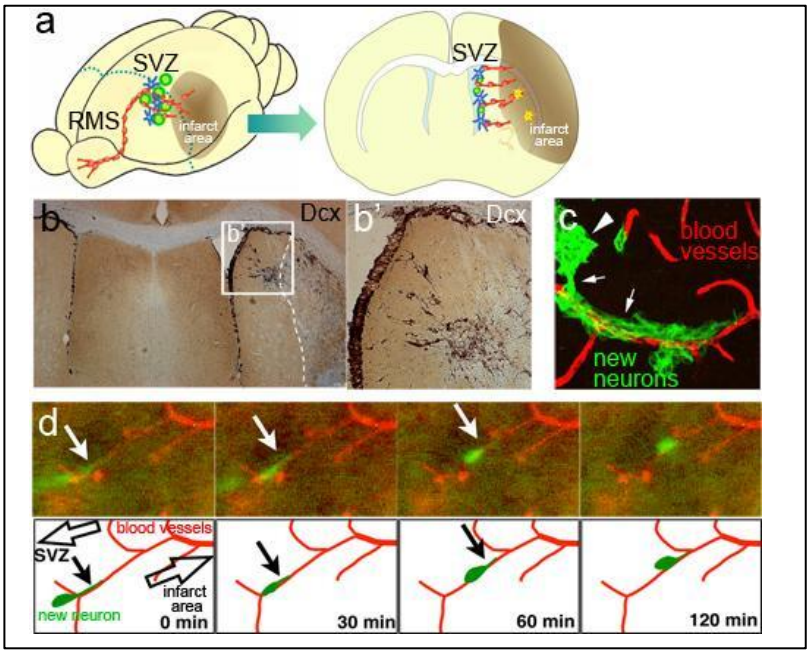

Figure I-14. Migration of new neurons to an infarcted area. (a) Schematic drawings of SVZ new neurons migrating toward an infarcted area; (b) Mouse brain section 18 days after experimental ischemic stroke stained with the new neuron marker DCX (brown). (c) Association of migrating new neurons with the vasculature. (d) Time lapse imaging of vascular scaffold for new neurons migrating toward the infarcted area. Adapted from Kaneko et al., 2011.

Other studies showed that after brain trauma, increased neuroblasts migration from the SVZ to the damaged cerebral cortex (Fig. I-15), a region recognized as non-neurogenic under normal conditions; white matter structures, and some contralateral regions (Nakayama et al., 2010; Ramaswamy et al., 2005; Saha et al., 2012; Urrea et al., 2007).

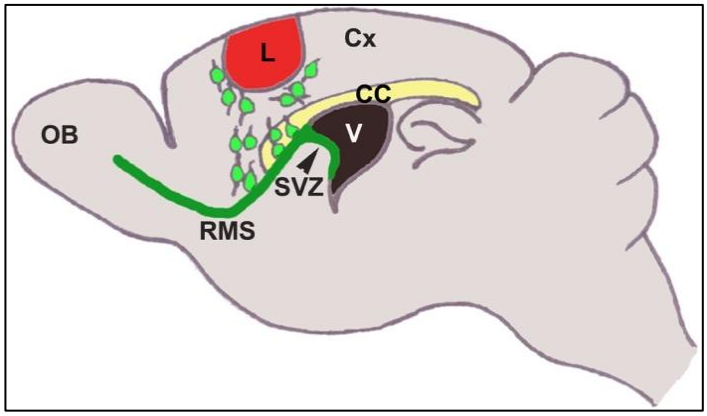

Figure I-15. Schematic representation of neural stem cells migrating to cortical lesion. In cortical lesion, neural stems cells in the SVZ (in green) proliferate to generate new neurons which migrate to the site of lesion (L, red). Lesion leads to up regulation of several molecules in the cortex around the injured area, which can affect this process. CC, Corpus Callosum; Cx, Cortex; L, lesion; V, Ventricle. Adapted from Saha et al., 2012.

A more recent study in newborn animals has shown that GFP-labeled neuroblasts can migrate radially to the cortex and that this migration is assisted by blood vessels (Le Magueresse et al., 2011).

Double-labeled studies have documented that many newborn doublecortin (DCX^+) positive neurons in the SVZ which migrate toward cerebral cortex lesions appear to differentiate into various adult cells, including astrocytes, oligodendrocytes, and neurons (Dash et al., 2001; Lu et al., 2007). Furthermore, other studies have shown that these new differentiated neurons expressed phenotypic markers of mature neurons, including neuronal-specific nuclear protein (NeuN), and region-specific mature neuronal markers, such as calbindin and dopamine (Arvidsson et al., 2002; Parent et al., 2002), and form some new synapses at the lesion site (Yamashita et al., 2006). Furthermore, there is evidence that following brain injury, supported by their local vasculature, NSC are thought to proliferate, migrate to and differentiate at injury sites, affecting variable degrees of structural and functional recovery (Fagel et al., 2006).

However, other studies showed that it is still not clear whether increased proliferation leads to increased neurogenesis in the SVZ after cortical lesion. Sundholm and co-workers using BrdU and DCX markers, reported no significant increase in $BrdU^+/DCX^+$ cell number in the SVZ 15 days after an aspiration lesion suggesting that there is no enhancement in neurogenesis in the SVZ (Sundholm-Peters et al., 2005). On the contrary, a previous finding by the same group demonstrated a delayed increase (after 25 days of lesion) in the number of PSA-NCAM (neuroblast marker) positive cells in the SVZ (Goings et al., 2002). Despite a general agreement that cortical lesions result in an increase in cell proliferation within the SVZ, observations on more aspects of proliferation are somewhat contradictory.

3.2 Are new neurons formed in the cortex after lesion?

It is established that the cerebral cortex of normal adults is non- neurogenic (Bhardwaj et al., 2006; Kornack and Rakic, 2001; Rakic, 2004). However, several groups have reported that in response to either TBI (Covey et al., 2010; Magavi et al., 2000) or stroke (Arvidsson et al., 2002; Jiang et al., 2001; Masuda et al., 2007; Parent et al., 2002), neurogenesis can be induced in non-neurogenic areas such as the cortex. Recent studies used more direct approaches to ascertain that these new neurons are indeed generated in the cortex. Application of Cytosine Arabinosine (Ara-C), which blocks SVZ “type C” cell proliferation for 7 days post-ischemia resulted in a reduction, but not complete absence of proliferative response around peri-infarct area and almost 15% of those proliferating cells were non-microglial and nestin positive (Leker et al., 2007). In another study, 3 days after a unilateral infrared-laser lesion in the rat visual cortex, BrdU positive cells, which also expressed markers for embryonic and adult neural

progenitor cells, were found to be around the lesion penumbra (Sirko et al., 2009). The 3-day time window it seems to be not long enough for cells to generate in the SVZ and migrate to the visual cortex in response to lesions (Saha et al., 2012).
These reports demonstrate that endogenous neural precursors can be induced in non-recognized neurogenic regions to differentiate into CNS neurons in a region specific manner.

Taken together, these findings show that brain injuries induce neurogenesis and angiogenesis. The demonstration of neurogenesis in damaged regions in adult brains and the presence of proliferating cells with the ability to give rise to neurons in the injured regions of brains after TBI open new possibilities and strategies of rebuilding damaged tissues by endogenous neural cell replacement. Despite the presence of endogenous NSC niche with an active angiogenic support, in the mammalian brain it is recognized that intrinsic "self-repair" activity for the most devastating of injuries is currently inadequate or ineffective (Monje et al., 2002). This poor regenerative ability, particularly in the postnatal and adult central nervous system (CNS), may be because of the limited number and restricted location of native NSCs niches, and/or limitations imposed by the surrounding microenvironment, which may not be supportive or instructive at all for neuronal regeneration (Saha et al., 2012).

3.3 Other important factors regulating brain repair process

Physical exercise and glial intervention can also influence effective repair process following injury.
Van Praag (van Praag et al., 1999) has shown that physical exercise increases neurogenesis in the mouse dentate gyrus. In normal adults, physical exercise enhances neurogenesis only in the hippocampus, but does not affect the SVZ (Brown et al., 2003a). Enhanced hippocampal neurogenesis was also observed after a lesion in the sensorimotor cortex in rats (Wurm et al., 2007). Early exercise (treadmill running for 28 days) after cerebral ischemia reduces infarct volume in rats indicating its involvement in proliferation and recruitment of cells in the damaged area. Exercise-induced increase in neurogenesis appears to be mediated by several neurotrophic factors (Matsuda et al., 2011).
On the other hand, glial intervention in injury induced repair process is primarily mediated by reactive astrocytes. Astrocytes play a bipartite role (neuroprotection as well as inhibition of axon regeneration) in injury-induced repair process. In moderate controlled cortical impact (CCI) model, ablation of proliferative reactive astrocytes resulted in severe neuronal degeneration and inflammation compared to control mice (Myer et al., 2006).

Astrocytic protection against neuronal degeneration has been well investigated in ischemic injury and was found to be multifactorial. Astrocytes prevent neurons from encountering severe post-injury metabolic insults/toxicity by scavenging oxygen free radicals, up taking extracellular glutamate and buffering extracellular K+ (Chen and Swanson, 2003). However, axonal regeneration, an important step for effective repair process, is negatively affected by astrocytes. Glial scars, formed at the lesion site, prevent regrowth of axons into the lesion area (Rudge and Silver, 1990) (see more details in Chapter 1).

4. Neuroregeneration treatment strategies

Efforts to treat traumatic CNS injures can be broadly divided into two categories: *neuroprotection*, the minimization of cell damage and death and axonal degeneration caused by the cascade of secondary events, and *neuroregeneration*, the promotion of plasticity and neuronal growth. For neuroregeneration following TBI, axonal growth is required across the injury site through the glial scar and to the appropriate target tissue. Elucidating secondary damage events and exploiting factors involved in endogenous neuroprotection and neuroregeneration may aid in developing more effective treatments for traumatic CNS injury. Although repairing the damaged brain is a daunting task, advances in regenerative medicine and tissue engineering are raising the possibility to repair injured tissue and neuronal circuits (Roberts et al., 1998).

4.1 Cell/Drug Delivery

The delivery of therapeutic compounds to repair injured brain has proved to be extremely complicated and challenging (Orive et al., 2009; Pangalos et al., 2007). Although drugs, cytokines or cell delivery with potential as neural repair molecular therapy do not repair directly injured brain yet, they might be important for minimizing the gliotic reaction and paving the way for neuronal and/or axonal regrowth.

Systemic delivery is the easiest route and it is suitable for molecules that can cross the blood brain barrier (BBB). The greatest advantage of systemic delivery approaches is their non-invasive nature and use of traditional routes of administration. However, approximately 98% of small molecular weight drugs and almost 100% of larger molecular weight peptides and proteins do not cross the BBB and often require high doses to achieve therapeutic concentrations with undesirable side effects (Pardridge, 2005). Moreover, the diffusion distance is limited in the brain, particularly for molecules for which there are unnecessary receptors in adjacent tissue (Krewson et al., 1995). An example is BDNF, which stimulate axonal and dendritic sprouting and promote neurogenesis (Binder and Scharfman, 2004). It is an attractive candidate for a neural repair molecular therapy when delivered through invasive cannulation, but does not significantly pass the BBB if it is delivered systemically (Zhang and Pardridge, 2001). Nevertheless, the past few years have seen some notable developments in systemic and local controlled- release nanosystems and microsystems for drug/cell delivery (Begley, 2004) for brain repair. However, local delivery systems require invasive surgery and do not allow dose adjustments once implanted.

The most recently investigated systemic and local systems exploited for drug and cell delivery to the brain are;

(a) ***Liposomes***, which have a long history as drug carrier systems because of their easy preparation, acceptable toxicity and biocompatibility profiles. They are spherical vesicles that comprise one or more lipid bilayer structures enclosing an aqueous core (Fig. I-16). Liposomes are high-potency carriers that protect encapsulated drugs from degradation and can also be functionalized to improve cell targeting and solubility (Sahoo and Labhasetwar, 2003; Schnyder and Huwyler, 2005).

(b) ***Polymeric nanoparticles***, which include nanospheres and nanocapsules, are solid carriers ranging from 10 to 1,000 nm in diameter made of natural or artificial polymers, which are generally biodegradable and in which therapeutic drugs can be adsorbed, dissolved, entrapped, encapsulated or covalently linked to the particle (Fig. I-16) (Lockman et al., 2002). Nanospheres and nanocapsules are basically used to transport materials. Nanospheres are typically solid polymers with drugs embedded in the polymer matrix. Nanocapsules are a shell with an inner space loaded with the drug of interest. Both are generally more stable than liposomes but are limited by poor pharmacokinetic properties and a poor ability to cross the blood–brain barrier. Similar to liposomes, the surface of nanoparticles can be coated with molecules to increase blood–brain barrier permeability and improve pharmacokinetics (Kreuter et al., 2003).

(c) ***Alternative nanocarriers***, such as solid lipid nanoparticles, micelles and dendrimers have been tested for brain drug delivery. Dendrimers might be the most versatile of all nanocarriers (Fig. I-16). They are highly branched polymers with a controlled three-dimensional structure around a central core. Dendrimers are easily functionalized and can accommodate more than 100 terminal groups. A micelle is a spherical conglomeration of amphiphilic molecules, such as cholesterol. They are easy to prepare and possess low cytotoxicity, good physical stability, can protect labile drugs from degradation and can provide controlled drug release (Blasi et al., 2007).

Finally there is a new delivery system involving cells, called ***cell-inmobilization system***. Cells that secrete therapeutically active agents are enclosed by selectively permeable materials to be protected from immune rejection by an artificial, semipermeable membrane (de Vos et al., 2009; Orive et al., 2009) (Fig. I-17). These cell-loaded capsules can be implanted into the damaged brain area favoring the local, targeted and long-term release of drugs or proteins.

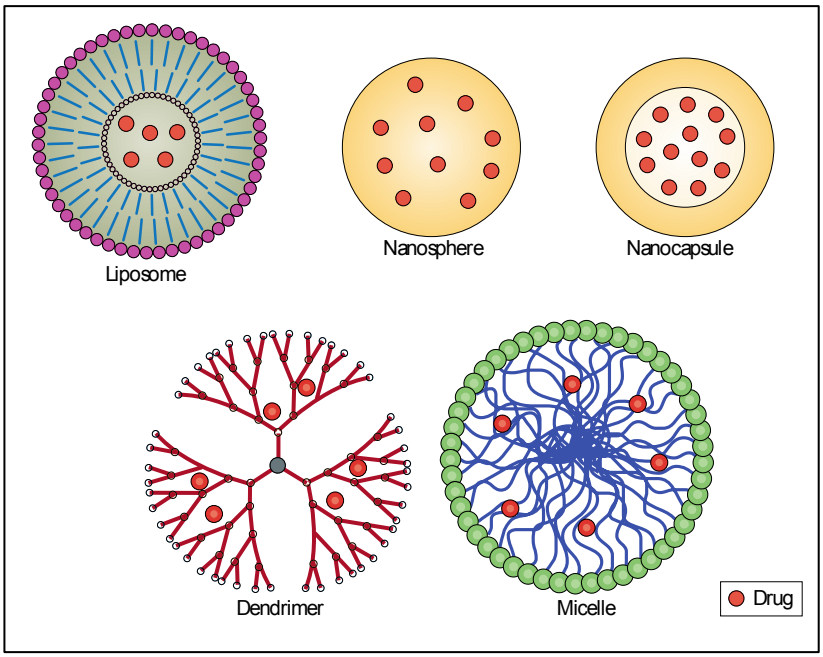

Figure I-16. Different technologies for drug/cell delivery into the brain. Structure of different nanocarriers (liposomes, nanospheres, nanocapsules, dendrimers and micelles) for brain drug delivery. Adapted from Orive et al., 2009.

All these nanosystems suggest that similar approaches could be used for the delivery of drugs or cells to promote neuroprotection, regeneration and/or repair. One important consideration in the use of nano-sized carriers or delivery systems is the largely unknown cytotoxicity that they might possess; especially if used on an intermittent to chronic basis.

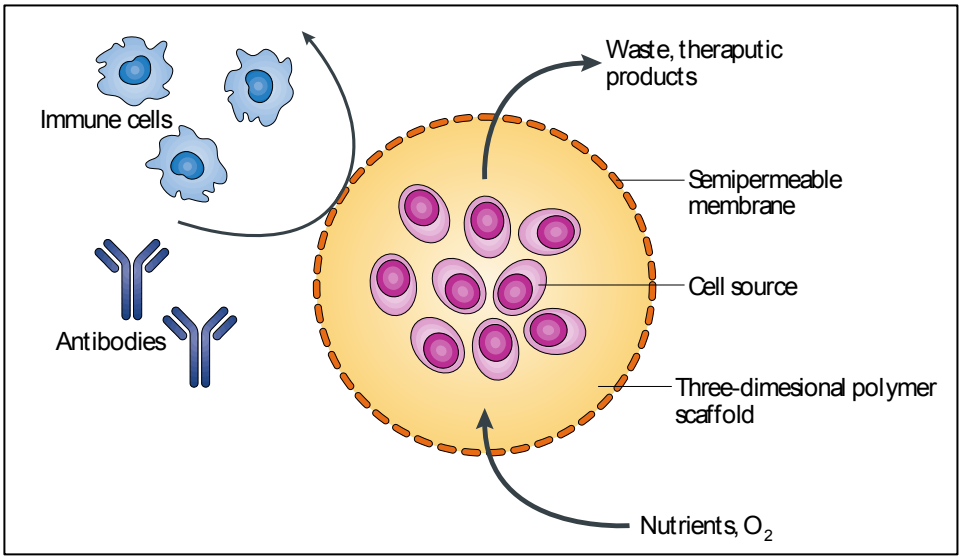

Figure 2 | **Different technologies for drug delivery into the brain. a** | Schematic

Figure I-17. Cell-immobilization system. Cell encapsulation consists of enclosing cells within a three-dimensional polymer scaffold surrounded by a semipermeable membrane that is designed to circumvent immune rejection. Adapted from Orive et al., 2009.

4.2 Cells for brain repair

4.2.1 Exogenous stem cell transplantation

Cell replacement therapy (CRT) and cell-based therapy (CBT) have provided promising therapeutic strategies for treatment of several neurological diseases and traumatic injuries for which no conventional treatment is available. Rapid progress in understanding the biology of NSCs has generated enthusiasm for the development of strategies for CNS insults using stem cells. In mammalian brain development, neural stem cells (NSCs) produce neural cells, including various types of neurons and glia (see Chapter 2). With recent technological developments, NSCs can be induced *in vitro* from pluripotent stem cells, including embryonic stem cells (ESCs) and/or induced-pluripotent stem cells (iPSCs) (Okada et al., 2008; Zhang et al., 2001) and then implanted into the damaged brain *in vivo* (Fig. I-18, left).The results of animal studies (Brustle, 1999; Keirstead et al., 2005; Wernig et al., 2008) support the possibility that the transplantation of exogenous NSCs and their progeny will be a powerful strategy for regenerating nervous system tissue damaged by disease or trauma, for which no conventional treatment is available (Figure I-18, left). However, there are some relevant problems, associated with regenerative medicine using cell-transplantation therapy that need to be solved before its clinical application (Kaneko et al., 2011); Cell survival is one of the most challenging technical issues as only a small percentage (10–30%) of implanted cells survive 2 weeks after transplantation (Brundin et al., 2000).

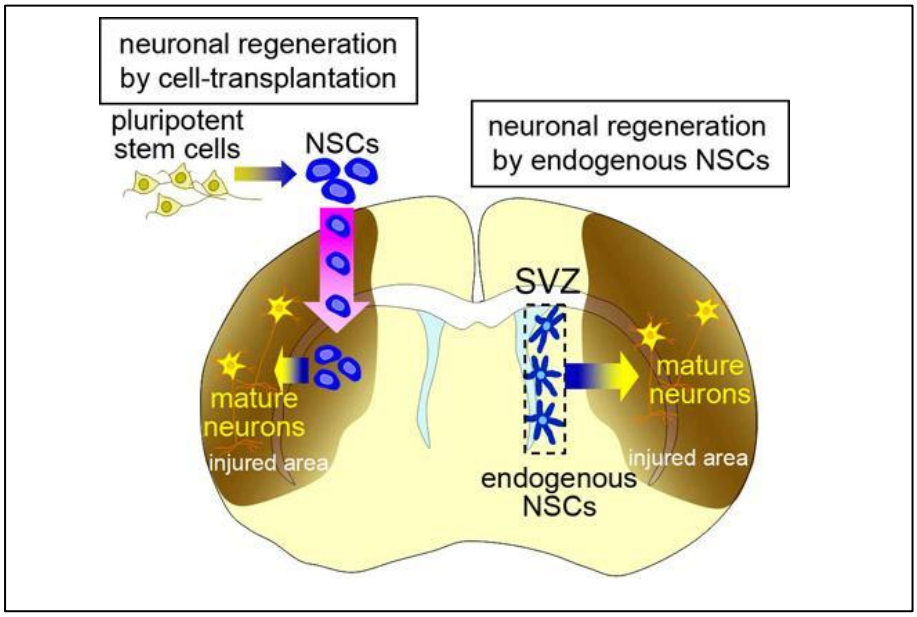

Figure I-18. Therapeutic strategies using exogenous and endogenous neural stem cells (NSCs). Schematic drawing of a model for the therapeutic use of exogenous (left) and endogenous (right) NSCs. Adapted from Kaneko et al., 2011.

Moreover, exogenous NSCs induce immunological responses, which need to be continuously suppressed. Another important question to solve is the tumorigenic risk from stem-cell transplantation (Amariglio et al., 2009) particularly because; given the limited size of the intracranial cavity, a space-occupying tumor could be fatal (Miura et al., 2009; Tsuji et al., 2010). The transplantation procedure itself also might injure the complicated neuronal circuitry, affecting neurological function and finally, a fundamental ethical problem lies in the therapeutic use of ESCs.

4.2.2 Endogenous neural stem cells

As explained before, the NSCs have the potential to "regenerate" lost neurons and glia in response to various pathological conditions (Kaneko and Sawamoto, 2009; Okano and Sawamoto, 2008) (Fig. I-18, right) (See chapter 2.4 and 3). However, this spontaneous regeneration is insufficient for structural or functional restoration of the injured brain. In spite of these apparent limitations to the regeneration of damaged brain tissue by endogenous NSCs, accumulating studies show beneficial effects of interventions that promote neurogenesis, including treatment with erythropoietin (Iwai et al., 2010), statins (Chen et al., 2003b), activated protein C (Thiyagarajan et al., 2008) HDAC inhibitors (Kim et al., 2009), and EGF/FGF-2 (Yoshikawa et al., 2010), on their functional recovery following a lesion. It has not been determined whether these effects depend directly on the promotion of neuronal regeneration by NSCs or whether accompanying events, such as enhanced glial regeneration and other types of trophic support, are more important. Further studies are needed to clarify how newly generated neurons are associated with neurological improvement and to elucidate the mechanisms regulating the endogenous regeneration system.

4.3 Tissue engineering and biomaterial strategies in the injured brain

Neural tissue engineering strategies include the introduction of natural or synthetic biomaterials based interventions as well as combinations of exogenous cells and bioactive scaffolds in the injured brain (Fig. I-19) that restore, maintain and/or improve neural tissue functions (Forraz et al., 2013). The specific combinations of cells and scaffolds can be designed to meet the needs of the different types of brain injury. However, biomaterial-based strategies include those where the biomaterials by themselves have some therapeutic benefit to help neural regeneration across scars, gaps, and cavities or serve as an extracellular matrix, with the goal of recruiting cells or enhancing axonal growth. In fact, they offer a wide range of possibilities since they can be designed to fit specific needs, such as promoting growth or recreating biochemical and topographical cues, and provide a suitable microenvironment for cell survival, tissue regeneration, and host tissue integration.

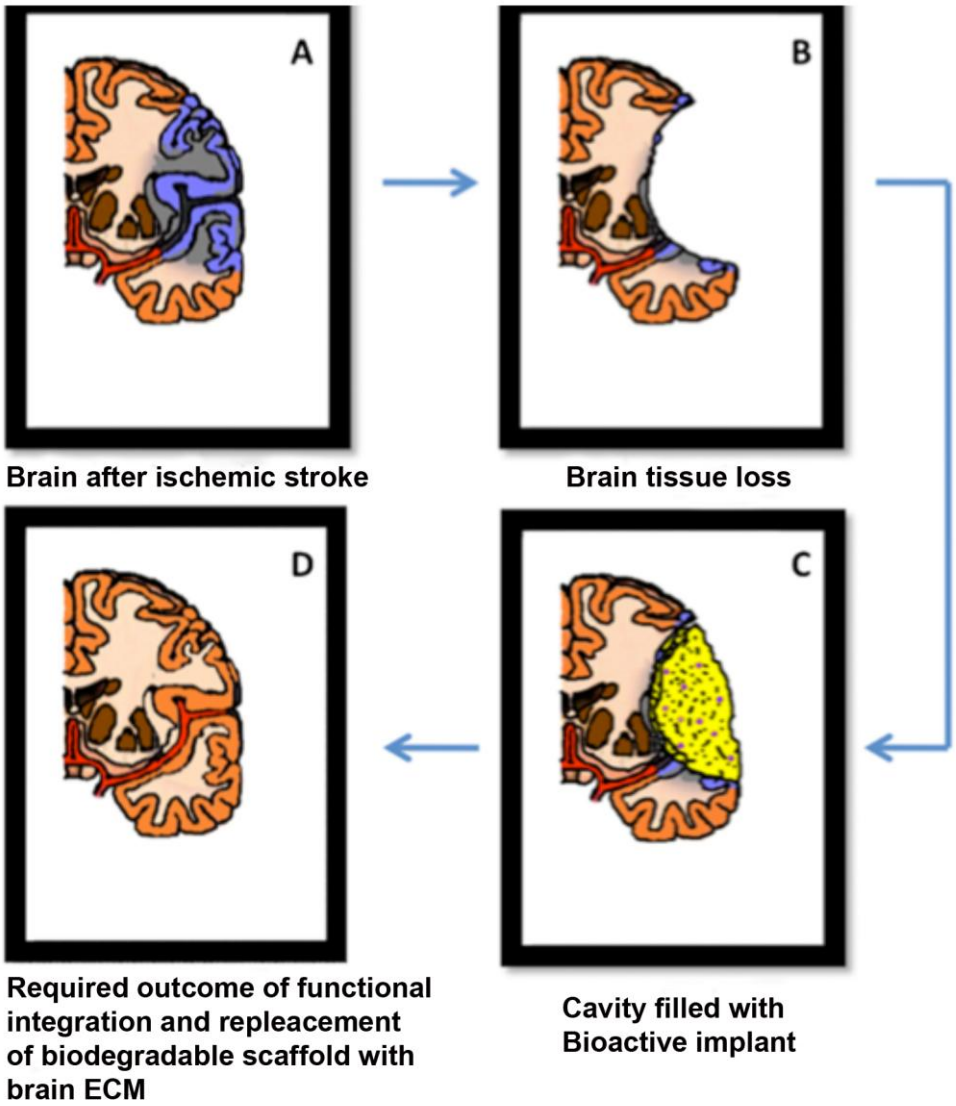

Figure I-19. A schematic diagram of the expected outcome in brain tissue engineering. A cell-seeded biomimetic scaffolds implanted into the human brain after ischemic stroke to assist with tissue repair and replacement**.** Adapted from Forraz et al., 2013.

5. Biomaterials design for brain repair

Damage to the brain produces immediate and delayed cell death leading to the formation of a lesion cavity and glial scar (Fitch et al., 1999). Placing a biomaterial scaffold into the brain damaged area or cavity may provide support for the surrounding brain tissue, function as a substrate for cell growth and proliferation, axon regeneration and neurite infiltration. Occasionally, they were designed to try to recapitulate some of the events that occur during embryogenesis recreating biochemical and topographical cues normally present in the neural stem cell (NSC) niche (Geller and Fawcett, 2002; Nomura et al., 2006; Piantino et al., 2006). In order to achieve these, a wide range of biomaterials have been used in brain tissue engineering. Scaffolds for brain repair are based either on biological or on artificial biomaterials, such as collagen, chitosan or poly (lactic acid) (PLA), used alone or in mixtures, providing scaffolds with different properties (Dalton and Mey, 2009; Potter et al., 2008).

1*) Biological biomaterials*

These are mainly natural polymers such as collagen, laminin, fibronectin, hyaluronic acid, agarose, alginate, and chitosan. The majority of them are derived directly from ECM and has been extensively studied due to their inherent merits including the presentation of biological receptor-binding ligands, the susceptibility to proteolytic degradation and remodeling *in vivo* (Ma, 2008). These natural macromolecules can be hydrated, and serve as bioscaffolds for various neural cells *in vivo* and *in vitro* (Gao et al., 2013). Major concerns regarding the clinical application of biologically derived materials include the problems with sustainable production, immunogenicity, and pathogen transmission as well as weak mechanical strength *in vivo* (Ma, 2008).

2*) Artificial biomaterials*

Compared to the natural polymers, artificial biomaterials could be designed and synthesized to mimic one or multiple desired characteristics of the natural ECM for specific purposes (biomimetic materials). For neural reparative applications, artificial polymers have the advantages of having great flexibility for design and modification so as to allow for the control of orientation and development of new-born tissue for better functional outcomes (Gao et al., 2013).

To better understand the requirements necessary for brain tissue regeneration some parameters are analyzed in both, biological and artificial biomaterials:

- *Surface properties*, such as charge and wettability, are of great importance. The first step following implantation of a scaffold within the brain is its coverage by a non-specific layer of proteins, a process mainly governed by surface hydrophobicity and hydrophilicity, which may contribute to the inflammation process, biocompatibility problems also as cell adhesion and survival (Fournier et al., 2006).

- *The biophysical parameters*, which contain the mechanical properties and architecture of the scaffold, are also taken in to account. Physical support must be offered to neural cells and axons, as well as physical properties similar to the native environment (e.g. elastic modulus). This possess a major scaffold design challenge because native brain tissue typically has an elastic modulus of 0.5–1 kPa, (Gefen and Margulies, 2004) softer than the majority of the materials. Neural cells sense mechanical properties such as matrix stiffness and respond through cell colonization, migration and differentiation, (Leipzig and Shoichet, 2009; Saha et al., 2008) altering neurite formation and trajectory (Balgude et al., 2001). For instance, after 8 days, stem cell cultures on methacrylamide chitosan hydrogels with stiffness between <1 and 7 kPa, showed different cell differentiation. The <1 kPa substrate produced 59% oligodendrocytes, 33% neurons, and 2% astrocytes, while the 7kPa substrate produced 72% oligodendrocytes, 12% neurons, and no astrocytes, while the 3.5kPa substrate generated intermediate values (Leipzig and Shoichet, 2009). The topology is another important characteristic of the scaffold. Recent findings suggest that cells often show a non-natural behavior when they are moved away from their natural niches and seeded onto flat substrates. Therefore, although 2D experiments represent a versatile and accurate way to screen the cell behavior, 3D experiments are designed to direct a progressive and steady reconstruction of the complexity that entails the native tissue (Fig. I-20) (Santos et al., 2012).

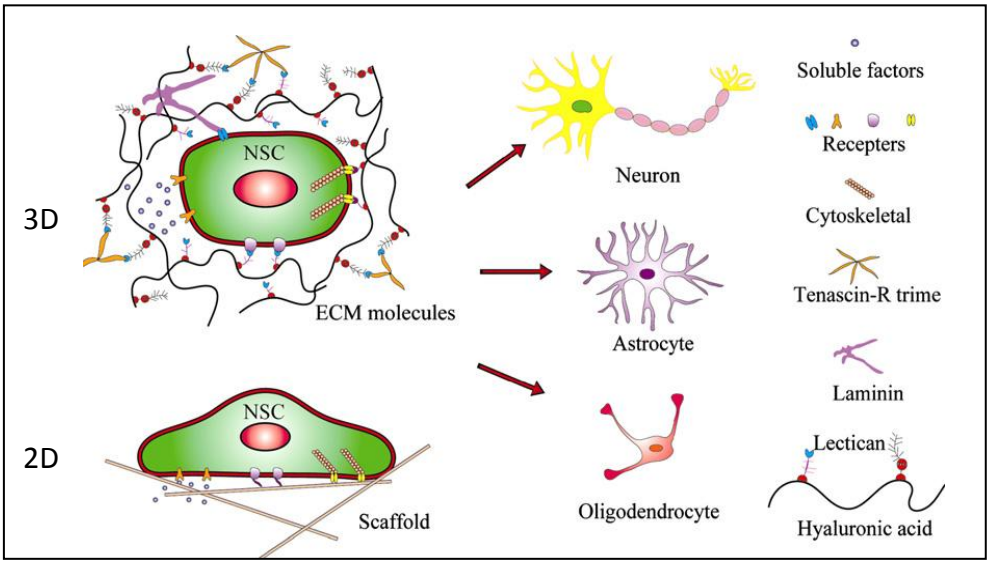

Figure I-20. Direct NSC cell fate with 2D or 3D scaffolds *in vitro*. Adapted from Yao et al., 2013.

Topography, i.e. outer architecture, but also inner architecture of the scaffolds can affects cell behavior once implanted into the brain. For example, the presence of pores and channels on the surface may enhance astrocytic infiltration and affect host cell migration (Wong et al., 2008). Moreover, access to nutrients such as glucose, is a critical parameter for neuronal cells. Therefore, if larger implants are used, vascularization is required for cell survival. In this sense, channeled/porous scaffolds, or scaffolds that become porous after implantation by degradation, may improve vascularization and cell infiltration problems.

- *Biodegradability and biocompatibility* of the biomaterials used for brain regeneration are two parameters of tremendous importance (Vert, 2009). Indeed, the adverse host cell response, such as glial scar and inflammation after scaffold implantation, has to be minimized.

a) Degradable materials

The concept of biodegradable scaffold has both benefits and drawbacks; however, this issue must be addressed in terms of the primary injury (Pettikiriarachchi et al., 2010). Although biodegradation enhances scaffold porosity over time and allows cell infiltration, it diminishes the mechanical integrity of the scaffold and can lead to build-up non-bioeliminable products by the body. Consequently, for small lesions in other parts of the body, it may be desirable to produce a biodegradable scaffold that deteriorates as cells deposit their own ECM. However, in the brain, particularly for large lesions such as those caused by TBI, it is more feasible to have a long-term scaffold providing architectural support of the adjacent brain parenchyma, while also supporting cell differentiation (Gritti and Bonfanti, 2007; Hatten, 1990; Nisbet et al., 2010). Due to the well-accepted biodegradability and biocompatibility one of the most studied family materials are the poly(α-hydroxyacids) which include synthetic polymers and copolymers such as poly(glycolic acid) (PGA), poly(lactic acid) (PLA), poly(lactic acid-co-glycolic acid) (PLGA), and poly(lactide-co-caprolactone) (PLCL). Several mechanisms have been identified for controlling the degradation and mechanical properties of these polymers including varying the ratio of monomer units, the stereochemistry of the monomer units (either D- or L-form), and the molecular weight distribution of chains. Since poly (α-hydroxyacids) degrades *in vivo* by hydrolysis and produce acidic degradation products that result in a transient pH decline, only a limited amount of polymers can be implanted (Park and Lakes, 1992). PLA and PGA, and their copolymers have been widely used to design scaffolds in diverse conditions for brain repair. PGA, PLA as well as PLCL have been approved by the FDA for use in the repair of human peripheral nerves, and this success has inspired investigation of their use in brain repair (Gautier et al., 1998; Oudega et al., 2001). These degradable materials can be also functionalized or tuned with different molecules, peptides, proteins….etc.; The hydrophobic surface properties in most of the synthetic biodegradable materials such as PLGA, PCL and PLA, may be modified

by coating them with ECM proteins components like laminin, fibronectin, collagen. Specific adhesion oligopeptide such as RGD and IKVAV, YIGSR may also be added to improve their adhesion properties for seeded cells (Samadikuchaksaraei, 2007).

b) Non-degradable materials

The use of synthetic non-degradable materials in neural repair is limited by their non-degradablilty and unbioabsorbility. Recently, electroactive polymers like polypyrole or hybrid conduct materials showed neuronal attachment and growth. The major concerns regarding these materials are related to immunorejection, chronic inflammatory responses, fibrous scarring, and the associated problems of neural compression and need for re-operation. These render non-degradable materials unsuitable for CNS repair (Cullen et al., 2008).

All these characteristics mentioned above are taken in to account to design the suitable scaffold for brain repair according to fit specific needs. A wide range of biomaterials are used to minimize and regenerate tissue lost after brain injury or stoke. The most desirable implantable materials are biodegradable and bioabsorbable materials such as polyethylene glycol (PEG), poly (lactic-co-glycolic acid) (PLGA), Poly (lactic acid) (PLA), collagen, dextran, gelatine and chitosan. 3D bioscaffolds can be used as supportive structures for endogenous or exogenous stem cells. As well as considering the mechanical properties of the scaffold for brain tissue engineering, it is essential that the surface properties are optimized to support endogenous or implanted cells and to possibly provide guided axonal growth. The trade-offs in bulk and surface properties may necessitate optimization of the scaffold through means such as incorporating biomolecules and surface treatment procedures for improved biorecognition.

The subsequent sections will review the various scaffolds and outline methods of modification employed to enhance neural integration and regeneration following implantation into the brain.

5.1 Types of scaffold

A range of scaffolds including hydrogels, self-assembling peptides, electrospun nanofibers and channeled scaffolds among others, have been investigated as candidates for neural tissue engineering within the brain.

5.1.1 Hydrogels

Hydrogels are hydrophilic polymer networks that can absorb ~30% (as a lower limit) of their dried weight in water (Park and Lakes, 1992). The mesh structure and highly interconnected porosity of hydrogels accounts for the high water content and enables rapid diffusion of

nutrients and metabolites to and from the cells (Woerly et al., 1999). Although these features make hydrogels compatible with surrounding tissue, it adversely affects the mechanical integrity of the scaffold and produce tissue expansion when they are implanted into the brain parenchyma. An advantage of hydrogels is that their mechanical properties can be tuned to be similar to that of soft tissue such as the brain. This can facilitate the transfer of mechanical stimuli to cells similar to the native tissue (Pettikiriarachchi et al., 2010). Some hydrogels exhibit a composition-dependent critical temperature at which gelation or phase separation occurs. Thermoresponsive gelation serves several functions such as facilitating injection of the scaffold into a lesion via a minimally invasive procedure, while also enabling the hydrogel to interface with irregular cavities (Crompton et al., 2007; Stabenfeldt et al., 2006; Wang et al., 2009b).

There are two types of hydrogels used in brain repair; biological derived and synthetic hydrogels.

Most biologically derived (natural) hydrogels are polysaccharides and glycosaminoglycans, some of which are constituents of the ECM such as hyaluronic acid (HA), found within the body (Lin and Metters, 2006). Natural hydrogels can possess inherent bioactivity eliminating the necessity for biomolecule functionalization to achieve cell–scaffold interactions. Although the use of these natural materials would be ideal, there are some inherent difficulties including undesirable immune responses (Hudson et al., 2000).

Huang and co-workers (Huang et al., 2012) use a collagen glycosaminoglycan (Collagen GAG or CG) hydrogel matrix after a surgical brain trauma. After 28 days, CG scaffold by itself reduces de lesion area, increases cell proliferation and also promotes an early migration and differentiation of endogenous neural precursor cells (Fig. I-21). However, they require a long time period to analyze the response of vascularization, glial cell scarring and infiltration and the immune response.

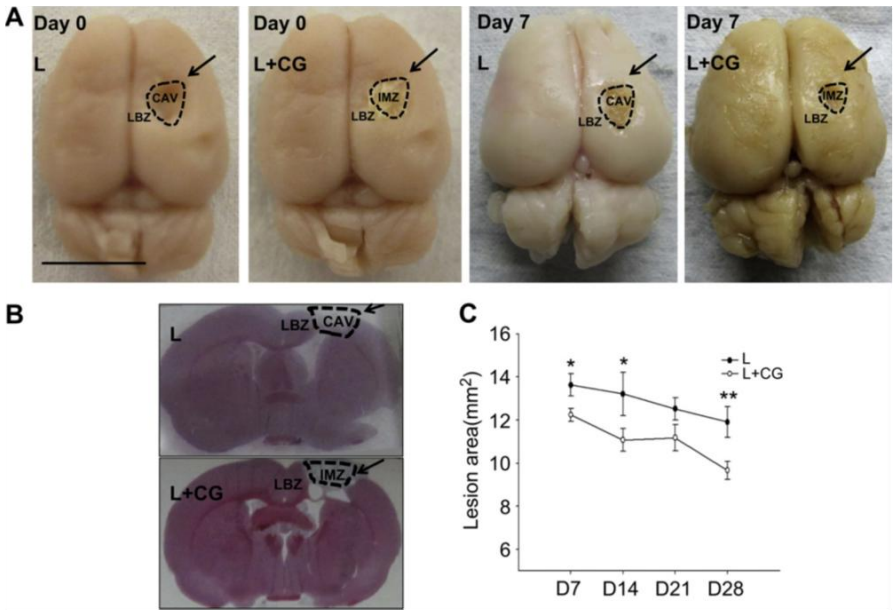

Figure I-21. **Morphological evidence of tissue repair in lesion area associated with CG matrix implantation.** (A) The appearance of brain immediately after surgery (Day 0) and 7 days after unilateral surgical brain lesion (Day 7). (L) in the right hemisphere with implantation of a CG hydrogel into the lesion area (L + CG) (right photo) as compared to that without the implantation (L) (left photo). Sites of lesions are indicated with the black arrows. LBZ = Lesion boundary zone, IMZ = Intra-matrix zone, CAV =Cavity (B) Images of hematoxylin and eosin (H&E)-stained coronal sections from an L or an L + CG brain. Black arrows show the site of lesion in L and CG matrix is shown as a gray insertion in the L + CG brain. (C) Section areas in the same cross section (2.0 mm anterior to the bregma). Adapted from Huang et al., 2012.

On the other hand, synthetic hydrogels are biologically inert and therefore have weak cell adherence. However, they are commonly chemically stable and can be optimized for neural engineering applications. Modified synthetic hydrogels avoid some drawbacks associated with natural polymers such as a superior tuning of mechanical properties, while the lack of biofunctionality can be solved binding cell adhesive peptide motifs and/or the incorporation of natural polymers.

Several synthetic hydrogels such as poly (N-2-(hydroxy-propyl)methacrylamide) (pHPMA) (oerly et al.,1), poly(hydroxyethyl- methacrylate) (p EMA) (Lesn et al., 2002), poly (e-caprolactone) (PCL), poly(L-lactic-co-glycolic acid) (PLGA) (Wong et al., 2007) and polyethylene glycol (PEG) have been used for the repair of brain lesions. Wong and co-workers evaluated the rat brain response to PLGA and PCL implant hydrogels. After 4 weeks, PCL and PLGA hydrogels decreased cell death and inflammation and supported neural cell growth and infiltration *in vivo* (Fig. I-22). However, no revascularization and glial effects were described, and the effect of degradation products at long times were not analyzed (Wong et al., 2007).

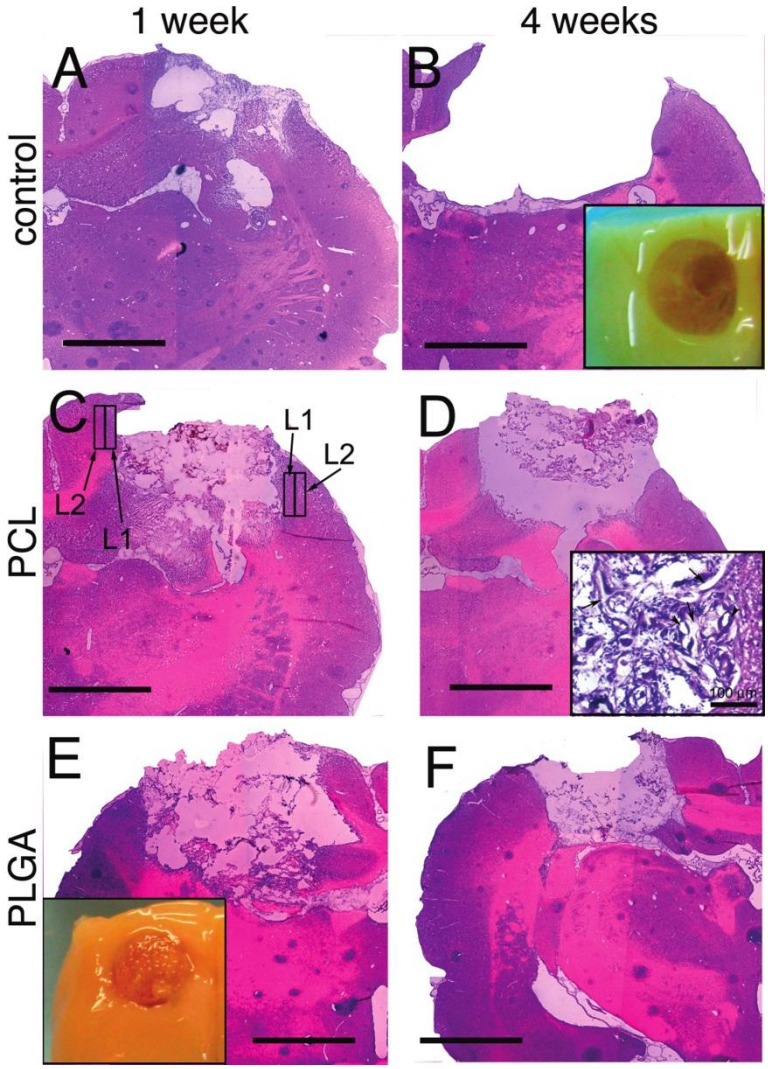

Figure I-22. Hematoxylin and eosin (H&E)-stained sections of polymer constructs in brain cavities. Control at (A) 1 week and (B) 4 weeks, poly(e-caprolactone) (PCL) at (C) 1 week and (D) 4 weeks, and poly (L-lactic-co-glycolic acid) (PLGA) at (E) 1 week and (F) 4 weeks (inset B and inset E). Gross images before sectioning illustrate the visual difference between (B) control and (E) a defect containing material (inset D). 10x mag of H&E section showing parenchyma at the bottom corner of a defect site on the right-hand side with PCL polymer (arrows) and blood vessels (arrow heads). Adapted from Wong et al., 2007.

In the literature, hydrogels demonstrate a capacity to encapsulate cells, regulate their behavior, and facilitate integration into host tissue. Further optimization of hydrogels for enhanced cell interactions and cell penetration is necessary before they can be applied to promote neural repair. In addition to their neuron regeneration capacity, the future of hydrogels will need to reverse not only the structural damage to the brain, also assess the functional recovery trying to restore the lost cognitive, sensory, and motor functions and the important issue of water absorption inside the brain.

5.1.2 Self-assembling peptides

An alternative form of hydrogels for brain tissue engineering is self-assembling peptide nanofiber scaffolds (SAPNS). These scaffolds are manufactured from various oligopeptides or amphiphilic molecules that spontaneously aggregate to form nanofibers, which subsequently form a fibrillar network in the presence of physiological ionic conditions (Jing et al., 2008). Amphiphile peptide molecules form nanofibers that are composed of a core of hydrophobic tails while the hydrophilic head-groups form a sheath (Jing et al., 2008). SAPNS are characterized by high porosity, tissue-like water content, and enhanced cell signaling by high-density presentation of bioactive peptide sequences (Silva et al., 2004). However, the high water content makes SAPNS mechanically weak, produces also tissue expansion once they implanted within the brain and the biological origins increase susceptibility to enzymatic degradation *in vivo*. SAPNS used in neural tissue engineering have predominantly involved two types of polymer peptides; an ECM-derived sequence isoleucine–lysine–valine–alanine–valine (IKVAV) and arginine–alanine–aspartate–alanine (RADA) (Fig. I-23). IKVAV-SAPNS induced selective differentiation of neural progenitor cells into neurons while down regulating astrocyte differentiation. This feature has been attributed to the capacity of SAPNS to amplify presentation of the neurite-promoting laminin epitope, IKVAV, on the surface (Silva et al., 2004).

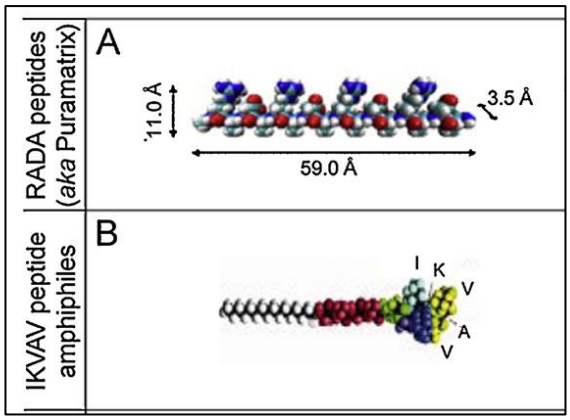

Figure I-23. Schematic of design strategies for self-assembling peptide nanofiber scaffolds. (A) Four repeats of the RADA amino acid sequence (Nagai et al., 2006). (B) Peptide amphiphiles self-assemble with cell-adhesive IKVAV sequences (Silva et al., 2004).

In contrast, RADA-SAPNS supported cell attachment, differentiation, and neurite outgrowth *in vitro* and functional synapse formation *in situ* without eliciting an immunogenic response (Fig. I-24) (Holmes et al., 2000).

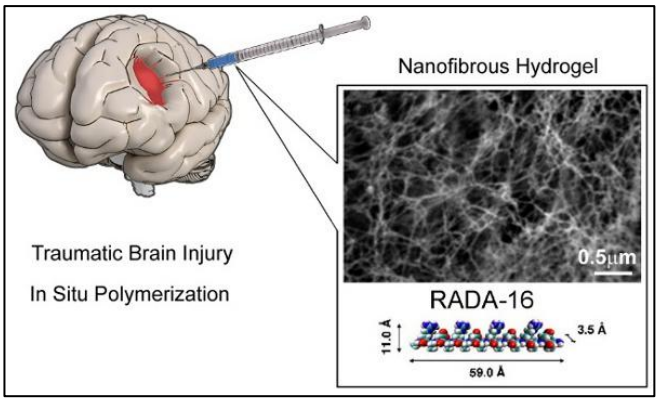

Figure I-24. ***In situ*** **hydrogel polymerization for instances where significant soft tissue damage occurs**. Inset shows the nanofibrillar arrangement of RADA-16 peptide amphiphiles. Adapted from Nagai et al., 2006.

Application of SAPNS in brain lesions virtually eliminated cavitation, with fewer astrocytes and macrophages present at the lesion site indicating low immunogenicity compared with controls exhibiting secondary tissue loss (Fig. I-25) (Guo et al., 2009). Although these primary *in vivo* studies provide promising results, SAPNS for use in neural brain repair are still in their infancy and deeper understanding and optimization and its interactions with neural tissue is necessary.

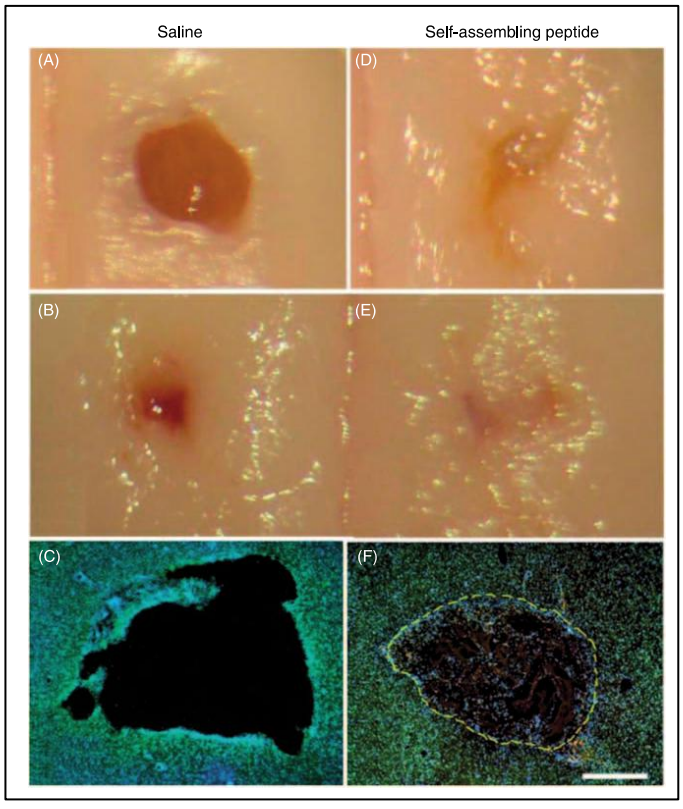

Figure I-25. Cortical tissue regeneration and reconstruction: control group treated by injection of saline (A, B and C) and experimental group treated with self- assembling peptide nanofiber scaffolds (SAPNS) (D, E right and F). C and F show Nissl staining (cell RNA in the rough endoplasmic reticulum of nuclei) and DAPI (nuclei) staining. Scale bar: Scale bar: 500 μm. Adapted from Guo et al., 2009.

5.1.3 Electrospun nanofibers

Electrospun scaffolds consist of a nanofibrous mesh formed by uniaxial stretching of a viscoelastic polymer solution under an applied voltage. The application of a voltage instigates accumulation to counteract the solution's surface tension, resulting in the formation of a taylor cone (Koh et al., 2008; Prabhakaran et al., 2008; Teo and Ramakrishna, 2009). At a critical voltage, a polymer jet is ejected from the cone tip and accelerated towards a collector. As the jet travels, whipping instabilities draw out the fiber to nanoscale diameters (Shin et al., 2001). There are several electrospinner configurations available today; however, electrospinning is a remarkably simple and versatile technique and it has been successfully applied to more than 100 different types of polymers (Pettikiriarachchi et al., 2010). Fig. I-26 shows a typical apparatus for electrospinning, which consists of three major components: a high-voltage power supply, a spinneret, and an electrically conductive collector. An ordinary hypodermic needle serves as the spinneret. The polymer to be electrospun may be in the form of a solution or melt that is typically loaded in a syringe (Xie et al., 2009).

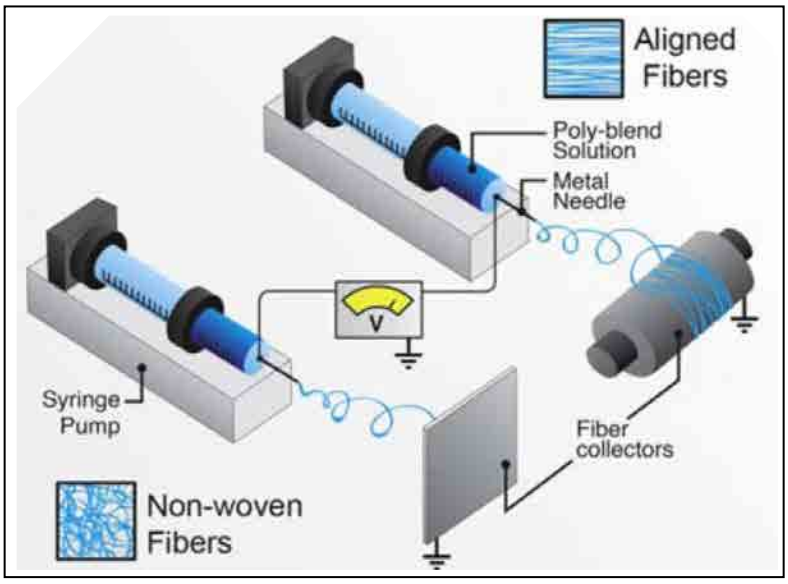

Figure I-26. Scheme of electrospinning apparatus. Polymer fibers captured on a flat surface produce nonwoven mats, whereas fibers can be aligned using a rotating spindle target**.** Adapted from Gunn and Zhang, 2010.

The electrospinning process basically consists of a jet produced by applying a high voltage onto the slurry through the charged metallic tip. When the charge is higher than the fluid surface tension, it produces the aforementioned jet, which usually goes to the grounded conductive collector, which is held at certain distance. The resulting nanofibers form either a nonwoven or aligned fibrous mesh depending upon the type of the collector used; nonwoven nanofibers were performed by a flat collector, while the aligned fibers were collected in a rotating disc (Fig. I-26) (Gunn and Zhang, 2010).

Interest in nanofibrous scaffolds for tissue engineering is based on the structural similarity to the fibrillar arrangement of collagen, laminin, and other fibrils of the ECM (Kumbar et al., 2008; Smith and Ma, 2004). The fiber diameters of electrospun scaffolds typically range from a few nanometers to few micrometers (Smith and Ma, 2004). Due to their submicron or even smaller sizes, electrospun nanofibers are supposed to be more physiologically relevant in terms of their potential to mimic the ECM. As an example, the highly anisotropic feature of aligned electrospun nanofibers has been employed to successfully guide the outgrowth of neurites.Yang and Ramakrishna found that scaffolds made of aligned nanofibers were better suited for culturing nerve stem cells *in vitro* than scaffolds of random microfibers (Yang et al., 2005). It is also noteworthy that aligned fibrous scaffolds prepared by electrospinning have demonstrated a capacity to orient neural cells and neurite growth *in vitro* in the same direction as fibers (Gupta et al., 2009; Wang et al., 2009a). However, guidance of neurite extension alone is insufficient for promoting nerve regeneration.

From another perspective, nanofibers mimic other ECM attributes such as a large surface, high porosity, and similar mechanical properties (Kumbar et al., 2008). High porosity and fibrillar traits facilitate cell and axon penetration, neurite contact guidance and diffusion of nutrients and waste, all of which act to enhance scaffold–tissue integration.

A variety of polymers have been electrospun with different fibers orientation for neural tissue engineering applications, including: poly (ε-caprolactone) (PCL) (Johnson et al., 2009; Xie et al., 2009), poly(lactic-co-glycolic acid) (PLGA), polypyrrole (Lee et al., 2009) polylactide (PLA) (Xie et al., 2009), polymethyl methacrylate (PMMA), and polyacrylic acid (PAA) (Li et al., 2008a) to name a few.

Randomly orientated and aligned PCL scaffolds were used to develop a system that simulates brain tumor migration *in vitro* (Johnson et al., 2009). Glioma (tumors) cells exhibited faster migration on aligned scaffolds, as the tortuous paths in random scaffolds are likely to decelerate cell migration. However, Nisbet et al. showed that when random and partially aligned electrospun PCL scaffolds were implanted in the adult rat brain to study endogenous cell migration, neurites existing at the scaffold–tissue interface displayed perpendicular axon guidance on partially aligned electrospun scaffolds, whereas a random scaffold promoted neurite penetration (Nisbet et al., 2009) (Fig. I-27).

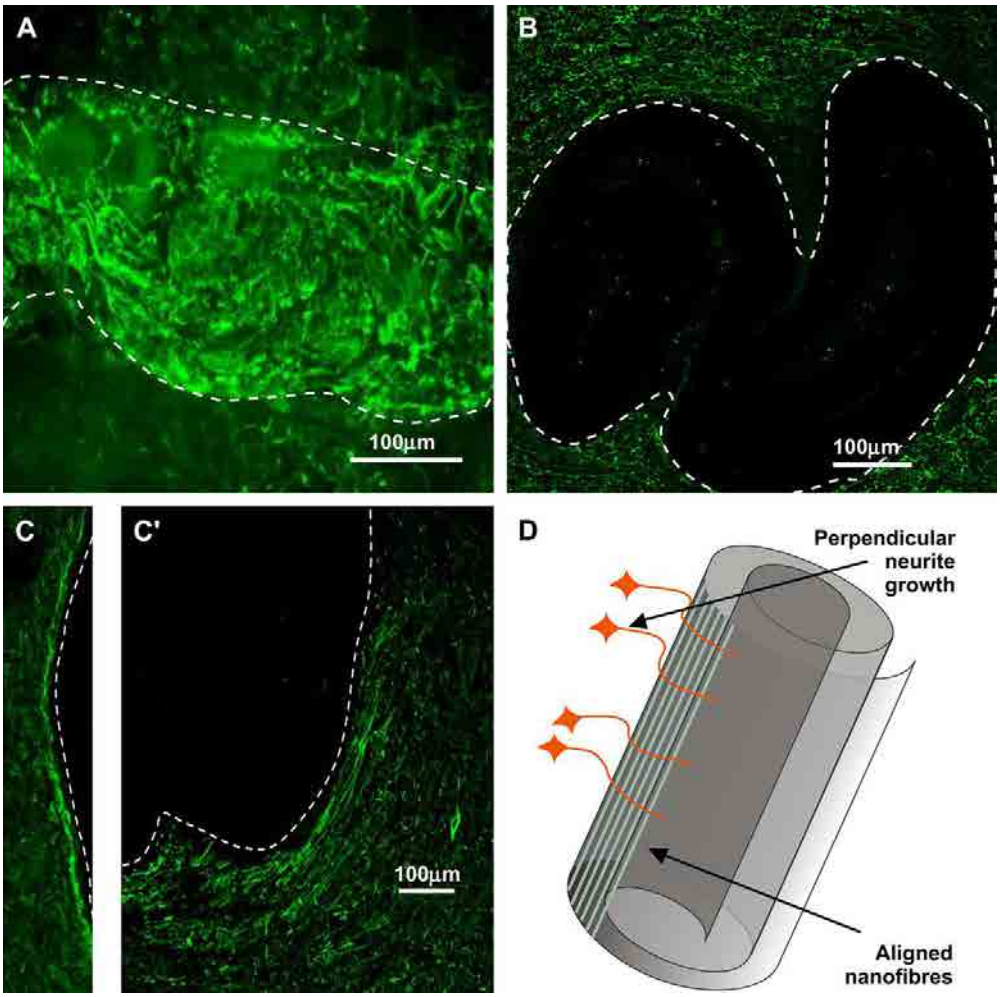

Figure I-27. Neurites interacting with the electrospun PCL scaffolds 60 days after implantation. The nanofibrous scaffolds have not been imaged. (A) PCL scaffold with random fiber alignment that has been sectioned parallel to the implantation to show the extent of neurite infiltration into the scaffold. (B) Partially aligned fibers sectioned perpendicular to the scaffold. (C) A higher magnification of the partially aligned fibers. (D) A schematic of how the neurites are interacting with the partially aligned fibers. The white dotted lines in the images represent the interface between the scaffold and the endogenous tissue. Adapted from Nisbet et al., 2009.

Contrasts in findings between such studies represent the dualities encountered in designing scaffolds that facilitate rapid cell migration and penetration. Porosity plays an important role in enabling cell penetration of the scaffolds; however, the tortuous paths sometimes create axonal delay inside the scaffold.

5.1.4 Channeled scaffolds and others

Recent studies in brain tissue regeneration showed that a suitable scaffold for neural tissue engineering should be porous to facilitate the accommodation of many cells and the diffusion of oxygen and nutrients from the host tissue, permitting also the neovascularization of the scaffold

(Martinez-Ramos et al., 2012). A recent example is the study by Pradas and his group. They studied the endogenous cell activation by implanting channeled scaffolds to different cortical zones in rat brains. They used acrylate scaffolds with aligned channels (40-80 um) implanted in two different regions (cortical plate and subventricular zone). After 8 weeks *in vivo*, immunohistochemical analysis for neuronal (Tuj-1^{+}) and endothelial (CD31) cells markers demonstrated that the scaffolds maintained continuity with the surrounding neural tissue. Moreover, GFAP^{+} cells colonized the entire scaffold and in the case of scaffolds implanted in contact with the subventricular zone also Tuj-1^{+} neurons were within the material (Fig. I-28). Local angiogenesis was also evidenced surrounding the scaffold and within the scaffold's pores (Martinez-Ramos et al., 2012).

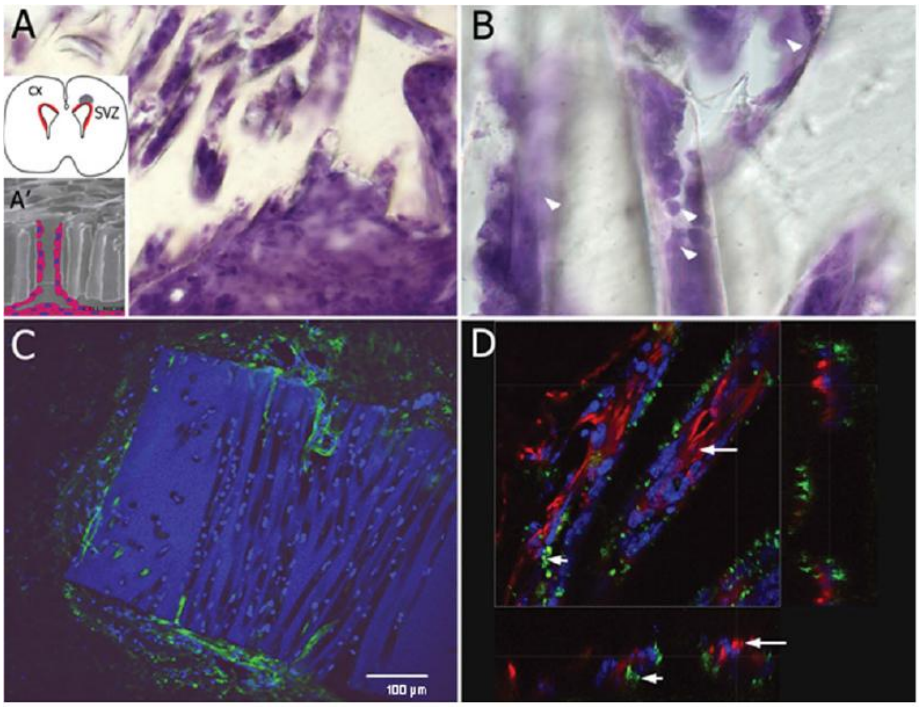

Figure I-28. Acrylate scaffolds implanted 8 weeks near the SVZ. A–B. Optical micrograph of a section stained with hematoxilin to reveal the presence of neural cells (the gray spot in the scheme of A indicates scaffold location; the SVZ is singled out in red in the scheme). Cells are shown at the scaffold–tissue interface (A), and a detail of a channel (B) reveals numerous cells. C. Glial cells immunoreactive for GFAP (green) around the scaffold. D. Reconstruction by confocal images of the longitudinal channels showing Tuj-1+ neurons (red) (white arrow) and CD 31+ cells (green) could be seen inside the channels, suggesting the presence of some new blood vessels (arrowhead in D). Blue in C, D,: nuclei stained with DAPI. Adapted from Martinez-Ramos et al., 2012.

Wong and co-workers showed also how important is to modify the architecture of the scaffold, including channels or pores, for brain cortex regeneration. By PCL matrices with unidirectional channels and microgrooves oriented longitudinally and orthogonally inside the cylinder they concluded that the architecture can benefit brain tissue regeneration. They integrated large

channels oriented toward the parenchyma in the material to increase astrocytic infiltration. They used microgrooves oriented in the desired direction of cellular migration or/and fully interconnecting channels for cellular migration and tissue integration (Fig. I-29) (Wong et al., 2008).

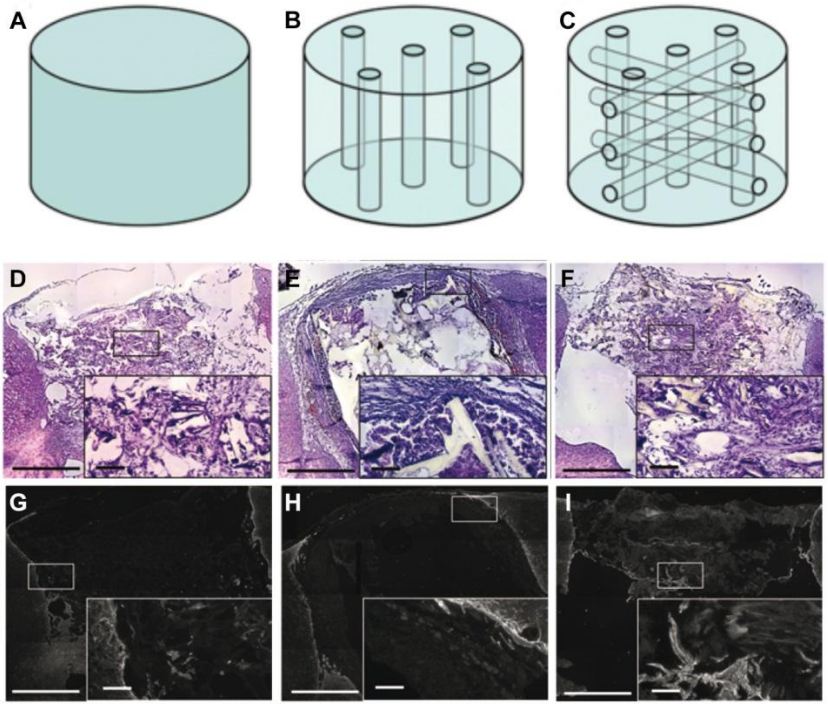

Figure I-29. PCL sponges implanted into the rat brain. Schematics illustrating a cylinder (A), channel (B), and orthogonal (C) scaffolds design. Photomicrographs revealing representative and corresponding sections (D-F) H & E stained and (G-I) labeled for GFAP at 8 weeks postimplantation. Each larger image has a higher-magnification inset indicated by the small boxes to show cellular details. Larger bar = 1 mm; smaller bar = 100 μm. Adapted from Wong et al., 2008.

Finally, others materials like electroactive scaffolds that can potentially facilitate communication between neurons in the brain have been of recent research interest. Polypyrrole is a highly conductive polyacetylene derivative that is becoming increasingly employed owing to its potential to stimulate signal transduction in neural cells (Lee et al., 2009). PCL and poly-l-lactide nanofibrous scaffolds were coated in polypyrrole via *in situ* polymerization to form conductive sheaths (Xie et al., 2009). The properties of nanofibrous scaffolds can also be enhanced through the attachment of biomolecules such as collagen to the surface to improve cell viability and attachment (Li et al., 2008a).

5.2 Functionalized scaffolds

Biomolecules form an integral part of neural regeneration through the regulation of cell adhesion, proliferation, migration, and differentiation. The incorporation of essential ECM proteins into scaffolds has been demonstrated as means of enhancing biocompatibility (Moore et al., 2006). Various proteins and ligands have been grafted or adsorbed onto scaffolds, in particular neurotrophins and factors associated with neural regeneration. There is a wide literature about biomolecules that have been coupled to scaffolds with potential for neural engineering applications. Some examples are shown here.

Hou and co-workers evaluated the ability to improve tissue reconstruction by hyaluronic acid (HA) hydrogels unmodified and modified with laminin into cortical defects mechanically created in rats (Fig. I-30) (Hou et al., 2005). Laminin is found in the ECM and represent the main non-collagenous component of the basal lamina. It is also a key substrate along which nerve axons will grow, both *in vivo* and *in vitro*, and has therefore been incorporated into scaffolds to enhance cell adhesion and migration. The cell-binding domains of laminin consist of the peptide sequences Ile-lys-Val-Ala-Val (IKVAV) and Tyr-Ile-Gly-Ser-Arg (YIGSr).

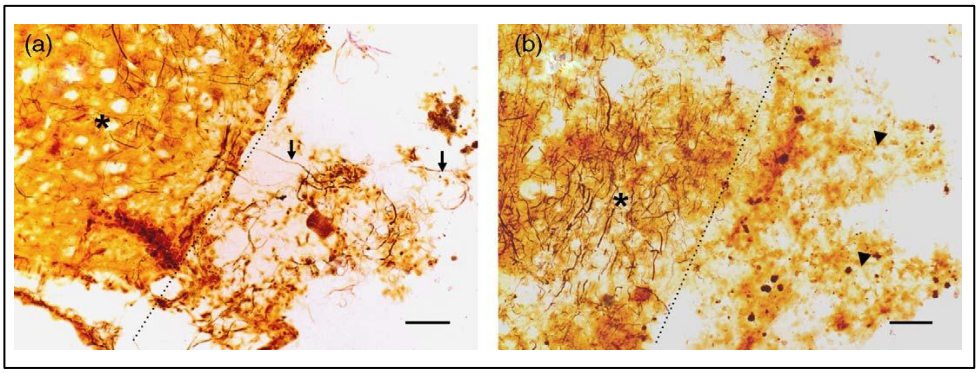

Figure I-30. Hydrogels implantation in the right hemisphere on a coronal section. A-B Silver staining on a coronal section**.** The implantation region is on the right of dotted line, and normal tissues (asterisks) on the left. Numerous processes (arrows) are revealed within the reconstructed lesion in the group of modified hydrogels, which are the same as the normal in morphology (a). However, new fibers are not observed within grafts (arrowhead) in the group of unmodified hydrogels (b). Scale bar = 20 um. Adapted from Hou et al., 2005.

The YIGSr sequence facilitates cell binding, whereas the IKVAV peptide facilitates neurite extension (Orive G., et al., 2009). The results showed that the HA hydrogels synthesized had mechanical properties similar to the brain tissue. After being implanted into the lesion of the cortex, the porous hydrogels created a scaffold, which could support angiogenesis and simultaneously inhibit the formation of glial scar. In addition, HA hydrogels modified with laminin could promote neurite extension in material-tissue interface (Fig. I-30) (Hou et al., 2005).

Zhang lab performed polydimethylsiloxane–tetraethoxysilane (PDMS-TEOS) gels with or without vascular endothelial growth factor (VEGF), which is crucial for new vessel formation (Zhang et al., 2007). When PDMS-TEOS scaffold was implanted into the artificial brain defect, it remained at the implanted site and kept the integrity of the brain shape. 30 days after the implantation, astrocytes and endothelial cells occupied the marginal territory of PDMS-TEOS scaffold. Addition of VEGF increased the newly produced tissue volume, and the immunohistochemical analysis showed that the number of astrocytes and endothelial cells were increased (Fig. I-31) (Zhang et al., 2007).

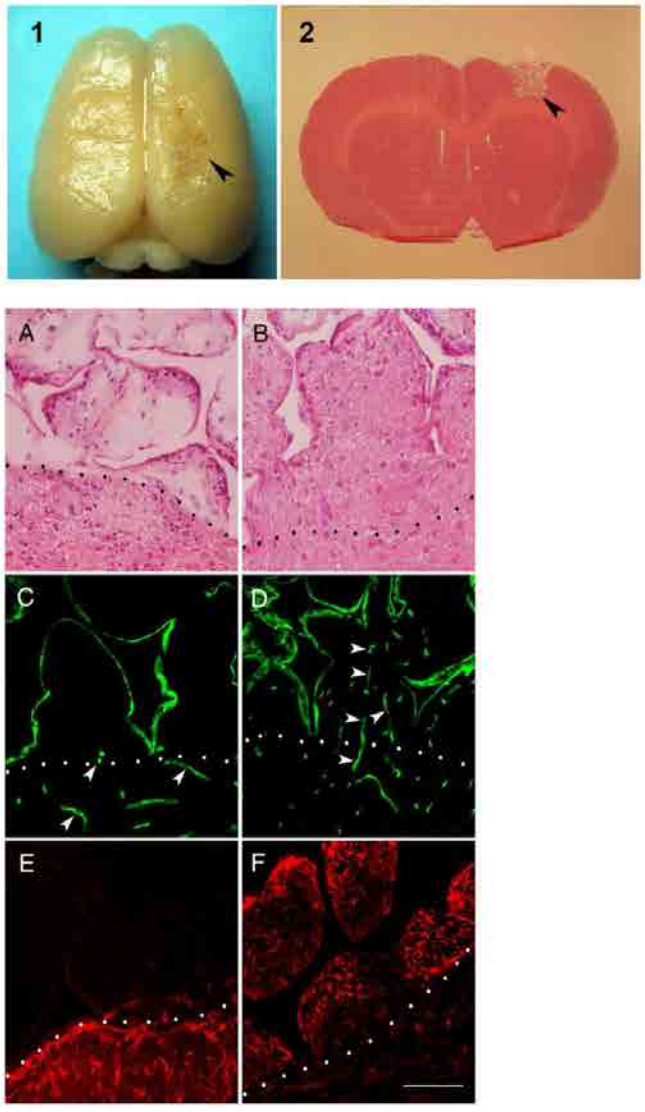

Figure I-31. **Brain regeneration with PDMS-TEOS implants**. Whole brain (1) and Hematoxilin Eosin (HE) stained brain section (2) with PDMS-TEOS+ VEGF scaffold implantation. HE staining (A, B) and histochemical analysis for endothelial cell (C, D) and astrocyte (E, F) markers at the marginal territory of PDMS-TEOS scaffold. (A, C, E) PDMS-TEOS scaffold without VEGF; (B, D and F) PDMS-TEOS scaffold with VEGF. Adapted from Zhang et al., 2007.

5.3 Cell-seeded scaffolds

Tissue engineering strategies often include implanting of constructs containing exogenous cells in a bioactive scaffold. A wide range of transplantable cells have been used in combination with scaffolds, including embryonic stem cells, neural stem cells, mesenchymal stem cells, Schwann cells and a variety of adult multipotent stem cell types (Gao et al., 2013). The underlying principle is that these engrafted cells may promote neural repair and regeneration by means of growth factor production, neuronal replacement and remyelination. Thus, cells, typically isolated from CNS, are grown in scaffolds *in vitro* and implanted within the injured brain (Fig. I-32). Generally, these scaffolds are designed to mimic some of the roles of natural extracellular matrix (ECM), which control tissue structure, regulate the function of the cells and allow the diffusion of nutrients, metabolites and soluble factors (Lee and Mooney, 2001).

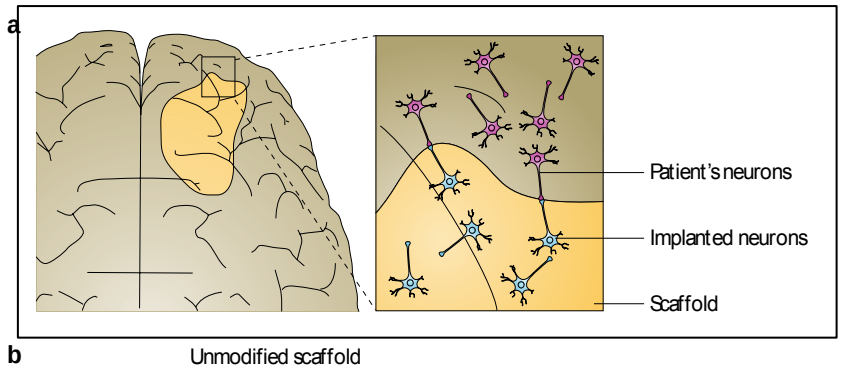

Figure I-32. Cell-seeded scaffolds. Placing scaffolds into a region of damaged brain tissue can provide structural support to the surrounding tissue and allow cells from the adjacent parenchyma to infiltrate the scaffold potentially promoting local tissue regeneration. Adapted from Orive et al., 2009.

In a cell-seeded scaffold, the interaction between the cells and scaffolds is crucial and can be regulated by controlling specific ligand receptor interactions; the physical properties of the scaffolds such as their mechanical properties and degradation rate, and the release of incorporated molecules such as growth factors or DNA from the scaffolds (Orive et al., 2009).

5.3.1 Stem cells and scaffolds

The use of neural stem cells for brain repair is intuitively attractive as they can differentiate into neurons and glia that functionally integrate into the damaged brain (See chapter 4.2). *In vitro*, biomaterials promote the attachment, growth and differentiation of neural stem cells, and their ability to do so is affected by the surface of the substrates, the presence or absence of neurotrophic factors, and cell seeding density (Bhang et al., 2007; Kulbatski et al., 2005; Levenberg et al., 2003) (Fig. I-33).

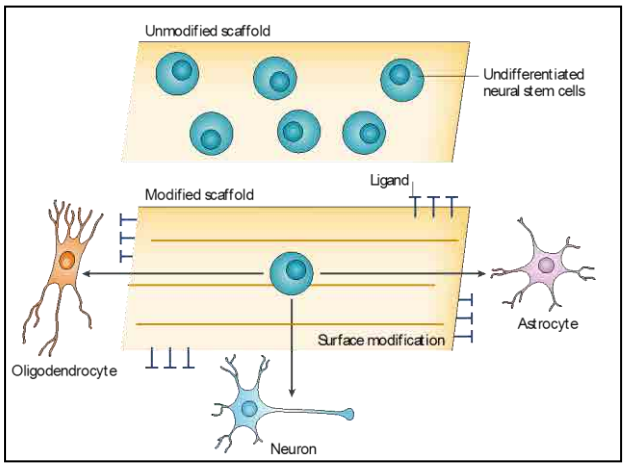

Figure I-33. Scaffolds can guide the NSC fate in brain repair processes. The scaffold can be modified to control and program neural stem cells; to provide local and sustained delivery of proteins, and the surface can be topographically altered (lines), coated with ligands or modified to possess a surface charge to promote attachment, growth and differentiation of neural stem cells. Adapted from Orive et al., 2009.

Whether the factors that provide an optimum cell culture environment can be translated directly to the *in vivo* environment, several other important issues including the optimum time frame for implantation of cell-loaded scaffolds into the damaged brain remain unknown. Park, and colleagues (Park et al., 2002), transplanted a PGA scaffold containing neural stem cells into the infarction cavity caused by hypoxia-ischemia (HI) in mice. As the scaffold degraded, new brain parenchyma was regenerated as evidenced by a reduction in the amount of damaged brain tissue (Fig. I-34). A plexus of host and graft-derived arborized neurites was also seen innervating the scaffold, which indicated that the scaffold altered the trajectory and complexity of cortical neurites and donor-derived neurons.

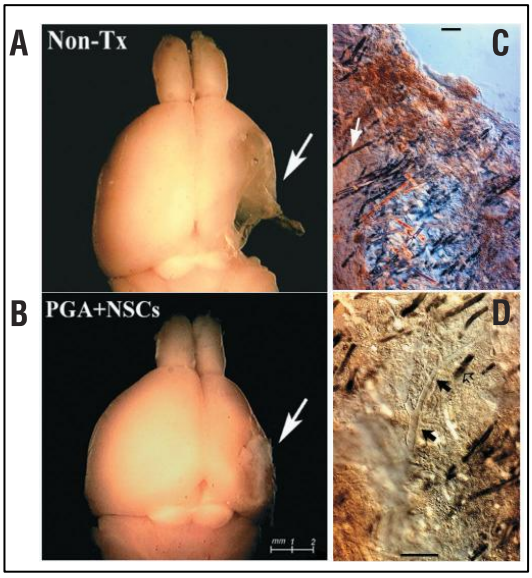

Figure I-34. Implantation of NSC–PGA complexes into a region of cavity formation following extensive HI brain injury. (A) Brain of an untransplanted mouse with extensive infarction of the right cortex, (arrow). (B) Brain of a similarly injured mouse implanted with an NSC-PGA complex generated in vitro. (C, D) Higher magnification of representative coronal sections through that region, in which parenchyma appears to have filled in spaces between the dissolving black polymer fibers (white arrow in (C)) and even to support neovascularization by host tissues, as seen in (D). A blood vessel is indicated by the closed black arrow in (D); open arrow in (D) points to degrading black polymer fiber. (C, D) 100 µm. Adapted from Park et al., 2002.

Elias and Spector investigated the survival and differentiation of hippocampal progenitor cells seeded in a collagen scaffold and implanted in a rat model brain injury. The cell-scaffold construct was implanted 1 week after injury and was observed to remain intact with open pores upon analysis 4 weeks later. Implanted neural progenitors were found to have survived within the scaffold (stained with the proliferative marker BrdU), and also to have migrated into some parts of the surrounding tissue (Fig. I-35). However, in some experiments, lack of scaffold integration was observed (Fig. I-34a inset) (Elias and Spector, 2009).

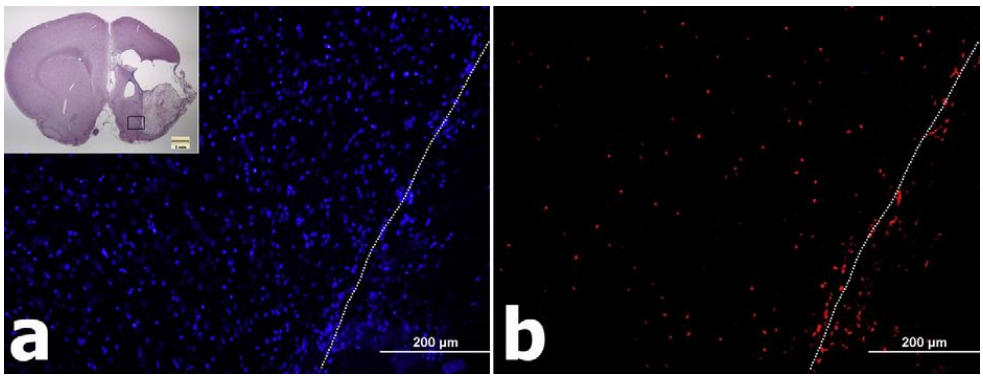

Figure I-35. BrdU labeled neural progenitors detected in vivo 4 weeks after implantation. (a) DAPI staining (blue) showing nuclei of cells near the scaffold border (white line) and within the brain. The field of view corresponds to the outlined rectangle in the H&E inset. (b) BrdU staining (red) showing implanted cells present in the brain after 4 weeks. Adapted from Elias and Spector, 2009.

Cheng et al. (Cheng et al., 2013) used a combination of physical, chemical and cellular cues to regenerate brain injury. Their purpose was providing a functional 3D SNAP scaffold with encapsulated neural stem cells to enhance the reconstruction of the injured brain (Fig. I-36). They specifically linked laminin-derived IKVAV motif on the C-terminal to enrich self-assembling peptide RADA16 as a functional peptide-based scaffold. The animal study was conducted in a rat brain surgery model. The results showed that the injected peptide solution immediately *in situ* formed the 3D hydrogel filling up the cavity and bridging the gaps. The histological analyses revealed that the RADA16-IKVAV self-assembling peptide not only enhanced survival of encapsulated NSCs but also reduced the formation of glial astrocytes. The peptide hydrogel with IKVAV extended motifs also showed the support of encapsulated NSCs in neuronal differentiation and the improvement in brain tissue regeneration after 6 weeks post-transplantation (Fig. I-36).

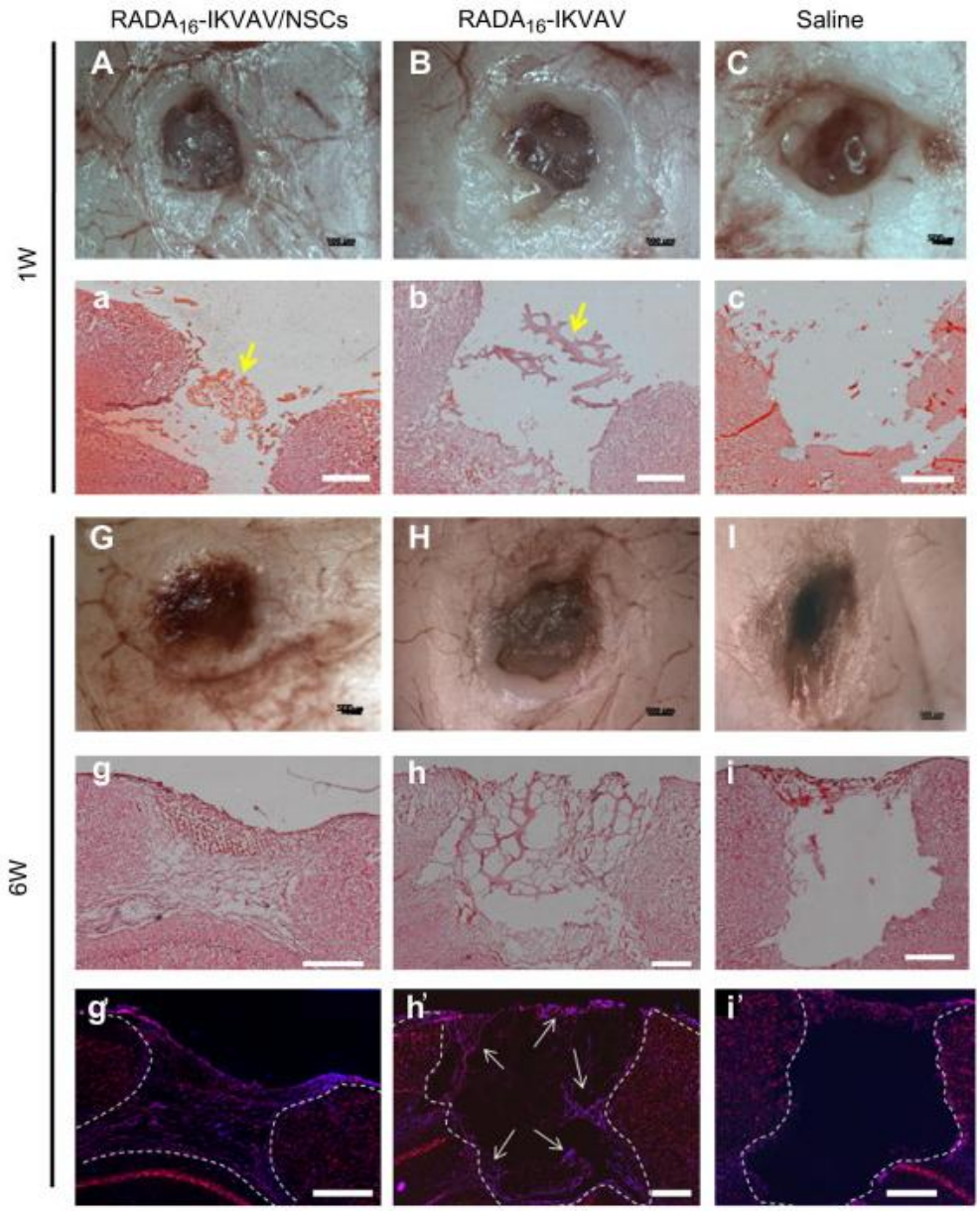

Figure I-36. Gross morphological examinations of brain wound defect on neural tissue in coronary sections. (A-I) macroscopic observation of cavities. (a-i). Neurons were labeled with red florescence Nissl stain and the nuclei were counterstained with blue florescence DAPI in coronal sections 6 weeks after surgery (g'-i'). The yellow arrow points out the remaining SNAP hydrogels in the injured cavities. The white dashed lines outline the wound margin to distinguish the area of original host tissue and neoregenerated neural tissue. Scale bar =200 mm. Adapted from Cheng et al., 2013.

Others studies showed that, incorporating neural stem cells into a laminin or fibronectin-based scaffolds also enhanced the distribution of grafted cells into the surrounding tissue following their transplantation into the traumatically injured brain of mice. Histological and imaging studies only confirmed that the scaffolds integrated efficiently within host tissue (Tate et al., 2009).

Finally, there are several studies that used different cell-seeded polymer scaffolds, which have been shown to increase cell adhesion, survival, and host-implant integration in the CNS with a sequential degradation of the implanted scaffold (Silva et al., 2004; Stabenfeldt et al., 2006; Tate et al., 2002; Teng et al., 2002). All these data provide evidence that the microenvironment can be synthetically recapitulated by controlling the interaction between the biomaterials and exogenous cells.

Although the successful results obtained in the last years, seeded-cells scaffolds still remain an emerging field for brain regeneration with many problems to solve such as ineffective scaffold integration; abortive vascularization, poor cell survival and defective cell differentiation (see 4.2.1).

6. New applications for a well-known biomaterial: Poly (lactic acid) for brain repair strategies

6.1 Poly (lactic acid) chemistry and synthesis

Recent advances in biodegradable polymers have been encouraged by intense interest in biomedical applications. In the last decades, numerous studies have focused on the utilization of poly (lactic acid) (PLA) as a promising biodegradable polymer for neural regeneration, owing to its mechanical properties, thermoplastic processibility and biological properties, such as biocompatibility and biodegradability. PLA is aliphatic polyester industrially obtained from renewable resources, such as corn or sugar beets (Auras et al., 2004).

The chemistry of PLA involves the processing and polymerization of lactic acid monomers. Lactic acid (2-hydroxy propionic acid, HOCH3CHCOOH) is the simplest hydroxyl acid with an asymmetric carbon atom, which exists as two enantiomers, L- and D-lactic acid, differing in their effect on polarized light (Fig. I-37A) (Samuel et al., 2013).

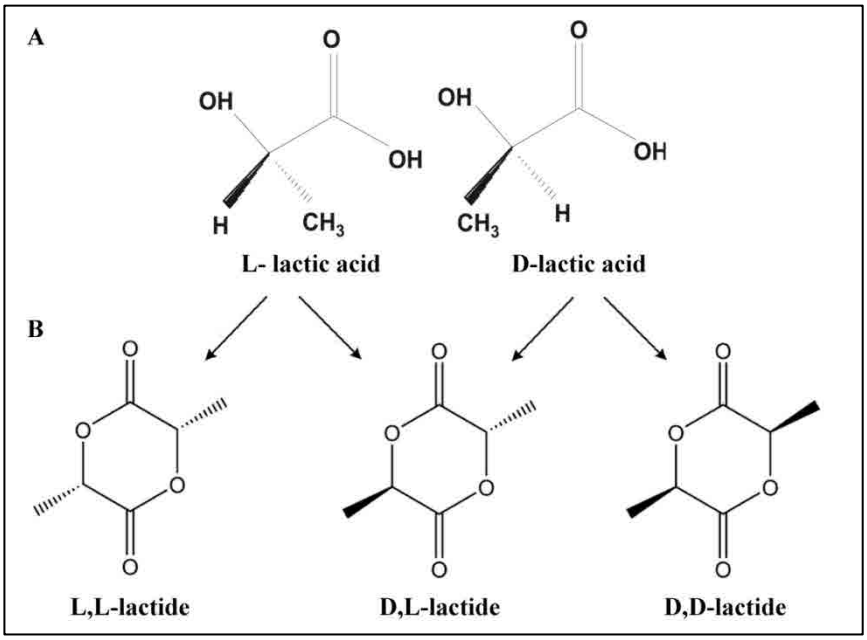

Figure I-37. Chemical structures of lactic acid. A. Optical isomers of lactic acid; L-lactic acid and D-lactic acid **B.** Chemical structures of dimers; D,D-lactide, L,L-lactide and D,L-lactide**.** Adapted from Samuel et al., 2013.

The L isomer rotates the plane of polarized light clockwise; the D isomer rotates it counterclockwise. The optically inactive D, L or meso form is an equimolar (racemic) mixture of D and L isomers (Lunt, 1998) (Fig. I-37A).

L-lactic acid is produced by mammalian cells during glycogenolysis and is involved in the Kreb's cycle through pyruvic acid and acetyl- CoA (Gupta et al., 2007). Lactic acid is produced commercially by fermentation or via petrochemical feedstock. Today the most popular route is

fermentation, in which corn starch or sugarcane is converted into lactic acid by bacterial fermentation using an optimized strain of Lactobacillus (Gupta et al., 2007) (Fig. I-38).

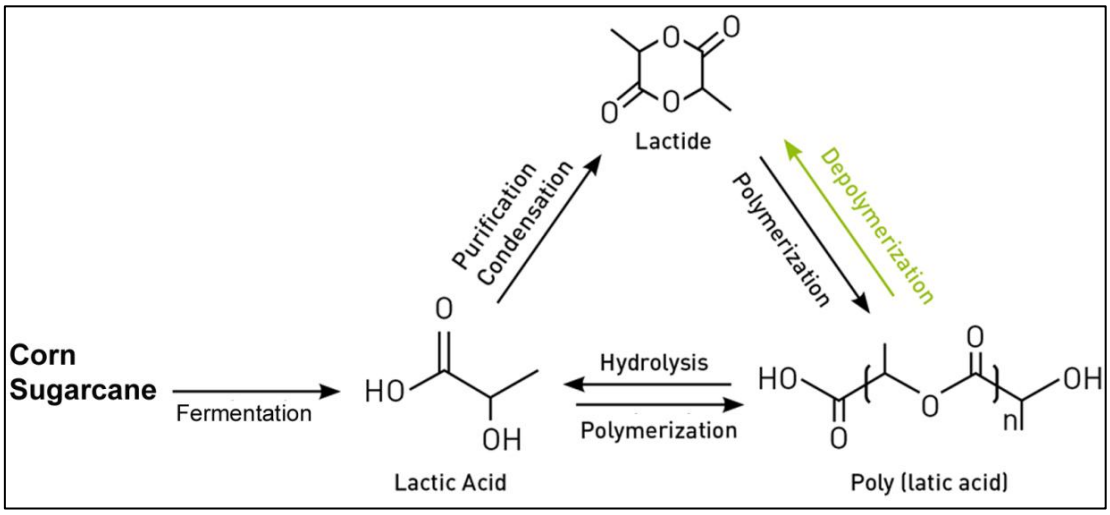

Figure I-38. Synthesis of high molecular weight PLA. Adapted from Gupta et al., 2007.

Polymerization of lactic acid to high molecular weight PLA can be achieved in two ways: (a) direct polymerization; and (b) polymerization through lactide formation (Fig.I-38). As direct polymerization is an expensive route, polymerization through lactide formation is by large the current method used for producing PLA (Auras et al., 2004). Lactide, the cyclic dimer of lactic acid, is formed by the condensation of two lactic acid molecules as follows: L-lactide (two L-lactic acid molecules), D-lactide (two D-lactic acid molecules) and meso-lactide (L-lactic acid and D-lactic acid molecule) (Fig.I-37B).

The properties of high molecular weight PLA are determined by the polymer architecture (i.e. the stereochemical makeup of the backbone) and the molecular mass, which is controlled by the addition of hydroxylic compounds. The ability to control the stereochemical architecture permits precise control over the speed of crystallization and finally the degree of crystallinity, the mechanical properties and the processing temperatures of the material. In addition, the degradation behavior strongly depends on the crystallinity of the samples (Auras et al., 2004). Fully amorphous materials can be made by the inclusion of relatively high D content (>20%) whereas highly crystalline material is obtained when the D content is low (<2%) (Cicero and Dorgan, 2001; Cicero et al., 2002; Lunt, 1998). By controlling residence time and temperature in combination with catalyst type and concentration, it is possible to control the ratio and sequence of D- and L-lactic acid units in the final polymer (Lunt, 1998). The degradation products of polylactides are nontoxic, which enhances practical applications in biomedicine (Eling et al., 1982; Penning et al., 1993). The environment significantly influences its degradation: e.g. water, air, pH, and temperature (Satyanarayana and Chatterji, 1993). The accessibility of the polymer to the external medium will be enhanced at low crystallinity (Gupta

et al., 2007). The PLA polymer may take 10 months to 4 years to degrade, depending on the microstructural factors such as chemical composition, porosity and crystallinity that may influence tensile strength for specific uses (Mäkelä et al., 1989) and the environment where polymer is placed.

6.2 PLA for brain regeneration

All these properties mentioned above, make PLA an ideal scaffold used for cell transplantation and neural tissue regeneration. In addition, PLA and its breakdown products were demonstrated to be biocompatible with brain tissue. PLA has been used for CNS regeneration in different conformations; as tubes (Oudega et al., 2001), macroporous scaffold (Tu et al., 2003), mesh of nanofibers (Hurtado et al., 2011), particles or gels (Piantino et al., 2006)…etc (Fig. I-39). However, the studies with PLA alone for brain regeneration have been very limited.

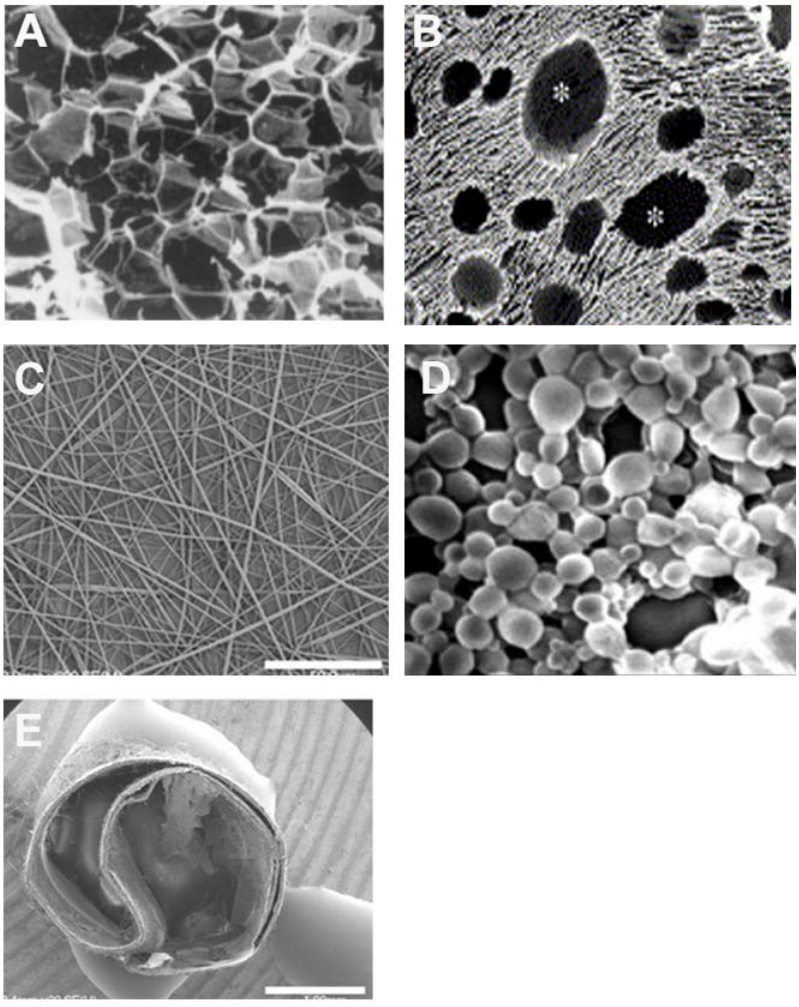

Figure I-39. Different PLA conformation scaffolds for CNS regeneration. A. Macroporous and B. Microporous scaffolds**, C.** Nanofibers **D.** Nanoparticles and **E.** Tubes or conduits. Adapted from Hurtado et al., 2011; Patist et al., 2004; Piantino et al., 2006; Tu et al., 2003; Wang et al., 2009a.

In the last years, more often investigations are carried out on copolymers of PLA with other polyesters, presumably because of the higher degradation rates and lower crystallinity of them, as mixed with poly caprolactone (Jin et al., 2011) or poly (glycolic acid) (Lee et al., 2009). PLA is also commonly functionalized with proteins or neurotrophins like laminin (Hurtado et al., 2011) or BDNF (Patist et al., 2004) for CNS regeneration (Fig. I-39). All these PLA scaffolds were used to try to regenerate glial and neuronal cells, induce neurite infiltration, promote angiogenesis and also generate a low inflammatory response after CNS injury.

6.3 The role of lactate in brain: the discoveries and the controversies

6.3.1 Lactate in brain metabolism

Cerebral energy metabolism is a highly compartmentalized and complex process in which trans-cellular trafficking of metabolites plays a pivotal role. The adult brain normally uses glucose as its primary energy source (Sokoloff, 1992). Glucose metabolism by different pathways has important functions related to energetics, neurotransmission, oxidation–reduction (redox) reactions, and biosynthesis of essential brain components (Dienel, 2011). For many decades, lactate production in the brain was viewed as a consequence of inadequate oxygen delivery, disruption of oxidative metabolism, or mismatch between glycolytic and oxidative rates (Folbergrova et al., 1978); but more recently, the conceptual role of lactate metabolism and function in the normal brain have undergone major changes, shifting from developmental fuel and glycolytic waste product to include its use as a supplemental fuel and signaling molecule (Dienel, 2011).

Before and immediately after birth, lactate is an important energy source because at this time the level of glucose in the blood is low but the lactate concentration is high (Dombrowski et al., 1989; Tabernero et al., 1996). Lactate is transported across cell membranes into the brain by monocarboxylate transporters (MCTs), among which MCT1-4 co-transports lactate with a proton (Halestrap and Meredith, 2004). In this context, monocarboxylate transporters are present in fetal brain at midgestation and their expression sharply increases during late fetal and neonatal period (Baud et al., 2003; Fayol et al., 2004), suggesting that the perinatal brain is able to take up lactate efficiently. This is in agreement with the early observation that lactate transport to the brain *in vivo* is very active during the perinatal period (Cremer, 1982). Lactate accumulates in fetal blood at the end of gestation although it is metabolized rapidly immediately after delivery. In fact, neurons and oligodendrocytes use lactate as preferential substrate, suggesting that lactate is essential for brain cell proliferation and differentiation (Medina and Tabernero, 2005). This is relevant in humans, in which key steps of brain development occur during the perinatal period. Moreover in adult brain, lactate production and accumulation occur not only during oxygen lack (anoxia, hypoxia, or ischemia) but also during cerebral stimulation

under normoxic conditions (Pellerin and Magistretti, 1994; Schurr et al., 1997) with values ranging from. 0.2 to 1 μmol/g and it doubles during brain activation (Dienel et al., 2007). Most of the lactate available to the brain is produced by the brain itself and need not enter via the blood-brain barrier.

Over the past decade, the lactate literature has been very extensive and has involved many different experimental systems. One of the first indications that lactate is not only a product of the metabolic chain but also a potentially important alternative neuronal energy substrate was documented more than two decades ago from the demonstration that lactate is able to support synaptic function in the absence of glucose in rat hippocampal slices (Schurr and Rigor, 1998).

Because neonatal brain actively uses lactate, Dringen et al., (Dringen et al., 1993) decided to investigate lactate metabolism in cultured brain cells. They discovered that lactate, not glucose, is released from cultured astrocytes during glycogenolysis, and suggested that lactate may function as fuel for neighboring cells. These and related *in vitro* studies (Alves et al., 1995; Vicario et al., 1993; Waagepetersen et al., 1998), underlie the widely held notion that astrocytes may be the major source of brain lactate, but the cellular origin and cellular metabolic fate of lactate *in vivo* remain to be experimentally established.

In 1994, Pellerin and Magistretti proposed that activated neurons use lactate which is provided by astrocytes. This concept, the astrocyte–neuron lactate shuttle hypothesis (ANLS), proposes a causal sequence of events (Fig. I-40). This hypothesis postulates that lactate is produced by astrocytes and used by neurons in an activity-dependent and glutamate-mediated manner (Pellerin and Magistretti, 1994).

Accordingly, glutamate released from neurons during synaptic activity induces glutamate uptake by glial cells, which triggers activation of glycolysis. Glial glycolysis then produces lactate which is released into the extracellular space by the MCT1 transporter and is later used as a major metabolic substrate by neurons expressing the MCT2 lactate transporter, present exclusively in this type of cell (Pellerin et al., 1998).

While there is a considerable support for the existence of an activity-dependent transfer of lactate between astrocytes and neurons, there are few diverging views that debate some aspects of the ANLS. Thus, one argument derived from modeling studies suggests that the glucose transport capacity is larger in neurons than in astrocytes (Mangia et al., 2009; Simpson et al., 2007), a prediction suggested being inconsistent with ANLS. Another modeling study by DiNuzzo and colleagues has suggested that glycogenolysis in astrocytes provides a mechanism to preserve glucose availability for neurons, rather than providing lactate to them (DiNuzzo et al., 2010). However, experimental data obtained *in vivo* described in (Suzuki et al., 2011) and reviewed in (Pellerin and Magistretti, 2012) is in contradiction with the mathematical model proposed.

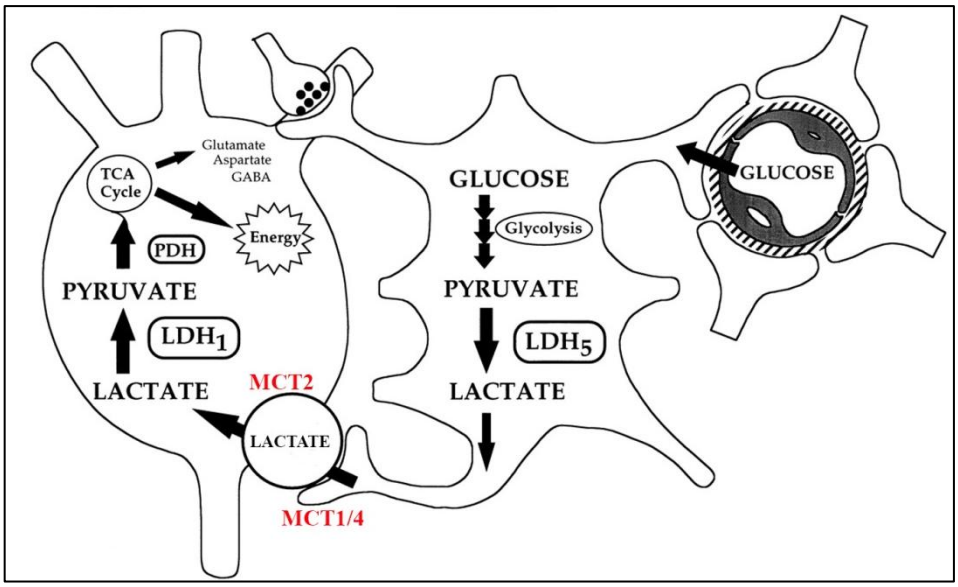

Figure I-40. Schematic representation of astrocyte-neuron lactate shuttle hypothesis. Glucose is processed glycolytically to lactate by astrocytes. The exchange of lactate between astrocytes and neurons is operated by monocarboxylate transporters (MCT1/4 in astrocytes and MCT2 in neurons, in red). Lactate is then converted to pyruvate. Pyruvate, via the formation of acetyl CoA by pyruvate dehydrogenase (PDH), enters the tricarboxylic acid (TCA) cycle. Some of the carbons in the lactate molecule could enter into amino acid pools such as the neurotransmitters glutamate, aspartate, and γ-aminobutyric acid (GABA). Adapted from Magistretti and Pellerin, 1999.

Finally, a critique that has been raised particularly at the early times of the formulation of the ANLS model was that it was largely based on *in vitro* data. However in the last decade, molecular description of the astroglial-based coupling mechanism relies on extensive *in vitro*, *ex vivo*, and *in vivo* investigations by several groups (Boumezbeur et al., 2010; Gallagher et al., 2009; van Hall et al., 2009).

6.3.2 Lactate and angiogenesis

Lactate is an important intermediate in the process of repair and regeneration, a role that has been largely ignored and it is now being (re)discovered (Fraisl et al., 2009).

It was found that after injury, disruption of microcirculation and subsequent increased oxygen consumption led to the production of lactate (Ghani et al., 2004). Under these conditions, some cells, particularly neutrophils, macrophages, and fibroblasts, depend to a large extent on glycolysis for cellular energy and produce large amounts of lactate (10-15mM) through aerobic glycolysis (Caldwell et al., 1984; Constant et al., 2000). Several studies have shown that lactate alone, even in the presence of oxygen, enhances collagen deposition and stimulates angiogenesis after a lesion (Constant et al., 2000; Trabold et al., 2003). This reaction can be described as a response to a metabolic demand precipitated in an environment that has little oxygen and/or a high level of lactate. In response to this, fibroblasts (and endothelial cells)

synthesize and secrete collagen (Ghani et al., 2003; Hunt et al., 1978; Trabold et al., 2003) and macrophages (and endothelial cells) elicit vascular endothelial growth factor (VEGF) production and keep it in an active form, which stimulates new vessel growth (Ghani et al., 2003; Sheikh et al., 2000; Trabold et al., 2003). The endothelial cell response terminates as the macrophage-derived angiogenic signals diminish.

6.3.3 The effect of lactate in brain injury

A key to understand traumatic brain injury is the energy crisis derived from decreased cerebral blood flow, increased energy demand and mitochondrial dysfunction. Although still controversial, both clinical and experimental studies demonstrate increased lactate in the injured brain (Bullock et al., 1995).

However, some studies in ischemia have reported that a high lactate level is correlated with a poor prognosis (Zauner et al., 1997). Other studies have also demonstrated extracellular lactate accumulation during cerebral ischemia and injury, which has led to the lactic acidosis hypothesis of ischemic damage, in which a high degree of tissue acidosis is thought to impair post-ischemic recovery (Inao et al., 1988; Kalimo et al., 1981; Siesjo et al., 1974).

Andersen and Marmarou (Andersen and Marmarou, 1992) have demonstrated that whole brain lactate increased after traumatic brain injury (TBI), even though simultaneously measured cerebral blood flow was unchanged, suggesting that TBI itself, rather than secondary ischemia, may cause this lactate increase. Marmarou's group proposed the ''energy compartmentalization'' hypothesis to explain these findings, suggesting, in common with other authors, that mitochondrial function is depressed after TBI, and that anaerobic glycolysis is therefore facilitated in compensation (Andersen and Marmarou, 1992). This increased glycolysis supports restoration of ionic homeostasis, and generates lactate (Pellerin and Magistretti, 1994).

Several reports indicate that lactate can also serve as an energy substrate for damaged and premature neonatal brains (Pellerin and Magistretti, 1994; Schurr et al., 1997). Schurr and Rigor (Schurr and Rigor, 1998) demonstrated that lactate is used as an aerobic energy substrate by neural tissue immediately following hypoxia *in vitro*. Even more recently, lactate was found to be a critical oxidative energy substrate immediately post-ischemia in rat brain *in vivo* (Schurr et al., 2001). Schurr and his group (Schurr et al., 1999) have demonstrated that lactate, not glucose, primarily fuel the recovery of synaptic function after hypoxia, upon reoxygenation in hippocampal slices and is a crucial aerobic energy substrate that enables neurons to endure activation. Moreover, other studies have shown that blood lactate may cross the blood-brain barrier (BBB) in increased amounts after the TBI (Chen et al., 2000a). In other study, ^{14}C-Lactate was used to test the hypothesis that blood lactate was acutely taken up by the injured

brain. They demonstrate that this metabolite was mainly concentrate in the injury site (2.5 times greater), although un-injured brain also took it up (Fig. I-41) (Chen et al., 2000b).

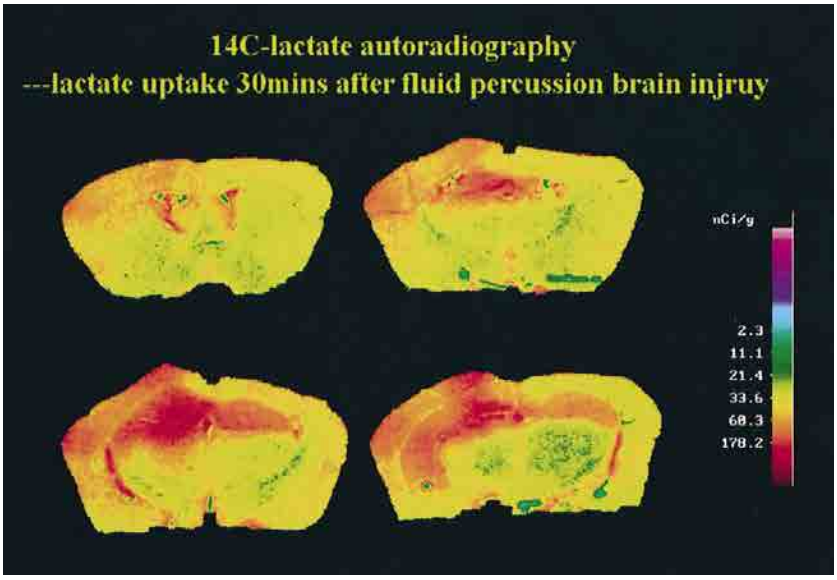

Figure 41. ^{14}C-Lactate distribution is increased at the injury site and in both hippocampi after the brain injury. Adapted from Chen et al., 2000b.

Moreover, new findings suggest that brain cells try to survive in injured conditions by metabolizing lactate as an energy substrate instead of glucose. Experimental and clinical data suggest that lactate, at least when exogenously administered, is transported from astrocytes to neurons for neuronal utilization, essentially bypassing the slow, catabolizing glycolysis process to quickly and efficiently produce ATP (Alessandri et al., 2009).

In this sense, treatment strategies using systemically applied lactate have proved to be protective in various experimental traumatic brain injury studies (Alessandri et al., 2009).

7. Challenges in brain repair: engineering artificial neural stem cell niches

Tissue-engineered scaffolds offer some scenarios for the treatment of brain injuries and neurodegenerative disorders. At present, the design and fabrication of scaffolds is still in its infancy and must overcome several problems before their employment in treatment. As scaffolds are designed to support neural cells (either transplanted or endogenous), the major obstacles related to modulating cell function is through optimization of surface functionality, mechanical properties, and biological activity. Therefore, the requirements of a scaffold to form a cellular microenvironment also translate to challenges for tissue engineers. Challenges encountered by scaffolds include limitations in porosity, pore dimensions, three-dimensionality, and surface functionality. Issues relating to toxicity of residual solvents, mechanical compatibility, biocompatibility, and degradation traits also need to be taken into consideration. Fabricating a scaffold that overcomes these morphological and biological limitations and also promotes integration with the native tissue and achieving functional recovery is a challenging task (Pettikiriarachchi et al., 2010).

Moreover, the biological activity of the scaffold should be tailored to address the necessities of individual neurological conditions due to differences in the way of injury (Lampe and Heilshorn, 2012). Although there are some *in vivo* investigations ascertaining scaffold biocompatibility and identifying the cell types that infiltrate the construct, the functional nature of the regenerating tissue remains to be explored.

Recent approaches in neural engineering have focused on the natural NSCs niche, which provides a model for designing a powerful artificial microenvironment to regulate the NSCs fate, which is essential for the CNS regeneration (Lampe and Heilshorn, 2012). Ideally, an engineered niche would include spatial organization, biochemical cues, soluble factors, extracellular matrix and also blood vessels to induce a dynamic modulation of cells. In order to study specific features of the NSC environment, many groups have attempted to engineer materials that allow isolation of individual variables, such as stiffness, without varying others. Diverse materials with tunable mechanical properties have been engineered to try to mediate NSC self-renewal and differentiation as well as astrocytic activation and glial scarring (Banerjee et al., 2009; Keung et al., 2010; Lampe and Heilshorn, 2012; Saha et al., 2008). Although currently available matrices often lack this level of complexity (Lutolf and Hubbell, 2005), new biomaterials strategies are being developed to address these needs.

GOALS

RATIONAL OF THE THESIS

In the embryonic brain, radial glia cells are neural stem cells (NSC) that serve as substrate for neuronal migration and are retained in the adult brain of species that regenerate. Radial glia are bipolar cells with long shafts (1-2μm thick) that span the entire cortical parenchyma forming a radial palisade. These cells contain high levels of glycogen and release L-lactate through MCT1 monocarboxylate transporters.

The main goal of this thesis is to perform a cell-free biomimetic scaffold to regenerate cortical brain injuries in mice. For this purpose, we are going to design an implantable material consisting of electrospun poly-lactic acid (PLA) fibers that by reproducing the 3D organization and supportive function of radial glia will mimic physical and biochemical characteristics of the embryonic NSC niche.

GOALS

1. Select a PLDLA polymer (PLDLA 95/5 and 70/30) with optimal degradation rate to support neural cells attachment, growth and differentiation.

2. Perform 3D electrospun nanofibers and analyze the effect of topology on neural cells in terms of cell adhesion, survival, proliferation, differentiation and migration in *vitro*.

3. Analyze the effect of D and L-lactate, the degradation products of PLDLA materials, on neural cells physiology *in vitro* and *in vivo*.

4. Study the neurogenic and angiogenic regenerative capacity of electrospun PLDLA lactate-releasing scaffolds when implanted into surgically made cavities in postnatal and adult mice brain.

MATERIALS and METHODS

PLDLA films fabrication

Poly-LL/DL lactic acid 95/5 (PLA95/5) (Purasorb PLLDL 9562, inherent viscosity midpoint 6.2 dl/g, Mw ≈ 125.000 g/mol) and Poly-LL/DL lactic acid 70/30 (PLA70/30) (Purasorb PLLDL 7038, inherent viscosity midpoint 3.8 dl/g, Mw ≈ 850.000 Da) were purchased from Purac Biomaterials (Gorinchem). 150 μm thick films of PLA95/5 and PLA70/30 were prepared by solvent casting. Briefly, 6.75 g of PLA were dissolved in 270 ml of chloroform (2.5% w/v). The solution was poured into Petri dishes with ø of 150 mm. The solvent was evaporated in a chloroform-saturated atmosphere for 48 hours.

PLDLA 70/30 nanofiber fabrication

Poly- LL/DL lactic acid 70/30 (PLA70/30) (Purasorb PLLDL 7038, inherent viscosity midpoint 3.8 DL/g, molecular mass ≈ 850,000 Da) was purchased from Purac Biomaterials (Gorinchem, The Netherlands). 238±18-μm-thick sheets of random and aligned PLA70/30 nanofibers were prepared by electrospinning. Briefly, 2.86 g (4% w/w) of PLA was dissolved in 50 ml of 2,2,2-trifluroethanol (99.8%; Panreac, Barcelona, Spain). The solution was electrospun with a grounded flat collector for randomly distributed fiber samples or with a grounded rotary collector with a diameter of 9 cm and a rotational speed of 1,000 rpm for aligned ones. The voltage was 8 kV, the distance between the tip and the collector was 12 cm, and the humidity was 20% at 23°C.

PLDLA films and fibers characterization

Characterization of PLA95/5, 70/30 films and fibers wettability was performed via contact-angle measurements using an OCA 20 system (Dataphysics, GmbH), using the captive bubble technique This method measures the equilibrium angle formed between a 3-μl air bubble and the PLA surface, both immersed in water. The measurements were performed in triplicate with at least three different data points for each sample. The ζ-potential was measured using a SurPASS electrokinetic analyzer and VisioLab software (Anton Paar Ltd., Graz, Austria). All measurements were done at a dynamic pH of the electrolyte (1 mM KCl, pH 3–8) after 1 h of equilibration and using the adjustable gap cell for small samples.

The stiffness and surface topography of PLA95/5, 70/30 films and fibers were measured using atomic force microscopy (AFM) (MultiMode 8 Atomic Force Microscope (Bruker)). Tests to failure to measure films tensile strength were performed using an Instron 5565 compression and tension tester (Instron Corp. Canton MA) with samples of 15x10 mm and thicknesses of 333±22 μm. The tensile stress test was monitored using a speed of 10 mm/min. For fibrous sheets were

determined with a Zwick-Roell Zwicki-Line Z0.5TN (Zwick-Roell, Ulm, Germany) universal testing machine, with ten samples of 40×10 mm.

A thermal characterization of the different materials was performed by Differential Scanning Calorimetry (DSC, for films; 2029 TAInstruments, New Castle, USA / For fibers; Mettler DSC-822e calorimeter with a TS0801RO robotic arm). For DSC test, approximately 5 mg of the sample were placed in aluminum crucibles under a nitrogen atmosphere and heated from room temperature up to 180°C at a rate of 10°C/min. The degree of crystallinity was calculated using the following equation (1):

$$\%Xc = \frac{(\Delta H_m - \Delta H_c)}{\Delta H_m^0} \times 100$$

where %Xc is the percentage of crystallinity, DH_m is the latent heat of melting, DH_c is the heat of the crystallization, and DH_m^0 is the heat of melting of a PLA with a supposed 100% degree of crystallinity (DH_m^0 = 93.1 J/g) (Fischer, 1973).

A X'Pert PRO diffractometer (Panalytical, Almelo, Netherlands) (CuKα λ=1.5406 Å radiation, 45 kV, 40 mA, and a step size of 0.026º) was used in θ/2θ 2–60º X-ray diffraction (XRD) analyses of PLA films and fibers.

Micro and nanomorphology were assessed using a field emission scanning electron microscope (Nova-Nano SEM-230; FEI Co., Netherlands), operating at 10 kV and with ultra-thin carbon coating of the fibers. The fiber sheets were cross-sectioned using the focused ion beam lithography technique (Strata DB235; FEI Co.).

For cell culture, PLA95/5 and 70/30 films were sterilized with 70% ethanol for 15 min and cut to fit in 60 mm ø tissue culture dishes. As PLA 70/30 fibers could not be sterilized with 70% ethanol due to the degradation/collapse of nanofibrous sheets after 2 minutes (Fig. M-1), fibers were sterilized with UV during 24h in a laminar flow hood.

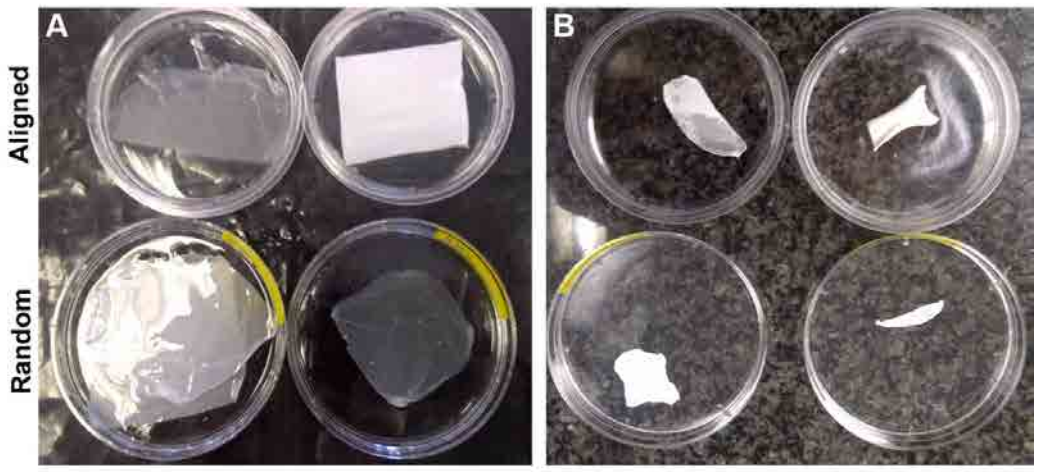

Figure M-1. PLA70/30 nanofibers sterilized with 70% ethanol. A. Random and aligned PLA fibers before been sterilized with ethanol 70%, **B.** and 2 minutes after been immersed in ethanol 70%.

Degradation study and L-lactate quantification

The degradation of PLA films *in vitro* was followed at 37ºC for four weeks. Four samples (~ 8mg) were immersed in Neurobasal A (NB^A, glucose- and pyruvate- free, Gibco, Auckland, New Zeland) and retrieved after 1, 3, 4, 5, 7, 15 and 21days *in vitro* (*div)*.

The degradation study of PLA nanofibers *in vitro* was followed at 37ºC for eight weeks. Four samples were immersed in Neurobasal A (NB^A, glucose- and pyruvate-free, Gibco) and retrieved after 5, 7, 21, 30, and 45 days *in vitro* (*div*).

The L-lactate concentration was determined using an enzymatic reaction based on the oxidation of L-lactate to pyruvate by lactate dehydrogenase (5 mg of the enzyme (Roche)/mL, 550 U/mg) in the presence of NAD (Sigma-Aldrich,St Louis, MO). In this assay, the amount of NADH produced in the reaction is proportional to the amount of L-lactate in the samples. With this enzymatic system, D-lactate is not detected.

All experiments were carried out at least three times and triplicate samples were diluted 1:20 with reaction mix [0.3M hydrazine sulfate (Merck, USA) and 0.87 M glycine (AppliChem, USA), pH 9.5; 2.5 M NAD^+ (Sigma-Aldrich), 0.19 M EDTA (Merck)]. Lactate dehydrogenase was added at a final concentration of 6.9 U/ml. The NADH concentration was determined by using the Fluostar Optima BMG Labtech system to measure absorbance (340 nm) and fluorescence (excitation 340 nm/emission 460 nm) 0 and 20 min after the start of the reaction. The endpoint of the reaction was set at 20 min and the corresponding values were used in the calculations. Different concentrations of sodium L-lactate (Sigma-Aldrich) served as the standard.

Glucose quantification

The concentration of glucose was determined by the glucose oxidase-peroxidase method using PGO enzymes (Peroxidase and Glucose Oxidase, Sigma-Aldrich). O-dianisidine dihydrochloride (ODD, Sigma) was utilized as a colorimetric substrate. Colorless ODD in reaction with H_2O_2 (produced by oxidation of glucose) changed to brown. The brown intensity was measured at 450nm using lector Tecan (Sunrise-Basic, ref. 16039400). For glucose determination, glucose standard (Sigma-Aldrich) was used to prepare the standard curve. The reaction proceeded for 30 min at 37ºC. The samples were analyzed in triplicate.

Cell culture

All animal housing and procedures were approved by the Institutional Animal Care and Use Committee, in accordance with Spanish and EU regulations. Glial cells were derived from the cerebral cortex of newborn mice (P0) as previously described (Mattotti et al., 2012). Briefly,

cerebral cortices were dissected free of meninges in dissection buffer (PBS 0.6% glucose (Sigma-Aldrich), 0.3% BSA (Sigma-Aldrich) and digested with trypsin (Biological Industries, Israel) and DNAse I (Sigma-Aldrich) for 10 min at 37º C. The tissue was dissociated in Dulbecco's Modified Eagle Medium (DMEM, Biological Industries), 10% normal horse serum (NHS, Gibco), 1% penicillin-streptomycin (pen-strep, Biological Industries) and 2mM L-glutamine (Biological Industries). After centrifugation and resuspension, cells were plated and grown to confluence at 37°C, 5% CO_2 (approximately 25-30 days *in vitro (div)*). The influence of the properties of the various materials used in this thesis on glial cell adhesion, morphology and differentiation was determined as follows: passage 1 (Ps1) cells were cultured at a density of 2×10^5 cells/cm^2 for 5 div in NB containing 3% normal human serum (NHS), 1% pen-strep, and 2 mM L-glutamine on uncoated PLA materials. Control Ps1 glial cells were cultured on non-coated culture plastic (for western blotting) or on glass coverslips (for immunocytochemistry) under the same conditions used for PLA substrates (films and fibers).

Neurons were obtained from embryonic brains as described elsewhere (Ortega and Alcantara, 2010). Briefly, a time-pregnant mouse was sacrificed by cervical dislocation and the embryos were extracted at embryonic day 16 (E16). Cerebral cortices were dissected free of meninges in a solution of PBS with 0.6% glucose (Sigma-Aldrich), 0.3% BSA (Sigma-Aldrich) and digested with trypsin (Biological Industries) DNAse I (Sigma-Aldrich) for 10 min at 37ºC. The tissue was mechanically dissociated, centrifuged and resuspended in CO_2-equilibrated Neurobasal^{TM} (NB), supplemented with 5% NHS, 1% pen-strep, 0.5mM L-glutamine, 5.8µl/ml $NaHCO_3$ (Sigma-Aldrich). The cell suspension was pre-plated at 37ºC. After 30 min, the supernatant was collected, centrifuged (1000g 5min) and resuspended in neuronal culture medium (NB, 1%NHS, 1% pen-strep, 0.5mM L-glutamine, 22µM glutamic acid (Sigma-Aldrich), 2% B27 (Gibco), 5.8µl/ml $NaHCO_3$. Cells were plated at a density of $1x10^5$-$2.5x10^5$ cells/cm^2 directly on top of films of PLA(95/5 and 70/30) and/or PLA70/30 fibers (random and aligned) and on poly-D-lysine (Sigma-Aldrich) coated tissue culture plate (for Western blotting) or poly-D-lysine coated glass (Lysglass, for ICC) as a positive control.

After 24h, the medium was changed to a serum free neuronal culture medium (1% pen-strep, 0.5mM L-glutamine, 2% B27 (Gibco), 5.8µl/ml $NaHCO_3$) during 1*div*, 3*div* and 5*div*. For co-cultures, neurons were plated directly on top of 5*div* glial cell cultures, and then cultured for 5 more days in neuronal culture medium.

Lactate treatments

In order to analyze the effect of lactate released by the material, neurons and glial cells were plated in the same conditions as described above for the first 24h in a glucose-free Neurobasal^{A} media (glucose-free, NB^{A}; Invitrogen, USA), with 3% NHS, 1% pen-strep, and 2 mM L-

glutamine during *5div* for glial cells, and 1%NHS, 1% pen-strep, 0.5mM L-glutamine, 22 µM glutamic acid, 1x B27, 5.8 µl/ml Na C O_3 for neuronal cell cultures. After 24h, the neuronal culture medium was changed again to a serum free NB^A with 1% pen-strep, 0.5mM L-glutamine, 1x B27, 5.8 µl/ml Na C O_3 and cultured during 4*div*.

P0 primary glial cultures and E16 neuronal cultures grown on tissue culture plate treated with L- or D-lactic acid (Sigma Aldrich) were growing in Neurobasal medium supplemented with 25 mM glucose (glucose medium) or with 25 mM glucose and 4 mM lactic acid ((glucose+lactate medium), or with 4 mM lactic acid only (glucose-free lactate medium). Neurons were cultured for 24 h in the above media supplemented with 1% NHS, 1% pen-strep, 0.5 mM L-glutamine, 22 µM glutamic acid, 1× B27, and 5.8 µL Na C O_3/mL. The medium was then replaced with the same medium but serum-free and the cultures incubated for 4 more days. The samples were either fixed in 4% paraformaldehyde for immunocytochemistry or used for protein extraction and western blot analysis.

Pharmacological inhibition of lactate transport and signaling

- **Neuronal cultures grown PLA fibers**

To analyze the effect of lactate, E16 neurons were cultured on aligned PLA70/30 nanofibers in Neurobasal™ media (with 25mM glucose, glucose-containing medium), or in free glucose Neurobasal^A medium (NB^A) supplemented with 1% NHS, 1% pen-strep, 0.5 mM L-glutamine, 22 µM glutamic acid, 1× B27, and 5.8 µl 7,5% $NaHCO_3$/ml for 24 h, after which the medium was replaced with serum-free neuronal medium in the presence or absence of 100 nM of the monocarboxylate transporter (MCT) 1/2 inhibitor AR-C155858 (AdooQ, Irvine CA, USA) or 1mM of the selective agonist of GPR81 lactate receptor 3, 5-Dihydroxybenzoic acid (3, 5-DHBA, Santa Cruz Biotechnology) for four more days. The samples were either fixed in 4% paraformaldehyde for immunocytochemistry.

- **Neuronal cultures treated with lactate**

Experiments testing the effects of MCT2 inhibition or the lactate receptor agonist GPR81 were carried out as follows: E16 primary neuronal cultures were treated with L- or D-lactic acid (Sigma Aldrich) and cultured in three different media: NB medium (with 25 mM glucose, glucose medium), NB medium supplemented with 4 mM lactic acid (glucose+lactate medium) or glucose-free NeurobasalA medium (NBA) supplemented with 4 mM lactic acid (lactate medium). Neurons were cultured for 24 h in these media, also containing 1% NHS, 1% pen-strep, 0.5 mM L-glutamine, 22 µM glutamic acid, 1× B27, and 5.8 µL Na CO3/mL. The

medium was then changed to serum-free formulations containing 1% pen-strep, 0.5 mM L-glutamine, 1× B27, 5.8μL Na C O3/mL and the presence or absence of the MCT2 inhibitor AR-C155858 (100 nM) or the GPR81 agonist, 3,5-dihydroxybenzoic acid (1 mM, 3,5-DHBA) for four more days.

In experiments testing the effects of PEPCK inhibition, the cells were cultured as described above, except that the serum-free medium contained DMSO (1:2000, Sigma-Aldrich) for control conditions or the PEPCK inhibitor 3-mercaptopicolinic acid (100 μM, 3MPA, Toronto Research Chemicals). The cells were then cultured for four more days. The samples were either fixed in 4% paraformaldehyde for immunocytochemistry or used for protein extraction and western blot analysis.

All experiments were carried out at least three times and triplicate samples were analyzed by Western blot, cell morphology was analyzed by immunofluorescence, and L-lactate and glucose in media were measured by spectrophotometry and fluorescence respectively.

Intraventricular brain injections in postnatal animals

Experiments were design to minimize the number of animals used in the procedure. All animal protocols were approved by the Institutional Animal Care and Use Committee in accordance with Spanish and European Union regulations. The brains of newborn (postnatal day 0, P0) mice were injected in the lateral ventricle 2 μL of lactic acid (5 mM, Sigma Aldrich, n=10), 3-mercaptopicolinic acid (100 μM, 3MPA, Toronto Research Chemicals, n=8), or vehicle (MiliQ water, n=8). Tissues for immunohistochemistry analysis were obtained at P3, by killing the animals by anesthetic overdose followed by a transcardiac perfusion with 4% paraformaldehyde (PFA) in 0.1 M phosphate buffer, pH 7.3. The mouse brains were post-fixed for 8–12 h, cryoprotected, and kept frozen. Coronal sections of 40 μm thickness were collected in a cryoprotective solution and stored at −20 °C until further use.

Implantation of PLA nanofibers tubes into the right hemisphere of injured brain

All animal housing and procedures were approved by the Institutional Animal Care and Use Committee in accordance with Spanish and EU regulations.

Four-day-old (P4) mice were anesthetized by immersion in ice for 5 min, placed in a stereotaxic apparatus for small animals (mouse and neonatal rat stereotaxic adaptor Stoelting Europe, Dublin, Ireland), and kept cold during surgery. A triangular tissue flap overlying the right somatosensory cortex was lifted with a surgical blade, carefully avoiding severing surface

blood vessels in the brain parenchyma. After opening the skull, PLA films were directly implanted or 1 mm^3 cavities were made by direct suction with a syringe connected to a blunt needle of 1 mm ø to implant tubes of PLA fibers (Fig. M-2).

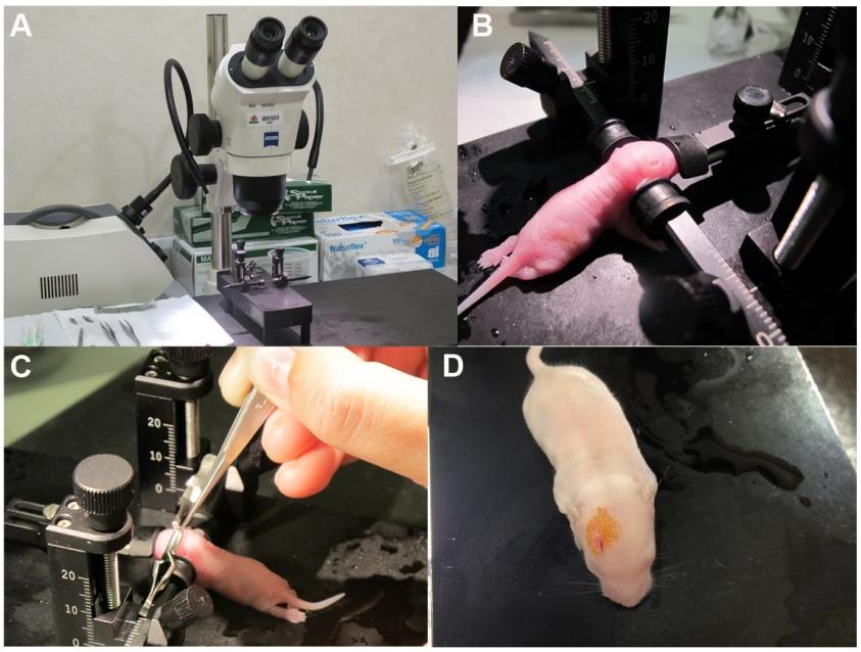

Figure M-2. Surgery procedure in postnatal mouse (P4). A. Stereotaxic apparatus for small animals (Stoelting mouse and neonatal rat stereotaxic adaptor). **B-D.** Surgery procedure in P4 mouse.

Tubes of PLA fiber sheets were folded in a 3 layer-tube and cut into $1mm^3$ following the procedure (Fig. M-3) adapted from Hurtado et al., 2011. Immediately after tissue removal, $1mm^3$ scaffolds soaked in Neurobasal™ (NB) with 1% pen-strep were implanted or the cavity left empty (Control) and the tissue flap put back in place.

Different fibers orientations were used to designed the scaffolds. Random (random scaffolds, n=29) and aligned PLA fiber scaffolds (aligned scaffolds, n=87) following the radial orientation of radial glia (radial scaffolds, n=77) or placed orthogonal to radial glia orientation (orthogonal scaffolds, n=10), were fitted into the brain cavity. The non-implanted injured cavities were used as control (control n= 27). Animals were warmed on a heating pad and returned to their mother after recovery. The brains were then analyzed at 2 and 7 days and at 2, 6, and 12–15 months post-surgery. After anesthetics overdose, animals were perfused using buffered 4% paraformaldehyde (Sigma–Aldrich). Brains were then removed, placed in a 30% sucrose/PBS mixture for 24h- 2 days and subsequently frozen with liquid nitrogen and stored at -80 ºC.

For immunohistochemistry brains were cryosectioned coronally at 40µm intervals and were processed for immunocytochemistry as described above.

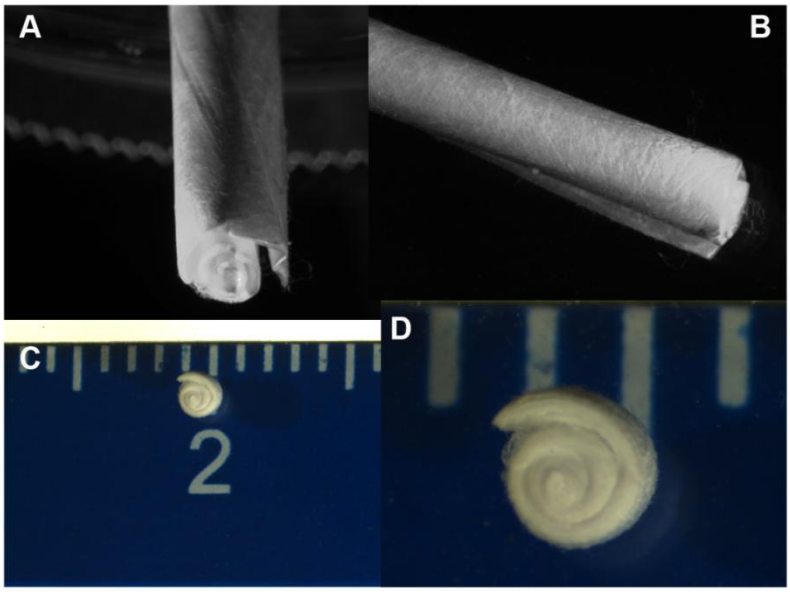

Figure M-3. Tubes of PLA fiber in the stereoscopic microscope. A-B Random PLA fiber sheet folded into 3 layers tube and **C-D** cut into 1mm^3 tubes**.**

Adult male/female Swiss Albino mice (3-6 months) weighing between 40-60 gr were anesthetized by intraperitoneal injection of Ketamine/Valium (150 μg/g, 5 μg/g) and placed in a stereotaxic apparatus. Surgery was performed under sterile conditions. A piece of skull over the right somatosensory/motor cortex was excised with a drill. 1 mm^3 cavities were made by direct suction with a syringe connected to a blunt needle of 1 mm ø. Those cavities were filled immediately after tissue removal with 1mm^3 aligned PLA fiber scaffolds (aligned scaffolds, n=4) soaked in NeurobasalTM (NB) with 1% pen-strep or left empty (Control n=4). After the surgery, the skin was sutured with 6.0 surgical sutures (Fig. M-4). The brains were then analyzed at 7 days and 3 months post-surgery after anesthetic overdose. Animals were perfused with buffered 4% paraformaldehyde (Sigma–Aldrich). Brains were then removed, placed in a 30% sucrose/PBS mixture for 24h- 2 days and subsequently frozen with liquid nitrogen and stored at -80 ºC.

For immunohistochemistry brains were cryosectioned coronally at 40μm intervals and were processed for immunocytochemistry as described above.

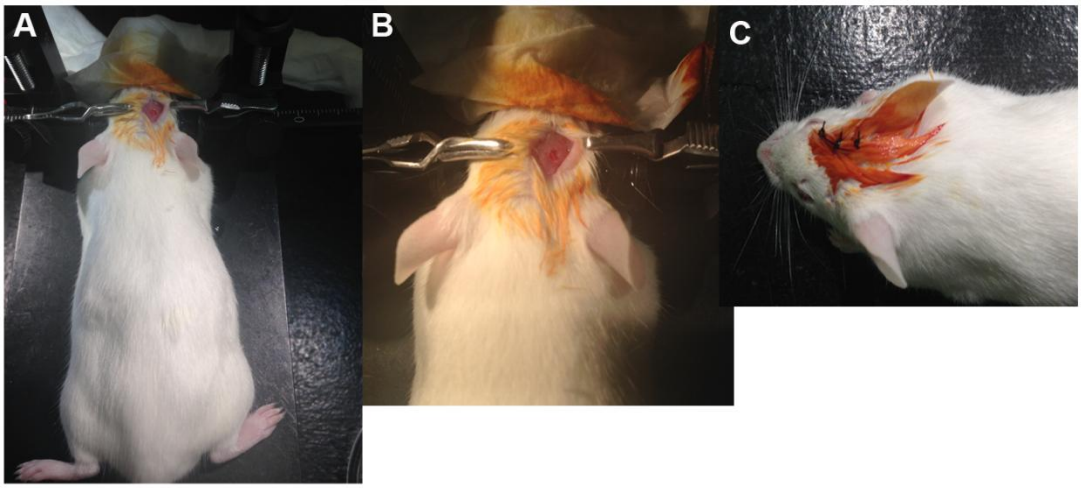

Figure M-4. Surgery procedure in adult mouse. A. Stereotaxic apparatus for animals (Stoelting mouse and neonatal rat stereotaxic adaptor). **B-D.** Surgery procedure for PLA scaffolds implantation in adult mouse.

Immunofluorescence and western blot analysis of culture cells

Total protein extracts for western blot analysis were prepared from primary neuronal and glial cultures, separated by SDS-polyacrylamide gel electrophoresis, and electro-transferred to a nitrocellulose membrane (Bio-Rad). The membranes were blocked with 5% bovine serum albumin (BSA, Sigma-Aldrich) and incubated overnight at 4°C first with primary antibodies and then with the corresponding secondary HRP-conjugated antibodies (1:3000; Santa Cruz Biotechnology). Protein signals were detected by the ECL chemiluminescent system (Amersham, GE Healthcare, Buckinghamshire, UK). Densitometry analysis, standardized to actin or total AKT as a control for protein loading, was carried out with ImageJ software (National Institutes of Health, USA). For quantification, triplicate samples were analyzed and at least three different experiments were performed.

For immunofluorescence, fixed primary cultures or tissue sections were incubated with primary antibodies overnight at 4°C and then with the appropriate Alexa 488 or Alexa 555 secondary antibodies (1:500, Molecular Probes, USA). TO-PRO-3 iodide (Topro, 1:500, Molecular Probes) was used to stain nuclei. Finally, the preparations were cover-slipped with Mowiol (Calbiochem, Billerica, USA) for imaging.

Detection and characterization of neural populations

To characterize the phenotype of the cells, the following primary antibodies were used: mouse anti-NeuN (Neuronal marker, 1:500, Abnova Corporation, Taiwan), rabbit anti-Parvalbumin (PV, gabaergic neuronal marker, 1:8000, Swant, Rumania), rabbit anti-glial-fibrillary-acidic-protein (GFAP, mature and reactive glial marker, 1:1000-1:8000, Dako, Denmark), rabbit anti-BLBP (radial glial marker, 1:1000-1:8000, Chemicon, Billerica, USA),rabbit anti-

EAAT1/GLAST-1 (GLAST, glial glutamate transporter marker, 1:1000, Abcam), mouse anti-Nestin (progenitor and radial glial marker, 1:250, Abnova Corporation), rat anti-F480 (macrophage marker, 1:1000, Chemicon, USA), goat anti-MCT2 (monocarboxylate transporter, 1:1000, Santa Cruz Biotechnology), PEPCK-M (mitochondrial phosphoenolpyruvate carboxykinase, 1:1000, Abcam, UK), goat anti- G-protein-coupled lactate receptor (GPR81, 1:500, Santa Cruz Biotechnology), goat anti-Iba1 (microglial and macrophages marker, 1:200, Abcam), rabbit anti-CX3CR1 (macrophage and microglial marker, 1:500, Abcam), rabbit anti-PH3 (mitosis cell marker, Millipore, USA), rabbit anti-Ki67 (cell cycle marker, 1:500, Abcam), goat anti-Actin (cytoskeleton Marker, 1:2000, Santa Cruz Biotechnology), mouse anti-Vinculin (cytoskeleton marker, 1:1000, Santa Cruz Biotechnology), goat anti-AKT (serine/threonine-specific protein kinase, 1:1000, Millipore), mouse anti-Tuj-1 (neuronal marker, 1:10000, Covance, USA), rabbit anti-MAP2 (neuronal cell bodies and dendritic marker, 1:2000, Covance), rabbit anti-Doublecortin (DCX, neuronal marker, 1:1000, Abcam), goat anti-FOXP2 (progenitor marker, 1:1000, Santa Cruz Biotechnology), rabbit anti-Pax6 (bipotential radial glial marker, 1:250, Abcam), rabbit anti-Tbr2 (neurogenic intermediate progenitor cell marker, 1:500, Abcam), rabbit anti-Sox2 (stem cell marker, 1:1000, Abcam), rat anti-CD31/PECAM (endothelial marker, 1:200, Abnova Corporation), rabbit anti-Laminin (extracellular matrix and blood vessel marker, 1:500, Sigma-Aldrich), rabbit anti-NG2 (oligodendrocyte precursor cells, 1:1000, Chemicon), rabbit anti-Olig2 (oligodendrocyte transcription factor 2, 1:200, Abcam), rabbit anti- myelin basic protein (MBP, oligodentrocyte marker, 1:1000, Covance), rabbit anti-PSD95 (postsynaptic marker, 1:1000, Abcam), mouse anti-SNAP25 (Presynaptic marker, 1:1000, Covance), mouse anti-synaptophysin (pre-synaptic neuronal marker, 1:1000, Abcam) and rabbit anti-caspase-3 (apoptosis marker 1:100, Santa Cruz Biotechnology).

BrdU labeling

Starting at different time points after scaffold implantation, 5-bromo-2'-deoxyuridine (BrdU, Sigma-Aldrich) was injected intraperitoneally (5 mg/10 gr body weight) every 24 h for a 5-day period. BrdU incorporation was analyzed by immunohistochemistry (rat-anti-BrdU, 1:1000; Abcam) at different time points after injection. Animals were killed at different time points after injection as follows (P indicates postnatal day): P6: 3 h after the first injection (n=5); P11: injections at P6–P10 (n=5); at 1 year: injections at P6–P10 (n=3); at 1 year: injections at 2 months (n=3); at 1 year: injections one week before death (n=3). The cell types that incorporated BrdU and their progeny were identified by double immunohistochemistry with BrdU antibodies and antibodies to Sox2, Tbr2, Pax6, DCX, NeuN, PV, GFAP, and Olig2.

Vascular labeling

10 ml of lipophilic carbocyanine dye DiI (100mg/20ml ethanol, Sigma-Aldrich) solution (PBS and 5% glucose dilution (1:4)) was injected during cardiac perfusion of the animals (Fig. M-5) as previously described (Li et al., 2008b). DiI-labeled vasculature was reconstructed on 300-µm-thick coronal sections in animals after 1-year post implantation (n=4 Aligned nanofibers, n=3 Random nanofibers, n= 2 Control).

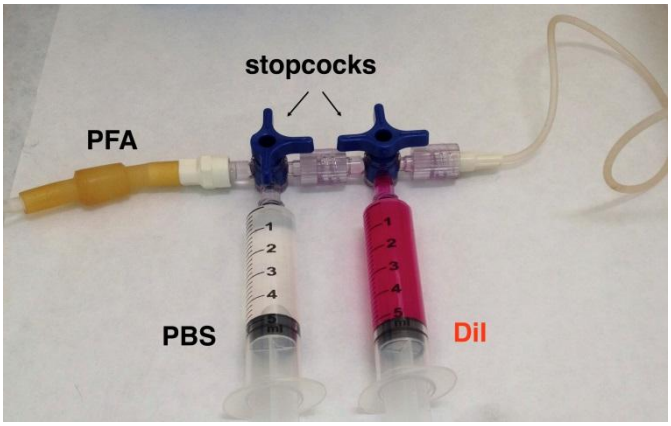

Figure M-5. DiI perfusion device. The main body of the perfusion device is two-way stopcocks connected in series. The inflow ports are connected to two 5-ml disposable syringes for PBS (left) and DiI solution (right) and a fixative solution.

1 year after the implant (n= 4 Aligned nanofibers), vasculature staining was performed by caudal vein perfusion with 1 mg/ml *Lycopersicon esculentum* (tomato) FITC-conjugated lectin (Sigma-Aldrich) according the protocol of Inoue and Sing, 1999, modified by Egeblad, 2004 (http://werblab.ucsf.edu/sites/werblab.ucsf.edu/files/protocol%20pdfs/Lectin_perfusion.pdf). Then, the animals were transcardially perfused with 4% paraformaldehyde (Sigma–Aldrich). The brains were then removed, frozen and cut as described above. Sections were processed for immunocytochemistry.

Retrograde neural tracing studies

One year after scaffold implantation, cholera toxin subunit B conjugated to Alexa fluor 555 (AF-CBT, Life technologies) was stereotactically injected (0.5%wt/vol in phosphate buffer) as described (Conte et al., 2009) into the intact contralateral somatosensory cortex of the 1year old mice. Control animals (n=2) and radial scaffold implanted animals (n=4) were transcardially perfused with 4% paraformaldehyde after 4 days of the injection and their brains were analyzed.

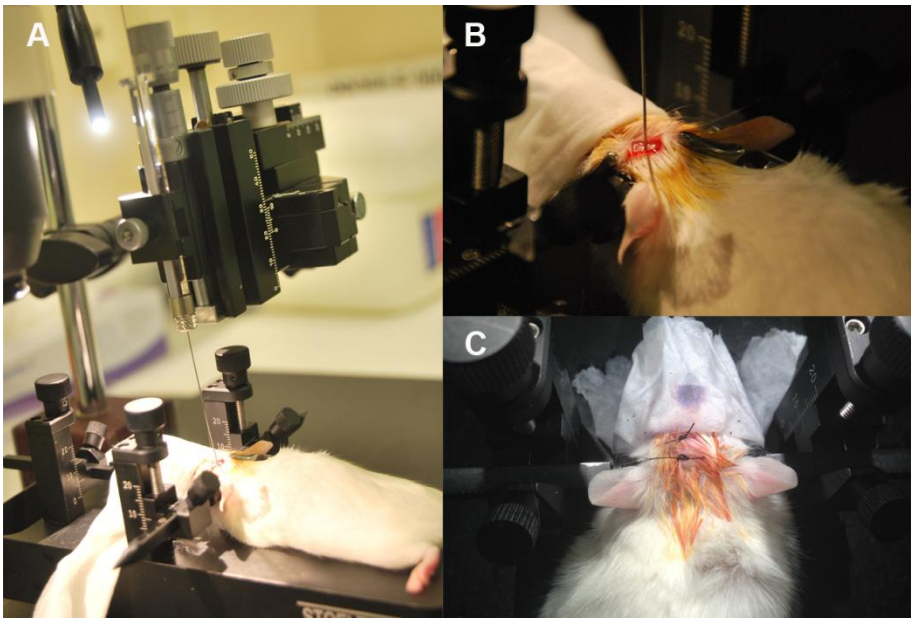

Figure M-6. Cholera toxin injections in adult mouse brain. A. Stereotaxic apparatus and micro-manipulator. **B-D.** Surgery procedure and Cholera toxin injection 1 year post-implantation.

Imaging and cell analysis

Digital images were taken throughout the study using a software-controlled digital camera. Fluorescent preparations were visualized and micrographs were captured with either a Leica TCS-SL Spectral confocal microscope (Leica Microsystems, Mannheim, Germany) or a Nikon Eclipse 800 light microscope (Nikon, Tokyo, Japan). The images were assembled in Adobe Photoshop (v. 7.0), with adjustments for contrast, brightness, and color balance to obtain optimum visual reproductions of the data. Morphometric and quantitative analyses were performed using ImageJ software (National Institutes of Health, USA). Confocal images were reconstructed using the Imaris program (Bitplane, Zurich, Switzerland) for 3D and 4D real-time interactive data viewing, with normal or shadow projections of coronal tissue sections screened under a Leica TCS-SL spectral confocal microscope.

For video time-lapse analysis, neurons were obtained from the cerebral cortex of E16 mice and cultured at low density on top of aligned PLA nanofibers. After 5 div, the cells were placed in the incubation chamber of an Observer Z1m inverted fluorescence microscope (Carl Zeiss, USA) at 37°C with 5% CO_2 and observed by phase-contrast microscopy. Images were obtained every minute for 15 h. Cell displacement; speed and trajectory were calculated using the "Manual Tracking" plug-in of the ImageJ software (National Institutes of Health, USA).

Magnetic resonance imaging (MRI)

MRI experiments were conducted on a 7.0 T BioSpec 70/30 horizontal animal scanner (Bruker BioSpin, Ettlingen, Germany) equipped with a 12-cm inner diameter actively shielded gradient system (400 mT/m). The receiver coil was a phased-array surface coil for mouse brain. The mice were placed in a supine position in a Plexiglas holder fitted with a nose cone for administering anesthetic gases (isofluorane in a mixture of 30% O_2 and 70% CO_2) and secured using a tooth bar, ear bars, and adhesive tape. Tripilot scans were used for accurate positioning of the animal's head in the isocenter of the magnet. High-resolution T2-weighted images were acquired using TurboRARE (rapid acquisition with rapid enhancement) sequences, with a repetition time = 2970 ms, echo time = 12 ms, RARE factor = 8, 10 averages, slice thickness = 0.3 mm, 25 slices for axial view and 40 slices for sagittal view, field of view = 25 × 25 mm, matrix size = 240 × 240 pixels, resulting in a spatial resolution of 0.104 × 0.104 mm for a slice thickness of 0.3 mm.

Statistical analyses

Cell counts were expressed as mean cells/mm^2 ± standard deviation. The values are the average of three replicates of at least two different experiments. Statistical analysis was performed using the Statgraphic-plus software and GraphPad Prism. One-way ANOVA and Fisher's least significant difference (LSD) procedure were used to discriminate between the means. Statistical significance was set at *$P < 0.05$ and ** $P < 0.001$.

RESULTS | CHAPTER 1

The effect of the composition of PLA films and lactate release on glial and neuronal maturation; Maintenance of the neuronal progenitor niche

To develop tissue engineering strategies useful for repairing damage in the central nervous system (CNS) it is essential to design scaffolds that emulate the neural stem cell (NSC) niche and its tight control of neural cell genesis, growth, and differentiation. In this first part of the results we tested two types of poly LL/DL lactic acid films; PLDLA95/5 (95% pure LL and 5% DL, PLA95/5) and PLDLA70/30 (70% pure LL and 30% DL, PLA70/30), as materials for nerve regeneration. In this chapter, we characterize the mechanical and chemical properties of both PLA and the different biological responses in terms of cell adhesion, survival, differentiation and the use of lactic acid by neurons, glial cells and neural progenitors cultured *in vitro*. At the end, we select one of those polymers to design three-dimensional patterns mimicking the architecture of the embryonic NSC niches.

1.1 Characterization of PLA 95/5 and 70/30 films

In addition to their distinct composition, glass, PLA95/5, 70/30 and culture plastic (polystyrene) are harder than brain and are considered stiff substrates. PLA95/5, 70/30 and glass were slightly hydrophobic and negatively charged (contact angle 75.6±5.2, 78.1±8.7, 73.9±2.8 respectively; Z potential at pH=7.4: -72.3±1.8 mV, -36.7±1.9 mV and -80±14 mV respectively), while culture plastic was slightly hydrophilic (contact angle: 58.3±1.3) and negatively charged (Z potential at pH=7.4: -124.±1.4 mV). To analyze the effect of degradation on wettability and surface charge, the measures were repeated on PLA films after 4 days in serum-free medium. Contact angle was slightly reduced in PLA95/5 (70.3±3.0), while on PLA70/30 there was a dramatic decrease (≤20), indicating a switch from slightly hydrophobic to hydrophilic. The Z potential becomes significantly more negative in both PLA (PLA95/5:-102.2±1.9 mV; PLA70/30:-82.2±2.5 mV).

AFM visualization of surface topography showed differences in the surface roughness in PLA95/5 and 70/30 (Fig. R-1A). In both cases the semi-crystalline domains (spherulites) of the polymeric network were visible. However, the semi-crystalline domains were larger in PLA95/5 than in PLA70/30, as expected for the different ratios of the L and DL monomers (Chen et al., 2003a; Tsuji and Ikarashi, 2004).

To confirm the difference in the amount of semi-crystalline domains, the crystallinity of PLA95/5 and 70/30 films was assessed by means of X-ray diffraction (XRD) and Differential Scanning Calorimetry (DSC) (Fig. R-1B). The XRD diffraction patterns showed the different crystallinity of the materials after the formation of the solvent-casting films.

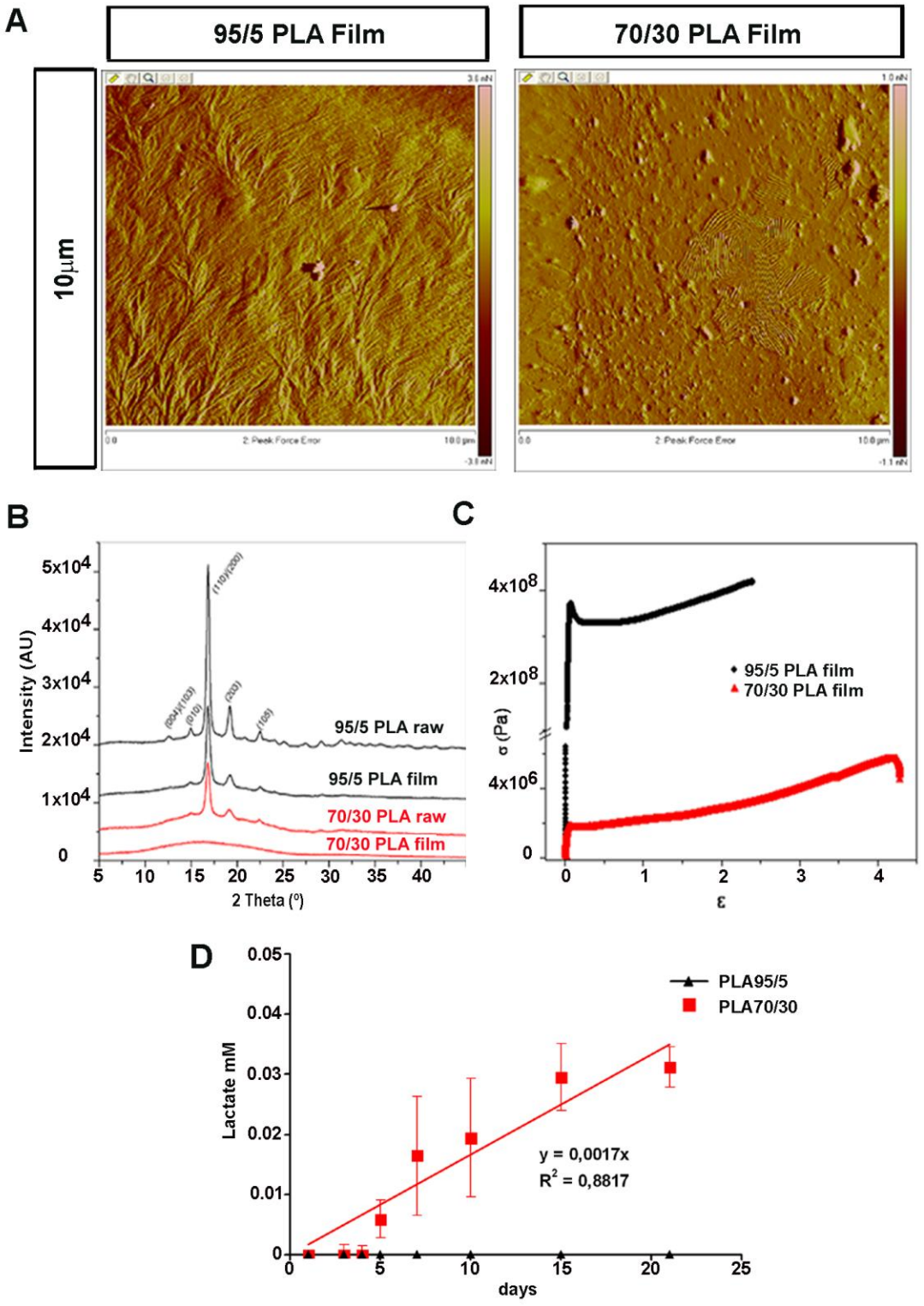

Figure R-1. Mechanical properties of PLA 95/5 and 70/30 films. **A.** 10x10µm Atomic Force Microscopy (AFM) images of PLA 95/5 and 70/30 films surface. **B.** θ/2θ 2-60º XRD analysis of PLA films and PLA powder. **C.** Tensile stress test of PLA95/5 film (Black) and PLA70/30 (red). **D.** Quantification of L-lactate release into the culture medium at 37ºC by PLA95/5 films (black) and 70/30 films (red) at different days *in vitro (div)* (1*div*, 3*div*, 4*div*, 5*div*, 7*div*, 15*div* and 21*div*). Error bars in **D.** indicate SD.

While both raw materials were semi-crystalline (due to the aging process), on formation of the films only PLA95/5 remained semi-crystalline (Fig. R-1B). DSC measurements confirmed these results, since the degree of crystallinity determined (%XC) was 18% for PLA95/5 and less than 5% for PLA70/30.

Tensile strength measurements were carried out for the different materials. PLA95/5, the most crystalline material, presented higher Young's Modulus (.5±0.3 GPa) than PLA70/30 (63.7±1.3 MPa). Correspondingly, the maximum stress to rupture was higher in PLA95/5 (428.5±118.1 MPa) than in PLA70/30 (5.7±0.1 MPa) (Fig. R-1C).

To determine differences in the degradation rate between the two PLA polymers, the presence of L-lactate released in the medium was analyzed by spectrophotometry and fluorescence (see materials and methods). PLA95/5 films did not release detectable amounts of L-lactate into the medium in the 21-day period analyzed. In contrast, PLA70/30 films, which are more amorphous, showed a linear release of L-lactate into the medium in the physiological range of μM, reaching a value of 31.2±0.3 μM after 21 days *in vitro* (Fig. R-1D).

1.2 Glial adhesion and differentiation on PLA 95/5 and 70/30 films

Firstly, *in vitro* studies with glial cells were performed with both PLA polymers. Primary glial cells attached to the three types of substrate, although the cell density differed significantly (control glass: 590±96, PLA95/5: 824±166 and PLA70/30: 1124±261, $p<0.001$). Phalloidin staining of F-actin cytoskeleton showed that glial cells grown on PLA95/5, 70/30 and control (glass) mainly adopted the spread morphology typical of mature astrocytes. In addition, small ramified cells and some bipolar radial glia-like cells (RGLS) were also present on control and PLA70/30 films (Fig. R-2A). Branched cytoskeleton arrangements typical of reactive glia were not observed in any of the conditions. To identify proliferative cells, we analyzed the expression of Ki67, a marker associated with proliferative cells during interphase. Ki67 staining was limited to a few cells on control and PLA95/5 films (3±2, 15±6 respectively), but was abundant in glial cells cultured on PLA70/30 films (49±15, $p<0.001$), indicating an active proliferative state (Fig. R-2A).

Western blot and densitometry analysis were used to quantify differences in the expression of glial cell maturation markers after 5 days *in vitro* (*div)* (Fig. R-2B, C). Glial cells grown on PLA95/5 films expressed similar levels of GFAP, PH3 and Nestin to control glia. However, glial cells grown on PLA70/30 films expressed higher levels of the immature glial marker Nestin and the proliferative marker PH3. Pax6 and Tbr2 progenitor markers were not expressed in these cultures. These results indicate that PLA70/30, but not 95/5 films or control glass, induced an immature and proliferative state in the glial cultures, and that no neurogenic progenitors were present. Afterward, the lactate released into the medium and glucose

consumption in the same glial cultures were analyzed (Fig. R-2D,E). As no lactate was initially present in the culture medium, the L-lactate concentration in the medium of glial cells cultured on the control substrate (6.46±1.04 mM) may derive exclusively from astrocyte release. In the case of glial cells grown in PLA substrates, L-lactate may also derive from PLA degradation.

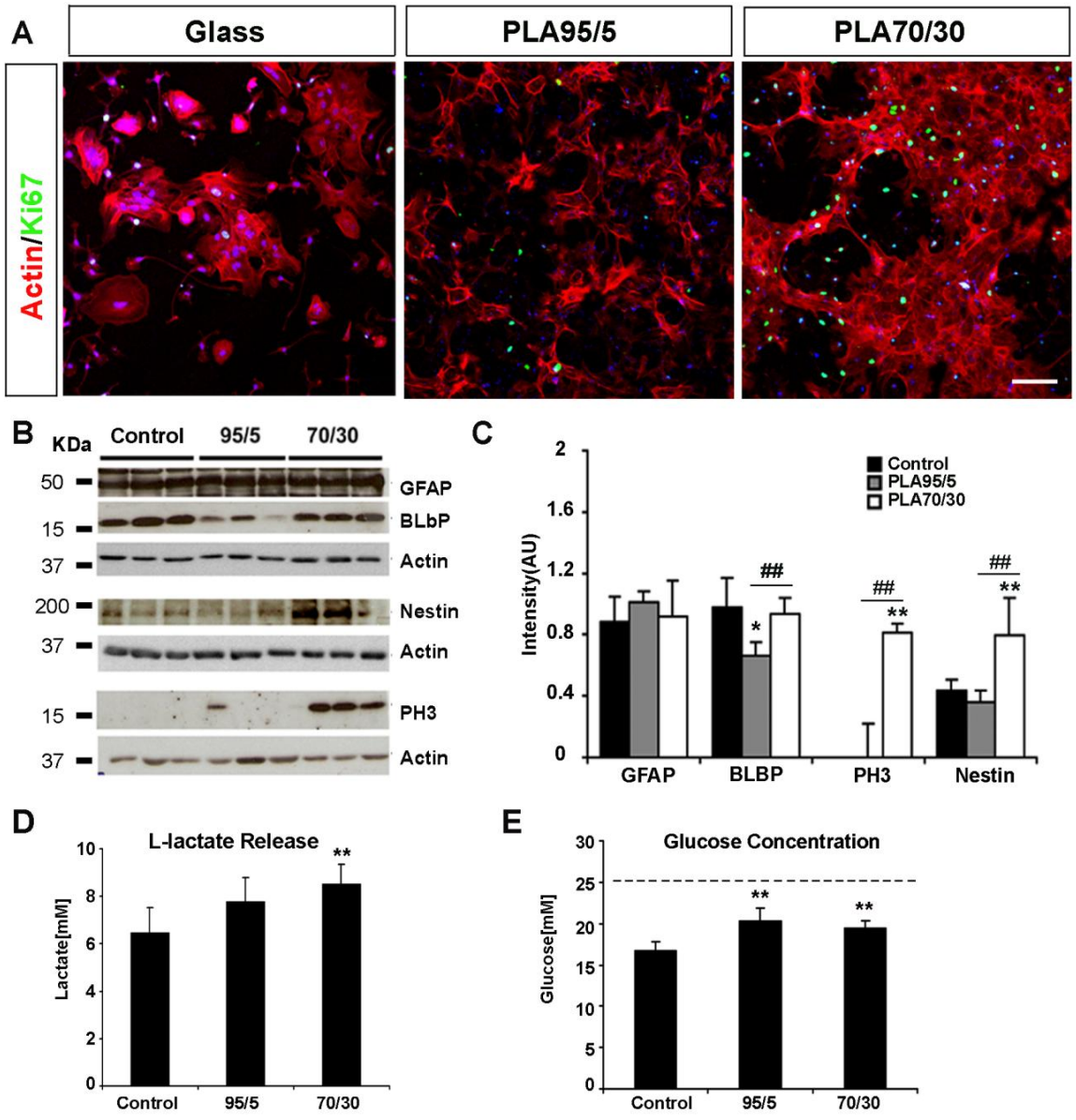

Figure R-2. Effect of PLA on glial cells morphology and phenotype. **A**. Confocal images of actin staining (Phalloidin, red), nuclei (Topro, blue) and proliferative nuclei (Ki67, green). **B.** Biochemical characterization of glial differentiation by Western blots showing the expression of different radial glia (Nestin, BLbP), mature glia (GFAP), and proliferative (PH3) markers. **C**. Quantitative representation of the western blot densitometry (intensity values normalized to actin). **D.** L-lactate release in glial cultures grown in the three substrates after 5*div*. **E**. Glucose quantification in the same cultures, dash line indicates the initial glucose concentration. Scale bar = 100µm. * $p<0.05$, ** $p<0.01$ indicate significant differences compared to control, and ## $p<0.01$ indicates significant differences between PLA95/5 and 70/30 conditions, LSD test. Error bars in **D-E** indicate SD.

L-lactate concentration in PLA95/5-derived medium was slightly (but not significantly) higher (7.78±1 mM) than controls, while L-lactate concentration increased significantly in 70/30-derived culture medium (8.53±0.81 mM, $p< 0.01$) (Fig. R-2D). Initial glucose concentration in the culture medium was 25 mM, and decreased after 5*div* in all conditions (Fig. R-2E). Glucose remained significantly higher in PLA95/5- and 70/30-derived media (20.35±1.54 mM and 19.42±0.87 mM respectively) than in the control-derived medium (16.73±1.12 mM, $p< 0.01$), suggesting that glucose consumption by glial cells decreased as the L-lactate concentration in the medium increased.

1.3 Neuronal cell adhesion and differentiation on PLA 95/5 and 70/30 films

β-III Tubulin (Tuj-1) staining revealed that cortical cells attached and differentiated into neurons in the control substrate (Lysglass), and their number remained constant during the culture period (1*div*:377±48; 5*div*:399±54) (Fig. R-3A). In contrast, cortical neurons hardly attached at all to PLA95/5 (1*div*:80±39; 5*div*:91±12), where they tended to aggregate in clusters sprouting small numbers of axons and dendrites after 5*div*. Surprisingly, neurons attached to and differentiated on PLA70/30, exhibiting a robust sprouting of axons and dendrites. Although initial adhesion was significantly lower in PLA 70/30 than in control ($p<0.01$), the number of cells in PLA 70/30 significantly increased after 5*div* (1*div*:234±49; 5*div*:311±58, $p<0.01$). Staining with the proliferative marker Ki67 revealed that after 1*div* the number of progenitor cells was similar in Lysglass and in PLA70/30 (65±14 and 53±15 respectively) while it fell notably in PLA95/5 (2±2). However, after 5*div* the situation changed dramatically: Ki67 progenitor cells almost disappeared in Lysglass and PLA95/5 (3±3 and 1±1 respectively) but remained stationary in PLA70/30 (68±19) (Fig. R-3A). This result indicates that, starting from a similar progenitor pool, PLA70/30 maintained the progenitor population over time, but Lysglass did not.

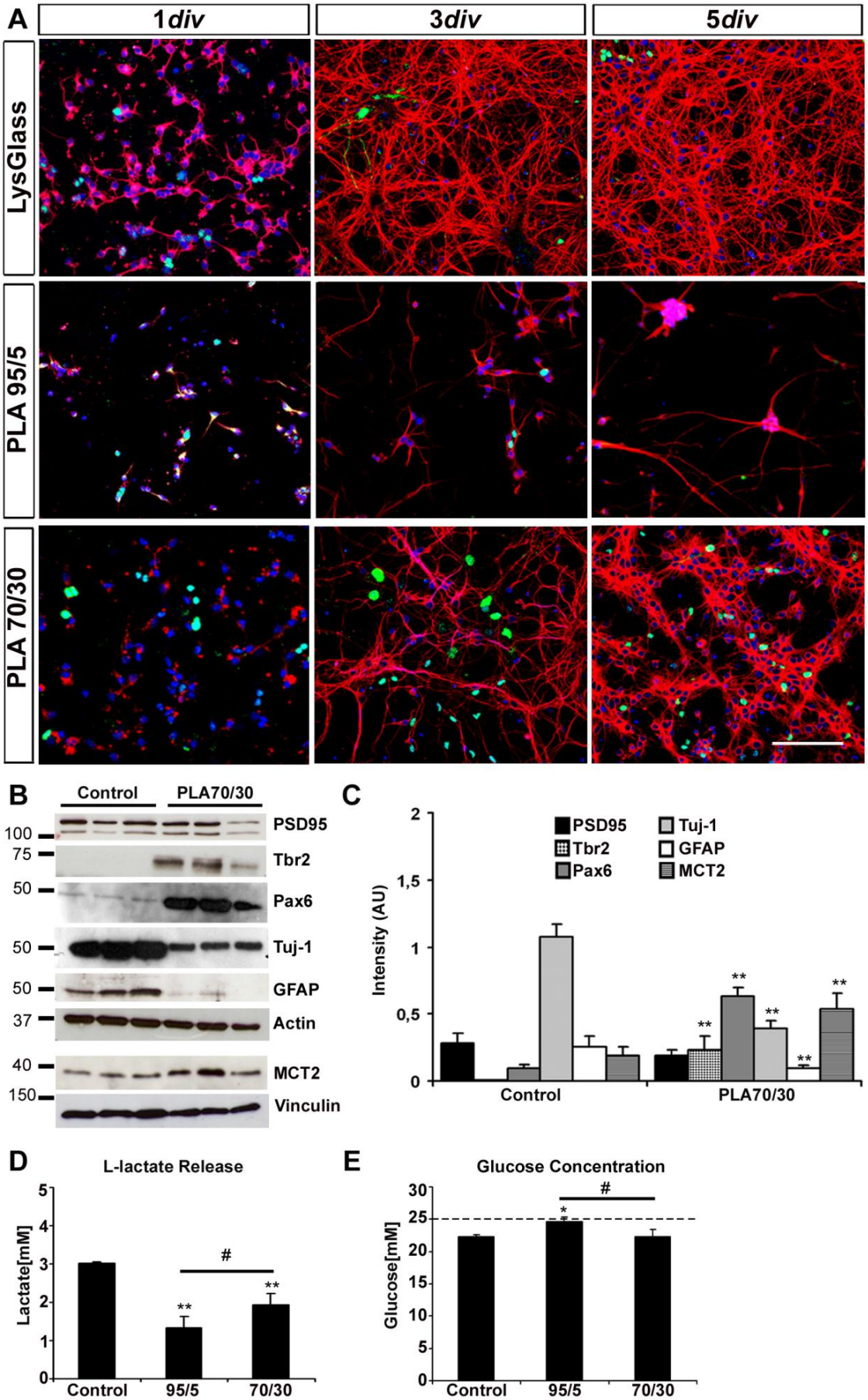
A
1div
3div
5div
LysGlass
PLA 95/5
PLA 70/30
B
Control
PLA70/30
PSD95
Tbr2
Pax6
Tuj-1
GFAP
Actin
MCT2
Vinculin
100
75
50
50
50
37
40
150
C
PSD95
Tbr2
Pax6
Tuj-1
GFAP
MCT2
Intensity (AU)
Control
PLA70/30
D
L-lactate Release
Lactate[mM]
Control
95/5
70/30
E
Glucose Concentration
Glucose[mM]
Control
95/5
70/30

Figure R-3. Effect of PLA on neuronal cultures growth and neural phenotype. A. Confocal images of neuronal cultures grown on PLA 95/5, 70/30 and Lysglass after different times (1*div*, 3*div* and 5*div*) showing neuronal cytoskeleton staining (Tuj-1, red), nuclei (Topro, blue) and proliferative nucleus (Ki67, green). **B**. Biochemical characterization by Western blot of neuronal cultures grown on PLA 70/30 films and tissue culture plate (Lys TCP) after 5*div,* showing the expression of progenitor cell markers (Pax6, Tbr2), post-mitotic neuronal markers (Tuj-1, PSD95, and MCT2) and the glial cell marker GFAP. **C.** Quantitative representation of the Western blot densitometry (intensity values normalized to actin or vinculin). **D.** L-lactate release in neuronal cultures grown in the three substrates after 5*div* **E**. Glucose concentration in medium in the same cultures; dashed line indicates the initial glucose concentration. Scale bar =100μm. Values are the average of three replicas. * $p<0.05$, ** $p<0.01$ indicate significant differences compared to control (TCP), and # $p<0.05$ indicate significant differences between PLA95/5 and 70/30 conditions, LSD test.

To investigate whether gliogenic or neurogenic progenitors were favored in PLA70/30 films with respect to the control substrate, we used Western blot and densitometry to analyze the expression of several lineage-specific markers after 5*div* (Fig. R-3B, C). This study was not possible with neuronal cultures on PLA 95/5 films due to the low amount of protein obtained. Neurons grown in the control substrate expressed high levels of mature neuronal markers Tuj-1 and the postsynaptic density marker PSD95. In addition, these neuronal cultures express GFAP, indicating the presence of mature astrocytes in the culture. In contrast, neurons cultured on PLA70/30 films expressed high levels of the progenitor markers Pax6 and Tbr2. Pax6 is a homeodomain transcription factor expressed in potential RGLC, and Tbr2 a T-domain transcription factor expressed by neuronal restricted progenitors/ IPCs and by early post-mitotic neurons. The decrease in the mature glial marker GFAP in PLA70/30 films corroborates the prevalence of neural progenitors and immature glia in these cultures. Finally, the expression of proton-linked monocarboxylate transporter MCT2, a neuronal restricted lactate transporter, was increased in neurons cultured in PLA70/30 with respect to the control substrate. The neural stem cell (NSC) marker Sox2 was not expressed in any condition.

We then quantified the release of L-lactate into the medium (Fig. R-3D) and glucose consumption (Fig. R-3E) in neuronal cultures. L-lactate concentration in neuronal cultures was significantly higher in the control condition (3.01±0.02 mM, $p<0.01$) than in PLA70/30 (1.93±0.29 mM) and 95/5 (1.33±0.29 mM) (Fig. R-3D). These data correlate well with the higher presence of mature GFAP positive astrocytes in control cultures. Analysis of glucose concentration revealed similar consumptions of neuronal cultures in control (Lysglass) and PLA70/30 (22.32±0.23 mM, 22.25±1.17 mM respectively) and lower consumption in neurons cultured on PLA95/5 films (24.64±0.71 mM), associated with the scarce cell presence in this last substrate (Fig. R-3E).

Taken together, these results indicate that PLA70/30 maintains the neuronal culture in a relatively immature state, preserving a pool of neuronal progenitors and inducing the expression of the neuron-specific lactate transporter MCT2.

1.4 Effect of lactate release by PLA70/30 films on neural cell cultures

To analyze the possibility that neural cells used the lactate released from the substrate, neurons and glial cells were cultured on control substrates and both PLA films in the absence of glucose (Neurobasal^{A} medium, NB^{A}). After 5*div,* glial cells were stained with Phalloidin and neurons with tuj-1 antibody for morphometric analysis, and both were co-stained with Ki67 antibody to identify proliferative cells (Fig. R-4A).

In the absence of glucose, the survival of glial cells was similar on PLA 70/30 films (186±40) and control (glass) (161±52); in both substrates they presented a spread and round morphology typical of mature astrocytes. In contrast, the number of astrocytes on 95/5 films was notably reduced (59±33) and they were smaller and less spread out (Fig. R-4A, B). Ki67^{+} proliferative glial cells were almost absent in all three conditions, indicating a quiescent state (Fig. R-4A). The L-lactate released by glial cells in glucose-free medium was around 20% of the amount observed in the presence of glucose (Fig. R-2D, 4C). L-lactate concentration in the medium from glial cultures grown on PLA70/30 was significantly higher than in the medium from control surface (1.48±0.05 mM and 1.33±0.09 mM respectively), while it was significantly lower on PLA95/5 (0.96±0.03 mM) (Fig. R-4C), in accordance with the reduced degradation rate and glial cell presence in this substrate. On the other hand, neuronal cultures did not survive on PLA95/5 films in the absence of glucose and barely survived on control substrate (64±36), while neurons attached to and grew well on PLA70/30 (158±50) (Fig. R-4A, B).

On the control substrate only some progenitor cells were stained with Ki67 (2±1) and a few poorly developed neurons were found, while on PLA70/30, neurons exhibited a well-developed neurite outgrowth and Ki67^{+} neuronal progenitors were abundant (33±6) (Fig. 4A).

L-lactate concentration in media from neuronal cultures grown on control substrate or PLA95/5 was at the limit of technical detection (0.61±1.6 μM, and 0.14±1.4 μM respectively).

L-lactate concentration on neuronal cultures grown on PLA70/30 was higher (3.4±0.07 μM) than in the other two substrates (Fig. R-4C), and within the range of values obtained from direct PLA70/30 degradation at similar times (Fig. R-1D). These results suggest that in the absence of glucose, lactate released from PLA70/30 degradation can provide an alternative energy substrate that is sufficient for neural cell growth.

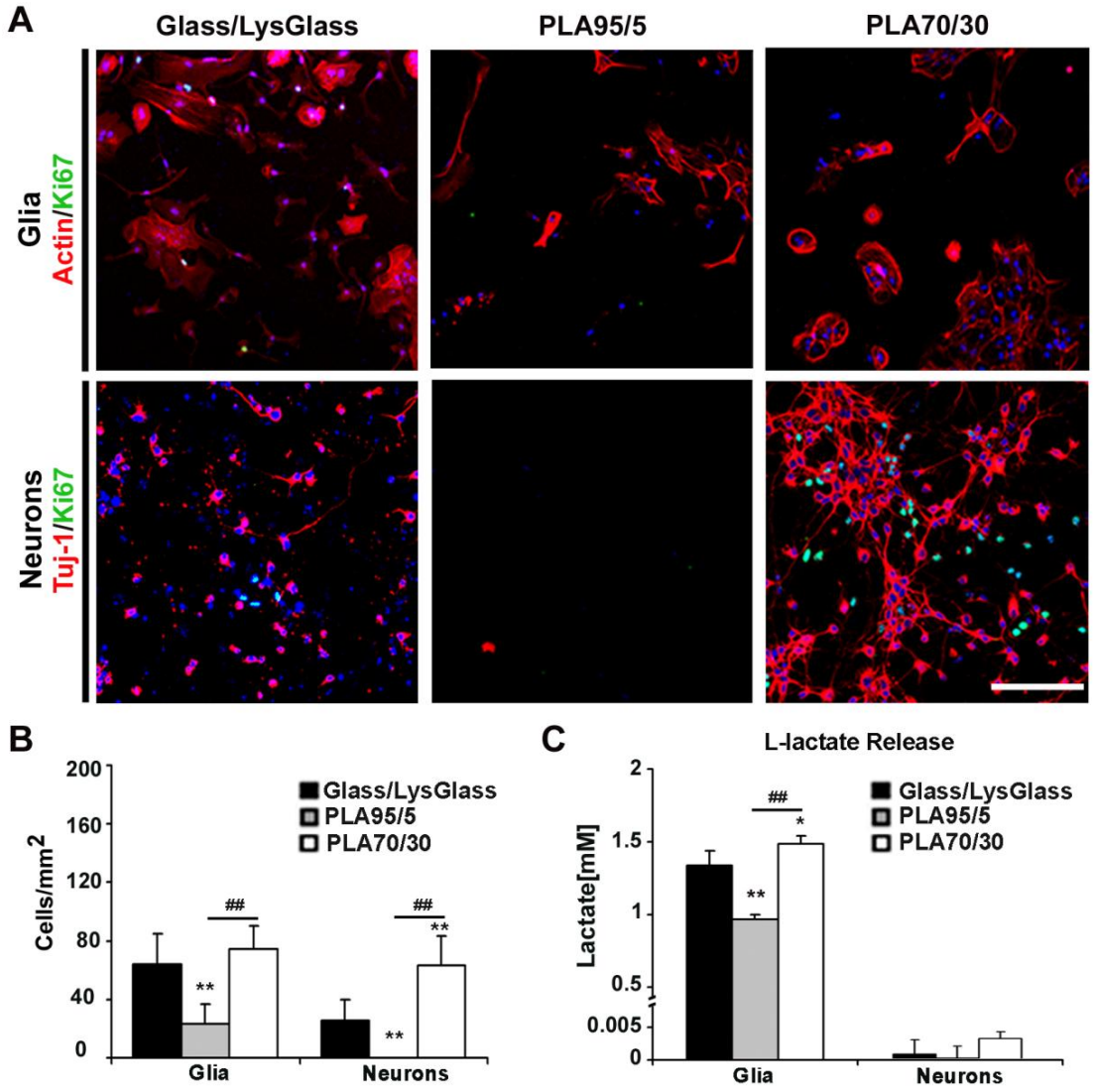

Figure R-4. Effect of lactate released by PLA on neural cultures. **A**. Images showing neuronal and glial cell cultures grown on the different substrates in glucose free medium (NB^A) during 5*div*. Cell nuclei are marked with Topro (blue), neurons with Tuj-1 antibody (red), glial cells with actin antibody (red), and proliferative cells with Ki67 (green). **B**. Cell quantification (glial cells and neurons) on glass/Lysglass, PLA95/5 and 70/30 in the same cultures shown in **A**. **C**. Lactate release quantification in glucose free medium after 5*div* (Glial cells and Neurons) on glass/Lysglass, PLA95/5 and 70/30. Scale bar =100µm. * $p<0.05$, ** $p<0.01$ indicate significant differences compared to control (Glass/LyasGlass), and ## $p<0.01$ indicate significant differences between PLA95/5 and 70/30 conditions, LSD test. Error bars in **B-C** indicate SD.

1.5 Differential effect of glucose and lactate as energy substrates for glial cultures

In order to explore the influence of lactate on glial cell phenotype, cells were treated with L-lactic acid or D-lactic acid; the degradation products of PLA material, in the presence or absence of glucose in the medium (see materials and methods). Glial cultures were grown in serum-free culture medium with glucose (25 mM glucose, glucose medium), glucose and L-lactate (25 mM glucose + 4 mM L-lactic acid, glucose+lactate medium), or L-lactate only (4

mM L-lactic acid, lactate medium). After 5*div*, glial cells grown on glass or culture plastic and in glucose medium or in glucose+L-lactate medium, adopted a flattened, well-spread morphology with a few proliferating Ki67^{+} cells present in both cultures. Nevertheless, there were significantly more cells in the glucose than in the glucose+L-lactate medium (685±103 and 322±101 respectively, $p<0.001$). Glial cells grown in L-lactate medium barely survived after 5*div* (92±33) and were shrunken and poorly developed (Fig. R-5A).

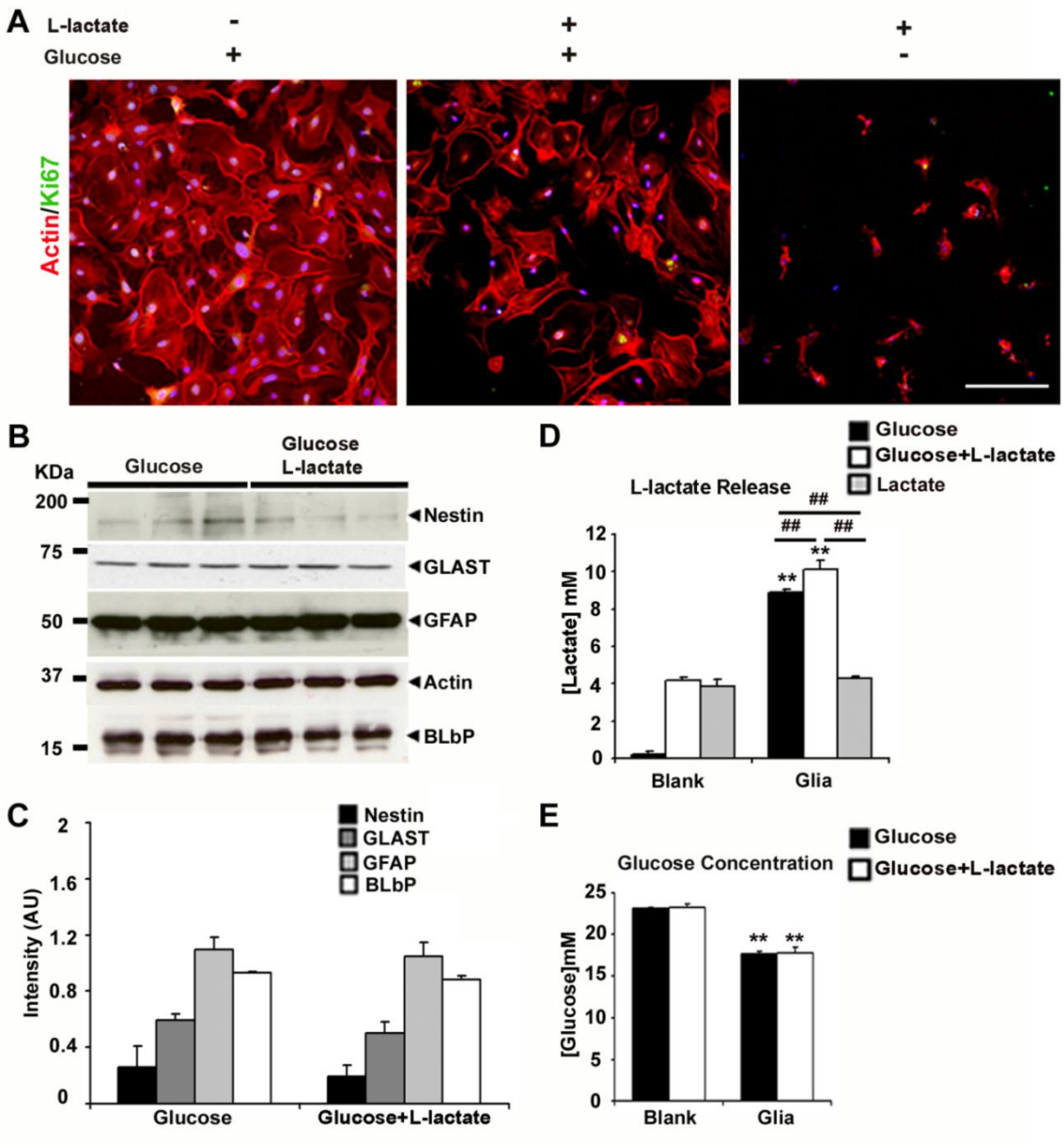

Figure R-5. Glial cell cultures treated with L-lactic acid. A. Confocal images of glial cell cultures grown in NB medium (glucose), in NB medium supplemented with L-lactic acid (glucose+L-lactate) and in glucose free NB^{A} medium supplemented with L-lactic acid (Lactate). Cytoskeleton is stained with Phalloidin (red), nuclei with Topro (blue) and proliferative nuclei with Ki67 (green). **B.** Western blots of GFAP (mature and reactive glial marker), BLbP (immature astrocyte marker), GLAST (astrocyte marker) and Nestin (radial glial marker) in similar cultures as showed in **A**. **C.** Graph summarizing Western blots quantification (intensity values normalized to actin). **D.** L-lactate quantification in the three condition media after 5*div*. **E.** Glucose quantification in the same media used in **D**. Scale bar =100µm. Values are the average of three replicas. * $p<0.05$, ** $p<0.01$ indicates significant differences respect to

the blank condition, and # $p<0.05$, ## $p<0.01$ indicate significant differences between treated conditions, LSD test. Error bars in **C-E** indicate SD.

Quantitative analysis of glial differentiation markers was performed by Western blot and densitometry (Fig. R-5B, C). Nestin, BLBP and GFAP glial differentiation markers and the glial glutamate transporter GLAST were similarly expressed in glial cells grown in the presence of glucose or with glucose+L-lactate. This analysis was not possible when only L-lactate was present in the medium due to the low amount of protein obtained. The bipotential RGLC marker Pax6 and the neural stem cell (NSC) marker Sox2 were not expressed in any condition.
The concentrations of L-lactate and glucose in media containing glucose or glucose+L-lactate were analyzed in order to estimate the consumption or release of each metabolite by the glial cells. In the presence of glucose, glial cells released high amounts of L-lactate into the medium (8.86±0.18 mM), a quantity that increased significantly in the glucose+L-lactate medium (10.16mM± 0.44) but was not as high as that suggested by direct calculation of the endogenous production plus the exogenously added L-lactate. Glial cells cultured in L-lactate medium maintained the initial amount of lactate (4.28±0.1 mM) (Fig. 5D). Analysis of glucose concentration revealed similar glucose consumption in the presence or absence of L-lactate in the medium (17.68±0.26 mM and 17.76±0.73 mM respectively; blank 23.10±0.16 mM) (Fig. R-5E).

When the non-metabolizable D-lactate was added in the presence or absence of glucose, glial cultures exhibited similar features to the respective control cultures, and only a mild reduction in the total number of cells (glucose: 567±152; glucose+D-lactate: 499±66; D-lactate: 354±84) and a very mild increase in Ki67 (glucose: 2±2; glucose+D-lactate: 4±3; D-lactate: 9±5) were observed in D-lactate medium (Fig. 6A, B).

These results strongly suggest that glial cells use glucose as the primary energy substrate, while the presence of L-lactate in the medium reduces lactate extrusion by glial cells.

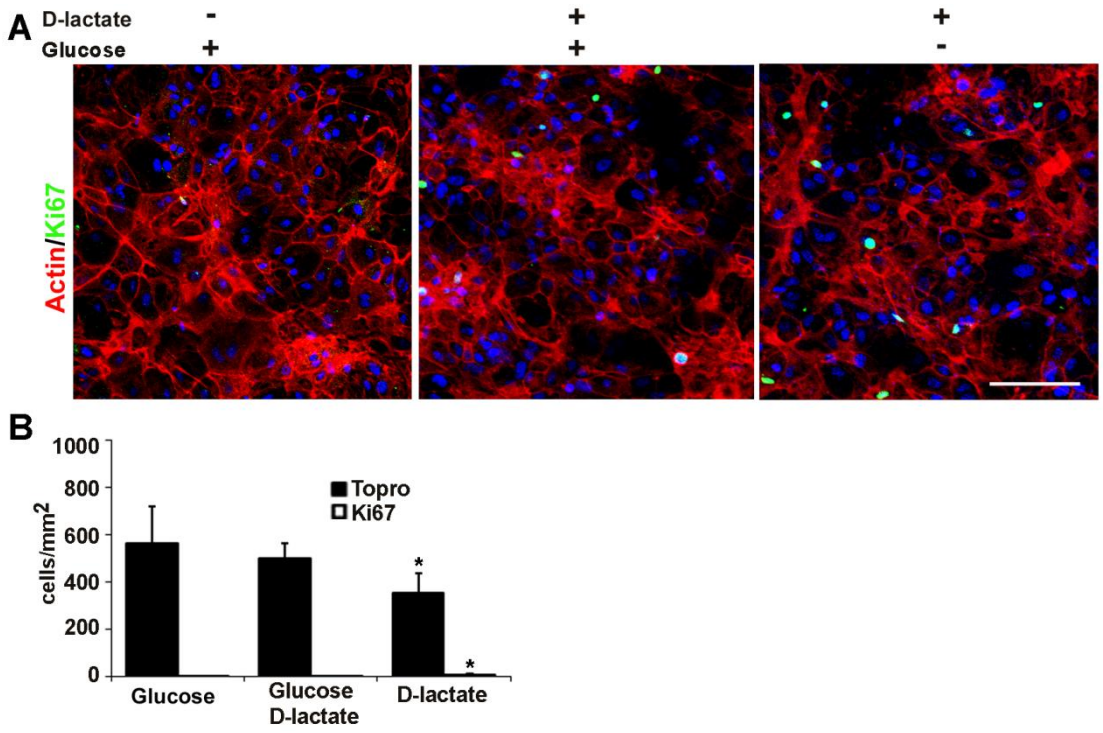

Figure R-6. Glial cell cultures treated with D-lactic acid. A. Confocal images of glial cell cultures grown in NB medium (glucose), in NB medium supplemented with D-lactic acid (glucose+D-lactate) and in glucose free NB^A medium supplemented with D-lactic acid (D-lactate). Cytoskeleton is stained with Phalloidin (red), nuclei are stained with Topro (blue) and proliferative nuclei with Ki67 (green). **B**. Quantification of the total number of cells (Topro) and proliferative cells (Ki67) after 5*div*. Scale bar =50µm. * $p<0.05$ indicates significant differences compared to glucose condition, # $p<0.05$ indicate significant differences between glucose+D-Lactate and D-Lactate, LSD test). Error bars indicate SD.

1.6 Differential effect of glucose and lactate as energy substrates for neuronal cultures

To explore the influence of L-lactate on the self-renewal and differentiation of neuronal progenitor's *in vitro*, embryonic neurons were cultured in the same conditions as those used for treated glial cell cultures (Fig. R-5). Under glucose medium, glucose+L-lactate medium, or L-lactate medium, cell adherence and survival were the same. After one day *in vitro* (1*div*) similar counts were obtained for both the total number of cells (glucose: 274±43, glucose+L-lactate: 243±46, and lactate: 246±36) and the number of $Ki67^+$ cycling progenitors (glucose: 38±9, glucose+ L-lactate: 44±14, and lactate: 55±14) (Fig. R-7). After 5*div*, the neuronal cultures showed signs of differentiation, and neurons identified by staining with the neuronal marker Tuj-1 exhibited well-developed neurites, particularly in glucose medium (Fig. R-7). At this time point, the total cell number in the glucose (375±47, $p<0.01$) and glucose+L-lactate (297±40, $p<0.05$) cultures were significantly higher than at 1*div* while in lactate medium there was no change (247±27). A similar comparison of $Ki67^+$ progenitors showed fewer numbers of these

cells in glucose medium (4±3, $p<0.01$), while the number remained constant in glucose+ L-lactate medium (57±19) and had significantly increased in lactate medium (79±18, $p<0.01$). As post-mitotic neurons cannot re-enter the cell cycle, the increase in cell number in 5*div* embryonic neuronal cultures can only be explained by the division of pre-existing $Ki67^{+}$ progenitors at 1*div*. Therefore, the increase in cell number and the depletion of progenitors after 5*div* in glucose medium is compatible with two rounds of progenitor division; first an asymmetric division giving rise to a progenitor and a differentiated cell, and then a symmetric division of the progenitor giving two differentiated cells. The observation in glucose+L-lactate medium of an increased number of cells together with progenitor maintenance is compatible with one round of asymmetric progenitor division giving rise to a self-renewing progenitor and a differentiated cell; and finally, the increase in progenitors but not in the total cell number in lactate medium suggests self-renewing symmetric divisions and an enrichment in progenitor cells compared to the initial pool of terminally differentiated cells.

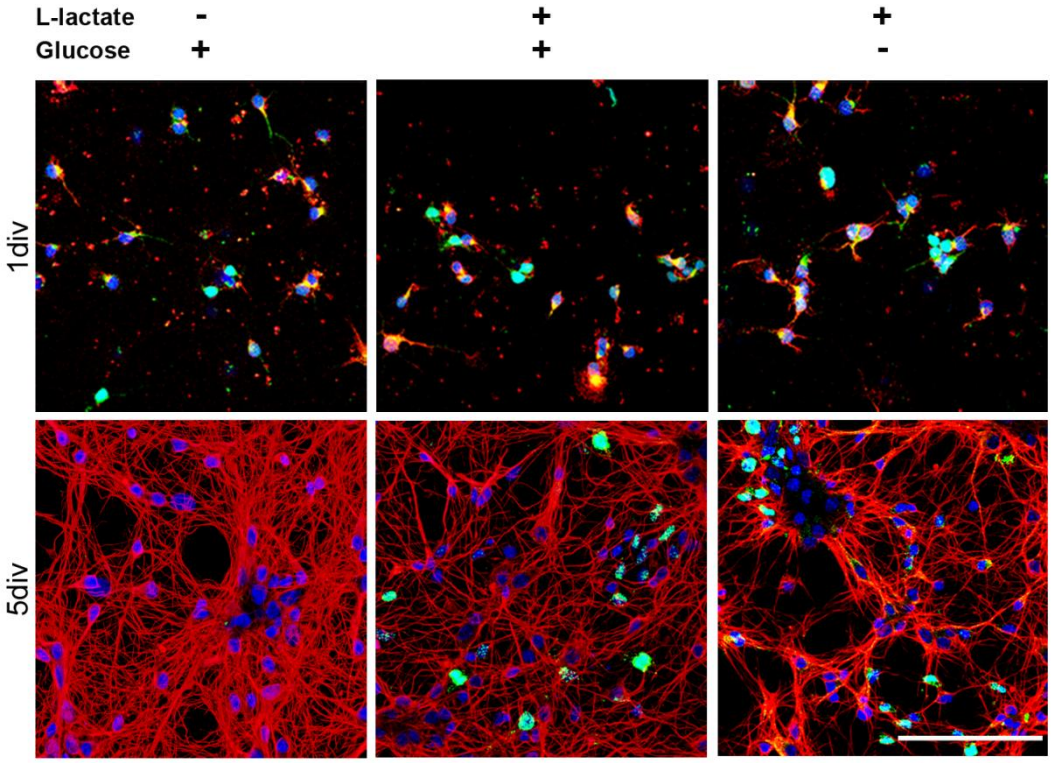

Figure R-7. Neuronal cultures treated with L-lactic acid. Confocal images of embryonic neuronal cell culture grown in NB medium (glucose), in NB medium supplemented with L-lactic acid (glucose+lactate) and in glucose free NBA medium supplemented with L-lactic acid (Lactate) after 1*div* and 5*div*. Neurons are stained with Tuj-1 (red), nuclei with Topro (blue), and proliferative nuclei with Ki67 (green). Scale bar =50µm.

Western blot and densitometry analysis were performed after 5*div* to quantify differences in the expression of neuronal, glial and progenitor markers (Fig. R-8A, B). Neuronal cultures grown in glucose or glucose+L-lactate media maintained the expression of the immature glial and progenitor marker Nestin and the mature astroglial marker GFAP.

However, the expression of GFAP and Nestin was dramatically reduced or even absent in lactate medium, indicative of a significant reduction in the population of glial cells. The expression of the neuronal marker Tuj-1 and the postsynaptic density marker PSD95 decreased in glucose+L-lactate and decreased even more notably in L-lactate with respect to the glucose media, indicating a delayed neuronal maturation in these cultures. In addition, the presence the high-affinity proton-linked monocarboxylate transporter MCT2 and the G-protein-coupled lactate receptor, GPR81, were abundantly expressed in neuronal cultures grown in glucose+L-lactate and lactate medium. Analysis of progenitor markers revealed high levels of Tbr2, a transcription factor associated with neuronal restricted intermediate progenitor cells and early post-mitotic neurons in glucose+L-lactate and more significantly in L-lactate with respect to the glucose medium. The bipotential RGLC marker Pax6 and the NSC marker Sox2 were not expressed in any condition. These results indicate that in the presence of L-lactate neuronal cultures were less differentiated and preserved a significant pool of neuronal restricted progenitors.

L-lactate release and glucose consumption were also analyzed in these neuronal cultures (Fig. R-8C, D). When grown in glucose medium, neuronal cultures released L-lactate (1.96±0.06 mM, Fig. R-8C), as did neuronal cultures grown in glucose+L-lactate medium (4.85±0.17 mM, blank 3.97±0.16 mM). As expected, neuronal cultures grown in L-lactate medium consumed L-lactate (1.93±0.77 mM, blank 3.97± 0.16 mM, Fig. R-8C). When neuronal cultures grown in glucose+L-lactate media, cells consumed significantly less glucose than when grown only with glucose (21.02±0.43 mM and 22.04±0.51 mM respectively, blank 23.01±0.16 mM, Fig. R-8D).

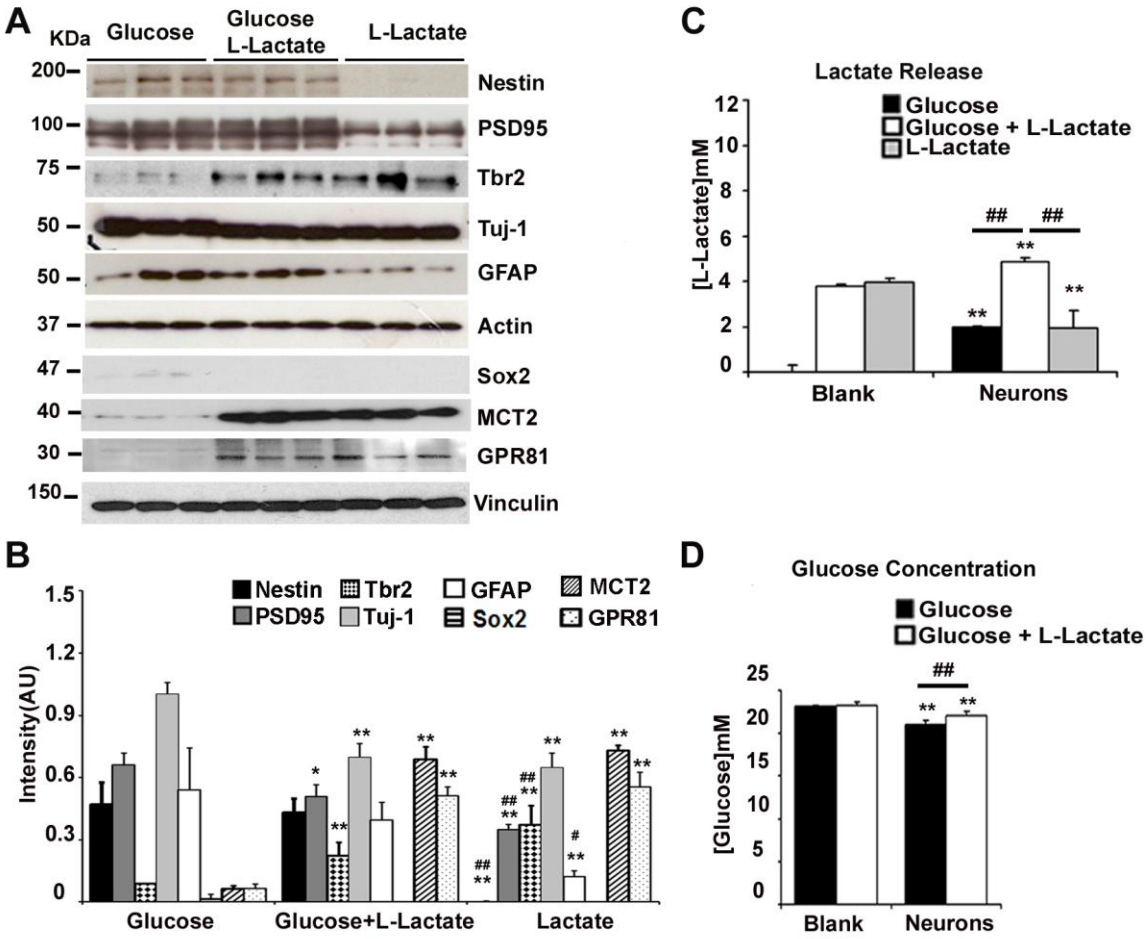

Figure R-8. Characterization of neuronal cultures treated with L-lactic acid after 5*div*. A. Western blot of Nestin (radial glial marker), PSD95 (post-synaptic density neuronal marker), Tbr2 (intermediate progenitor marker), Tuj-1 (post-mitotic neuronal marker), GFAP (mature astroglial marker), Sox2 (NSC marker), MCT2 (neuronal monocarboxylate transporter) and GPR81 (lactate receptor) in neuronal cultures grown in the same conditions as in Figure R-7 after 5*div*. **B**. Graph summarizing Western blot quantification (intensity values normalized to actin or vinculin). **C**. Lactate quantification in culture media in the three conditions described above. **D**. Glucose quantification in the same media used in **C**. * $p<0.05$, ** $p<0.01$ indicate significant differences compared to blank condition, and # $p<0.05$, ## $p<0.01$ indicate significant differences between treated conditions, LSD test. Error bars in **B-D** indicate SD.

When D-lactate was added in the presence of glucose, neuronal cultures exhibited similar features to the control medium (glucose: 508±70; glucose+D-lactate: 395±69) and no $Ki67^+$ cells were observed, while D-lactate did not support neuronal growth (D-lactate: 1±1) in the absence of glucose (Fig. R-9A, B).

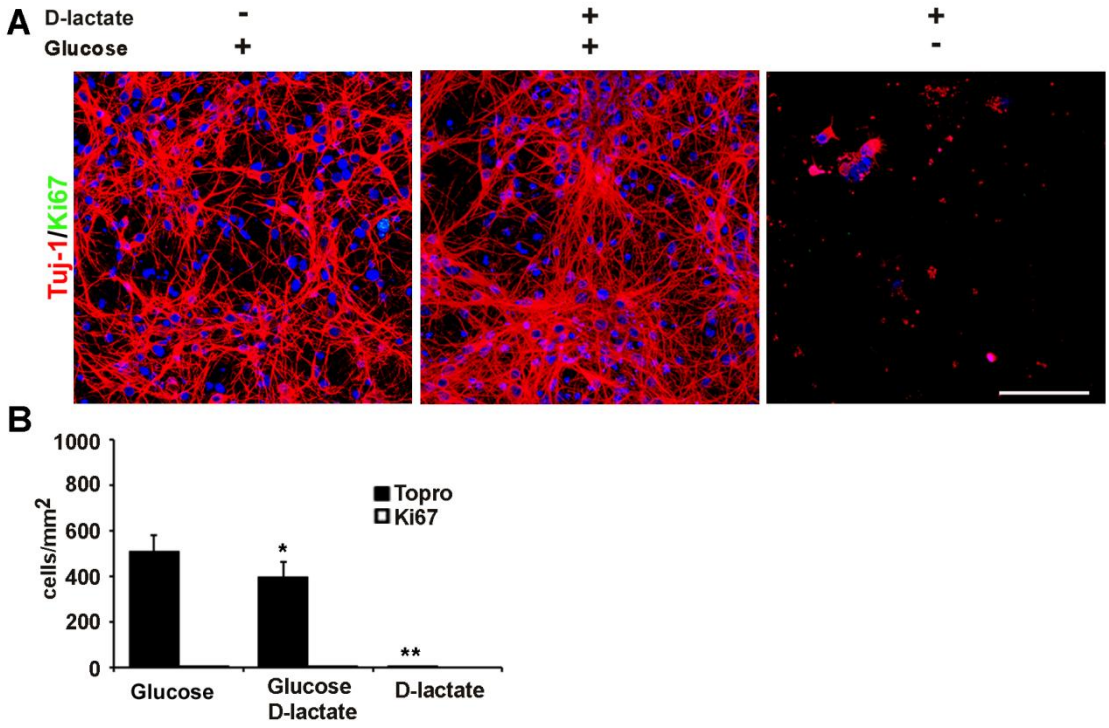

Figure R-9. Neuronal cultures treated with D-lactic acid. A. Confocal images of embryonic neuronal cell cultures in NB medium (glucose), in NB medium supplemented with D-lactic acid (glucose+D-lactate) and in glucose free NB^A medium supplemented with D-lactic acid (D-lactate). Neuronal cytoskeleton is stained with Tuj-1 (red), nuclei are stained with Topro (blue) and proliferative nuclei with Ki67 (green). **B.** Cells (Topro) and Ki67 quantification after 5*div*. Scale bar =75µm. * $p<0.05$, ** $p<0.01$ compared to glucose, LSD test; ## $p<0.001$ between glucose+D-lactate and D-lactate condition, LSD test. Error bars indicate the SD.

Taken together, these data suggest that neurons preferred L-lactate as primary energy source, unlike glial cells. In the presence of this metabolite, neuronal cultures maintained an immature phenotype and preserved the pool of neurogenic Tbr2 progenitors.

1.7 Effect of L-lactate on neuronal progenitor survival and differentiation.

Based on these observations, we speculated that glucose promotes the differentiation of neuronal progenitors while L-lactate is required for their self-renewal. To test this hypothesis, neuronal cultures were grown in L-lactate medium for 5*div* and then for 2 more days either in the same medium or in glucose medium (Fig. R-10A). After the 7 days, there were significantly fewer $Ki67^+$ progenitors in glucose than in lactate medium (10±1 and 63±5 respectively, $p< 0.001$, Fig. R-10B), while the total number of cells was significantly higher in glucose than in lactate cultures (220±41 and 170±23 respectively, $p< 0.001$, Fig. R-10C). These results suggested that glucose medium induced a terminal division of Ki67 progenitors whereas in lactate medium these cells remained mostly quiescent. When the opposite experiment was done, i.e., neuronal cultures were grown in glucose medium for 5*div* and then for 2 more days either

in the same medium or in lactate medium (Fig. R-10D), there were no changes either in the total number of cells (glucose: 260±34; lactate: 228±44, Fig. R-10F) or in the number of Ki67$^+$ progenitors (glucose: 2±2 and lactate: 1±1, Fig. R-10E), indicating that lactate cannot reprogram the terminal progenitor differentiation induced by glucose.

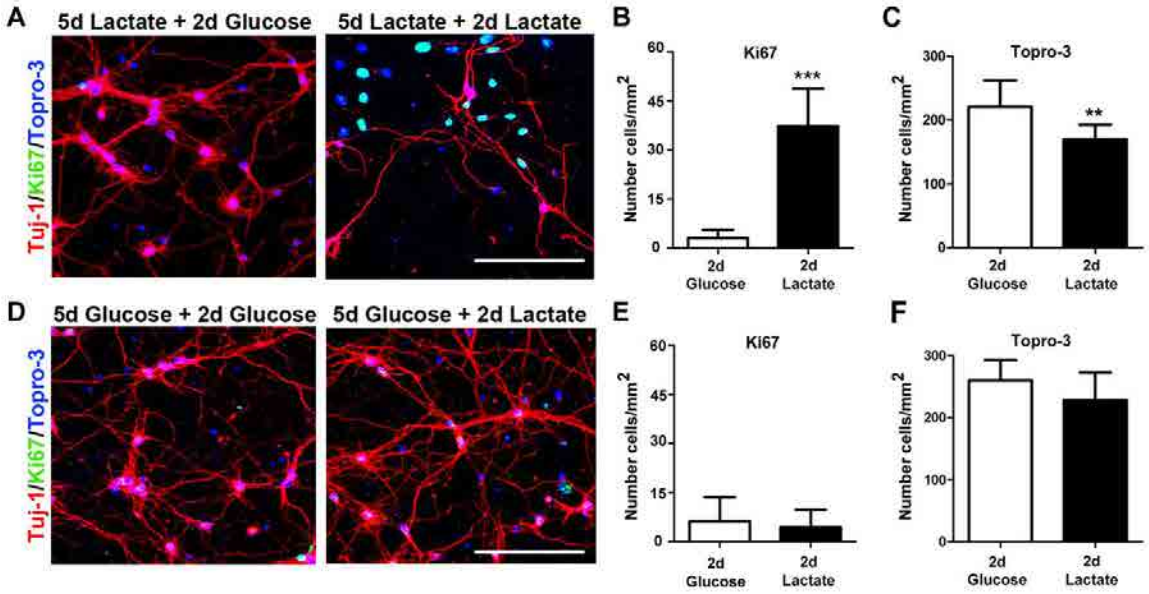

Figure R-10. Lactate as an energy source that maintains neuronal progenitors *in vitro*. A. Confocal images showing neurons (Tuj-1, red), nuclei (Topro, blue), and proliferative cells (Ki67, green) in neuronal cultures grown in lactate medium for 5*div* followed by 2 more days either in glucose medium or in lactate medium. **B, C**. Quantification of Ki67$^+$ (proliferative cells) and Topro (nuclei) under the same conditions as in **A**. **D**. Confocal images of neuronal cultures grown in glucose medium for 5*div* followed by 2 more days either in lactate medium or in glucose medium. The cells were stained for the cytoskeleton (Tuj-1, red), nuclei (Topro, blue), and proliferation (Ki67, green). **E, F**. Quantification of Ki67$^+$ cells (proliferative cells) and Topro (nuclei) in cells cultured as in **D.** Scale bar =50µm (A, D). ** p<0.01, *** p<0.001 indicate significant differences compared to glucose LSD test. Error bars in **B, C, E** and **F** indicate SD.

We then examined whether lactate induced the formation of reactive oxygen species, leading to oxidative stress and cell death and therefore the observed differences in cell number. Neuronal cultures were grown in L-lactate medium for 5*div* and then in the same medium or in glucose medium for 1h or 2 days more. After 1 h or 2 days, the cells were treated with CellROX, an indicator of oxidative stress, for 30 min before fixation. After 1 h, CellROX fluorescence was higher in neuronal cultures grown in glucose than in lactate medium (21±3 and 16±2 cells respectively, p< 0.001) (Fig. R-11A, B). After 2 days, however, CellROX intensity decreased and the differences disappeared (glucose: 10±1 cells, lactate: 10±5 cells) (Fig. R-11B). As an indicator of cell death, the number of caspase-3$^+$ cells was analyzed under the same experimental conditions. The percentage of dead cells was very low in either medium although

at 1 h it was slightly higher in the lactate- than in the glucose-containing cultures (glucose: 2±2 and lactate: 5±3, p< 0.05, Fig. R-11C, D). These differences were no longer observed after 2*div* (glucose: 3±3 and lactate: 2±3, Fig. R-11D). These results suggested that lactate did not induce the formation of more reactive oxygen spices and consequently cell death than glucose medium.

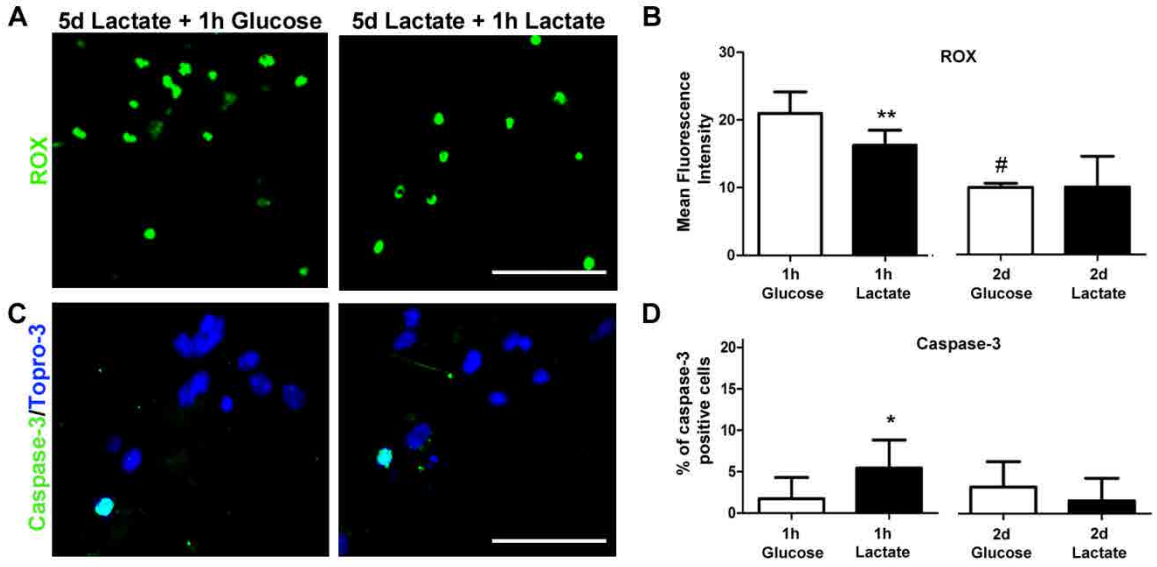

Figure R-11. Metabolic stress of neuronal culture in presence of lactate. A. Images showing ROX staining (green) in neuronal cell cultures grown in lactate medium for 5*div* followed by either 1 h or 2 days in glucose medium or in lactate medium. **B**. Quantification of ROX intensity in cells cultured as in **A**. **C.** Images showing cell death stained with caspase-3 (green) and nuclei stained with Topro (blue) in cells cultured as in **A**. **D.** Percentage of death cells (caspase-3^{+}) in cultures grown as in **C.** Scale bar =50µm (A), 25 µm (C). * p<0.05, ** p<0.01 indicate significant differences compared to glucose, and p<0.05 indicate significant differences compared to 1h condition, LSD test. Error bars in **B and D** indicate SD.

Author Contribution

Many authors have collaborated in this chapter. Dr. Oscar Castaño and Dr. Miguel Angel Mateos-Timoneda characterized PLA films at the Institute for Bioengineering of Catalonia (IBEC). Petra Hyrossova and Dr. Jose C. Perales performed the glucose and lactate measurements at the Physiological Sciences II department (Bellvitge Campus, UB).

RESULTS | CHAPTER 2

Characterization of 3D PLA70/30 nanofibers scaffold; the role of lactate and topology on neural cell fate

In the previous chapter we concluded that PLA70/30 film was better substrate for cortical neural cells growth and also maintained the pools of neuronal and glial progenitor cells *in vitro* compared with PLA95/5. In this second chapter, we would demonstrate how important the control of topography to dedifferentiate glial and neuronal cells is. Thus, the scaffold used in this part combines the neurogenic properties of lactate-releasing PLA70/30 and a topology performed by electrospinning technique, creating aligned and random three-dimensional organization to characterize neural cells response *in vitro*.

2.1 Fabrication and characterization of random and aligned PLA nanofibers

The production of 238±18 μm nanofiber sheets with the PLA nanofibers in two different conformations, random and aligned, was successfully achieved by the electrospinning method (Fig. R-12A, B). We obtained continuous and homogeneous fibers thicknesses (657 ± 101 nm for random and 568 ± 81 nm for aligned nanofibers), with no bead content. Focused ion beam cross-sectional images of an aligned fibrous sheet (Fig. R-12B inset) showed that the nanofibers were hollow (~500 nm inner diameter) because of the Kirkendall effect (Fan et al., 2007). On AFM imaging, the single aligned nanofibers were smooth (RMS value of 14.2 ± 0.3 nm) (Fig. R-12C) and relatively soft (DMT modulus of 3.0 ± 0.004 MPa) (Fig. R-12D). Tensile strain differed between the two conformations. Thus, the Young's modulus of the random nanofibers was isotropic (41.4 ± 13.7MPa) while the aligned nanofibers showed an anisotropic Young's modulus almost four-fold higher, as determined in a uniaxial assay parallel to the direction of the nanofibers (142.7 ± 14.1 MPa; Fig. R-12H). The amorphous nature of the nanofibers was characterized by XRD (Fig. R-12E) and DSC (Fig. R-12F), neither of which showed evidence of crystallization or melting peaks, indicating a nearly null crystallinity. Both PLA fiber conformations were hydrophobic (contact angle of 137º±14º for aligned and 128º±17º for random conformations) and negatively charged (ζ-potential at pH 7.4 = -41±43 mV) and the degradation rates were similar (vLac-random = 458 nM·h-1 and vLac-aligned = 467 nM·h-1) (Fig. R-12G). However, it should be taken into account that the enzymatic reaction indicative of degradation only allows the detection of L-lactate monomers. Soluble PLA oligomers and D-lactate monomers are undetectable by this technique.

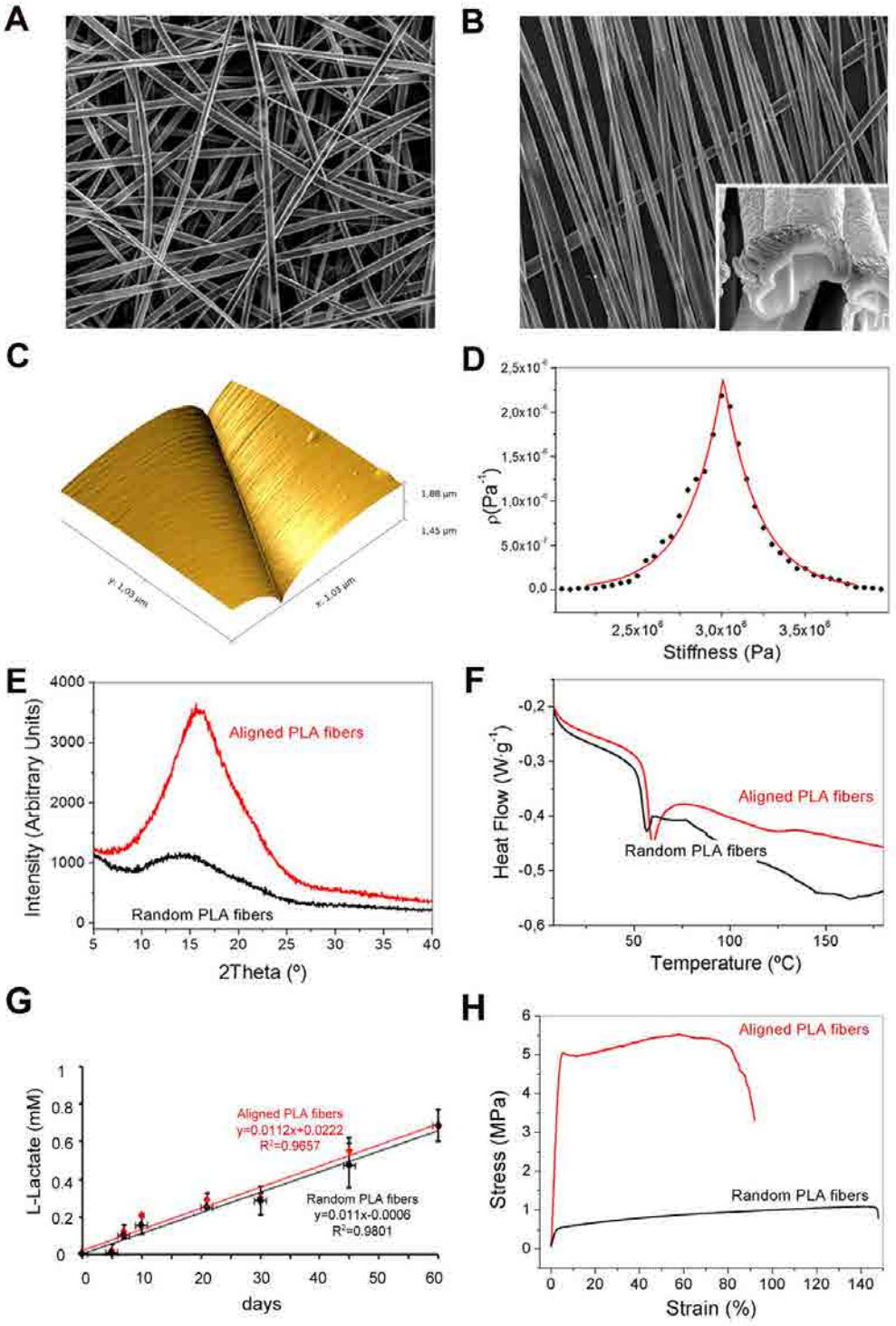

Figure R-12. Nanofibers characterization. A, B. Field emission scanning electron microscopy images of **A**. random and **B.** aligned nanofibers viewed from above, with a cross-section of aligned nanofibers produced by focused ion beam shown in the inset in **B**. **C**. Atomic force microscopy (AFM) topographic plot of the interface of two parallel nanofibers (RMS value of 14.2 ± 0.3 nm). Stiffness value distribution based on **D**. the DMT modulus measured by AFM, showing a peak at 3.01 ± 0.004 MPa, and **E**. X-ray diffraction. **F**. Differential scanning calorimetry spectra of random (black) and aligned (red) nanofiber conformations, showing the amorphous nature of the fibers. **G.** Plot of lactate release vs. time of random (black, vLac-random = 458 nM·h-1) and aligned (red, vLac-aligned = 467 nM·h-1) nanofiber sheets. **H**. Mechanical assays after tensile loading of the two nanofiber conformations. Scale bars: 5 µm (A, B); 500 nm (B inset).

2.2 Effect of PLA nanofibers on neuronal and glial cultures

For cell culture, uncoated three dimensional (238±18 μm) random and aligned PLA 70/30 fiber sheets were used as the substrates. Both types of electrospun fibers, random and aligned, supported neuronal and glial cells growth (Fig. R-13), but only on aligned electrospun fibers, neural cells adopted bipolar shapes following the direction of the fibers.

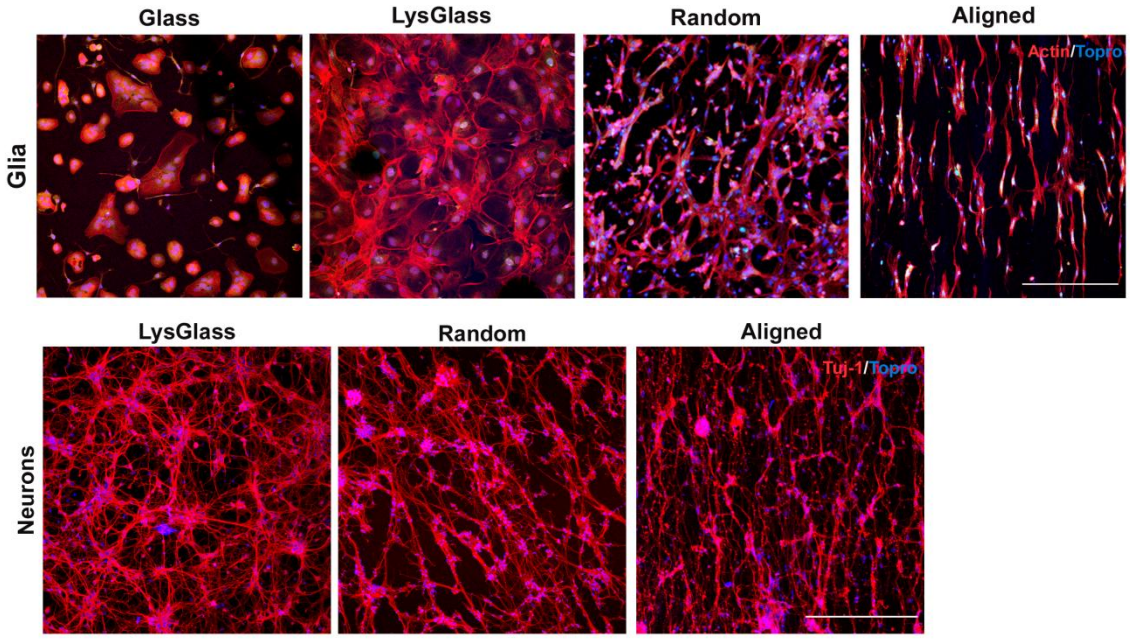

Figure R-13. Glial and neuronal cultures on random and aligned PLA fibers. Confocal images of glial cells stained with actin (red) and neurons stained with Tuj-1 (red) on glass and lyglass (Controls), random and aligned fibers after 5*div*. Topro (blue) stains nucleus. Scale bars: 100μm.

Glial cells (Fig. R-14A) and aligned axons (Fig. R-14B) invaded the entire thickness of 3D aligned nanofibers scaffold. Surprisingly, neuronal somas were mainly located in the middle of the aligned scaffold (Fig. R-14B inset), while axons were mainly located on the top.

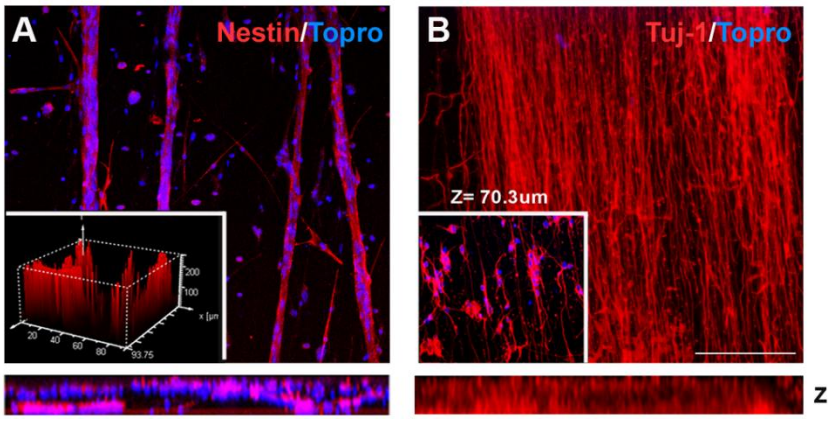

Figure R-14. Response of neural cells on aligned PLA nanofibers. Confocal images of **A**. glial cells stained with Nestin (red) and **B**. neurons stained with Tuj-1(red) on aligned PLA nanofibers after 5*div*. Glial cells colonized an

area of 200 μm in the z plane of the scaffold (**A, inset**) while neuronal somas localized in the middle of the scaffold (**B, inset**). Nuclei are stained with Topro (blue). Scale bars: 100μm **(A, B).**

Neurons and glial cells were cultured together during 10 *div*. Neurons were identified by immunoreactivity to β-III tubulin (Tuj-1) and glial cells to BLbP (Feng et al 1994) (Fig. R-15). On random scaffolds, neurons and glial cells grew on the surface and adopted multipolar shapes (Fig. R-15A), while in aligned scaffolds they maintained their bipolar shape oriented in the fibers direction (Fig. R-15B) and invaded the entire thickness (Supplementary video 1). Aligned neurons and glia mimicked the organization of embryonic radial glia and migrating neurons observed during brain development (Fig. R-15C).

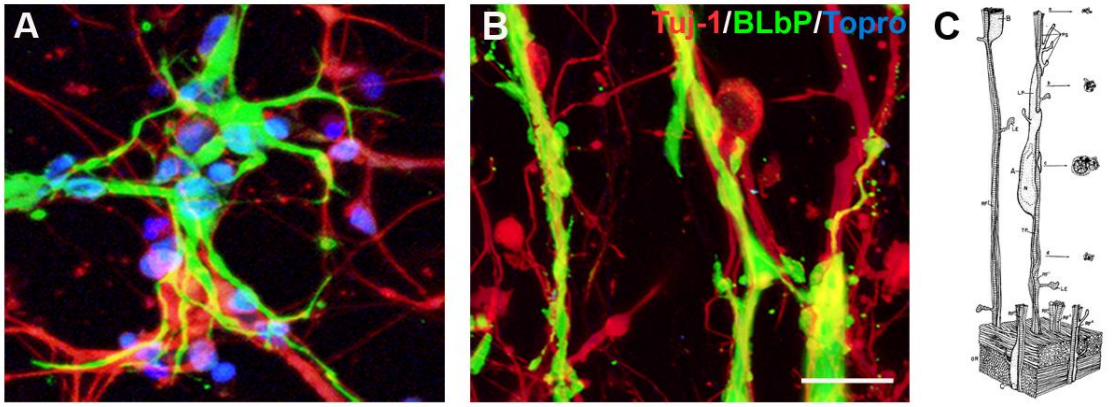

Figure R-15. **Co-culture grown on PLA nanofibers *in vitro*. A, B.** Morphology of $BLbP^+$ glia (green) and $Tuj\text{-}1^+$ neurons (red) on random **A.** and aligned nanofibers **B.** after 10*div*. **C**. Picture of migrating neuron on radial glia based originally on electron micrographs of serial sections of the monkey fetal cerebral wall. Adapted from (Rakic, 1972). Nuclei are stained with Topro (blue) Scale bars: 20μm **(A, B)**.

2.3 PLA fibers induce radial glia like and neuronal progenitor migrating phenotypes *in vitro*

In the developing CNS, new-born neurons attach to radial glia, which is the main substrate for neuronal migration. Thus, we analyzed by video time-lapse microscopy the neuronal supportive behavior of PLA nanofiber as RGLC. After 5 days *in vitro*, neurons migrated on PLA nanofibers showing the adherence of embryonic neurons without the need of radial glia as a supportive substrate (Fig. R-16 and Supplementary video 2) (Rakic, 2003).

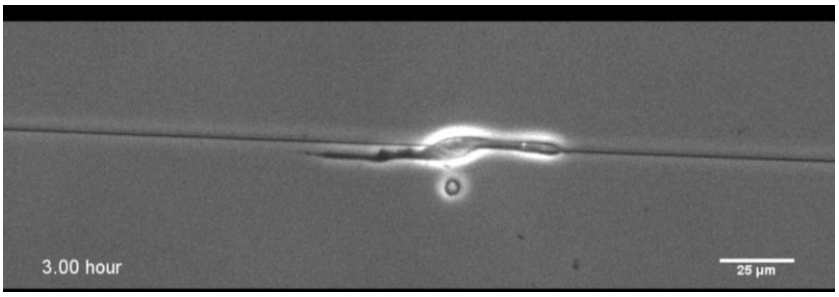

Figure R-16. Live-imaging of a neuron migrating on an aligned PLA fiber. Representative live-imaging shows an embryonic neuron migrating on top of an aligned PLA fiber after 5 days *in vitro*. Images were captured once a minute using an Axiovert 40 CFL light-inverted microscope (20× lens). Images were processed using the Image J program. Total time =13 h 50 min. Scale bar: 25µm (See Supplementary video 2).

The expression of cell-type molecular determinants of neurogenic niches (Englund et al., 2005b; Hsieh, 2012; Suh et al., 2007) was then analyzed by immunocytochemistry and western blot. After 5*div* on PLA fibers scaffolds, glial cultures dramatically increased their expression of the radial glia markers Nestin and Pax6 compared to control condition, and decreased their expression of the astroglial marker GFAP (Fig. R-17A, B).

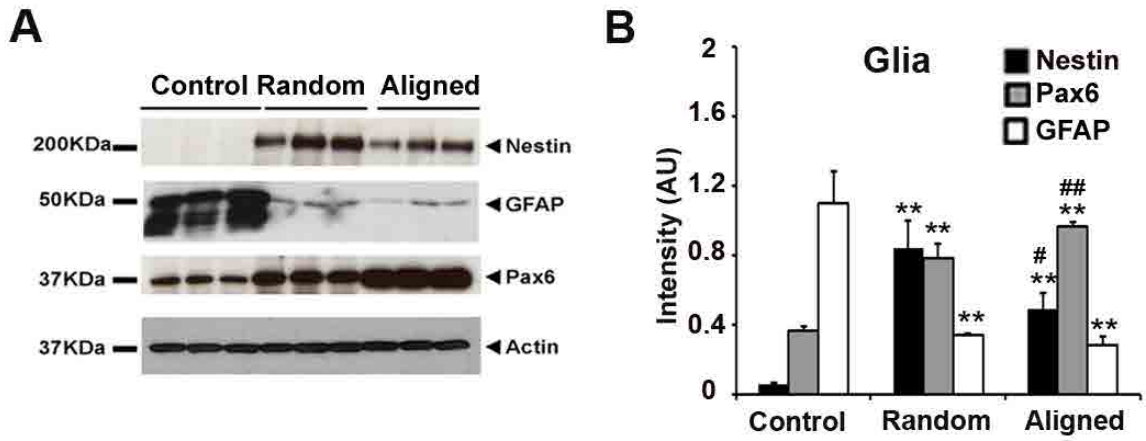

Figure R-17. Biochemical characterization of glial cells on PLA fibers. A. Western blots show the expression of Nestin, Pax6 and GFAP markers in glial cell cultures after 5*div*. **B.** Western blot densitometry (intensity values normalized to actin).* $p < 0.05$, ** $p < 0.001$, indicate significant differences compared to control, and # $p < 0.05$, ## $p < 0.001$ indicate significant differences between random and aligned, LSD test n=5. Error bars indicate the SD.

Similarly, compared to control condition, neuronal cultures on PLA fiber scaffolds dramatically increased their expression of $Ki67^{+}$ cycling progenitors (Fig. R-19), the neuronal progenitor marker Tbr2 and the NSC marker Sox2, whereas expression of the post-mitotic neuron marker Tuj-1 was lower (Fig. R-18A, B).

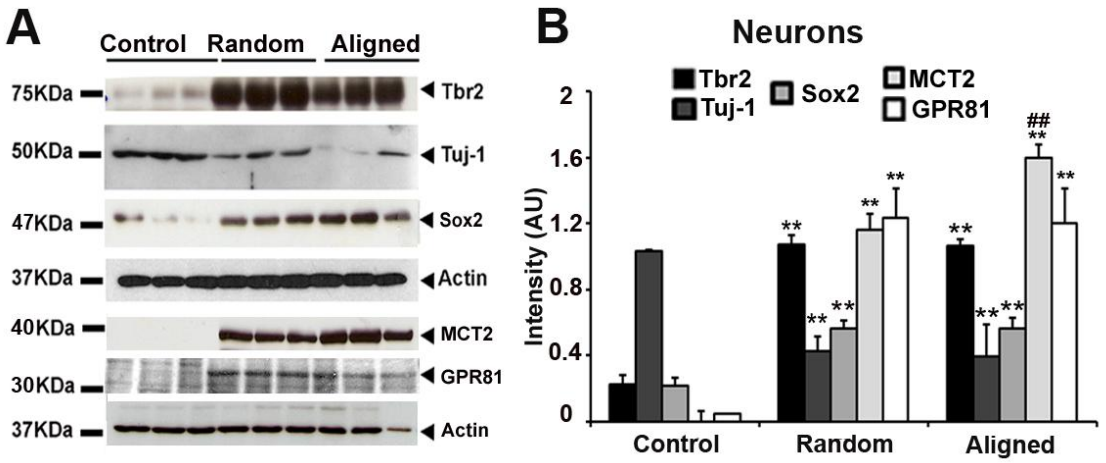

Figure R-18. Biochemical characterization of neuronal cells on PLA fibers. A. Western blots show the expression of Tbr2, Tuj-1,Sox2, MCT2 and GPR81 in neuronal cultures after 5 *div*. **B.** Western blot densitometry (intensity values normalized to actin).** p <0.001, indicate significant differences compared to control, and ## p <0.001 indicate significant differences between random and aligned, n=5. Error bars indicate the SD.

Moreover, in contrast to random scaffolds, aligned scaffolds better reproduced neurogenic niche properties as the expression of both Pax6 and Sox2 increased significantly (Fig. R-17 and 18 respectively).

Finally, in neuronal cultures, lactate released from PLA scaffold degradation induces a large increase in the proton-linked monocarboxylate transporter MCT2 (Halestrap and Wilson, 2012) and the G-protein-coupled lactate receptor, GPR81 (Lauritzen et al., 2013).

2.4 Effect of lactate released from PLA scaffold degradation on lactate-signaling and metabolism

As we demonstrated in the first part of results, postnatal glial cells didn't use lactate as energy source, however lactate maintained the pool of neural progenitors and neuron immaturity. Thus, we corroborated by immunocytochemistry the results obtained by western blot, whether the presence of lactate released from PLA nanofibers affected the expression of the monocarboxylate transporter MCT2 and the G-protein-coupled lactate receptor, GPR81, on progenitors and neuronal cells (Fig. R-19). After 5*div,* neurons cultured on control condition (tissue culture plate, TCP) expressed low levels of proton-linked monocarboxylate transporter MCT2 and the G-protein-coupled lactate receptor, GPR81. However, neuronal MCT2 and GPR81 were abundantly expressed in membranes and in the cytosol of neuronal cells and by some but not all $Ki67^{+}$ progenitors when neurons grown on PLA fibers (Fig. R-19).

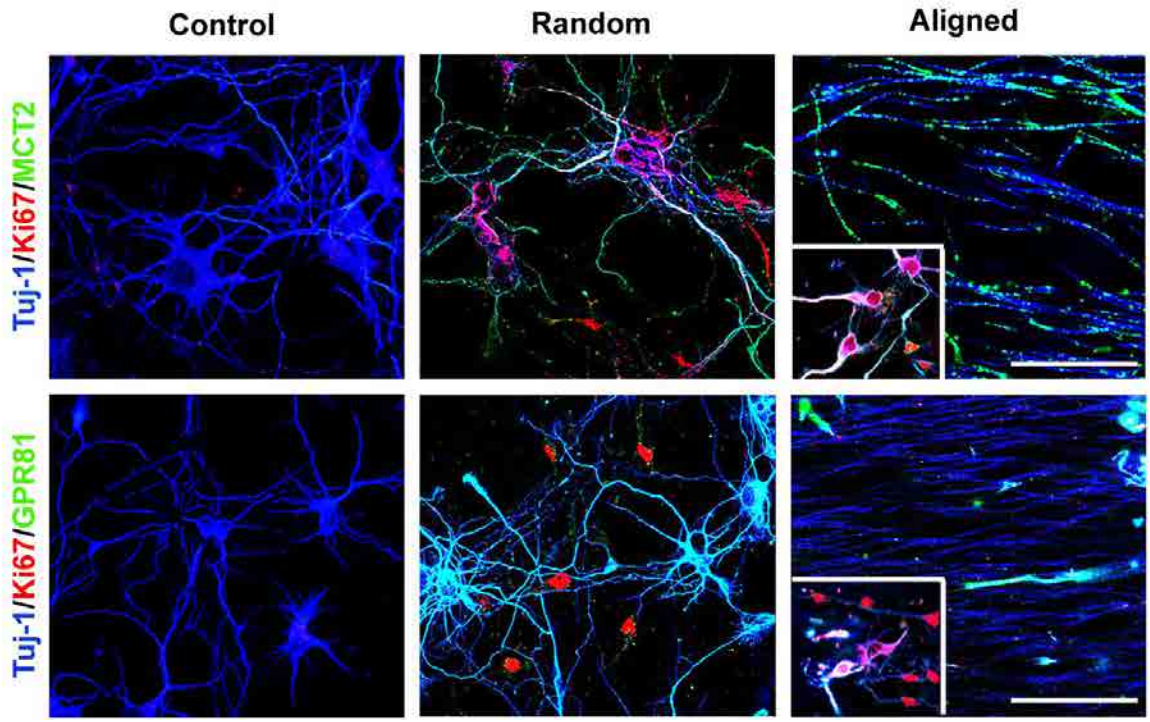

Figure R-19. Effect of lactate released by PLA nanofibers on progenitors and neuronal cell cultures. Confocal images of neuronal cultures grown on poly-D-lysine coated (Control), random (Random) and aligned PLA nanofibers (Aligned) after 5*div*, showing post-mitotic neurons (Tuj-1, blue), cycling cells (Ki67, red), neuronal lactate monocarboxylate transporter (MCT2, green), and G-protein-coupled lactate receptor (GPR81, green). Scale bars = 30 and 50μm.

On the other hand, when neurons were grown on TCP treated with glucose+L-lactate and L-lactate, they showed a similar expression patterns as neuronal cell cultures on PLA nanofibers (Fig. R-20).

After 5*div* in glucose medium, MCT2 and GPR81 were detected at low levels in neuronal membranes (Fig. R-20). However, in lactate conditions, MCT2 was abundantly expressed in membranes and cytosol of neurons, in $Ki67^+$ progenitors (Fig. R-20) and in $Tbr2^+$ neuronal restricted progenitors (Supplementary fig. 1), the principal type of precursor induced by lactate treatments (Chapter 1, Fig. R-8). By contrast, GPR81 was expressed in neuronal membranes and by some but not all $Ki67^+$ progenitors (Fig. R-20) and $Tbr2^+$ neuronal progenitors (Supplementary fig. 1) in lactate conditions.

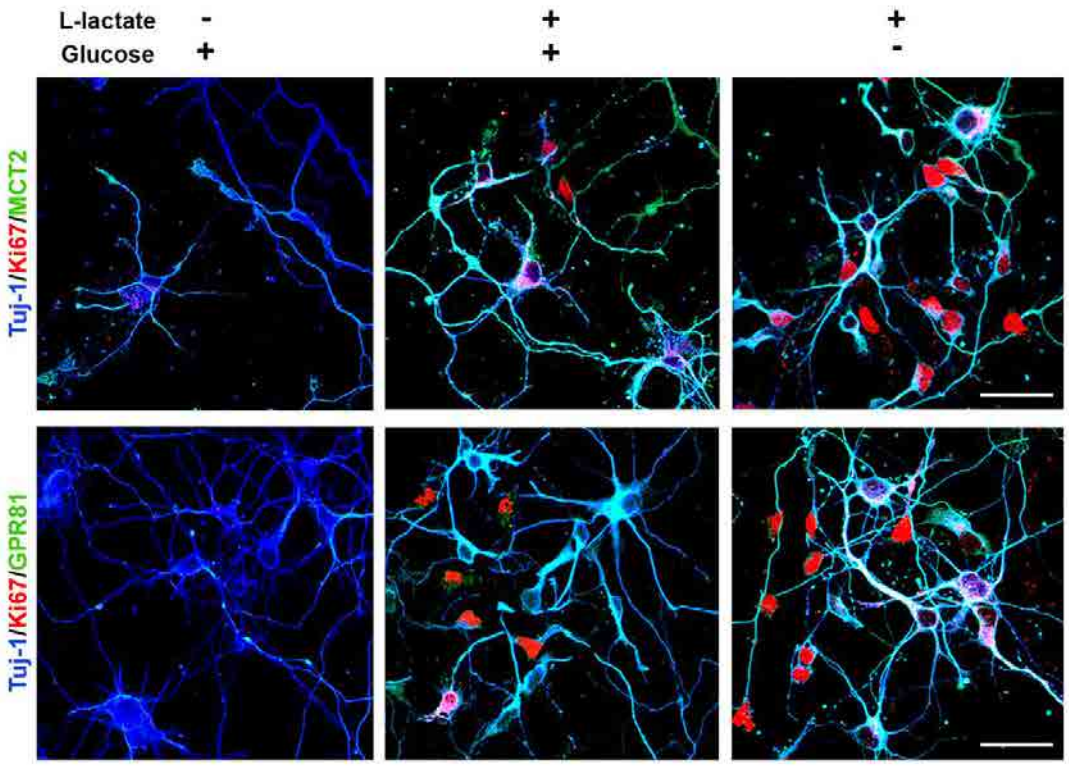

Figure R-20. Expression of lactate metabolic machinery in neuronal cell cultures treated with L-lactate. Confocal images of neuronal cell cultures grown in glucose, glucose+L-lactate, or lactate medium. Triple immunostaining of Tuj-1$^+$ neurons (blue), Ki67$^+$ proliferative cells (red), and cells expressing the lactate H^+/monocarboxylate transporter MCT2 (green) or the lactate receptor GPR81 (green). Scale bar = 40µm.

In a pharmacological approach we sought to answer the question whether neuronal survival and progenitor maintenance required lactate intake, either through monocarboxylate transporters, activation of the GPR81 lactate receptor, or a combination of both. Thus, neuronal cultures were grown on aligned nanofibers for 5*div* with or without glucose in the medium and treated with 100 nM of AR-C155858, an inhibitor of MCT1/2 that blocks lactate entrance into cells (Ovens et al., 2010), beginning at 1*div*.

Pharmacological blockade of lactate transport induced Ki67$^+$ progenitor depletion even in the presence of glucose, and neuronal death in the absence of glucose (Fig. R-21A-D). Thus, lactate released by PLA nanofibers apparently acts as an alternative fuel for neurons and is required for NSC/progenitor maintenance.

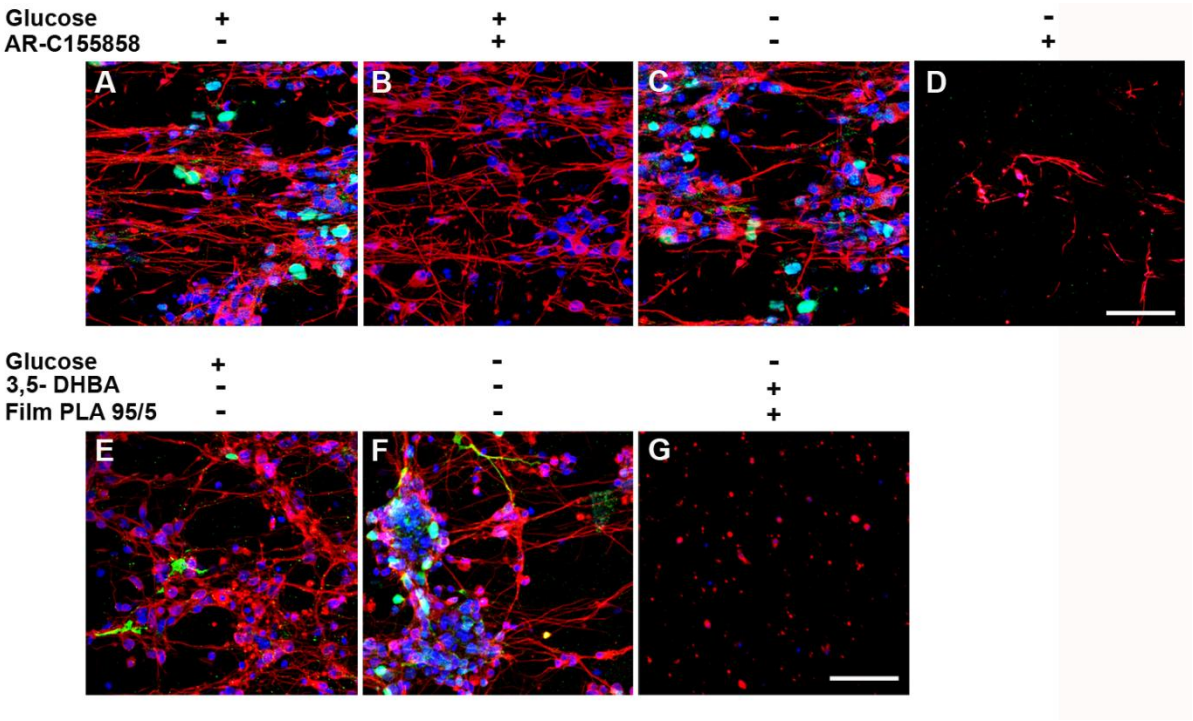

Figure R-21. **Inhibition of lactate released from PLA scaffolds.** Confocal images of neuronal cultures grown with or without glucose **A-D** on PLA70/30 nanofibers in the presence or absence of AR-C155858, an inhibitor of monocarboxylate transporters 1/2; **E-G.** on PLA70/30 nanofibers or PLA95/5films in the presence or absence of the lactate receptor agonist 3,5-DHBA for 5*div*. Neurons are stained with Tuj-1 antibody (red), cell nuclei with Topro (blue), and proliferative cells with Ki67 (green). Scale bars: 50 µm.

In a second set of experiments, 1mM of 3, 5-Dihydroxybenzoic acid (3, 5-DHBA), a selective agonist of lactate receptor GPR81, was added with or without glucose. In the presence of the agonist, neuronal death occurred when a not degradable PLA substrate was used (Fig. R-21E-G). Thus, lactate released by PLA nanofibers apparently acts as an alternative fuel for neurons using the MCT2 and is required for NSC/progenitor maintenance.

Then, neuronal cultures were grown on TCP treated with lactic acid using the same pharmacological approach as described for PLA experiments. With these experiments we determine whether neuronal survival and progenitor's maintenance required lactate *per se*.
Neuronal cultures were grown for 5*div* in the presence or absence of 100 nM of the MCT1/2 inhibitor AR-C155858 beginning at 1*div*. When added to glucose+L-lactate medium, the inhibitor induced $Ki67^{+}$ progenitor depletion (22±5 and 0±1 respectively, $p<0,001$), without affecting neuronal survival (211±51 and 240±24 respectively, Fig. R-22A, B), whereas when added to L-lactate medium it induced massive cell death (159±35 and 0, respectively, Fig. R-22C, D).

In another set of experiments, 3,5-DHBA, was added to glucose medium or to glucose/lactate-free medium beginning at 1*div*. In glucose medium, the agonist did not modify either the total number of cells (glucose: 255±46, glucose+agonist: 216±79, respectively, FigR-22E, F) or the number of Ki67^{+} progenitors (glucose: 0±0, glucose+agonist: 0±0) after 5*div*, nor did it promote cell survival in glucose/lactate-free medium (Fig. R-22G, H).

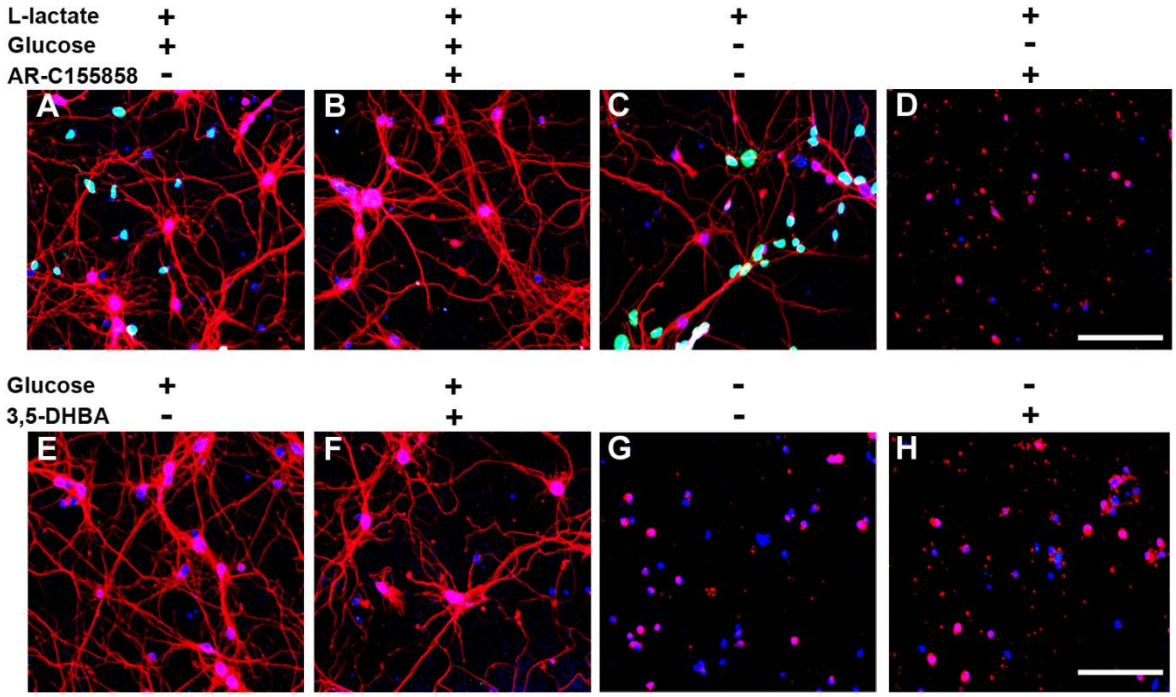

Figure R-22. L-Lactate inhibition on neuronal progenitor cells *in vitro*. A-D. Confocal images of neuronal cell cultures grown in glucose+L-lactate medium or in lactate medium in the presence or absence of AR-C155858, an inhibitor of monocarboxylate transporters 1/2, for 5*div*. **E-H.** Confocal images of neuronal cell cultures grown with or without glucose for 5*div* in the presence or absence of the lactate receptor agonist 3,5-DHBA. Neurons are stained with Tuj-1 antibody (red), cell nuclei with Topro (blue), and proliferative cells with Ki67 (green). Scale bars: 50 µm.

Moreover, the effects of L-lactate on neuronal cultures were not mimicked by D-lactate (Fig. R-23). D-lactate did not maintain Ki67^{+} cells (Fig. R-23 A, B, E, and F) and as neurons cannot use it as an energetic metabolite, there was no difference between the pharmacological treatment with AR-C155858 or 3, 5-DHBA and their respective controls (Fig. R-23C, D, G and H).

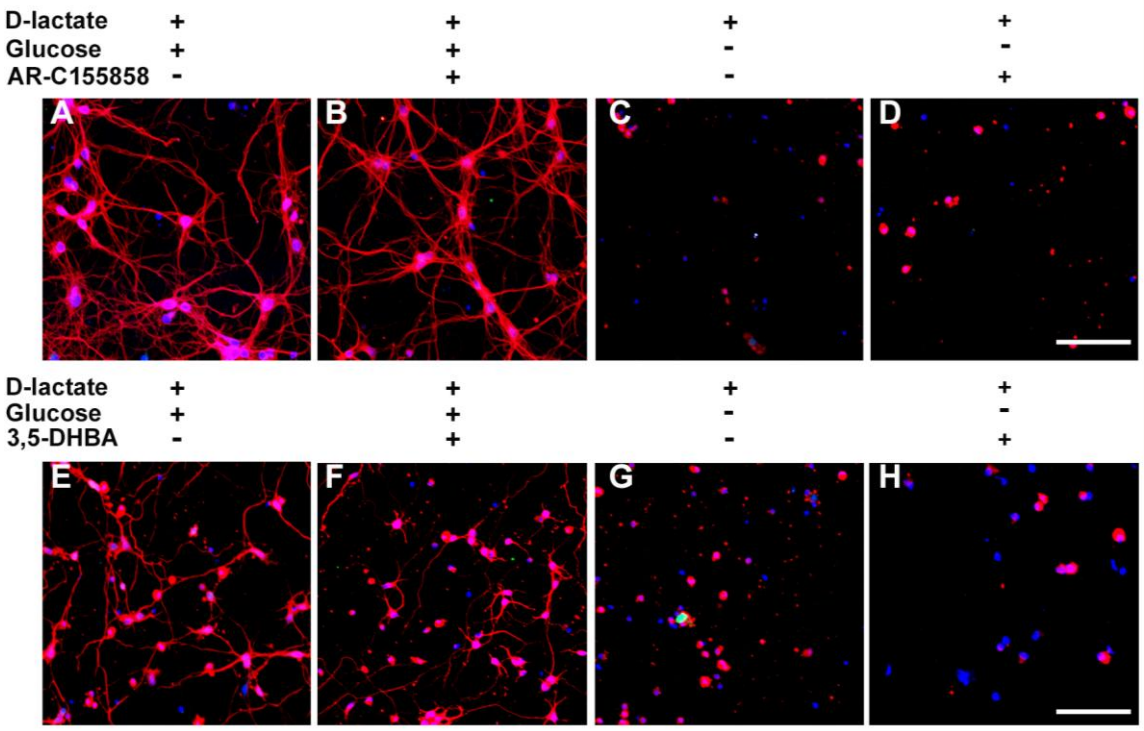

Figure R-23. Inhibitory effect of D-lactate on neuronal progenitor cells *in vitro*. A-D. Confocal images of neuronal cell cultures grown in glucose medium supplemented with D-lactic acid (D-lactate) and in D-lactate medium in the presence or absence of AR-C155858, an inhibitor of monocarboxylate transporters 1/2 for 5*div*. **E-H.** Confocal images of neuronal cell cultures grown in glucose medium supplemented with D-lactic acid (D-lactate), and in D-lactate medium for 5*div* in the presence or absence of the lactate receptor agonist 3,5-DHBA. Neurons are stained with Tuj-1 antibody (red), cell nuclei with Topro (blue), and proliferative cells with Ki67 (green). Scale bar =50 μm.

2.5 Lactate-associated changes in the metabolic profile of neuroprogenitor cells

Next, we analyzed whether the presence of lactate in the medium affected the expression of the mitochondrial enzyme PEPCK-M, required for the anabolic use of L-lactate (Supplementary fig. 2). After 5*div* in glucose medium, PEPCK-M was detected at low levels with a punctate distribution in the neuronal soma, whereas in lactate or on PLA70/30 fibers conditions, both neurons and progenitors expressed very high levels of the enzyme (Fig. R-24A). The absence of astrocytes and other type of progenitors in lactate conditions (see chapter 1 Figure R-8) suggested that the $Ki67^+$ progenitors were mostly $Tbr2^+$ neuronal progenitors and that lactate and PEPCK-M activity allowed the avoidance of differentiation, perhaps by promoting the maintenance of self-renewal. Quantitative analysis by Western blot and densitometry corroborated the significant increase of Tbr2 and PEPCK-M proteins (Fig. R-24B, C).

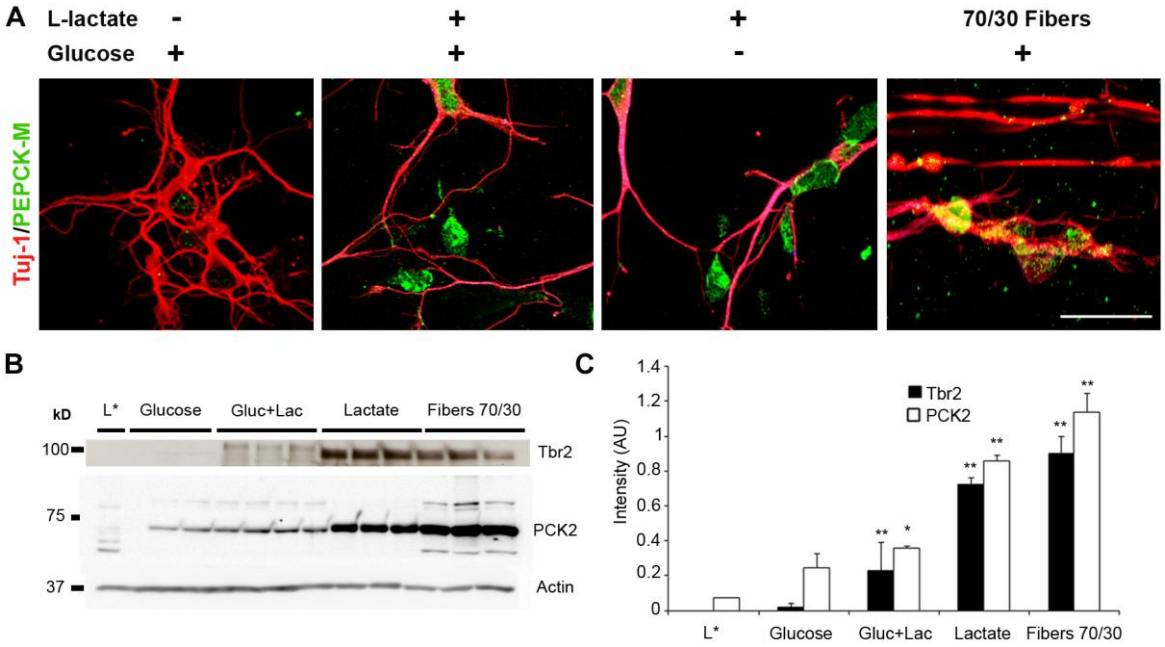

Figure R-24. Expression of PEPCK-M in neuronal cell cultures. Confocal images of neuronal cell cultures grown in glucose, glucose+L-lactate, lactate medium and cultured on aligned PLA70/30 fibers. **A.** Double immunostaining of Tuj-1+ neurons (red) and PEPCK-M (green). **B.** Western blot showing lactate-induced expression PEPCK-M and neuronal restricted progenitors Tbr2 in neuronal cultures grown as described in **A**. Actin were used as loading controls. **C.** Graph summarizing western blot quantification (densitometric intensity values normalized to actin). L= liver (positive control). Scale bar = and 20 µm. * $p<0.05$, and ** $p<0.01$ compared to glucose condition, LSD test. Error bars indicate the SD.

To specifically examine the potential role of PEPCK-M in the observed effects of lactate, we treated cultures with 3-mercaptopicolinic acid (3MPA), an inhibitor of PEPCK-M activity, or with DMSO as the control, from 1*div* to 5*div* (Fig. R-25A, B). In glucose medium, PEPCK-M inhibition did not affect the total number of cells (256±50 DMSO; 252±54 3MPA) or the number of $Ki67^+$ progenitors (1±2 DMSO; 1±2 3MPA).

However, in glucose+L-lactate or L-lactate medium, the lack of PEPCK-M activity corresponded with a significant reduction in the total number of cells (from 204±47 to 150±46 in glucose+L-lactate and from 121±50 to 79±34 in lactate, $p<0.01$) as well as the complete depletion of $Ki67^+$ progenitors (from 12±5 glucose+L-lactate, 15±6 lactate to 0, $p<0.01$), indicating that in the presence of lactate PEPCK-M inhibition leads to progenitor cell death. Consistent with this finding, lactate consumption decreased in the presence of 3MPA (from 0.7±0.1 to 0.2 mM in glucose+L-lactate, and from1.7±0.1 to 1.5±0.2 mM in lactate, $p<0.05$) (Fig. R-25C).

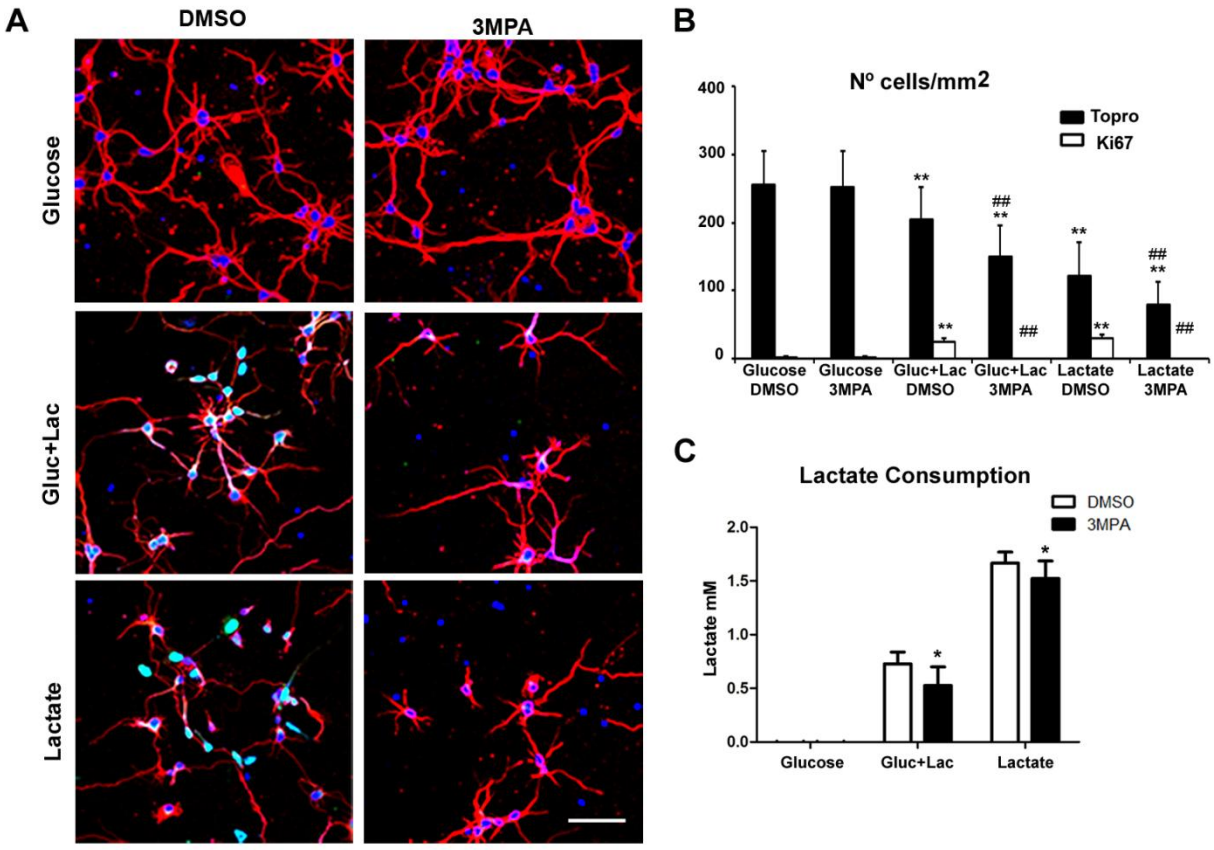

Figure R-25. Effect of 3MPA on neuronal progenitors. A. Confocal images of neuronal cell cultures grown in glucose, glucose+L-lactate, or lactate medium and treated with the PEPCK-M inhibitor 3MPA for 5*div*. Neurons are stained with Tuj-1 antibody (red), cell nuclei with Topro (blue), and proliferative cells with Ki67 (green). **B.** Quantification of the total number of cells (Topro) and of $Ki67^{+}$ proliferative cells after 5*div* in neuronal cultures grown as in **A**. **C.** Quantification of L-lactate in medium obtained from cells cultured as in **A.** Scale bar =75 µm. Values are the average of three replicas. * $p<0.05$, ** $p<0.01$ compared to glucose condition, and ## $p< 0.01$ between 3MPA and DMSO conditions, LSD test. Error bars indicate the SD.

Taken together these data suggest stereospecific effects of L-lactate on neuronal survival and progenitor self-renewal. These effects are apparently mediated by the cellular entry of L-lactate through MCT1/2 receptors and its metabolism at the TCA junction, represented by PEPCK-M catalytic activity.

Lactate restriction of neuronal progenitors implies that lactate metabolism also plays a crucial role in sustaining the increase in biomass that occurs during the cell cycle and in the extracellular matrix (ECM) production characteristic of these cells.

In this context, PEPCK-M is the only pathway that can export carbons from lactate and other tricarboxylic acid (TCA) cycle intermediates (i.e., glutamine) into the triose and hexose pools, through phosphoenolpyruvate (PEP) synthesis (Mendez-Lucas et al., 2013). Therefore, we evaluated whether the presence of lactate and the inhibition of PEPCK-M activity using 3MPA altered the synthesis of laminin, a highly glycosylated ECM protein that serves as a marker of

synthetic activity in neuronal progenitors (Kazanis et al., 2010). Indeed, lactate significantly increased the laminin content of neuroprogenitor cultures mainly associated with progenitor cells (Fig. R-26A-C), while in the presence of lactate and 3MPA there was a substantial decrease in the laminin content of neuroprogenitor cultures as shown by western blot (Fig. R-26D, E). This result suggested that the PEPCK-M pathway is relevant to link the glycolytic pools of building blocks necessary to sustain biosynthetic processes.

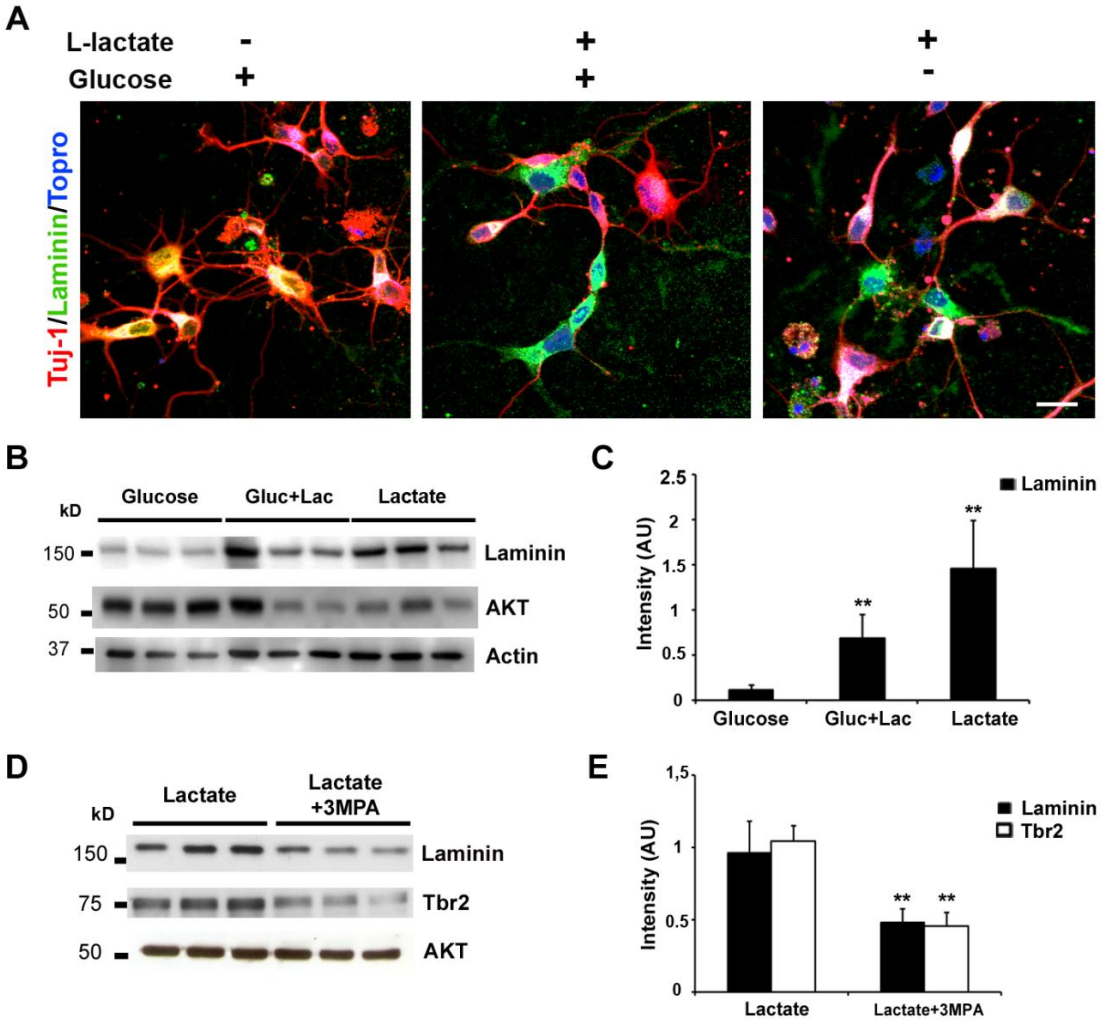

Figure R-26. Effect of 3MPA on laminin expression in neuronal cultures treated with L-lactate. A. Confocal images of neuronal cell cultures grown in glucose, glucose+L-lactate, or in lactate medium for 5*div* and stained with Tuj-1 (neurons, red), laminin (basal lamina, green), and Topro (nuclei, blue). **B.** Western blot of laminin (basal lamina marker) in neuronal cultures grown as in **A**. AKT and actin were used as controls. **C.** Quantitative representation of the Western blot (densitometric intensity values normalized to AKT). **D.** Western blot of laminin and the intermediate progenitor marker Tbr2 in neuronal cultures grown in lactate medium and treated or not with 3MPA for 24h after 4*div* in culture. AKT was used as the loading control. **E.** Quantitative representation of the Western blot (densitometric intensity values normalized to AKT). Scale bar = 20 µm. Values are the average of three replicas. ** $p<0.01$ compared to glucose condition, LSD test. Error bars indicate the SD.

2.6 PEPCK-M is required for the lactate-dependent increase in cycling cells *in vivo*

Finally, we tested whether progenitor self-renewal in the cerebral cortex was effectively mediated by L-lactate and PEPCK-M catalytic activity. In this *in vivo* experiment, 2 μL of either L-lactate (5 mM), 3MPA (100 μM), or vehicle was injected into the lateral ventricle of new-born (postnatal day 0, P0) mice. The effects on PEPCK-M expression and in the number of $Ki67^+$ cycling cells, $Sox2^+$ NSC/progenitors, and $Tbr2^+$ neuronal progenitors were analyzed in the ventricular/subventricular and intermediate zones (VZ/SVZ, IZ) at P3 (Fig. R-27).

The results showed an increase in PEPCK-M expression in the germinal VZ/SVZ of lactate-injected brains (Fig. R-27A) together with significant increases in the number of $Ki67^+$ progenitors (vehicle: 79±14, lactate: 129±37, 3MPA: 47±15; Fig. R-27B, C), $Sox2^+$ NSC/progenitors (vehicle: 85±10, lactate: 102±21, 3MPA: 57±9; Fig. R-27D, E), and $Tbr2^+$ neuronal progenitors (vehicle: 60±8, lactate: 72±14, 3MPA: 23±8; Fig. R-27F, G). Conversely, the numbers of all these cells significantly decreased in mice injected with 3MPA. Moreover, compared to the vehicle control, laminin expression in the germinal VZ/SVZ dramatically increased in lactate-injected animals but decreased in 3MPA-injected animals (Fig. R-27H). Taken together these data provide *in vivo* corroboration of the lactate dependence of neural progenitors.

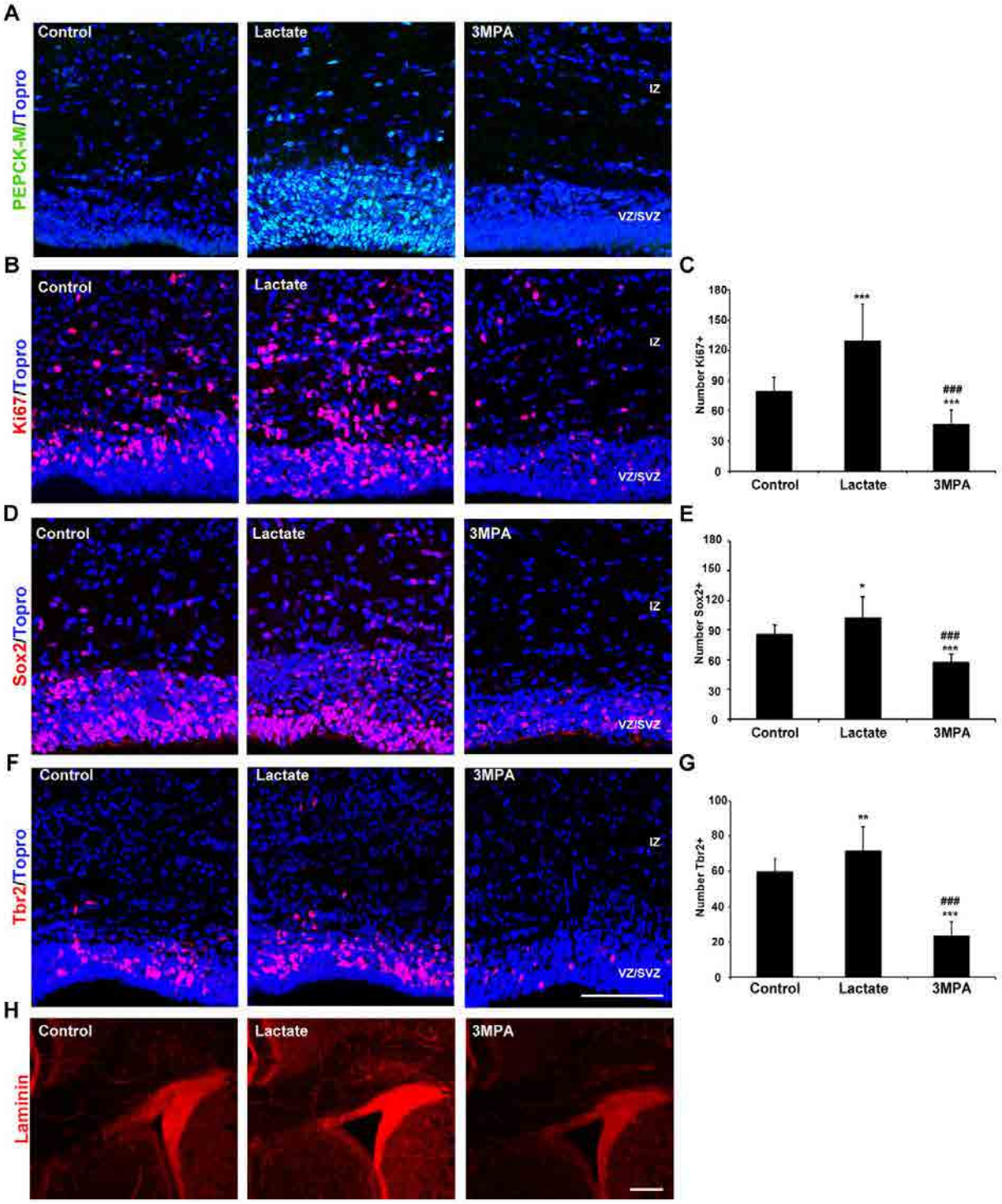

Figure R-27. Effect of lactate and 3MPA on cycling cells *in vivo*. (A, B, D, F, and H) Coronal sections of postnatal day 3 (P3) mouse cerebral cortex injected at P0 with vehicle (control), L-lactic acid (lactate), or the PEPCK-M inhibitor 3MPA and stained with **A.** PEPCK-M (mitochondrial enzyme, green), **B.** Ki67 (proliferative marker, red), **D.** Sox2 (NSC/progenitors, red), **F.** Tbr2 (intermediate progenitor marker, red), and **H.** laminin (basal lamina). Quantification of **C.** $Ki67^+$ cycling cells, **E.** $Sox2^+$ NSCs, and **G.** $Tbr2^+$ neuronal progenitors in the ventricular/subventricular and intermediate zones of animals treated as described in **B**, **D, and F**, respectively**.** Cell nuclei are stained with Topro (blue). Scale bar =100 µm (**A**–**F**), 500 µm (**H**). Values are the average of 8-10 animals. * p<0,05, ** p<0.01, *** p<0.001 indicate significant differences compared to control, and ### p< 0.001 compared between treatments, LSD test. Error bars indicate the SD.

Author Contribution

Many authors have collaborated in this chapter. Dr. Oscar Castaño and Dr. Miguel Angel Mateos-Timoneda designed and characterized PLA scaffolds at the Institute for Bioengineering of Catalonia (IBEC). Petra Hyrossova and Dr. Jose C. Perales performed the glucose and lactate measurements and some lactate-related experiments at the Physiological Sciences II department (Bellvitge Campus, UB).

RESULTS | CHAPTER 3

Neurogenesis and vascularization of the damaged brain using a lactate-releasing biomimetic scaffold

In the previous chapter, we demonstrated that the topology of PLA70/30 nanofibers support neuronal migration and induce radial glia and neuronal migrating phenotypes, while L-lactate from PLA degradation act as alternative fuel for neurons and is strictly required for progenitors maintenance. In this last part of results, we design an implantable biomaterial scaffold that reproduces the 3D organization and supportive function of embryonic radial glia. Thus, we implanted PLA70/30 scaffolds into postnatal and adult mice brain and characterized the response of the endogenous central nervous system progenitors and the regenerative capacity of the PLA implants.

3.1 Implantation of PLA scaffolds in injured brain

During the first postnatal week, cortical gliogenesis is still very active whereas neurogenesis is mostly completed prenatally (Miller and Gauthier, 2007), with the exception of life-span neurogenesis in adult neurovascular niches (Tavazoie et al., 2008). To analyze the regenerative potential of PLA, we implanted 500µm x150µm PLA70/30 films into the right somatosensory cortex of four day-old mice (P4). Implanted animals were analyzed after 15 days (Fig. R-28). The capacity of PLA films for inducing brain tissue regeneration was characterized by immunofluorescence. In P18 animals, no reactive astrogliosis were observed in the surround tissue and only a thin glial scar surrounding the material was observed (Fig. R-28). Due to the absence of channels/porosity in the 2D films there was no cell infiltration.

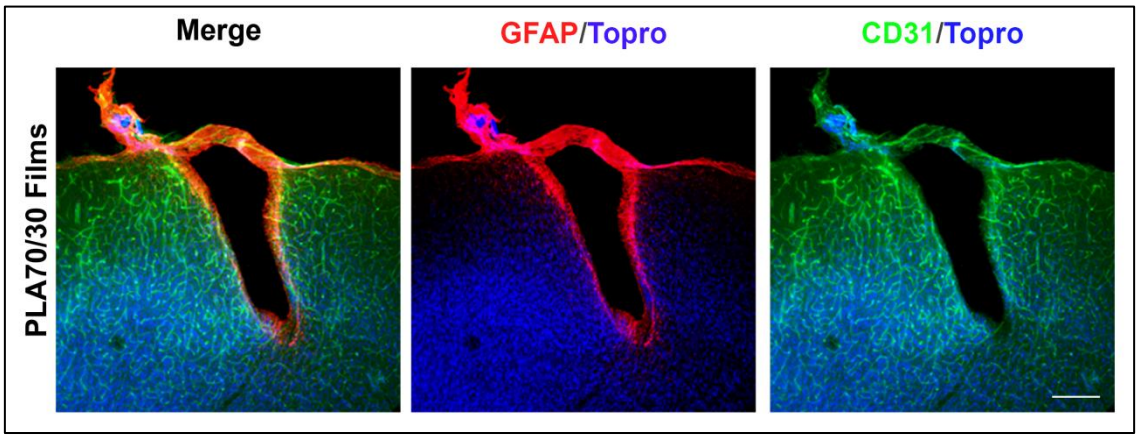

Figure R-28. Glial response in animals implanted with PLA films. Confocal images of coronal sections in cerebral cortex of P19 brains implanted with PLA 70/30 films. Confocal images of the material area (black) show the distribution of $GFAP^+$ astroglia (red) and $CD31^+$ endothelial cells (green). Topro (blue) stains nuclei. Scale bars; 500µm.

3.2 Implantation of PLA fiber scaffolds in aspiration brain cavities

After testing different conformations of PLA70/30 (films and sheets of fibers) implanted into cavities made in postnatal mouse (P4) cortex with variable results, we started implanting tubes of PLA fibers following the procedure used by (Hurtado et al., 2011) for spinal cord repair (Fig. R-29).

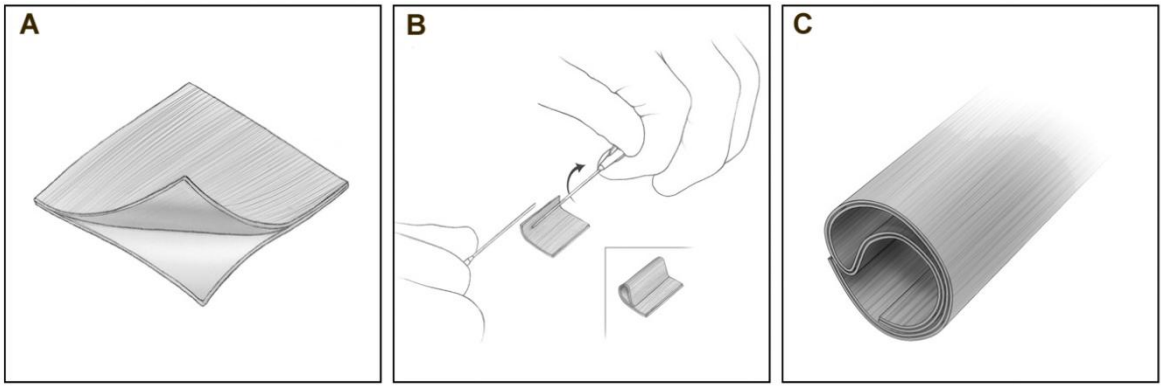

Figure R-29. Schematic photos of conduit assembly sheets with electrospun fibers. A. peeled from coverslips and **B.** rolled **C.** into tubes. Adapted from Hurtado et al., 2011.

To analyze the regenerative potential of PLA fiber scaffolds *in vivo,* we used a model of traumatic brain injury in 4-day-old (P4) mice, consisting of the aspiration of a $1mm^3$ cylindrical piece spanning almost the entire cortical thickness of the right somatosensory cortex (Fig. R-30A). PLA fiber sheets were folded and cut into $1mm^3$ tubes (Fig. R-30B, C) (see materials and methods). Random (random scaffolds, n=29, Fig. R-31) and aligned PLA fiber scaffolds (aligned scaffolds, n=87) following the radial orientation of radial glia (radial scaffolds, n=77, Fig. R-30D-F) or placed orthogonal to the orientation of radial glia (orthogonal scaffolds, n=10, Fig. R-31), were fitted into the brain cavity just after tissue removal. Control lesion (Fig. R-31) and implanted animals were analyzed at different times from 7 days to 15 months. PLA fiber scaffolds refilled the cavity and became incorporated into the surrounding parenchyma. The non-implanted brain cavities (control, n=20) remained empty (Fig. R-31) with no signs of brain tissue regeneration even 15 months after surgery. Abnormal neurological behavior was not observed in any experimental group or in mice of any age.

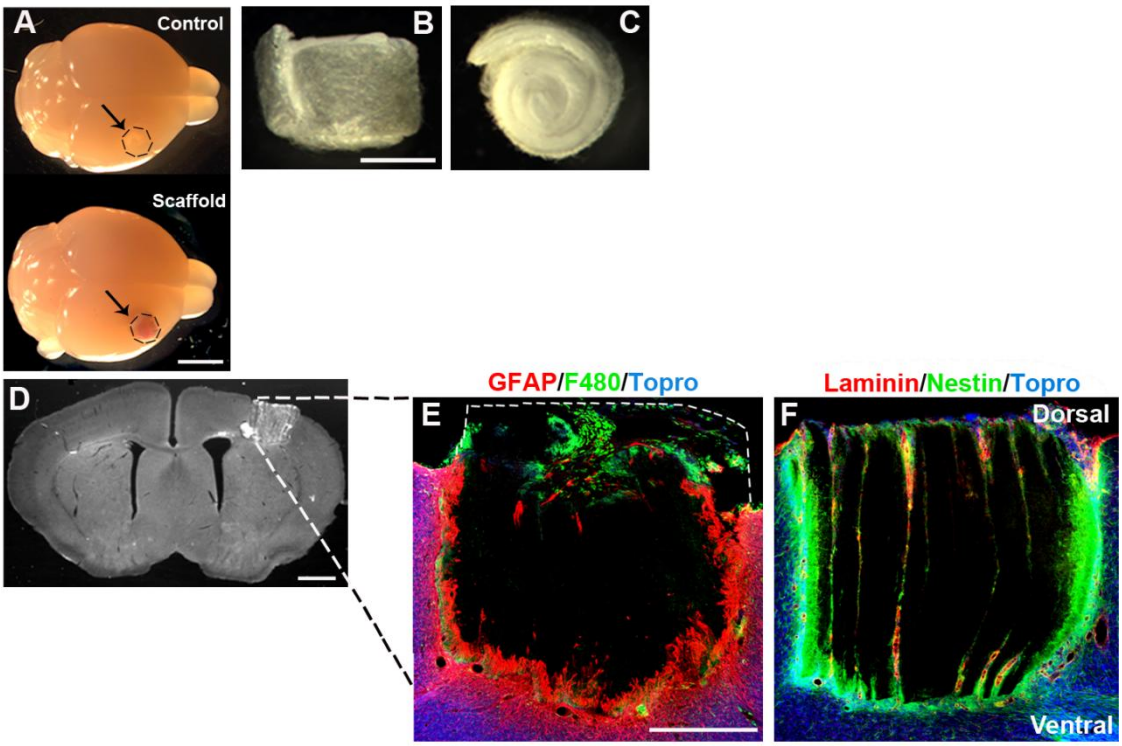

Figure R-30. Neurovascular bridges inside radial scaffolds. A. Macroscopic view of postnatal day 11 (P11) mouse brains with control injury (Control) or with an implanted PLA scaffold (Scaffold) in the right cortex; **B, C.** Lateral and top views of the scaffold before implantation. **D.** Bright-field coronal section showing the implanted radial scaffold. Confocal images showing **(E)** $GFAP^+$ astroglia (red) and $F480^+$ macrophages (green) surrounding the scaffold and **F.** $Nestin^+$ radial glia (green) and laminin basal lamina (red) forming radial neurovascular bridges inside the scaffold. Scale bar: 2mm **(A)**; 500µm **(B, C);** 1mm **(D)**; 400µm **(E, F).**

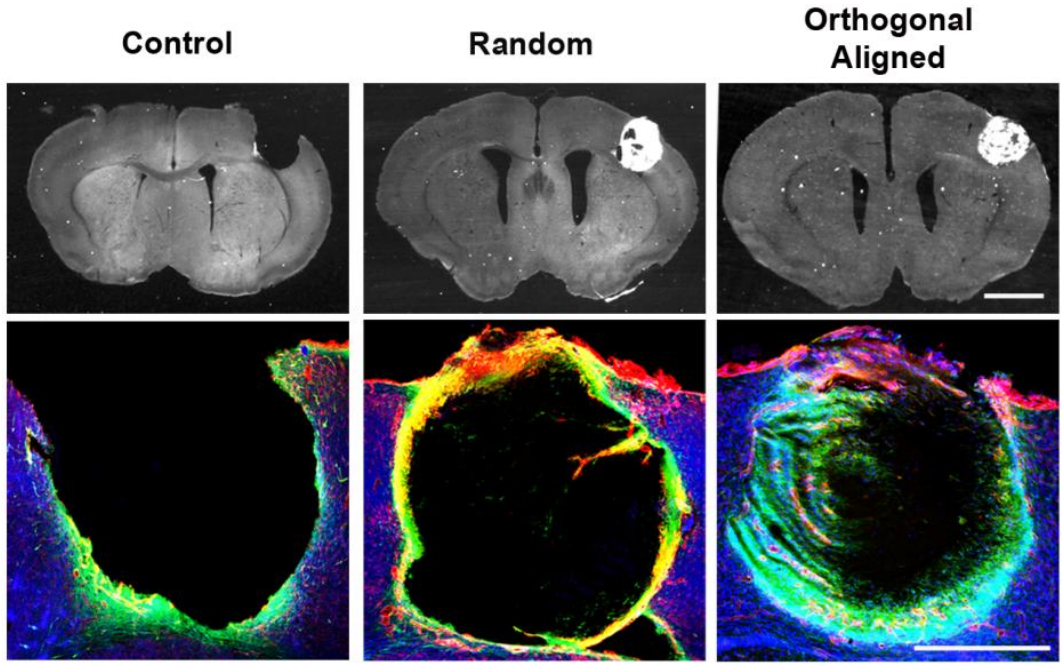

Figure R-31. Glial response in control lesions and in mice implanted with scaffolds of different fiber conformations at P11. Bright-field images of coronal sections of P11 mouse brains with aspiration lesion at P4 that were left untreated (Control) or implanted with either random nanofibers (Random) or with orthogonally aligned

nanofibers (Orthogonal aligned). Confocal images of the lesion area show the distribution of Nestin$^+$ radial glia (green) and laminin$^+$ basal lamina (red). Nuclei were stained with Topro (blue). Scale bars: bright field: 1mm, confocal images: 500µm.

3.3 Brain tissue regeneration inside PLA fiber scaffolds in *vivo*

Brain tissue regeneration was assessed by immunofluorescence microscopy. One week after surgery (P11), immune system activation was shown by the presence of F480$^+$ mature macrophages at the border of the lesion site and at the tissue–implant interface, but not far from the injury place (Fig. R-30E). Iba1$^+$ microglial cells were not present. Moreover, one week after surgery, GFAP$^+$ activated astrocytes were detected at the border of the lesion site and at the tissue–implant interface (Fig. R-30E).

At this time, Nestin$^+$ radial glia dramatically increased around and inside the aligned scaffolds, as did laminin, an adhesive extracellular matrix glycoprotein mainly secreted by glial and endothelial cells (Fig. R-30F; 33A). Newly generated tissue formed neurovascular bridges that crossed the scaffolds, following radial (Fig. R-30F, 32) or orthogonal trajectories to the brain surface, depending on the disposition of the aligned nanofibers (Fig. R-31). By contrast, in random scaffolds, despite similar fiber composition and size, cells were only present at the tissue-implant interface (Fig. R-31). Therefore, in subsequent experiments we used radial scaffolds for brain regeneration studies and random scaffolds as controls.

At the cell level, radial glial populations Nestin$^+$ and BLbP$^+$ were organized around a central blood vessel surrounded by a laminin-rich basal lamina (Fig. R-32, 33A, E and Supplementary video 3). Moreover, bridges of heterogeneous population of NG2$^+$ cells (Fig. R-32, 33F) including oligodendrocyte progenitors (OPCs) (Robel et al., 2011) entered inside the radial scaffold, while Olig-2$^+$ oligodendrocytes were absent. CX3CR1$^+$ resolving macrophages (Shechter et al., 2013) were also seen at the border and entering radial scaffolds from the meninges (Fig. R-33B).

Transcardiac perfusion with the lipophilic tracer DiI revealed an effective connection between this radial vascular network inside the scaffold and the host vasculature as well as the perfusion of the newly formed vessels (Fig. R-33D). As described above, GFAP$^+$ astroglia was only found at the tissue-scaffold interface (Fig. R-30E, 32, 33C) following the orientation of the fibers. At this early time point, embryonic neurons expressing the transcription factors Foxp-2 (Hisaoka et al., 2010) from the surrounding tissue were start entering the scaffold (Fig. R-32, 33F). The regeneration of neurogenic niches inside radial scaffold was also analyzed 1 week after surgery.

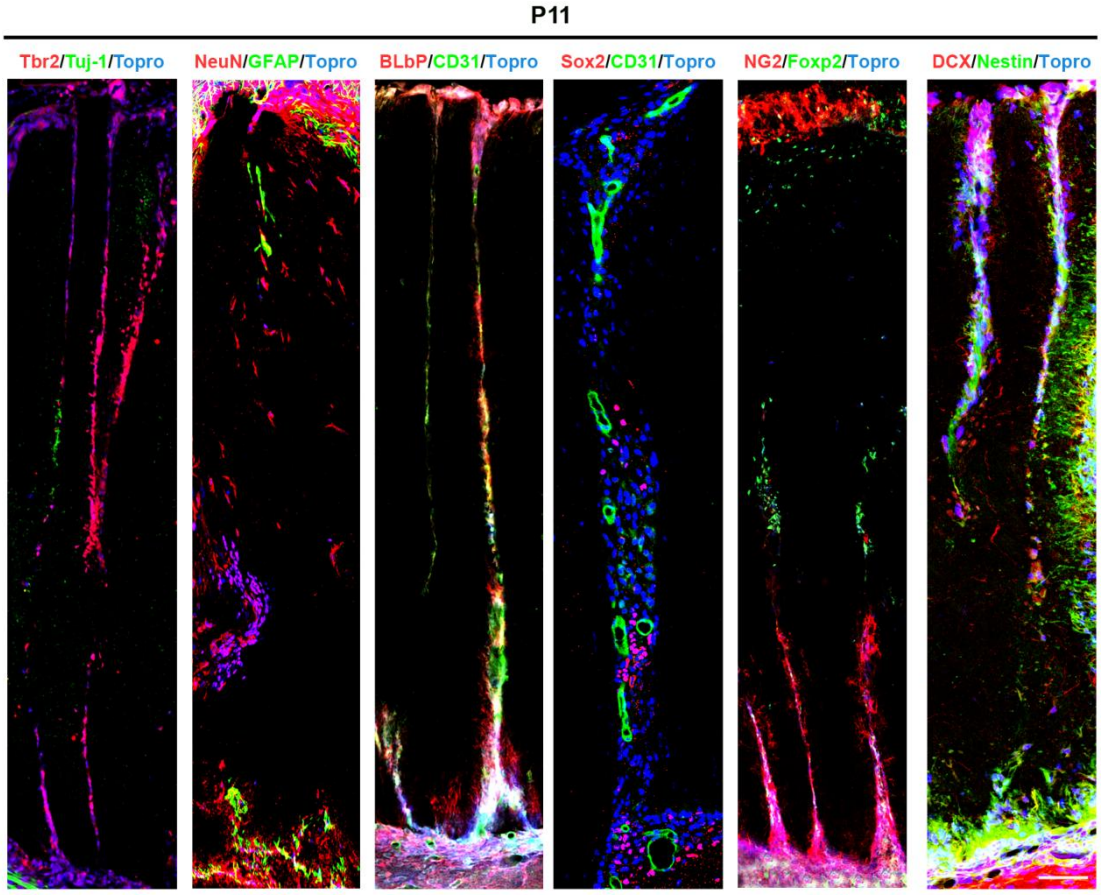

Figure R-32. Neurovascular bridges inside radially aligned fiber scaffolds implanted in P4 mice. Reconstruction of neurovascular bridges that reconnect the basal and meningeal sides of radially aligned fiber scaffolds 7 days after implantation (P11). $Tbr2^+$ intermediate progenitors (red); $NeuN^+$ neurons (red) and $GFAP^+$ astroglia (green); $BLbP^+$ immature glia (red) and $CD31^+$ endothelial cells (green); $Sox2^+$ stem cells (red) and $CD31^+$ endothelial cells (green); DCX^+ immature neurons (red) and $Nestin^+$ radial glia (green). Nuclei were stained with Topro (blue). Scale bar: 25 μm.

After one week, $Ki67^+$ cycling cells were found in close association with blood vessels ($CD31^+$) (Tavazoie et al., 2008) in the tissue surrounding the scaffold and in the neurovascular bridges (Fig. R-34A). The analysis of progenitor determinants revealed a highly heterogeneous population of neuronal and glial progenitors. The distribution of $Sox2^+$ NSC (Fig. R-32, 34B), the neuronal restricted progenitor transcription factor Tbr2 (Fig. R-32, 34C, H), which is expressed in the intermediate progenitor cells (IPCs) of the SVZ (Englund et al., 2005b; Sessa et al., 2008) and $Pax6^+$ bipotential radial glia (Fig. R-34G) was similar to that of $Ki67^+$ cells (Fig. R-34A).

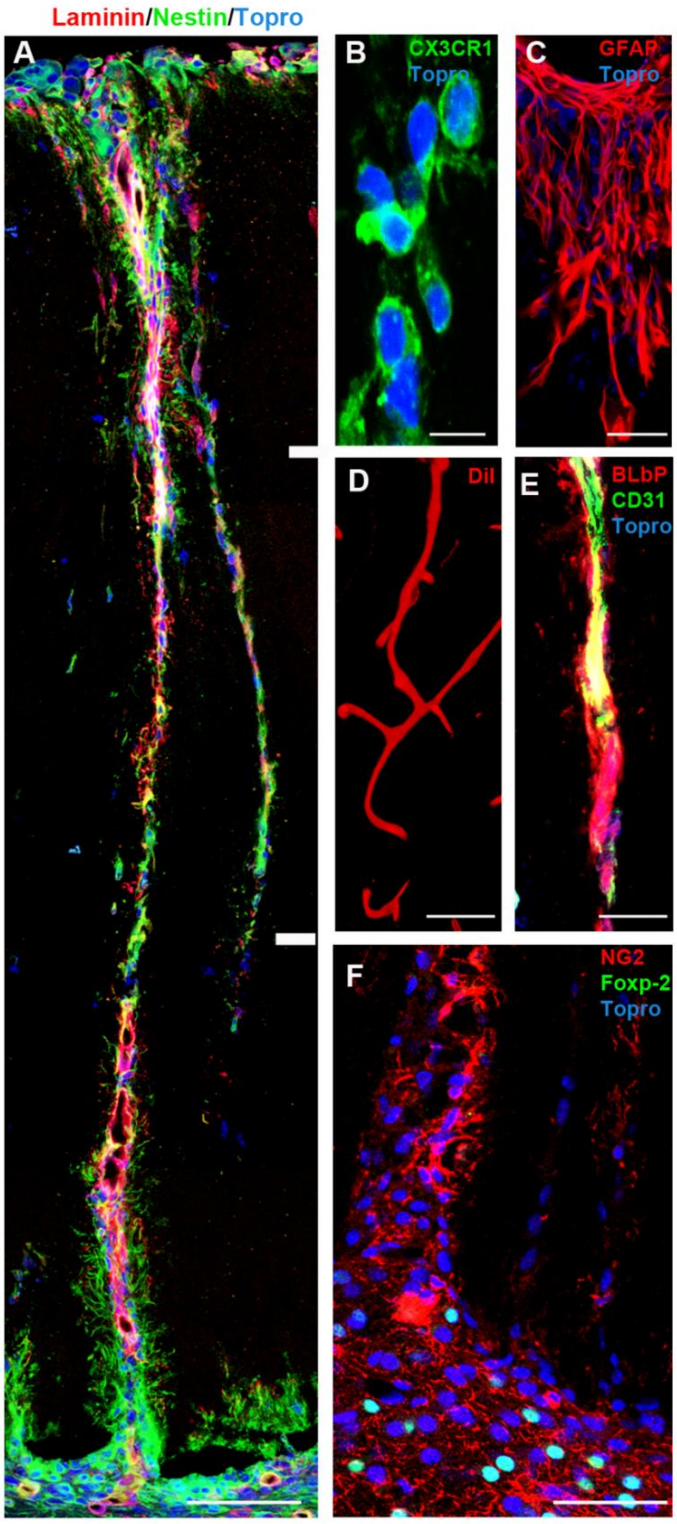

Figure R-33. Neurovascular bridges inside radial scaffolds at P11. Confocal images were showing **A**. Nestin^{+} radial glia (green) and laminin basal lamina (red) forming a neurovascular bridge reconnecting basal and meningeal zones. **B, C.** Higher magnifications showing **B.** resolving macrophages stained with CX3CR1 (green) and **C.** GFAP^{+} astroglia (red) in the upper third of the implant. **D.** Functional blood vessels stained by DiI perfusion. **E.** Proximity of BLbP^{+} radial glia (red) and CD31^{+} endothelial cells (green). **F.** NG2^{+} cells (red) entering the scaffold and FOXP-2^{+} neurons (green) remaining in the lower layers. Nuclei were stained with Topro (blue). Scale bars: 50µm **(A);** 20µm **(C, E);** 10µm **(B, D, F).**

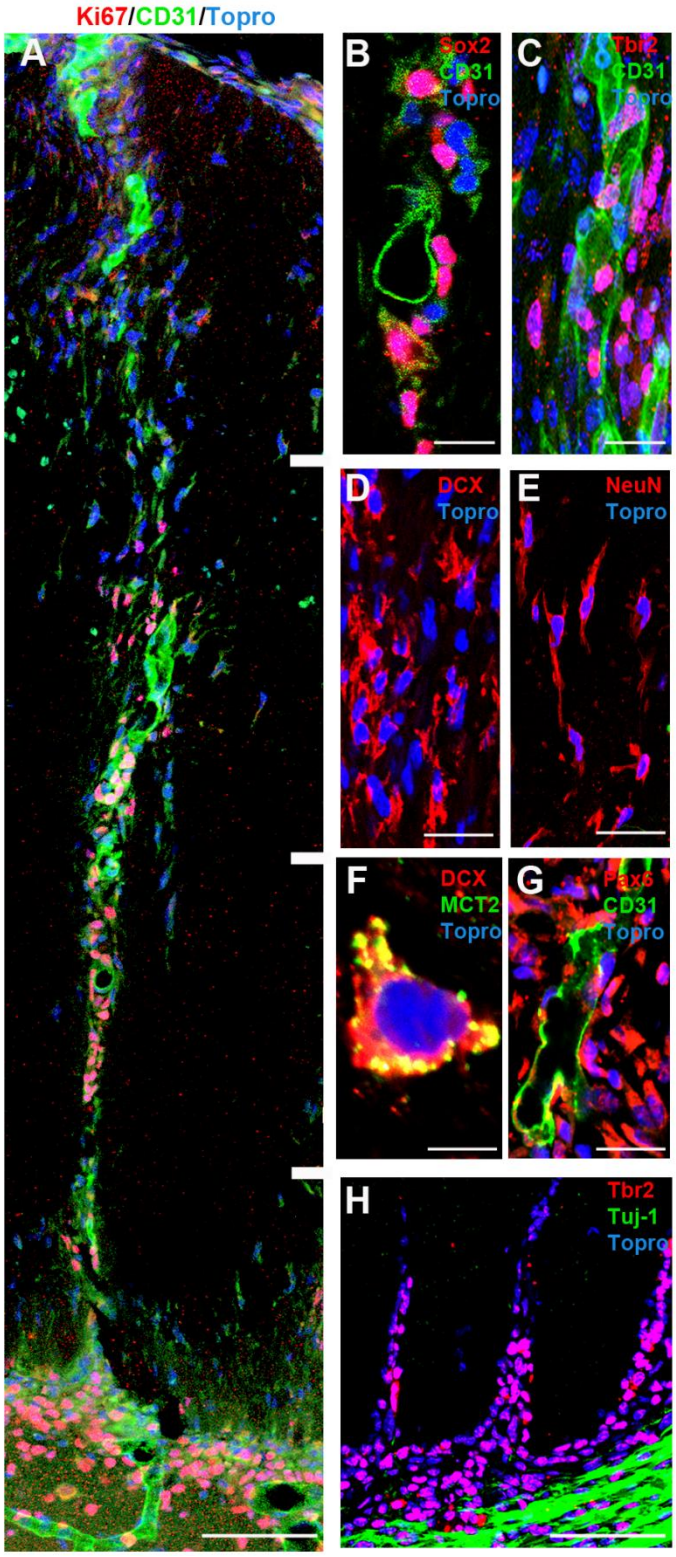

Figure R-34. Distribution of neural progenitors inside radial scaffolds at P11. Confocal images showing **A.** $CD31^+$ endothelial cells (green) in a neurovascular bridge surrounded by $Ki67^+$ cycling progenitors, by **B.** $Sox2^+$ stem cells (red) **C.** and by $Tbr2^+$ neurogenic progenitors (red). **D.** DCX^+ immature neurons and **E.** $NeuN^+$ neurons. **F.** DCX^+ cells (red) expressing MCT2 lactate transporter (green). **G.** $CD31^+$ endothelial cells (green) surrounded by $Pax6^+$ bipotential progenitors (red). **H.** $Tbr2^+$ progenitors (red) entering the scaffold and $Tuj\text{-}1^+$ axons (green) at the material-tissue interface. Nuclei were stained with Topro (blue). Scale bars: 50µm **(A, H)**; 10µm **(B, C, D, E, G),** 2µm **(F).**

Immature bipolar neurons expressing DCX, a microtubule-associated protein required for neuronal migration, and the neuronal transcription factor NeuN (Magavi, et al., 2000) were also detected in the neurovascular bridges after 1 week (Fig. R-32, 34D- F). The high-affinity proton-linked monocarboxylate transporter MCT2 (Halestrap and Wilson, 2012) required for the anabolic use of lactate were analyzed in immature neurons inside the scaffold. After one week, the DCX^+ cells showed high expression of the MCT2 in their soma (Fig. R-34F). Finally, neurons expressing the neuronal marker $Tuj\text{-}1^+$ (Hisaoka et al., 2010) from the surrounding tissue were excluded from entering the scaffold (Fig. R-34H).

3.4 Radial scaffolds induced long-term functional vascularization and brain tissue regeneration

To analyze long-term viability and effective brain tissue regeneration, implanted brains were analyzed 12-15 months post-surgery. After 1 year, the initially narrow neurovascular bridges had formed large areas of regenerated tissue, containing blood vessels, neurons, and glial cells, inside the radial scaffolds (Fig. R-35, 36). Despite evident signs of fiber degradation, PLA fiber scaffolds were clearly visible 15 months after implantation (Fig. R-35, 37E). Since the amount of new tissue generated inside the radial scaffolds increased over time, most of the data reported below correspond to the experiment's end-point at 15 months (radial scaffolds n=21, random scaffolds n=11 and control injury n=8).

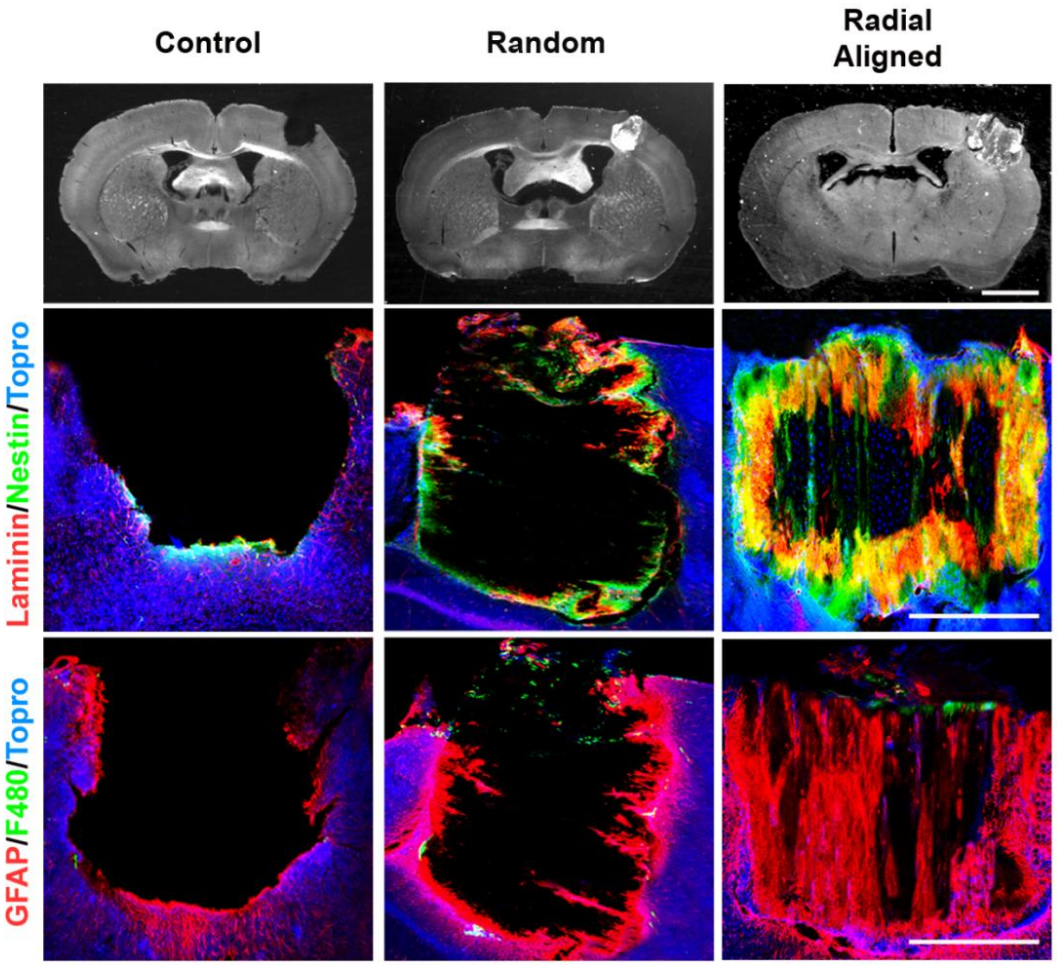

Figure R-35. Glial and immune response in control lesions and in animals implanted with scaffolds of different fiber conformations 1 year after surgery. Bright-field images of coronal sections of 1-year-old mouse brains with aspiration lesion at P4 that were left untreated (Control) or implanted with either random nanofibers (Random) or with radially aligned nanofibers (Radial aligned). Confocal images of the lesion area show the distribution of Nestin^{+} radial glia (green) and laminin^{+} basal lamina (red), and F480-macrophages (green) and GFAP^{+} astroglia (red). Nuclei were stained with Topro (blue). Scale bars; bright field: 1mm, confocal images: 500µm.

Nestin$^+$ and GFAP$^+$ glial cells were abundant and widely distributed inside the radial scaffolds (Fig. R-35, 36 and 37), maintaining the elongated shape and radial organization of embryonic radial glia and a laminin-rich extracellular matrix (Fig. R-35, 36). Immune activation was residual after 1 year, with scarce F480$^+$ macrophages at the tissue–implant interface (Fig. R-35). At 1 year, mature neurons expressing Tuj-1 (Fig. R-36, 37F, 38A, E) and MAP-2 (Fig. R-37G) were abundant and formed a rich neuronal meshwork inside the radial scaffold.

At the cellular level, some GABAergic neurons that stained with Parvalbumin (PV) and had well-developed morphology (Fig. R-36, 38H) were also found inside the implant. CX3CR1-resolving macrophages were largely absent and a few Iba1$^+$ ramified resting microglia were found inside radial scaffolds (Fig. R-38F).

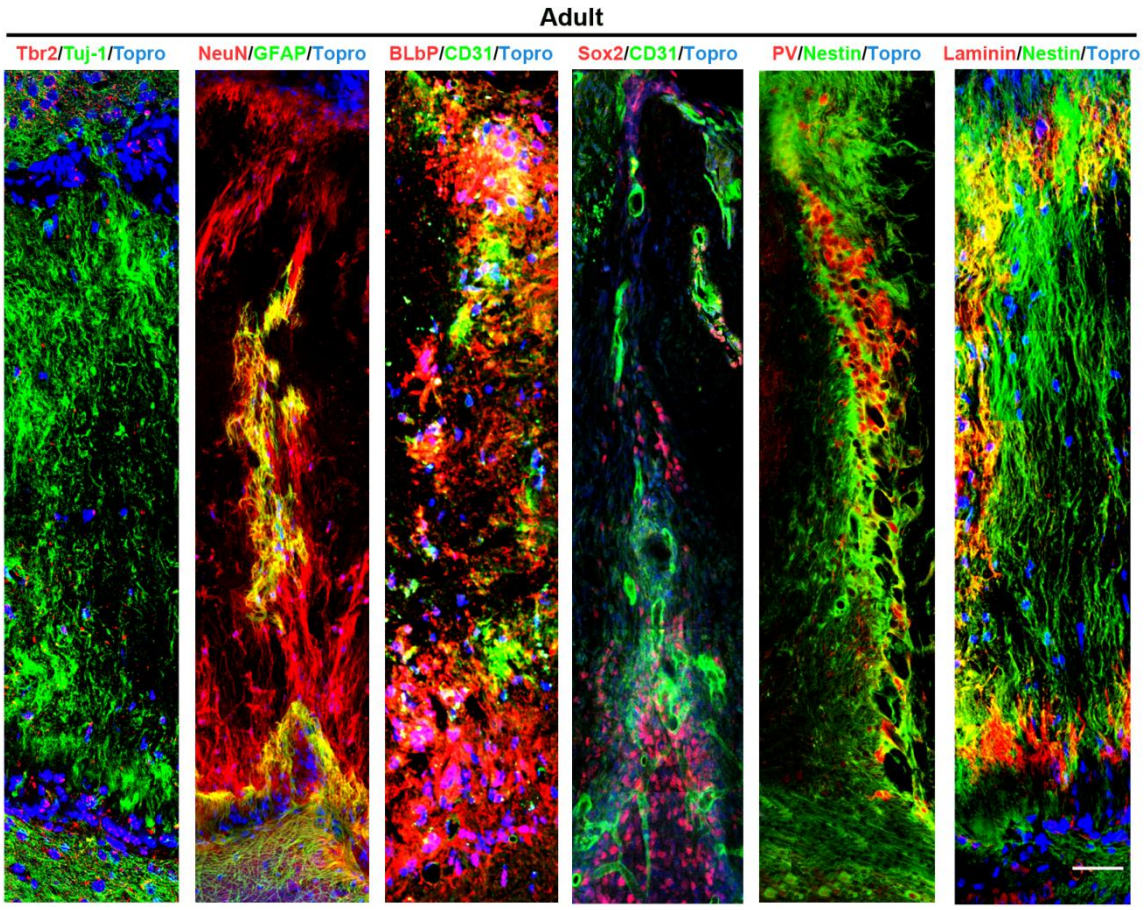

Figure R-36. Neurovascular bridges inside radially aligned fiber scaffolds 1 year after surgery. Reconstruction of neurovascular bridges that reconnect basal and meningeal sides of radially aligned fiber scaffolds 1 year after implantation (Adult). Tbr2$^+$ intermediate progenitors (red); Tuj-1$^+$ neurons (green); NeuN$^+$ neurons (red) and GFAP$^+$ astroglia (green); BLbP$^+$ immature glia (red) and CD31$^+$ endothelial cells (green); Sox2$^+$ stem cells (red); PV$^+$ GABAergic neurons (red); Nestin$^+$ radial glia (green) and laminin$^+$ basal lamina (red). Topro (blue) stains nucleus. Scale bar: 25µm.

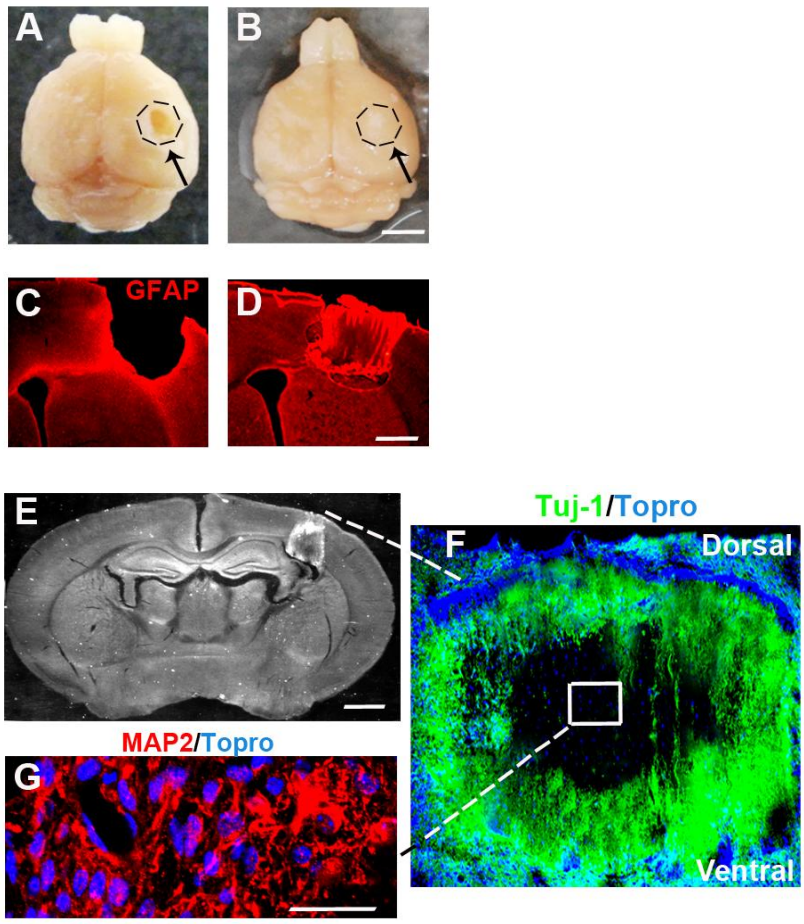

Figure R-37. Extent of brain tissue regeneration and vascularization after 1 year. Macroscopic view of brains with **A.** control lesion and **B.** radial scaffold 1 year after implantation. Coronal sections showing GFAP$^+$ astroglia around **C.** a control lesion and **D.** in the radial scaffold. **E.** Bright-field coronal section showing the material remaining. **F.** Magnification showing extensive colonization by Tuj-1$^+$ neurons. **G.** Mature neurons stained with MAP-2 in the middle of the scaffold. Nuclei were stained with Topro (blue). Scale bars: 1mm **(A, B)**; 500µm **(C, D)**; 1mm **(E)**; 200µm **(F)**; 25µm **(H)**.

The oligodendroglial lineage was now well represented and in addition to NG2$^+$ (Fig. R-38C), Olig-2$^+$ oligodendrocytes progenitor cells (OPCs) (Fig. R-38G) was also observed inside the scaffold. Moreover, myelin basic protein (MBP) typical of mature oligodendrocytes was present inside the scaffold (Fig. R-38D).

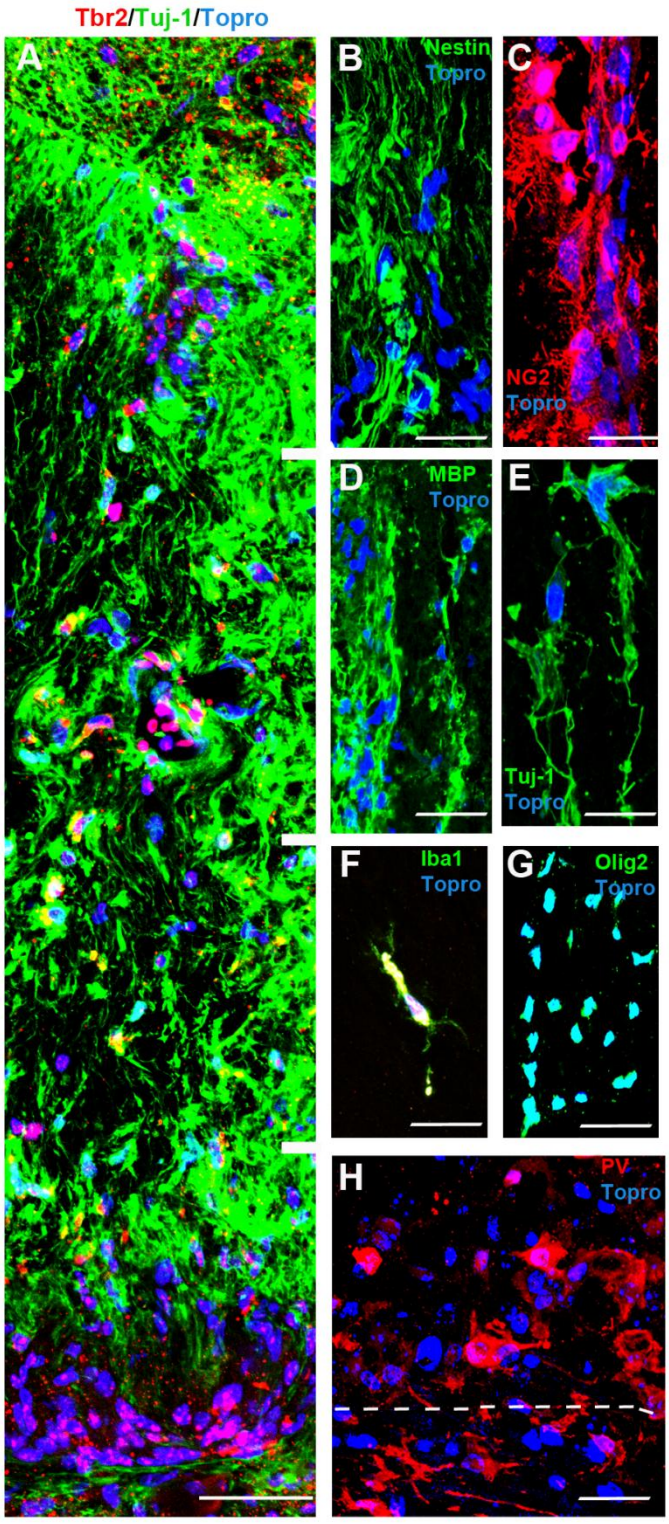

Figure R-38. Neuronal population inside radially aligned fiber scaffolds 1 year after surgery. Magnification **A.** showing Tuj-1^{+} neurons (green) and Tbr2 neural progenitors (red) following the radial organization of the nanofibers. **B.** Nestin^{+} radial glia **C.** NG2^{+} cells, **D.** MBP^{+} mature oligodendrocytes and **E.** Tuj-1^{+} neurons in the middle of the scaffold. **F.** Iba-1^{+} ramified microglia. **G.** Olig-2^{+} oligodendrocytes progenitors. **H.** PV^{+} GABAergic neurons on both sides of the tissue-scaffold interface. Nuclei were stained with Topro (blue). Scale bars: 25µm **(A, B, C)**; 20µm **(E, H)**; 10µm **(D, F, G)**.

At 1 year, DiI perfusion delineated large radial vessels that entered the radial scaffold before profusely branching (Fig. R-39, 40, 41B, 42A and Supplementary video 4). This vascular organization closely reproduced the normal organization of blood vessels in the contralateral brain tissue (Fig. R-41A and Supplementary video 5) whereas inside random scaffolds a similar vasculature was completely absent (Fig. R-41C and Supplementary video 6).

The radial scaffold removed from the brain 1-year after surgery showed a high vascularization surrounding and inside the aligned radial scaffold (Fig. R-40A, B).

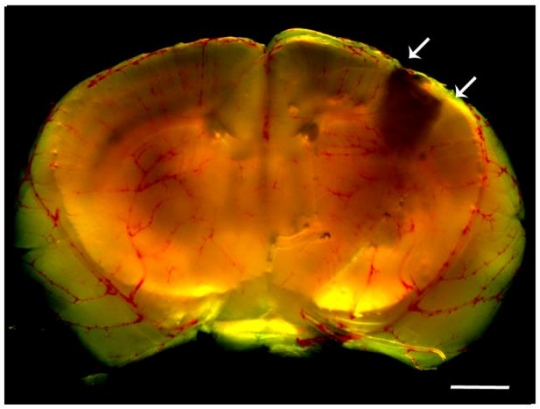

Figure R-39. DiI perfusion in adult mice. Coronal section of 300µm-thick showing aligned PLA tube (arrows) implanted in somatosensory cortex. Blood vessels were labeled by transcardiac perfusion with DiI (red) and visualized by stereoscopic microscope. Scale Bar: 1mm

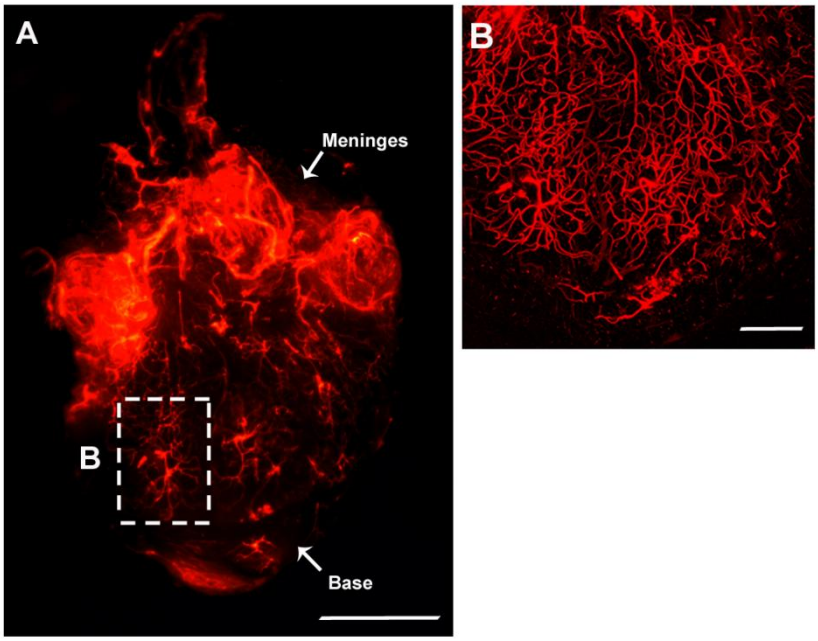

Figure R-40. Vascularization inside radially aligned fiber scaffolds 1 year after implantation. A. Radially aligned fiber tube perfused with DiI visualized by stereoscopic microscope. **B.** Magnification showing blood vessels stained with DiI (red) surrounding the material. Scale bars: 500µm **(A)**, 50µm **(B)**.

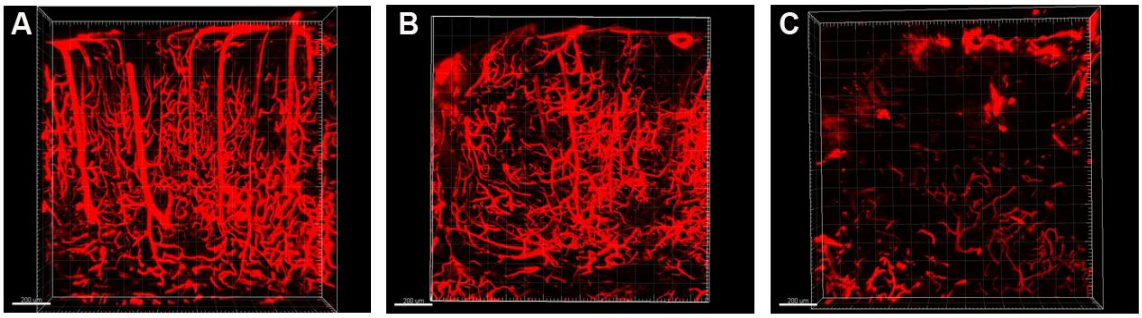

Figure R-41. Reconstruction of vascularization. The vascular network **A.** of the intact contralateral cortex, **B.** inside radially aligned nanofibers and **C.** inside a random fiber scaffold 1 year after implantation perfused with DiI (red). Coronal tissue sections (300 µm thick) were screened using a Leica TCS-SL spectral confocal microscope (10× lens). Confocal images were reconstructed using the Imaris program (Bitplane scientific software) for 3D and 4D real-time interactive data viewing. Scale bar: 200 µm. (See Supplementary video 4, 5 and 6).

The persistence of the regenerated neurovascular niche inside aligned scaffold was also analyzed after 1 year. A functional microvasculature associated with the neurogenic niche was revealed by CD31 expression or tomato lectin perfusion through the caudal vein (Fig. R-42). NSCs and progenitors expressing Sox2, Pax6, or Tbr2 (Fig. R-42D-F) were present inside radial scaffolds in close association with tomato-lectin-labeled microvasculature.
Finally, neurons expressing nuclear NeuN marker and immature neurons expressing microtubule-associated protein DCX required for neuronal migration, were still present after 1 year (Fig. R-42B, C).

Taken together, these results indicate that the implanted scaffold elicited neither a foreign body reaction nor encapsulation. Vascular sprouts, radial glia, and neural progenitors invaded radial scaffolds during the first week, suggesting that the neurogenic neurovascular niches were reconstituted early on inside the scaffolds and were still active after 1 year

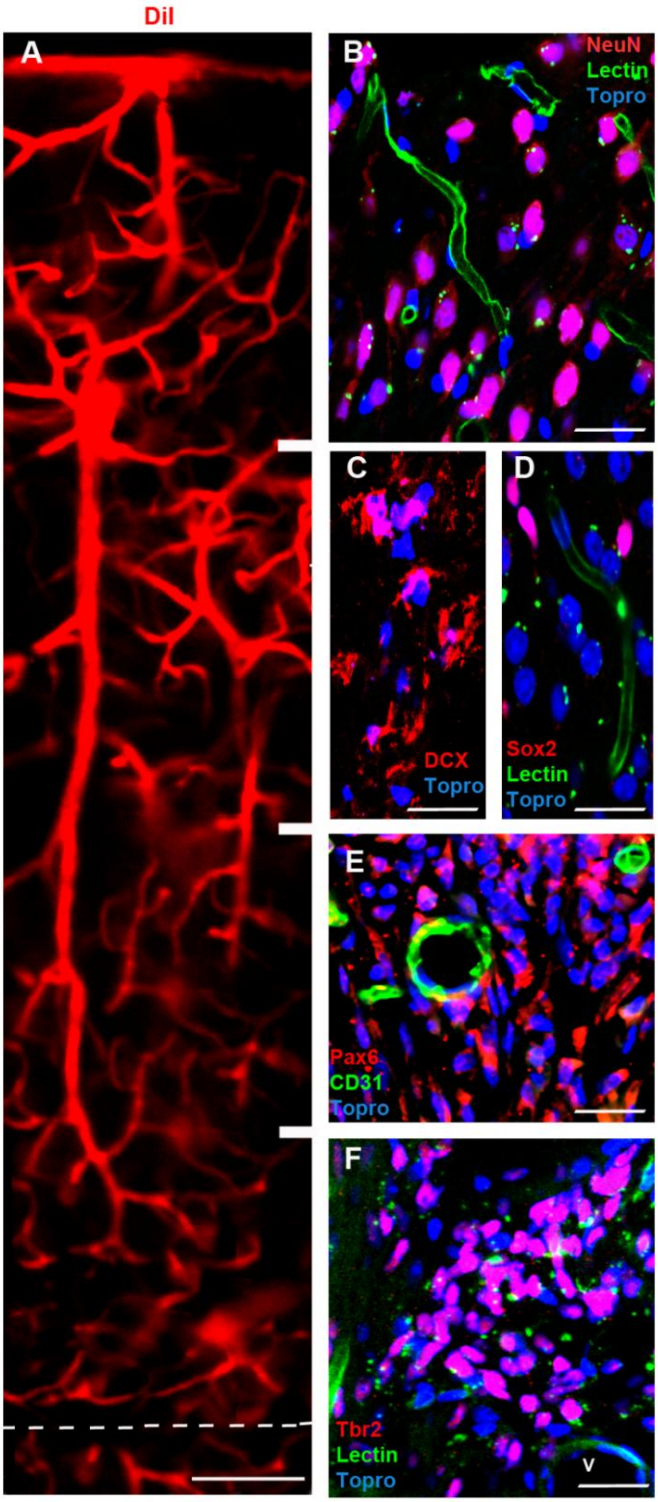

Figure R-42. Distribution of neural progenitors inside radial scaffolds 1 year after surgery. A. Reconstruction at 300 µm of blood vessels perfused with DiI inside an aligned scaffold. **B.** The vicinity of $NeuN^+$ neurons (red) and the microvasculature labeled by lectin perfusion (green). **C.** DCX^+ immature neurons. **D-F.** Lectin/CD31 blood vessels (green) surrounded by $Sox2^+$ stem cells (red) **(D)**, $Pax6^+$ bipotential progenitors (red) **(E)** and $Tbr2^+$ neural progenitors (red) **(F)**. Nuclei were stained with Topro (blue). Scale bars: 25µm **(A)**; 20µm **(B-F)**.

3.5 Induction and maintenance of functional neurogenic niches inside radial scaffolds

To confirm the activity of neurogenic niches, we examined the fates of dividing cells using markers for DNA replication (BrdU, a thymidine analogue) and progressive neuronal differentiation. At the time of implantation (P4), BrdU was incorporated in cells mostly located in the ventricular zone/subventricular zone (VZ/SVZ) and in a few cells scattered through the cortex. Only a few cells were double-labeled with BrdU and Sox2, Tbr2, Pax6, or DCX, while BrdU and NeuN colocalization was seen in SVZ neuroblasts (Fig. R-43).

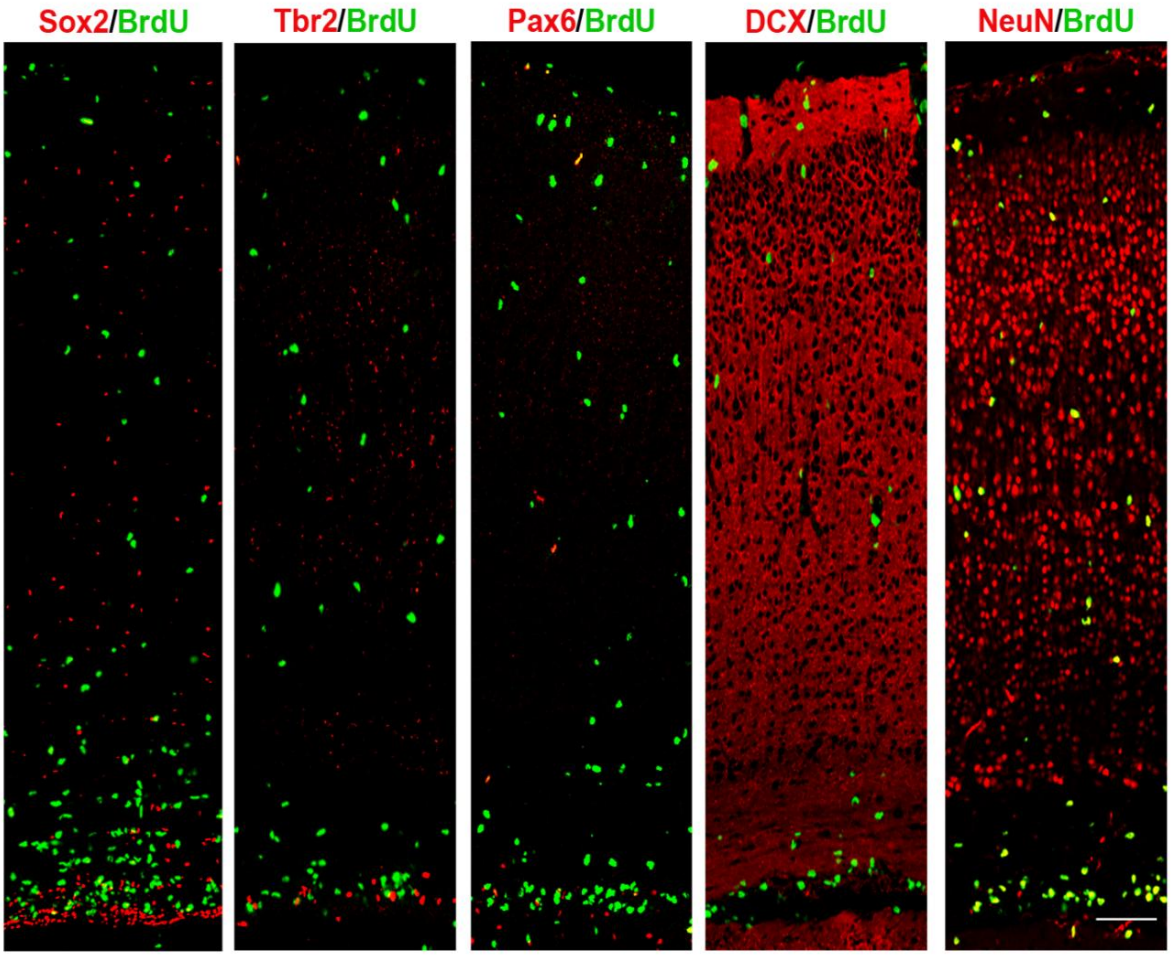

Figure R-43. Laminar distribution of the distinct progenitor types that incorporate BrdU in the cerebral cortex of P4 mice. Reconstructions of the entire thickness of P4 mouse cerebral cortex 3 h after BrdU injection. BrdU fluoresces green and $Sox2^+$ stem cells, $Tbr2^+$ neural restricted progenitors, $Pax6^+$ bipotential progenitors, DCX^+ immature neurons, and $NeuN^+$ neurons red. Scale bar: 25 μm.

When injected during the first week after surgery (1 injection/day for 5 days, P6–P11), BrdU was incorporated dramatically around and inside the radial scaffold (Fig. R-44, 45), but not on the contralateral side (Fig. R-46). Three hours after the first injection (P6), BrdU was found in progenitors expressing Tbr2 and Pax6 and in neuroblasts expressing DCX and NeuN. Only a few $Sox2^+$ NSCs incorporated BrdU, but their number increased at P11, after 5 consecutive

injections, suggesting the slow cycling of these progenitors. In the regenerated tissue, BrdU persisted in Sox2, Tbr2, and Pax6 progenitors for more than 1 year, indicating that they underwent very few rounds of cell division. After 1 year, abundant DCX^+ and $NeuN^+$ neurons (Fig. R-44) also co-localized with BrdU.

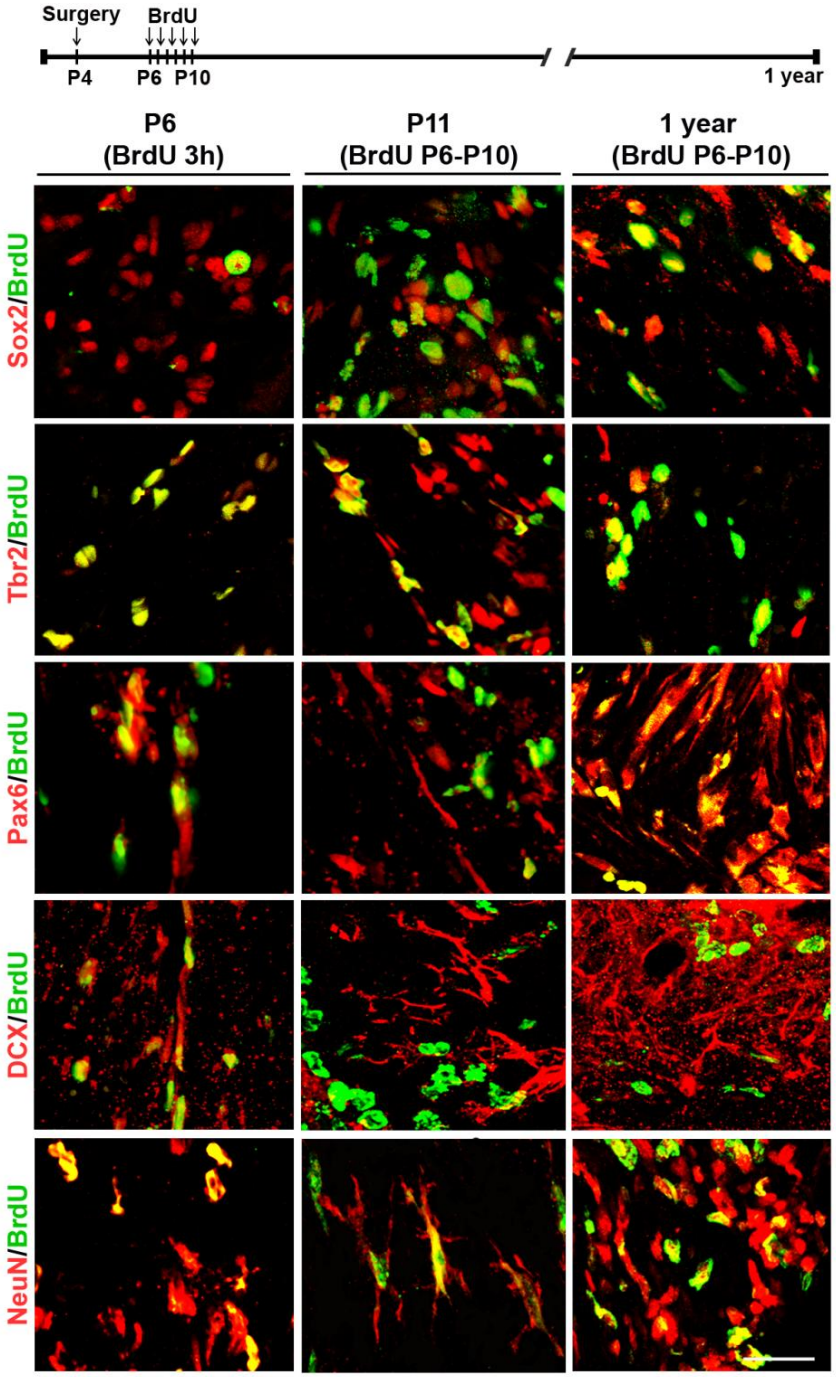

Figure R-44. BrdU incorporation into NSC/progenitors and neurons inside radial scaffolds. BrdU was injected intraperitoneally for 5 consecutive days, from P6 (2 days after scaffold implantation) to P10, and then analyzed 3h after the first BrdU injection, 7 days after implantation (P11), and 1 year after implantation. BrdU immunostaining (green) and colocalization inside the implant with molecular markers (red) of stem cells (Sox2), neuron-restricted progenitors (Tbr2), bipotential progenitors (Pax6), and neurons (DCX, NeuN).Scale bar: 20μm.

Some PV^+ GABAergic neurons, $GFAP^+$ astrocytes, and Olig-2^+ oligodendrocytes (Fig. R-45) co-localized with the BrdU inside the scaffold after 1 year. These data were consistent with both extensive neurogenesis and gliogenesis soon after radial scaffold implantation and the long-term survival of the newly generated neurons and glial cells.

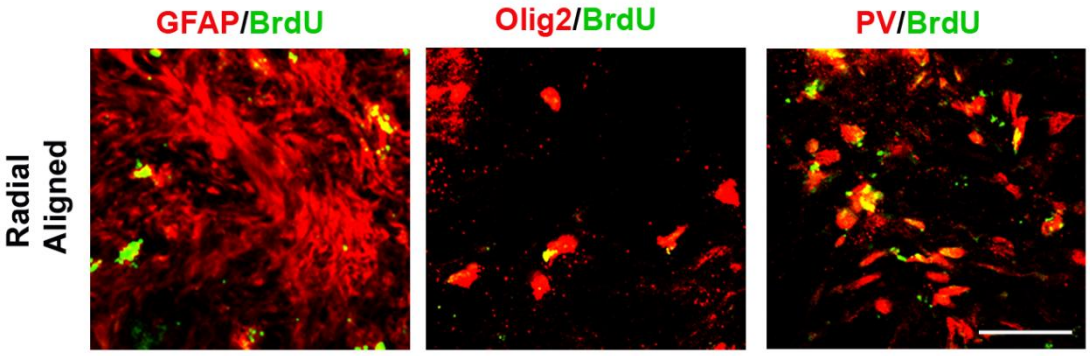

Figure R-45. Long-term survival of glial and neuronal populations in adult mice implanted at P4. BrdU injected for five consecutive days (from P6 to P10) in P4 mice implanted with radially aligned fiber scaffolds and analyzed at 1 year. Confocal images of radially aligned fiber scaffolds 1 year after implantation show double immunostaining for BrdU in green, and GFAP (astroglial marker), Olig-2 (oligodendroglial marker), and PV (GABAergic neurons marker) in red. Scale bar: 20 μm.

When BrdU was injected 2 months after radial scaffold implantation, it was incorporated into $Sox2^+$ and $Pax6^+$ progenitors and into DCX^+ and $NeuN^+$ neurons (Fig. R-47A), whereas when injected at 1 year it was seen only in $Pax6^+$ progenitors and DCX^+ and $NeuN^+$ neurons (Fig. R-47B). These data suggest that substantial neurogenesis continues in the implant, although the progenitor types and generated neurons probably vary.

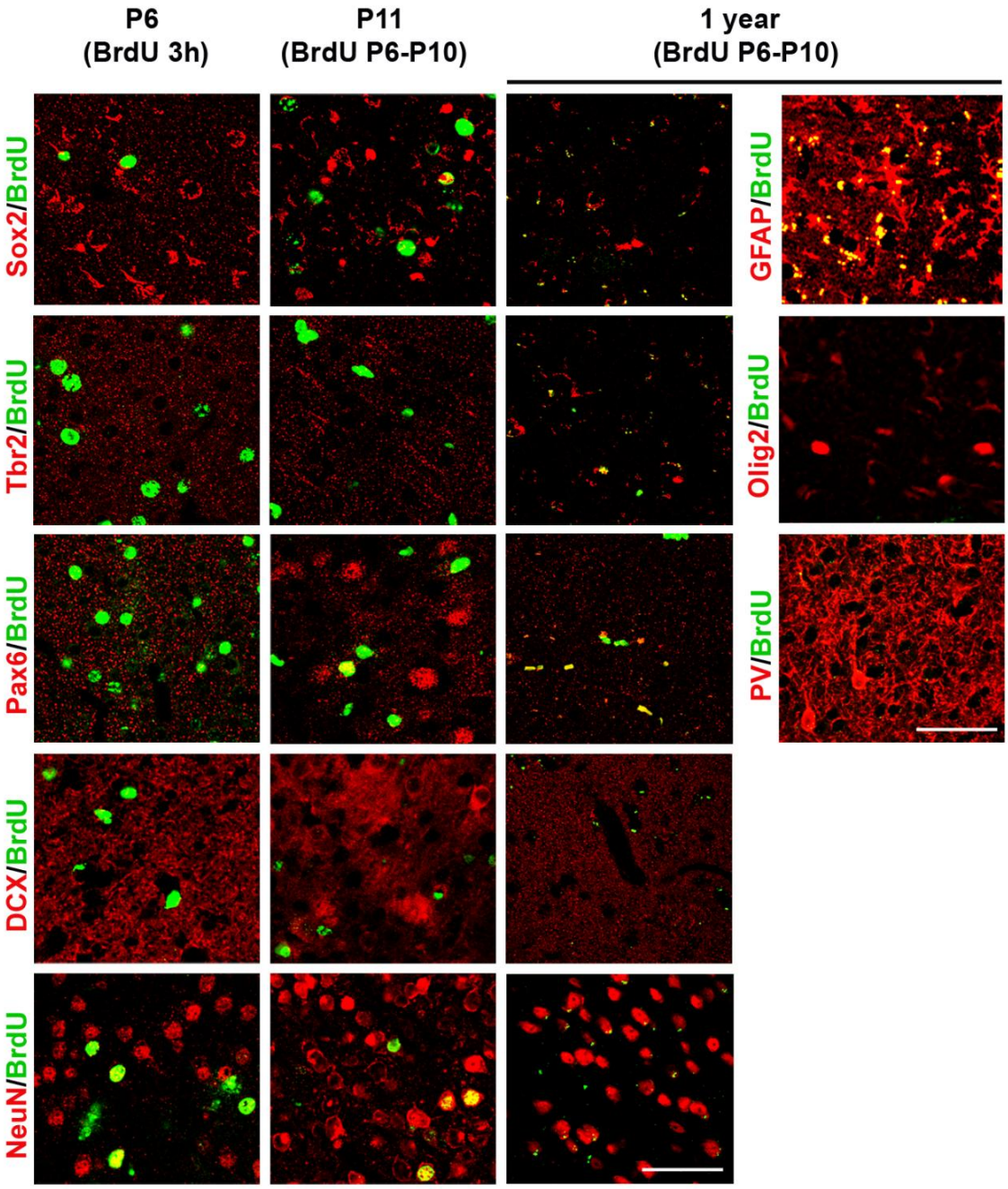

Figure R-46. BrdU incorporation and survival in the intact left hemisphere of mice implanted in the right hemisphere with radial fiber scaffolds. BrdU was injected for five consecutive days (from P6 to P10) in P4 mice implanted with radially aligned fiber scaffolds and analyzed 3 h, 2 months, and 1 year after the first BrdU injection. Confocal images show double immunostaining for BrdU in green, and Sox2 (stem cell marker), Tbr2 (neuron-restricted progenitor), Pax6 (bipotential progenitor), DCX (immature neurons), NeuN (neurons), GFAP (astroglial marker), Olig-2 (oligodendroglial marker) and parvalbumin (GABAergic neurons marker) in red. Scale bars: 20 µm.

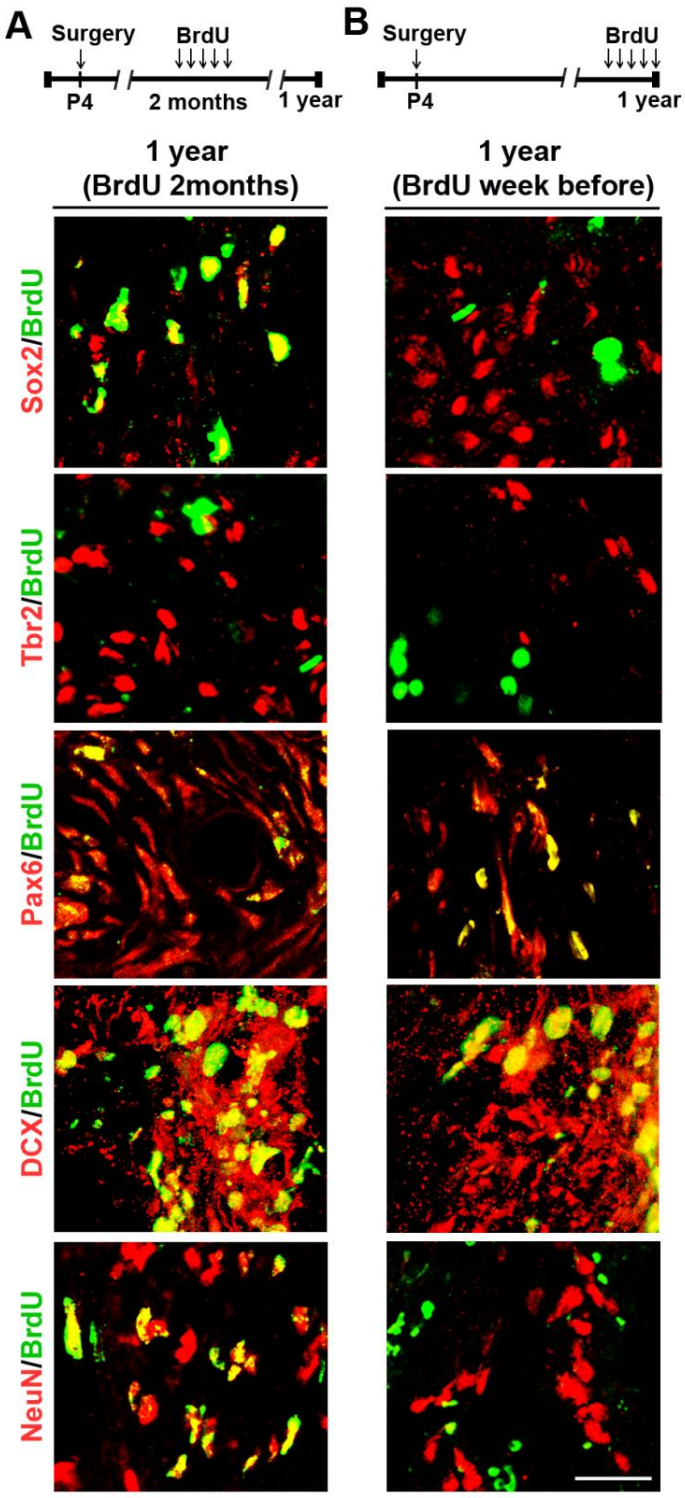

Figure R-47. BrdU incorporation into NSC/progenitors and neurons inside radial scaffolds at long times. A. BrdU was injected intraperitoneally for 5 consecutive days 2 months after implantation and analyzed at 1 year. **B**. BrdU was injected intraperitoneally for 5 consecutive days 1 year after implantation and analyzed the day after the last injection. BrdU immunostaining (green) and colocalization inside the implant with molecular markers (red) of stem cells (Sox2), neuron-restricted progenitors (Tbr2), bipotential progenitors (Pax6), and neurons (DCX, NeuN). Scale bar: 20 μm.

3.6 Newly generated neurons in radial scaffolds became anatomically integrated into functional circuits

Implant integration into the surrounding tissue was assessed by MRI in a group of mice (n=8). Six to 12 months after implantation, the meninges and skull had regenerated and the scaffold limits were clearly visible in the right motor/somatosensory cortex. Signal intensity inside the implant was similar to that in the surrounding tissue (Fig. R-48A). Unfortunately, the system's limits of resolution in mice did not permit functional MRI. Instead, integration of the newly generated neurons inside the radial scaffold into brain circuitry was analyzed by retrograde tracing of commissural neurons 1 year after implantation. Cholera toxin subunit B conjugated to Alexa fluor (AF-CTB) was injected into the contralateral hemispheres of mice with implanted radial scaffolds (Fig. R-48B) and of uninjured control animals. Four days after AF-CTB injection, retrograde transport of the tracer through the corpus callosum was evident, as was the staining of two bands of pyramidal neurons in layers VI–V and II-III in control animals (Fig. R-48C, E). Many retrogradely labeled pyramidal neurons were also found inside radial scaffolds, with a distribution that suggested a certain degree of anatomical and functional laminar organization within the regenerated tissue (Fig. R-48D, F), as inside the scaffold they roughly reproduced the normal bilaminar distribution of callosal neurons (Fame et al., 2011).

The presence of a functional synaptic machinery in the regenerated tissue was confirmed by the immunohistochemical detection of postsynaptic density protein 95 (PSD95) and synaptosomal-associated protein 25 (SNAP25). Both proteins were expressed in neurons inside the regenerated tissue and their distribution resembled that in the adult cortex (Fig. R-48G, H).

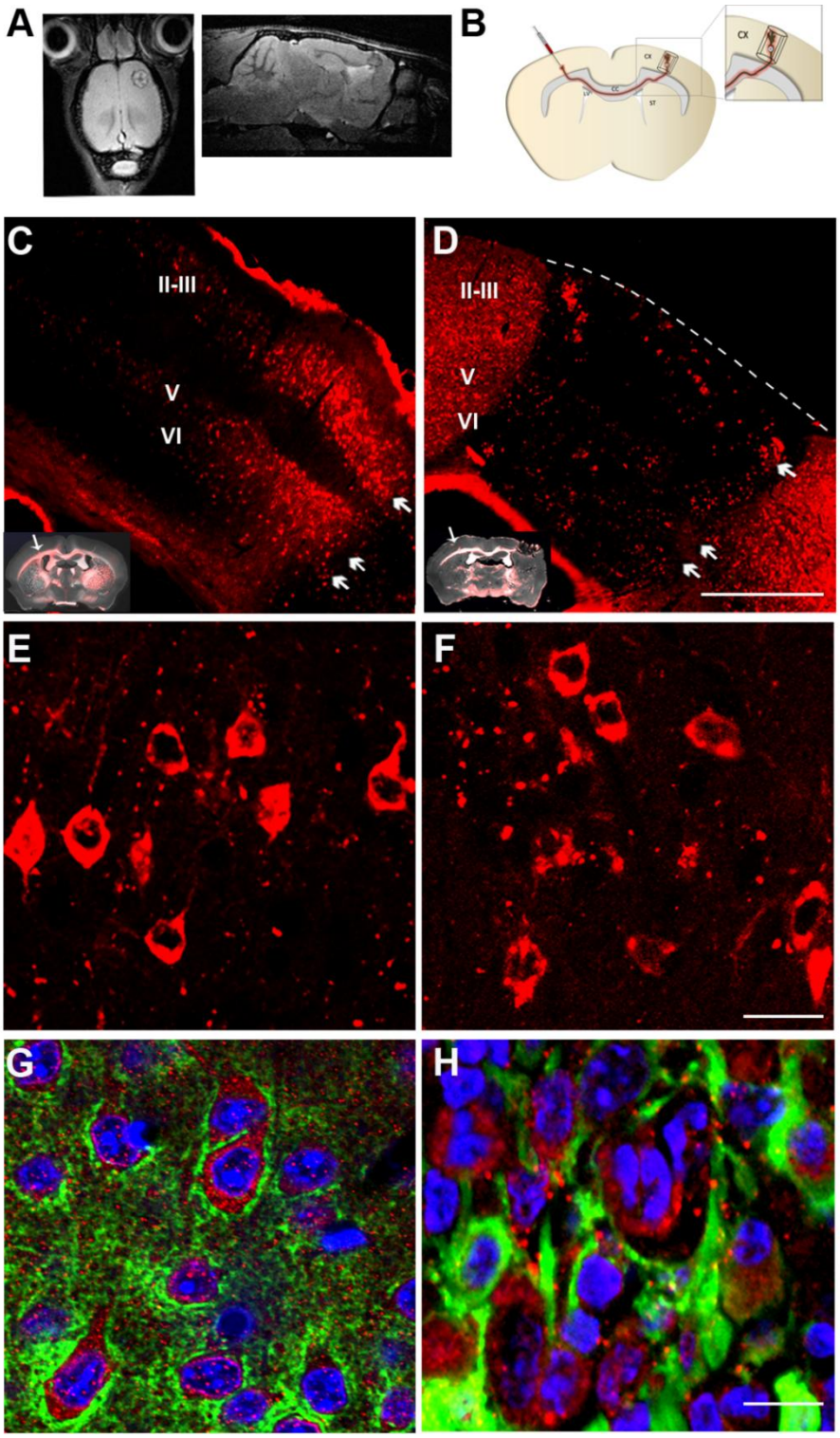

Figure R-48. Functional integration of newly generated neurons in radial scaffolds. A. Horizontal and parasagittal MRI showing the integration of a radial scaffold 1 year after implantation. **B.** Diagram of the retrograde tracing of commissural neurons following the injection of AF-CBT in the contralateral cortex of the radial scaffold implant. **C-D.** Distribution of AF-CTB labeled commissural neurons (arrows) **C.** in the contralateral hemisphere of an uninjured control brain and **D**. inside a radial implant. Insets in **(C)** and **(D)** are superimposed images of differential interference contrast and fluorescence (red), showing the exact area of AF-CTB injection (arrow). **E-F.** Magnification showing retrograde-labeled pyramidal neurons **E.** in the contralateral hemisphere to the injection in a control **F.** and in an implanted brain. **G-H.** Presynaptic SNAP25 (green) and postsynaptic PSD95 (red) labeling in **G.** control cortex

and **H.** inside a radial scaffold 1 year after implantation. Cortical layers II–III, V, and VI. Scale bars: 250 μm **(C, D)**; 20 μm **(E, F);** 10 μm **(G, H)**.

3.7 Radially aligned fiber scaffolds implanted into adult brains

To analyze the regenerative capacity of adult brain, radially aligned fiber scaffolds were implanted in the somatosensory cortex of 3 months-old mice. After the aspiration of a 1mm^3 cylindrical piece, tubes were immediately implanted in the same conditions as described for P4 mice. Control lesion and implanted animals were analyzed 7 days and 3 months after surgery.

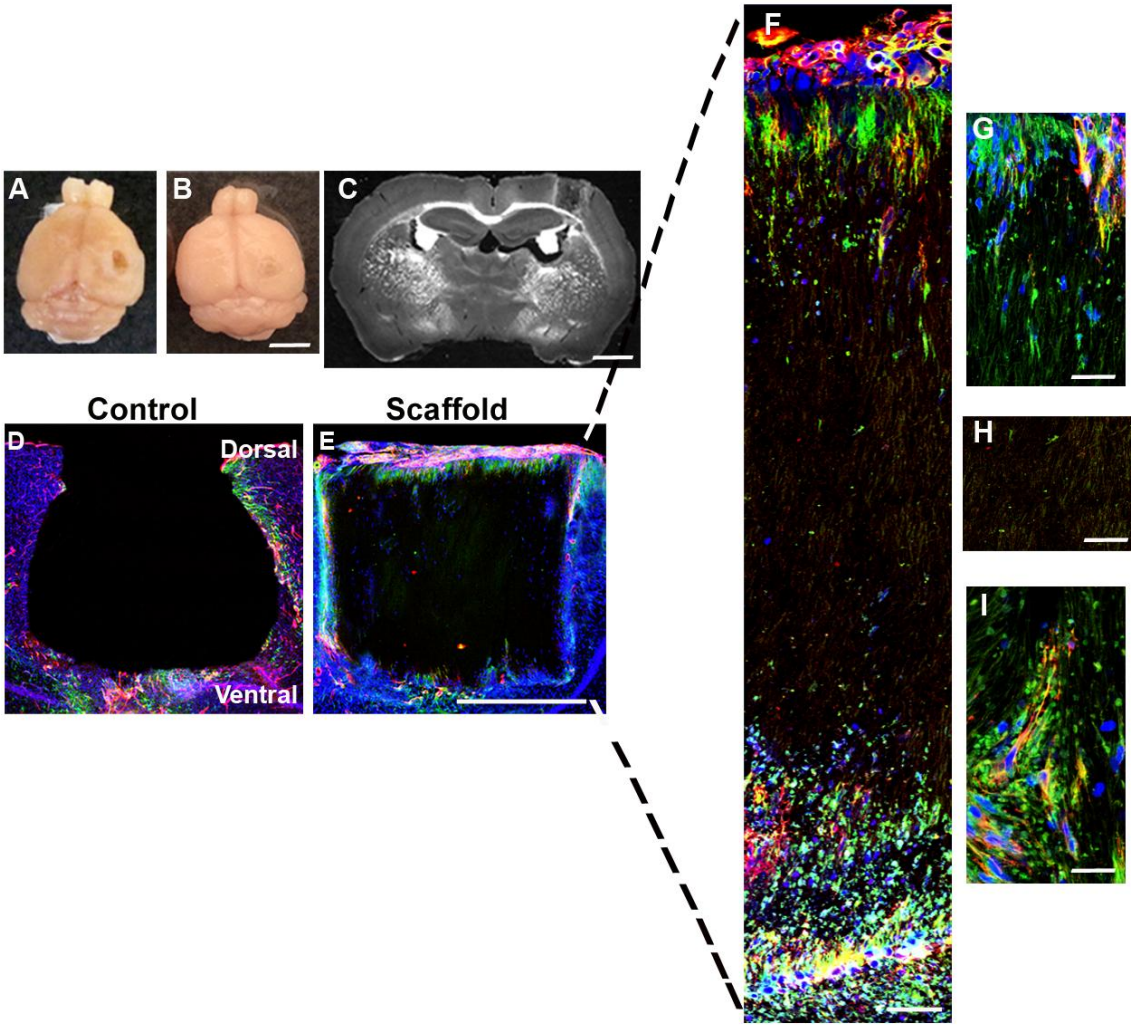

Figure R-49. Adult brain regeneration 1 week after surgery. Macroscopic view of adult brains with **A.** control lesion and **B.** radial scaffold 1 week after implantation. **C**. Bright field coronal section showing the material. **D-E.** Magnification showing Nestin$^+$ radial glia (green) and laminin$^+$ basal lamina (red) **(D)** around control lesion and **(E)** in the radial scaffold. **F-I** Nestin$^+$ radial glia (green) and laminin$^+$ basal lamina (red) surrounding the scaffold and following the radial organization of nanofibers. Nuclei were stained with Topro (blue). Scale bars: 1mm **(A, B)**; 500μm **(C, D, E)**; 50μm **(F)**; 25μm **(H)**.

After 1 week, radially aligned fiber scaffolds refilled the cavity and became incorporated into the surrounding parenchyma (Fig. R-49B, C, E) as occurred when scaffolds were implanted at

P4 mice. The control brains remained empty with some Nestin^{+} cells surrounding the hole (Fig. R-49A, D).By contrast, in aligned fiber scaffolds, Nestin^{+} radial glia cells and laminin, an adhesive extracellular matrix glycoprotein mainly secreted by glial and endothelial cells, dramatically increased basically around the scaffold entering into it, following the fiber orientation (Fig. R-49F-I).

After 3 months, in control lesion, the hole remained intact with no signs of regeneration and radial glial cells stained with Nestin were completely absent (Fig. R-50A, C). Concerning radially aligned fiber scaffolds (Fig. R-50B), Nestin^{+} radial glia increased around and inside the aligned scaffolds, as did laminin, forming neurovascular bridges reconnecting basal and meningeal zones (Fig R-50D and 51A).

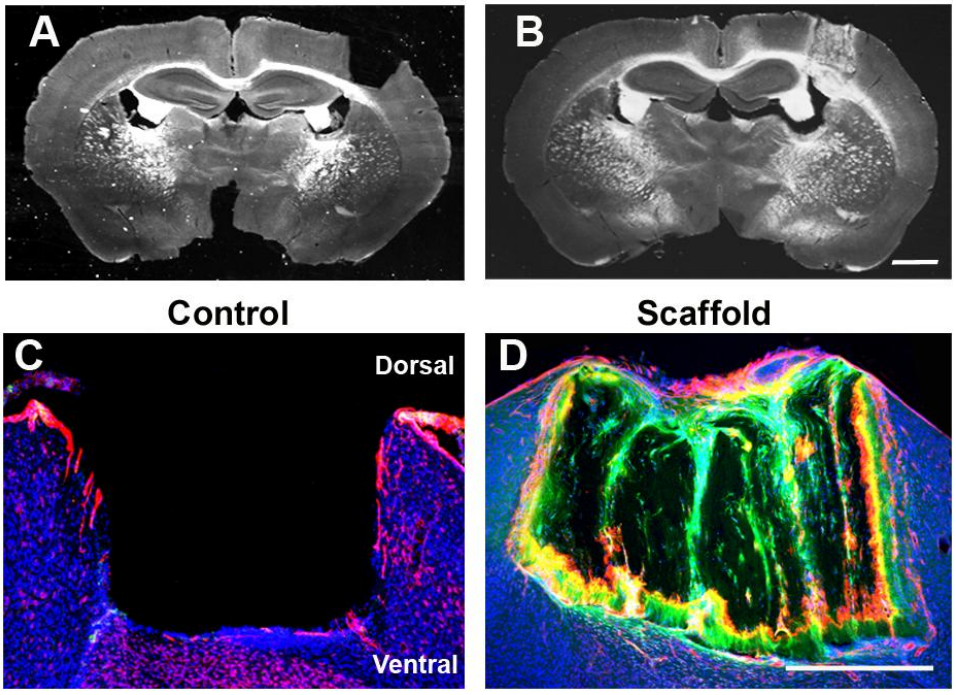

Figure R-50. Adult brain regeneration 3 months after surgery. Bright field coronal section showing **A.** the control lesion and **B.** the implanted radial scaffold in adult. Confocal images showing Nestin^{+} radial glia (green) and laminin^{+} basal lamina (red) **C.** around a control lesion and **D.** in the radial scaffold. Nuclei were stained with Topro (blue). Scale bars: 1mm **(A, B)**; 500µm **(C, D).**

The regeneration of neurogenic niches inside radial scaffolds was also analyzed. 3 months after surgery, the distribution of the neuronal restricted progenitor transcription factor Tbr2 (Fig. R-51B), the neuronal marker NeuN (Fig. R-51C) and Ki67^{+} cycling cells (Fig. R-51D) were detected in close association with blood vessels (CD31^{+}). The results obtained after 3 months were similar to that observed 1 week after radial scaffold implantation in postnatal animals.

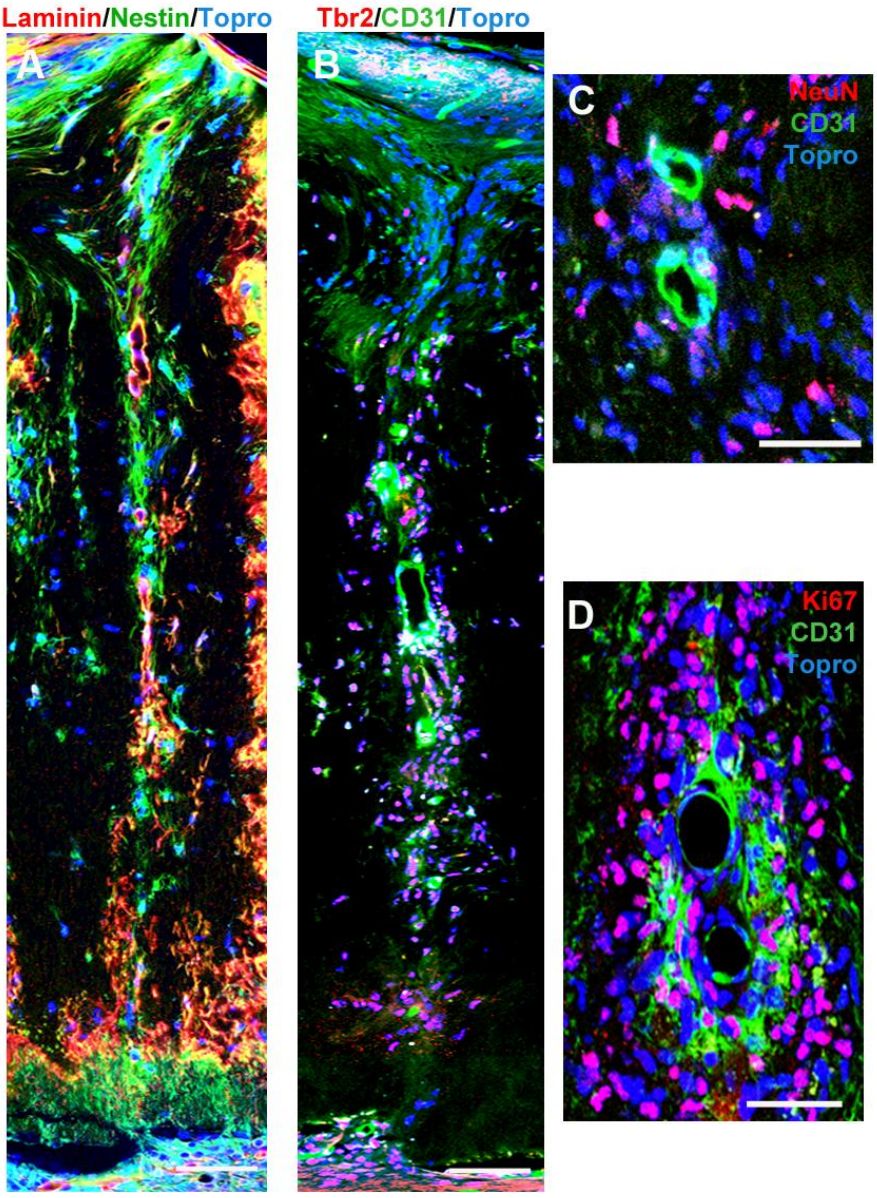

Figure R-51. Neurovascular bridges in the adult brain 3 months after surgery. Confocal images of **A.** of Nestin^{+} radial glia (green) and laminin^{+} basal lamina (red), showing a neurovascular bridge reconnecting basal and meningeal zones. **B.** CD31^{+} endothelial cells (green) surrounded by Tbr2 neural progenitors (red) following the radial organization of the nanofibers. **C, D**. High magnification showing CD31^{+} endothelial cells (green) surrounded by **C.** NeuN^{+} neurons (red) and **D.** by Ki67^{+} cycling progenitors (red). Nuclei were stained with Topro (blue). Scale bars: 40µm **(A, B)**; 20µm **(C, D).**

Although more experiments are required, these results showed that radially aligned PLA70/30 nanofibers recapitulate some of the organizational aspects of the embryonic NSC niche properties promoting neurogenesis and vascularization also when implanted into the adult lesioned brain.

DISCUSSION

The regenerative capacity of a tissue relies on the maintenance of a population of stem cells which self-renew and produce a committed daughter cell able to differentiate. Those properties are regulated by the niche, a dynamic microenvironment in which stem cells reside. The CNS has only limited capacity for self-repair after injury despite the presence of NSC, therefore a fuller understanding is needed of the physical nature of the NSC niches and the molecular mechanisms that govern them (Kazanis, 2012; Miller and Gauthier-Fisher, 2009). Recent approaches have focused on the use of biomaterials to investigate what controls NSC fate. Polyesters like polyglycolic, polylactic or polylactic-co-glicolic acids have been used for CNS implantation, and parameters like mechanical stiffness, surface properties and degradation kinetics are important to control cell behavior (Discher et al., 2009; Keung et al., 2010; Vazin and Schaffer, 2010). Although hydrophobicity, slow degradation rates and release of acidic products from PLA based scaffolds have been reported as limitations for biomedical applications (Kim et al., 2003), the main findings of this thesis show that;

PLA obtained from combination of L/L- and D/L-lactic acid in a 70/30 ratio (PLA30/70) has specific effects on the adhesion, growth and differentiation of neurons, glia, and progenitor cells without the need for activation or protein coatings. PLA70/30 is a truly biodegradable polymer derived from lactic acid, and the initial L/DL distribution determines the potential for PLA crystallization (Auras et al., 2004). The two types of films (PLA95/5 and PLA70/30) analyzed here supported glial cell growth, However, PLA70/30 also allowed neuronal adhesion and growth. These films have similar hydrophobicity, although they differ in crystallinity, stiffness, charge, and in degradation rate. Therefore, the better performance of PLA70/30 was probably related to its more amorphous, soft and elastic characteristics as a result of the lower proportion of the L isomer. CNS tissue elasticity is below 1 KPa, and soft substrates direct stem cell differentiation to a neuronal lineage (Discher et al., 2009; Engler et al., 2006; Keung et al., 2010). PLA70/30 elasticity in dry state was of a few MPa while PLA95/5 has a supra physiological stiffness in the range of GPa. Due to its more amorphous structure, PLA70/30 started to degrade when immersed in culture medium at physiological temperature unlike PLA95/5, which presented no significant degradation throughout the study. Although both PLA materials were initially hydrophobic, PLA70/30 becomes hydrophilic and more negatively charged as degradation proceeds. Hence, degradation of polyesters like PLA increase the exposure of free carboxyl (-COOH) groups which increases their negative charge and hydrophilicity (Atthoff and Hilborn, 2007), modifications that favor the interaction with matrix proteins and cell adhesion (Ren et al., 2009).

Another question is the effect of PLA70/30 on glial and neuronal dedifferentiation *in vitro*. Glial cells grown on PLA70/30 films tend to express more immature and proliferation markers such as Nestin, Ki67 and PH3 than those grown in control conditions or on PLA95/5 (Table D-1). When topology was introduced in PLA70/30 (nanofibers), the immaturity of glial cells culture

significantly increased respect to that observed on films, founding all markers mentioned above and also Pax6 positive cells, a marker expressed by radial glia cell progenitors (Englund et al., 2005b) (Table D-1). This undifferentiated and proliferative glial phenotype resembles that observed when glial cells were grown on textured PMMA films (Mattotti et al., 2012). Although PLA70/30 is biodegradable and PMMA is not, both polymers have similar initial hydrophobicity and negative charge (Mattotti et al., 2012), properties that have been related with low cell adhesion and increased proliferation (Biran et al., 1999). These results support the idea that a loose adhesion may be a requisite for maintaining NSC competence and proliferative capacity.

	Control (Glass/TCP)	PLA95/5 Films	PLA70/30 Films	Random 70/30 Fibers	Aligned 70/30 Fibers
Glial Culture	GFAP BLbP Nestin (-)	GFAP BLbP Nestin (-)	GFAP BLbP Nestin Ki67/PH3	GFAP BLBP Nestin (+) Ki67 Pax6 (-)	GFAP BLBP Nestin Ki67 Pax6 (+)
Neuronal Culture	Tuj-1 GFAP (-) Nestin (-) MCT2 (-)	Tuj-1 -- -- --	Tuj-1 -- -- MCT2 Tbr2 Pax6 Ki67	Tuj-1(-) -- -- MCT2/GPR81 Tbr2 -- Ki67 Sox2	Tuj-1(-) -- -- MCT2/GPR81 Tbr2 -- Ki67 Sox2

Grey: Decrease
Red : Increase
(-): Low expression
(+): High expression
-- : No expression

Table D-1. Expression of glial and neuronal markers in neural cultures grown on different substrates during 5 days *in vitro*.

A part from that, the orientation of PLA fibers plays an important role in cell behavior. On aligned fibers glial cells adopted a bipolar shape and induced a high expression of Pax6, while on random nanofibers glial cells showed a ramified morphology and there was a reduction of Pax6 expression (Table D-1). Aligned fibers conformation allows bipolar glial cells to invade the entire thickness of the scaffold. In contrast, in random fibers multipolar glial cells could not access to the entire mesh of fibers. This different invasive behavior might relay in the different

cell shape induced by fiber topology and probably also in differences in scaffold's porosity and tortuosity, although these parameters were not possible to measure in this work.

On the other hand, embryonic neurons grown on PLA70/30 films also maintained an immature phenotype. An unexpected but exciting observation was the robust maintenance of the bipotential Pax6 and neuronal restricted and/or early post mitotic Tbr2 progenitor pools (Englund et al., 2005b) in neuronal cultures grown on PLA70/30 films (Table D-1). In these cultures, the number of neurons increased with time while the number of $Ki67^+$ progenitors was similar throughout the time of culture. Quantitative analysis showed in chapter 1, revealed that this could be explained if each $Ki67^+$ progenitor divided asymmetrically once, suggesting that in PLA70/30 a neuronal progenitor pool with self-renewing capacity was preserved throughout the culture period. When neurons were cultured on PLA70/30 fibers, the expression of neural progenitor markers also increased as occurred in glial cell cultures. Neuronal cultures in PLA fibers maintained $Tbr2^+$ cells and for the first time we observed high expression of $Sox2^+$ cells; a marker of neural stem cell populations with self-renewing capacity (Table D-1). $Sox2^+$ cells with NSC characteristics were rarely seen in neuronal cultures *in vitro* in control conditions. While $Tbr2^+$ progenitors are induced by a flat substrate of PLA, $Sox2^+$ progenitors/NSC are induced when the same PLA is molded as a 3D mesh of nanofibers; an organization that mimics the three dimensional ECM and the embryonic niche (Table D-1). The topology of fibers plays also an important role in neuronal behavior. As in glial cells cultures, neurons cultured in aligned fibers invaded the scaffold using the mesh of nanofibers to extend their axons. However neurons cultured in random fibers could grow only in the surface of the scaffold.

An important property of PLA substrates is their release of active metabolites. PLA essentially degrades to L-lactic acid, a terminal metabolite of anaerobic glycolysis, and to a lesser degree D-lactic acid that is not metabolizable (Cassady et al., 2001). Metabolism is an important indicator of cell function, since it shifts together with differentiation, growth, and anabolic capacities. For example, undifferentiated stem cells preferentially rely on glycolysis whereas differentiated cells up-regulate oxidative metabolism to support their anabolic or biological potential (Facucho-Oliveira and St John, 2009; Ivanovic, 2009; Simsek et al., 2010). Traditionally, L-lactate was considered to be a metabolite that was toxic for brain cells and should be evacuated from the brain parenchyma (Dienel and Hertz, 2001). However, in the last 50 years it has been demonstrated that L-lactate represents an alternative oxidative substrate for neurons *in vitro* and in *vivo* (Itoh et al., 2003; Pellerin and Magistretti, 2003). L-lactate is mainly released by glial cells and, when present together with glucose, it is largely preferred to glucose as an oxidative energy substrate by neurons in physiological conditions (Bouzier-Sore et al., 2003; Itoh et al., 2003; Ivanov et al., 2011). Moreover, in the developing brain, NSC/radial glia progenitors are in charge of sourcing the various differentiated cell types (Rowitch and Kriegstein, 2010). Several studies have shown that the highly hypoxic

environment characteristic of the stem cell and NSC niche favors glycolysis and lactate production at sites of unrestricted progenitor cell proliferation (Mohyeldin et al., 2010). As NSCs mature, their specific lineage restriction is likely to be accompanied by a shift in their metabolic needs (De Filippis and Delia, 2011; Goldman and Chen, 2011; Stubbs et al., 2009). This shift might explain the role of L-lactate, to be a critical substrate of the developing brain (Medina and Tabernero, 2005; Rinholm et al., 2011). Indeed, the results provided in this thesis evidence of a lactate-restricted metabolic requirement to fulfill the biosynthetic needs for neuronal-restricted progenitors (summarized in Fig. D-1).

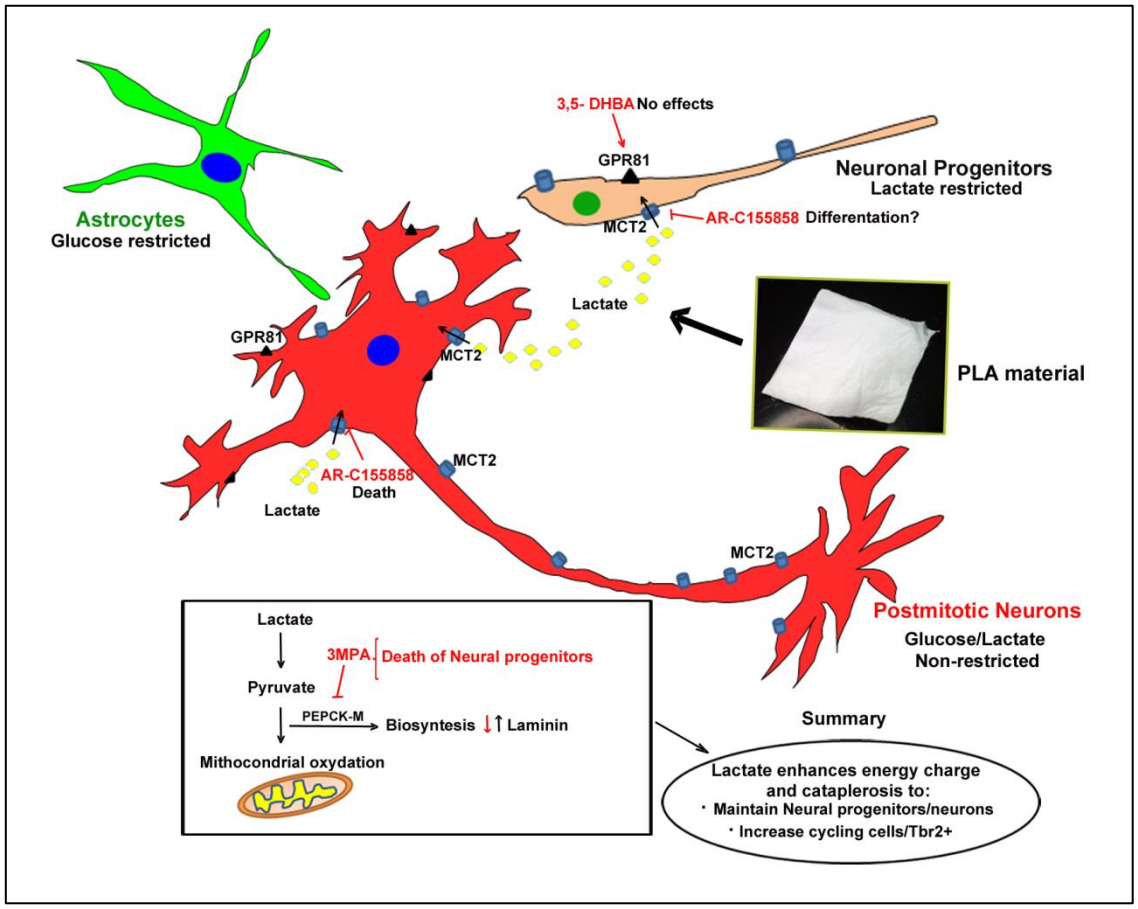

Figure D-1. Schematic representation of the proposed effect of lactate in neuronal and progenitor cells.

Aerobic glycolysis is a functional marker of the specialized phenotype of dividing cells, whether they arise from physiologic tissue components (i.e., stem cells or endothelial cells) or after pathologic dedifferentiation (tumor cells) (De Bock et al., 2013; Suda et al., 2011; Takubo et al., 2013). This seemingly inefficient, partial oxidation of glucose nonetheless provides both a rapid source of energy and the anabolic building blocks to support cell division, but it reduces the cellular capacity to integrate into a functional, complex tissue. The same can be said for NSC metabolism (Rafalski and Brunet, 2011; Yamasaki et al., 2001) and for radial glia

progenitors and astrocytes, which are also essentially glycolytic (Tsacopoulos and Magistretti, 1996; Yamasaki et al., 2001).

By contrast, in this thesis we showed that when L-lactate was directly added to the neuronal culture medium grown on tissue culture plate (TCP), the presence of neuronal restricted $Tbr2^+$ cells, but not radial glia cells or neuronal stem cell progenitors ($Pax6^+$ and $Sox2^+$) increased (Table D-2). These results suggested the possibility that the local regulation of lactate availability in the NSC niche may be an important issue to support neuronal progenitor physiology. Moreover, Tbr2 neuronal-restricted progenitors have a highly oxidative metabolic profile that is entirely dependent on lactate as a carbon source. The neuronal progenitor cells examined in neuronal cultures treated with L-lactate underwent a single round of cell division during their 5 days *in vitro,* which can produce two progenitors or one progenitor and one neuron depending on the absence or present of glucose. However, in the presence of glucose, lactate withdrawal induces progenitor terminal division and differentiation to a neuronal fate.

Glass/ TCP	Glucose(Control)	Glucose+Lactate	Lactate
Glial Culture	GFAP BLbP GLAST Nestin (-)	GFAP BLbP GLAST Nestin (-)	--------
Neuronal Culture	Tuj-1 GFAP (-) Nestin (-) MCT2 (-) PSD95	Tuj-1 GFAP (-) Nestin(-) MCT2/GPR81 PSD95 Tbr2 Ki67	Tuj-1 GFAP -- MCT2/GPR81 PSD95 Tbr2 Ki67

Grey: Decrease
Red : Increase
(-): Low expression
-- : No expression
---------: Death

Table D-2. Expression of glial and neuronal markers in neural cultures treated with glucose or/and lactate grown on glass/TCP during 5 days *in vitro*.

On the other hand, when L-lactate was directly added to the glial culture medium, glial cells grown on TCP, hardly survive in glucose-free lactate medium, while when grown on PLA they reduced its glucose consumption, indicating a change in their metabolism. The somewhat deleterious effect of L-lactate on glial cultures may be related to its effect on glycolytic metabolism rather than on pH acidification, as mild acidosis has been described as neuroprotective (Tombaugh and Sapolsky, 1990). Exposure to mM L-lactate inhibits glycolysis in glial cells, but does not have a significant effect in neurons whose metabolism is essentially oxidative (Sotelo-Hitschfeld et al., 2012). This inhibitory feedback may also account for the

reduction of lactate release by astrocytes when 4mM L-lactate was added to the culture medium but not when astrocytes were cultured on PLA70/30 films or fibers, which lactate release was in the range of 0.05 μM – 1 mM.

Taken together, these results suggest that PLA mechanical properties have a role in maintain bipotential and glial progenitors (Pax6 and Nestin) survival giving a physical environment to growth (Table D-1). L-lactate, the degradation product of PLA scaffolds, is used as a metabolic substrate to preserved the self-renewal of neurogenic progenitors (Tbr2), maintaining the immaturity of neuronal cultures *in vitro*. Finally, the introduction of the topology into PLA scaffolds induces high expression of the NSC marker Sox2.

Another point is the possibility of shuttling lactate between brain cell types, determined by the expression of specific transporters exhibiting different kinetics. Indeed, modeling studies have demonstrated a key role for monocarboxylate transporters (MCT) in regulating lactate influx and efflux (Aubert et al., 2005). MCT1 is expressed mainly in the brain blood barrier and astrocytes and MCT2 in neurons (Pierre and Pellerin, 2005). Energy substrate utilization may be limited by L-lactate receptor GPR81, the transport capacity, and the affinity for D- and L-lactate, which is much higher for MCT2 than for MCT1 (K_m of 0.7mM and 3 to 5mM respectively) suggesting that neurons may use lactate more efficiently than glial cells (Simpson et al., 2007). In this regard, MCT2 overexpression increased neuronal lactate transport and utilization (Pierre et al., 2009). In our results, MCT2 overexpression increased in neuronal cultures grown on PLA70/30 substrates (Table D-1) and in L-lactate treatments (Table D-2). The direct determination of the role of lactate transporters MCT1/2 and receptor GPR81 on neuronal and progenitor's survival on PLA70/30 fibers or in L-Lactate treatments was evaluated by pharmacological approaches. The addition of MCT1/2 inhibitor or an agonist of GPR81 answer the question whether neuronal survival and progenitor maintenance required lactate intake only through monocarboxylate transporters and not through the activation of the GPR81 lactate receptor. Moreover, the inhibition of the mitochondrial enzyme PEPCK-M by 3MPA, blocking lactate metabolic use, corroborates the utilization of L-lactate by neuronal progenitors (Fig. D-1). Our results indicate that, the effects of neuronal survival and progenitor self-renewal are apparently mediated by the cellular entry of L-lactate through MCT1/2 receptors and it metabolism represented by PEPCK-M catalytic activity.

PEPCK activity is present in the cytosol (PEPCK-C) and in mitochondria (PEPCK-M), reflecting the expression of two different nuclear genes, PCK1 and PCK2, respectively. As we mentioned in chapter 2, in neural progenitors only the mitochondrial isoform, PEPCK-M, was detected, with no measurable cytosolic protein found. PEPCK-M catalyzes the GTP-dependent decarboxylation of mitochondrial oxaloacetate to produce PEP, which is then exported into the

cytosol where it feeds the reverse glycolytic pathway (Mendez-Lucas et al., 2013; Stark et al., 2009). It is noteworthy that PEPCK-M is the only known pathway that can communicate mitochondrial carbon intermediates directly to the glycolytic pool, because of the irreversible nature of the pyruvate kinase step. We also found that laminin, an integral component of the ECM of neurogenic niches and secreted by neural cells and progenitors, was sensitive to the PEPCK inhibitor 3MPA. We propose that neuronal progenitors have a role in maintaining the ECM of the neurogenic niche and in the secretion of factors necessary for the neurogenic environment.

In vivo, in addition to increase PEPCK-M expression, laminin synthesis and neuronal-restricted Tbr2+ progenitors, lactate also induced an increase in Sox2+ progenitors. These data are in accordance with our results demonstrating the requirement of the NSC niche specific topographical cues for the maintenance of the undifferentiated progenitor's subpopulations.

Taken together, this part of results support the strict dependence of neuronal-restricted progenitors ($Tbr2^{+}$) on lactate metabolism and on the provision of ECM components of the neurogenic niche by the anabolic activity of PEPCK-M. Nevertheless, in the *in vivo* niche, other physical and/or biochemical cues might cooperate with lactate to maintain different progenitor populations.

Moving to *in vivo* applications, PLA70/30 film is not an appropriate material formulation for in vivo implantation as did not allow cell infiltration after a lesion. The addition of three-dimensional patterns mimicking the architecture of the embryonic NSC niches (like electrospun fibers) potentiate PLA70/30 physical and surface properties, allowing cell invasion, driving endogenous astrocytes into a radial glia-like cell progenitor phenotype, sustained neurogenesis and vascularization in vivo.

Several different mechanisms might cooperate in driving the reactivation of neurogenic and angiogenic programs by lactate-releasing PLA nanofiber scaffolds in vivo.

First, the results corroborated that PLA70/30 and L-lactate are required to maintain the metabolism and self-renewal of neurogenic progenitors as we showed in chapter 1 and 2 (Speder et al., 2011) and both induce angiogenesis (Polet and Feron, 2013).

Second, PLA nanofibers are hydrophobic, with the same size, shape, and negative superficial charge as radial glia shafts (Anton et al., 1997; Freire et al., 2004). Accordingly, the surface properties of PLA nanofibers may well be similar to those of negatively charged lipids on the surface of astrocytes and radial glia, controlling the extracellular polymerization of laminin (Freire et al., 2004) that, as we explained before, is an intrinsic component of the extracellular matrix of neurogenic NSC niches (Lathia et al., 2007). Laminin was strongly up-regulated in cells around and inside the scaffold implanted in postnatal and adult animals. It is known that 3D architecture of the cell environment modulates its morphology and differentiation state

(Keung et al., 2010). The appropriate orientation of vascular sprouts and radial glia in the regenerating tissue was only achieved when the topology of the PLA nanofibers reproduced that of embryonic radial glia organization. Consequently, radially aligned electrospun PLA70/30 fibers implanted in postnatal and adult mice cortices reproduce the 3D organization and supportive function of embryonic radial glia and migrating neurons *in vivo*. Random PLA nanofibers did not allow vascular invasion inside the scaffold, demonstrating the relevance of scaffold topology in CNS regeneration. The robust functional vascularization induced by aligned PLDLA nanofibers implanted in cortices contrasts with the poor vascularization reported when aligned PLLA (pure L isomer) microfibers were implanted into the transected spinal cord (Hurtado et al., 2011). The principal difference between the two fiber types is that mismatching of the chains in PLDLA results in less order, less crystallinity, and a higher degree of amorphicity, and therefore, a higher polymer degradation rate. It is known that lactate is a common cue that supports neuronal and NSC/progenitor metabolism (Speder et al., 2011) and induces angiogenesis in the presence of glucose and fluctuating oxygen levels (Polet and Feron, 2013). These results are in agreement with the results discussed in chapter 2, in which the induction of NSC progenitor and laminin expression was associated to lactate injections in the brain cortex. Taken together, these data indicate that topology is necessary but not sufficient for vascularization and that lactate release is also a requirement. Recent studies similarly demonstrated that lactate-releasing radial glia are essential in guiding and stabilizing the nascent brain vascular network (Ma et al., 2013). Interactions between laminin and its receptors in vascular cells, NSCs/precursors, and migrating neuroblasts are thought to regulate NSC/precursor activation and cell migration (Belvindrah et al., 2007; Kazanis et al., 2010; Loulier et al., 2009). Laminin deposition around PLA fibers might also help in directing the formation of endothelial sprouts and the stabilization of new blood vessels (Simon-Assmann et al., 2011) that direct radial glial cells migration and the formation of neurovascular bridges in postnatal and adults animals. However, in adults the formation of these bridges required longer times. Despite the presence of endogenous niche with an active angiogenic support, in the adult brain, it is recognized that intrinsic “self-repair” activity after an injury is currently insignificant (Monje et al., 2002). This poor regenerative ability in adults may be because of the limited number and restricted location of native NSCs niches, and/or limitations imposed by the surrounding microenvironment, which may not be supportive or instructive at all for neuronal regeneration and vascularization (Saha et al., 2012).

On the other hand, glial and immune responses after a lesion contribute to tissue repair by limiting and resolving blood extravasations and promoting neurogenesis from NSC (Anton et al., 1997; Magavi et al., 2000). PLA scaffolds might also favor inflammation resolution by recruiting the $CX3CR1^{+}$-resolving macrophages (Shechter et al., 2013).

Another important question is the original lineage of the activated neuronal progenitors. BrdU analyses indicated that the newly generated cells comprise a heterogeneous population of radial glia (Pax6), NSCs (Sox2), intermediate progenitors (Tbr2), neurons (NeuN and PV), glial cells (GFAP) and oligodendrocyte progenitors (Olig2). The observed temporal changes in progenitor pool activation and in the neuronal and glial types that incorporated BrdU suggested that the contributions of the different progenitor types to neurogenesis differed throughout the life span of the implant. Neurogenic radial glia progenitors are a constant in embryonic and adult neurogenic niches (Tanaka and Ferretti, 2009; Weissman et al., 2003). In the newly lesioned brain, activated SVZ progenitors generate protective astrogenesis (Benner et al., 2013) and, to a much lesser extent, give rise to neurons that migrate and integrate into the subjacent cortex (Covey et al., 2010; Magavi et al., 2000; Saha et al., 2013). In our implants in postnatal and adult mice, substantial vascular and progenitor invasion occurred from the meningeal and lateral sides; however, tissue regeneration was considerably reduced when the entire VZ/SVZ was surgically destroyed (data not shown), suggesting that these zones are an important but not exclusive progenitor source. In addition, direct dedifferentiation of mature glia into neurogenic progenitors has been described after Sox2 transfection (Niu et al., 2013) and in response to extracellular cues (Robel et al., 2011). Although the exact progenitor source of the newly generated neurons and glial cells remains unclear, our data suggest that progenitors with multiple origins and different time-dependent activation contributed to brain tissue regeneration in the radial PLA nanofiber scaffolds. A scheme summarizing neural cell populations at 1 week and 1-year after surgery inside radial aligned PLA fiber scaffolds was represented in Fig. D-2.

The newly generated neurons were also functional, integrating into brain circuitry and establishing synaptic contacts, as demonstrated by retrograde AF-CTB labeling and the expression of pre- and postsynaptic proteins 1-year post implantation.

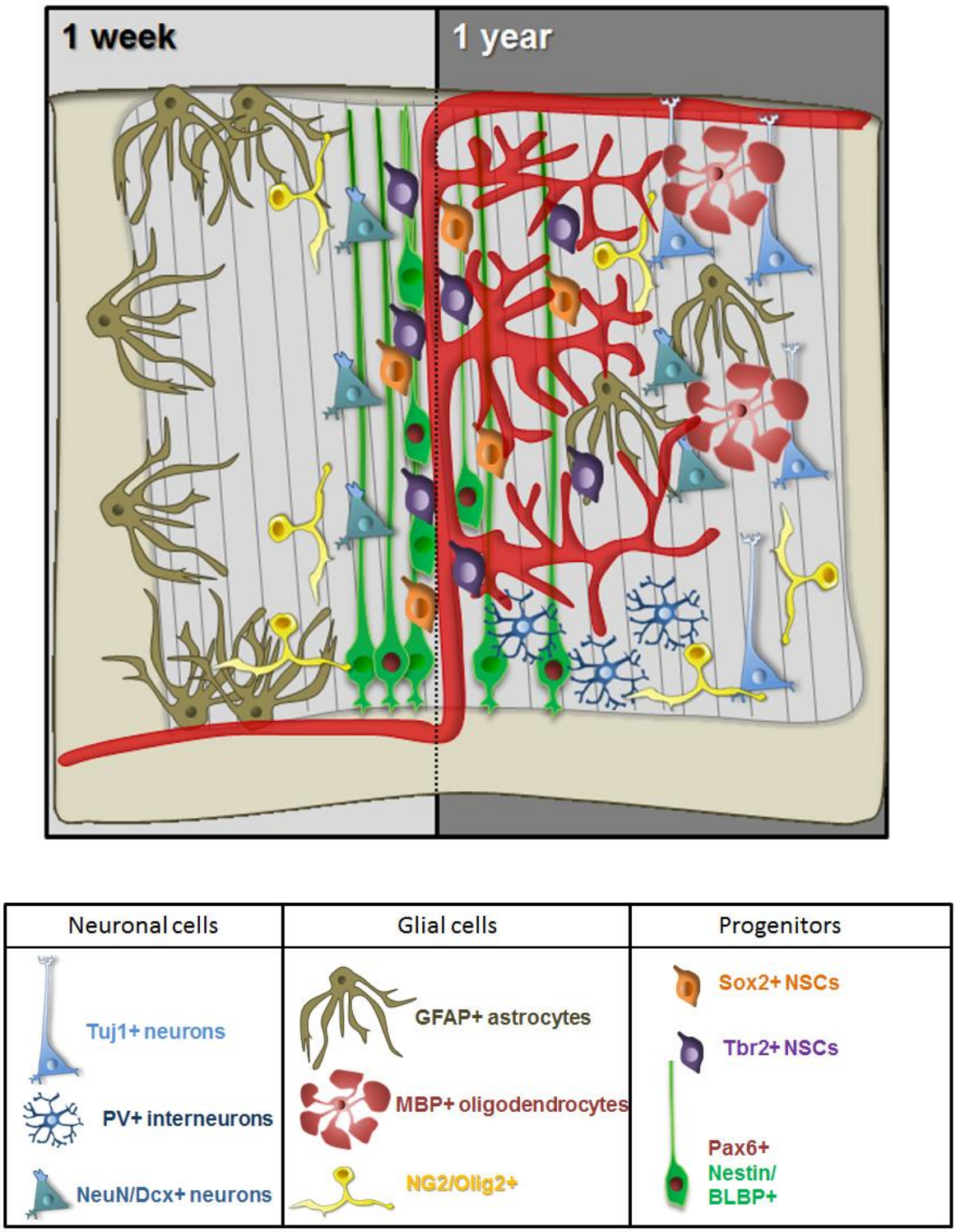

Figure D-2. Schematic representation of neural cell populations 1 week and 1 year after radially aligned PLA scaffold implantation.

Some limitations have been found using electrospun PLA scaffolds during the *in vivo* experiments. First of all, the "low" degradation rate of the scaffold made that at long time points *in vivo* the material became crystalline reducing it degradation rate and probably cell infiltration. The long term material presence and consequently a lactate release maintain the immaturity of neural cell populations inside the scaffold during more than one year in brain cortices, causing a delay in cell maturation. In the future, new formulations of PLDLA will be taken into account to help cell maturation and infiltration inside the scaffold. Another question to solve is the poor regeneration capacity inside the implant when VZ/SVZ was destroyed surgically. In this sense, it might be necessary to design a scaffold that could reconnect the destroyed VZ/SVZ with the surrounded tissue. In addition, a direct demonstration of the functionality of the regenerated tissue was not possible due to technical limitations of functional MRI in mice and due to mechanical interference of the implanted scaffold with the glass micropipettes required for electrophysiological recordings. Other animal models (rat, mini-pig…) more relevant and closer to human applications will be used in future.

Finally, one of the undesirable associated risks of therapies based on cell reprogramming or dedifferentiation is the induction of neuroglial tumors. This possibility was carefully checked in the implanted animals and neither brain tumors nor the expression of CD133, a molecular marker of glioma-initiating cells (Christensen et al., 2008), was found (data not shown).

Although there is a long way to go before these experiments can be translated to the clinic, our results open new possibilities to understand the regenerative capacity of CNS and open up unexpected and exciting perspectives in the design of cell-free implantable devices. By mimicking embryonic radial glia function and organization, it is possible to induce endogenous CNS regeneration through *in vivo* dedifferentiation induced by biophysical and metabolic cues, with no need for exogenous cells, growth factors or genetic manipulation.

CONCLUSIONS

CONCLUSIONS

1. The mechanical and surface properties of PLA70/30 films and their lactate release, support cortical neural cell adhesion and differentiation while maintaining proliferation and the pools of neuronal and glial progenitor cells *in vitro*.

2. PLDLA70/30 nanofibers support neuronal migration and induce neural stem cells, radial glia and progenitors expressing Sox2, Nestin, Pax6 and Tbr2 respectively, as well as differentiated glial cells and neurons *in vitro*.

3. L-lactate, the metabolically active PLA degradation product, is sufficient to maintain neuronal restricted progenitors (Tbr2), but not neural stem cells (Sox2) and radial glia progenitors (Nestin, Pax6), which required the mechanical and topographical cues of PLA scaffolds.

4. Lactate support of neuronal progenitors and laminin synthesis rely in MCT2-mediated intake and oxidative metabolism through the mitochondrial phosphoenolpyruvate carboxykinase (PEPCK-M) pathway *in vivo* and *in vitro*.

5. Scaffolds consisting of radially aligned electrospun PLA70/30 fibers implanted into brain cortex, release L-lactate, induce robust vascularization, laminin synthesis and sustain the generation of several types of progenitors, neurons and glial cells. The newly generated neurons survive for more than 1 year, express synaptic proteins and integrate into normal brain circuits.

6. Although preliminary, our results support that radial PLA scaffolds reactivate neurovascular niches promoting neurogenesis and vascularization also when implanted into the adult lesioned brain.

7. We propose that cell-free implantable devices based on radial glia biomimetic scaffolds, are a good starting point for the design of future implantable devices that activate resident neurogenic neural stem cells niches and induce vascularization, boosting the central nervous system regenerative response *in situ*.

BIBLIOGRAPHY

Abbott, N. J., Ronnback, L., and Hansson, E. (2006). Astrocyte-endothelial interactions at the blood-brain barrier. Nat Rev Neurosci *7*, 41-53.

Alessandri, B., Gugliotta, M., Levasseur, J. E., and Bullock, M. R. (2009). Lactate and glucose as energy substrate and their role in traumatic brain injury and therapy. Future Neurology *4*, 209-228.

Allen, N. J., and Barres, B. A. (2005). Signaling between glia and neurons: focus on synaptic plasticity. Curr Opin Neurobiol *15*, 542-548.

Allen, N. J., and Barres, B. A. (2009). Neuroscience: Glia - more than just brain glue. Nature *457*, 675-677.

Altman, J. (1969). Autoradiographic and histological studies of postnatal neurogenesis. IV. Cell proliferation and migration in the anterior forebrain, with special reference to persisting neurogenesis in the olfactory bulb. J Comp Neurol *137*, 433-457.

Altman, J., and Das, G. D. (1964). Autoradiographic Examination of the Effects of Enriched Environment on the Rate of Glial Multiplication in the Adult Rat Brain. Nature *204*, 1161-1163.

Alvarez-Buylla, A., and Garcia-Verdugo, J. M. (2002). Neurogenesis in adult subventricular zone. J Neurosci *22*, 629-634.

Alvarez-Buylla, A., Garcia-Verdugo, J. M., and Tramontin, A. D. (2001). A unified hypothesis on the lineage of neural stem cells. Nat Rev Neurosci *2*, 287-293.

Alves, P. M., McKenna, M. C., and Sonnewald, U. (1995). Lactate metabolism in mouse brain astrocytes studied by [13C]NMR spectroscopy. Neuroreport *6*, 2201-2204.

Amariglio, N., Hirshberg, A., Scheithauer, B. W., Cohen, Y., Loewenthal, R., Trakhtenbrot, L., Paz, N., Koren-Michowitz, M., Waldman, D., Leider-Trejo, L., *et al.* (2009). Donor-derived brain tumor following neural stem cell transplantation in an ataxia telangiectasia patient. PLoS Med *6*, e1000029.

Andersen, B. J., and Marmarou, A. (1992). Post-traumatic selective stimulation of glycolysis. Brain Res *585*, 184-189.

Anderson, C. M., and Swanson, R. A. (2000). Astrocyte glutamate transport: review of properties, regulation, and physiological functions. Glia *32*, 1-14.

Anthony, T. E., Klein, C., Fishell, G., and Heintz, N. (2004). Radial glia serve as neuronal progenitors in all regions of the central nervous system. Neuron *41*, 881-890.

Anton, E. S., Marchionni, M. A., Lee, K. F., and Rakic, P. (1997). Role of GGF/neuregulin signaling in interactions between migrating neurons and radial glia in the developing cerebral cortex. Development *124*, 3501-3510.

Arvidsson, A., Collin, T., Kirik, D., Kokaia, Z., and Lindvall, O. (2002). Neuronal replacement from endogenous precursors in the adult brain after stroke. Nat Med *8*, 963-970.

Atthoff, B., and Hilborn, J. (2007). Protein adsorption onto polyester surfaces: is there a need for surface activation? J Biomed Mater Res B Appl Biomater *80*, 121-130.

Aubert, A., Costalat, R., Magistretti, P. J., and Pellerin, L. (2005). Brain lactate kinetics: Modeling evidence for neuronal lactate uptake upon activation. Proc Natl Acad Sci U S A *102*, 16448-16453.

Auras, R., Harte, B., and Selke, S. (2004). An overview of polylactides as packaging materials. Macromol Biosci *4*, 835-864.

Balgude, A. P., Yu, X., Szymanski, A., and Bellamkonda, R. V. (2001). Agarose gel stiffness determines rate of DRG neurite extension in 3D cultures. Biomaterials *22*, 1077-1084.

Bandtlow, C. E., and Schwab, M. E. (2000). NI-35/250/nogo-a: a neurite growth inhibitor restricting structural plasticity and regeneration of nerve fibers in the adult vertebrate CNS. Glia *29*, 175-181.

Banerjee, A., Arha, M., Choudhary, S., Ashton, R. S., Bhatia, S. R., Schaffer, D. V., and Kane, R. S. (2009). The influence of hydrogel modulus on the proliferation and differentiation of encapsulated neural stem cells. Biomaterials *30*, 4695-4699.

Barry, D., and McDermott, K. (2005). Differentiation of radial glia from radial precursor cells and transformation into astrocytes in the developing rat spinal cord. Glia *50*, 187-197.

Baud, O., Fayol, L., Gressens, P., Pellerin, L., Magistretti, P., Evrard, P., and Verney, C. (2003). Perinatal and early postnatal changes in the expression of monocarboxylate transporters MCT1 and MCT2 in the rat forebrain. J Comp Neurol *465*, 445-454.

Beattie, M. S., Bresnahan, J. C., and Lopate, G. (1990). Metamorphosis alters the response to spinal cord transection in Xenopus laevis frogs. J Neurobiol *21*, 1108-1122.

Begley, D. J. (2004). Delivery of therapeutic agents to the central nervous system: the problems and the possibilities. Pharmacol Ther *104*, 29-45.

Belvindrah, R., Graus-Porta, D., Goebbels, S., Nave, K. A., and Muller, U. (2007). Beta1 integrins in radial glia but not in migrating neurons are essential for the formation of cell layers in the cerebral cortex. J Neurosci *27*, 13854-13865.

Benner, E. J., Luciano, D., Jo, R., Abdi, K., Paez-Gonzalez, P., Sheng, H., Warner, D. S., Liu, C., Eroglu, C., and Kuo, C. T. (2013). Protective astrogenesis from the SVZ niche after injury is controlled by Notch modulator Thbs4. Nature *497*, 369-373.

Bentivoglio, M., and Mazzarello, P. (1999). The history of radial glia. Brain Res Bull *49*, 305-315.

Bertrand, N., Castro, D. S., and Guillemot, F. (2002). Proneural genes and the specification of neural cell types. Nat Rev Neurosci *3*, 517-530.

Beschorner, R., Simon, P., Schauer, N., Mittelbronn, M., Schluesener, H. J., Trautmann, K., Dietz, K., and Meyermann, R. (2007). Reactive astrocytes and activated microglial cells express EAAT1, but not EAAT2, reflecting a neuroprotective potential following ischaemia. Histopathology *50*, 897-910.

Bhang, S. H., Lim, J. S., Choi, C. Y., Kwon, Y. K., and Kim, B. S. (2007). The behavior of neural stem cells on biodegradable synthetic polymers. J Biomater Sci Polym Ed *18*, 223-239.

Bhardwaj, R. D., Curtis, M. A., Spalding, K. L., Buchholz, B. A., Fink, D., Bjork-Eriksson, T., Nordborg, C., Gage, F. H., Druid, H., Eriksson, P. S., and Frisen, J. (2006). Neocortical neurogenesis in humans is restricted to development. Proc Natl Acad Sci U S A *103*, 12564-12568.

Binder, D. K., and Scharfman, H. E. (2004). Brain-derived neurotrophic factor. Growth Factors *22*, 123-131.

Biran, R., Noble, M. D., and Tresco, P. A. (1999). Characterization of cortical astrocytes on materials of differing surface chemistry. J Biomed Mater Res *46*, 150-159.

Blasi, P., Giovagnoli, S., Schoubben, A., Ricci, M., and Rossi, C. (2007). Solid lipid nanoparticles for targeted brain drug delivery. Adv Drug Deliv Rev *59*, 454-477.

Bonfanti, L., and Peretto, P. (2007). Radial glial origin of the adult neural stem cells in the subventricular zone. Prog Neurobiol *83*, 24-36.

Bonfanti, L., and Theodosis, D. T. (1994). Expression of polysialylated neural cell adhesion molecule by proliferating cells in the subependymal layer of the adult rat, in its rostral extension and in the olfactory bulb. Neuroscience *62*, 291-305.

Boumezbeur, F., Petersen, K. F., Cline, G. W., Mason, G. F., Behar, K. L., Shulman, G. I., and Rothman, D. L. (2010). The contribution of blood lactate to brain energy metabolism in humans measured by dynamic 13C nuclear magnetic resonance spectroscopy. J Neurosci *30*, 13983-13991.

Bouzier-Sore, A. K., Voisin, P., Canioni, P., Magistretti, P. J., and Pellerin, L. (2003). Lactate is a preferential oxidative energy substrate over glucose for neurons in culture. J Cereb Blood Flow Metab *23*, 1298-1306.

Brazel, C. Y., Romanko, M. J., Rothstein, R. P., and Levison, S. W. (2003). Roles of the mammalian subventricular zone in brain development. Prog Neurobiol *69*, 49-69.

Brown, J., Cooper-Kuhn, C. M., Kempermann, G., Van Praag, H., Winkler, J., Gage, F. H., and Kuhn, H. G. (2003a). Enriched environment and physical activity stimulate hippocampal but not olfactory bulb neurogenesis. Eur J Neurosci *17*, 2042-2046.

Brown, J. P., Couillard-Despres, S., Cooper-Kuhn, C. M., Winkler, J., Aigner, L., and Kuhn, H. G. (2003b). Transient expression of doublecortin during adult neurogenesis. J Comp Neurol *467*, 1-10.

Brundin, P., Karlsson, J., Emgard, M., Schierle, G. S., Hansson, O., Petersen, A., and Castilho, R. F. (2000). Improving the survival of grafted dopaminergic neurons: a review over current approaches. Cell Transplant *9*, 179-195.

Brustle, O. (1999). Building brains: neural chimeras in the study of nervous system development and repair. Brain Pathol *9*, 527-545.

Buffo, A., Rite, I., Tripathi, P., Lepier, A., Colak, D., Horn, A. P., Mori, T., and Gotz, M. (2008). Origin and progeny of reactive gliosis: A source of multipotent cells in the injured brain. Proc Natl Acad Sci U S A *105*, 3581-3586.

Buffo, A., Rolando, C., and Ceruti, S. (2010). Astrocytes in the damaged brain: molecular and cellular insights into their reactive response and healing potential. Biochem Pharmacol *79*, 77-89.

Bullock, R., Zauner, A., Myseros, J. S., Marmarou, A., Woodward, J. J., and Young, H. F. (1995). Evidence for prolonged release of excitatory amino acids in severe human head trauma. Relationship to clinical events. Ann N Y Acad Sci *765*, 290-297; discussion 298.

Bullon, M. M., Alvarez-Gago, T., Fernandez-Ruiz, B., and Aguirre, C. (1984). Glial fibrillary acidic protein (GFAP) in spinal cord of postnatal rat. An immunoperoxidase study in semithin sections. Brain Res *316*, 129-133.

Cajal, R. y. (1928). Degeneration and regeneration of the nervous system (London, Oxford University).

Caldwell, M. D., Shearer, J., Morris, A., Mastrofrancesco, B., Henry, W., and Albina, J. E. (1984). Evidence for aerobic glycolysis in lambda-carrageenan-wounded skeletal muscle. J Surg Res *37*, 63-68.

Cameron, R. S., and Rakic, P. (1991). Glial cell lineage in the cerebral cortex: a review and synthesis. Glia *4*, 124-137.

Campbell, K., and Gotz, M. (2002). Radial glia: multi-purpose cells for vertebrate brain development. Trends Neurosci *25*, 235-238.

Campos, L. S., Leone, D. P., Relvas, J. B., Brakebusch, C., Fassler, R., Suter, U., and ffrench-Constant, C. (2004). Beta1 integrins activate a MAPK signalling pathway in neural stem cells that contributes to their maintenance. Development *131*, 3433-3444.

Cassady, C. J., Phillis, J. W., and O'Regan, M. H. (2001). Further studies on the effects of topical lactate on amino acid efflux from the ischemic rat cortex. Brain Res *901*, 30-37.

Chang, A., Nishiyama, A., Peterson, J., Prineas, J., and Trapp, B. D. (2000). NG2-positive oligodendrocyte progenitor cells in adult human brain and multiple sclerosis lesions. J Neurosci *20*, 6404-6412.

Chen, C. C., Chueh, J. Y., Tseng, H., Huang, H. M., and Lee, S. Y. (2003a). Preparation and characterization of biodegradable PLA polymeric blends. Biomaterials *24*, 1167-1173.

Chen, J., Zhang, Z. G., Li, Y., Wang, Y., Wang, L., Jiang, H., Zhang, C., Lu, M., Katakowski, M., Feldkamp, C. S., and Chopp, M. (2003b). Statins induce angiogenesis, neurogenesis, and synaptogenesis after stroke. Ann Neurol *53*, 743-751.

Chen, T., Qian, Y. Z., Di, X., Rice, A., Zhu, J. P., and Bullock, R. (2000a). Lactate/glucose dynamics after rat fluid percussion brain injury. J Neurotrauma *17*, 135-142.

Chen, T., Qian, Y. Z., Rice, A., Zhu, J. P., Di, X., and Bullock, R. (2000b). Brain lactate uptake increases at the site of impact after traumatic brain injury. Brain Res *861*, 281-287.

Chen, Y., and Swanson, R. A. (2003). The glutamate transporters EAAT2 and EAAT3 mediate cysteine uptake in cortical neuron cultures. J Neurochem *84*, 1332-1339.

Cheng, T. Y., Chen, M. H., Chang, W. H., Huang, M. Y., and Wang, T. W. (2013). Neural stem cells encapsulated in a functionalized self-assembling peptide hydrogel for brain tissue engineering. Biomaterials *34*, 2005-2016.

Christensen, K., Schroder, H. D., and Kristensen, B. W. (2008). CD133 identifies perivascular niches in grade II-IV astrocytomas. J Neurooncol *90*, 157-170.

Cicero, J. A., and Dorgan, J. R. (2001). Physical properties and fiber morphology of poly(lactic acid) obtained from continous two-step melting spinning. J Polym and Enviro *9*, 1-10.

Cicero, J. A., Dorgan, J. R., Janzen, J., Garrett, J., Runt, J., and Lin, J. S. (2002). Supramolecular morphology of two-step, melt-spun poly(lactic acid) fibers. J Appl Polym Sci *86*, 2828-2838.

Constant, J. S., Feng, J. J., Zabel, D. D., Yuan, H., Suh, D. Y., Scheuenstuhl, H., Hunt, T. K., and Hussain, M. Z. (2000). Lactate elicits vascular endothelial growth factor from macrophages: a possible alternative to hypoxia. Wound Repair Regen *8*, 353-360.

Conte, W. L., Kamishina, H., and Reep, R. L. (2009). Multiple neuroanatomical tract-tracing using fluorescent Alexa Fluor conjugates of cholera toxin subunit B in rats. Nat Protoc *4*, 1157-1166.

Correale, J., and Villa, A. (2004). The neuroprotective role of inflammation in nervous system injuries. J Neurol *251*, 1304-1316.

Corvino, V., Businaro, R., Geloso, M. C., Bigini, P., Cavallo, V., Pompili, E., Mennini, T., Fumagalli, L., and Michetti, F. (2003). S100B protein and 4-hydroxynonenal in the spinal cord of wobbler mice. Neurochem Res *28*, 341-345.

Covey, M. V., Jiang, Y., Alli, V. V., Yang, Z., and Levison, S. W. (2010). Defining the critical period for neocortical neurogenesis after pediatric brain injury. Dev Neurosci *32*, 488-498.

Cremer, J. E. (1982). Substrate utilization and brain development. J Cereb Blood Flow Metab *2*, 394-407.

Crespo, D., Asher, R. A., Lin, R., Rhodes, K. E., and Fawcett, J. W. (2007). How does chondroitinase promote functional recovery in the damaged CNS? Exp Neurol *206*, 159-171.

Crompton, K. E., Goud, J. D., Bellamkonda, R. V., Gengenbach, T. R., Finkelstein, D. I., Horne, M. K., and Forsythe, J. S. (2007). Polylysine-functionalised

thermoresponsive chitosan hydrogel for neural tissue engineering. Biomaterials *28*, 441-449.

Culican, S. M., Baumrind, N. L., Yamamoto, M., and Pearlman, A. L. (1990). Cortical radial glia: identification in tissue culture and evidence for their transformation to astrocytes. J Neurosci *10*, 684-692.

Cullen, D. K., A, R. P., Doorish, J. F., Smith, D. H., and Pfister, B. J. (2008). Developing a tissue-engineered neural-electrical relay using encapsulated neuronal constructs on conducting polymer fibers. J Neural Eng *5*, 374-384.

Curtis, M. A., Kam, M., Nannmark, U., Anderson, M. F., Axell, M. Z., Wikkelso, C., Holtas, S., van Roon-Mom, W. M., Bjork-Eriksson, T., Nordborg, C., *et al.* (2007). Human neuroblasts migrate to the olfactory bulb via a lateral ventricular extension. Science *315*, 1243-1249.

Dahl, D. (1981). The vimentin-GFA protein transition in rat neuroglia cytoskeleton occurs at the time of myelination. J Neurosci Res *6*, 741-748.

Dalton, P. D., and Mey, J. (2009). Neural interactions with materials. Front Biosci (Landmark Ed) *14*, 769-795.

Dash, P. K., Mach, S. A., and Moore, A. N. (2001). Enhanced neurogenesis in the rodent hippocampus following traumatic brain injury. J Neurosci Res *63*, 313-319.

Davalos, D., Grutzendler, J., Yang, G., Kim, J. V., Zuo, Y., Jung, S., Littman, D. R., Dustin, M. L., and Gan, W. B. (2005). ATP mediates rapid microglial response to local brain injury in vivo. Nat Neurosci *8*, 752-758.

Davies, S. J., Fitch, M. T., Memberg, S. P., Hall, A. K., Raisman, G., and Silver, J. (1997). Regeneration of adult axons in white matter tracts of the central nervous system. Nature *390*, 680-683.

De Bock, K., Georgiadou, M., and Carmeliet, P. (2013). Role of endothelial cell metabolism in vessel sprouting. Cell Metab *18*, 634-647.

De Filippis, L., and Delia, D. (2011). Hypoxia in the regulation of neural stem cells. Cell Mol Life Sci *68*, 2831-2844.

de Vos, P., Bucko, M., Gemeiner, P., Navratil, M., Svitel, J., Faas, M., Strand, B. L., Skjak-Braek, G., Morch, Y. A., Vikartovska, A., *et al.* (2009). Multiscale requirements for bioencapsulation in medicine and biotechnology. Biomaterials *30*, 2559-2570.

Deuel, T. A., Liu, J. S., Corbo, J. C., Yoo, S. Y., Rorke-Adams, L. B., and Walsh, C. A. (2006). Genetic interactions between doublecortin and doublecortin-like kinase in neuronal migration and axon outgrowth. Neuron *49*, 41-53.

Dienel, G. A. (2011). Brain lactate metabolism: the discoveries and the controversies. J Cereb Blood Flow Metab *32*, 1107-1138.

Dienel, G. A., Ball, K. K., and Cruz, N. F. (2007). A glycogen phosphorylase inhibitor selectively enhances local rates of glucose utilization in brain during sensory stimulation of conscious rats: implications for glycogen turnover. J Neurochem *102*, 466-478.

Dienel, G. A., and Hertz, L. (2001). Glucose and lactate metabolism during brain activation. J Neurosci Res *66*, 824-838.

DiNuzzo, M., Mangia, S., Maraviglia, B., and Giove, F. (2010). Glycogenolysis in astrocytes supports blood-borne glucose channeling not glycogen-derived lactate shuttling to neurons: evidence from mathematical modeling. J Cereb Blood Flow Metab *30*, 1895-1904.

Discher, D. E., Mooney, D. J., and Zandstra, P. W. (2009). Growth factors, matrices, and forces combine and control stem cells. Science *324*, 1673-1677.

do Carmo Cunha, J., de Freitas Azevedo Levy, B., de Luca, B. A., de Andrade, M. S., Gomide, V. C., and Chadi, G. (2007). Responses of reactive astrocytes containing S100beta protein and fibroblast growth factor-2 in the border and in the adjacent preserved tissue after a contusion injury of the spinal cord in rats: implications for wound repair and neuroregeneration. Wound Repair Regen *15*, 134-146.

Doetsch, F. (2003). A niche for adult neural stem cells. Curr Opin Genet Dev *13*, 543-550.

Doetsch, F., and Alvarez-Buylla, A. (1996). Network of tangential pathways for neuronal migration in adult mammalian brain. Proc Natl Acad Sci U S A *93*, 14895-14900.

Doetsch, F., Caille, I., Lim, D. A., Garcia-Verdugo, J. M., and Alvarez-Buylla, A. (1999). Subventricular zone astrocytes are neural stem cells in the adult mammalian brain. Cell *97*, 703-716.

Doetsch, F., Garcia-Verdugo, J. M., and Alvarez-Buylla, A. (1997). Cellular composition and three-dimensional organization of the subventricular germinal zone in the adult mammalian brain. J Neurosci *17*, 5046-5061.

Doetsch, F., and Scharff, C. (2001). Challenges for brain repair: insights from adult neurogenesis in birds and mammals. Brain Behav Evol *58*, 306-322.

Dombrowski, G. J., Jr., Swiatek, K. R., and Chao, K. L. (1989). Lactate, 3-hydroxybutyrate, and glucose as substrates for the early postnatal rat brain. Neurochem Res *14*, 667-675.

Dringen, R., Wiesinger, H., and Hamprecht, B. (1993). Uptake of L-lactate by cultured rat brain neurons. Neurosci Lett *163*, 5-7.

Eddleston, M., and Mucke, L. (1993). Molecular profile of reactive astrocytes--implications for their role in neurologic disease. Neuroscience *54*, 15-36.

Elias, P. Z., and Spector, M. (2009). Implantation of a collagen scaffold seeded with adult rat hippocampal progenitors in a rat model of penetrating brain injury. J Neurosci Methods *209*, 199-211.

Eling, B., Gogolewski, S., and Pennings, A. J. (1982). Biodegradable materials of poly (L-lactic acid):1. Melt-spun and solution spun fibers. Polymer *23*, 1587-1593.

Emsley, J. G., and Hagg, T. (2003). alpha6beta1 integrin directs migration of neuronal precursors in adult mouse forebrain. Exp Neurol *183*, 273-285.

Eng, L. F., Lee, Y. L., and Miles, L. E. (1976). Measurement of glial fibrillary acidic protein by a two-site immunoradiometric assay. Anal Biochem *71*, 243-259.

Eng, L. F., Vanderhaeghen, J. J., Bignami, A., and Gerstl, B. (1971). An acidic protein isolated from fibrous astrocytes. Brain Res *28*, 351-354.

Engler, A. J., Sen, S., Sweeney, H. L., and Discher, D. E. (2006). Matrix elasticity directs stem cell lineage specification. Cell *126*, 677-689.

Englund, C., Alvord, E. C., Jr., Folkerth, R. D., Silbergeld, D., Born, D. E., Small, R., and Hevner, R. F. (2005a). NeuN expression correlates with reduced mitotic index of neoplastic cells in central neurocytomas. Neuropathol Appl Neurobiol *31*, 429-438.

Englund, C., Fink, A., Lau, C., Pham, D., Daza, R. A., Bulfone, A., Kowalczyk, T., and Hevner, R. F. (2005b). Pax6, Tbr2, and Tbr1 are expressed sequentially by radial glia, intermediate progenitor cells, and postmitotic neurons in developing neocortex. J Neurosci *25*, 247-251.

Ergul, A., Alhusban, A., and Fagan, S. C. (2012). Angiogenesis: a harmonized target for recovery after stroke. Stroke *43*, 2270-2274.

Eriksson, P. S., Perfilieva, E., Bjork-Eriksson, T., Alborn, A. M., Nordborg, C., Peterson, D. A., and Gage, F. H. (1998). Neurogenesis in the adult human hippocampus. Nat Med *4*, 1313-1317.

Facucho-Oliveira, J. M., and St John, J. C. (2009). The relationship between pluripotency and mitochondrial DNA proliferation during early embryo development and embryonic stem cell differentiation. Stem Cell Rev *5*, 140-158.

Fagel, D. M., Ganat, Y., Silbereis, J., Ebbitt, T., Stewart, W., Zhang, H., Ment, L. R., and Vaccarino, F. M. (2006). Cortical neurogenesis enhanced by chronic perinatal hypoxia. Exp Neurol *199*, 77-91.

Fame, R. M., MacDonald, J. L., and Macklis, J. D. (2011). Development, specification, and diversity of callosal projection neurons. Trends Neurosci *34*, 41-50.

Fan, H. J., Knez, M., Scholz, R., Hesse, D., Nielsch, K., Zacharias, M., and Gosele, U. (2007). Influence of surface diffusion on the formation of hollow nanostructures induced by the Kirkendall effect: the basic concept. Nano Lett *7*, 993-997.

Fawcett, J. W., and Asher, R. A. (1999). The glial scar and central nervous system repair. Brain Res Bull *49*, 377-391.

Fayol, L., Baud, O., Monier, A., Pellerin, L., Magistretti, P., Evrard, P., and Verney, C. (2004). Immunocytochemical expression of monocarboxylate transporters in the human visual cortex at midgestation. Brain Res Dev Brain Res *148*, 69-76.

Fischer EW, S. H., Wegner G (1973). Investigation of the structure of solution grown crystals of lactide copolymers by means of chemical reactions. Colloid Polym Sci *251*, 980-990.

Fitch, M. T., Doller, C., Combs, C. K., Landreth, G. E., and Silver, J. (1999). Cellular and molecular mechanisms of glial scarring and progressive cavitation: in vivo and in vitro analysis of inflammation-induced secondary injury after CNS trauma. J Neurosci *19*, 8182-8198.

Fitch, M. T., and Silver, J. (2008). CNS injury, glial scars, and inflammation: Inhibitory extracellular matrices and regeneration failure. Exp Neurol *209*, 294-301.

Folbergrova, J., Nilsson, B., Nordstrom, C. H., and Siesjo, B. K. (1978). Energy flux and lactate production in rat cerebral cortex during the first 5-10 s of bicuculline-induced seizures. J Neurochem *31*, 1533-1535.

Forraz, N., Wright, K. E., Jurga, M., and McGuckin, C. P. (2013). Experimental therapies for repair of the central nervous system: stem cells and tissue engineering. J Tissue Eng Regen Med *7*, 523-536.

Fournier, A. E., Takizawa, B. T., and Strittmatter, S. M. (2003). Rho kinase inhibition enhances axonal regeneration in the injured CNS. J Neurosci *23*, 1416-1423.

Fournier, E., Passirani, C., Colin, N., Sagodira, S., Menei, P., Benoit, J. P., and Montero-Menei, C. N. (2006). The brain tissue response to biodegradable poly(methylidene malonate 2.1.2)-based microspheres in the rat. Biomaterials *27*, 4963-4974.

Fraisl, P., Mazzone, M., Schmidt, T., and Carmeliet, P. (2009). Regulation of angiogenesis by oxygen and metabolism. Dev Cell *16*, 167-179.

Freire, E., Gomes, F. C., Jotha-Mattos, T., Neto, V. M., Silva Filho, F. C., and Coelho-Sampaio, T. (2004). Sialic acid residues on astrocytes regulate neuritogenesis by controlling the assembly of laminin matrices. J Cell Sci *117*, 4067-4076.

Fuchs, E., Tumbar, T., and Guasch, G. (2004). Socializing with the neighbors: stem cells and their niche. Cell *116*, 769-778.

Gaetz, M. (2004). The neurophysiology of brain injury. Clin Neurophysiol *115*, 4-18.

Gage, F. H. (2000). Mammalian neural stem cells. Science *287*, 1433-1438.

Gallagher, C. N., Carpenter, K. L., Grice, P., Howe, D. J., Mason, A., Timofeev, I., Menon, D. K., Kirkpatrick, P. J., Pickard, J. D., Sutherland, G. R., and Hutchinson, P. J. (2009). The human brain utilizes lactate via the tricarboxylic acid cycle: a 13C-

labelled microdialysis and high-resolution nuclear magnetic resonance study. Brain *132*, 2839-2849.

Gallien, L., and Beetschen, J. C. (1951). [Extent and limits of the regenerative power of the extremities in Xenopus laevis Daudin after metamorphosis]. C R Seances Soc Biol Fil *145*, 874-876.

Gao, M., Guo, J., Keung, G. K. K., and Wu, W. (2013). Use of Self-Assempling nanofibre biomaterials for neural repair after injury.

Gautier, S. E., Oudega, M., Fragoso, M., Chapon, P., Plant, G. W., Bunge, M. B., and Parel, J. M. (1998). Poly(alpha-hydroxyacids) for application in the spinal cord: resorbability and biocompatibility with adult rat Schwann cells and spinal cord. J Biomed Mater Res *42*, 642-654.

Gefen, A., and Margulies, S. S. (2004). Are in vivo and in situ brain tissues mechanically similar? J Biomech *37*, 1339-1352.

Geller, H. M., and Fawcett, J. W. (2002). Building a bridge: engineering spinal cord repair. Exp Neurol *174*, 125-136.

Ghani, Q. P., Wagner, S., Becker, H. D., Hunt, T. K., and Hussain, M. Z. (2004). Regulatory role of lactate in wound repair. Methods Enzymol *381*, 565-575.

Ghani, Q. P., Wagner, S., and Hussain, M. Z. (2003). Role of ADP-ribosylation in wound repair. The contributions of Thomas K. Hunt, MD. Wound Repair Regen *11*, 439-444.

Gilyarov, A. V. (2008). Nestin in central nervous system cells. Neurosci Behav Physiol *38*, 165-169.

Goetz, A. K., Scheffler, B., Chen, H. X., Wang, S., Suslov, O., Xiang, H., Brustle, O., Roper, S. N., and Steindler, D. A. (2006). Temporally restricted substrate interactions direct fate and specification of neural precursors derived from embryonic stem cells. Proc Natl Acad Sci U S A *103*, 11063-11068.

Goings, G. E., Wibisono, B. L., and Szele, F. G. (2002). Cerebral cortex lesions decrease the number of bromodeoxyuridine-positive subventricular zone cells in mice. Neurosci Lett *329*, 161-164.

Goldberg, J. S., and Hirschi, K. K. (2009). Diverse roles of the vasculature within the neural stem cell niche. Regen Med *4*, 879-897.

Goldman, S. A., and Chen, Z. (2011). Perivascular instruction of cell genesis and fate in the adult brain. Nat Neurosci *14*, 1382-1389.

Gotts, J. E., and Chesselet, M. F. (2005). Vascular changes in the subventricular zone after distal cortical lesions. Exp Neurol *194*, 139-150.

Gotz, M., and Huttner, W. B. (2005). The cell biology of neurogenesis. Nat Rev Mol Cell Biol *6*, 777-788.

Gould, E. (2007). How widespread is adult neurogenesis in mammals? Nat Rev Neurosci *8*, 481-488.

Gould, E., Reeves, A. J., Fallah, M., Tanapat, P., Gross, C. G., and Fuchs, E. (1999a). Hippocampal neurogenesis in adult Old World primates. Proc Natl Acad Sci U S A *96*, 5263-5267.

Gould, E., Reeves, A. J., Graziano, M. S., and Gross, C. G. (1999b). Neurogenesis in the neocortex of adult primates. Science *286*, 548-552.

Gritti, A., and Bonfanti, L. (2007). Neuronal-glial interactions in central nervous system neurogenesis: the neural stem cell perspective. Neuron Glia Biol *3*, 309-323.

Gunn, J., and Zhang, M. (2010). Polyblend nanofibers for biomedical applications: perspectives and challenges. Trends Biotechnol *28*, 189-197.

Guo, J., Leung, K. K., Su, H., Yuan, Q., Wang, L., Chu, T. H., Zhang, W., Pu, J. K., Ng, G. K., Wong, W. M., *et al.* (2009). Self-assembling peptide nanofiber scaffold promotes the reconstruction of acutely injured brain. Nanomedicine *5*, 345-351.

Gupta, B., Revagade, N., and Hilborn, J. (2007). Poly(lactic acid) fiber: An overview. Progress in Polymer Science *32*, 455-482.

Gupta, D., Venugopal, J., Prabhakaran, M. P., Dev, V. R., Low, S., Choon, A. T., and Ramakrishna, S. (2009). Aligned and random nanofibrous substrate for the in vitro culture of Schwann cells for neural tissue engineering. Acta Biomater *5*, 2560-2569.

Halestrap, A. P., and Meredith, D. (2004). The SLC16 gene family-from monocarboxylate transporters (MCTs) to aromatic amino acid transporters and beyond. Pflugers Arch *447*, 619-628.

Halestrap, A. P., and Wilson, M. C. (2012). The monocarboxylate transporter family--role and regulation. IUBMB Life *64*, 109-119.

Hamill, C. E., Goldshmidt, A., Nicole, O., McKeon, R. J., Brat, D. J., and Traynelis, S. F. (2005). Special lecture: glial reactivity after damage: implications for scar formation and neuronal recovery. Clin Neurosurg *52*, 29-44.

Hartfuss, E., Galli, R., Heins, N., and Gotz, M. (2001). Characterization of CNS precursor subtypes and radial glia. Dev Biol *229*, 15-30.

Hatten, M. E. (1990). Riding the glial monorail: a common mechanism for glial-guided neuronal migration in different regions of the developing mammalian brain. Trends Neurosci *13*, 179-184.

Hatten, M. E. (2002). New directions in neuronal migration. Science *297*, 1660-1663.

Hisaoka, T., Nakamura, Y., Senba, E., and Morikawa, Y. (2010). The forkhead transcription factors, Foxp1 and Foxp2, identify different subpopulations of projection neurons in the mouse cerebral cortex. Neuroscience *166*, 551-563.

Holmes, T. C., de Lacalle, S., Su, X., Liu, G., Rich, A., and Zhang, S. (2000). Extensive neurite outgrowth and active synapse formation on self-assembling peptide scaffolds. Proc Natl Acad Sci U S A *97*, 6728-6733.

Hou, S., Xu, Q., Tian, W., Cui, F., Cai, Q., Ma, J., and Lee, I. S. (2005). The repair of brain lesion by implantation of hyaluronic acid hydrogels modified with laminin. J Neurosci Methods *148*, 60-70.

Hsieh, J. (2012). Orchestrating transcriptional control of adult neurogenesis. Genes Dev *26*, 1010-1021.

Huang, K. F., Hsu, W. C., Chiu, W. T., and Wang, J. Y. (2012). Functional improvement and neurogenesis after collagen-GAG matrix implantation into surgical brain trauma. Biomaterials *33*, 2067-2075.

Hudson, T. W., Evans, G. R., and Schmidt, C. E. (2000). Engineering strategies for peripheral nerve repair. Orthop Clin North Am *31*, 485-498.

Hunt, T. K., Conolly, W. B., Aronson, S. B., and Goldstein, P. (1978). Anaerobic metabolism and wound healing: an hypothesis for the initiation and cessation of collagen synthesis in wounds. Am J Surg *135*, 328-332.

Hurtado, A., Cregg, J. M., Wang, H. B., Wendell, D. F., Oudega, M., Gilbert, R. J., and McDonald, J. W. (2011). Robust CNS regeneration after complete spinal cord transection using aligned poly-L-lactic acid microfibers. Biomaterials *32*, 6068-6079.

Inao, S., Marmarou, A., Clarke, G. D., Andersen, B. J., Fatouros, P. P., and Young, H. F. (1988). Production and clearance of lactate from brain tissue, cerebrospinal fluid, and serum following experimental brain injury. J Neurosurg *69*, 736-744.

Itoh, Y., Esaki, T., Shimoji, K., Cook, M., Law, M. J., Kaufman, E., and Sokoloff, L. (2003). Dichloroacetate effects on glucose and lactate oxidation by neurons and astroglia in vitro and on glucose utilization by brain in vivo. Proc Natl Acad Sci U S A *100*, 4879-4884.

Ivanov, A., Mukhtarov, M., Bregestovski, P., and Zilberter, Y. (2011). Lactate Effectively Covers Energy Demands during Neuronal Network Activity in Neonatal Hippocampal Slices. Front Neuroenergetics *3*, 2.

Ivanovic, Z. (2009). Hypoxia or in situ normoxia: The stem cell paradigm. J Cell Physiol *219*, 271-275.

Iwai, M., Stetler, R. A., Xing, J., Hu, X., Gao, Y., Zhang, W., Chen, J., and Cao, G. (2010). Enhanced oligodendrogenesis and recovery of neurological function by erythropoietin after neonatal hypoxic/ischemic brain injury. Stroke *41*, 1032-1037.

Jakovcevic, D., and Harder, D. R. (2007). Role of astrocytes in matching blood flow to neuronal activity. Curr Top Dev Biol *79*, 75-97.

Javaherian, A., and Kriegstein, A. (2009). A stem cell niche for intermediate progenitor cells of the embryonic cortex. Cereb Cortex *19 Suppl 1*, i70-77.

Jiang, W., Gu, W., Brannstrom, T., Rosqvist, R., and Wester, P. (2001). Cortical neurogenesis in adult rats after transient middle cerebral artery occlusion. Stroke *32*, 1201-1207.

Jiao, J., and Chen, D. F. (2008). Induction of neurogenesis in nonconventional neurogenic regions of the adult central nervous system by niche astrocyte-produced signals. Stem Cells *26*, 1221-1230.

Jin, G. Z., Kim, M., Shin, U. S., and Kim, H. W. (2011). Neurite outgrowth of dorsal root ganglia neurons is enhanced on aligned nanofibrous biopolymer scaffold with carbon nanotube coating. Neurosci Lett *501*, 10-14.

Jing, P., Rudra, J. S., Herr, A. B., and Collier, J. H. (2008). Self-assembling peptide-polymer hydrogels designed from the coiled coil region of fibrin. Biomacromolecules *9*, 2438-2446.

Johnson, J., Nowicki, M. O., Lee, C. H., Chiocca, E. A., Viapiano, M. S., Lawler, S. E., and Lannutti, J. J. (2009). Quantitative analysis of complex glioma cell migration on electrospun polycaprolactone using time-lapse microscopy. Tissue Eng Part C Methods *15*, 531-540.

Kageyama, R., Ohtsuka, T., and Kobayashi, T. (2007). The Hes gene family: repressors and oscillators that orchestrate embryogenesis. Development *134*, 1243-1251.

Kalimo, H., Rehncrona, S., Soderfeldt, B., Olsson, Y., and Siesjo, B. K. (1981). Brain lactic acidosis and ischemic cell damage: 2. Histopathology. J Cereb Blood Flow Metab *1*, 313-327.

Kaneko, N., Kako, E., and Sawamoto, K. (2011). Prospects and limitations of using endogenous neural stem cells for brain regeneration. Genes (Basel) *2*, 107-130.

Kaneko, N., and Sawamoto, K. (2009). Adult neurogenesis and its alteration under pathological conditions. Neurosci Res *63*, 155-164.

Kato, H., and Walz, W. (2000). The initiation of the microglial response. Brain Pathol *10*, 137-143.

Kawano, H., Kimura-Kuroda, J., Komuta, Y., Yoshioka, N., Li, H. P., Kawamura, K., Li, Y., and Raisman, G. (2012). Role of the lesion scar in the response to damage and repair of the central nervous system. Cell Tissue Res *349*, 169-180.

Kazanis, I. (2012). Can adult neural stem cells create new brains? Plasticity in the adult mammalian neurogenic niches: realities and expectations in the era of regenerative biology. Neuroscientist *18*, 15-27.

Kazanis, I., Lathia, J. D., Vadakkan, T. J., Raborn, E., Wan, R., Mughal, M. R., Eckley, D. M., Sasaki, T., Patton, B., Mattson, M. P., *et al.* (2010). Quiescence and activation of stem and precursor cell populations in the subependymal zone of the mammalian brain are associated with distinct cellular and extracellular matrix signals. J Neurosci *30*, 9771-9781.

Keirstead, H. S., Nistor, G., Bernal, G., Totoiu, M., Cloutier, F., Sharp, K., and Steward, O. (2005). Human embryonic stem cell-derived oligodendrocyte progenitor cell transplants remyelinate and restore locomotion after spinal cord injury. J Neurosci *25*, 4694-4705.

Kerever, A., Schnack, J., Vellinga, D., Ichikawa, N., Moon, C., Arikawa-Hirasawa, E., Efird, J. T., and Mercier, F. (2007). Novel extracellular matrix structures in the neural stem cell niche capture the neurogenic factor fibroblast growth factor 2 from the extracellular milieu. Stem Cells *25*, 2146-2157.

Kernie, S. G., Erwin, T. M., and Parada, L. F. (2001). Brain remodeling due to neuronal and astrocytic proliferation after controlled cortical injury in mice. J Neurosci Res *66*, 317-326.

Keung, A. J., Healy, K. E., Kumar, S., and Schaffer, D. V. (2010). Biophysics and dynamics of natural and engineered stem cell microenvironments. Wiley Interdiscip Rev Syst Biol Med *2*, 49-64.

Kim, H., Cooke, M. J., and Shoichet, M. S. (2012). Creating permissive microenvironments for stem cell transplantation into the central nervous system. Trends Biotechnol *30*, 55-63.

Kim, H. J., Leeds, P., and Chuang, D. M. (2009). The HDAC inhibitor, sodium butyrate, stimulates neurogenesis in the ischemic brain. J Neurochem *110*, 1226-1240.

Kim, K., Yu, M., Zong, X., Chiu, J., Fang, D., Seo, Y. S., Hsiao, B. S., Chu, B., and Hadjiargyrou, M. (2003). Control of degradation rate and hydrophilicity in electrospun non-woven poly(D,L-lactide) nanofiber scaffolds for biomedical applications. Biomaterials *24*, 4977-4985.

Kim, S. U., and de Vellis, J. (2005). Microglia in health and disease. J Neurosci Res *81*, 302-313.

Knoth, R., Singec, I., Ditter, M., Pantazis, G., Capetian, P., Meyer, R. P., Horvat, V., Volk, B., and Kempermann, G. (2010). Murine features of neurogenesis in the human hippocampus across the lifespan from 0 to 100 years. PLoS One *5*, e8809.

Koh, H. S., Yong, T., Chan, C. K., and Ramakrishna, S. (2008). Enhancement of neurite outgrowth using nano-structured scaffolds coupled with laminin. Biomaterials *29*, 3574-3582.

Kojima, T., Hirota, Y., Ema, M., Takahashi, S., Miyoshi, I., Okano, H., and Sawamoto, K. (2010). Subventricular zone-derived neural progenitor cells migrate along a blood vessel scaffold toward the post-stroke striatum. Stem Cells *28*, 545-554.

Kokovay, E., Shen, Q., and Temple, S. (2008). The incredible elastic brain: how neural stem cells expand our minds. Neuron *60*, 420-429.

Kornack, D. R., and Rakic, P. (2001). Cell proliferation without neurogenesis in adult primate neocortex. Science *294*, 2127-2130.

Kreuter, J., Ramge, P., Petrov, V., Hamm, S., Gelperina, S. E., Engelhardt, B., Alyautdin, R., von Briesen, H., and Begley, D. J. (2003). Direct evidence that polysorbate-80-

coated poly(butylcyanoacrylate) nanoparticles deliver drugs to the CNS via specific mechanisms requiring prior binding of drug to the nanoparticles. Pharm Res *20*, 409-416.

Kreutzberg, G. W. (1996). Microglia: a sensor for pathological events in the CNS. Trends Neurosci *19*, 312-318.

Krewson, C. E., Klarman, M. L., and Saltzman, W. M. (1995). Distribution of nerve growth factor following direct delivery to brain interstitium. Brain Res *680*, 196-206.

Kriegstein, A. R., and Gotz, M. (2003). Radial glia diversity: a matter of cell fate. Glia *43*, 37-43.

Kruger, S., Sievers, J., Hansen, C., Sadler, M., and Berry, M. (1986). Three morphologically distinct types of interface develop between adult host and fetal brain transplants: implications for scar formation in the adult central nervous system. J Comp Neurol *249*, 103-116.

Kulbatski, I., Mothe, A. J., Nomura, H., and Tator, C. H. (2005). Endogenous and exogenous CNS derived stem/progenitor cell approaches for neurotrauma. Curr Drug Targets *6*, 111-126.

Kumbar, S. G., James, R., Nukavarapu, S. P., and Laurencin, C. T. (2008). Electrospun nanofiber scaffolds: engineering soft tissues. Biomed Mater *3*, 034002.

Ladeby, R., Wirenfeldt, M., Garcia-Ovejero, D., Fenger, C., Dissing-Olesen, L., Dalmau, I., and Finsen, B. (2005). Microglial cell population dynamics in the injured adult central nervous system. Brain Res Brain Res Rev *48*, 196-206.

Lampe, K. J., and Heilshorn, S. C. (2012). Building stem cell niches from the molecule up through engineered peptide materials. Neurosci Lett *519*, 138-146.

Lander, A. D., Kimble, J., Clevers, H., Fuchs, E., Montarras, D., Buckingham, M., Calof, A. L., Trumpp, A., and Oskarsson, T. (2012). What does the concept of the stem cell niche really mean today? BMC Biol *10*, 19.

Lathia, J. D., Rao, M. S., Mattson, M. P., and Ffrench-Constant, C. (2007). The microenvironment of the embryonic neural stem cell: lessons from adult niches? Dev Dyn *236*, 3267-3282.

Lauritzen, K. H., Morland, C., Puchades, M., Holm-Hansen, S., Hagelin, E. M., Lauritzen, F., Attramadal, H., Storm-Mathisen, J., Gjedde, A., and Bergersen, L. H. (2013). Lactate Receptor Sites Link Neurotransmission, Neurovascular Coupling, and Brain Energy Metabolism. Cereb Cortex.

Lavezzi, A. M., Corna, M. F., and Matturri, L. (2013). Neuronal nuclear antigen (NeuN): a useful marker of neuronal immaturity in sudden unexplained perinatal death. J Neurol Sci *329*, 45-50.

Le Magueresse, C., Alfonso, J., Khodosevich, K., Arroyo Martin, A. A., Bark, C., and Monyer, H. (2011). "Small axonless neurons": postnatally generated neocortical interneurons with delayed functional maturation. J Neurosci *31*, 16731-16747.

Lee, J. Y., Bashur, C. A., Goldstein, A. S., and Schmidt, C. E. (2009). Polypyrrole-coated electrospun PLGA nanofibers for neural tissue applications. Biomaterials *30*, 4325-4335.

Lee, K. Y., and Mooney, D. J. (2001). Hydrogels for tissue engineering. Chem Rev *101*, 1869-1879.

Leipzig, N. D., and Shoichet, M. S. (2009). The effect of substrate stiffness on adult neural stem cell behavior. Biomaterials *30*, 6867-6878.

Leker, R. R., Soldner, F., Velasco, I., Gavin, D. K., Androutsellis-Theotokis, A., and McKay, R. D. (2007). Long-lasting regeneration after ischemia in the cerebral cortex. Stroke *38*, 153-161.

Leone, D. P., Relvas, J. B., Campos, L. S., Hemmi, S., Brakebusch, C., Fassler, R., Ffrench-Constant, C., and Suter, U. (2005). Regulation of neural progenitor proliferation and survival by beta1 integrins. J Cell Sci *118*, 2589-2599.

Levenberg, S., Huang, N. F., Lavik, E., Rogers, A. B., Itskovitz-Eldor, J., and Langer, R. (2003). Differentiation of human embryonic stem cells on three-dimensional polymer scaffolds. Proc Natl Acad Sci U S A *100*, 12741-12746.

Levitt, P., and Rakic, P. (1980). Immunoperoxidase localization of glial fibrillary acidic protein in radial glial cells and astrocytes of the developing rhesus monkey brain. J Comp Neurol *193*, 815-840.

Li, W., Guo, Y., Wang, H., Shi, D., Liang, C., Ye, Z., Qing, F., and Gong, J. (2008a). Electrospun nanofibers immobilized with collagen for neural stem cells culture. J Mater Sci Mater Med *19*, 847-854.

Li, Y., Song, Y., Zhao, L., Gaidosh, G., Laties, A. M., and Wen, R. (2008b). Direct labeling and visualization of blood vessels with lipophilic carbocyanine dye DiI. Nat Protoc *3*, 1703-1708.

Lie, D. C., Song, H., Colamarino, S. A., Ming, G. L., and Gage, F. H. (2004). Neurogenesis in the adult brain: new strategies for central nervous system diseases. Annu Rev Pharmacol Toxicol *44*, 399-421.

Lin, C. C., and Metters, A. T. (2006). Enhanced protein delivery from photopolymerized hydrogels using a pseudospecific metal chelating ligand. Pharm Res *23*, 614-622.

Lin, R., Kwok, J. C., Crespo, D., and Fawcett, J. W. (2008). Chondroitinase ABC has a long-lasting effect on chondroitin sulphate glycosaminoglycan content in the injured rat brain. J Neurochem *104*, 400-408.

Lo, E. H., Dalkara, T., and Moskowitz, M. A. (2003). Mechanisms, challenges and opportunities in stroke. Nat Rev Neurosci *4*, 399-415.

Lockman, P. R., Mumper, R. J., Khan, M. A., and Allen, D. D. (2002). Nanoparticle technology for drug delivery across the blood-brain barrier. Drug Dev Ind Pharm *28*, 1-13.

Lois, C., and Alvarez-Buylla, A. (1994). Long-distance neuronal migration in the adult mammalian brain. Science *264*, 1145-1148.

Loulier, K., Lathia, J. D., Marthiens, V., Relucio, J., Mughal, M. R., Tang, S. C., Coksaygan, T., Hall, P. E., Chigurupati, S., Patton, B., *et al.* (2009). beta1 integrin maintains integrity of the embryonic neocortical stem cell niche. PLoS Biol *7*, e1000176.

Lu, D., Qu, C., Goussev, A., Jiang, H., Lu, C., Schallert, T., Mahmood, A., Chen, J., Li, Y., and Chopp, M. (2007). Statins increase neurogenesis in the dentate gyrus, reduce delayed neuronal death in the hippocampal CA3 region, and improve spatial learning in rat after traumatic brain injury. J Neurotrauma *24*, 1132-1146.

Lunt, J. (1998). Large scale production, properties and commercial applications of polylactic acid polymers. Polym Deg Stab *59*, 145-152.

Luskin, M. B. (1993). Restricted proliferation and migration of postnatally generated neurons derived from the forebrain subventricular zone. Neuron *11*, 173-189.

Lutolf, M. P., and Hubbell, J. A. (2005). Synthetic biomaterials as instructive extracellular microenvironments for morphogenesis in tissue engineering. Nat Biotechnol *23*, 47-55.

Ma, P. X. (2008). Biomimetic materials for tissue engineering. Adv Drug Deliv Rev *60*, 184-198.

Ma, S., Kwon, H. J., Johng, H., Zang, K., and Huang, Z. (2013). Radial glial neural progenitors regulate nascent brain vascular network stabilization via inhibition of Wnt signaling. PLoS Biol *11*, e1001469.

Madri, J. A. (2009). Modeling the neurovascular niche: implications for recovery from CNS injury. J Physiol Pharmacol *60 Suppl 4*, 95-104.

Magavi, S. S., Leavitt, B. R., and Macklis, J. D. (2000). Induction of neurogenesis in the neocortex of adult mice. Nature *405*, 951-955.

Magistretti, P. J., and Pellerin, L. (1999). Cellular mechanisms of brain energy metabolism and their relevance to functional brain imaging. Philos Trans R Soc Lond B Biol Sci *354*, 1155-1163.

Mäkelä, E. A., Vainionpää, S., Vihtonen, K., Mero, M., Helevirta, P., Törmälä, P., and Rokkanen, P. (1989). Te effet of a penetrating biodegradable implant on the growth plate. Clin Orthopaed *241*, 677-690.

Malatesta, P., Hartfuss, E., and Gotz, M. (2000). Isolation of radial glial cells by fluorescent-activated cell sorting reveals a neuronal lineage. Development *127*, 5253-5263.

Mangia, S., Simpson, I. A., Vannucci, S. J., and Carruthers, A. (2009). The in vivo neuron-to-astrocyte lactate shuttle in human brain: evidence from modeling of measured lactate levels during visual stimulation. J Neurochem *109 Suppl 1*, 55-62.

Martinez-Ramos, C., Valles-Lluch, A., Verdugo, J. M., Ribelles, J. L., Barcia Albacar, J. A., Orts, A. B., Soria Lopez, J. M., and Pradas, M. M. (2012). Channeled scaffolds implanted in adult rat brain. J Biomed Mater Res A *100*, 3276-3286.

Massey, J. M., Hubscher, C. H., Wagoner, M. R., Decker, J. A., Amps, J., Silver, J., and Onifer, S. M. (2006). Chondroitinase ABC digestion of the perineuronal net promotes functional collateral sprouting in the cuneate nucleus after cervical spinal cord injury. J Neurosci *26*, 4406-4414.

Masuda, T., Isobe, Y., Aihara, N., Furuyama, F., Misumi, S., Kim, T. S., Nishino, H., and Hida, H. (2007). Increase in neurogenesis and neuroblast migration after a small intracerebral hemorrhage in rats. Neurosci Lett *425*, 114-119.

Matsuda, F., Sakakima, H., and Yoshida, Y. (2011). The effects of early exercise on brain damage and recovery after focal cerebral infarction in rats. Acta Physiol (Oxf) *201*, 275-287.

Mattotti, M., Alvarez, Z., Ortega, J. A., Planell, J. A., Engel, E., and Alcantara, S. (2012). Inducing functional radial glia-like progenitors from cortical astrocyte cultures using micropatterned PMMA. Biomaterials *33*, 1759-1770.

McKerracher, L., David, S., Jackson, D. L., Kottis, V., Dunn, R. J., and Braun, P. E. (1994). Identification of myelin-associated glycoprotein as a major myelin-derived inhibitor of neurite growth. Neuron *13*, 805-811.

McKerracher, L., and Higuchi, H. (2006). Targeting Rho to stimulate repair after spinal cord injury. J Neurotrauma *23*, 309-317.

Medina, J. M., and Tabernero, A. (2005). Lactate utilization by brain cells and its role in CNS development. J Neurosci Res *79*, 2-10.

Mendez-Lucas, A., Duarte, J. A., Sunny, N. E., Satapati, S., He, T., Fu, X., Bermudez, J., Burgess, S. C., and Perales, J. C. (2013). PEPCK-M expression in mouse liver potentiates, not replaces, PEPCK-C mediated gluconeogenesis. J Hepatol *59*, 105-113.

Mercier, F., Kitasako, J. T., and Hatton, G. I. (2002). Anatomy of the brain neurogenic zones revisited: fractones and the fibroblast/macrophage network. J Comp Neurol *451*, 170-188.

Mercier, F., Kitasako, J. T., and Hatton, G. I. (2003). Fractones and other basal laminae in the hypothalamus. J Comp Neurol *455*, 324-340.

Miller, F. D., and Gauthier-Fisher, A. (2009). Home at last: neural stem cell niches defined. Cell Stem Cell *4*, 507-510.

Miller, F. D., and Gauthier, A. S. (2007). Timing is everything: making neurons versus glia in the developing cortex. Neuron *54*, 357-369.

Mirzadeh, Z., Merkle, F. T., Soriano-Navarro, M., Garcia-Verdugo, J. M., and Alvarez-Buylla, A. (2008). Neural stem cells confer unique pinwheel architecture to the ventricular surface in neurogenic regions of the adult brain. Cell Stem Cell *3*, 265-278.

Miura, K., Okada, Y., Aoi, T., Okada, A., Takahashi, K., Okita, K., Nakagawa, M., Koyanagi, M., Tanabe, K., Ohnuki, M., *et al.* (2009). Variation in the safety of induced pluripotent stem cell lines. Nat Biotechnol *27*, 743-745.

Miyake, T., Hattori, T., Fukuda, M., Kitamura, T., and Fujita, S. (1988). Quantitative studies on proliferative changes of reactive astrocytes in mouse cerebral cortex. Brain Res *451*, 133-138.

Mobley, A. K., Tchaicha, J. H., Shin, J., Hossain, M. G., and McCarty, J. H. (2009). Beta8 integrin regulates neurogenesis and neurovascular homeostasis in the adult brain. J Cell Sci *122*, 1842-1851.

Mohyeldin, A., Garzon-Muvdi, T., and Quinones-Hinojosa, A. (2010). Oxygen in stem cell biology: a critical component of the stem cell niche. Cell Stem Cell *7*, 150-161.

Monje, M. L., Mizumatsu, S., Fike, J. R., and Palmer, T. D. (2002). Irradiation induces neural precursor-cell dysfunction. Nat Med *8*, 955-962.

Moore, K., MacSween, M., and Shoichet, M. (2006). Immobilized concentration gradients of neurotrophic factors guide neurite outgrowth of primary neurons in macroporous scaffolds. Tissue Eng *12*, 267-278.

Morganti-Kossmann, M. C., Rancan, M., Stahel, P. F., and Kossmann, T. (2002). Inflammatory response in acute traumatic brain injury: a double-edged sword. Curr Opin Crit Care *8*, 101-105.

Morgenstern, D. A., Asher, R. A., and Fawcett, J. W. (2002). Chondroitin sulphate proteoglycans in the CNS injury response. Prog Brain Res *137*, 313-332.

Morshead, C. M., and van der Kooy, D. (2004). Disguising adult neural stem cells. Curr Opin Neurobiol *14*, 125-131.

Mukhopadhyay, G., Doherty, P., Walsh, F. S., Crocker, P. R., and Filbin, M. T. (1994). A novel role for myelin-associated glycoprotein as an inhibitor of axonal regeneration. Neuron *13*, 757-767.

Mullen, R. J., Buck, C. R., and Smith, A. M. (1992). NeuN, a neuronal specific nuclear protein in vertebrates. Development *116*, 201-211.

Myer, D. J., Gurkoff, G. G., Lee, S. M., Hovda, D. A., and Sofroniew, M. V. (2006). Essential protective roles of reactive astrocytes in traumatic brain injury. Brain *129*, 2761-2772.

Nagai, Y., Unsworth, L. D., Koutsopoulos, S., and Zhang, S. (2006). Slow release of molecules in self-assembling peptide nanofiber scaffold. J Control Release *115*, 18-25.

Nakayama, D., Matsuyama, T., Ishibashi-Ueda, H., Nakagomi, T., Kasahara, Y., Hirose, H., Kikuchi-Taura, A., Stern, D. M., Mori, H., and Taguchi, A. (2010). Injury-induced neural stem/progenitor cells in post-stroke human cerebral cortex. Eur J Neurosci *31*, 90-98.

Neuwelt, E. A., Bauer, B., Fahlke, C., Fricker, G., Iadecola, C., Janigro, D., Leybaert, L., Molnar, Z., O'Donnell, M. E., Povlishock, J. T., *et al.* (2011). Engaging

neuroscience to advance translational research in brain barrier biology. Nat Rev Neurosci *12*, 169-182.

Nicholls, J., and Saunders, N. (1996). Regeneration of immature mammalian spinal cord after injury. Trends Neurosci *19*, 229-234.

Nieto, M., Monuki, E. S., Tang, H., Imitola, J., Haubst, N., Khoury, S. J., Cunningham, J., Gotz, M., and Walsh, C. A. (2004). Expression of Cux-1 and Cux-2 in the subventricular zone and upper layers II-IV of the cerebral cortex. J Comp Neurol *479*, 168-180.

Nisbet, D. R., Rodda, A. E., Horne, M. K., Forsythe, J. S., and Finkelstein, D. I. (2009). Neurite infiltration and cellular response to electrospun polycaprolactone scaffolds implanted into the brain. Biomaterials *30*, 4573-4580.

Nisbet, D. R., Rodda, A. E., Horne, M. K., Forsythe, J. S., and Finkelstein, D. I. (2010). Implantation of functionalized thermally gelling xyloglucan hydrogel within the brain: associated neurite infiltration and inflammatory response. Tissue Eng Part A *16*, 2833-2842.

Nishiyama, A. (2007). Polydendrocytes: NG2 cells with many roles in development and repair of the CNS. Neuroscientist *13*, 62-76.

Niu, W., Zang, T., Zou, Y., Fang, S., Smith, D. K., Bachoo, R., and Zhang, C. L. (2013). In vivo reprogramming of astrocytes to neuroblasts in the adult brain. Nat Cell Biol *15*, 1164-1175.

Noctor, S. C., Martinez-Cerdeno, V., Ivic, L., and Kriegstein, A. R. (2004). Cortical neurons arise in symmetric and asymmetric division zones and migrate through specific phases. Nat Neurosci *7*, 136-144.

Nomura, H., Tator, C. H., and Shoichet, M. S. (2006). Bioengineered strategies for spinal cord repair. J Neurotrauma *23*, 496-507.

O'Kusky, J., and Colonnier, M. (1982). Postnatal changes in the number of astrocytes, oligodendrocytes, and microglia in the visual cortex (area 17) of the macaque monkey: a stereological analysis in normal and monocularly deprived animals. J Comp Neurol *210*, 307-315.

Obermeier, B., Daneman, R., and Ransohoff, R. M. (2013). Development, maintenance and disruption of the blood-brain barrier. Nat Med *19*, 1584-1596.

Ohab, J. J., Fleming, S., Blesch, A., and Carmichael, S. T. (2006). A neurovascular niche for neurogenesis after stroke. J Neurosci *26*, 13007-13016.

Okada, M., Murase, K., Makino, A., Nakajima, M., Kaku, T., Furukawa, S., and Furukawa, Y. (2008). Effects of estrogens on proliferation and differentiation of neural stem/progenitor cells. Biomed Res *29*, 163-170.

Okano, H., and Sawamoto, K. (2008). Neural stem cells: involvement in adult neurogenesis and CNS repair. Philos Trans R Soc Lond B Biol Sci *363*, 2111-2122.

Orive, G., Anitua, E., Pedraz, J. L., and Emerich, D. F. (2009). Biomaterials for promoting brain protection, repair and regeneration. Nat Rev Neurosci *10*, 682-692.

Ortega, J. A., and Alcantara, S. (2010). BDNF/MAPK/ERK-induced BMP7 expression in the developing cerebral cortex induces premature radial glia differentiation and impairs neuronal migration. Cereb Cortex *20*, 2132-2144.

Otto, V. I., Gloor, S. M., Frentzel, S., Gilli, U., Ammann, E., Hein, A. E., Folkers, G., Trentz, O., Kossmann, T., and Morganti-Kossmann, M. C. (2002). The production of macrophage inflammatory protein-2 induced by soluble intercellular adhesion molecule-1 in mouse astrocytes is mediated by src tyrosine kinases and p42/44 mitogen-activated protein kinase. J Neurochem *80*, 824-834.

Oudega, M., Gautier, S. E., Chapon, P., Fragoso, M., Bates, M. L., Parel, J. M., and Bunge, M. B. (2001). Axonal regeneration into Schwann cell grafts within resorbable poly(alpha-hydroxyacid) guidance channels in the adult rat spinal cord. Biomaterials *22*, 1125-1136.

Ovens, M. J., Davies, A. J., Wilson, M. C., Murray, C. M., and Halestrap, A. P. (2010). AR-C155858 is a potent inhibitor of monocarboxylate transporters MCT1 and MCT2 that binds to an intracellular site involving transmembrane helices 7-10. Biochem J *425*, 523-530.

Palmer, T. D., Willhoite, A. R., and Gage, F. H. (2000). Vascular niche for adult hippocampal neurogenesis. J Comp Neurol *425*, 479-494.

Pangalos, M. N., Schechter, L. E., and Hurko, O. (2007). Drug development for CNS disorders: strategies for balancing risk and reducing attrition. Nat Rev Drug Discov *6*, 521-532.

Pardridge, W. M. (2005). The blood-brain barrier and neurotherapeutics. NeuroRx *2*, 1-2.

Parent, J. M., Vexler, Z. S., Gong, C., Derugin, N., and Ferriero, D. M. (2002). Rat forebrain neurogenesis and striatal neuron replacement after focal stroke. Ann Neurol *52*, 802-813.

Park, J. B., and Lakes, R. S. (1992). Biomaterials: an Introduction, Second edn (New York).

Park, K. I., Teng, Y. D., and Snyder, E. Y. (2002). The injured brain interacts reciprocally with neural stem cells supported by scaffolds to reconstitute lost tissue. Nat Biotechnol *20*, 1111-1117.

Patist, C. M., Mulder, M. B., Gautier, S. E., Maquet, V., Jerome, R., and Oudega, M. (2004). Freeze-dried poly(D,L-lactic acid) macroporous guidance scaffolds impregnated with brain-derived neurotrophic factor in the transected adult rat thoracic spinal cord. Biomaterials *25*, 1569-1582.

Pellerin, L., and Magistretti, P. J. (1994). Glutamate uptake into astrocytes stimulates aerobic glycolysis: a mechanism coupling neuronal activity to glucose utilization. Proc Natl Acad Sci U S A *91*, 10625-10629.

Pellerin, L., and Magistretti, P. J. (2003). How to balance the brain energy budget while spending glucose differently. J Physiol *546*, 325.

Pellerin, L., and Magistretti, P. J. (2012). Sweet sixteen for ANLS. J Cereb Blood Flow Metab *32*, 1152-1166.

Pellerin, L., Pellegri, G., Martin, J. L., and Magistretti, P. J. (1998). Expression of monocarboxylate transporter mRNAs in mouse brain: support for a distinct role of lactate as an energy substrate for the neonatal vs. adult brain. Proc Natl Acad Sci U S A *95*, 3990-3995.

Penning, J. P., Dijikstra, H., and Pennings, A. J. (1993). Preparation and characterization of absorvable fibers from L-lactide copolymers. polymer *34*, 942-951.

Pettikiriarachchi, J. T. S., Parish, C. L., Shoichet, M. S., Forsythe, J. S., and Nisbet, D. R. (2010). Biomaterials for brain tissue engineering. Australian Journal of Chemistry *63*, 1143-1154.

Piantino, J., Burdick, J. A., Goldberg, D., Langer, R., and Benowitz, L. I. (2006). An injectable, biodegradable hydrogel for trophic factor delivery enhances axonal rewiring and improves performance after spinal cord injury. Exp Neurol *201*, 359-367.

Pierre, K., Chatton, J. Y., Parent, A., Repond, C., Gardoni, F., Di Luca, M., and Pellerin, L. (2009). Linking supply to demand: the neuronal monocarboxylate transporter MCT2 and the alpha-amino-3-hydroxyl-5-methyl-4-isoxazole-propionic acid

receptor GluR2/3 subunit are associated in a common trafficking process. Eur J Neurosci *29*, 1951-1963.

Pierre, K., and Pellerin, L. (2005). Monocarboxylate transporters in the central nervous system: distribution, regulation and function. J Neurochem *94*, 1-14.

Pinto, G. R., Clara, C. A., Santos, M. J., Almeida, J. R., Burbano, R. R., Rey, J. A., and Casartelli, C. (2007). Mutation analysis of gene PAX6 in human gliomas. Genet Mol Res *6*, 1019-1025.

Plumpe, T., Ehninger, D., Steiner, B., Klempin, F., Jessberger, S., Brandt, M., Romer, B., Rodriguez, G. R., Kronenberg, G., and Kempermann, G. (2006). Variability of doublecortin-associated dendrite maturation in adult hippocampal neurogenesis is independent of the regulation of precursor cell proliferation. BMC Neurosci *7*, 77.

Polet, F., and Feron, O. (2013). Endothelial cell metabolism and tumour angiogenesis: glucose and glutamine as essential fuels and lactate as the driving force. J Intern Med *273*, 156-165.

Ponti, G., Obernier, K., Guinto, C., Jose, L., Bonfanti, L., and Alvarez-Buylla, A. (2013). Cell cycle and lineage progression of neural progenitors in the ventricular-subventricular zones of adult mice. Proc Natl Acad Sci U S A *110*, E1045-1054.

Pontious, A., Kowalczyk, T., Englund, C., and Hevner, R. F. (2008). Role of intermediate progenitor cells in cerebral cortex development. Dev Neurosci *30*, 24-32.

Popovich, P. G., and Longbrake, E. E. (2008). Can the immune system be harnessed to repair the CNS? Nat Rev Neurosci *9*, 481-493.

Potter, W., Kalil, R. E., and Kao, W. J. (2008). Biomimetic material systems for neural progenitor cell-based therapy. Front Biosci *13*, 806-821.

Prabhakaran, M. P., Venugopal, J. R., Chyan, T. T., Hai, L. B., Chan, C. K., Lim, A. Y., and Ramakrishna, S. (2008). Electrospun biocomposite nanofibrous scaffolds for neural tissue engineering. Tissue Eng Part A *14*, 1787-1797.

Quaegebeur, A., Segura, I., and Carmeliet, P. (2010). Pericytes: blood-brain barrier safeguards against neurodegeneration? Neuron *68*, 321-323.

Quinones-Hinojosa, A., Sanai, N., Soriano-Navarro, M., Gonzalez-Perez, O., Mirzadeh, Z., Gil-Perotin, S., Romero-Rodriguez, R., Berger, M. S., Garcia-Verdugo, J. M., and Alvarez-Buylla, A. (2006). Cellular composition and cytoarchitecture of the adult human subventricular zone: a niche of neural stem cells. J Comp Neurol *494*, 415-434.

Rafalski, V. A., and Brunet, A. (2011). Energy metabolism in adult neural stem cell fate. Prog Neurobiol *93*, 182-203.

Raff, M. C., Miller, R. H., and Noble, M. (1983). Glial cell lineages in the rat optic nerve. Cold Spring Harb Symp Quant Biol *48 Pt 2*, 569-572.

Rakic, P. (1971). Neuron-glia relationship during granule cell migration in developing cerebellar cortex. A Golgi and electronmicroscopic study in Macacus Rhesus. J Comp Neurol *141*, 283-312.

Rakic, P. (1972). Mode of cell migration to the superficial layers of fetal monkey neocortex. J Comp Neurol *145*, 61-83.

Rakic, P. (1988). Specification of cerebral cortical areas. Science *241*, 170-176.

Rakic, P. (2003). Developmental and evolutionary adaptations of cortical radial glia. Cereb Cortex *13*, 541-549.

Rakic, P. (2004). Neuroscience. Genetic control of cortical convolutions. Science *303*, 1983-1984.

Ramaswamy, S., Goings, G. E., Soderstrom, K. E., Szele, F. G., and Kozlowski, D. A. (2005). Cellular proliferation and migration following a controlled cortical impact in the mouse. Brain Res *1053*, 38-53.

Reillo, I., de Juan Romero, C., Garcia-Cabezas, M. A., and Borrell, V. (2010). A role for intermediate radial glia in the tangential expansion of the mammalian cerebral cortex. Cereb Cortex *21*, 1674-1694.

Ren, Y. J., Zhang, H., Huang, H., Wang, X. M., Zhou, Z. Y., Cui, F. Z., and An, Y. H. (2009). In vitro behavior of neural stem cells in response to different chemical functional groups. Biomaterials *30*, 1036-1044.

Rhodes, K. E., and Fawcett, J. W. (2004). Chondroitin sulphate proteoglycans: preventing plasticity or protecting the CNS? J Anat *204*, 33-48.

Ribak, C. E., Korn, M. J., Shan, Z., and Obenaus, A. (2004). Dendritic growth cones and recurrent basal dendrites are typical features of newly generated dentate granule cells in the adult hippocampus. Brain Res *1000*, 195-199.

Rinholm, J. E., Hamilton, N. B., Kessaris, N., Richardson, W. D., Bergersen, L. H., and Attwell, D. (2011). Regulation of oligodendrocyte development and myelination by glucose and lactate. J Neurosci *31*, 538-548.

Riquelme, P. A., Drapeau, E., and Doetsch, F. (2008). Brain micro-ecologies: neural stem cell niches in the adult mammalian brain. Philos Trans R Soc Lond B Biol Sci *363*, 123-137.

Robel, S., Berninger, B., and Gotz, M. (2011). The stem cell potential of glia: lessons from reactive gliosis. Nat Rev Neurosci *12*, 88-104.

Roberts, I., Schierhout, G., and Alderson, P. (1998). Absence of evidence for the effectiveness of five interventions routinely used in the intensive care management of severe head injury: a systematic review. J Neurol Neurosurg Psychiatry *65*, 729-733.

Rola, R., Mizumatsu, S., Otsuka, S., Morhardt, D. R., Noble-Haeusslein, L. J., Fishman, K., Potts, M. B., and Fike, J. R. (2006). Alterations in hippocampal neurogenesis following traumatic brain injury in mice. Exp Neurol *202*, 189-199.

Rolls, A., Shechter, R., and Schwartz, M. (2009). The bright side of the glial scar in CNS repair. Nat Rev Neurosci *10*, 235-241.

Rousselot, P., Lois, C., and Alvarez-Buylla, A. (1995). Embryonic (PSA) N-CAM reveals chains of migrating neuroblasts between the lateral ventricle and the olfactory bulb of adult mice. J Comp Neurol *351*, 51-61.

Rowitch, D. H., and Kriegstein, A. R. (2010). Developmental genetics of vertebrate glial-cell specification. Nature *468*, 214-222.

Rudge, J. S., and Silver, J. (1990). Inhibition of neurite outgrowth on astroglial scars in vitro. J Neurosci *10*, 3594-3603.

Saha, B., Jaber, M., and Gaillard, A. (2012). Potentials of endogenous neural stem cells in cortical repair. Front Cell Neurosci *6*, 14.

Saha, B., Peron, S., Murray, K., Jaber, M., and Gaillard, A. (2013). Cortical lesion stimulates adult subventricular zone neural progenitor cell proliferation and migration to the site of injury. Stem Cell Res *11*, 965-977.

Saha, K., Keung, A. J., Irwin, E. F., Li, Y., Little, L., Schaffer, D. V., and Healy, K. E. (2008). Substrate modulus directs neural stem cell behavior. Biophys J *95*, 4426-4438.

Sahoo, S. K., and Labhasetwar, V. (2003). Nanotech approaches to drug delivery and imaging. Drug Discov Today *8*, 1112-1120.

Samadikuchaksaraei, A. (2007). An overview of tissue engineering approaches for management of spinal cord injuries. J Neuroeng Rehabil *4*, 15.

Samuel, C., Cayuela, J., Barakat, I., Muller, A. J., Raquez, J. M., and Dubois, P. (2013). Stereocomplexation of polylactide enhanced by poly(methyl methacrylate): improved processability and thermomechanical properties of stereocomplexable polylactide-based materials. ACS Appl Mater Interfaces *5*, 11797-11807.

Santos, E., Hernandez, R. M., Pedraz, J. L., and Orive, G. (2012). Novel advances in the design of three-dimensional bio-scaffolds to control cell fate: translation from 2D to 3D. Trends Biotechnol *30*, 331-341.

Satyanarayana, D., and Chatterji, P. R. (1993). Biodegradable polymers: challenges and strategies. J M S-Rev Macromol Chem Phys *C33*, 349-368.

Schmidt, O. I., Heyde, C. E., Ertel, W., and Stahel, P. F. (2005). Closed head injury--an inflammatory disease? Brain Res Brain Res Rev *48*, 388-399.

Schnyder, A., and Huwyler, J. (2005). Drug transport to brain with targeted liposomes. NeuroRx *2*, 99-107.

Schurr, A., Payne, R. S., Miller, J. J., and Rigor, B. M. (1997). Brain lactate, not glucose, fuels the recovery of synaptic function from hypoxia upon reoxygenation: an in vitro study. Brain Res *744*, 105-111.

Schurr, A., Payne, R. S., Miller, J. J., Tseng, M. T., and Rigor, B. M. (2001). Blockade of lactate transport exacerbates delayed neuronal damage in a rat model of cerebral ischemia. Brain Res *895*, 268-272.

Schurr, A., Payne, R. S., Tseng, M. T., Miller, J. J., and Rigor, B. M. (1999). The glucose paradox in cerebral ischemia. New insights. Ann N Y Acad Sci *893*, 386-390.

Schurr, A., and Rigor, B. M. (1998). Brain anaerobic lactate production: a suicide note or a survival kit? Dev Neurosci *20*, 348-357.

Schwab, M. E., and Bartholdi, D. (1996). Degeneration and regeneration of axons in the lesioned spinal cord. Physiol Rev *76*, 319-370.

Schwartz, M. (2000). Autoimmune involvement in CNS trauma is beneficial if well controlled. Prog Brain Res *128*, 259-263.

Schwartz, M., and Yoles, E. (2005). Macrophages and dendritic cells treatment of spinal cord injury: from the bench to the clinic. Acta Neurochir Suppl *93*, 147-150.

Scolding, N. J., Rayner, P. J., and Compston, D. A. (1999). Identification of A2B5-positive putative oligodendrocyte progenitor cells and A2B5-positive astrocytes in adult human white matter. Neuroscience *89*, 1-4.

Sessa, A., Mao, C. A., Hadjantonakis, A. K., Klein, W. H., and Broccoli, V. (2008). Tbr2 directs conversion of radial glia into basal precursors and guides neuronal amplification by indirect neurogenesis in the developing neocortex. Neuron *60*, 56-69.

Shechter, R., London, A., Varol, C., Raposo, C., Cusimano, M., Yovel, G., Rolls, A., Mack, M., Pluchino, S., Martino, G., *et al.* (2009). Infiltrating blood-derived macrophages are vital cells playing an anti-inflammatory role in recovery from spinal cord injury in mice. PLoS Med *6*, e1000113.

Shechter, R., Miller, O., Yovel, G., Rosenzweig, N., London, A., Ruckh, J., Kim, K. W., Klein, E., Kalchenko, V., Bendel, P., *et al.* (2013). Recruitment of beneficial M2 macrophages to injured spinal cord is orchestrated by remote brain choroid plexus. Immunity *38*, 555-569.

Shechter, R., Raposo, C., London, A., Sagi, I., and Schwartz, M. (2011). The glial scar-monocyte interplay: a pivotal resolution phase in spinal cord repair. PLoS One *6*, e27969.

Sheikh, A. Y., Gibson, J. J., Rollins, M. D., Hopf, H. W., Hussain, Z., and Hunt, T. K. (2000). Effect of hyperoxia on vascular endothelial growth factor levels in a wound model. Arch Surg *135*, 1293-1297.

Shen, Q., Goderie, S. K., Jin, L., Karanth, N., Sun, Y., Abramova, N., Vincent, P., Pumiglia, K., and Temple, S. (2004). Endothelial cells stimulate self-renewal and expand neurogenesis of neural stem cells. Science *304*, 1338-1340.

Shen, Q., Wang, Y., Kokovay, E., Lin, G., Chuang, S. M., Goderie, S. K., Roysam, B., and Temple, S. (2008). Adult SVZ stem cells lie in a vascular niche: a quantitative analysis of niche cell-cell interactions. Cell Stem Cell *3*, 289-300.

Sherwood, L. (2001). Human Physiology: From Cells to Systems., 4th edn).

Shin, Y. M., Hohmann, M. M., Brenner, M. P., and Rutledge, G. C. (2001). Experimental characterization of electrospinning: the elctrically forced jet and instabilities. Polymer *42*, 09955-09967.

Shoichet, M. S., Tate, C. C., Baumann, M. D., and LaPlaca, M. C. (2008). Strategies for Regeneration and Repair in the Injured Central Nervous System Environment.

Siesjo, B. K., Johannsson, H., Ljunggren, B., and Norberg, K. (1974). Brain dysfunction in cerebral hypoxia and ischemia. Res Publ Assoc Res Nerv Ment Dis *53*, 75-112.

Silva, G. A., Czeisler, C., Niece, K. L., Beniash, E., Harrington, D. A., Kessler, J. A., and Stupp, S. I. (2004). Selective differentiation of neural progenitor cells by high-epitope density nanofibers. Science *303*, 1352-1355.

Silver, J., and Miller, J. H. (2004). Regeneration beyond the glial scar. Nat Rev Neurosci *5*, 146-156.

Simon-Assmann, P., Orend, G., Mammadova-Bach, E., Spenle, C., and Lefebvre, O. (2011). Role of laminins in physiological and pathological angiogenesis. Int J Dev Biol *55*, 455-465.

Simpson, I. A., Carruthers, A., and Vannucci, S. J. (2007). Supply and demand in cerebral energy metabolism: the role of nutrient transporters. J Cereb Blood Flow Metab *27*, 1766-1791.

Sims, K. D., and Robinson, M. B. (1999). Expression patterns and regulation of glutamate transporters in the developing and adult nervous system. Crit Rev Neurobiol *13*, 169-197.

Simsek, T., Kocabas, F., Zheng, J., Deberardinis, R. J., Mahmoud, A. I., Olson, E. N., Schneider, J. W., Zhang, C. C., and Sadek, H. A. (2010). The distinct metabolic profile of hematopoietic stem cells reflects their location in a hypoxic niche. Cell Stem Cell *7*, 380-390.

Sirko, S., Neitz, A., Mittmann, T., Horvat-Brocker, A., von Holst, A., Eysel, U. T., and Faissner, A. (2009). Focal laser-lesions activate an endogenous population of neural stem/progenitor cells in the adult visual cortex. Brain *132*, 2252-2264.

Skihar, V., Silva, C., Chojnacki, A., Doring, A., Stallcup, W. B., Weiss, S., and Yong, V. W. (2009). Promoting oligodendrogenesis and myelin repair using the multiple sclerosis medication glatiramer acetate. Proc Natl Acad Sci U S A *106*, 17992-17997.

Smith, L. A., and Ma, P. X. (2004). Nano-fibrous scaffolds for tissue engineering. Colloids Surf B Biointerfaces *39*, 125-131.

Sofroniew, M. V. (2005). Reactive astrocytes in neural repair and protection. Neuroscientist *11*, 400-407.

Sokoloff, L. (1992). Energy metabolism and effects of energy depletion or exposure to glutamate. Can J Physiol Pharmacol *70 Suppl*, S107-112.

Sotelo-Hitschfeld, T., Fernandez-Moncada, I., and Barros, L. F. (2012). Acute feedback control of astrocytic glycolysis by lactate. Glia *60*, 674-680.

Speder, P., Liu, J., and Brand, A. H. (2011). Nutrient control of neural stem cells. Curr Opin Cell Biol *23*, 724-729.

Stabenfeldt, S. E., Garcia, A. J., and LaPlaca, M. C. (2006). Thermoreversible laminin-functionalized hydrogel for neural tissue engineering. J Biomed Mater Res A *77*, 718-725.

Stark, R., Pasquel, F., Turcu, A., Pongratz, R. L., Roden, M., Cline, G. W., Shulman, G. I., and Kibbey, R. G. (2009). Phosphoenolpyruvate cycling via mitochondrial phosphoenolpyruvate carboxykinase links anaplerosis and mitochondrial GTP with insulin secretion. J Biol Chem *284*, 26578-26590.

Strack, A., Asensio, V. C., Campbell, I. L., Schluter, D., and Deckert, M. (2002). Chemokines are differentially expressed by astrocytes, microglia and inflammatory leukocytes in Toxoplasma encephalitis and critically regulated by interferon-gamma. Acta Neuropathol *103*, 458-468.

Stubbs, D., DeProto, J., Nie, K., Englund, C., Mahmud, I., Hevner, R., and Molnar, Z. (2009). Neurovascular congruence during cerebral cortical development. Cereb Cortex *19 Suppl 1*, i32-41.

Suda, T., Takubo, K., and Semenza, G. L. (2011). Metabolic regulation of hematopoietic stem cells in the hypoxic niche. Cell Stem Cell *9*, 298-310.

Suh, H., Consiglio, A., Ray, J., Sawai, T., D'Amour, K. A., and Gage, F. H. (2007). In vivo fate analysis reveals the multipotent and self-renewal capacities of Sox2+ neural stem cells in the adult hippocampus. Cell Stem Cell *1*, 515-528.

Sundholm-Peters, N. L., Yang, H. K., Goings, G. E., Walker, A. S., and Szele, F. G. (2005). Subventricular zone neuroblasts emigrate toward cortical lesions. J Neuropathol Exp Neurol *64*, 1089-1100.

Suzuki, T., Sugiyama, M., Wakazono, K., Kaneko, Y., and Harashima, S. (2011). Lactic-acid stress causes vacuolar fragmentation and impairs intracellular amino-acid homeostasis in Saccharomyces cerevisiae. J Biosci Bioeng *113*, 421-430.

Szele, F. G., and Chesselet, M. F. (1996). Cortical lesions induce an increase in cell number and PSA-NCAM expression in the subventricular zone of adult rats. J Comp Neurol *368*, 439-454.

Tabata, H., Yoshinaga, S., and Nakajima, K. (2012). Cytoarchitecture of mouse and human subventricular zone in developing cerebral neocortex. Exp Brain Res *216*, 161-168.

Tabernero, A., Vicario, C., and Medina, J. M. (1996). Lactate spares glucose as a metabolic fuel in neurons and astrocytes from primary culture. Neurosci Res *26*, 369-376.

Takubo, K., Nagamatsu, G., Kobayashi, C. I., Nakamura-Ishizu, A., Kobayashi, H., Ikeda, E., Goda, N., Rahimi, Y., Johnson, R. S., Soga, T., *et al.* (2013). Regulation of glycolysis by Pdk functions as a metabolic checkpoint for cell cycle quiescence in hematopoietic stem cells. Cell Stem Cell *12*, 49-61.

Tam, S. J., and Watts, R. J. (2010). Connecting vascular and nervous system development: angiogenesis and the blood-brain barrier. Annu Rev Neurosci *33*, 379-408.

Tanaka, E. M., and Ferretti, P. (2009). Considering the evolution of regeneration in the central nervous system. Nat Rev Neurosci *10*, 713-723.

Tanaka, K. (2007). Role of glutamate transporters in astrocytes. Brain Nerve *59*, 677-688.

Tarabykin, V., Stoykova, A., Usman, N., and Gruss, P. (2001). Cortical upper layer neurons derive from the subventricular zone as indicated by Svet1 gene expression. Development *128*, 1983-1993.

Tate, C. C., Shear, D. A., Tate, M. C., Archer, D. R., Stein, D. G., and LaPlaca, M. C. (2009). Laminin and fibronectin scaffolds enhance neural stem cell transplantation into the injured brain. J Tissue Eng Regen Med *3*, 208-217.

Tate, C. C., Tate, M. C., and LaPlaca, M. C. (2007). Fibronectin and laminin increase in the mouse brain after controlled cortical impact injury. J Neurotrauma *24*, 226-230.

Tate, M. C., Shear, D. A., Hoffman, S. W., Stein, D. G., Archer, D. R., and LaPlaca, M. C. (2002). Fibronectin promotes survival and migration of primary neural stem cells transplanted into the traumatically injured mouse brain. Cell Transplant *11*, 283-295.

Tavazoie, M., Van der Veken, L., Silva-Vargas, V., Louissaint, M., Colonna, L., Zaidi, B., Garcia-Verdugo, J. M., and Doetsch, F. (2008). A specialized vascular niche for adult neural stem cells. Cell Stem Cell *3*, 279-288.

Teng, Y. D., Lavik, E. B., Qu, X., Park, K. I., Ourednik, J., Zurakowski, D., Langer, R., and Snyder, E. Y. (2002). Functional recovery following traumatic spinal cord injury mediated by a unique polymer scaffold seeded with neural stem cells. Proc Natl Acad Sci U S A *99*, 3024-3029.

Teo, W. E., and Ramakrishna, S. (2009). Electrospun nanofibers as a plataform for multifunctional, hierarchically organized nanocomposite. Compos Sci Technol *69*, 1804-1817.

Thiyagarajan, M., Fernandez, J. A., Lane, S. M., Griffin, J. H., and Zlokovic, B. V. (2008). Activated protein C promotes neovascularization and neurogenesis in postischemic brain via protease-activated receptor 1. J Neurosci *28*, 12788-12797.

Thored, P., Wood, J., Arvidsson, A., Cammenga, J., Kokaia, Z., and Lindvall, O. (2007). Long-term neuroblast migration along blood vessels in an area with transient angiogenesis and increased vascularization after stroke. Stroke *38*, 3032-3039.

Tom, V. J., Doller, C. M., Malouf, A. T., and Silver, J. (2004). Astrocyte-associated fibronectin is critical for axonal regeneration in adult white matter. J Neurosci *24*, 9282-9290.

Tombaugh, G. C., and Sapolsky, R. M. (1990). Mechanistic distinctions between excitotoxic and acidotic hippocampal damage in an in vitro model of ischemia. J Cereb Blood Flow Metab *10*, 527-535.

Trabold, O., Wagner, S., Wicke, C., Scheuenstuhl, H., Hussain, M. Z., Rosen, N., Seremetiev, A., Becker, H. D., and Hunt, T. K. (2003). Lactate and oxygen constitute a fundamental regulatory mechanism in wound healing. Wound Repair Regen *11*, 504-509.

Trotter, J. (2005). NG2-positive cells in CNS function and the pathological role of antibodies against NG2 in demyelinating diseases. J Neurol Sci *233*, 37-42.

Tsacopoulos, M., and Magistretti, P. J. (1996). Metabolic coupling between glia and neurons. J Neurosci *16*, 877-885.

Tsang, K. Y., Cheung, M. C., Chan, D., and Cheah, K. S. (2010). The developmental roles of the extracellular matrix: beyond structure to regulation. Cell Tissue Res *339*, 93-110.

Tsuji, H., and Ikarashi, K. (2004). In vitro hydrolysis of poly(L-lactide) crystalline residues as extended-chain crystallites. Part I: long-term hydrolysis in phosphate-buffered solution at 37 degrees C. Biomaterials *25*, 5449-5455.

Tsuji, O., Miura, K., Okada, Y., Fujiyoshi, K., Mukaino, M., Nagoshi, N., Kitamura, K., Kumagai, G., Nishino, M., Tomisato, S.*, et al.* (2010). Therapeutic potential of appropriately evaluated safe-induced pluripotent stem cells for spinal cord injury. Proc Natl Acad Sci U S A *107*, 12704-12709.

Tu, C., Cai, Q., Yang, J., Wan, Y., Bei, J., and Wang, S. (2003). The fabrication and characterization of poly (lacticacid) scaffolds for tissue engineering by improved solid–liquid phase separation. Polymer for advanced Technologies *14*, 565-573.

Urrea, C., Castellanos, D. A., Sagen, J., Tsoulfas, P., Bramlett, H. M., and Dietrich, W. D. (2007). Widespread cellular proliferation and focal neurogenesis after traumatic brain injury in the rat. Restor Neurol Neurosci *25*, 65-76.

van Hall, G., Stromstad, M., Rasmussen, P., Jans, O., Zaar, M., Gam, C., Quistorff, B., Secher, N. H., and Nielsen, H. B. (2009). Blood lactate is an important energy source for the human brain. J Cereb Blood Flow Metab *29*, 1121-1129.

van Praag, H., Kempermann, G., and Gage, F. H. (1999). Running increases cell proliferation and neurogenesis in the adult mouse dentate gyrus. Nat Neurosci *2*, 266-270.

Vasudevan, A., and Bhide, P. G. (2008). Angiogenesis in the embryonic CNS: a new twist on an old tale. Cell Adh Migr *2*, 167-169.

Vazin, T., and Schaffer, D. V. (2010). Engineering strategies to emulate the stem cell niche. Trends Biotechnol *28*, 117-124.

Verma, A. (2000). Opportunities for neuroprotection in traumatic brain injury. J Head Trauma Rehabil *15*, 1149-1161.

Vert, M. (2009). Bioabsorbable polymers in medicine: an overview. EuroIntervention *5 Suppl F*, F9-F14.

Vicario, C., Tabernero, A., and Medina, J. M. (1993). Regulation of lactate metabolism by albumin in rat neurons and astrocytes from primary culture. Pediatr Res *34*, 709-715.

Vijayan, V. K., Lee, Y. L., and Eng, L. F. (1990). Increase in glial fibrillary acidic protein following neural trauma. Mol Chem Neuropathol *13*, 107-118.

Vives, V., Alonso, G., Solal, A. C., Joubert, D., and Legraverend, C. (2003). Visualization of S100B-positive neurons and glia in the central nervous system of EGFP transgenic mice. J Comp Neurol *457*, 404-419.

Waagepetersen, H. S., Bakken, I. J., Larsson, O. M., Sonnewald, U., and Schousboe, A. (1998). Comparison of lactate and glucose metabolism in cultured neocortical neurons and astrocytes using 13C-NMR spectroscopy. Dev Neurosci *20*, 310-320.

Wang, H. B., Mullins, M. E., Cregg, J. M., Hurtado, A., Oudega, M., Trombley, M. T., and Gilbert, R. J. (2009a). Creation of highly aligned electrospun poly-L-lactic acid fibers for nerve regeneration applications. J Neural Eng *6*, 016001.

Wang, Q., Li, S., Wang, Z., Liu, H., and Li, C. (2009b). Preparation and characterization of a positive thermoresponsive hydrogel for drug loading and release. Journal of Applied Polymer Science *111*, 1417-1425.

Weiss, S., Reynolds, B. A., Vescovi, A. L., Morshead, C., Craig, C. G., and van der Kooy, D. (1996). Is there a neural stem cell in the mammalian forebrain? Trends Neurosci *19*, 387-393.

Weissman, T., Noctor, S. C., Clinton, B. K., Honig, L. S., and Kriegstein, A. R. (2003). Neurogenic radial glial cells in reptile, rodent and human: from mitosis to migration. Cereb Cortex *13*, 550-559.

Wen, J., Hu, Q., Li, M., Wang, S., Zhang, L., Chen, Y., and Li, L. (2008). Pax6 directly modulate Sox2 expression in the neural progenitor cells. Neuroreport *19*, 413-417.

Wernig, M., Zhao, J. P., Pruszak, J., Hedlund, E., Fu, D., Soldner, F., Broccoli, V., Constantine-Paton, M., Isacson, O., and Jaenisch, R. (2008). Neurons derived from reprogrammed fibroblasts functionally integrate into the fetal brain and improve

symptoms of rats with Parkinson's disease. Proc Natl Acad Sci U S A *105*, 5856-5861.

White, R. E., and Jakeman, L. B. (2008). Don't fence me in: harnessing the beneficial roles of astrocytes for spinal cord repair. Restor Neurol Neurosci *26*, 197-214.

Wiltrout, C., Lang, B., Yan, Y., Dempsey, R. J., and Vemuganti, R. (2007). Repairing brain after stroke: a review on post-ischemic neurogenesis. Neurochem Int *50*, 1028-1041.

Woerly, S., Petrov, P., Sykova, E., Roitbak, T., Simonova, Z., and Harvey, A. R. (1999). Neural tissue formation within porous hydrogels implanted in brain and spinal cord lesions: ultrastructural, immunohistochemical, and diffusion studies. Tissue Eng *5*, 467-488.

Wong, D. Y., Hollister, S. J., Krebsbach, P. H., and Nosrat, C. (2007). Poly(epsilon-caprolactone) and poly (L-lactic-co-glycolic acid) degradable polymer sponges attenuate astrocyte response and lesion growth in acute traumatic brain injury. Tissue Eng *13*, 2515-2523.

Wong, D. Y., Krebsbach, P. H., and Hollister, S. J. (2008). Brain cortex regeneration affected by scaffold architectures. J Neurosurg *109*, 715-722.

Wu, L. J., Vadakkan, K. I., and Zhuo, M. (2007). ATP-induced chemotaxis of microglial processes requires P2Y receptor-activated initiation of outward potassium currents. Glia *55*, 810-821.

Wurm, F., Keiner, S., Kunze, A., Witte, O. W., and Redecker, C. (2007). Effects of skilled forelimb training on hippocampal neurogenesis and spatial learning after focal cortical infarcts in the adult rat brain. Stroke *38*, 2833-2840.

Xie, J., MacEwan, M. R., Schwartz, A. G., and Xia, Y. (2009). Electrospun nanofibers for neural tissue engineering. Nanoscale *2*, 35-44.

Yamasaki, M., Yamada, K., Furuya, S., Mitoma, J., Hirabayashi, Y., and Watanabe, M. (2001). 3-Phosphoglycerate dehydrogenase, a key enzyme for l-serine biosynthesis, is preferentially expressed in the radial glia/astrocyte lineage and olfactory ensheathing glia in the mouse brain. J Neurosci *21*, 7691-7704.

Yamashita, T., Ninomiya, M., Hernandez Acosta, P., Garcia-Verdugo, J. M., Sunabori, T., Sakaguchi, M., Adachi, K., Kojima, T., Hirota, Y., Kawase, T., *et al.* (2006). Subventricular zone-derived neuroblasts migrate and differentiate into mature neurons in the post-stroke adult striatum. J Neurosci *26*, 6627-6636.

Yang, F., Murugan, R., Wang, S., and Ramakrishna, S. (2005). Electrospinning of nano/micro scale poly(L-lactic acid) aligned fibers and their potential in neural tissue engineering. Biomaterials *26*, 2603-2610.

Yao, S., Liu, X., Wang, X., Merolli, A., Chen, X., and Cui, F. (2013). Directing neural stem cell fate with biomaterial parameters for injured brain regeneration. Prog in Natural Science: Materials International *23*, 103-112.

Yoshikawa, G., Momiyama, T., Oya, S., Takai, K., Tanaka, J., Higashiyama, S., Saito, N., Kirino, T., and Kawahara, N. (2010). Induction of striatal neurogenesis and generation of region-specific functional mature neurons after ischemia by growth factors. Laboratory investigation. J Neurosurg *113*, 835-850.

Zauner, A., Doppenberg, E., Woodward, J. J., Allen, C., Jebraili, S., Young, H. F., and Bullock, R. (1997). Multiparametric continuous monitoring of brain metabolism and substrate delivery in neurosurgical patients. Neurol Res *19*, 265-273.

Zhang, H., Hayashi, T., Tsuru, K., Deguchi, K., Nagahara, M., Hayakawa, S., Nagai, M., Kamiya, T., Osaka, A., and Abe, K. (2007). Vascular endothelial growth factor

promotes brain tissue regeneration with a novel biomaterial polydimethylsiloxane-tetraethoxysilane. Brain Res *1132*, 29-35.

Zhang, S. C., Wernig, M., Duncan, I. D., Brustle, O., and Thomson, J. A. (2001). In vitro differentiation of transplantable neural precursors from human embryonic stem cells. Nat Biotechnol *19*, 1129-1133.

Zhang, Y., and Pardridge, W. M. (2001). Conjugation of brain-derived neurotrophic factor to a blood-brain barrier drug targeting system enables neuroprotection in regional brain ischemia following intravenous injection of the neurotrophin. Brain Res *889*, 49-56.

Zhao, C., Deng, W., and Gage, F. H. (2008). Mechanisms and functional implications of adult neurogenesis. Cell *132*, 645-660.

Zuo, J., Ferguson, T. A., Hernandez, Y. J., Stetler-Stevenson, W. G., and Muir, D. (1998). Neuronal matrix metalloproteinase-2 degrades and inactivates a neurite-inhibiting chondroitin sulfate proteoglycan. J Neurosci *18*, 5203-5211.

APPENDIX I

Supplementary Information

Supplementary Figures

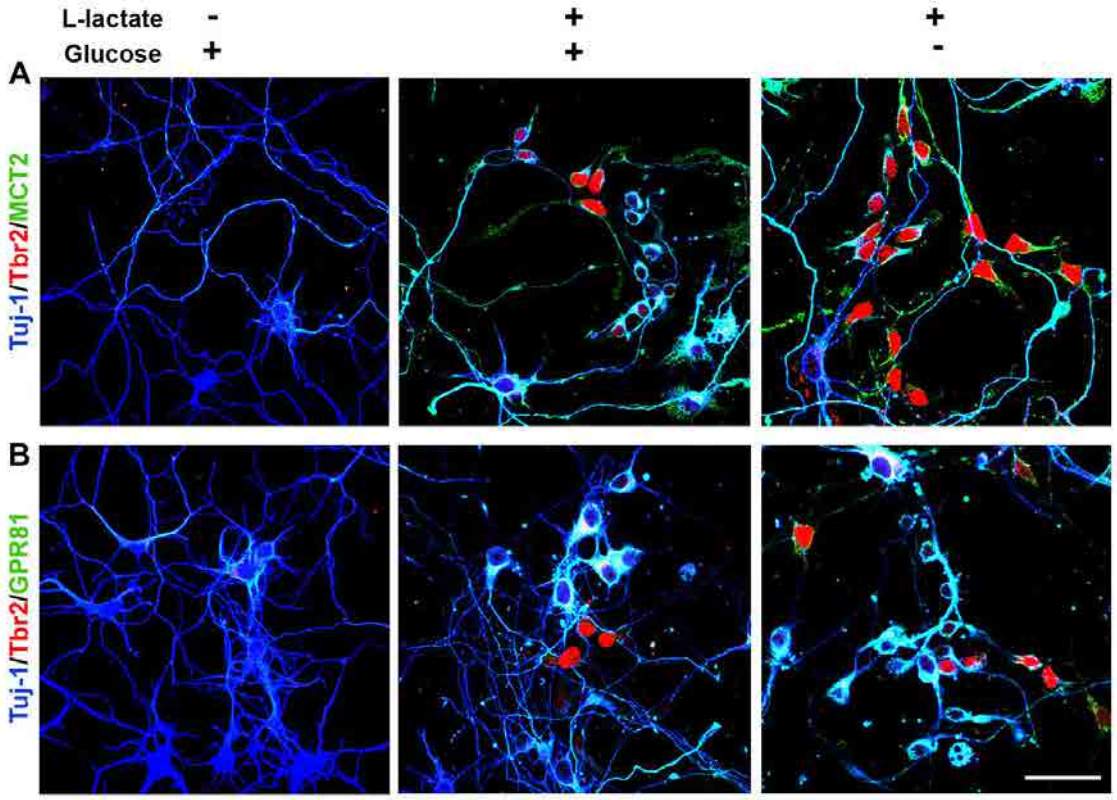

Supplementary figure 1. Expression of the lactate metabolic machinery in neuronal cell cultures treated with L-lactate. Confocal images of neuronal cell cultures grown in glucose, glucose+L-lactate, or lactate medium. **A.** Triple immunostaining of Tuj-1^{+} neurons (blue), Tbr2^{+} neuronal progenitor cells (red), and cells expressing the lactate H+/monocarboxylate transporter MCT2 (green). **B.** Triple immunostaining of Tuj-1^{+} neurons (blue), Tbr2^{+} neuronal progenitor cells (red), and cells expressing the lactate receptor GPR81 (green). Scale bar = 40μm.

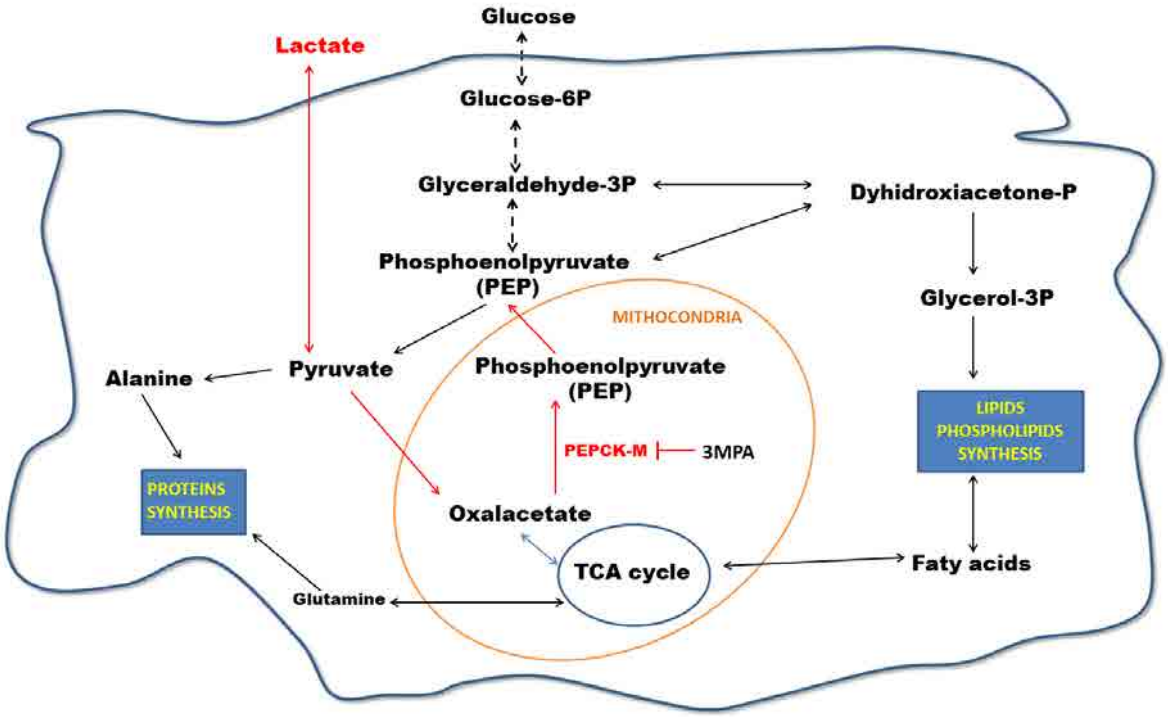

Supplementary figure 2. Scheme of lactate metabolism via PEPCK-M cataplerosis pathway (red arrows).

Supplementary Videos

Supplementary video 1. Reconstruction of neural cells cultured on aligned fibers. Confocal images of BLbP$^+$ glia (green) and Tuj-1$^+$ neurons (red) on aligned nanofibers after 10*div*. Cells colonized an area of 173μm in the z plane of the scaffold screened under Spectral Leica TCS-SL confocal microscope (x10 lens). Confocal images were processed using the Leica TCS-SL confocal software. Scale Bar: 20μm.

Supplementary video 2. Live-imaging of a neuron migrating on an aligned PLA fiber. Representative live-imaging shows an embryonic neuron migrating on top of an aligned PLA fiber after 5 days *in vitro*. Images were captured once a minute using an Axiovert 40 CFL light-inverted microscope (20× lens). Images were processed using the Image J program. Total time =13 h 50 min. Scale bar: 25μm.

Supplementary video 3. Neurovascular bridge at P11. Biobridges inside radial scaffolds were organized by glial populations composed of nestin+ radial glia (green) around a central blood vessel formed by endothelial cells surrounded by a laminin-rich basal lamina (red). Nuclei were stained with Topro (blue). Coronal tissue sections (50 μm thick) were screened using a Leica TCS-SL spectral confocal microscope (63× oil immersion objective). Confocal images were reconstructed in 3D using the Imaris program (Bitplane scientific software) for 3D and 4D real-time interactive data viewing using shadow projections. Scale bar: 40 μm.

Supplementary video 4. Reconstruction of the vascularization inside an aligned fiber scaffold 1 year after implantation. The vascular network of 1-year-old mouse brains, with aspiration lesions created at P4, implanted with radially aligned nanofibers and labeled by transcardiac perfusion with DiI (red). Coronal tissue sections (300 μm thick) were screened using a Leica TCS-SL spectral confocal microscope (10× lens). Confocal images were reconstructed using the Imaris program (Bitplane scientific software) for 3D and 4D real-time interactive data viewing. Scale bar: 200μm.

Supplementary video 5. Reconstruction of cortical vascularization in the intact contralateral cortex 1 year after implantation. Similar to the procedure in Supplementary video 3.

Supplementary video 6. Reconstruction of vascularization inside a random fiber scaffold 1 year after implantation. Similar to the procedure in Supplementary video 3.

APPENDIX II

-Scientific Communications-

Oral Presentation

Zaida Álvarez, Miguel Angel Mateos, Petra Hyrossova, Oscar Castaño, Josep A. Planell, J.Carlos Perales, Elisabeth Engel, Soledad Alcántara; "Effect of PLA 5/5 and 70/30 films on glial and neuronal maturation: role of lactate in maintaining the neuronal progenitor niche". 25th European Conference on Biomaterials (ESB), 8th-12th September 2013, Madrid, Spain.

Zaida Álvarez, Oscar Castaño, Josep A. Planell., Soledad Alcántara and Elisabeth Engel; "Response of neural cells to different types of Poly Lactic Acid". V European Chapter of The Tissue Engineering And Regenerative Medicine International Society (TERMIS), 7th-10th June 2011, Granada, Spain.

Oral flash poster presentation (3-5min)

Zaida Álvarez, Oscar Castaño, Josep A. Planell, Elisabeth Engel and Soledad Alcantàra. "3D electrospun Polylactic acid nanofibers induce radial glia like cells and neurons migrating phenotypes". 2nd Brain Extracellular Matrix in Health and Disease (ECMNET) Conference, 12-13th July 2012, Barcelona, Spain,.

Zaida Álvarez, Oscar Castaño, Josep A. Planell., Soledad Alcántara and Elisabeth Engel; "Nanofibers of Poly Lactic acid for nerve regeneration". 4th IBEC Symposium and Workshop on Bioengineering and Nanomedicine, 18th of October 2011, Barcelona, Spain.

Poster Presentations

Zaida Álvarez, Oscar Castaño, Josep A. Planell, Elisabeth Engel and Soledad Alcantàra. "3D Nanofibres Scaffold mimics neural progenitor niches". FENS Featured Regional Meeting, 11-14th September 2013, Prague, Czech Republic.

Zaida Álvarez, Oscar Castaño, Miguel A. Mateos-Timoneda, Josep A. Planell, Soledad Alcantàra and Elisabeth Engel. "3D Nanofibres Scaffold mimics neural progenitor

niches". 6th IBEC Symposium on Bioengineering and Nanomedicine, 11th June 2013, Barcelona, Spain.

Zaida Álvarez, Benjamín Torrejón-Escribano, Soledad Alcántara, "New improvments in optical clearing protocol for imaging of organs, embryos and little animals". 1st Congress Red Española Microscopía Optica Avanzada (REMOA), 20-22nd November 2012, Barcelona, Spain.

Zaida Álvarez , Josep A. Planell , Elisabeth Engel and Soledad Alcántara, "Nanofibers of Poly Lactic acid for nerve regeneration". 24th European Conference on Biomaterials, 5-9th September 2012, Dublin, Ireland.

Zaida Álvarez, Oscar Castaño, Josep A. Planell, Elisabeth Engel and Soledad Alcantàra. 3D electrospun Polylactic acid nanofibers induce radial glia like cells and neurons migrating phenotypes. 8th Federation of European Neuroscience Societies Forum (FENS), 14-18th July 2012, Barcelona, Spain.

Zaida Álvarez, Oscar Castaño, Josep A. Planell, Soledad Alcantàra and Elisabeth Engel. "Aligned Polylactic acid nanofibers induce inmature phenotypes on brain cortex cells *in vitro* and *in vivo*". 5h IBEC Symposium on Bioengineering and Nanomedicine, 11th June 2012, Barcelona, Spain.

Zaida Álvarez, Oscar Castaño, Josep A. Planell, Soledad Alcantàra and Elisabeth Engel. "3D scaffolds of PLA induce neural and blood vessels invasion *in vivo*". th World Biomaterials Congress, 1-5th June 2012, Chengdu, China.

Marta Mattotti, **Zaida Alvarez**, Josep.A. Planell, Elisabeth Engel and Soledad Alcántara, "Inducing in vitro astrocytes de-differentiation using a micropatterned polymer". 7th Federation of European Neuroscience Societies Forum (FENS), 2-7th July 2010, Amsterdam, Netherlands.

Zaida Álvarez , Josep A. Planell , Soledad Alcantàra and Elisabeth Engel, "Response of neural cells to Poly L/DL Lactic Acid 95/5 and 70/30". 3rd IBEC Symposium on Bioengineering and Nanomedicine, 1-2nd June 2010, Barcelona.

Meeting Attendance

2nd Spinal Cord Repair Meeting, 26-27th April 2013, Barcelona, Spain.

2nd Annual Conference of COST Action ECMNET: Brain Extracellular Matrix in Health and Disease, 12-13th July 2012, Barcelona, Spain.

CIBICAT, Global Questions on Advanced Biology, 9-12th July 2012, Barcelona, Spain.

2nd China-Europe Symposium on Biomaterials in Regenerative Medicine, 16-20th November 2009, Barcelona, Spain.

Awards

Best oral presentation at 25th European Conference of Biomaterials (ESB) and the 10th Young Scientific Forum, 8th-12th September 2013, Madrid, Spain. Entitled: "Effect of PLA95/5 and 70/30 films on glial and neuronal maturation: role of lactate in maintaining the neuronal progenitor niche".

Best oral presentation at 5th European Chapter of The Tissue Engineering and Regenerative Medicine International Society (TERMIS), 7th-10th June 2011, Granada, Spain. Entitled: "Response of neural cells to different types of poly lactic acid".

Best poster at 6th IBEC Symposium on Bioengineering and Nanomedicine, 11th June 2013, Barcelona, Spain. Entitled: "3D nanofibers scaffolds mimics neural progenitor niches".

APPENDIX III

PUBLICATIONS

PUBLICATIONS RELATED WITH THIS THESIS

Álvarez Z., Castaño O., Castells Alba A., Mateos-Timoneda, Planell J.A., Engel E., Alcántara S. Neurogenesis and vascularization of the damaged brain using a lactate-releasing biomimetic scaffold. Biomaterials, Volume 35, Issue 17, Pages 4769–4781, June 2014.

Álvarez Z., Mateos-Timoneda M.A., yroššová P., Castaño O., Planell J.A., Perales J.C., Engel E., Alcántara S. The effect of the composition of PLA films and lactate release on glial and neuronal maturation and the maintenance of the neuronal progenitor niche. Biomaterials, Volume 34, Issue 9, Pages 2221-2233, March 2013.

Álvarez Z.*, yroššová P.*, Engel E., Alcántara S., Perales J.C. Neuronal progenitor maintenance requires lactate metabolism and PEPCK-M directed cataplerosis. Cerebral Cortex, *Submitted June 2014.*

PUBLICATIONS UNRELATED WITH THIS THESIS

Álvarez Z., Sena E., Mattotti M., Engel E., Alcántara S. An efficient and reproducible method to culture Bergmann radial glia using textured PMMA. Journal of Neuroscience Methods, Volume 232, Pages 93-101, July 2014.

Mattotti M., **Álvarez Z**., Ortega J.A., Planell J.A., Engel E., Alcántara S. Inducing functional radial glia-like progenitors from cortical astrocyte cultures using micropatterned PMMA. Biomaterials, Volume 33, Issue 6, Pages 1759-1770, February 2012.

*Equal contribution authors

Biomaterials 35 (2014) 4769–4781

Contents lists available at ScienceDirect

Biomaterials

journal homepage: www.elsevier.com/locate/biomaterials

Neurogenesis and vascularization of the damaged brain using a lactate-releasing biomimetic scaffold

Zaida Álvarez [a,b,d], Oscar Castaño [a,c,d], Alba A. Castells [b], Miguel A. Mateos-Timoneda [a,d], Josep A. Planell [a], Elisabeth Engel [a,c,d], Soledad Alcántara [b,*]

[a] Institute for Bioengineering of Catalonia-IBEC, Barcelona, Spain
[b] Dpt. of Pathology and Experimental Therapeutics, Medical School (Bellvitge Campus), University of Barcelona-UB, Barcelona, Spain
[c] Dpt. Material Science and Metallurgical Engineering, Technical University of Catalonia-UPC, Barcelona, Spain
[d] CIBER en Bioingeniería, Biomateriales y Nanomedicina (CIBER-BBN), Barcelona, Spain

ARTICLE INFO

Article history:
Received 2 January 2014
Accepted 22 February 2014
Available online 15 March 2014

Keywords:
Nanofibers
Lactate
Regeneration
Neural stem cells
Vascularization
Neurogenesis

ABSTRACT

Regenerative medicine strategies to promote recovery following traumatic brain injuries are currently focused on the use of biomaterials as delivery systems for cells or bioactive molecules. This study shows that cell-free biomimetic scaffolds consisting of radially aligned electrospun poly-L/DL lactic acid (PLA70/30) nanofibers release L-lactate and reproduce the 3D organization and supportive function of radial glia embryonic neural stem cells. The topology of PLA nanofibers supports neuronal migration while L-lactate released during PLA degradation acts as an alternative fuel for neurons and is required for progenitor maintenance. Radial scaffolds implanted into cavities made in the postnatal mouse brain fostered complete implant vascularization, sustained neurogenesis, and allowed the long-term survival and integration of the newly generated neurons. Our results suggest that the endogenous central nervous system is capable of regeneration through the *in vivo* dedifferentiation induced by biophysical and metabolic cues, with no need for exogenous cells, growth factors, or genetic manipulation.

1. Introduction

Stroke and traumatic injury are common causes of disability, with loss of nerve tissue due to secondary degeneration, gliosis, and often the formation of cavities that inhibit neural cell growth [1,2]. Unfortunately, the clinical efficacy of regenerative medicine strategies for nerve tissue regeneration has been limited by the poor effective integration, vascularization, and survival of the implants and the defective differentiation of exogenous neural stem cells (NSCs) [3–6]. Recent attempts at neural cell regeneration have therefore focused on the use of engineering materials that mimic the adult NSC niche, in order to establish an adequate environment for neurogenesis and differentiation. Biophysical cues and the release of biochemical factors are the principal parameters that regulate NSC survival and differentiation [4,7]. However, because the adult mammalian NSC niche has limited regenerative capacities, effective regeneration of the central nervous system (CNS) requires the reconstitution of its embryonic counterpart [8–11]. During development, radial glia are the principal NSCs that generate neurons and glia. Radial glia span the entire CNS parenchyma and serve as substrates for neuronal migration [12–14]. During early neurogenesis, blood vessels invade the CNS and interact with NSCs, giving rise to the neurovascular niche [15,16]. In the adult brain, neurogenic radial glia can be regained, at least to some extent, after injury [17,18], indicating an endogenous attempt at reconstitution of the embryonic NSC niche.

The goal of this study was to design an implantable biomaterial scaffold that reproduces the 3D organization and supportive function of embryonic radial glia. Radial glia are bipolar cells with 1- to 2-μm-thick shafts that form a palisade [19]. They contain high levels of glycogen and release L-lactate [20], a common cellular cue that induces angiogenesis [21] and supports neuronal and NSC/progenitor metabolism [22]. Lactate is also a component of widely used biobased plastics made from poly-lactic-acid polymers. In a previous work we observed that poly(L-lactide-co-D,L-lactide)

* Corresponding author. Cell Biology Unit, Department of Experimental Pathology and Therapeutics, School of Medicine (Bellvitge Campus), University of Barcelona, 08907 L'Hospitalet de Llobregat, Barcelona, Spain. Tel./fax: +34 934024288.
E-mail address: salcantara@ub.edu (S. Alcántara).

http://dx.doi.org/10.1016/j.biomaterials.2014.02.051
0142-9612/

(PLDLLA) 70/30 (70% pure L, and 30% DL) films were better *in vitro* substrates than PLDLLA 95/5 (95% pure L, and 5% DL) in terms of cortical neural cell growth and the maintenance of pools of neuronal and glial progenitor cells [23]. The difference between PLDLLA 70/30 and the usual PLLA (pure L isomer) is that in the former mismatching of the polymer chains promotes less order, less crystallinity, a higher degree of amorphicity, and therefore, a higher degradation rate. We also demonstrated the importance of controlling topography in order to dedifferentiate glial cells [24]. Thus, the biomimetic scaffold used in the present work combines the neurogenic and radial-glia-inducing properties of lactate-releasing PLDLLA 70/30 (PLA) with a topology that mimics their 3D organization of radial glia.

Here we show that L-lactate released by PLA nanofibers is required for NSC/progenitor maintenance. Radially aligned PLA nanofiber scaffolds implanted into cavities made in the postnatal mouse brain were observed to mimic some of the physical and biochemical characteristics of radial glia *in vivo*. This enabled robust and functional vascularization in the direction of fiber orientation, NSC niche activation, neurogenesis, and neuronal survival and integration into normal brain circuits for more than 1 year. Our results suggest the possibility of endogenous central nervous system regeneration through *in vivo* dedifferentiation induced by biophysical and metabolic cues, with no need for exogenous cells, growth factors, or genetic manipulation.

2. Materials and methods

2.1. PLA70/30 nanofiber characterization

Poly-L/DL lactic acid 70/30 (PLA70/30) (Purasorb PLDL 7038, inherent viscosity midpoint 3.8 DL/g, molecular mass ≈ 850,000 Da) was purchased from Purac Biomaterials (Gorinchem, The Netherlands). The 238 ± 18-μm-thick sheets of random and aligned PLA70/30 nanofibers were prepared by electrospinning. Briefly, 2.86 g (4% w/w) of PLA was dissolved in 50 ml of 2,2,2-trifluroethanol (99.8%; Panreac, Barcelona, Spain). The solution was electrospun with a grounded flat collector for randomly distributed fiber samples or with a grounded rotary collector with a diameter of 9 cm and a rotational speed of 1000 rpm for aligned ones. The voltage was 8 kV, the distance between the tip and the collector was 12 cm, and the humidity was 20% at 23 °C.

PLA70/30 wettability was characterized by contact-angle measurements with an OCA 20 system (Dataphysics GmbH, Filderstadt, Germany), using the captive bubble technique. This method measures the equilibrium angle formed between a 3-ml air bubble and the PLA surface, both immersed in water. The measurements were performed in triplicate with at least three different data points for each sample.

The ζ-potential was measured using a SurPASS electrokinetic analyzer and VisioLab software (Anton Paar Ltd., Graz, Austria). All measurements were done at a dynamic pH of the electrolyte (1 mM KCl, pH 3–8) after 1 h of equilibration and using the adjustable gap cell for small samples.

The stiffness and surface topography of PLA70/30 nanofibers were measured by atomic force microscopy (AFM) (MultiMode 8 atomic force microscope; Bruker). Young's modulus and the tensile strength of the fibrous sheets were determined with a Zwick-Roell Zwicki-Line Z0.5TN (Zwick-Roell, Ulm, Germany) universal testing machine, with ten samples of 40 × 10 mm. The tensile stress test was monitored at a speed of 10 mm/min.

The two conformations of the PLA70/30 nanofibers were characterized by differential scanning calorimetry (DSC, Mettler DSC-822e calorimeter with a TS0801RO robotic arm). Samples of approximately 5 mg were placed in aluminum crucibles under a nitrogen atmosphere and heated from room temperature up to 180 °C at a rate of 10 °C/min. The degree of crystallinity was assessed by the following equation (1):

$$\%\chi_c = \frac{(\Delta H_m - \Delta H_c)}{\Delta H_m^0} \quad (1)$$

where $\%\chi_c$ is the percentage crystallinity, ΔH_m is the latent heat of melting, ΔH_c is the heat of the crystallization, and ΔH_m^0 is the melting heat of PLA with an assumed degree of crystallinity of 100% ($\Delta H_m^0 = 93.1$ J/g).

An X'Pert PRO diffractometer (Panalytical, Almelo, Netherlands) (CuKα $\lambda = 1.5406$ Å radiation, 45 kV, 40 mA, and a step size of 0.026°) was used in $\theta/2\theta$ 2–60° X-ray diffraction (XRD) analyses of PLA films.

Micro- and nano-morphologies were assessed using a field emission scanning electron microscope (Nova-Nano SEM-230; FEI Co., Netherlands), operating at 10 kV and with ultra-thin carbon coating of the fibers. The fiber sheets were cross-sectioned using the focused ion beam lithography technique (Strata DB235; FEI Co.).

2.2. Degradation study and L-lactate quantification

The degradation of PLA nanofibers *in vitro* was followed at 37 °C for eight weeks. Four samples were immersed in glucose- and pyruvate-free Neurobasal A (NB-A; Gibco) and retrieved after 5, 7, 21, 30, and 45 days *in vitro* (div). The L-lactate concentration was determined as previously described [23].

2.3. Cell culture

All animal housing and procedures were approved by our institution's Animal Care and Use Committee, in accordance with Spanish and EU regulations. Glial cells were derived from the cerebral cortex of newborn mice (P0) as previously described [24]. The influence of the properties of the various materials used in this study on glial cell adhesion, morphology and differentiation was determined as follows: passage 1 (Ps1) cells were cultured at a density of 2×10^5 cells/cm^2 for 5 div in NB containing 3% normal human serum (NHS), 1% penicillin–streptomycin (pen–strep), and 2 mM L-glutamine on uncoated PLA70/30 nanofibers. Control Ps1 glial cells were cultured on non-coated culture plastic (for western blotting) or on glass coverslips (for immunocytochemistry) under the same conditions used for PLA nanofibers. Both the cell composition and the biochemical characterization of control and reference glial conditions were described previously [24].

Neurons were obtained from embryonic brains as described elsewhere [23]. The cells were plated at a density of 2.5×10^5 cells/cm^2 directly, either on top of random and aligned nanofibers or, as a positive control, on poly-D-lysine (Sigma–Aldrich) coated tissue culture plates (for western blotting) or glass coverslips (for immunocytochemistry) for 5 div. In co-cultures, embryonic-day 16 (E16) neurons were plated at a density of 2.5×10^5 cells/cm^2 directly on top of 5-div glial cell cultures and then cultured for 5 more days in serum-free NB supplemented with 1% pen-strep, 0.5 mM L-glutamine, 1× B27 (Gibco), 5.8 μl/ml 7.5% $NaHCO_3$ (neuronal medium). To analyze the effect of lactate, E16 neurons were cultured on aligned PLA70/30 nanofibers in glucose-containing NB or in glucose-free NBA supplemented with 1% NHS, 1% pen-strep, 0.5 mM L-glutamine, 22 μM glutamic acid, 1× B27, and 5.8 μl 7.5% $NaHCO_3$/ml for 24 h, after which the medium was replaced with serum-free neuronal medium in the presence or absence of 100 nM of the monocarboxylate transporter (MCT) 1/2 inhibitor AR-C155858 (AdooQ, Irvine, CA, USA) for four more days. The samples were either fixed in 4% paraformaldehyde for immunocytochemistry or used for protein extraction and western blot analysis.

2.4. Video time-lapse microscopy

For video time-lapse analysis, neurons were obtained from the cerebral cortex of E16 mice and cultured at low density on top of aligned PLA nanofibers. After 5 div, the cells were placed in the incubation chamber of an Observer Z1m inverted fluorescence microscope (Carl Zeiss, USA) at 37 °C with 5% CO_2 and observed by phase-contrast microscopy. Images were obtained every minute for 15 h. Cell displacement, speed, and trajectory were calculated using the "Manual Tracking" plug-in of the ImageJ software (National Institutes of Health, USA).

2.5. Implantation of PLA nanofiber tubes into the right hemisphere of the injured mouse brain

Four-day-old (P4) mice were anesthetized by immersion in ice for 5 min, placed in a stereotaxic apparatus for small animals (Stoelting Europe, Dublin, Ireland mouse and neonatal rat stereotaxic adaptor), and kept cold during surgery. A triangular tissue flap overlying the right somatosensory cortex was lifted with a surgical blade, carefully avoiding severing surface blood vessels in the brain parenchyma. After opening the skull, 1-mm^3 cavities were made by direct suction with a syringe connected to a blunt needle (1 mm ø). Immediately after tissue removal, 1-mm^3 nanofiber tubes were soaked in NB containing 1% pen–strep and implanted into the cavity ($n = 96$). As a control, the cavity was left empty and the tissue flap put back in place. The mice were then warmed on a heating pad and returned to their mother after recovery. The two groups of mice were killed at 2 or 7 days or at 2, 6, 12, or 15 months following implantation, and the brains were processed for immunocytochemistry as described above.

2.6. Immunofluorescence of cultured cells and western blot analysis

Total protein extracts for western blot analysis were prepared from primary neuronal and glial cultures, separated by SDS-polyacrylamide gel electrophoresis, and electro-transferred to a nitrocellulose membrane (Bio-Rad). The membranes were blocked with 5% bovine serum albumin (BSA, Sigma–Aldrich) and incubated overnight at 4 °C first with primary antibodies and then with the corresponding secondary HRP-conjugated antibodies (1:3000; Santa Cruz Biotechnology). Protein signals were detected by the ECL chemiluminescent system (Amersham, GE Healthcare). Densitometry analysis, standardized to actin as a control for protein loading, was carried out with ImageJ software (National Institutes of Health, USA). For quantification, triplicate samples were analyzed and at least three different experiments were performed.

For immunofluorescence, fixed primary cultures or tissue sections were incubated with primary antibodies overnight at 4 °C and then with the appropriate Alexa 488 or Alexa 555 secondary antibodies (1:500, Molecular Probes). To-Pro-3 iodide (TOPRO-3, 1:500, Molecular Probes) was used to stain nuclei. Finally, the preparations were cover-slipped with Mowiol (Calbiochem) for imaging.

2.7. Detection and characterization of neural populations

The mice were perfused with 4% paraformaldehyde and their brains were removed and cryosectioned coronally at 40-μm intervals. To characterize the phenotype of the cells inside the scaffold, the following primary antibodies were used: mouse anti-NeuN (neuronal marker, 1:500; Abnova Corp., Taipei, Taiwan), rabbit anti-parvalbumin (PV, gabaergic neuronal marker, 1:8000; Swant, Switzerland), rabbit anti-glial-fibrillary-acidic-protein (GFAP, a mature and reactive glial cell marker, 1:1000–1:8000; Dako, Glostrup, Denmark), rabbit anti-BLBP (radial glial marker, 1:1000–1:8000; Chemicon, Temecula, CA, USA), mouse anti-nestin (progenitor and radial glial marker, 1:250; Abnova Corp.), rat anti-F480 (macrophage marker, 1:1000; Chemicon), goat anti-MCT2 (1:1000; Santa Cruz Biotechnology, Delaware, CA, USA), goat anti-GPR81 (G-protein-coupled lactate receptor, 1:500; Santa Cruz Biotechnology), goat anti-Iba1 (microglial and macrophage marker, 1:200; Abcam, Cambridge, UK), rabbit anti-CX3CR1 (microglial and macrophage marker, 1:500; Abcam), rabbit anti-Ki67 (cell cycle marker, 1:500; Abcam), goat anti-actin (cytoskeletal marker, 1:2000; Santa Cruz Biotechnology), mouse anti-Tuj-1 (neuronal marker, 1:10,000; Covance, Princeton, NJ, USA), rabbit anti-MAP2 (neuronal cell bodies and dendritic marker, 1:2000; Covance), rabbit anti-doublecortin (DCX, neuronal marker, 1:1000; Abcam), goat anti-FOXP2 (progenitor marker, 1:1000; Santa Cruz Biotechnology), rabbit anti-Pax6 (bipotential radial glial marker, 1:250; Abcam), rabbit anti-Tbr2 (neurogenic intermediate progenitor cell marker, 1:500; Abcam), rabbit anti-Sox2 (stem cell marker, 1:1000; Abcam), rat anti-CD31/PECAM (endothelial marker, 1:200; Abnova Corp.), rabbit anti-laminin (extracellular matrix and blood vessel marker, 1:500; Sigma–Aldrich), rabbit anti-NG2 (oligodendrocyte precursor cells, 1:1000; Chemicon), rabbit anti-olig2 (oligodendrocyte transcription factor 2, 1:200; Abcam), rabbit anti-PSD95 (postsynaptic marker, 1:1000; Abcam), or mouse anti-SNAP25 (presynaptic marker, 1:1000; Covance).

2.8. BrdU labeling

Starting at different time points after scaffold implantation, 5-bromo-2′-deoxyuridine (BrdU, Sigma–Aldrich) was injected intraperitoneally (5 mg/10 gr body weight) every 24 h for a 5-day period. BrdU incorporation was analyzed by immunohistochemistry (rat-anti-BrdU, 1:1000; Abcam) at different time points after injection. The injection protocol was as follows (in which P indicates postnatal day): P6: 3 h after the first injection ($n = 5$); P11: injections at P6–P10 ($n = 5$); at 1 year: injections at P6–P10 ($n = 3$); at 1 year: injections at 2 months ($n = 3$); at 1 year: injections one week before death ($n = 3$). The cell types that incorporated BrdU and their progeny were identified by double immunohistochemistry with BrdU antibodies and antibodies to Sox2, Tbr2, Pax6, DCX, NeuN, PV, GFAP, and olig2.

2.9. Vascular labeling

The lipophilic carbocyanine dye DiI (Sigma–Aldrich) was injected during cardiac perfusion of the animals, as previously described [25]. DiI-labeled vasculature was reconstructed on 300-μm-thick coronal sections ($n = 4$ aligned nanofibers; $n = 3$ random nanofibers). Vasculature staining with 1 mg/ml *Lycopersicon esculentum* (tomato) FITC-conjugated lectin (Sigma–Aldrich) was performed by caudal vein perfusion according the following protocol (http://werblab.ucsf.edu/sites/werblab.ucsf.edu/files/protocol%20pdfs/Lectin_perfusion.pdf).

2.10. Retrograde neural tracing studies

One year after scaffold implantation, cholera toxin subunit B conjugated to Alexa fluor 555 (AF-CBT) was stereotactically injected as described [26] into the intact contralateral somatosensory cortex of the mice. Control animals ($n = 2$) and radial scaffold implanted animals ($n = 4$) were killed after 4 days and their brains were analyzed.

2.11. Imaging and cell analysis

Cells were observed *in vivo* using an Axiovert 40 CFL light-inverted microscope (Carl Zeiss, USA). Digital images were acquired throughout the experiments using a digital camera controlled by software. Fluorescent preparations were viewed and micrographs were taken with either a Leica TCS-SL spectral confocal microscope (Leica Microsystems, Mannheim, Germany) or a Nikon Eclipse 800 light microscope (Nikon, Tokyo, Japan). Images were assembled in Adobe Photoshop (v. 7.0), with adjustments for contrast, brightness, and color balance to obtain optimum visual reproductions. Morphometric, quantitative, and live-image analyses were performed using ImageJ software (National Institutes of Health, USA).

Confocal images were reconstructed using the Imaris program (Bitplane, Zurich, Switzerland) for 3D and 4D real-time interactive data viewing, with normal or shadow projections of coronal tissue sections screened under a Leica TCS-SL spectral confocal microscope.

2.12. Magnetic resonance imaging (MRI)

MRI experiments were conducted on a 7.0 T BioSpec 70/30 horizontal animal scanner (Bruker BioSpin, Ettlingen, Germany) equipped with a 12-cm inner diameter actively shielded gradient system (400 mT/m). The receiver coil was a phased-array surface coil for mouse brain. The mice were placed in a supine position in a Plexiglas holder fitted with a nose cone for administering anesthetic gases (isofluorane in a mixture of 30% O_2 and 70% CO_2) and secured using a tooth bar, ear bars, and adhesive tape. Tripilot scans were used for accurate positioning of the animal's head in the isocenter of the magnet. High-resolution T2-weighted images were acquired using TurboRARE (rapid acquisition with rapid enhancement) sequences, with a repetition time = 2970 ms, echo time = 12 ms, RARE factor = 8, 10 averages, slice thickness = 0.3 mm, 25 slices for axial view and 40 slices for sagittal view, field of view = 25 × 25 mm, matrix size = 240 × 240 pixels, resulting in a spatial resolution of 0.104 × 0.104 mm for a slice thickness of 0.3 mm.

2.13. Statistical analyses

Statistical analyses were performed using Statgraphic-plus software. One-way ANOVA and Fisher's least significant difference (LSD) procedure were used to distinguish the means. Statistical significance was set at $P < 0.05$ (*) and $P < 0.001$ (**).

3. Results

3.1. Effect of PLA nanofibers on neuronal and glial cultures

The production of 238 ± 18-μm nanofiber sheets with the PLA nanofibers in two different conformations, random and aligned, was successfully achieved by the electrospinning method (Fig. 1A, B). We obtained continuous and homogeneous fiber thicknesses (657 ± 101 nm for random and 568 ± 81 nm for aligned nanofibers), with no bead content. Focused ion beam cross-sectional images of an aligned fibrous sheet (Fig. 1B inset) showed that the nanofibers were hollow (~500 nm inner diameter) because of the Kirkendall effect [27]. On AFM imaging, the single aligned nanofibers were smooth (RMS value of 14.2 ± 0.3 nm) (Fig. 1C) and relatively soft (DMT modulus of 3.0 ± 0.004 MPa) (Fig. 1D). Tensile strain differed between the two conformations. Thus, the Young's modulus of the random nanofibers was isotropic (41.4 ± 13.7 MPa) while the aligned nanofibers showed an anisotropic Young's modulus almost four-fold higher, as determined in a uniaxial assay parallel to the direction of the nanofibers (142.7 ± 14.1 MPa; Fig. 1H). The amorphous nature of the nanofibers was characterized by XRD (Fig. 1E) and DSC (Fig. 1F), neither of which showed evidence of crystallization or melting peaks, indicating a nearly null crystallinity. Both PLA fiber conformations were hydrophobic (contact angle of 137° ± 14° for aligned and 128° ± 17° for random conformations) and negatively charged (ζ-potential at pH 7.4 = −41 ± 43 mV) and the degradation rates were similar (νLac-random = 458 nM·h-1 and νLac-aligned = 467 nM·h-1) (Fig. 1G). However, it should be taken into account that the enzymatic reaction indicative of degradation only allows the detection of L-lactate monomers. Soluble PLA oligomers and D-lactate monomers are undetectable by this technique.

For cell culture, uncoated random and aligned fiber sheets were used as the substrates. Neurons and glial cells were identified by their immunoreactivity to β-III tubulin (Tuj-1) and BLbP, respectively [28]. On random scaffolds, neurons and glial cells grew on the surface and adopted multipolar shapes (Fig. 2A), while in aligned scaffolds they were bipolar, oriented in the fiber direction, and invaded the entire thickness (Fig. 2B–D). Neuronal migration in PLA nanofibers was analyzed by video time-lapse microscopy, which showed the adherence of embryonic neurons to single nanofibers and their migration alongside them (Supplementary video 1), mimicking neuronal behavior on radial glia during brain development [14].

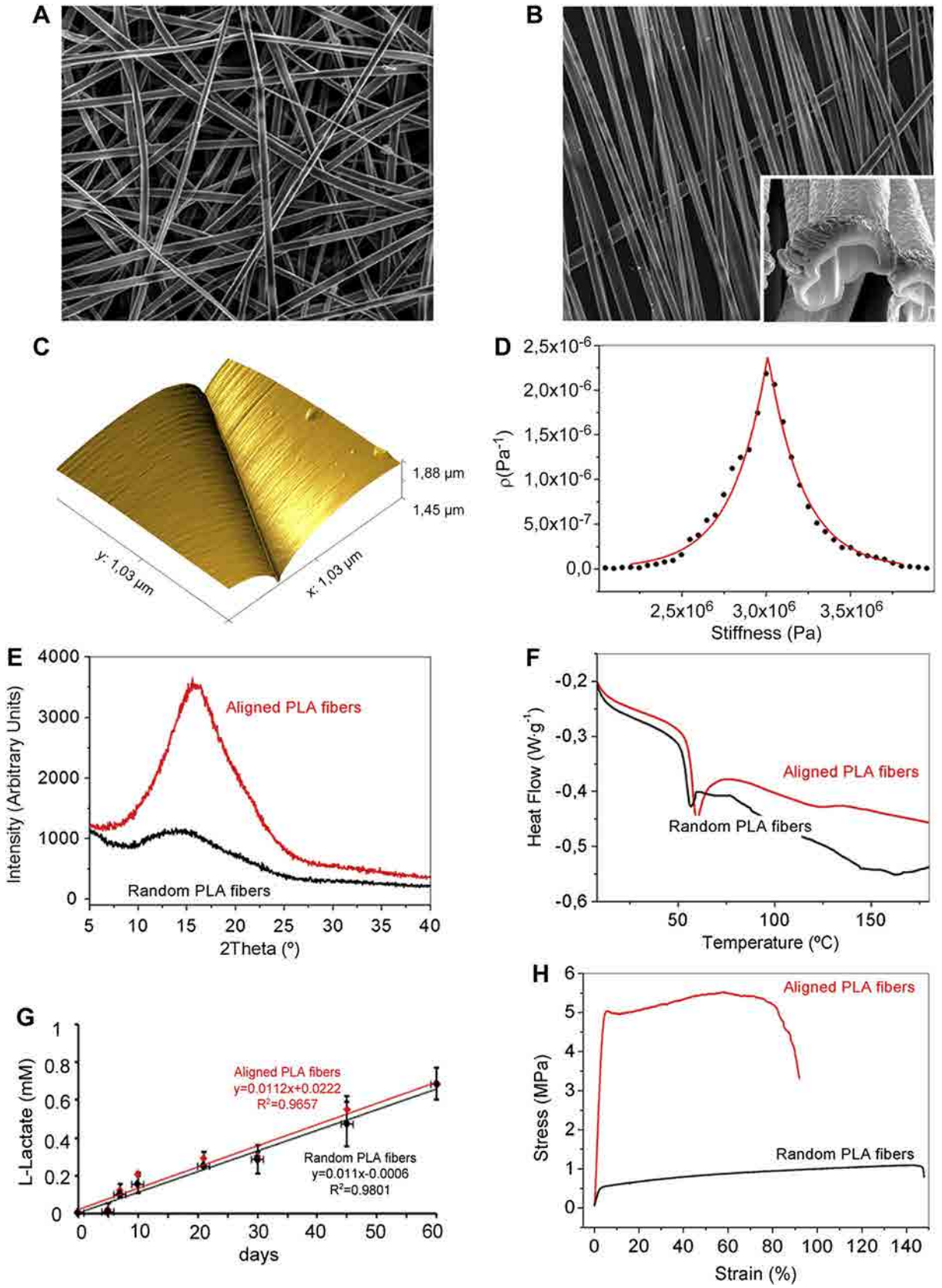

Fig. 1. Material characterization. **(A, B)** Field emission scanning electron microscopy images of **(A)** random and **(B)** aligned nanofibers viewed from above, with a cross-section of aligned nanofibers produced by focused ion beam shown in the inset in **B**. **(C)** Atomic force microscopy (AFM) topographic plot of the interface of two parallel nanofibers (RMS value of 14.2 ± 0.3 nm). Stiffness value distribution based on **(D)** the DMT modulus measured by AFM, showing a peak at 3.01 ± 0.004 MPa, and **(E)** X-ray diffraction. **(F)** Differential scanning calorimetry spectra of random (black) and aligned (red) nanofiber conformations, showing the amorphous nature of the fibers. **(G)** Plot of lactate release vs. time of random (black, νLac-random = 458 nM h^{-1}) and aligned (red, νLac-aligned = 467 nM h^{-1}) nanofiber sheets. **(H)** Mechanical assays after tensile loading of the two nanofiber conformations. Scale bars: 5 μm **(A, B)**; 500 nm **(B inset)**. (For interpretation of the references to color in this figure legend, the reader is referred to the web version of this article.)

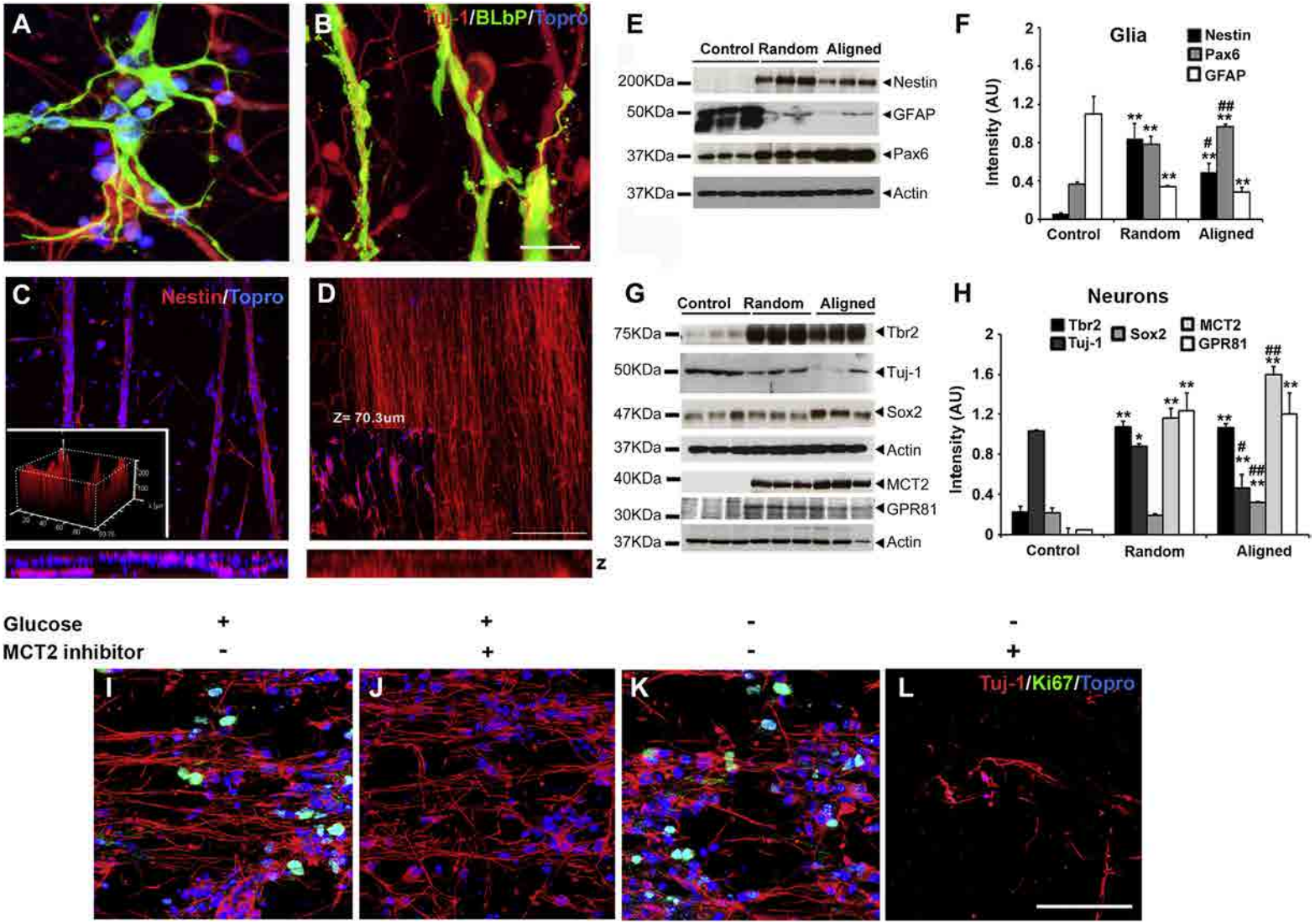

Fig. 2. Lactate released by PLA nanofibers induces radial glia and neurogenic progenitors. **(A, B)** Morphology of BLbP+ glia (green) and Tuj-1+ neurons (red) on random **(A)** and aligned **(B)** nanofibers after 10 div. Confocal images of **(C)** glial cells stained with nestin (red) and **(D)** neurons stained with Tuj-1 (red) on aligned PLA nanofibers after 5 div. Glial cells colonized an area of 200 μm in the *z* plane of the scaffold **(C, inset)** while neuronal somas localized in the middle of the scaffold **(D, inset)**. Western blots show the expression of nestin, Pax6, and GFAP markers in glial cell cultures **(E)** and of Tbr2, Tuj-1,Sox2, MCT2 and GPR81 in neuronal cultures **(G)** after 5 div. **(F, H)** Western blot densitometry (intensity values normalized to actin). **(I–L)** Confocal images of neuronal cultures grown on aligned nanofibers in NB medium **(I, J)** or in glucose-free NB-A medium **(K, L)** after 5 div in the presence or absence of AR-C155858, an inhibitor of monocarboxylate transporters (MCT) 1/2. Neurons are stained with Tuj-1 antibody (red) and proliferative cells with Ki67 (green). Nuclei are stained with TOPRO-3 (blue).*$P < 0.05$, **$P < 0.001$, LSD test (compared with control); #$P < 0.05$, ##$P < 0.001$, LSD test (random vs. aligned nanofibers), $n = 5$. Scale bars: 20 μm **(A, B)**; 100 μm **(C, D)**; 50 μm **(I–L)**. (For interpretation of the references to color in this figure legend, the reader is referred to the web version of this article.)

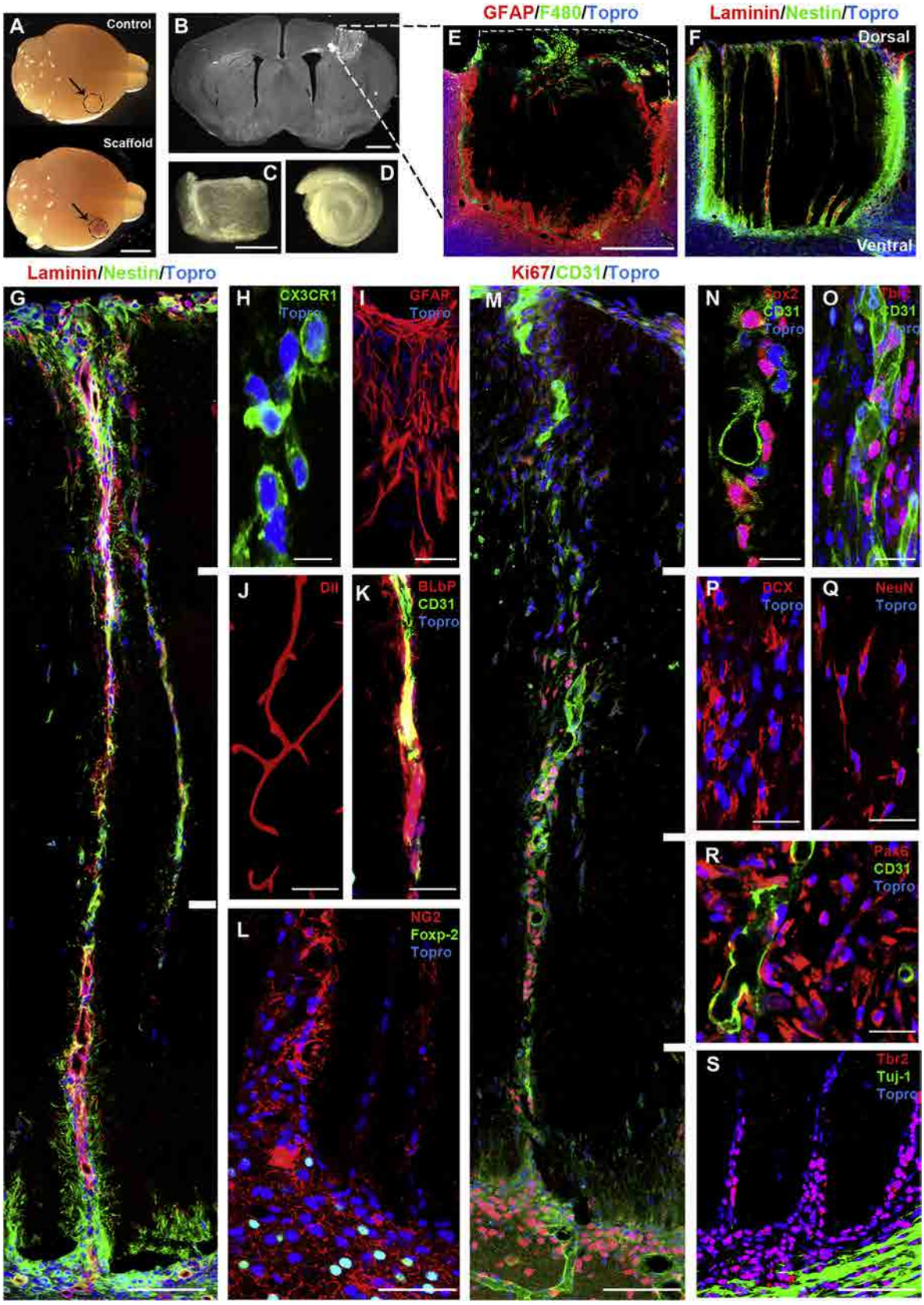

Fig. 3. Neurovascular bridges inside radial scaffolds. (A) Macroscopic view of postnatal day 11 (P11) mouse brains with control injury (Control) or with an implanted PLA scaffold (Scaffold) in the right cortex. **(B)** Bright-field coronal section showing the implanted radial scaffold. **(C, D)** Lateral and top views of the scaffold before implantation. Confocal images showing **(E)** GFAP+ astroglia (red) and F480+ macrophages (green) surrounding the scaffold and **(F)** nestin+ radial glia (green) and laminin basal lamina (red) forming radial neurovascular bridges inside the scaffold. **(G)** High magnification of **(F)**, showing a neurovascular bridge reconnecting basal and meningeal zones. **(H, I)** Higher magnifications show resolving macrophages stained with CX3CR1 (green) **(H)** and GFAP+ astroglia (red) **(I)** in the upper third of the implant. **(J)** Functional blood vessels stained by DiI perfusion. **(K)**

Supplementary video related to this article can be found at http://dx.doi.org/10.1016/j.biomaterials.2014.02.051.

The expression of cell-type molecular determinants of neurogenic niches [29–31] was then analyzed by immunocytochemistry and western blot. After 5 div on PLA fiber scaffolds, glial cultures dramatically increased their expression of the radial glia markers nestin and Pax6 and decreased their expression of the astroglial marker GFAP (Fig. 2E, F). Similarly, compared to control cultures, neuronal cultures on PLA fiber scaffolds dramatically increased their expression of Ki67+ cycling progenitors, the neuronal progenitor marker Tbr2, and the NSC marker Sox2, whereas expression of the post-mitotic neuron marker Tuj-1 was lower (Fig. 2G, H, Supplementary Fig. 1). Moreover, in contrast to random scaffolds, aligned scaffolds better reproduced neurogenic niche properties, as the expression of both Sox2 and Pax6 increased significantly (Fig. 2F, H).

In neuronal cultures, lactate released from PLA scaffold degradation induced a large increase in MCT2 and GPR81 (Fig. 2G, H). Next, neuronal cultures were grown on aligned nanofibers with or without glucose in the medium and treated with AR-C155858, an inhibitor of MCT1/2 [32] that blocks lactate entrance into cells. Pharmacological blockade of lactate transport induced KI67+ progenitor depletion even in the presence of glucose, and neuronal death in the absence of glucose (Fig. 2I–L). Thus, lactate released by PLA nanofibers apparently acts as an alternative fuel for neurons and is required for NSC/progenitor maintenance.

3.2. Implantation of PLA fiber scaffolds in vivo

During the first postnatal week, cortical gliogenesis is still very active whereas neurogenesis is mostly completed prenatally [33], with the exception of life-span neurogenesis in adult neurovascular niches [34]. To analyze the regenerative potential of PLA fiber scaffolds *in vivo*, we used a model of traumatic brain injury in 4-day-old (P4) mice. One-mm^3 random (random scaffolds, $n = 29$) and aligned PLA fiber scaffolds (aligned scaffolds, $n = 87$) following the radial orientation of radial glia (radial scaffolds, $n = 77$) or placed orthogonal to the orientation of radial glia (orthogonal scaffolds, $n = 10$) were fitted into the brain cavity just after tissue removal (Fig. 3A–D). The brains were then analyzed at 2 and 7 days and at 2, 6, and 12–15 months post-surgery. The non-implanted brain cavities (control, $n = 20$) remained empty, with no sign of brain tissue regeneration even 15 months after surgery (Supplementary Fig. 2). By contrast, despite evident signs of fiber degradation, the PLA fiber scaffolds were clearly visible 15 months after implantation (Supplementary Fig. 2). Since the amount of new tissue generated inside the radial scaffolds increased over time, most of the data reported below correspond to post-implantation days and to the experiment's end-point at 12–15 months. Abnormal neurological behavior was not observed in any experimental group or in mice of any age.

3.3. Brain tissue regeneration inside PLA fiber scaffolds in vivo

Brain tissue regeneration was assessed by immunofluorescence microscopy. One week after surgery, immune system activation was shown by the presence of F480+ mature macrophages at the border of the lesion site and at the tissue–implant interface (Fig. 3E). CX3CR1+ resolving macrophages [35] were also seen at the border and entering radial scaffolds from the meninges (Fig. 3H). Immune activation was residual after 1 year, with scarce F480+ macrophages at the tissue–implant interface (Supplementary Fig. 2B) and a few Iba1+ ramified resting microglia inside the radial scaffolds (Fig. 4M). One week after surgery, GFAP+ activated astrocytes were detected at the border of the lesion site and at the tissue–implant interface (Fig. 3E, I). At this time, nestin+ radial glia dramatically increased around and inside the aligned scaffolds, as did laminin, an adhesive extracellular matrix glycoprotein mainly secreted by glial and endothelial cells (Fig. 3F; Supplementary Fig. 2A). Newly generated tissue formed neurovascular bridges that crossed the scaffolds, following radial (Fig. 3F) or orthogonal (Supplementary Fig. 2A) trajectories to the brain surface, depending on the disposition of the aligned nanofibers. At this early time point, embryonic neurons expressing the transcription factors Foxp-2 [36] and Bhlhb5 (not shown) and Tuj1+ axons from the surrounding tissue were excluded from entering the scaffold (Fig. 3L, S). After 1 year, the initially narrow neurovascular bridges had formed large areas of regenerated tissue, containing blood vessels, neurons, and glial cells, inside the radial scaffolds (Fig. 4). Nestin+ and GFAP+ glial cells were abundant and widely distributed inside the scaffolds, maintaining the elongated shape and radial organization of embryonic radial glia and a laminin-rich extracellular matrix (Fig. 4C, D, J; Supplementary Fig. 2B). By contrast, in random scaffolds, despite similar fiber composition and size, these cells were only present at the tissue–implant interface (Supplementary Fig. 2B). Therefore, in subsequent experiments we used radial scaffolds for brain regeneration studies and random scaffolds as controls.

At the cell level, neurovascular bridges were organized around a central blood vessel formed by CD31+ endothelial cells [34] surrounded by a laminin-rich basal lamina (Fig. 3G, M). Glial populations around central vessels included nestin+ and BLbP+ radial glia (Fig. 3G, K; Supplementary video 2) and a heterogeneous population of NG2+ cells (Fig. 3L), including oligodendrocyte progenitors [9], while olig2+ oligodendrocytes were absent. The same populations persisted after 1 year, at which time olig2+ oligodendrocytes were also observed inside the scaffold (Fig. 4J, K, N). Transcardiac perfusion with the lipophilic tracer DiI revealed an effective connection between this radial vascular network inside the scaffold and the host vasculature as well as the perfusion of the newly formed vessels (Fig. 3J). At 1 year, DiI perfusion delineated large radial vessels that entered the radial scaffold before profusely branching (Fig. 4G, P; Supplementary video 3). This vascular organization closely reproduced the normal organization of blood vessels in the contralateral brain tissue (Supplementary video 4) whereas inside random scaffolds a similar vasculature was completely absent (Supplementary video 5).

Supplementary video related to this article can be found at http://dx.doi.org/10.1016/j.biomaterials.2014.02.051.

The regeneration of neurogenic niches inside radial scaffolds was also analyzed. After one week, Ki67+ cycling cells were found in close association with blood vessels in the tissue surrounding the scaffold and in the neurovascular bridges (Fig. 3M). The analysis of progenitor determinants revealed a highly heterogeneous population of neuronal and glial progenitors. The distribution of Sox2+ NSC, Pax6+ bipotential radial glia, and Tbr2+ neuronal restricted progenitors was similar to that of Ki67+ cells (Fig. 3M–O, R, S; Supplementary Fig. 3) and was maintained after 1 year. A functional

Proximity of BLbP+ radial glia (red) and CD31+ endothelial cells (green). **(L)** NG2+ cells (red) entering the scaffold and FOXP-2+ neurons (green) remaining in the lower layers. **(M)** CD31+ endothelial cells (green) in a neurovascular bridge surrounded by Ki67+ cycling progenitors, by Sox2+ stem cells (red) **(N)**, and by Tbr2+ neurogenic progenitors (red) **(O)**. **(P)** DCX+ and (**Q**) NeuN+ immature neurons. **(R)** CD31+ endothelial cells (green) surrounded by Pax6+ bipotential progenitors (red). **(S)** Tbr2+ progenitors (red) entering the scaffold and Tuj-1+ axons (green) at the material–tissue interface. Nuclei were stained with TOPRO-3 (blue). Scale bars: 2 mm **(A)**; 1 mm **(B)**; 500 μm **(C, D)**; 400 μm **(E, F)**; 50 μm **(G, M, S)**; 20 μm **(I, K)**; 10 μm **(H, J, L, N–R)**. (For interpretation of the references to color in this figure legend, the reader is referred to the web version of this article.)

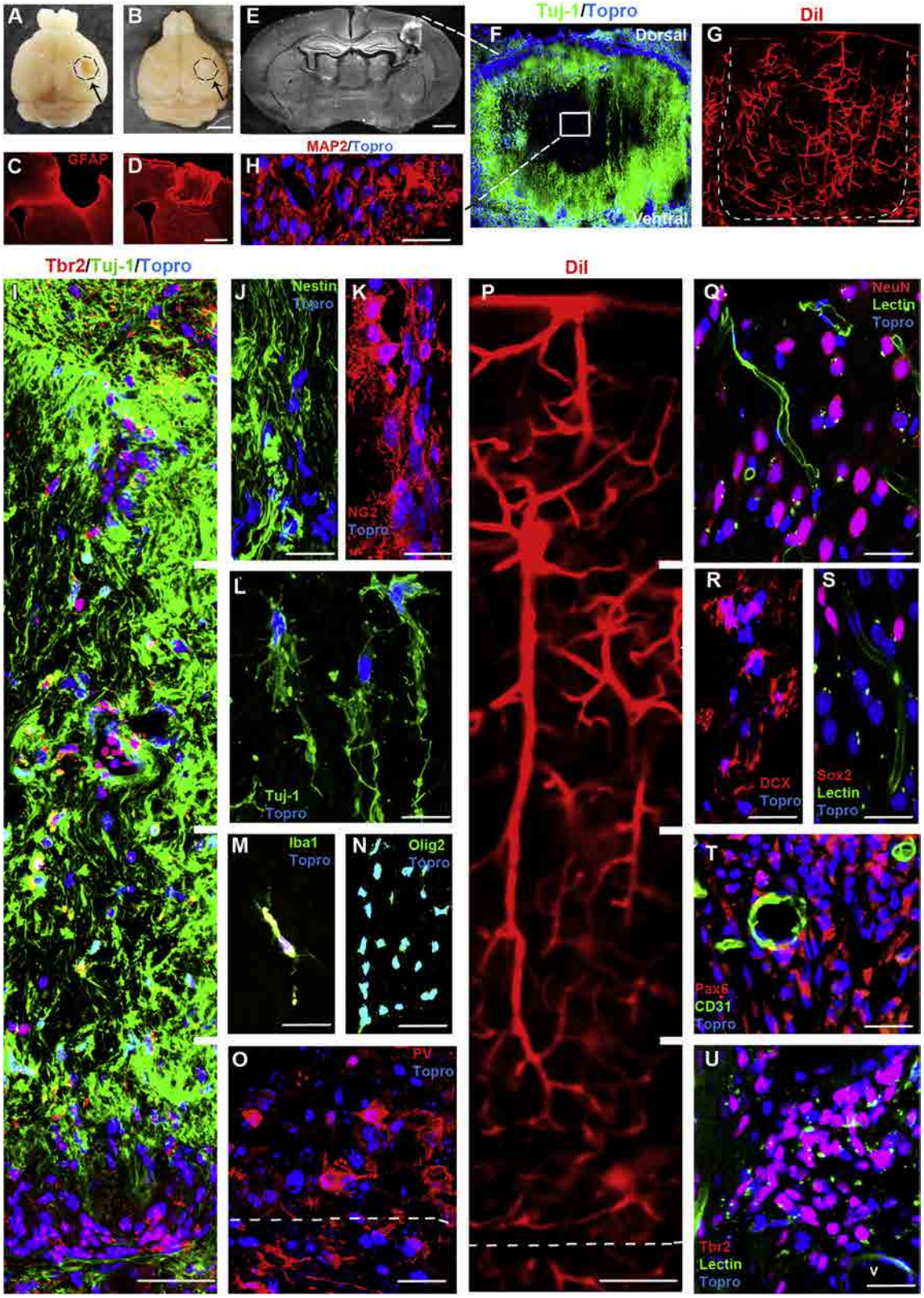

Fig. 4. Extent of brain tissue regeneration and vascularization after 1 year. Macroscopic view of brains with **(A)** control lesions and **(B)** radial scaffolds 1 year after implantation. Coronal sections showing GFAP+ astroglia around **(C)** a control lesion and **(D)** in the radial scaffold. **(E)** Bright-field coronal section showing the material remaining. **(F)** Magnification showing extensive colonization by Tuj-1+ neurons and **(G)** blood vessels labeled by DiI perfusion. **(H)** Mature neurons stained with MAP-2 in the middle of the scaffold. **(I)** Magnification of **(F)**, showing Tuj-1+ neurons (green) and Tbr2 neural progenitors (red) following the radial organization of the nanofibers. Nestin+ radial glia **(J)**, NG2+ cells **(K)**, and Tuj-1+ neurons **(L)** in the middle of the scaffold. **(M)** Iba-1+ ramified microglia. **(N)** Olig2+ oligodendrocytes. **(O)** PV+ GABAergic neurons on both sides of the tissue–scaffold interface. **(P)** Reconstruction at 300 μm of blood vessels perfused with DiI inside an aligned scaffold. **(Q)** The vicinity of NeuN+ neurons (red) and the microvasculature labeled by lectin perfusion (green). **(R)** DCX+ immature neurons. **(S–U)** Lectin/CD31+ blood vessels (green) surrounded by Sox2+ stem cells (red) **(S)**, Pax6+ bipotential progenitors (red) **(T)**, and Tbr2+ neural progenitors (red) **(U)**. Nuclei were stained with TOPRO-3 (blue). Scale bars: 1 mm **(A, B)**; 500 μm **(C, D)**; 1 mm **(E)**; 200 μm **(F, G)**; 25 μm **(H, J, P, O)**; 20 μm **(J, K, L, Q–U)**; 10 μm **(M, N)**. (For interpretation of the references to color in this figure legend, the reader is referred to the web version of this article.)

microvasculature associated with the neurogenic niche was revealed by CD31 expression or tomato lectin perfusion through the caudal vein. NSCs and progenitors expressing Sox2, Pax6, or Tbr2 (Fig. 4I, S–U) were present inside radial scaffolds in close association with tomato-lectin-labeled microvasculature.

Finally, immature bipolar neurons expressing DCX, a microtubule-associated protein required for neuronal migration, and the neuronal transcription factor NeuN [37] were also detected in the neurovascular bridges after 1 week (Fig. 2P, Q; Supplementary Fig. 3). DCX+ immature neurons were still present after 1 year (Fig. 4R), at which time neurons expressing Tuj-1 (Fig. 4F, I, L), MAP-2 (Fig. 4H), and nuclear NeuN (Fig. 4Q) were abundant and formed a rich neuronal meshwork (Fig. 4F, H). Some GABAergic neurons that stained with PV and had a well-developed morphology were also found inside the scaffold (Fig. 4O).

Taken together, these results indicate that neither a foreign body reaction nor encapsulation were elicited by the implanted scaffold. Radial scaffolds were invaded by vascular sprouts, radial glia, and neural progenitors during the first week, suggesting that the neurogenic neurovascular niches were reconstituted early on inside the scaffolds and were still active after 1 year.

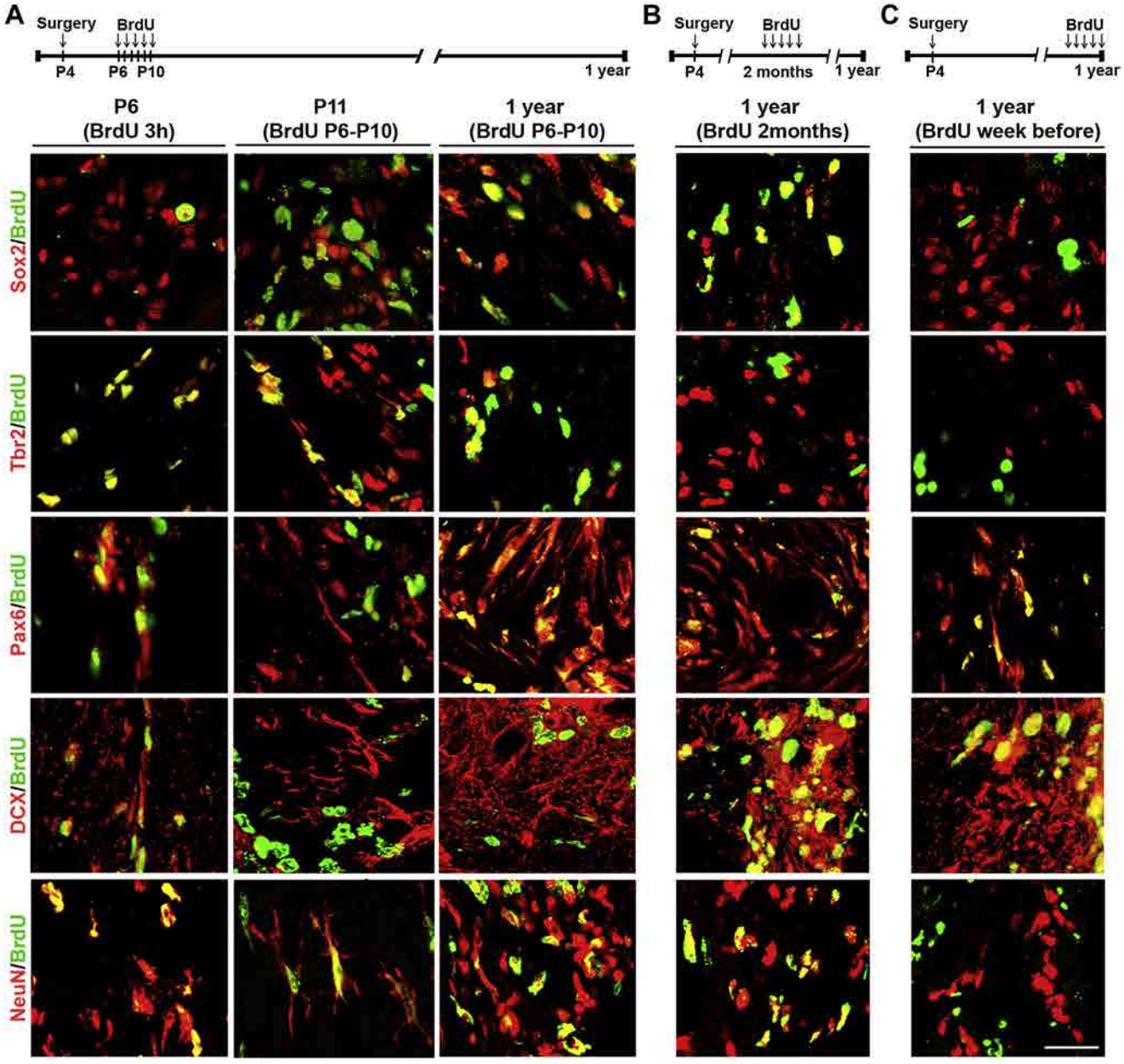

Fig. 5. BrdU incorporation into NSC/progenitors and neurons inside radial scaffolds. BrdU immunostaining (green) and colocalization inside the implant with molecular markers (red) of stem cells (Sox2), neuron-restricted progenitors (Tbr2), bipotential progenitors (Pax6), and neurons (DCX, NeuN). **(A)** BrdU was injected intraperitoneally for 5 consecutive days, from P6 (2 days after scaffold implantation) to P10, and then analyzed 3 h after the first BrdU injection, 7 days after implantation (P11), and 1 year after implantation. **(B)** BrdU was injected intraperitoneally for 5 consecutive days 2 months after implantation and analyzed at 1 year. **(C)** BrdU was injected intraperitoneally for 5 consecutive days 1 year after implantation and analyzed the day after the last injection. Scale bar: 20 μm. (For interpretation of the references to color in this figure legend, the reader is referred to the web version of this article.)

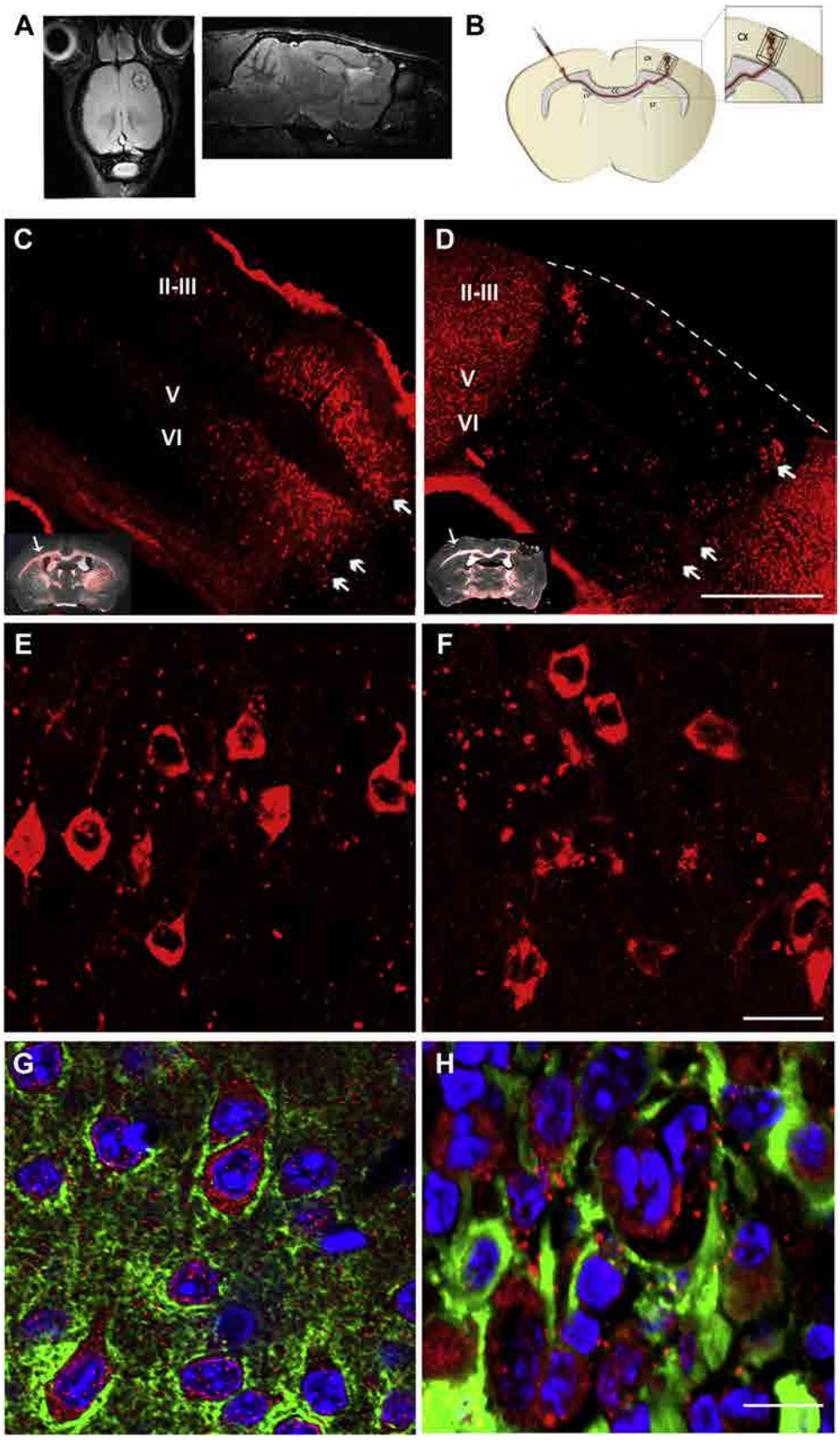

Fig. 6. Functional integration of newly generated neurons in radial scaffolds. **(A)** Horizontal and parasagittal MRI showing the integration of a radial scaffold 1 year after implantation. **(B)** Diagram of the retrograde tracing of commissural neurons following the injection of AF-CBT in the contralateral cortex of the radial scaffold implant. **(C)** Distribution of AF-CTB labeled commissural neurons (arrows) in the contralateral hemisphere of an uninjured control brain and inside a radial implant **(D)**. Insets in **(C)** and **(D)** are superimposed images of differential interference contrast and fluorescence (red), showing the exact area of AF-CTB injection (arrow). **(E, F)** Magnification showing retrograde-labeled pyramidal neurons in the contralateral hemisphere to the injection in a control **(E)** and in an implanted **(F)** brain. **(G, H)** Presynaptic SNAP25 (green) and postsynaptic PSD95 (red) labeling in control cortex **(G)** and inside a radial scaffold 1 year after implantation **(H)**. Cortical layers II–III, V, VI. Scale bars: 250 μm **(C, D)**; 20 μm **(E, F)**; 10 μm **(G, H)**. (For interpretation of the references to color in this figure legend, the reader is referred to the web version of this article.)

3.4. Neurogenesis and neuronal differentiation inside radial scaffolds

To confirm the activity of neurogenic niches, we examined the fates of dividing cells using markers for DNA replication (BrdU, a thymidine analog) and progressive neuronal differentiation. At the time of implantation (P4), BrdU was incorporated in cells mostly located in the ventricular zone/subventricular zone (VZ/SVZ) and in a few cells scattered through the cortex. Only a few cells were double-labeled with BrdU and Sox2, Tbr2, Pax6, or DCX, while extensive BrdU and NeuN colocalization was seen in SVZ neuroblasts (Supplementary Fig. 4). When injected during the first week after surgery (1 injection/day for 5 days, P6–P11), BrdU was incorporated dramatically around and inside the radial scaffold (Fig. 5A), but not on the contralateral side (Supplementary Fig. 5). Three hours after the first injection (P6), BrdU was found in progenitors expressing Tbr2 and Pax6 and in neuroblasts expressing DCX and NeuN. Only a few Sox2+ NSCs incorporated BrdU, but their number increased at P11, after 5 consecutive injections, suggesting the slow cycling of these progenitors. In the regenerated tissue, BrdU persisted in Sox2, Tbr2, and Pax6 progenitors for more than 1 year, indicating that they underwent very few rounds of cell division. After 1 year, abundant DCX+ or NeuN+ neurons (Fig. 5A) and some PV+ GABAergic neurons, GFAP+ astrocytes, and olig2+ oligodendrocytes (Supplementary Fig. 6) co-localized with the BrdU inside the scaffold. These data were consistent with both extensive neurogenesis and gliogenesis soon after radial scaffold implantation and the long-term survival of the newly generated neurons and glial cells. When BrdU was injected 2 months after radial scaffold implantation, it was incorporated into Sox2+ and Pax6+ progenitors and into DCX+ and NeuN+ neurons (Fig. 5B), whereas when injected at 1 year it was seen only in Pax6+ progenitors and DCX+ and NeuN+ neurons (Fig. 5C). These data suggest that substantial neurogenesis continues in the implant, although the progenitor types and generated neurons probably vary.

Implant integration into the surrounding tissue was assessed by MRI in a group of mice ($n = 8$). Six to 12 months after implantation, the meninges and skull had regenerated and the scaffold limits were clearly visible in the right motor/somatosensory cortex. Signal intensity inside the implant was similar to that in the surrounding tissue (Fig. 6A). Unfortunately, the system's limits of resolution in mice did not permit functional MRI. Instead, integration of the newly generated neurons inside the radial scaffold into brain circuitry was analyzed by retrograde tracing of commissural neurons 1 year after implantation. AF-CTB was injected into the contralateral hemispheres of mice with implanted radial scaffolds (Fig. 6B) and of uninjured control animals. Four days after AF-CTB injection, retrograde transport of the tracer through the corpus callosum was evident, as was the staining of two bands of pyramidal neurons in layers VI–V and II–III in control animals (Fig. 6C, E). Many retrogradely labeled pyramidal neurons were also found inside radial scaffolds, with a distribution that suggested a certain degree of anatomical and functional laminar organization within the regenerated tissue (Fig. 6D, F), as inside the scaffold they roughly reproduced the normal bilaminar distribution of callosal neurons [38]. The presence of a functional synaptic machinery in the regenerated tissue was confirmed by the immunohistochemical detection of postsynaptic density protein 95 (PSD95) and synaptosomal-associated protein 25 (SNAP25). Both proteins were expressed in neurons inside the regenerated tissue and their distribution resembled that in the adult cortex (Fig. 6G, H).

4. Discussion

Our results demonstrate that lactate-releasing PLA70/30 radially aligned fiber scaffolds reproduce some of the organizational and functional aspects of the embryonic NSC niche, including induction of the robust and sustained generation of several types of neurons and glial cells, and accompanied by complete vascularization of the implant. The new neurons survived for more than 1 year and differentiated inside the scaffold, receiving synapses and sending axons that became integrated into functional brain circuits.

Several different mechanisms might cooperate in driving the reactivation of embryonic neurogenic and angiogenic programs by lactate-releasing PLA nanofiber scaffolds. First, the present and previous data demonstrated that PLA70/30 and L-lactate are required to maintain the metabolism and self-renewal of neurogenic progenitors [22,23] and both induce angiogenesis [21]. Second, PLA nanofibers are hydrophobic, with the same size, shape, and negative superficial charge as radial glia shafts [19,39]. Accordingly, the surface properties of PLA nanofibers may well be similar to those of negatively charged lipids on the surface of astrocytes and radial glia, controlling the extracellular polymerization of laminin [39], an intrinsic component of the extracellular matrix of neurogenic NSC niches [40]. Laminin was strongly up-regulated in cells around and inside the scaffold. The appropriate orientation of vascular sprouts and radial glia in the regenerating tissue was only achieved when the topology of the PLA nanofibers reproduced that of embryonic radial glia organization. Random PLA nanofibers did not allow vascular invasion inside the scaffold, demonstrating the relevance of scaffold topology in CNS regeneration. The robust functional vascularization induced by aligned PLDLA nanofibers contrasts with the poor vascularization reported when aligned PLA (pure L isomer) microfibers were implanted into the transected spinal cord [41]. The principal difference between the two fiber types is that mismatching of the chains in PLDLA results in less order, less crystallinity, and a higher degree of amorphicity, and therefore, a higher polymer degradation rate. It is known that lactate is a common cue that supports neuronal and NSC/progenitor metabolism [22,23] and induces angiogenesis in the presence of glucose and fluctuating oxygen levels [21]. Taken together, these data indicate that topology is necessary but not sufficient for vascularization and that lactate release is also a requirement. Recent studies similarly demonstrated that lactate-releasing radial glia are essential in guiding and stabilizing the nascent brain vascular network [42].

Laminin deposition around PLA fibers might also help in directing the formation of endothelial sprouts and the stabilization of new blood vessels inside the scaffold [43]. Moreover, interactions between laminin and its receptors in vascular cells, NSCs/precursors, and migrating neuroblasts are thought to regulate NSC/precursor activation and cell migration [44–46]. PLA scaffolds might also limit inflammation, by recruiting the CX3CR1+-resolving macrophages required for its resolution [35].

Another important question is the original lineage of the dedifferentiated neuronal progenitors. BrdU analyses indicated that the newly generated cells comprise a heterogeneous population of radial glia, NSCs, intermediate progenitors, neurons, and glial cells. The observed temporal changes in progenitor pool activation and in the neuronal and glial types that incorporated BrdU suggested that the contributions of the different progenitor types to neurogenesis differed throughout the life span of the implant. Neurogenic radial glia progenitors are a constant in embryonic and adult neurogenic niches [10,11]. In the newly lesioned brain, activated SVZ progenitors generate protective astrogenesis [47] and, to a much lesser extent, give rise to neurons that migrate and integrate into the subjacent cortex [18,37,48]. In our implants in neonatal mice, substantial vascular and progenitor invasion occurred from the meningeal and lateral sides; however, tissue regeneration was considerably reduced when the entire VZ/SVZ was surgically destroyed (data not shown), suggesting that these zones are an

important but not exclusive progenitor source. In addition, direct dedifferentiation of mature glia into neurogenic progenitors has been described after Sox2 transfection [49] and in response to extracellular cues [9,24]. Although the exact progenitor source of the newly generated neurons and glial cells remains unclear, our data suggest that progenitors with multiple origins and different time-dependent activation contributed to brain tissue regeneration in the radial PLA nanofiber scaffolds. The newly generated neurons were also functional, integrating into brain circuitry and establishing synaptic contacts, as demonstrated by retrograde AF-CTB labeling and the expression of pre- and postsynaptic proteins. Unfortunately, a direct demonstration of the functionality of the regenerated tissue was not possible due to technical limitations of functional MRI in mice and to mechanical interference of the implanted scaffold with the glass micropipettes required for electrophysiological recordings.

Finally, one of the undesirable associated risks of therapies based on cell reprogramming or dedifferentiation is the induction of neuroglial tumors. This possibility was carefully checked in the implanted animals and neither brain tumors nor the expression of CD133, a molecular marker of glioma-initiating cells [50], was found (data not shown).

5. Conclusions

This study demonstrated that biomimetic scaffolds consisting of radially aligned electrospun PLA70/30 fibers release L-lactate and reproduce the 3D organization and supportive function of embryonic radial glia, thus mimicking some of the physical and biochemical characteristics of the embryonic NSC niche. Radial scaffolds implanted into brain cavities induced robust and functional vascularization in the fiber orientation from 1 week to 15 months, neurogenesis for more than 1 year, and the survival and integration of the newly generated neurons into normal brain circuits. Although there is a long way to go before their clinical translation, our results open up unexpected and exciting perspectives in the design of cell-free implantable devices. By means of tuned biomaterials it may be possible to regulate biophysical and metabolic parameters to reproduce embryonic neurovascular niches inducing gliogenesis, neurogenesis, and vascularization, leading to the restoration of functional CNS tissue lost after a lesion without the need for exogenous cells, growth factors, or genetic manipulation.

Acknowledgments

This study was supported by grants from Spain's Ministerio de Economía y Competitividad (MINECO) [MAT2011-29778-C02-02] and [MAT2011-29778-C02-01], co-financed by the European Regional Development Fund, to S.A. and O.C., respectively; from 2009 SGR 719 to S.A.; and from fellowship IBEC 10-2009-01 to Z.A. O.C. acknowledges the Spanish MINECO for the Ramon y Cajal contract. We are grateful to Wendy Ran for editorial assistance, to P. Hyroššová for helping with lactate degradation studies, to J.C. Perales and J. Domingo for critical reading of the manuscript, to J.A. Ortega for the drawing in Figure 6, to B. Torrejón from the UB's Scientific-Technical Services (Bellvitge Campus) for technical support in confocal microscopy, to X. Ramis for DSC measurements and technical support, to the Experimental 7T MRI Unit (IDIBAPS) and to F. Artigas and M.P. Celada for electrophysiological studies.

Appendix A. Supplementary data

Supplementary data related to this article can be found at http://dx.doi.org/10.1016/j.biomaterials.2014.02.051.

References

[1] Bigler ED. Neuroinflammation and the dynamic lesion in traumatic brain injury. Brain 2013;136:9–11.
[2] Frontczak-Baniewicz M, Chrapusta SJ, Sulejczak D. Long-term consequences of surgical brain injury – characteristics of the neurovascular unit and formation and demise of the glial scar in a rat model. Folia Neuropathol 2011;49(3):204–18.
[3] Forraz N, Wright KE, Jurga M, McGuckin CP. Experimental therapies for repair of the central nervous system: stem cells and tissue engineering. J Tissue Eng Regen Med 2013;7:523–36.
[4] Orive G, Anitua E, Pedraz JL, Emerich DF. Biomaterials for promoting brain protection, repair and regeneration. Nat Rev Neurosci 2009;10:682–92.
[5] Bible E, Chau DY, Alexander MR, Price J, Shakesheff KM, Modo M. The support of neural stem cells transplanted into stroke-induced brain cavities by PLGA particles. Biomaterials 2009;30:2985–94.
[6] Park KI, Teng YD, Snyder EY. The injured brain interacts reciprocally with neural stem cells supported by scaffolds to reconstitute lost tissue. Nat Biotechnol 2002;20:1111–7.
[7] Volpato FZ, Fuhrmann T, Migliaresi C, Hutmacher DW, Dalton PD. Using extracellular matrix for regenerative medicine in the spinal cord. Biomaterials 2013;34:4945–55.
[8] Saha B, Jaber M, Gaillard A. Potentials of endogenous neural stem cells in cortical repair. Front Cell Neurosci 2012;6:14.
[9] Robel S, Berninger B, Gotz M. The stem cell potential of glia: lessons from reactive gliosis. Nat Rev Neurosci 2011;12:88–104.
[10] Weissman T, Noctor SC, Clinton BK, Honig LS, Kriegstein AR. Neurogenic radial glial cells in reptile, rodent and human: from mitosis to migration. Cereb Cortex 2003;13:550–9.
[11] Tanaka EM, Ferretti P. Considering the evolution of regeneration in the central nervous system. Nat Rev Neurosci 2009;10:713–23.
[12] Anthony TE, Klein C, Fishell G, Heintz N. Radial glia serve as neuronal progenitors in all regions of the central nervous system. Neuron 2004;41:881–90.
[13] Kriegstein A, Alvarez-Buylla A. The glial nature of embryonic and adult neural stem cells. Annu Rev Neurosci 2009;32:149–84.
[14] Rakic P. Developmental and evolutionary adaptations of cortical radial glia. Cereb Cortex 2003;13:541–9.
[15] Stubbs D, DeProto J, Nie K, Englund C, Mahmud I, Hevner R, et al. Neurovascular congruence during cerebral cortical development. Cereb Cortex 2009;19:32–41.
[16] Tam SJ, Watts RJ. Connecting vascular and nervous system development: angiogenesis and the blood-brain barrier. Annu Rev Neurosci 2010;33:379–408.
[17] Buffo A, Rolando C, Ceruti S. Astrocytes in the damaged brain: molecular and cellular insights into their reactive response and healing potential. Biochem Pharmacol 2010;79:77–89.
[18] Covey MV, Jiang Y, Alli VV, Yang Z, Levison SW. Defining the critical period for neocortical neurogenesis after pediatric brain injury. Dev Neurosci 2010;32:488–98.
[19] Anton ES, Marchionni MA, Lee KF, Rakic P. Role of GGF/neuregulin signaling in interactions between migrating neurons and radial glia in the developing cerebral cortex. Development 1997;124:3501–10.
[20] Baud O, Fayol L, Gressens P, Pellerin L, Magistretti P, Evrard P, et al. Perinatal and early postnatal changes in the expression of monocarboxylate transporters MCT1 and MCT2 in the rat forebrain. J Comp Neurol 2003;465:445–54.
[21] Polet F, Feron O. Endothelial cell metabolism and tumour angiogenesis: glucose and glutamine as essential fuels and lactate as the driving force. J Intern Med 2013;273:156–65.
[22] Speder P, Liu J, Brand AH. Nutrient control of neural stem cells. Curr Opin Cell Biol 2011;23:724–9.
[23] Alvarez Z, Mateos-Timoneda MA, Hyrossova P, Castano O, Planell JA, Perales JC, et al. The effect of the composition of PLA films and lactate release on glial and neuronal maturation and the maintenance of the neuronal progenitor niche. Biomaterials 2013;34:2221–33.
[24] Mattotti M, Alvarez Z, Ortega JA, Planell JA, Engel E, Alcantara S. Inducing functional radial glia-like progenitors from cortical astrocyte cultures using micropatterned PMMA. Biomaterials 2012;33:1759–70.
[25] Li Y, Song Y, Zhao L, Gaidosh G, Laties AM, Wen R. Direct labeling and visualization of blood vessels with lipophilic carbocyanine dye DiI. Nat Protoc 2008;3:1703–8.
[26] Conte WL, Kamishina H, Reep RL. Multiple neuroanatomical tract-tracing using fluorescent Alexa Fluor conjugates of cholera toxin subunit B in rats. Nat Protoc 2009;4:1157–66.
[27] Fan HJ, Knez M, Scholz R, Hesse D, Nielsch K, Zacharias M, et al. Influence of surface diffusion on the formation of hollow nanostructures induced by the Kirkendall effect: the basic concept. Nano Lett 2007;7:993–7.
[28] Feng L, Hatten ME, Heintz N. Brain lipid-binding protein (BLBP): a novel signaling system in the developing mammalian CNS. Neuron 1994;12:895–908.
[29] Englund C, Fink A, Lau C, Pham D, Daza RA, Bulfone A, et al. Pax6, Tbr2, and Tbr1 are expressed sequentially by radial glia, intermediate progenitor cells, and postmitotic neurons in developing neocortex. J Neurosci 2005;25:247–51.

[30] Suh H, Consiglio A, Ray J, Sawai T, D'Amour KA, Gage FH. In vivo fate analysis reveals the multipotent and self-renewal capacities of Sox2+ neural stem cells in the adult hippocampus. Cell Stem Cell 2007;1:515–28.
[31] Hsieh J. Orchestrating transcriptional control of adult neurogenesis. Genes Dev 2012;26:1010–21.
[32] Ovens MJ, Davies AJ, Wilson MC, Murray CM, Halestrap AP. AR-C155858 is a potent inhibitor of monocarboxylate transporters MCT1 and MCT2 that binds to an intracellular site involving transmembrane helices 7–10. Biochem J 2010;425:523–30.
[33] Miller FD, Gauthier AS. Timing is everything: making neurons versus glia in the developing cortex. Neuron 2007;54:357–69.
[34] Tavazoie M, Van der Veken L, Silva-Vargas V, Louissaint M, Colonna L, Zaidi B, et al. A specialized vascular niche for adult neural stem cells. Cell Stem Cell 2008;3:279–88.
[35] Shechter R, Miller O, Yovel G, Rosenzweig N, London A, Ruckh J, et al. Recruitment of beneficial M2 macrophages to injured spinal cord is orchestrated by remote brain choroid plexus. Immunity 2013;38:555–69.
[36] Hisaoka T, Nakamura Y, Senba E, Morikawa Y. The forkhead transcription factors, Foxp1 and Foxp2, identify different subpopulations of projection neurons in the mouse cerebral cortex. Neuroscience 2010;166:551–63.
[37] Magavi SS, Leavitt BR, Macklis JD. Induction of neurogenesis in the neocortex of adult mice. Nature 2000;405:951–5.
[38] Fame RM, MacDonald JL, Macklis JD. Development, specification, and diversity of callosal projection neurons. Trends Neurosci 2011;34:41–50.
[39] Freire E, Gomes FC, Jotha-Mattos T, Neto VM, Silva Filho FC, Coelho-Sampaio T. Sialic acid residues on astrocytes regulate neuritogenesis by controlling the assembly of laminin matrices. J Cell Sci 2004;117:4067–76.
[40] Lathia JD, Rao MS, Mattson MP, Ffrench-Constant C. The microenvironment of the embryonic neural stem cell: lessons from adult niches? Dev Dyn 2007;236:3267–82.
[41] Hurtado A, Cregg JM, Wang HB, Wendell DF, Oudega M, Gilbert RJ, et al. Robust CNS regeneration after complete spinal cord transection using aligned poly-L-lactic acid microfibers. Biomaterials 2011;32:6068–79.
[42] Ma S, Kwon HJ, Johng H, Zang K, Huang Z. Radial glial neural progenitors regulate nascent brain vascular network stabilization via inhibition of Wnt signaling. PLoS Biol 2013;11:e1001469.
[43] Simon-Assmann P, Orend G, Mammadova-Bach E, Spenle C, Lefebvre O. Role of laminins in physiological and pathological angiogenesis. Int J Dev Biol 2011;55:455–65.
[44] Kazanis I, Lathia JD, Vadakkan TJ, Raborn E, Wan R, Mughal MR, et al. Quiescence and activation of stem and precursor cell populations in the subependymal zone of the mammalian brain are associated with distinct cellular and extracellular matrix signals. J Neurosci 2010;30:9771–81.
[45] Belvindrah R, Graus-Porta D, Goebbels S, Nave KA, Muller U. Beta1 integrins in radial glia but not in migrating neurons are essential for the formation of cell layers in the cerebral cortex. J Neurosci 2007;27:13854–65.
[46] Loulier K, Lathia JD, Marthiens V, Relucio J, Mughal MR, Tang SC, et al. beta1 integrin maintains integrity of the embryonic neocortical stem cell niche. PLoS Biol 2009;7:e1000176.
[47] Benner EJ, Luciano D, Jo R, Abdi K, Paez-Gonzalez P, Sheng H, et al. Protective astrogenesis from the SVZ niche after injury is controlled by Notch modulator Thbs4. Nature 2013;497:369–73.
[48] Saha B, Peron S, Murray K, Jaber M, Gaillard A. Cortical lesion stimulates adult subventricular zone neural progenitor cell proliferation and migration to the site of injury. Stem Cell Res 2013;11:965–77.
[49] Niu W, Zang T, Zou Y, Fang S, Smith DK, Bachoo R, et al. In vivo reprogramming of astrocytes to neuroblasts in the adult brain. Nat Cell Biol 2013;15:1164–75.
[50] Christensen K, Schroder HD, Kristensen BW. CD133 identifies perivascular niches in grade II–IV astrocytomas. J Neurooncol 2008;90:157–70.

Biomaterials 34 (2013) 2221–2233

Contents lists available at SciVerse ScienceDirect

Biomaterials

journal homepage: www.elsevier.com/locate/biomaterials

The effect of the composition of PLA films and lactate release on glial and neuronal maturation and the maintenance of the neuronal progenitor niche

Zaida Álvarez [a,b,d], Miguel A. Mateos-Timoneda [d,a], Petra Hyroššová [e], Oscar Castaño [a,c,d], Josep A. Planell [a,c,d], José C. Perales [e], Elisabeth Engel [a,c,d], Soledad Alcántara [b,*]

[a] Institute for Bioengineering of Catalonia-IBEC, Barcelona, Spain
[b] Department of Pathology and Experimental Therapeutics, Medical School (Bellvitge Campus), University of Barcelona-UB, Barcelona, Spain
[c] Department of Material Science and Metallurgical Engineering, Technical University of Catalonia-UPC, Barcelona, Spain
[d] CIBER en Bioingeniería, Biomateriales y Nanomedicina (CIBER-BBN), Barcelona, Spain
[e] Department of Physiological Sciences, Medical School (Bellvitge Campus), University of Barcelona-UB, Barcelona, Spain

ARTICLE INFO

Article history:
Received 3 October 2012
Accepted 9 December 2012
Available online 28 December 2012

Keywords:
Polylactic acid
Degradation
Neurons
Progenitors
Lactate
Glial cells
NSC niche

ABSTRACT

To develop tissue engineering strategies useful for repairing damage in the central nervous system (CNS) it is essential to design scaffolds that emulate the NSC niche and its tight control of neural cell genesis, growth, and differentiation. In this study we tested two types of poly L/DL lactic acid (PLA95/5 and PLA70/30), a biodegradable material permissive for neural cell adhesion and growth, as materials for nerve regeneration. Both PLA were slightly hydrophobic and negatively charged but differed in crystallinity, stiffness and degradation rate. PLA95/5 films were highly crystalline, stiff (GPa), and did not degrade significantly in the one-month period analyzed in culture. In contrast, PLA70/30 films were more amorphous, softer (MPa) and degraded faster, releasing significant amounts of lactate into the culture medium. PLA70/30 performs better than PLA95/5 for primary cortical neural cell adhesion, proliferation and differentiation, maintaining the pools of neuronal and glial progenitor cells *in vitro*. L-lactate in the medium recapitulated PLA70/30's maintenance of neuronal restricted progenitors but did not sustain bipotential or glial restricted progenitors in the cultures, as occurred when neural cells were grown on PLA70/30. Our results suggest that PLA70/30 may mimic some of the physical and biochemical characteristics of the NSC niche. Its mechanical and surface properties may act synergistically in the modulation of bipotential and glial restricted progenitor phenotypes, while it is L-lactate, either added to the medium or released by the film that drives the maintenance of neuronal restricted progenitor cell phenotypes.

1. Introduction

Despite advances in the knowledge of the mechanisms of nerve injury and repair, regeneration strategies for the damaged central nervous system (CNS) are still in their infancy. The development of tissue engineering opened up a new chapter for biomaterials and their potential applications in this field. Biomaterials can be used as mediators to help nerve regeneration across scars, gaps, and cavities resulting from injuries. In fact, they offer a wide range of possibilities since they can be designed to fit specific needs, such as promoting growth or recreating biochemical and topographical cues normally present in the neural stem cell (NSC) niche [1,2].

A variety of materials, in particular polymers, have been investigated in order to establish their suitability for tissue engineering applications. Among them, polylactic acid (PLA) is a promising polymer for neural regeneration owing to its thermoplastic processability and mechanical and biological properties, such as its lack of immunogenicity and its biodegradability [3]. Moreover, though it is known that D-lactic acid does not act as metabolic substrate, L-lactic acid, the principal degradation product of PLA material, is an intermediate metabolite of anaerobic glycolysis and consequently a possible alternative energy substrate for neural cells [4,5].

* Corresponding author. Cell Biology Unit, Department of Experimental Pathology and Therapeutics, School of Medicine (Bellvitge Campus), University of Barcelona, 08907 L'Hospitalet de Llobregat, Spain. Tel./fax: +34934024288.
E-mail address: salcantara@ub.edu (S. Alcántara).

0142-9612/$ – see front matter © 2012 Elsevier Ltd. All rights reserved.
http://dx.doi.org/10.1016/j.biomaterials.2012.12.001

Cerebral energy metabolism is a highly compartmentalized and complex process in which trans-cellular trafficking of metabolites plays a pivotal role. The adult brain normally uses glucose as its primary energy source [6]. However, before and immediately after birth, lactate is also an important energy source because at this time the level of glucose in the blood is low but the lactate concentration is high [7,8]. Lactate is transported across cell membranes into the brain by monocarboxylate transporters (MCTs), among which MCT1–4 co-transports lactate with a proton [9].

Over the past decade, a role for lactate in fueling the energetic requirements of neurons has emerged, not only during the perinatal period but also in adulthood. It is not fully understood how the switch from glucose to lactate neuronal metabolism is achieved but the astrocyte-neuron lactate shuttle seems to be involved. This hypothesis postulates that lactate is produced by astrocytes and used by neurons in an activity-dependent and glutamate-mediated manner [10]. Accordingly, glutamate released from neurons during synaptic activity induces glutamate uptake by glial cells, which triggers activation of glycolysis. Glial glycolysis then produces lactate which is released into the extracellular space by the MCT1 transporter and is later used as a major metabolic substrate by neurons expressing the MCT2 lactate transporter, present exclusively in this type of cell [11]. Emerging evidence suggests that the metabolisms of NSC, neurons and astrocytes differ and that energy-dependent processes may influence the balance between NSC self-renewal and differentiation [12]. Recent work in drosophila revealed that NSC proliferation is controlled by diet-dependent insulin/TOR signaling [13]. However, it is not known whether a similar system operates in the mammalian brain; nor is it clear whether glucose or lactate is the main NSC metabolic substrate.

We investigated the different biological responses *in vitro* in terms of cell adhesion, survival, differentiation and the use of lactic acid by neurons, glial cells and neural progenitors, cultured on two different uncoated PLA-based polymers. PLA95/5 and 70/30 films contain different proportions of D- and L-lactic acid, which confer different mechanical surface properties and degradation rates.

2. Materials and methods

2.1. PLA95/5 and 70/30 films characterization

Poly-L/DL lactic acid 95/5 (PLA95/5) (Purasorb PLDL 9562, inherent viscosity midpoint 6.2 dl/g, $M_w \approx 125{,}000$ g/mol) and Poly-L/DL lactic acid 70/30 (PLA70/30) (Purasorb PLDL 7038, inherent viscosity midpoint 3.8 dl/g, $M_w \approx 850{,}000$ Da) were purchased from Purac Biomaterials (Gorinchem). 150 μm thick films of PLA95/5 and PLA70/30 were prepared by solvent casting. Briefly, 6.75 g of PLA were dissolved in 270 ml of chloroform (2.5% *w*/*v*). The solution was poured into Petri dishes with ø of 150 mm. The solvent was evaporated in a chloroform-saturated atmosphere for 48 h. For cell culture, PLA95/5 and 70/30 films were sterilized with 70% ethanol for 15 min and cut to fit in 60 mm ø tissue culture dishes.

Characterization of PLA95/5 and 70/30 wettability was performed via contact-angle measurements using an OCA 20 system (Dataphysics, GmbH). Advancing contact angle measurements were taken using the captive bubble technique. This method consists in the measurement of the equilibrium angle formed between a 3 ml air bubble and the surface of the PLA, both immersed in water. The measurements were performed in triplicate with at least three different data points for each sample.

Z-potential measurements were carried out using a SurPASS apparatus and VisioLab software (Anton Paar Ltd.). All the measurements were performed at a dynamic pH of the electrolyte (KCl 1 mM, pH 3–8) after 2 h of equilibration using the Adjustable Gap Cell for small samples. The young modulus and surface topography of PLA95/5 and PLA70/30 films were measured using atomic force microscopy (AFM) (MultiMode 8 Atomic Force Microscope (Bruker)).

Tests to failure to measure films tensile strength were performed using an Instron 5565 compression and tension tester (Instron Corp. Canton MA) with samples of 15 × 10 mm and thicknesses of 333 ± 22 μm. The tensile stress test was monitored using a speed of 10 mm/min.

A thermal characterization of the two different materials was performed by Differential Scanning Calorimetry (DSC, 2029 TA). PLA films were prepared by solvent casting following the protocol described above. For each DSC test, about 5 mg of material were loaded in the furnace of the instrument and were heated from room temperature up to 175 °C (heating rate 10 °C/min). The degree of crystallinity was calculated using the following Equation (1):

$$\%X_c = \frac{(\Delta H_m - \Delta H_c)}{\Delta H_m^0} \times 100 \quad (1)$$

where $\%X_c$ is the percentage of crystallinity, ΔH_m is the latent heat of melting, ΔH_c is the heat of the crystallization, and ΔH_m^0 is the heat of melting of a PLA with a supposed 100% degree of crystallinity ($\Delta H_m^0 = 93.1$ J/g) [14].

$\theta/2\theta$ 2–60° XRD analysis of PLA films were performed using a Panalytical X'Pert PRO Diffractometer using a CuKα $\lambda = 1.5406$ Å radiation, 45 kV, 40 mA and a step size of 0.026°.

Micro and nanomorphology was assessed using a Nova™ NanoSEM Scanning Electron Microscope at 10 kV and ultra-thin carbon coatings.

2.2. Cell culture

All animal housing and procedures were approved by the Institutional Animal Care and Use Committee in accordance with Spanish and EU regulations. Glial cells were derived from the cerebral cortex of newborn mice (P0) as described elsewhere [15]. Briefly, cerebral cortices were dissected free of meninges in dissection buffer (PBS 0.6% glucose (Sigma–Aldrich), 0.3% BSA (Sigma–Aldrich)) and digested with trypsin (Biological Industries) and DNAse I (Sigma–Aldrich) for 10 min at 37 °C. The tissue was dissociated in Dulbecco's Modified Eagle Medium (DMEM, Biological Industries), 10% normal horse serum (NHS, GIBCO), 1% penicillin–streptomycin (Pen-Strep, Biological Industries) and 2 mM L-glutamine (Biological Industries). After centrifugation and resuspension, cells were plated and grown to confluence at 37 °C, 5% CO_2 (approximately 25–30 days *in vitro (div)*). All the experiments were performed using glial cells from the first passage (Ps1).

To assess the influence of material properties on glial cell adhesion, morphology and differentiation, Ps1 cells were cultured at a density of 2×10^5 cells/cm^2 for 5*div* in Neurobasal™ (NB), 3% NHS, 1% Pen-Strep, and 2 mM L-glutamine on uncoated PLA95/5 and PLA70/30 films. Control glia were Ps1 glial cells cultured on non-coated culture plastic (for Western blotting) or glass (for ICC) under the same conditions as for PLA films. The cellular composition and biochemical characterization of control and reference glial conditions have been described previously [15].

Neurons were obtained from embryonic brains as described elsewhere [16]. Briefly, a time pregnant mouse was sacrificed by cervical dislocation and the embryos were extracted at embryonic day 16 (E16). Cerebral cortices were dissected free of meninges in a solution of PBS with 0.6% glucose (Sigma–Aldrich), 0.3% BSA (Sigma–Aldrich) and digested with trypsin (Biological Industries) DNAse I (Sigma–Aldrich) for 10 min at 37 °C. The tissue was mechanically dissociated, centrifuged and resuspended in CO_2-equilibrated DMEM supplemented with 10% NHS, 1% Pen-Strep, 0.5 mM L-Glutamine, 5.8 μl/ml $NaHCO_3$ (Sigma–Aldrich). The cell suspension was pre-plated at 37 °C. After 30 min, the supernatant was collected, centrifuged (1000 *g* 5 min), resuspended in neuronal culture medium (NB, 1%NHS, 1% Pen-Strep, 0.5 mM L-glutamine, 22 μM glutamic acid (Sigma–Aldrich), 2% B27(Gibco), 5.8 μl/ml $NaHCO_3$) and plated at a density of 2.5×10^5 cells/cm^2 directly on top of films of PLA95/5, 70/30 or on poly-D-lysine (Sigma–Aldrich) coated tissue culture plate (for Western blotting) or glass (Lysglass, for ICC) as a positive control. After 24 h, the medium was changed to a serum free neuronal culture medium (1% Pen-Strep, 0.5 mM L-Glutamine, 2% B27 (Gibco), 5.8 μl/ml $NaHCO_3$) during 1*div*, 3*div* and 5*div*. By using these conditions, neuron-enriched culture contained around 10% of glial cells.

In order to analyze the effect of lactate released by the material, neurons and glial cells were plated in the same conditions as described above for the first 24 h in a glucose-free Neurobasal^A media (glucose-free, NB^A; Invitrogen), with 3% NHS, 1% Pen-Strep, and 2 mM L-glutamine for glial cells, and 1%NHS, 1% Pen-Strep, 0.5 mM L-glutamine, 22 μM glutamic acid, 1× B27, 5.8 μl/ml $NaHCO_3$ for neuronal cell cultures. After 24 h, the neuronal culture medium was changed again to a serum free NB^A with 1% Pen-Strep, 0.5 mM L-glutamine, 1× B27, 5.8 μl/ml $NaHCO_3$ and culture during 4*div*.

The samples were either fixed in 4% PFA for 15 min at room temperature for immunochemistry, or used for protein extraction and Western blot analysis. Media were collected to measure lactate and glucose concentration.

2.3. Western blot/immunocytochemistry

For Western blot analysis, protein extracts were obtained from primary cultures and total protein extracts were separated by SDS- polyacrylamide gel and electro-transferred to a nitrocellulose membrane (Bio-Rad). Membranes were blocked with 5% bovine serum albumin (BSA, Sigma–Aldrich) and incubated firstly with primary antibodies overnight at 4 °C, and then with their corresponding secondary HRP-conjugated antibodies (1:3000; Santa Cruz Biotechnology). Protein signal was detected using the ECL chemiluminescent system (Amersham, GE Healthcare). Densitometry analysis, standardized to actin/vinculin as a control for protein loading, was performed using ImageJ software. For quantification, triplicate samples were analyzed and at least two different experiments were used.

For immunofluorescence, fixed samples (4% PFA for 15 min at RT) were incubated with primary antibodies and appropriate Alexa 488 or Alexa 555 secondary

antibodies (1:500, Molecular Probes). Phalloidin was used to stain F-actin (1:2000, Sigma–Aldrich) and To-Pro-3 iodide (1:500, Molecular Probes) to stain nuclei. Finally, the preparations were coverslipped with Mowiol (Calbiochem) for imaging.

The following primary antibodies were used; rabbit anti-GFAP (mature and reactive glial marker, 1:500–1:8000, Dako), rabbit anti-BLBP (radial glial marker, 1:1000–1:8000, Chemicon), mouse anti-Nestin (progenitor and radial glial marker, 1:250, Abnova Corporation), goat anti-Actin (cytoskeleton Marker, 1:2000, Santa Cruz Biotechnology), mouse anti-Tuj-1 (neuronal marker 1:10,000, Covance), rabbit anti-PH3 (proliferation marker, 1:250, Millipore), goat anti-Pax6 (neurogenic radial glial marker, 1:250, Santa Cruz Biotechnology), rabbit anti-Tbr2 (neurogenic intermediate progenitor cells marker, 1:500, Abcam), rabbit anti-EAAT1/GLAST-1 (glial glutamate transporter marker, 1:1000, Abcam), rabbit anti-Ki67 (proliferation marker, 1:500, Abcam), mouse anti- Synaptophysin (pre-synaptic neuronal marker, 1:1000, Dako), rabbit anti-PSD95 (post-synaptic neuronal marker, 1:1000, Abcam) and goat anti-MCT2 (neuronal monocarboxylate transporter marker 1:500, Santa Cruz Biotechnology).

2.4. Degradation study and L-lactate quantification

The degradation of PLA films *in vitro* was followed at 37 °C over a period of four weeks. Four samples (~8 mg) were immersed in Neurobasal A (NB^A, glucose and pyruvate free Gibco) and retrieved on different days *in vitro* (1*div*, 3*div*, 4*div*, 5*div*, 7*div*, 15*div* and 21*div*).

The concentration of L-lactate was determined using an enzymatic reaction based on the oxidation of L-lactate to pyruvate by lactate dehydrogenase (LDH; Roche) (5 mg/ml, 550 U/mg) in presence of NAD (Sigma–Aldrich). The amount of NADH produced in the reaction is proportional to the amount of the L-lactate in the samples. With this enzymatic system, D-lactate was not detected.

All experiments were carried out at least three times, and triplicate samples were diluted 1:20 with reaction mix (buffer of 0.3 M hydrazine sulphate (Merck) and 0.87 M glycine (AppliChem) with pH 9.5, 2.5 M NAD (Sigma–Aldrich), 0.19 M EDTA (Merck)). LDH was added at a final concentration of 6.9 U/ml. NADH concentration was determined by measuring absorbance (340 nm) and fluorescence (excitation 340 nm and emission 460 nm) using Fluostar Optima BMG Labtech at 0 and 20 min after starting the reaction. 20 min was taken as the endpoint of the reaction and used in the calculations. Different concentrations of sodium L-lactate (Sigma–Aldrich) were used as a standard.

2.5. Glucose quantification

The concentration of glucose was determined by the glucose oxidase–peroxidase method using PGO enzymes (Peroxidase and Glucose Oxidase, Sigma). O-dianisidine dihydrochloride (ODD, Sigma) was utilized as a colorimetric substrate. Colorless ODD in reaction with H_2O_2 (produced by oxidation of glucose) changed to brown. The brown intensity was measured at 450 nm using lector Tecan (Sunrise-Basic, ref. 16039400). For glucose determination, glucose standard (Sigma) was used to prepare the standard curve. The reaction proceeded for 30 min at 37 °C. The samples were analyzed in triplicate.

2.6. Lactate treatments

In some experiments, E16 primary neuronal cultures and P0 glial cultures were treated with L-lactic acid or D-Lactic acid (Sigma Aldrich). Cells were cultured in three different media; Neurobasal™ medium (with 25 mM glucose, glucose medium), Neurobasal™ medium supplemented with lactic acid (4 mM) (glucose + lactate medium) or in a free glucose Neurobasal^A medium (NB^A) supplemented with lactic acid (4 mM) (lactate medium). Glial cells were cultured with 3% NHS, 1% Pen-Strep, and 2 mM L-glutamine for 5*div*. Neurons were cultured for 24 h in 1%NHS, 1% Pen-Strep, 0.5 mM L-glutamine, 22 μM glutamic acid, 1× B27, 5.8 μl/ml $NaHCO_3$ and the medium was then changed then to a serum-free medium, 1% Pen-Strep, 0.5 mM L-glutamine, 1× B27, 5.8 μl/ml $NaHCO_3$ for four more *div*.

All experiments were carried out at least three times and triplicate samples were analyzed by Western blot, cell morphology was analyzed by ICC, and L-lactate and Glucose in media were measured by spectrophotometry and fluorescence respectively.

2.7. Light and confocal microscopy

Micrographs were captured with a light microscope Nikon Eclipse 800 (Nikon) or with a spectral confocal microscope Leica TCS-SL (Leica Microsystems). Images were assembled in Adobe Photoshop (v. 7.0), with similar adjustments for contrast, brightness, and color balance to obtain optimum visual reproduction of the data.

2.8. Statistical analyses

Cell counts were expressed as mean cells/mm^2 ± standard deviation. Values were the average of three replicas of at least two different experiments. Statistical analysis was performed using the Statgraphic-plus software. One-way ANOVA and Fisher's least significant difference (LSD) procedure were used to discriminate between the means. Statistical significance was set at $p < 0.05$.

3. Results

3.1. Characterization of PLA95/5 and 70/30 films

In addition to their distinct composition, glass, PLA95/5, 70/30 and culture plastic (polystyrene) are harder than brain and are considered stiff substrates. PLA95/5, 70/30 and glass were slightly hydrophobic and negatively charged (contact angle 75.6 ± 5.2, 78.1 ± 8.7, 73.9 ± 2.8 respectively; *Z* potential at pH = 7.4: −72.3 ± 1.8 mV, −36.7 ± 1.9 mV and −80 ± 14 mV respectively), while culture plastic was slightly hydrophilic (contact angle: 58.3 ± 1.3) and negatively charged (*Z* potential at pH = 7.4: −124 ± 1.4 mV). To analyze the effect of degradation on wettability and surface charge, the measures were repeated on PLA films after 4 days in serum-free medium. Contact angle was slightly reduced in PLA95/5 (70.3 ± 3.0), while on PLA70/30 there was a dramatic decrease (≤20), indicating a switch from slightly hydrophobic to hydrophilic. The *Z* potential becomes significantly more negative in both PLA (PLA95/5:−102.2 ± 1.9 mV; PLA70/30:−82.2 ± 2.5 mV).

AFM visualization of surface topography showed differences in the surface roughness in PLA95/5 and 70/30 (Fig. 1A). In both cases the semi-crystalline domains (spherulites) of the polymeric network were visible. However, the semi-crystalline domains were larger in PLA95/5 than in PLA70/30, as expected for the different ratios of the L and DL monomers [17,18].

To confirm the difference in the amount of semi-crystalline domains, the crystallinity of PLA95/5 and 70/30 films was assessed by means of X-ray diffraction (XRD) and Differential Scanning Calorimetry (DSC). The XRD diffraction patterns showed the different crystallinity of the materials after the formation of the solvent-casting films. While both raw materials were semi-crystalline (due to the aging process), on formation of the films only PLA95/5 remained semi-crystalline (Fig. 1B). DSC measurements confirmed these results, since the degree of crystallinity determined (%XC) was 18% for PLA95/5 and less than 5% for PLA70/30.

Tensile strength measurements were carried out for the different materials. PLA95/5, the most crystalline material, presented higher Young's Modulus (9.5 ± 0.3 GPa) than PLA70/30 (63.7 ± 1.3 MPa). Correspondingly, the maximum stress to rupture was higher in PLA95/5 (428.5 ± 118.1 MPa) than in PLA70/30 (5.7 ± 0.1 MPa) (Fig. 1C).

To determine differences in the degradation rate between the two PLA polymers, the presence of L-lactate released in the medium was analyzed by spectrophotometry and fluorescence (see material and methods). PLA95/5 films did not release detectable amounts of L-lactate into the medium in the 21-day period analyzed. In contrast, PLA70/30 films, which are more amorphous, showed a linear release of L-lactate into the medium in the physiological range of μM, reaching a value of 31.2 ± 0.3 μM after 21 days *in vitro* (Fig. 1D).

3.2. Glial adhesion and differentiation in PLA95/5 and 70/30 films

Firstly, *in vitro* studies with glial cells were performed with both PLA polymers. Primary glial cells attached to the three types of substrate, although the cell density differed significantly (control glass:590 ± 96, PLA95/5:824 ± 166 and PLA70/30:1124 ± 261, $p < 0.001$). Phalloidin staining of F-actin cytoskeleton showed that glial cells grown on PLA95/5, 70/30 and control (glass) mainly adopted the spread morphology typical of mature astrocytes. In addition, small ramified cells and some bipolar radial glia-like cells

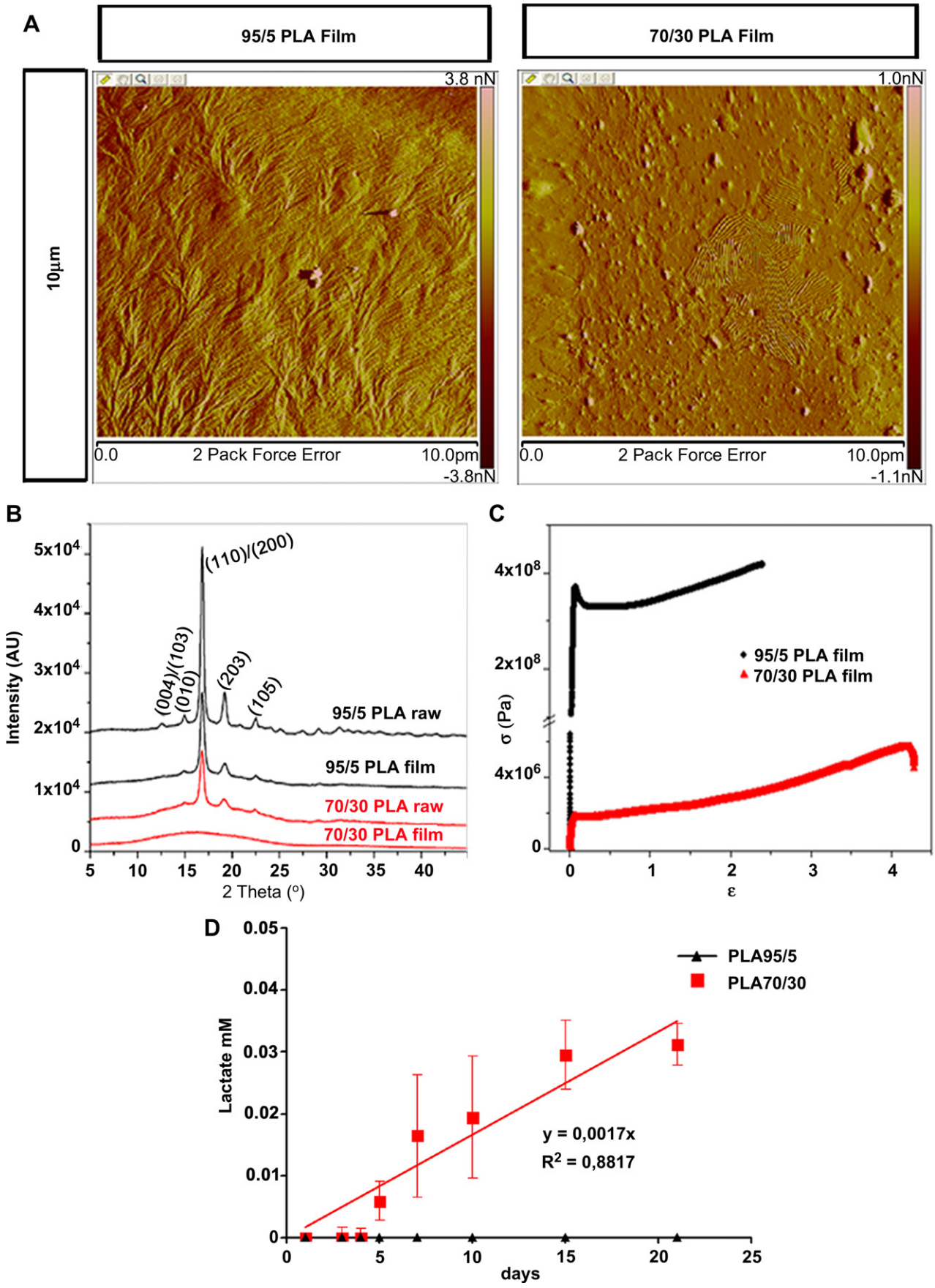

Fig. 1. Mechanical properties of PLA95/5 and 70/30 films. A. 10 × 10 µm Atomic Force Microscopy (AFM) images of PLA95/5 and 70/30 films surface. B. $\theta/2\theta$ 2–60° XRD analysis of PLA films and PLA powder. C. Tensile stress test of PLA95/5 film (Black) and PLA70/30 (red). D. Quantification of L-lactate release into the culture medium at 37 °C by PLA95/5 films (black) and 70/30 films (red) at different times (1*div*, 3*div*, 4*div*, 5*div*, 7*div*, 15*div* and 21*div*). Error bars in D. indicate SD. (For interpretation of the references to color in this figure legend, the reader is referred to the web version of this article.)

(RGLS) were also present on control and PLA70/30 films (Fig. 2A). Branched cytoskeleton arrangements typical of reactive glia were not observed in any of the conditions. To identify proliferative cells, we analyzed the expression of Ki67, a marker associated with proliferative cells during interphase. Ki67 staining was limited to a few cells on control and PLA95/5 films ($3 \pm 2, 15 \pm 6$ respectively), but was abundant in glial cells cultured on PLA70/30 films (49 ± 15, $p < 0.001$), indicating an active proliferative state (Fig. 2A).

Western blot and densitometry analysis were used to quantify differences in the expression of glial cell maturation markers after 5*div* (Fig. 2B and C). Glial cells grown on PLA95/5 films expressed similar levels of GFAP, PH3, BLBP and nestin to control glia. However, glial cells grown on PLA70/30 films expressed higher levels of the immature glial marker nestin and the proliferative marker PH3. Pax6 and Tbr2 progenitor markers were not expressed in these cultures. These results indicate that PLA70/30, but not 95/5 films or control glass, induced an immature and proliferative state in the glial cultures, and that no neurogenic progenitors were present.

Afterward, the lactate released into the medium and glucose consumption in the same glial cultures were analyzed. As no lactate was initially present in the culture medium, the L-lactate concentration in the medium of glial cells cultured on the control substrate (6.46 ± 1.04 mM) may derive exclusively from astrocyte release. In

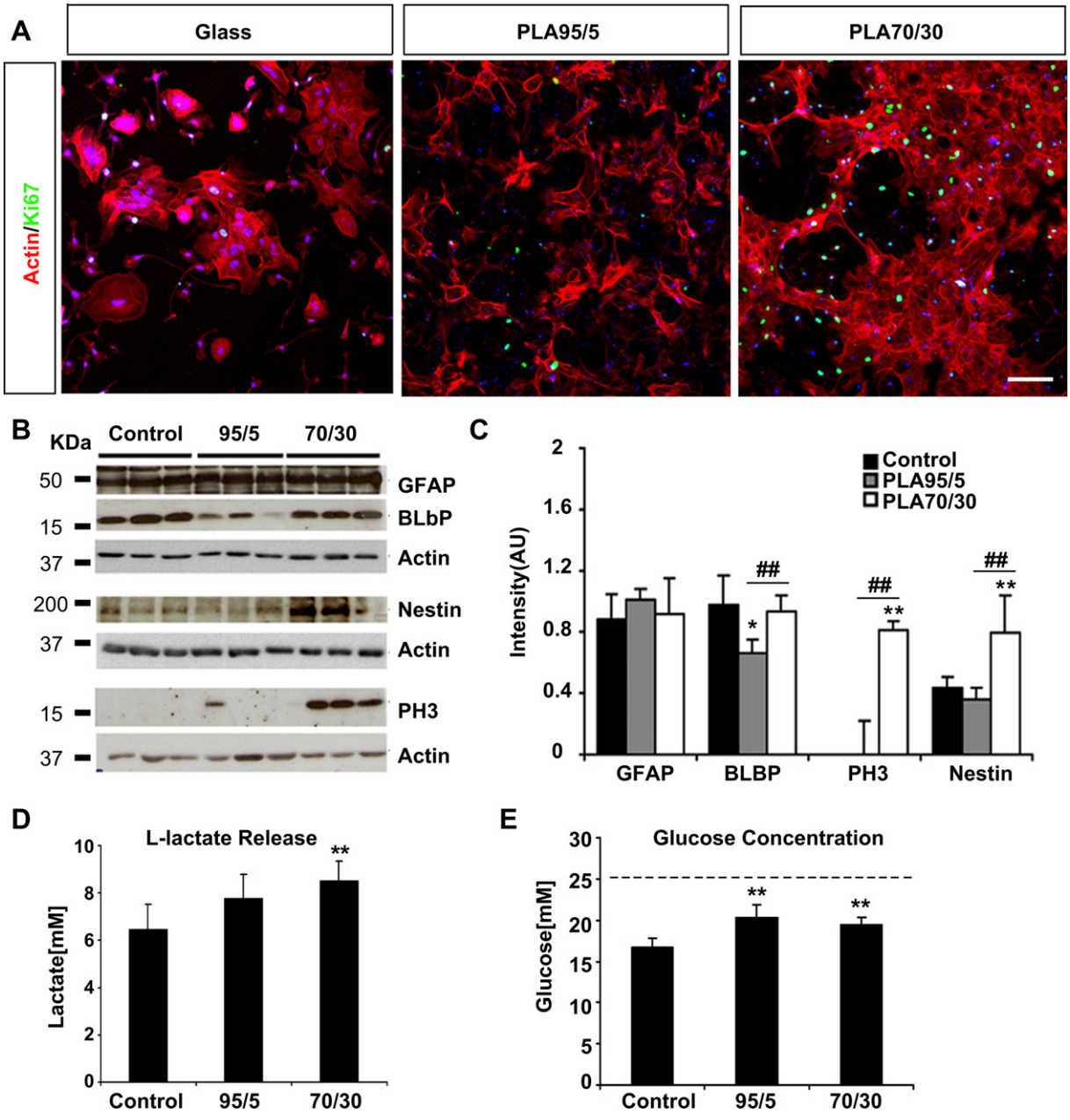

Fig. 2. Effect of PLA on glial cells morphology and phenotype. A. Confocal images of actin staining (phalloidin, red), nuclei (TO-PRO-3, blue) and proliferative nuclei (Ki67, green). B. Biochemical characterization of glial differentiation by Western blots showing the expression of different radial glia (Nestin, BLbP), mature glia (GFAP), and proliferative (PH3) markers. C. Quantitative representation of the western blot densitometry (intensity values normalized to actin). D. L-lactate release in glial cultures grown in the three substrates after 5*div*. E. Glucose quantification in the same cultures, dash line indicates the initial glucose concentration. Scale bar = 100 μm. Asterisks indicate statistical significance respect to control (*$p < 0.05$, **$p < 0.01$, LSD test) and hash indicates significant differences between PLA95/5 and 70/30 conditions (##$p < 0.01$, LSD test). Error bars in D–E indicate SD. (For interpretation of the references to color in this figure legend, the reader is referred to the web version of this article.)

the case of glial cells grown in PLA substrates, L-lactate may also derive from PLA degradation. L-lactate concentration in PLA95/5-derived medium was slightly (but not significantly) higher (7.78 ± 1 mM) than controls, while L-lactate concentration increased significantly in 70/30-derived culture medium (8.53 ± 0.81 mM, $p < 0.01$) (Fig. 2D). Initial glucose concentration in the culture medium was 25 mM, and decreased after 5*div* in all conditions (Fig. 2E). Glucose remained significantly higher in PLA95/5- and 70/30-derived media (20.35 ± 1.54 mM and 19.42 ± 0.87 mM respectively) than in the control-derived medium (16.73 ± 1.12 mM, $p < 0.01$), suggesting that glucose consumption by glial cells decreased as the L-lactate concentration in the medium increased.

3.3. Neuronal cell adhesion and differentiation on PLA95/5 and 70/30 films

β-III Tubulin (Tuj-1) staining revealed that cortical cells attached and differentiated into neurons in the control substrate (Lysglass), and their number remained constant during the culture period (1*div*:377 ± 48; 5*div*:399 ± 54) (Fig. 3A). In contrast, cortical neurons hardly attached at all to PLA95/5 (1*div*:80 ± 39; 5*div*:91 ± 12), where they tended to aggregate in clusters sprouting small numbers of axons and dendrites after 5*div*. Surprisingly, neurons attached to and differentiated on PLA70/30, exhibiting a robust sprouting of axons and dendrites. Although initial adhesion was significantly lower in PLA70/30 than in control ($p < 0.01$), the number of cells in PLA70/30 significantly increased after 5*div* (1*div*:234 ± 49; 5*div*:311 ± 58, $p < 0.01$). Staining with the proliferative marker Ki67 revealed that after 1*div* the number of progenitor cells was similar in Lysglass and in PLA70/30 (65 ± 14 and 53 ± 15 respectively) while it fell notably in PLA95/5 (2 ± 2). However, after 5*div* the situation changed dramatically: Ki67 progenitor cells almost disappeared in Lysglass and PLA95/5 (3 ± 3 and 1 ± 1 respectively) but remained stationary in PLA70/30 (68 ± 19) (Fig. 3A). This result indicates that, starting from a similar progenitor pool, PLA70/30 maintained the progenitor population over time, but Lysglass did not.

To investigate whether gliogenic or neurogenic progenitors were favored in PLA70/30 films with respect to the control substrate, we used Western blot and densitometry to analyze the expression of several lineage-specific markers after 5*div* (Fig. 3B, C). This study was not possible with neuronal cultures on PLA95/5 films due to the low amount of protein obtained. Neurons grown in the control substrate expressed high levels of mature neuronal markers Tuj-1 and the postsynaptic density marker PSD95. In addition, these neuronal cultures express GFAP, indicating the presence of mature astrocytes in the culture. In contrast, neurons cultured on PLA70/30 films expressed high levels of the progenitor markers Pax6 and Tbr2. Pax6 is a homeodomain transcription factor expressed in potential RGLC, and Tbr2 a T-domain transcription factor expressed by neuronal restricted progenitors and by early post-mitotic neurons. The decrease in the mature glial marker GFAP in PLA70/30 films corroborates the prevalence of neural progenitors and immature glia in these cultures. Finally, the expression of proton-linked monocarboxylate transporter MCT2, a neuronal restricted lactate transporter, was increased in neurons cultured in PLA70/30 with respect to the control substrate.

We then quantified the release of L-lactate into the medium (Fig. 3D) and glucose consumption (Fig. 3E) in neuronal cultures. L-lactate concentration in neuronal cultures was significantly higher in the control condition (3.01 ± 0.02 mM, $p < 0.01$) than in PLA70/30 (1.93 ± 0.29 mM) and 95/5 (1.33 ± 0.29 mM) (Fig. 3D). These data correlate well with the higher presence of mature GFAP positive astrocytes in control cultures. Analysis of glucose concentration revealed similar consumptions of neuronal cultures in control (Lysglass) and PLA70/30 (22.32 ± 0.23 mM, 22.25 ± 1.17 mM respectively) and lower consumption in neurons cultured on PLA95/5 films (24.64 ± 0.71 mM), associated with the scarce cell presence in this last substrate (Fig. 3E).

Taken together, these results indicate that PLA70/30 maintains the neuronal culture in a relatively immature state, preserving a pool of neuronal progenitors and inducing the expression of the neuron-specific lactate transporter MCT2.

3.4. Effect of lactate release by PLA70/30 films on neural cell cultures

To analyze the possibility that neural cells used the lactate released from the substrate, neurons and glial cells were cultured on control substrates and both PLA films in the absence of glucose (Neurobasal A medium, NB^A). After 5*div*, glial cells were stained with phalloidin and neurons with tuj-1 antibody for morphometric analysis, and both were co-stained with Ki67 antibody to identify proliferative cells (Fig. 4A).

In the absence of glucose, the survival of glial cells was similar on PLA70/30 films (186 ± 40) and control (glass) (161 ± 52); in both substrates they presented a spread and round morphology typical of mature astrocytes. In contrast, the number of astrocytes on 95/5 films was notably reduced (59 ± 33) and they were smaller and less spread out. Ki67 + proliferative glial cells were almost absent in all three conditions, indicating a quiescent state (Fig. 4B). The L-lactate released by glial cells in glucose-free medium was around 20% of the amount observed in the presence of glucose (Fig. 2D and Fig. 4C). L-lactate concentration in the medium from glial cultures grown on PLA70/30 was significantly higher than in the medium from control surface (1.48 ± 0.05 mM and 1.33 ± 0.09 mM respectively), while it was significantly lower on PLA95/5 (0.96 ± 0.03 mM) (Fig. 4C), in accordance with the reduced degradation rate and glial cell presence in this substrate.

On the other hand, neuronal cultures did not survive on PLA95/5 films in the absence of glucose and barely survived on control substrate (64 ± 36), while neurons attached to and grew well on PLA70/30 (158 ± 50) (Fig. 4A). On the control substrate only some progenitor cells were stained with Ki67 (2 ± 1) and a few poorly developed neurons were found, while on PLA70/30, neurons exhibited a well-developed neurite outgrowth and Ki67 positive neuronal progenitors were abundant (33 ± 6) (Fig. 4B). L-lactate concentration in media from neuronal cultures grown on control substrate or PLA95/5 was at the limit of technical detection (0.61 ± 1.6 μM, and 0.14 ± 1.4 μM respectively). L-lactate concentration on neuronal cultures grown on PLA70/30 was higher (3.4 ± 0.07 μM) than in the other two substrates (Fig. 4C), and within the range of values obtained from direct PLA70/30 degradation at similar times (Fig. 1D). These results suggest that in the absence of glucose, lactate released from PLA70/30 degradation can provide an alternative energy substrate that is sufficient for neural cell growth.

3.5. Differential effect of glucose and L-lactate as energy substrates for glial cultures

In order to explore the influence of lactate on glial cell phenotype, cells were treated with L-lactic acid or D-lactic acid; the degradation products of PLA material, in the presence or absence of glucose in the medium (see material and methods). After 5*div*, glial cells grown on glass or culture plastic and in control medium conditions (25 mM glucose, glucose medium) or in the presence of glucose and L-lactate (25 mM glucose + 4 mM L-lactic acid, glucose + L-lactate medium), adopted a flattened, well-spread morphology with a few proliferating Ki67 positive cells present in both cultures. Nevertheless, there were significantly more cells in the glucose than in the

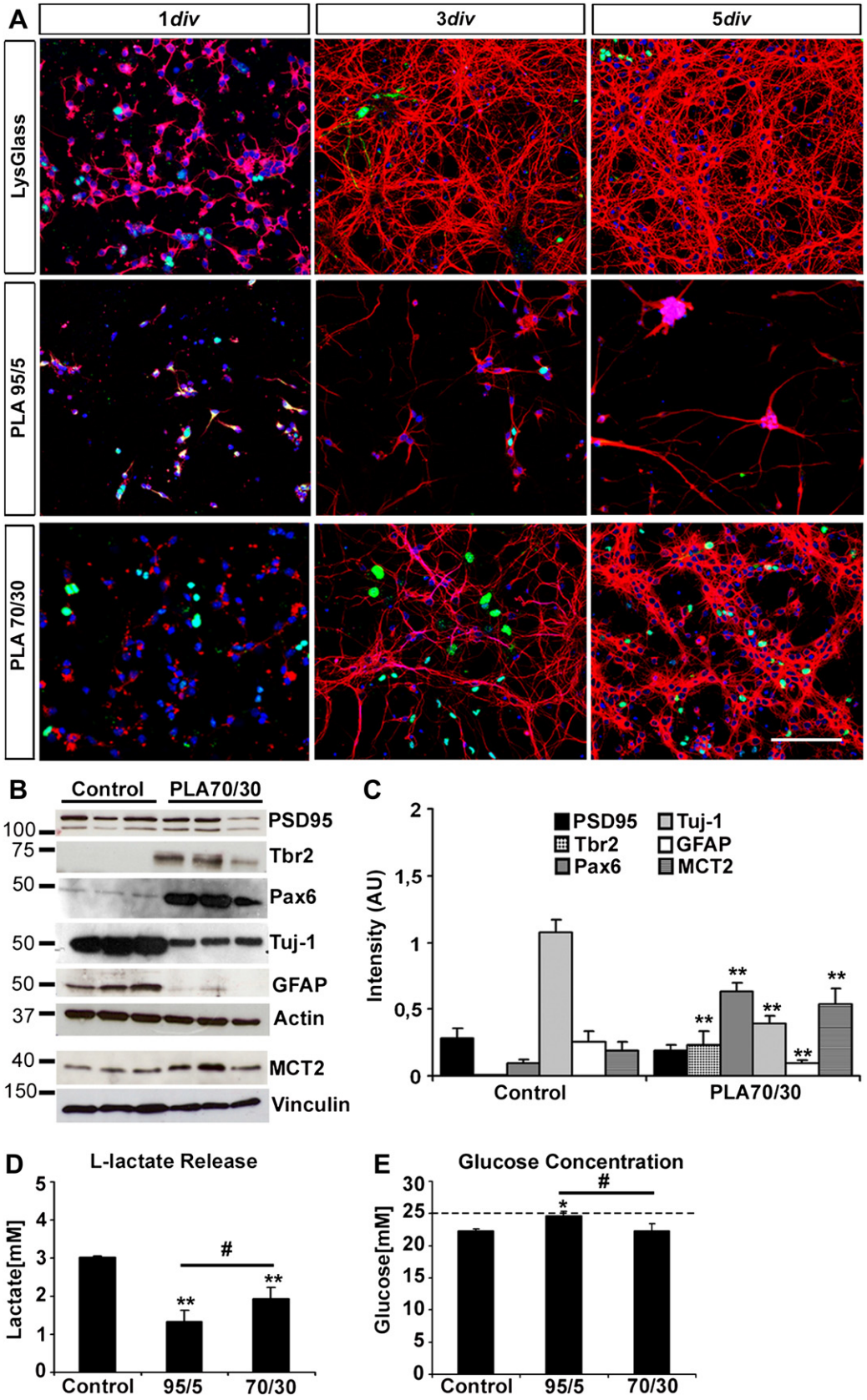

Fig. 3. Effect of PLA on neuronal cultures growth and neural phenotype A. Confocal images of neuronal cultures grown on PLA95/5, 70/30 and Lysglass after different times (1*div*, 3*div* and 5*div*) showing neuronal cytoskeleton staining (Tuj-1, red), nuclei (TO-PRO-3, blue) and proliferative nucleus (Ki67, green). B. Biochemical characterization by Western blot of neuronal cultures grown on PLA70/30 films and tissue culture plate (Lys TCP) after *5div,* showing the expression of progenitor cell markers (Pax6, Tbr2), post-mitotic neuronal markers (Tuj-1, PSD95, and MCT2) and the glial cell marker GFAP. C. Quantitative representation of the Western blot densitometry (intensity values normalized to actin or vinculin). D. L-lactate release in neuronal cultures grown in the three substrates after 5*div* E. Glucose concentration in medium in the same cultures; dashed line indicates the initial glucose concentration. Scale bar = 100 μm. Values are the average of three replicas. Asterisks indicate significant differences with respect to control (*5div*) ($^{*}p < 0.05$, $^{**}p < 0.01$, LSD test) and hash marks indicate significant differences between PLA95/5 and 70/30 conditions ($\#p < 0.05$, LSD test). (For interpretation of the references to color in this figure legend, the reader is referred to the web version of this article.)

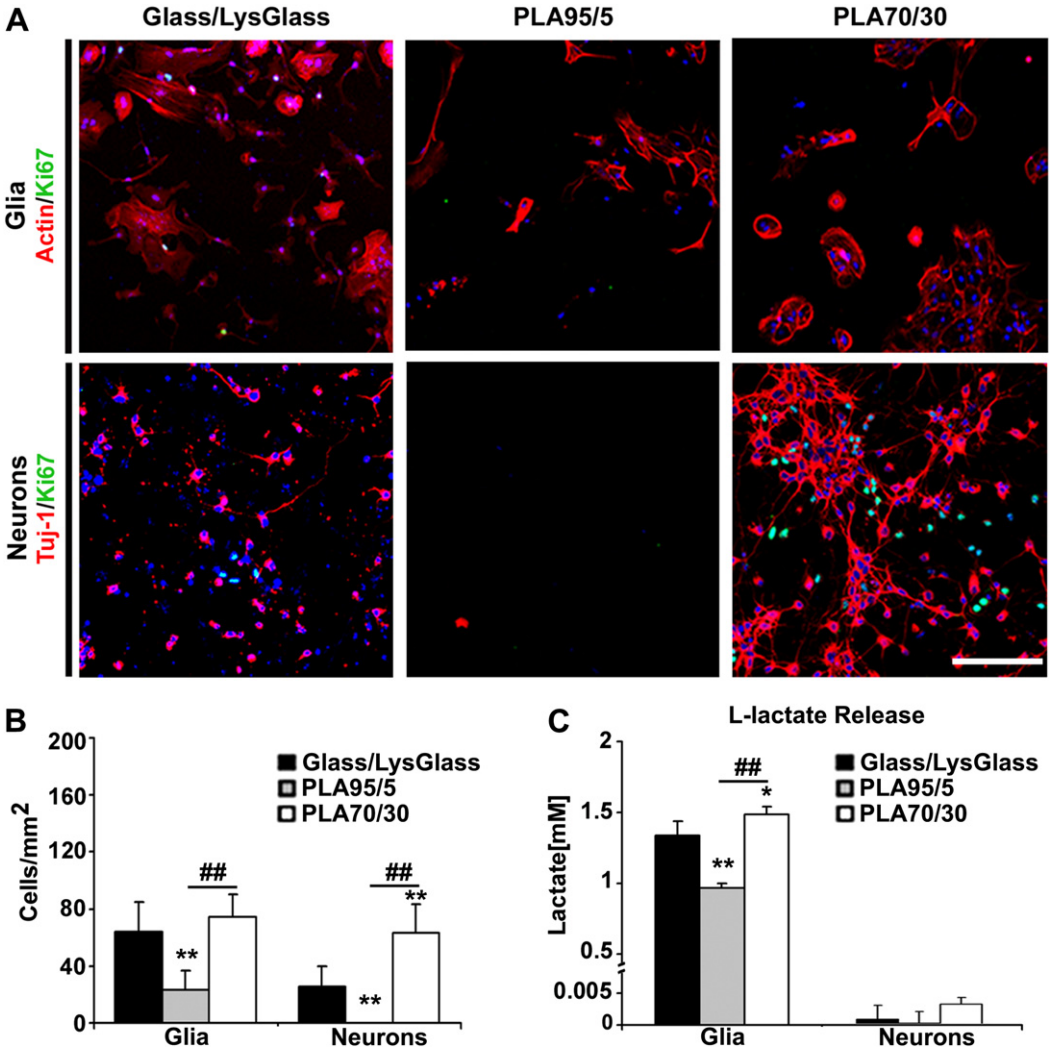

Fig. 4. Effect of lactate released by PLA on neural cultures. A. Images showing neuronal and glial cell cultures grown on the different substrates in glucose free medium (NB^A) during 5*div*. Cell nuclei are marked with TO-PRO-3 (blue), neurons with Tuj-1 antibody (red), glial cells with actin antibody (red), and proliferative cells with Ki67 (green). B. Cell quantification (glial cells and neurons) on glass/Lysglass, PLA95/5 and 70/30 in the same cultures shown in A. C. Lactate release quantification in glucose free medium after 5*div* (Glial cells and Neurons) on glass/Lysglass, PLA95/5 and 70/30. Scale bar = 100 μm. Asterisks indicate significant differences with respect to controls (*$p < 0.05$, **$p < 0.01$, LSD test) and hash marks indicate significant differences between PLA95/5 and 70/30 conditions (##$p < 0.01$, LSD test). Error bars in B and C indicate SD. (For interpretation of the references to color in this figure legend, the reader is referred to the web version of this article.)

glucose + L-lactate medium (685 ± 103 and 322 ± 101 respectively, $p < 0.001$). Glial cells grown in the absence of glucose (NB^A medium supplemented with 4 mM L-lactic acid, L-lactate medium) barely survived after 5*div* (92 ± 33) and were shrunken and poorly developed (Fig. 5A). When the non-metabolizable D-lactate was added in the presence or absence of glucose, glial cultures exhibited similar features to the respective control cultures, and only a mild reduction in the total number of cells and a very mild increase in Ki67 were observed in D-lactate medium (Supplementary Fig. 1).

Quantitative analysis of glial differentiation markers was performed by Western blot and densitometry (Fig. 5B and C). Nestin, BLBP and GFAP glial differentiation markers and the glial glutamate transporter GLAST were similarly expressed in glial cells grown in the presence of glucose or with glucose + L-lactate. This analysis was not possible when only L-lactate was present in the medium due to the low amount of protein obtained.

The concentrations of L-lactate and glucose in media containing glucose or glucose + L-lactate were analyzed in order to estimate the consumption or release of each metabolite by the glial cells. In the presence of glucose, glial cells released high amounts of L-lactate into the medium (8.86 ± 0.18 mM), a quantity that increased significantly in the glucose + L-lactate medium (10.16 mM ± 0.44) but was not as high as that suggested by direct calculation of the endogenous production plus the exogenously added L-lactate. Glial cells cultured in L-lactate medium maintained the initial amount of lactate (4.28 ± 0.1 mM) (Fig. 5D). Analysis of glucose concentration revealed similar glucose consumption in the presence or absence of L-lactate in the medium (17.68 ± 0.26 mM and 17.76 ± 0.73 mM respectively; blank 23.10 ± 0.16 mM) (Fig. 5E). These results strongly suggest that glial cells use glucose as the primary energy substrate, while the presence of L-lactate in the medium reduces lactate extrusion by glial cells.

3.6. Differential effect of glucose and L-lactate as energy substrates for neuronal cultures

To explore the influence of lactate on neuronal cell phenotype, embryonic neurons were cultured in the same conditions as those used for the glial cultures described above. After 5*div*, neurons attached to and grew in the three conditions: glucose,

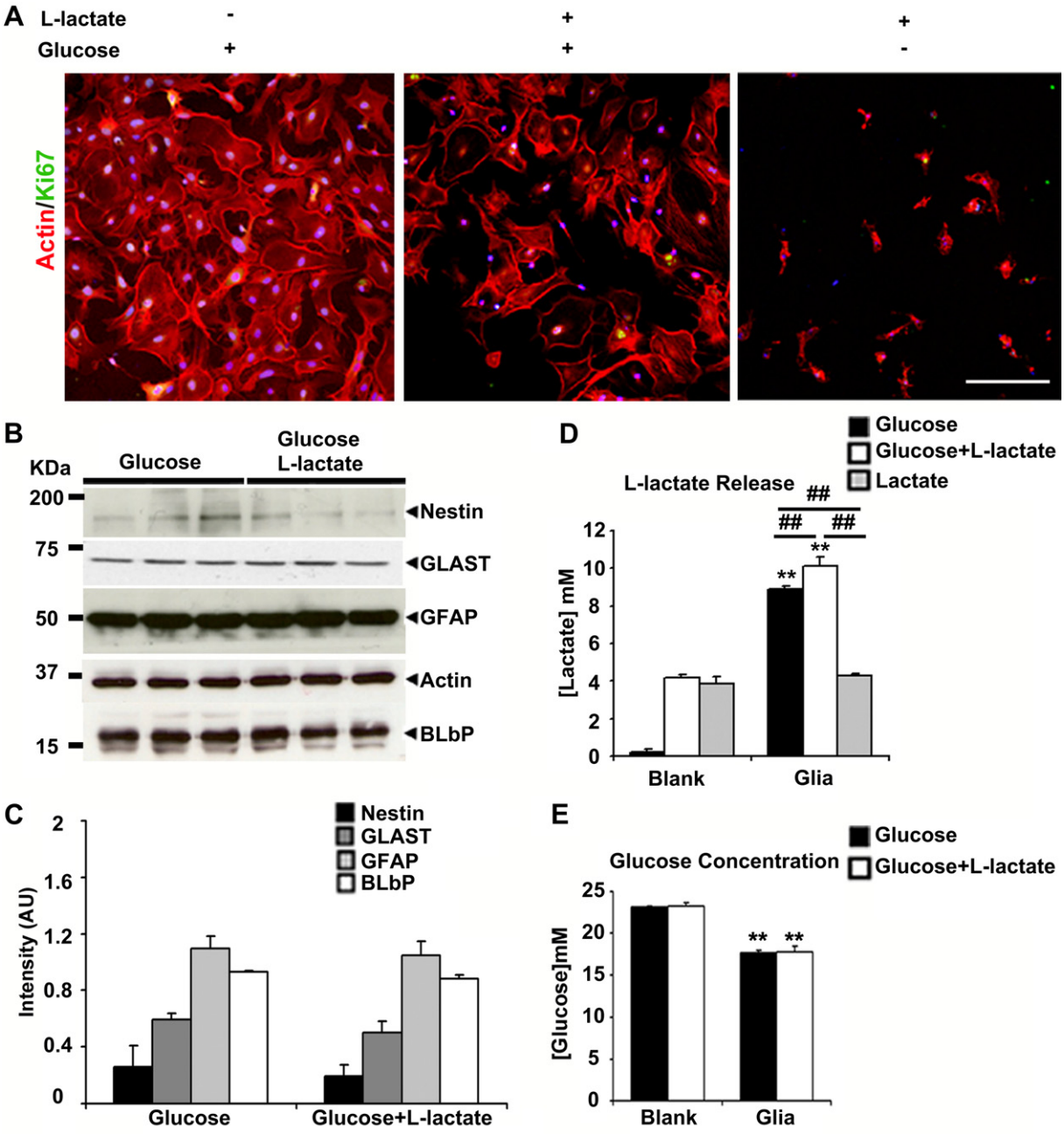

Fig. 5. Glial cell cultures treated with L-lactic acid. A. Confocal images of glial cell cultures grown in NB medium (Glucose), in NB medium supplemented with L-lactic acid (Glucose + L-lactate) and in glucose free NB^A medium supplemented with L-lactic acid (Lactate). Cytoskeleton is stained with phalloidin (red), nuclei with TO-PRO-3 (blue) and proliferative nuclei with Ki67 (green). B. Western blots of GFAP (mature and reactive glial marker), BLbP (immature astrocyte marker), GLAST (astrocyte marker) and nestin (radial glial marker) in similar cultures as showed in A. C. Graph summarizing Western blots quantification (intensity values normalized to actin). D. L-lactate quantification in the three condition media after 5*div*. E. Glucose quantification in the same media used in D. Scale bar = 100 μm. Values are the average of three replicas. Asterisk indicates significant differences with respect to the glucose condition ($^{**}p < 0.01$, LSD test) and hash marks indicate significant differences between Glucose + lactate and lactate ($\#\#p < 0.01$, LSD test). Error bars in C-E indicate SD. (For interpretation of the references to color in this figure legend, the reader is referred to the web version of this article.)

glucose + L-lactate and L-lactate media (Fig. 6A). In the glucose medium, neurons differentiated and exhibited well-developed axons and dendrites identified by Tuj-1 staining, whereas in glucose + L-lactate medium and most notably in the L-lactate medium there was a significant reduction in the total cell number (350 ± 41, 281 ± 30 and 213 ± 41 respectively, $p < 0.001$), and the neuritic differentiation was less developed. Conversely, proliferative cells identified by Ki67 expression were rare in the glucose medium (4 ± 3) whereas their number increased significantly in glucose + L-lactate and most notably in L-lactate (57 ± 19, 79 ± 18 respectively, $p < 0.001$). When D-lactate was added in the presence of glucose, neuronal cultures exhibited similar features to the control medium, while D-lactate did not support neuronal growth in the absence of glucose (Supplementary Fig. 2).

Western blot and densitometry analysis were performed to quantify differences in the expression of neuronal glial and progenitor markers (Fig. 6B and C). Neuronal cultures grown in glucose or glucose + L-lactate media maintained the expression of the immature glial and progenitor marker nestin and the mature

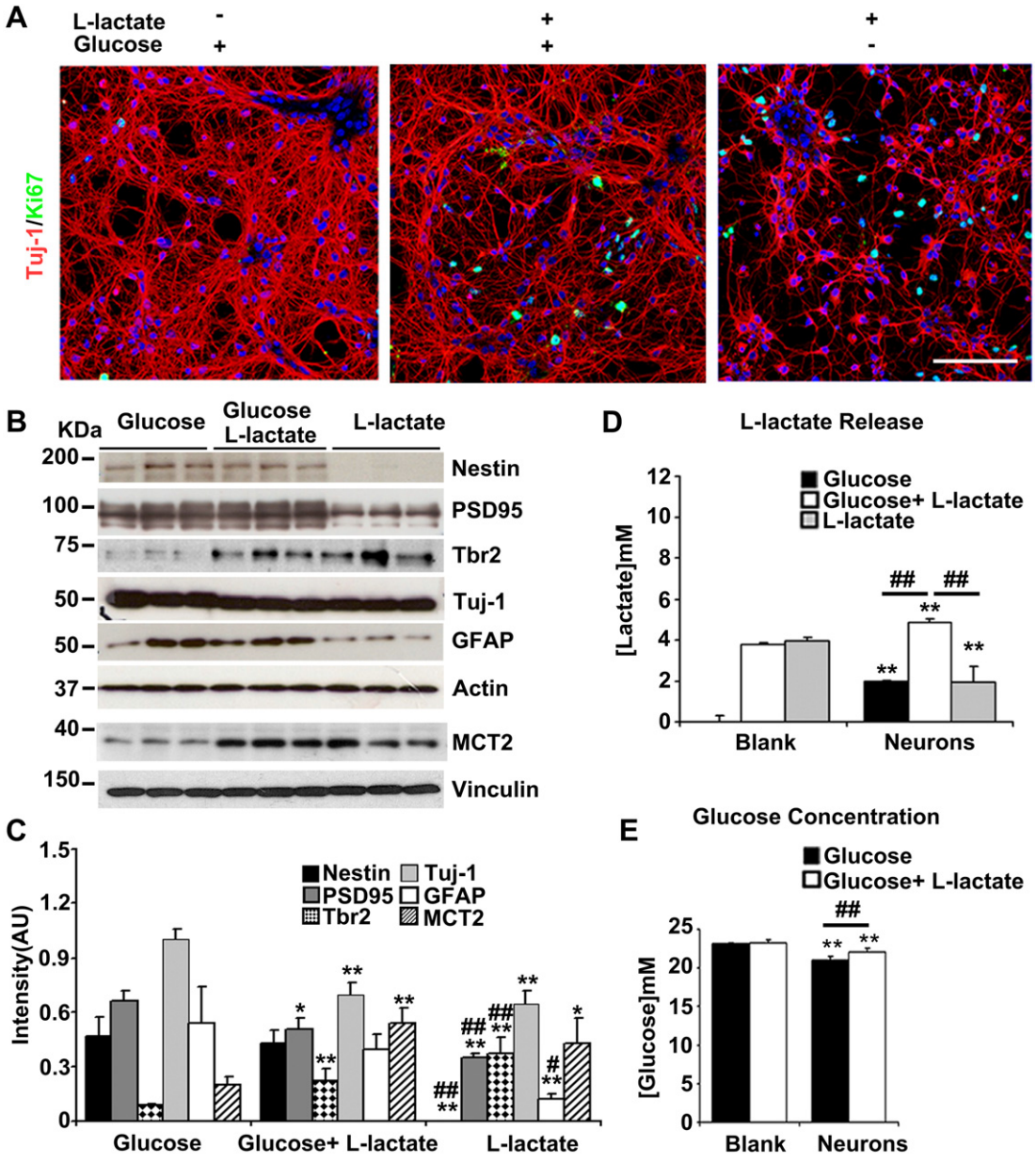

Fig. 6. Neuronal cultures treated with L-lactic acid. A. Confocal images of embryonic neuronal cell culture grown in NB medium (Glucose), in NB medium supplemented with L-lactic acid (Glucose + lactate) and in glucose free NB^A medium supplemented with L-lactic acid (lactate). Neuronal cytoskeleton is stained with Tuj-1 (red), nuclei are stained with TO-PRO-3 (blue) and proliferative nuclei with Ki67 (green). B. Western blot of nestin (radial glial marker), PSD95 (post-synaptic density neuronal marker), Tbr2 (intermediate progenitor marker), Tuj-1 (post-mitotic neuronal marker), GFAP (mature astroglial marker), and MCT2 (neuronal monocarboxylate transporter) in neuronal cultures grown in the same conditions as in A. C. Graph summarizing Western blot quantification (intensity values normalized to actin or vinculin). D. Lactate quantification in culture media in the three conditions described above. E. Glucose quantification in the same media used in D. Scale bar = 100 μm. Asterisks indicate significant differences respect to glucose condition ($^*p < 0.05$, $^{**}p < 0.01$, LSD test) and hash marks indicate significant differences between Glucose + lactate and lactate ($\#p < 0.05$, $\#\#p < 0.01$, LSD test). Error bars in C–E indicate SD. (For interpretation of the references to color in this figure legend, the reader is referred to the web version of this article.)

astroglial marker GFAP. However, the expression of GFAP and nestin was dramatically reduced or even absent in lactate medium, indicative of a significant reduction in the population of glial cells. The expression of the neuronal marker Tuj-1 and the postsynaptic density marker PSD95 decreased in glucose + L-lactate and decreased even more notably in L-lactate with respect to the glucose media, indicating a delayed neuronal maturation in these cultures. In addition, the presence of L-lactate induced neuronal monocarboxylate transporter MCT2 expression in these cultures. Analysis of progenitor markers revealed high levels of Tbr2, a transcription factor associated with neuronal restricted intermediate progenitor cells and early post-mitotic neurons in glucose + L-lactate and more significantly in L-lactate with respect to the glucose medium. The bipotential RGLC marker Pax6 was not expressed in any condition. These results indicate that in the presence of L-lactate neuronal cultures were less differentiated and preserved a significant pool of neuronal restricted progenitors.

Finally, L-lactate release and glucose consumption were also analyzed in these neuronal cultures (Fig. 6D and E). When grown in glucose medium, neuronal cultures released L-lactate (1.96 ± 0.06 mM), as did neuronal cultures grown in glucose + L-lactate medium (4.85 ± 0.17 mM, blank 3.97 ± 0.16 mM). As expected, neuronal cultures grown in L-lactate medium consumed L-lactate (1.93 ± 0.77 mM, blank 3.97 ± 0.16 mM). When grown in

glucose + L-lactate media, neuronal cultures consumed significantly less glucose than when grown only with glucose (21.02 ± 0.43 mM and 22.04 ± 0.51 mM respectively, blank 23.01 ± 0.16 mM). Taken together, these data suggest that neurons preferred L-lactate as primary energy source, unlike glial cells. In the presence of this metabolite, neuronal cultures maintained an immature phenotype and preserved the pool of neurogenic Tbr2 progenitors.

4. Discussion

The regenerative capacity of a tissue relies on the maintenance of a population of stem cells which self-renew by asymmetrical division and produce a committed daughter cell able to differentiate. Those properties are regulated by the niche, a dynamic microenvironment in which stem cells reside. The CNS has only limited capacity for self-repair after injury despite the presence of NSC, therefore a fuller understanding is needed of the physical nature of the NSC niches and the molecular mechanisms that govern them [19,20]. Recent approaches have focused on the use of biomaterials to investigate what controls NSC fate. Polyesters like polyglycolic, polylactic and polylactic-co-glicolic acids have been used for CNS implantation, and parameters like mechanical stiffness, surface properties and degradation kinetics are important to control cell behavior [2,21,22]. Although hydrophobicity, slow degradation rates and release of acidic products from PLA based scaffolds have been reported as limitations for biomedical applications [23], the main findings of this study show that PLA films obtained from combination of L- and D/L-lactic acid in a 70/30 ratio (PLA30/70) have specific effects on the adhesion, growth and differentiation of neurons, glia, and progenitor cells without the need for activation or protein coating. The physical properties of PLA70/30 films mainly accounted for neuronal and glial cell adhesion and the maintenance of glial nestin + progenitors and Pax6 + RGLC, while the L-lactate metabolite derived from PLA degradation was responsible for the maintenance of the neuronal restricted Tbr2 + progenitor pool.

PLA is a truly biodegradable polymer derived from lactic acid, and the initial D/L isomer distribution determines the potential for PLA crystallization [3]. The two films of PLA95/5 and PLA70/30 analyzed here supported glial cell growth, although PLA70/30 also allowed neuronal adhesion and growth. The two films have similar hydrophobicity, although they differ in crystallinity, stiffness, charge, and in degradation rate. Therefore, the better performance of PLA70/30 was probably related to its more amorphous, soft and elastic characteristics as a result of the lower proportion of the L isomer. CNS tissue elasticity is below 1 kPa, and soft substrates direct stem cell differentiation to a neuronal lineage [2,21,24]. PLA70/30 elasticity in dry state was of a few MPa while PLA95/5 has a supra physiological stiffness in the range of GPa. Due to its more amorphous structure, PLA70/30 started to degrade when immersed in culture medium at physiological temperature – unlike PLA95/5, which presented no significant degradation throughout the study. Although both PLA materials were initially hydrophobic, PLA70/30 becomes hydrophilic and more negatively charged as degradation proceeds. In this sense, degradation of polyesters like PLA increase the exposure of free carboxyl (–COOH) groups which increases their negative charge and hydrophilicity [25], modifications that favor the interaction with matrix proteins and cell adhesion [26].

Glial cells grown on PLA70/30 tend to express more immaturity and proliferation markers such as nestin, Ki67 and PH3 than those grown in control conditions. This undifferentiated and proliferative glial phenotype resembles that observed when glial cells were grown on PMMA films [15]. Although PLA70/30 is biodegradable and PMMA is not, both polymers have similar initial hydrophobicity and negative charge [15], properties that have been related with low cell adhesion and increased proliferation [27]. Taken together, the present results support the idea that a loose adhesion may be a requisite for maintaining NSC competence and proliferative capacity.

On the other hand, embryonic neurons grown on PLA70/30 also maintained an immature phenotype, increasing the expression of bipotential and neuron restricted progenitor markers Pax6 and Tbr2 after 5*div*, while control cultures exhibited a more mature phenotype. On PLA70/30 the number of neurons increased with time while the number of Ki67 positive progenitors was similar throughout the time of culture. Quantitative analysis revealed that the increase in neurons from 1 to 5*div* in these cultures can be explained if each Ki67 positive progenitor divided asymmetrically once, suggesting that in PLA70/30 a neuronal progenitor pool with self-renewing capacity was preserved throughout the culture period.

One important property of PLA substrates is their release of active metabolites. PLA essentially degrades to L-lactic acid, a terminal metabolite of anaerobic glycolysis, and to a lesser degree D-lactic acid that is not a metabolic substrate [4]. Although PLA surface properties might have a role in glial progenitor survival, collectively our results (Fig. 6 and Supplementary Fig. 2) support the idea that L-lactate, as a metabolic substrate, is responsible for the effects observed in neuronal cultures. Moreover, in favor of this hypothesis, one might argue that energy requirements for neuronal survival and growth in glucose and L-lactate free medium must be provided by L-lactate from PLA70/30 degradation (Fig. 4).

Traditionally, L-lactate was considered to be a metabolite that was toxic for brain cells and should be evacuated from the brain parenchyma [28]. However, in the last 50 years it has been demonstrated that L-lactate represents an alternative oxidative substrate for neurons *in vitro* and *in vivo* [29,30]. L-lactate is mainly released by glial cells and, when present together with glucose, it is largely preferred to glucose as an oxidative energy substrate by neurons in physiological conditions [5,31,32]. Moreover, a recent study demonstrated that neurons and NSC survive *in vitro* in glucose-free lactate medium [33]. The possibility of shuttling lactate between brain cell types is determined by the expression of specific transporters exhibiting different kinetics. Indeed, modeling studies have demonstrated a key role for monocarboxylate transporters (MCT) in regulating lactate influx and efflux [34]. MCT1 is expressed mainly in the brain blood barrier and astrocytes and MCT2 in neurons, where it is expressed in dendrites and associated with postsynaptic densities [35]. Energy substrate utilization may be limited by the transport capacity, and the affinity for D- and L-lactate is much higher for MCT2 than for MCT1 (K_m of 0.7 mM and 3–5 mM respectively) suggesting that neurons may use lactate more efficiently than glial cells [36]. In this regard, MCT2 overexpression increased neuronal lactate transport and utilization [37] and in the present study, MCT2 expression increased in neuronal cultures grown in PLA70/30 or after L-lactate addition to the culture medium.

On the other hand, glial cells hardly survive in glucose-free lactate medium, while glial cells grown on PLA reduced its glucose consumption, indicating a change in their metabolism. The somewhat deleterious effect of L-lactate on glial cultures may be related to its effect on glycolytic metabolism rather than on pH acidification, as mild acidosis has been described as neuroprotective [38], while exposure to mM L-lactate inhibits glycolysis in glial cells, but does not have a significant effect in neurons whose metabolism is essentially oxidative [39]. This inhibitory feedback at the micromolar range may also account for the reduction of lactate release by astrocytes when 4 mM L-lactate was added to the culture medium but not when astrocytes were cultured on PLA70/30, which releases lactate at the μM range.

Nevertheless, to conclusively establish that the effect of L-lactate on neural cells was exclusively metabolic the direct determination

of the role of lactate receptors and/or transporters on the neuronal and progenitors survival on PLA70/30 would be required.

An unexpected but exciting observation was the robust maintenance of potential Pax6 and neuronal restricted Tbr2 progenitor pools in neuronal cultures grown on PLA70/30.

Pax6 is expressed by neuronal/glial bipotential radial glia cell progenitors, while Tbr2 is expressed by neural restricted progenitors and by early postmitotic neurons [40]. The presence of neuronal restricted but not bipotential progenitors when L-lactate was directly added to the neuronal culture medium highlights the possibility that local regulation of lactate availability in the NSC niche may be an important issue to support neuronal progenitor physiology. The maintenance of glial and bipotential neuronal/glial progenitors may depend more on the structure and physical properties of the niche.

Although PLA70/30 film is not an appropriate material formulation for *in vivo* implantation after a lesion, other formulations such as microspheres or electrospun microfibers may better fulfill the requirements for implantable scaffolds. The addition of three-dimensional patterns mimicking the architecture of the embryonic NSC niches may also potentiate PLA70/30 physical and surface properties in driving endogenous astrocytes into an RGLC progenitor phenotype. L-lactate, the degradation product of PLA, may induce or activate resident NSC and/or progenitors to self-renew and produce new neurons, boosting a regenerative response *in situ*.

5. Conclusions

This study demonstrated that PLA70/30 films are good substrates for primary cortical neural cell adhesion, proliferation and differentiation, while also maintaining the pools of neuronal and glial progenitor cells *in vitro*. Moreover, the presence of the metabolically active PLA degradation product L-lactate in the medium is sufficient to maintain neuronal restricted progenitors, but not bipotential or glial restricted progenitors, in the cultures, indicating that different progenitors may use different metabolic pathways. Taken together, our results suggest that PLA70/30 films may mimic some of the physical and biochemical characteristics of the NSC niche. Mechanical and surface properties of PLA70/30 may act synergistically in the modulation of bipotential and glial restricted progenitor phenotypes, while released L-lactate may drive the maintenance of neuronal restricted progenitor cells. The design of three-dimensional patterns mimicking the architecture of the embryonic NSC niches on PLA70/30 based scaffolds may be a good starting point for future implantable devices that induce or activate resident neural progenitors to self-renew and to produce new neurons, boosting the CNS regenerative response *in situ*.

Acknowledgments

This study was supported in part by grants from Spain's Ministerio de Economía y Competitividad [MAT2011-29778-C02-02] and [MAT2011-29778-C02-01], co-financed by the European Regional Development Fund, to S.A. and J.A.P. respectively; from 2009 SGR 719 to S.A. O.C acknowledges the Spanish MINECO for the Ramon y Cajal contract. We are grateful to Michael Maudsley for editorial assistance and to B. Torrejón from the Scientific-Technical Services UB (Campus Bellvitge) for technical support in confocal microscopy.

Appendix A. Supplementary data

Supplementary data related to this article can be found, in the online version, at http://dx.doi.org/10.1016/j.biomaterials.2012.12.001.

References

[1] Yucel D, Kose GT, Hasirci V. Polyester based nerve guidance conduit design. Biomaterials 2010;31:1596–603.
[2] Keung AJ, Healy KE, Kumar S, Schaffer DV. Biophysics and dynamics of natural and engineered stem cell microenvironments. Wiley Interdiscip Rev Syst Biol Med 2010;2:49–64.
[3] Auras R, Harte B, Selke S. An overview of polylactides as packagingmaterials. Macromol Biosci 2004;4:835–64.
[4] Cassady CJ, Phillis JW, O'Regan MH. Further studies on the effects of topical lactate on amino acid efflux from the ischemic rat cortex. Brain Res 2001;901:30–7.
[5] Ivanov A, Mukhtarov M, Bregestovski P, Zilberter Y. Lactate effectively covers energy demands during neuronal network activity in neonatal hippocampal slices. Front Neuroenergetics 2011;3:2.
[6] Sokoloff L. The brain as a chemical machine. Prog Brain Res 1992;94:19–33.
[7] Dombrowski Jr GJ, Swiatek KR, Chao KL. Lactate 3-hydroxybutyrate, and glucose as substrates for the early postnatal rat brain. Neurochem Res 1989;14:667–75.
[8] Tabernero A, Vicario C, Medina JM. Lactate spares glucose as a metabolic fuel in neurons and astrocytes from primary culture. Neurosci Res 1996;26:369–76.
[9] Halestrap AP, Meredith D. The SLC16 gene family—from monocarboxylate transporters (MCTs) to aromatic amino acid transporters and beyond. Pflugers Arch 2004;447:619–28.
[10] Pellerin L, Magistretti PJ. Glutamate uptake into astrocytes stimulates aerobic glycolysis: a mechanism coupling neuronal activity to glucose utilization. Proc Natl Acad Sci U S A 1994;91:10625–9.
[11] Pellerin L, Pellegri G, Martin JL, Magistretti PJ. Expression of monocarboxylate transporter mRNAs in mouse brain: support for a distinct role of lactate as an energy substrate for the neonatal vs. adult brain. Proc Natl Acad Sci U S A 1998;95:3990–5.
[12] Rafalski VA, Brunet A. Energy metabolism in adult neural stem cell fate. Prog Neurobiol 2011;93:182–203.
[13] Chell JM, Brand AH. Nutrition-responsive glia control exit of neural stem cells from quiescence. Cell 2010;143:1161–73.
[14] Fischer EW, Sterzel HJ, Wegner G. Investigation of the structure of solution grown crystals of lactide copolymers by means of chemical reactions. Colloid Polym Sci 1973;251:980–90.
[15] Mattotti M, Álvarez Z, Ortega JA, Planell JA, Engel E, Alcántara S. Inducing functional radial glia-like progenitors from cortical astrocyte cultures using micropatterned PMMA. Biomaterials 2012;33:1759–70.
[16] Ortega JA, Alcántara S. BDNF/MAPK/ERK-induced BMP7 expression in the developing cerebral cortex induces premature radial glia differentiation and impairs neuronal migration. Cereb Cortex 2010;20:2132–44.
[17] Tsuji H, Ikarashi K. In vitro hydrolysis of poly(L-lactide) crystalline residues as extended-chain crystallites. Part I: long-term hydrolysis in phosphate buffered solution at 37 degrees C. Biomaterials 2004;25:5449–55.
[18] Chen CC, Chueh JY, Tseng H, Huang HM, Lee SY. Preparation and characterization of biodegradable PLA polymeric blends. Biomaterials 2003;24:1167–73.
[19] Miller FD, Gauthier-Fisher A. Home at last: neural stem cell niches defined. Cell Stem Cell 2009;4:507–10.
[20] Kazanis I. Can adult neural stem cells create new brains? Plasticity in the adult mammalian neurogenic niches: realities and expectations in the era of regenerative biology. Neuroscientist 2012;18:15–27.
[21] Discher DE, Mooney DJ, Zandstra PW. Growth factors, matrices, and forces combine and control stem cells. Science 2009;324:1673–7.
[22] Vazin T, Schaffer DV. Engineering strategies to emulate the stem cell niche. Trends Biotechnol 2010;28:117–24.
[23] Kim K, Yu M, Zong X, Chiu J, Fang D, Seo YS, et al. Control of degradation rate and hydrophilicity in electrospun non-woven poly(D, L-lactide) nanofiber scaffolds for biomedical applications. Biomaterials 2003;24:4977–85.
[24] Engler AJ, Sen S, Sweeney HL, Discher DE. Matrix elasticity directs stem cell lineage specification. Cell 2006;126:677–89.
[25] Atthoff B, Hilborn J. Protein adsorption onto polyester surfaces: is there a need for surface activation? J Biomed Mater Res B Appl Biomater 2007;80:121–30.
[26] Ren YJ, Zhang H, Huang H, Wang XM, Zhou ZY, Cui FZ, et al. In vitro behavior of neural stem cells in response to different chemical functional groups. Biomaterials 2009;30:1036–44.
[27] Biran R, Noble MD, Tresco PA. Characterization of cortical astrocytes on materials of differing surface chemistry. J Biomed Mater Res 1999;46:150–9.
[28] Dienel GA, Hertz L. Glucose and lactate metabolism during brain activation. J Neurosci Res 2001;66:824–38.
[29] Pellerin L, Magistretti PJ. How to balance the brain energy budget while spending glucose differently. J Physiol 2003;546:325.
[30] Boumezbeur F, Petersen KF, Cline GW, Mason GF, Behar KL, Shulman GI, et al. The contribution of blood lactate to brain energy metabolism in humans measuredby dynamic 13C nuclear magnetic resonance spectroscopy. J Neurosci 2010;30:3983–91.
[31] Itoh Y, Esaki T, Shimoji K, Cook M, Law MJ, Kaufman E, et al. Dichloroacetate effects on glucose and lactate oxidation by neurons and astroglia in vitro and on glucose utilization by brain in vivo. Proc Natl Acad Sci U S A 2003;100:4879–84.

[32] Bouzier-Sore AK, Voisin P, Canioni P, Magistretti PJ, Pellerin L. Lactate is a preferential oxidative energy substrate over glucose for neurons in culture. J Cereb Blood Flow Metab 2003;23:1298–306.
[33] Wohnsland S, Bürgers HF, Kuschinsky W, Maurer MH. Neurons and neuronal stem cells survive in glucose-free lactate and in high glucose cell culture medium during normoxia and anoxia. Neurochem Res 2010;35:1635–42.
[34] Aubert A, Costalat R, Magistretti PJ, Pellerin L. Brain lactate kinetics: modeling evidence for neuronal lactate uptake upon activation. Proc Natl Acad Sci U S A 2005;102:16448–53.
[35] Pierre K, Pellerin L. Monocarboxylate transporters in the central nervous system: distribution, regulation and function. J Neurochem 2005;94:1–14.
[36] Simpson IA, Carruthers A, Vannucci SJ. Supply and demand in cerebral energy metabolism: the role of nutrient transporters. J Cereb Blood Flow Metab 2007; 27:1766–91.
[37] Pierre K, Chatton JY, Parent A, Repond C, Gardoni F, Di Luca M, et al. Linking supply to demand: the neuronal monocarboxylate transporter MCT2 and the α-amino-3- hydroxyl-5-methyl-4-isoxazole-propionic acid receptor GluR2/3 subunit are associated in a common trafficking process. Eur J Neurosci 2009; 29:1951–63.
[38] Tombaugh GC, Sapolsky RM. Mechanistic distinctions between excitotoxic and acidotic hippocampal damage in an in vitro model of ischemia. J Cereb Blood Flow Metab 1990;10:527–35.
[39] Sotelo-Hitschfeld T, Fernandez-Moncada I, Barros LF. Acute feedback control of astrocytic glycolysis by lactate. Glia 2012;60:674–80.
[40] Englund C, Fink A, Lau C, Pham D, Daza RA, Bulfone A, et al. Pax6, Tbr2, and Tbr1 are expressed sequentially by radial glia, intermediate progenitor cells, and postmitotic neurons in developing neocortex. J Neurosci 2005;25: 247–51.

Neuronal progenitor maintenance requires lactate metabolism and PEPCK-M-directed cataplerosis

Authors: Zaida Álvarez[1,2,4*], Petra Hyroššová[3*], José Carlos Perales[3#] and Soledad Alcántara[2#]

Affiliations

[1]Institute for Bioengineering of Catalonia-IBEC, Barcelona, Spain; Dpts. of [2]Pathology and Experimental Therapeutics, and [3]Physiological Sciences II, Medical School (Bellvitge Campus), University of Barcelona-UB, Barcelona, Spain.; [4]CIBER en Bioingeniería, Biomateriales y Nanomedicina (CIBER-BBN), Barcelona, Spain; [5]Dpt. Material Science and Metallurgical Engineering, Technical University of Catalonia-UPC, Barcelona, Spain.

***Equal contribution authors**

#Corresponding authors:

Soledad Alcantara: Cell Biology Unit, Department of Experimental Pathology and Therapeutics. School of Medicine (Bellvitge Campus), University of Barcelona, 08907 L'Hospitalet de Llobregat, Spain.

Phone number: +34 934024288

Email: salcantara@ub.edu

Jose C. Perales: Department of Physiological Sciences II, School of Medicine (Bellvitge Campus), University of Barcelona, 08907 L'Hospitalet de Llobregat, Spain.

Phone number: +34 934024292

Email: jperales@ub.edu

Running Title: Neuronal progenitors require lactate metabolism

Abstract

This study investigated the metabolic requirements for neuronal progenitor maintenance *in vitro* and *in vivo* by examining the metabolic adaptations that support neuronal progenitors and neural stem cells (NSCs) in their undifferentiated state. We demonstrate that neuronal progenitors are strictly dependent on lactate metabolism, while glucose induces their neuronal differentiation. Lactate receptor agonists, in the absence of lactate, are incapable of maintaining the progenitor phenotype. The consequences of lactate metabolism include increased mitochondrial and oxidative metabolism, with a strict reliance on cataplerosis through the mitochondrial phosphoenolpyruvate carboxykinase (PEPCK-M) pathway to support anabolic functions, such as the production of extracellular matrix. *In vivo,* lactate maintains/induces populations of neuronal progenitors/NSCs in postnatal NSC niches in a PEPCK-M-dependent manner. Taken together, our data suggest that lactate and other physical/biochemical cues maintain NSCs/progenitors with a metabolic signature that is classically found in tissues with high anabolic capacity.

Key words: lactate, metabolism, neurons, neural progenitors, PEPCK-M.

Introduction

Glucose is still considered the major fuel for the adult brain, even though lactate signaling or utilization by neurons has been commonly observed both *in vitro* and *in vivo* (Bouzier-Sore AK et al. 2003; Gallagher CN et al. 2009; Wohnsland S et al. 2010). This is especially the case in the developing brain, where lactate is a major substrate for oxidative metabolism in addition to being selectively utilized as an anabolic source for cell proliferation and differentiation (Bolanos JP and JM Medina 1993; Nehlig A and A Pereira de Vasconcelos 1993; Medina JM et al. 1996; Medina JM and A Tabernero 2005; Zilberter Y et al. 2010). In neurons, lactate is transported across the cell membrane by the monocarboxylate transporter 2 (MCT2) (Pellerin L et al. 1998; Debernardi R et al. 2003) and subsequently converted to pyruvate, which can be further oxidized or used as an initial substrate in anabolic pathways. By contrast, astroglial cells release lactate to the extracellular milieu through the transporters MCT1 and MCT4 (Rafiki A et al. 2003; Pierre K and L Pellerin 2005). Lactate is also involved in the maintenance of brain energy turnover and neurovascular coupling, by regulating cyclic AMP (cAMP) formation through GPR81 receptor activation, a process independent of lactate metabolism (Bergersen LH and A Gjedde 2012; Bozzo L et al. 2013; Lauritzen KH et al. 2013).

Tissue remodeling and regeneration depend on adult stem cells and their progenitor properties, which are mostly regulated by the cellular microenvironment, or niche (Scadden DT 2006; Ivanovic Z 2009; Nakada D et al. 2011; Gattazzo F et al. 2014). Neural stem cells (NSCs) of the central nervous system (CNS) reside in niches that are in close contact with the vasculature (Shen Q et al. 2008; Tavazoie M et al. 2008; Goldman SA and Z Chen 2011). These neurogenic neurovascular niches contain a extracellular matrix (ECM) rich in laminins, type IV collagen, nidogen, and highly

glycosylated sulfate proteoglycans (Yanagisawa M and RK Yu 2007; Miner JH 2008; Shen Q *et al.* 2008; Nasu M et al. 2012). The balance between cellular self-renewal and differentiation is mediated by cell adhesion to the ECM, and by local cytokines, systemic hormones, and oxygen and nutrient supplies (De Filippis L and D Delia 2011; Lehtinen MK et al. 2011; Nakada D *et al.* 2011; Ziegler AN et al. 2012).

Our previous work showed that neuronal cultures grown on lactate-releasing biomimetic materials composed of poly-L/DL-lactate or treated with L-lactate were maintained in a less differentiated state in which a significant pool of neuronal progenitors was preserved (Alvarez Z et al. 2013). Our group has also shown that the biophysical properties and topography of the supplied substrate are essential for NSC and glial progenitor maintenance (Mattotti M et al. 2012; Alvarez Z et al. 2014). In this study, to explore the role of lactate in the NSC niche, we examined the differential effects of lactate and glucose on the cellular fate, metabolism, and anabolic capacities of neural progenitors *in vitro* and *in vivo*. Our results provide evidence that lactate intake through MCT2 and its subsequent oxidative metabolism direct progenitor commitment to a neuronal progenitor fate. The consequences of lactate metabolism are increased mitochondrial oxidation and a dependence on cataplerosis through the mitochondrial phosphoenolpyruvate carboxykinase (PEPCK-M) pathway. PEPCK-M enhances tricarboxylic acid (TCA) cycle flux and phosphoenolpyruvate (PEP) export to feed-forward carbons into the cytosolic 3-carbon pool, thus effectively promoting the cellular anabolic potential and ECM production. Taken together, these results indicate the coexistence in the neurovascular niche of NSC and progenitors with different metabolic signatures.

Materials and methods

Cell culture/intraventricular brain injections in postnatal animals

All animal housing and procedures were approved by the Institutional Animal Care and Use Committee of our institution in accordance with Spanish and EU regulations.

The brains of newborn (postnatal day 0, P0) mice were injected in the lateral ventricle with 2 μL of lactic acid (5 mM, Sigma Aldrich, n=10), 3-mercaptopicolinic acid (100 μM, 3MPA, Toronto Research Chemicals, n=8), or vehicle (MiliQ water, n=8). Tissues for immunohistochemistry analysis were obtained at P3, by killing the animals followed by a transcardial perfusion with 4% paraformaldehyde (PFA) in 0.1 M phosphate buffer, pH 7.3. The mouse brains were post-fixed for 8–12 h, cryoprotected, and kept frozen. Coronal sections of 40 μm thickness were collected in a cryoprotective solution and stored at −30 °C until further use.

Neurons were obtained from embryonic brains as described elsewhere (Ortega JA and S Alcantara 2010). Briefly, a time-pregnant mouse was killed by cervical dislocation and the embryos extracted at embryonic day 16 (E16).

Cerebral cortices were dissected free of the meninges in a solution of PBS with 0.6% glucose (Sigma-Aldrich, St. Louis, MO) and 0.3% bovine serum albumin (Sigma-Aldrich) and then digested with trypsin (Biological Industries, Israel) and DNAse I (Sigma-Aldrich) for 10 min at 37ºC. The tissue was mechanically dissociated, centrifuged, and resuspended in CO_2-equilibrated Dulbecco's modified Eagle's medium supplemented with 10% normal horse serum (NHS), 1% pen-strep, 0.5 mM L-glutamine, and 5.8 μL $NaHCO_3$ (Sigma-Aldrich)/mL. The cell suspension was pre-plated at 37ºC. After 30 min, the supernatant was collected, centrifuged (1000 g for 5 min), resuspended in NB neuronal culture medium (1% NHS, 1% pen-strep, 0.5 mM L-glutamine, 22 μM glutamic acid (Sigma-Aldrich), 2% B27 (Gibco, USA), and 5.8 μL

$NaHCO_3$/mL), and plated at a density of 2.5×10^5 cells/cm^2 directly on tissue culture plates coated with poly-D-lysine (Sigma-Aldrich). After 24 h, the medium was replaced with serum-free neuronal culture medium (1% pen-strep, 0.5 mM L-glutamine, 2% B27, 5.8 µL $NaHCO_3$/mL) during 1*div*, 3*div*, and 5*div*. With these conditions, we obtained a neuron-enriched culture in which about 10% of the cells were glial cells.

The samples were fixed in 4% PFA for 15 min at room temperature (RT) for immunofluorescence, protein extraction and western blot analysis, and ATP measurements. Media were collected to measure lactate and glucose concentrations.

Western blot/Immunofluorescence

For western blot analysis, protein extracts were obtained from primary cultures. Total cell proteins were separated by SDS-PAGE and electro-transferred from the gel to a nitrocellulose membrane (Bio-Rad). The membranes were blocked and then incubated first with primary antibodies overnight at 4°C, and then with their corresponding secondary HRP-conjugated antibodies (1:3000; Santa Cruz Biotechnology). Protein signals were detected using the ECL chemiluminescent system (Amersham, GE Healthcare, PA, USA). Densitometry analysis, standardized to F-actin as a control for protein loading, was performed using ImageJ software. For quantification, triplicate samples were analyzed and at least two different experiments were conducted.

For immunofluorescence, fixed samples (4% PFA for 15 min at RT) were incubated with primary antibodies and appropriate Alexa 488 or Alexa 555 secondary antibodies (1:500, Molecular Probes, USA). The following primary antibodies were used: goat anti-actin (cytoskeleton marker, 1:2000, Santa Cruz Biotechnology, USA), mouse anti-Tuj-1 (neuronal marker 1:10000, Covance), rabbit anti-Tbr2 (neurogenic intermediate progenitor cells marker, 1:500, Abcam, UK), rabbit anti-Ki67 (proliferation marker, 1:500, Abcam), rabbit anti-Sox2 (NSC/non-restricted progenitor marker, 1:1000,

Abcam) goat anti-MCT2 (neuronal monocarboxylate transporter marker 1:500, Santa Cruz Biotechnology), rabbit anti-PEPCK-M (mitochondrial phosphoenolpyruvate carboxykinase, 1:1000, Abcam), goat anti-GPR81 (G-protein-coupled receptor 1:500, Santa Cruz Biotechnology), rabbit anti-VDAC (voltage-dependent anion channel 1:1000, Cell Signaling), rabbit anti-phospho-AMPKα (adenosine monophosphate-activated protein kinase marker 1:1000, Cell Signaling), rabbit anti-Sirt1 (NAD-dependent deacetylase sirtuin-1 marker 1:1000, Upstate), rabbit anti-phospho-PDH-E1α (phosphorylated pyruvate dehydrogenase E1-alpha, 1:5000, Millipore), rabbit anti-AKT (serine/threonine-specific protein kinase, 1:1000, Millipore), rabbit anti-laminin-EHS (1:500, Sigma Aldrich, S9393), rabbit anti-caspase-3 (apoptosis marker 1:100, Santa Cruz Biotechnology), MitoTracker (250 nM, mitochondria marker, Invitrogen), and To-Pro-3 iodide (Topro) (nuclear stain, 1:500, Molecular Probes). Finally, the preparations were coverslipped with Mowiol (Calbiochem) for imaging.

Lactate Treatments

E16 primary neuronal cultures treated with L- or D-lactic acid (Sigma Aldrich) were cultured in Neurobasal medium supplemented with 25 mM glucose (glucose medium) or with 25 mM glucose and 4 mM lactic acid ((glucose+lactate medium), or with 4 mM lactic acid only (glucose-free lactate medium). Neurons were cultured for 24 h in the above media supplemented with 1% NHS, 1% pen-strep, 0.5 mM L-glutamine, 22 μM glutamic acid, 1× B27, and 5.8 μL NaHCO3/mL. The medium was then replaced with the same medium but serum-free and the cultures incubated for 4 more days.

In some experiments, lactate or glucose medium was replaced after 5*div* with glucose or lactate medium for 1 h (short incubation) or 2 days (long incubation). All experiments were carried out at least three times and triplicate samples from each were analyzed by

western blot, Inmunofluorescence (as a measure of cell death), or spectrophotometrically (to determine the lactate content of the medium).

ATP measurements

ATP in cell extracts was measured using a luciferin/luciferase assay (BioVision). Cell extracts were prepared in a single-step boiling water procedure (Yang NC et al. 2002). In brief, the cells were washed twice with PBS and then suspended in 200 µL of boiling water. The cell suspension was centrifuged (12000 g, 5 min, 4°C) and the resulting supernatant was assayed. Ten µL of the cell suspension was mixed with 10 µL of luciferin/luciferase reagent and 80 µL of deionized water. Light emission was measured on a TD 20/20 luminometer (Turner Designs, Houston, USA). A standard ATP curve was obtained by serial dilutions of 10 mM ATP (Sigma-Aldrich). The amount of ATP in the cell extracts was normalized to the cellular protein concentration.

Oxidative stress

Oxidative stress was measured using the cell-permeable fluorogenic probe CellROX Green (Invitrogen) as recommended by the manufacturer. In its reduced state CellROX Green is weakly fluorescent whereas upon oxidation by reactive oxygen species it binds to DNA and exhibits bright green fluorescence (excitation/emission: 485/520 nm). Cells assayed by this method were cultured in lactate medium as described above; after 5*div* they were shifted to glucose or lactate medium for either 1 h (short incubation) or 2 days (long incubation). The CellROX Green reagent was added at final concentration of 5 µM and the cultures were incubated at 37°C for 30 min. The cells were fixed with 4% PFA, mounted with Mowiol, and their fluorescence was then analyzed using ImageJ software (National Institutes of Health, USA).

Inhibitors

Experiments testing the effects of MCT2 inhibition or the lactate receptor agonist GPR81 were carried out as follows: E16 primary neuronal cultures were treated with L- or D-lactic acid (Sigma Aldrich) and cultured in three different media: NB medium (with 25 mM glucose, glucose medium), NB medium supplemented with 4 mM lactic acid (glucose+lactate medium) or glucose-free Neurobasal^{A} medium (NBA) supplemented with 4 mM lactic acid (lactate medium). Neurons were cultured for 24 h in these media, also containing 1% NHS, 1% pen-strep, 0.5 mM L-glutamine, 22 µM glutamic acid, 1× B27, and 5.8 µL $NaHCO_3$/mL. The medium was then changed to serum-free formulations containing 1% pen-strep, 0.5 mM L-glutamine, 1× B27, 5.8µL $NaHCO_3$/mL and the presence or absence of the MCT2 inhibitor AR-C155858 (100 nM, Adooq) or the GPR81 agonist, 3,5-dihydroxybenzoic acid (1 mM, 3,5-DHBA, Santa Cruz) for four more days.

In experiments testing the effects of PEPCK inhibition, the cells were cultured as described above, except that the serum-free medium contained either DMSO (1:2000, Sigma-Aldrich) for control conditions or the PEPCK inhibitor 3-mercaptopicolinic acid (100 µM, 3MPA, Toronto Research Chemicals). The cells were then cultured for four more days.

L-Lactate Assay

The concentration of L-lactate was determined using an enzymatic reaction based on the oxidation of L-lactate to pyruvate by lactate dehydrogenase (5 mg of the enzyme (Roche)/mL, 550 U/mg) in the presence of NAD (Sigma-Aldrich). In this assay, the amount of NADH produced in the reaction is proportional to the amount of L-lactate in the samples. With this enzymatic system, D-lactate is not detected.

All experiments were carried out at least three times and in triplicate samples. The latter were diluted 1:20 with reaction mix [0.3M hydrazine sulfate (Merck) and 0.87 M glycine (AppliChem), pH 9.5; 2.5 M NAD^+ (Sigma-Aldrich), 0.19 M EDTA (Merck)]. Lactate dehydrogenase was added at a final concentration of 6.9 U/ml. The NADH concentration was determined by using the Fluostar Optima BMG Labtech system to measure absorbance (340 nm) and fluorescence (excitation 340 nm/emission 460 nm) 0 and 20 min after the start of the reaction. The endpoint of the reaction was set at 20 min and the corresponding values were used in the calculations. Different concentrations of sodium L-lactate (Sigma-Aldrich) served as the standard.

Imaging and cell analysis

Digital images were taken throughout the study using a software-controlled digital camera. Fluorescent preparations were visualized and micrographs were captured with either a Leica TCS-SL Spectral confocal microscope (Leica Microsystems, Mannheim, Germany) or a Nikon Eclipse 800 light microscope (Nikon, Tokyo, Japan). The images were assembled in Adobe Photoshop (v. 7.0), with identical adjustments for contrast, brightness, and color balance to obtain optimum visual reproductions of the data. Morphometric and quantitative analyses were performed using ImageJ software (National Institutes of Health, USA).

Statistical analysis

Cell counts were expressed as mean cells/mm^2 ± standard deviation. The values are the average of three replicates of at least two different experiments. Statistical analysis was performed using the Statgraphic-plus software and GraphPad Prism. One-way ANOVA and Fisher's least significant difference (LSD) procedure were used to discriminate between the means.

Results

Effect of lactate on neuronal progenitor survival and differentiation

To explore the influence of L-lactate on the self-renewal and differentiation of neuronal progenitors *in vitro*, primary embryonic neuronal cultures were grown in serum-free culture medium with glucose (25 mM glucose, glucose medium), glucose and L-lactate (25 mM glucose + 4 mM L-lactic acid, glucose+lactate medium), or L-lactate only (4 mM L-lactic acid, lactate medium) (see Material and methods). Under these three conditions, initial cell adherence was the same while in the presence of lactate, glial content was residual or mostly absent (Alvarez Z *et al.* 2013). After one day *in vitro* (1*div*) (Fig. 1A) similar counts were obtained for both the total number of cells (glucose: 274±43, glucose+lactate: 243±46, and lactate: 246±36) and the number of Ki67+ cycling progenitors (glucose: 38±9, glucose+lactate: 44±14, and lactate: 55±14) (Fig. 1C). After 5*div*, the neuronal cultures showed signs of differentiation, and neurons identified by staining with the neuronal marker Tuj-1 exhibited well-developed neurites, particularly in glucose medium (Fig. 1B). At this time point, the total cell numbers in the glucose (375±47, $p<0.01$) and glucose+lactate (297±40, $p<0.05$) cultures were significantly higher than at 1*div* while in lactate medium there was no change (247±27). A similar comparison of Ki67+ progenitors (Fig. 1D) showed fewer numbers of these cells in glucose medium (4±3, $p<0.01$), while the number remained constant in glucose+lactate medium (57±19) and had significantly increased in lactate medium (79±18, $p<0.01$). As post-mitotic neurons cannot re-enter the cell cycle, the increase in cell number in 5*div* embryonic neuronal cultures can be explained by the division of pre-existing Ki67+ progenitors at 1*div*. Therefore, the increase in cell number and the depletion of progenitors after 5*div* in glucose medium is compatible with two rounds of progenitor division; first an asymmetric division giving rise to a progenitor and a

differentiated cell, and then a symmetric division of the progenitor giving two differentiated cells. The observation in glucose+lactate medium of an increased number of cells together with progenitor maintenance is compatible with one round of asymmetric progenitor division giving rise to a self-renewing progenitor and a differentiated cell; and finally, the increase in progenitors but not in the total cell number in lactate medium suggests self-renewing symmetric divisions and an enrichment in progenitor cells compared to the initial pool of terminally differentiated cells.

Based on these observations, we speculated that glucose promotes the differentiation of neuronal progenitors while lactate is required for their self-renewal. To test this hypothesis, neuronal cultures were grown in lactate medium for 5*div* and then for 2 more days either in the same medium or in glucose medium (Fig. 2A). After the 7 days, there were significantly fewer Ki67+ progenitors in glucose than in lactate medium (10±1 and 63±5 respectively, $p<0.001$, Fig. 2B), while the total number of cells was significantly higher in glucose than in lactate cultures (220±41 and 170±23 respectively, $p<0.001$, Fig. 2C). These results suggested that glucose medium induced one terminal division of Ki67 progenitors whereas in lactate medium these cells remained mostly quiescent. When the opposite experiment was done, i.e., neuronal cultures were grown in glucose medium for 5*div* and then for 2 more days either in the same medium or in lactate medium (Fig. 2D), there were no changes either in the total number of cells (260±34 glucose; 228±44 lactate) or in the number of Ki67+ progenitors (2±2 glucose; 1±1 lactate) (Fig. 2E, F), indicating that lactate cannot reprogram the terminal progenitor differentiation induced by glucose.

We then examined whether lactate induced the formation of reactive oxygen species, leading to oxidative stress and cell death and therefore the observed differences in cell

number. Neuronal cultures were grown in lactate medium for 5*div* and then in the same medium or in glucose medium. After either 1 h or 2 days, the cells were treated with CellROX, an indicator of oxidative stress, for 30 min before fixation. After 1 h, CellROX fluorescence was higher in neuronal cultures grown in glucose than in lactate medium (21±3 and 16±2 cells respectively, $p<0.001$). After 2 days, however, CellROX intensity decreased and the differences disappeared (glucose: 10±1 cells, lactate: 10±5 cells) (Fig. 2G, H). As an indicator of cell death, the number of caspase-3+ cells was analyzed under the same experimental conditions. The percentage of dead cells was very low in either medium although at 1 h it was slightly higher in the lactate- than in the glucose-containing cultures (glucose: 2±2, lactate: 5±2, $p<0.05$). These differences were no longer observed after 2*div* (glucose: 3±3, lactate: 2±3) (Fig. 2I, J).

Effect of lactate on lactate-signaling and metabolism

Next, we analyzed whether the presence of lactate in the medium affected the expression of lactate-related machinery, i.e., the high-affinity proton-linked monocarboxylate transporter MCT2 (Halestrap AP and MC Wilson 2012), the G-protein-coupled lactate receptor, GPR81 (Lauritzen KH *et al.* 2013), and the mitochondrial enzyme PEPCK-M, required for the anabolic use of lactate in the liver (Mendez-Lucas A et al. 2013). After 5*div* in glucose medium, MCT2 (Fig. 3A, B) was detected at low levels in neuronal membranes. In lactate media MCT2 was abundantly expressed in membranes and cytosol of neurons, Ki67+ progenitors and Tbr2+ neuronal restricted progenitors (Sessa A et al. 2008), the principal type of progenitor induced by lactate treatments (Alvarez Z *et al.* 2013). By contrast, GPR81 (Fig. 3C) was expressed in neuronal membranes in glucose medium and by some but not all Ki67+ progenitors (not shown) and Tbr2+ neuronal progenitors in lactate conditions. Similarly, in glucose medium, PEPCK-M was detected at low levels, with a punctate distribution in the

neuronal soma, whereas in the presence of lactate both neurons and progenitors expressed very high levels of the enzyme (Fig. 3D). Quantitative analysis by Western blot and densitometry (Fig. 3E-F) corroborated the significant lactate-related increases of these four proteins, MCT2, GPR81 and PEPCK-M, and Tbr2. Moreover, PEPCK-M and Tbr2 expression was significantly higher in lactate than in glucose+lactate medium. The absence of Sox2+ progenitors (Fig. 3E-F) and astrocytes (Alvarez Z *et al.* 2013) in lactate cultures suggested that the Ki67+ progenitors were mostly Tbr2+ neuronal progenitors and that lactate and PEPCK-M activity allowed the avoidance of differentiation, perhaps by promoting the maintenance of self-renewal.

In a pharmacological approach we sought to answer the question whether neuronal survival and progenitor maintenance required lactate intake, either through monocarboxylate transporters, activation of the GPR81 lactate receptor, PEPCK-M catalytic activity, or a combination of all three. Thus, neuronal cultures were grown for 5*div* in the presence or absence of 100 nM of the MCT1/2 inhibitor AR-C155858 beginning at 1*div*. When added to glucose+lactate medium, the inhibitor induced Ki67+ progenitor depletion (22±5 and 0±1 respectively, $p<0,001$), without affecting neuronal survival (211±51 and 240±24 respectively), whereas when added to lactate medium it induced massive cell death (159±35 and 0, respectively) (Fig. 4A). In a second set of experiments, 3,5-DHBA, a selective agonist of GPR81, was added to glucose medium or to glucose/lactate-free medium beginning at 1*div*. After 5*div* in glucose medium, the agonist did not modify either the total number of cells (glucose: 255±46, glucose+agonist: 216±79) or the number of Ki67+ progenitors (glucose: 0±0, glucose+agonist: 0±0), nor did it promote cell survival in glucose/lactate-free medium (Fig. 4B). Moreover, the effects of L-lactate on neuronal cultures were not mimicked by D-lactate (Supplementary Fig. 1).

To specifically examine the potential role of PEPCK in the observed effects of lactate, we treated cultures with 3-mercaptopicolinic acid (3MPA), an inhibitor of PEPCK activity, or with DMSO as the control, from 1*div* to 5*div* (Fig. 4C, D). In glucose medium, PEPCK inhibition did not affect the total number of cells (256±50 DMSO; 252±54 3MPA) or the number of Ki67+ progenitors (1±2 DMSO; 1±2 3MPA). However, in glucose+lactate or lactate medium, the lack of PEPCK activity corresponded with a significant reduction in the total number of cells (from 204±47 to 150±46 in glucose+lactate and from 121±50 to 79±34 in lactate, $p<0.01$) as well as the complete depletion of Ki67+ progenitors (from 12±5 glucose+lactate, 15±6 lactate to 0, $p<0.01$), indicating that in the presence of lactate, PEPCK-M inhibition leads to progenitor cell death. Consistent with this finding, lactate consumption decreased in the presence of 3MPA (from 0.7±0.1 to 0.2 mM in glucose+lactate, and from1.7±0.1 to 1.5±0.2 mM in lactate, $p<0.05$) (Fig. 4E).

Taken together these data suggest stereospecific effects of L-lactate on neuronal survival and progenitor self-renewal. These effects are apparently mediated by the cellular entry of L-lactate through MCT1/2 receptors and its metabolism at the TCA junction, represented by PEPCK-M catalytic activity.

Lactate-associated changes in the metabolic profile of neuroprogenitor cells

To investigate changes in the metabolic profile of self-renewing progenitor cells in the presence of lactate several key elements of metabolic regulation were analyzed. Differences in mitochondrial distribution were visualized by epifluorescence using MitoTracker, a cell-permeable mitochondrial marker. In neuronal cultures grown in glucose, glucose+lactate, or lactate medium for 5*div* well-developed neurons stained with the neuronal marker Tuj-1 contained fewer mitochondria than young neurons and progenitors (Tuj-1 negative), which showed intense mitochondrial labeling (Fig. 5A).

Consistent with progenitor enrichment, mitochondrial staining was highest in lactate medium, while there was no medium-related difference in ATP levels (Fig. 5B). Western blot and densitometry analysis showed slightly higher levels of phosphorylated AMPK (AMPK-P) in glucose+lactate medium, without concomitant changes in NAD-dependent deacetylase sirtuin-1 (Sirt1) or phospho-pyruvate dehydrogenase (PDH)-E1-α [PDH E1α-P(Ser^{293})], whereas AMPK-P, Sirt1, and phospho-PDH-E1-α levels were much lower in lactate condition (Fig. 5C, D) than in either of the glucose-containing media, indicating striking increased in the energy charge, redox potential, and mitochondrial metabolism of lactate through PDH. These data are consistent with a dramatic shift to oxidative metabolism as lactate becomes the main energy and carbon source in the cell. The metabolic profile described is a newly identified hallmark of neuron-restricted progenitor cells and contrasts with the glycolytic profile of glucose-restricted cells (mainly the glial component).

Lactate restriction of neuronal progenitors implies that lactate metabolism also plays a crucial role in sustaining the increase in biomass that occurs during the cell cycle and in the ECM production characteristic of these cells. In this context, PEPCK-M is the only pathway that can export carbons from lactate and other TCA cycle intermediates (i.e., glutamine) into the triose and hexose pools, through PEP synthesis (Mendez-Lucas A *et al.* 2013). Therefore, we evaluated whether the presence of lactate and the inhibition of PEPCK-M activity using 3MPA altered the synthesis of laminin, a highly glycosylated ECM protein that serves as a marker of synthetic activity in neuronal progenitors (Kazanis I et al. 2010). Indeed, lactate significantly increased the laminin content of neuronal cultures (Fig. 5E, F), mainly associated with progenitor cells (Supplementary Fig. 2). In the presence of lactate and 3MPA there was a substantial decrease in the laminin content as well as in Tbr2+ neuronal progenitors as shown by western blot (Fig.

5G, H). This result suggested that the PEPCK-M pathway is relevant to link the mitochondrial and glycolytic pools of building blocks necessary to sustain biosynthetic processes.

PEPCK-M is required for the lactate-dependent increase in cycling cells *in vivo*

Finally, we tested whether progenitor maintenance in the cerebral cortex was effectively mediated by L-lactate and PEPCK-M catalytic activity. In this *in vivo* experiment, 2 µL of either L-lactate (5 mM), 3MPA (100 µM), or vehicle was injected into the lateral ventricle of newborn (postnatal day 0, P0) mice. The effects on PEPCK-M expression and in the number of Ki67+ cycling cells, Sox2+ NSC/non-restricted progenitors, and Tbr2+ neuronal progenitors were analyzed in the ventricular/subventricular and intermediate zones (VZ/SVZ, IZ) at P3 (Fig. 6). The results showed an increase in PEPCK-M expression in the germinal VZ/SVZ of lactate-injected brains (Fig. 6A) together with significant increases in the number of Ki67+ progenitors (vehicle: 79±14, lactate: 129±37, 3MPA: 47±15; Fig. 6B, C), Sox2+ NSC/progenitors (vehicle: 85±10, lactate: 102±21, 3MPA: 57±9; Fig. 6D, E), and Tbr2+ neuronal progenitors (vehicle: 60±8, lactate: 72±14, 3MPA: 23±8; Fig. 6F, G). Conversely, the numbers of all these cells significantly decreased in mice injected with 3MPA. Moreover, compared to the vehicle control, laminin expression in the germinal VZ/SVZ dramatically increased in lactate-injected animals but decreased in 3MPA-injected animals (Fig. 6H). Taken together these data provide *in vivo* corroboration of the lactate dependence of neural progenitors.

Discussion

Metabolism is an important indicator of cell function, since it shifts together with differentiation, growth, or anabolic capacities. For example, undifferentiated stem cells

preferentially rely on glycolysis whereas differentiated cells up-regulate oxidative metabolism to support their anabolic or biological potential (Facucho-Oliveira JM and JC St John 2009; Ivanovic Z 2009; Simsek T et al. 2010). In the developing brain, NSC/radial glia progenitors generate the various differentiated cell types (Rowitch DH and AR Kriegstein 2010). Several studies have shown that the highly hypoxic environment characteristic of the stem cell and NSC niche favors glycolysis and lactate production at sites of unrestricted progenitor cell proliferation (Mohyeldin A et al. 2010). As NSCs mature, their specific lineage restriction is likely to be accompanied by a shift in their metabolic needs (Stubbs D et al. 2009; De Filippis L and D Delia 2011; Goldman SA and Z Chen 2011). This shift might explain the role of L-lactate, previously shown to be a critical substrate of the developing brain (Medina JM and A Tabernero 2005; Rinholm JE et al. 2011). Indeed, our results provide evidence of a lactate-restricted metabolic requirement to fulfill the biosynthetic needs of neuronal-restricted progenitors (summarized in Fig. 7).

Aerobic glycolysis is a functional marker of the specialized phenotype of dividing cells, whether they arise from physiologic tissue components (i.e., stem cells or endothelial cells) or after pathologic dedifferentiation (tumor cells) (De Bock K et al. 2013); (Suda T et al. 2011; Takubo K et al. 2013). This seemingly inefficient, partial oxidation of glucose nonetheless provides both a rapid source of energy and the anabolic building blocks to support cell division, but it reduces the cellular capacity to integrate into a functional, complex tissue. The same can be said for NSC metabolism (Yamasaki M et al. 2001; Rafalski VA and A Brunet 2011) and of radial glia progenitors and astrocytes, which are also essentially glycolytic (Tsacopoulos M and PJ Magistretti 1996; Yamasaki M *et al.* 2001). By contrast, in this work we showed that neuronal-restricted progenitors have a highly oxidative metabolic profile that is entirely dependent on lactate as a

carbon source. In the presence of glucose, lactate withdrawal induces progenitor differentiation to a neuronal fate.

Phosphorylation of the E1α domain of PDH by PDK1-4 regulates this enzyme and therefore the terminal oxidation of pyruvate in the mitochondria, a pathway that is actively regulated during hypoxia (Kim JW et al. 2006). Consistently, key metabolic markers of oxidative metabolism, including increased mitochondrial content and high PDH activity (reduced phosphorylation), are classically found in differentiated cells with a high anabolic capacity, such as liver, heart and slow-twitch muscle, and pancreatic β-cells. Terminal oxidative phosphorylation of pyruvate, whether from glucose or lactate sources, ensures the appropriate redox potential and energy charge needed to sustain biosynthesis at a high level of efficiency; while ensuring a minimal rate of cell division. The progenitors examined in this study underwent one or two rounds of cell division during their 5 days in culture, even though in all cases their nuclei were Ki67+. The cellular redox state contributes to the determination of cell fate. Thus, for example, increases in Sirt1 activity under oxidizing conditions induce neural progenitors to adopt a glial fate (Prozorovski T et al. 2008), while under basal non-oxidizing conditions these progenitors differentiate along a neural line (Hisahara S et al. 2008). Our data showed low-level Sirt1 expression, consistent with an increased redox potential, in parallel with a restriction to a neuronal progenitor fate. Also, diminished AMP-K phosphorylation suggested that when lactate is the main carbon source both redox potential and energy charge are increased, in line with the requirements of a mainly anabolic metabolism. Hence, we propose that Tbr2+ neuronal progenitors have a role in maintaining the ECM of the neurogenic niche and in the secretion of factors necessary for the neurogenic environment. Laminin is an integral component of the ECM of neurogenic niches (Kazanis I *et al.* 2010) and, as shown in the present work

and in a previous study (Alvarez Z *et al.* 2014), it is secreted by neural cells and progenitors exposed to lactate. Indeed, we found that laminin production was sensitive to the PEPCK inhibitor 3MPA, suggesting that both PEP and TCA flux are necessary to support biosynthetic processes, such as laminin production and glycosylation. PEPCK activity is present in the cytosol (PEPCK-C) and in mitochondria (PEPCK-M), reflecting the expression of two different nuclear genes, PCK1 and PCK2, respectively. In neural progenitors, only the mitochondrial isoform, PEPCK-M, was detected, with no measurable cytosolic protein found (data not shown). PEPCK-M catalyzes the GTP-dependent decarboxylation of mitochondrial oxaloacetate to produce PEP, which is then exported into the cytosol where it feeds the reverse glycolytic pathway (Stark R et al. 2009; Mendez-Lucas A *et al.* 2013). PEPCK-M has important advantages over PEPCK-C, since the shuttling of malate is not required and enzyme activity is coupled to TCA cycle flux through the recycling of GTP produced in the succinyl-CoA synthase reaction (Stark R *et al.* 2009). This pathway also shuttles carbons from lactate into the triose-phosphate intermediate pool for the synthesis of serine/glycine or glycerol-3P, or into hexose-phosphate intermediates for protein glycosylation, in the absence of oxidative phosphorylation (Nye C et al. 2008; Yang J et al. 2009; Kalhan SC and RW Hanson 2012). It is noteworthy that PEPCK-M is the only known pathway that can communicate mitochondrial carbon intermediates directly to the glycolytic pool, because of the irreversible nature of the pyruvate kinase step. In our *in vitro* neuronal cultures, Sox2+ cells with NSC characteristics were rarely seen. *In vivo*, in addition to increase PEPCK-M expression, laminin synthesis and neuronal-restricted Tbr2+ progenitors, lactate also induced an increase in Sox2+ progenitors. These data are in accordance with previous results demonstrating the requirement of the NSC niche for specific topographical cues. Thus, while Tbr2+ progenitors are induced by a flat

substrate of lactate-releasing polylactic acid (PLA), Sox2+ progenitors/NSC are only induced when the same PLA substrate is molded as aligned nanofibers, a 3D organization that reproduces the aligned palisade of embryonic radial glia (Alvarez Z *et al.* 2013; Alvarez Z *et al.* 2014).

Taken together, our results support the strict dependence of neuronal-restricted progenitors on lactate metabolism and on the provision of ECM components of the neurogenic niche by the anabolic activity of PEPCK-M. In the *in vivo* niche, other physical and/or biochemical cues might cooperate with lactate to maintain different progenitor populations.

Acknowledgments

This study was supported in part by grants from Spain's Ministerio de Economía y Competitividad [MAT2011-29778-C02-02] and [BFU2012-37177], co-financed by the European Regional Development Fund, to J.C.P and S.A. Z.A acknowledges the fellowship from IBEC 10-2009-01 and P.H was supported by a fellowship from the Ministerio de Educación y Ciencia (FPU). We are grateful to Wendy Ran for editorial assistance and to B. Torrejón from the Scientific-Technical Services UB (Campus Bellvitge) for technical support in confocal microscopy.

References

Alvarez Z, Castano O, Castells AA, Mateos-Timoneda MA, Planell JA, Engel E, Alcantara S. 2014. Neurogenesis and vascularization of the damaged brain using a lactate-releasing biomimetic scaffold. Biomaterials 35:4769-4781.

Alvarez Z, Mateos-Timoneda MA, Hyrossova P, Castano O, Planell JA, Perales JC, Engel E, Alcantara S. 2013. The effect of the composition of PLA films and lactate release on glial and neuronal maturation and the maintenance of the neuronal progenitor niche. Biomaterials 34:2221-2233.

Bergersen LH, Gjedde A. 2012. Is lactate a volume transmitter of metabolic states of the brain? Front Neuroenergetics 4:5.

Bolanos JP, Medina JM. 1993. Lipogenesis from lactate in fetal rat brain during late gestation. Pediatr Res 33:66-71.

Bouzier-Sore AK, Voisin P, Canioni P, Magistretti PJ, Pellerin L. 2003. Lactate is a preferential oxidative energy substrate over glucose for neurons in culture. J Cereb Blood Flow Metab 23:1298-1306.

Bozzo L, Puyal J, Chatton JY. 2013. Lactate modulates the activity of primary cortical neurons through a receptor-mediated pathway. PLoS One 8:e71721.

De Bock K, Georgiadou M, Carmeliet P. 2013. Role of endothelial cell metabolism in vessel sprouting. Cell Metab 18:634-647.

De Filippis L, Delia D. 2011. Hypoxia in the regulation of neural stem cells. Cell Mol Life Sci 68:2831-2844.

Debernardi R, Pierre K, Lengacher S, Magistretti PJ, Pellerin L. 2003. Cell-specific expression pattern of monocarboxylate transporters in astrocytes and neurons observed in different mouse brain cortical cell cultures. J Neurosci Res 73:141-155.

Facucho-Oliveira JM, St John JC. 2009. The relationship between pluripotency and

mitochondrial DNA proliferation during early embryo development and embryonic stem cell differentiation. Stem Cell Rev 5:140-158.

Gallagher CN, Carpenter KL, Grice P, Howe DJ, Mason A, Timofeev I, Menon DK, Kirkpatrick PJ, Pickard JD, Sutherland GR, Hutchinson PJ. 2009. The human brain utilizes lactate via the tricarboxylic acid cycle: a 13C-labelled microdialysis and high-resolution nuclear magnetic resonance study. Brain 132:2839-2849.

Gattazzo F, Urciuolo A, Bonaldo P. 2014. Extracellular matrix: A dynamic microenvironment for stem cell niche. Biochim Biophys Acta.

Goldman SA, Chen Z. 2011. Perivascular instruction of cell genesis and fate in the adult brain. Nat Neurosci 14:1382-1389.

Halestrap AP, Wilson MC. 2012. The monocarboxylate transporter family--role and regulation. IUBMB Life 64:109-119.

Hisahara S, Chiba S, Matsumoto H, Tanno M, Yagi H, Shimohama S, Sato M, Horio Y. 2008. Histone deacetylase SIRT1 modulates neuronal differentiation by its nuclear translocation. Proc Natl Acad Sci U S A 105:15599-15604.

Ivanovic Z. 2009. Hypoxia or in situ normoxia: The stem cell paradigm. J Cell Physiol 219:271-275.

Kalhan SC, Hanson RW. 2012. Resurgence of serine: an often neglected but indispensable amino Acid. J Biol Chem 287:19786-19791.

Kazanis I, Lathia JD, Vadakkan TJ, Raborn E, Wan R, Mughal MR, Eckley DM, Sasaki T, Patton B, Mattson MP, Hirschi KK, Dickinson ME, ffrench-Constant C. 2010. Quiescence and activation of stem and precursor cell populations in the subependymal zone of the mammalian brain are associated with distinct cellular and extracellular matrix signals. J Neurosci 30:9771-9781.

Kim JW, Tchernyshyov I, Semenza GL, Dang CV. 2006. HIF-1-mediated expression of

pyruvate dehydrogenase kinase: a metabolic switch required for cellular adaptation to hypoxia. Cell Metab 3:177-185.

Lauritzen KH, Morland C, Puchades M, Holm-Hansen S, Hagelin EM, Lauritzen F, Attramadal H, Storm-Mathisen J, Gjedde A, Bergersen LH. 2013. Lactate Receptor Sites Link Neurotransmission, Neurovascular Coupling, and Brain Energy Metabolism. Cereb Cortex.

Lehtinen MK, Zappaterra MW, Chen X, Yang YJ, Hill AD, Lun M, Maynard T, Gonzalez D, Kim S, Ye P, D'Ercole AJ, Wong ET, LaMantia AS, Walsh CA. 2011. The cerebrospinal fluid provides a proliferative niche for neural progenitor cells. Neuron 69:893-905.

Mattotti M, Alvarez Z, Ortega JA, Planell JA, Engel E, Alcantara S. 2012. Inducing functional radial glia-like progenitors from cortical astrocyte cultures using micropatterned PMMA. Biomaterials 33:1759-1770.

Medina JM, Tabernero A. 2005. Lactate utilization by brain cells and its role in CNS development. J Neurosci Res 79:2-10.

Medina JM, Tabernero A, Tovar JA, Martin-Barrientos J. 1996. Metabolic fuel utilization and pyruvate oxidation during the postnatal period. J Inherit Metab Dis 19:432-442.

Mendez-Lucas A, Duarte JA, Sunny NE, Satapati S, He T, Fu X, Bermudez J, Burgess SC, Perales JC. 2013. PEPCK-M expression in mouse liver potentiates, not replaces, PEPCK-C mediated gluconeogenesis. J Hepatol 59:105-113.

Miner JH. 2008. Laminins and their roles in mammals. Microsc Res Tech 71:349-356.

Mohyeldin A, Garzon-Muvdi T, Quinones-Hinojosa A. 2010. Oxygen in stem cell biology: a critical component of the stem cell niche. Cell Stem Cell 7:150-161.

Nakada D, Levi BP, Morrison SJ. 2011. Integrating physiological regulation with stem

cell and tissue homeostasis. Neuron 70:703-718.

Nasu M, Takata N, Danjo T, Sakaguchi H, Kadoshima T, Futaki S, Sekiguchi K, Eiraku M, Sasai Y. 2012. Robust formation and maintenance of continuous stratified cortical neuroepithelium by laminin-containing matrix in mouse ES cell culture. PLoS One 7:e53024.

Nehlig A, Pereira de Vasconcelos A. 1993. Glucose and ketone body utilization by the brain of neonatal rats. Prog Neurobiol 40:163-221.

Nye C, Kim J, Kalhan SC, Hanson RW. 2008. Reassessing triglyceride synthesis in adipose tissue. Trends Endocrinol Metab 19:356-361.

Ortega JA, Alcantara S. 2010. BDNF/MAPK/ERK-induced BMP7 expression in the developing cerebral cortex induces premature radial glia differentiation and impairs neuronal migration. Cereb Cortex 20:2132-2144.

Pellerin L, Pellegri G, Martin JL, Magistretti PJ. 1998. Expression of monocarboxylate transporter mRNAs in mouse brain: support for a distinct role of lactate as an energy substrate for the neonatal vs. adult brain. Proc Natl Acad Sci U S A 95:3990-3995.

Pierre K, Pellerin L. 2005. Monocarboxylate transporters in the central nervous system: distribution, regulation and function. J Neurochem 94:1-14.

Prozorovski T, Schulze-Topphoff U, Glumm R, Baumgart J, Schroter F, Ninnemann O, Siegert E, Bendix I, Brustle O, Nitsch R, Zipp F, Aktas O. 2008. Sirt1 contributes critically to the redox-dependent fate of neural progenitors. Nat Cell Biol 10:385-394.

Rafalski VA, Brunet A. 2011. Energy metabolism in adult neural stem cell fate. Prog Neurobiol 93:182-203.

Rafiki A, Boulland JL, Halestrap AP, Ottersen OP, Bergersen L. 2003. Highly differential expression of the monocarboxylate transporters MCT2 and MCT4 in the developing rat brain. Neuroscience 122:677-688.

Rinholm JE, Hamilton NB, Kessaris N, Richardson WD, Bergersen LH, Attwell D. 2011. Regulation of oligodendrocyte development and myelination by glucose and lactate. J Neurosci 31:538-548.

Rowitch DH, Kriegstein AR. 2010. Developmental genetics of vertebrate glial-cell specification. Nature 468:214-222.

Scadden DT. 2006. The stem-cell niche as an entity of action. Nature 441:1075-1079.

Sessa A, Mao CA, Hadjantonakis AK, Klein WH, Broccoli V. 2008. Tbr2 directs conversion of radial glia into basal precursors and guides neuronal amplification by indirect neurogenesis in the developing neocortex. Neuron 60:56-69.

Shen Q, Wang Y, Kokovay E, Lin G, Chuang SM, Goderie SK, Roysam B, Temple S. 2008. Adult SVZ stem cells lie in a vascular niche: a quantitative analysis of niche cell-cell interactions. Cell Stem Cell 3:289-300.

Simsek T, Kocabas F, Zheng J, Deberardinis RJ, Mahmoud AI, Olson EN, Schneider JW, Zhang CC, Sadek HA. 2010. The distinct metabolic profile of hematopoietic stem cells reflects their location in a hypoxic niche. Cell Stem Cell 7:380-390.

Stark R, Pasquel F, Turcu A, Pongratz RL, Roden M, Cline GW, Shulman GI, Kibbey RG. 2009. Phosphoenolpyruvate cycling via mitochondrial phosphoenolpyruvate carboxykinase links anaplerosis and mitochondrial GTP with insulin secretion. J Biol Chem 284:26578-26590.

Stubbs D, DeProto J, Nie K, Englund C, Mahmud I, Hevner R, Molnar Z. 2009. Neurovascular congruence during cerebral cortical development. Cereb Cortex 19 Suppl 1:i32-41.

Suda T, Takubo K, Semenza GL. 2011. Metabolic regulation of hematopoietic stem cells in the hypoxic niche. Cell Stem Cell 9:298-310.

Takubo K, Nagamatsu G, Kobayashi CI, Nakamura-Ishizu A, Kobayashi H, Ikeda E,

Goda N, Rahimi Y, Johnson RS, Soga T, Hirao A, Suematsu M, Suda T. 2013. Regulation of glycolysis by Pdk functions as a metabolic checkpoint for cell cycle quiescence in hematopoietic stem cells. Cell Stem Cell 12:49-61.

Tavazoie M, Van der Veken L, Silva-Vargas V, Louissaint M, Colonna L, Zaidi B, Garcia-Verdugo JM, Doetsch F. 2008. A specialized vascular niche for adult neural stem cells. Cell Stem Cell 3:279-288.

Tsacopoulos M, Magistretti PJ. 1996. Metabolic coupling between glia and neurons. J Neurosci 16:877-885.

Wohnsland S, Burgers HF, Kuschinsky W, Maurer MH. 2010. Neurons and neuronal stem cells survive in glucose-free lactate and in high glucose cell culture medium during normoxia and anoxia. Neurochem Res 35:1635-1642.

Yamasaki M, Yamada K, Furuya S, Mitoma J, Hirabayashi Y, Watanabe M. 2001. 3-Phosphoglycerate dehydrogenase, a key enzyme for l-serine biosynthesis, is preferentially expressed in the radial glia/astrocyte lineage and olfactory ensheathing glia in the mouse brain. J Neurosci 21:7691-7704.

Yanagisawa M, Yu RK. 2007. The expression and functions of glycoconjugates in neural stem cells. Glycobiology 17:57R-74R.

Yang J, Kalhan SC, Hanson RW. 2009. What is the metabolic role of phosphoenolpyruvate carboxykinase? J Biol Chem 284:27025-27029.

Yang NC, Ho WM, Chen YH, Hu ML. 2002. A convenient one-step extraction of cellular ATP using boiling water for the luciferin-luciferase assay of ATP. Anal Biochem 306:323-327.

Ziegler AN, Schneider JS, Qin M, Tyler WA, Pintar JE, Fraidenraich D, Wood TL, Levison SW. 2012. IGF-II promotes stemness of neural restricted precursors. Stem Cells 30:1265-1276.

Zilberter Y, Zilberter T, Bregestovski P. 2010. Neuronal activity in vitro and the in vivo reality: the role of energy homeostasis. Trends Pharmacol Sci 31:394-401.

Captions to figures

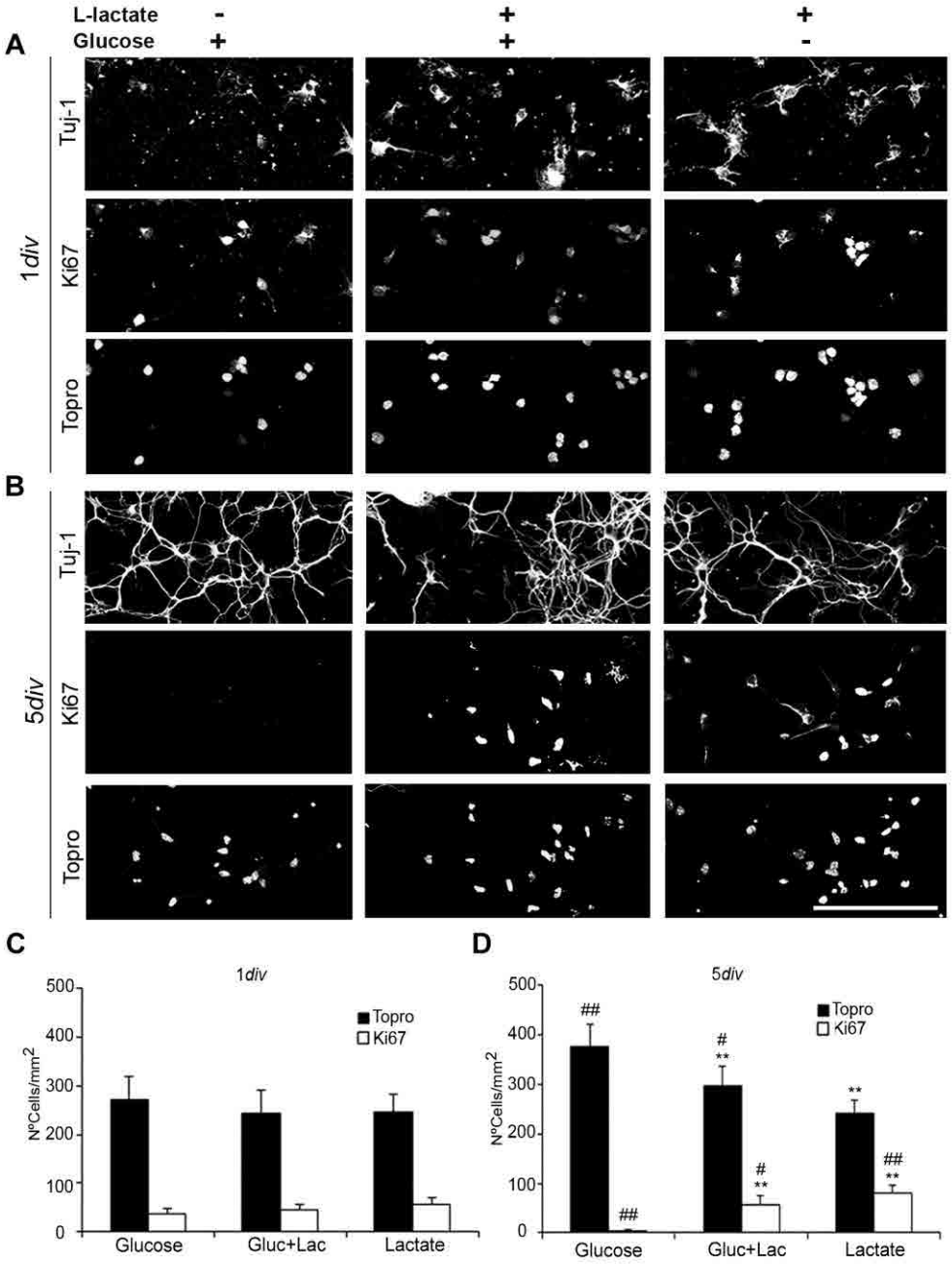

Figure 1. Effect of lactate on embryonic neuronal and progenitor cells. (A, B) Confocal images of embryonic neuronal cell cultures grown in glucose, glucose+lactate, or lactate medium after **(A)** 1 and **(B)** 5 days *in vitro* (*div*). Neurons are stained with Tuj-1, nuclei with Topro, and proliferative nuclei with Ki67. **(C-D)** Quantification of the total number of cells (Topro) and proliferative cells (Ki67) after **(C)** 1*div* and **(B)** 5*div*. Scale bar =50 μm. * $p<0.05$ and ** $p<0.01$ compared to cells cultured in glucose; #

p<0.05; ## p< 0.01 in a comparison between 1*div* and 5*div*, LSD test. Error bars indicate the SD.

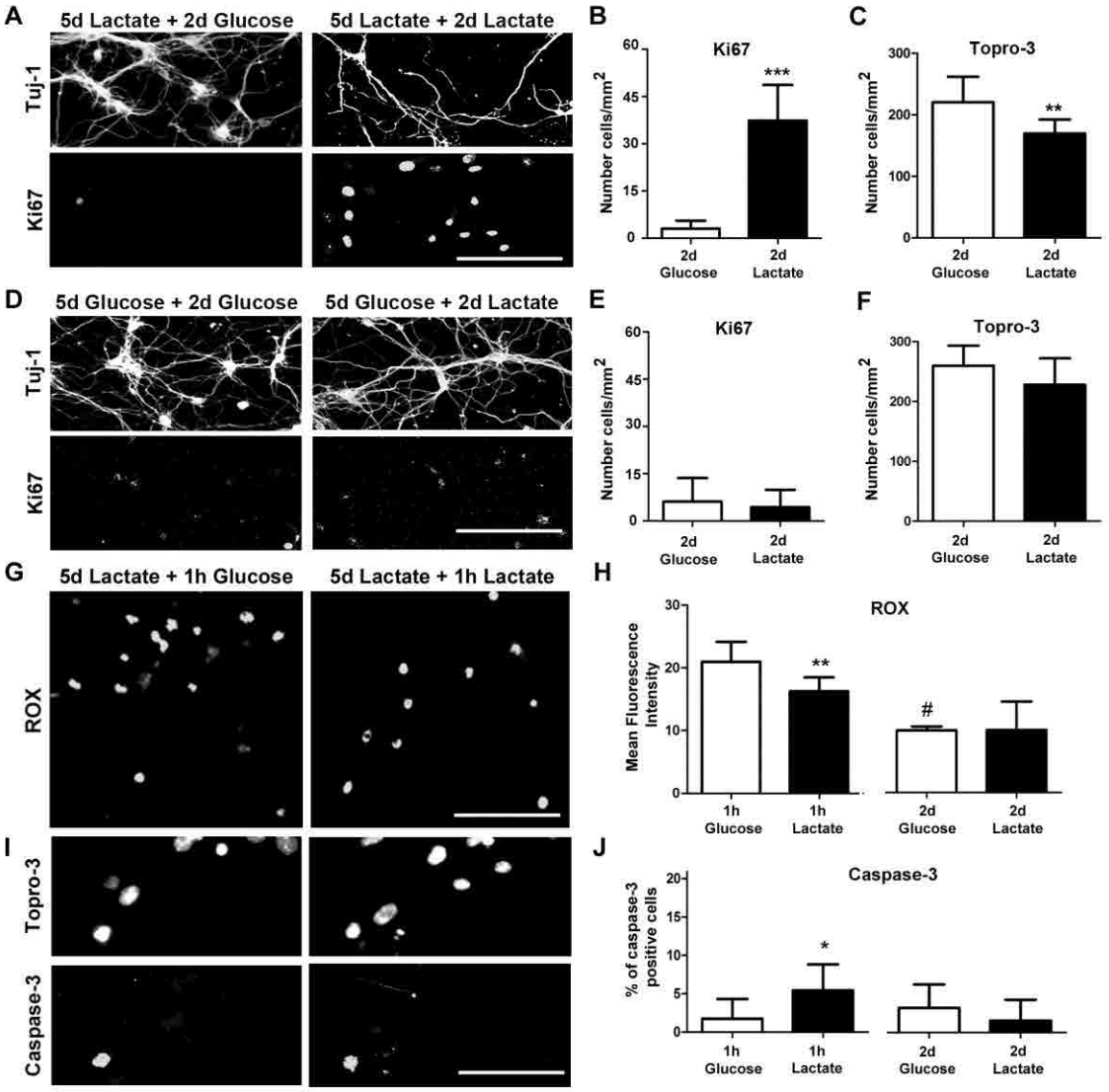

Figure 2. Lactate as an energy source that maintains neuronal progenitors *in vitro*. (**A)** Confocal images showing neurons (Tuj-1), and proliferative cells (Ki67) in neuronal cultures grown in lactate medium for 5*div* followed by 2 more days either in glucose or in lactate medium. (**B, C)** Quantification of Ki67+ (proliferative cells) and Topro (nuclei) under the same conditions as in **A**. (**D)** Confocal images of neuronal cultures showing neurons (Tuj-1), and proliferative cells (Ki67) grown in glucose medium for 5 *div* followed by 2 more days either in lactate or in glucose medium. **(E,**

F) Quantification of Ki67+ cells and Topro in neuronal cultures as in **D. (G)** Images showing ROX staining in neuronal cell cultures grown in lactate medium for 5*div* followed by either 1 h or 2 days in glucose medium or in lactate medium. **(H)** Quantification of ROX intensity in cells cultured as in **G**. **(I)** Images showing cell death (caspase-3) and nuclei (Topro) in cells cultured as in **G**. **(J)** Percentage of death cells (caspase-3+) in cultures grown as in **I.** Scale bar =50 μm (**A, D** and **G**), 25 μm (**I**). * $p<0.05$, ** $p<0.01$, *** $p<0.001$ compared to glucose; # $p<0.05$ compared to 1h, LSD test. Error bars indicate the SD.

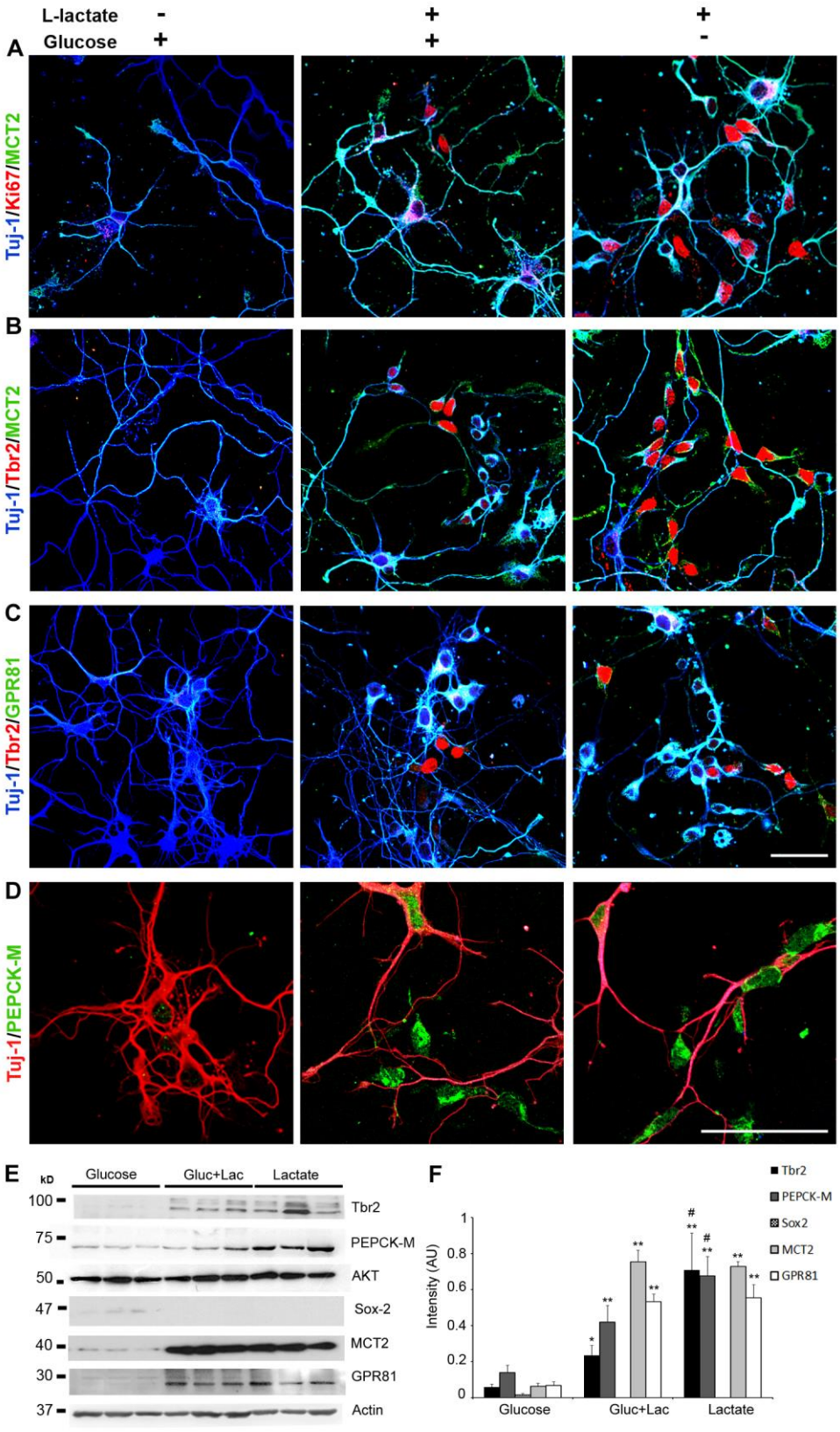

Figure 3. Expression of the lactate metabolic machinery in neuronal cell cultures. Confocal images of neuronal cell cultures grown in glucose, glucose+lactate, or lactate

medium. Triple immunostaining of **(A)** Tuj-1+ neurons (blue), Ki67+ progenitor cells (red), and cells expressing the lactate H+/monocarboxylate transporter MCT2 (green). **(B)** Tuj-1+ neurons (blue), Tbr2+ the intermediate progenitor cells (red), and cells expressing the lactate H+/monocarboxylate transporter MCT2 (green) and **(C)** Tuj-1+ neurons (blue), Tbr2+ the intermediate progenitor cells (red), and cells expressing the lactate receptor GPR81 (green). **(D)** Double immunostaining of Tuj-1+ neurons (red) and PEPCK-M (green). **(E)** Western blot showing lactate-induced expression of the intermediate progenitor marker Tbr2, the NSC/progenitor marker Sox2, and the lactate metabolic machinery proteins PEPCK-M, MCT2, and GPR81 in neuronal cultures grown as described in **A–D.** AKT and actin were used as loading controls. **(F)** Graph summarizing western blot quantification (densitometric intensity values normalized to AKT). Scale bar = 40 μm (**A-C**) and 20 μm (**D**). * $p<0.05$, ** $p<0.01$ compared to glucose; # $p<0.05$ compared to glucose+lactate condition, LSD test. Error bars indicate the SD.

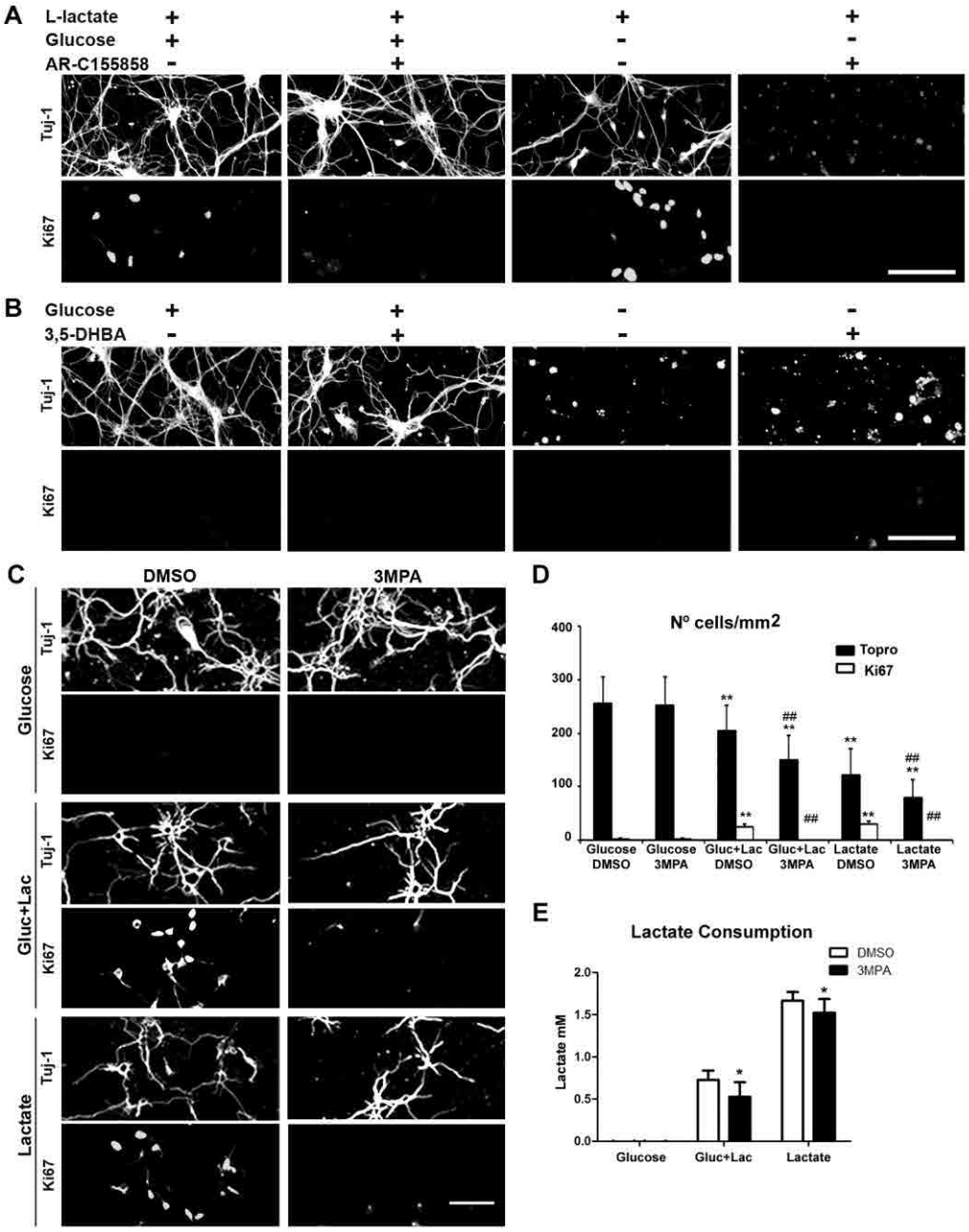

Figure 4. L-Lactate inhibition of neuronal progenitor cells *in vitro*. Confocal images of neuronal cell cultures grown in **(A)** glucose+lactate medium or in lactate medium for 5*div* in the presence or absence of AR-C155858, an inhibitor of monocarboxylate transporters 1/2; **(B)** glucose+lactate medium or in lactate medium for 5*div* in the presence or absence of the lactate receptor agonist 3,5-DHBA; and **(C)** glucose, glucose+lactate, or lactate medium and treated with the PEPCK-M inhibitor 3MPA for 5*div*. Neurons were stained with Tuj-1 antibody and proliferative cells with Ki67. **(D)**

Quantification of the total number of cells (Topro) and of Ki67+ proliferative cells after 5*div* in neuronal cultures grown as in **C. (E)** Quantification of L-lactate in medium obtained from cells cultured as in **C**. Scale bar =75 μm. Values are the average of three replicas. * $p<0.05$, ** $p<0.01$ compared to the glucose condition; ## $p< 0.01$ between 3MPA and DMSO, LSD test. Error bars indicate the SD.

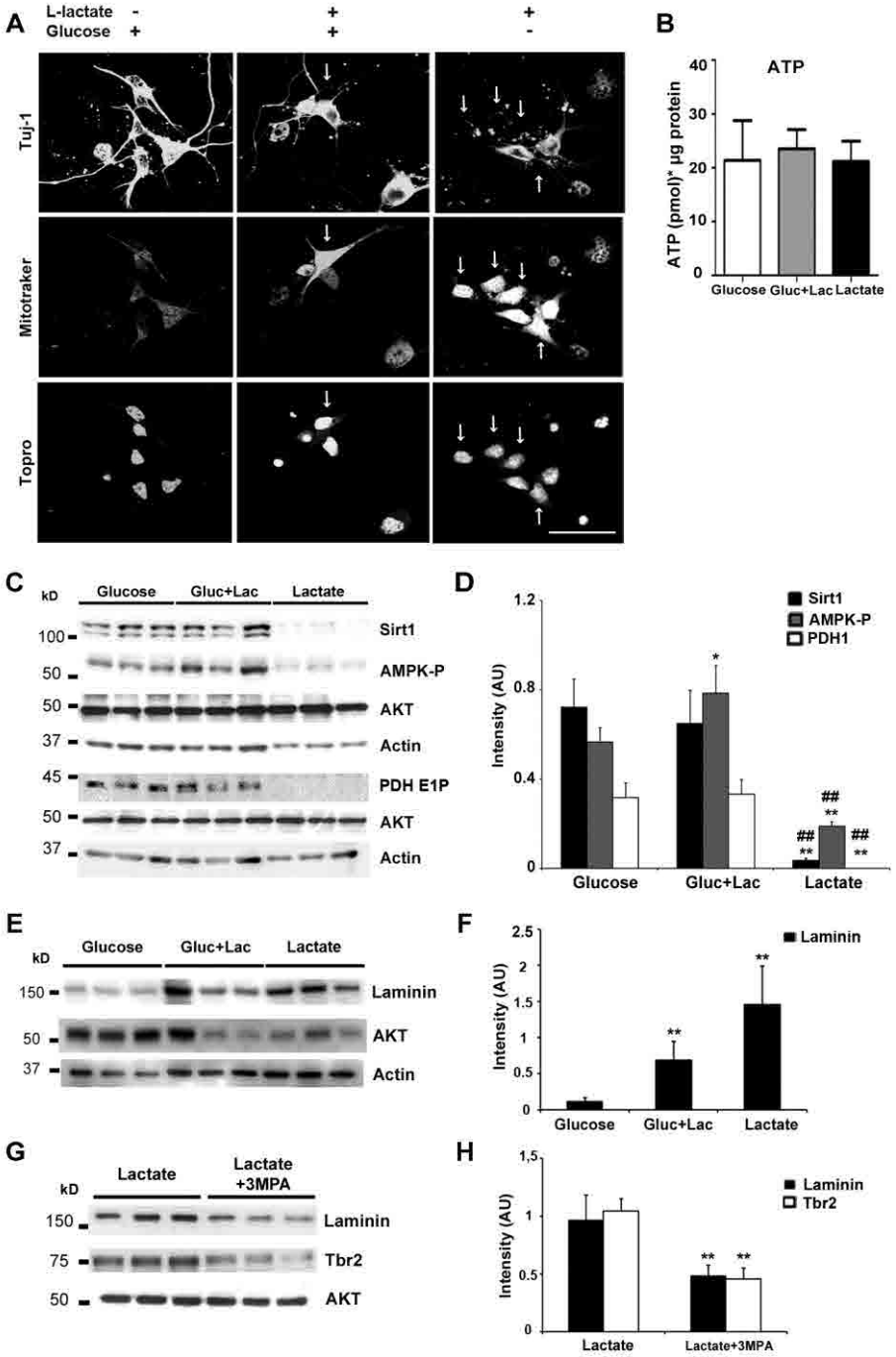

Figure 5. Metabolic profile of neuronal cultures. (A) Confocal images of neuronal cell cultures grown in glucose, glucose+lactate, or in lactate medium for 5*div* stained for neurons (Tuj-1), mitochondria (MitoTracker), and nuclei (Topro). **(B)** ATP quantification in cells cultured as in **A**. **(C)** Western blot of Sirt1 (NAD-dependent deacetylase sirtuin-1), AMPK-P (adenosine monophosphate-activated protein kinase), and pyruvate dehydrogenase E1α-P(Ser^{293}) in neuronal cultures grown as in **A.** AKT

and actin were used as loading controls. **(D)** Quantitative representation of the Western blot (densitometric intensity values normalized to that of AKT). **(E)** Western blot of laminin (basal lamina marker) in neuronal cultures grown as in **A**. AKT and actin were used as controls. **(F)** Quantitative representation of the Western blot (densitometric intensity values normalized to AKT). **(G)** Western blot of laminin and the intermediate progenitor marker Tbr2 in neuronal cultures grown in lactate medium and treated or not with 3MPA for 1*div*. AKT was used as the loading control. **(H)** Quantitative representation of the Western blot (densitometric intensity values normalized to AKT). Scale bar =40 μm. Values are the average of three replicas. * $p<0.05$, ** $p<0.01$ compared to glucose in **D**, **F**, or lactate in **H**; ## $p<0.01$ compared to the glucose+lactate condition, LSD test. Error bars indicate the SD.

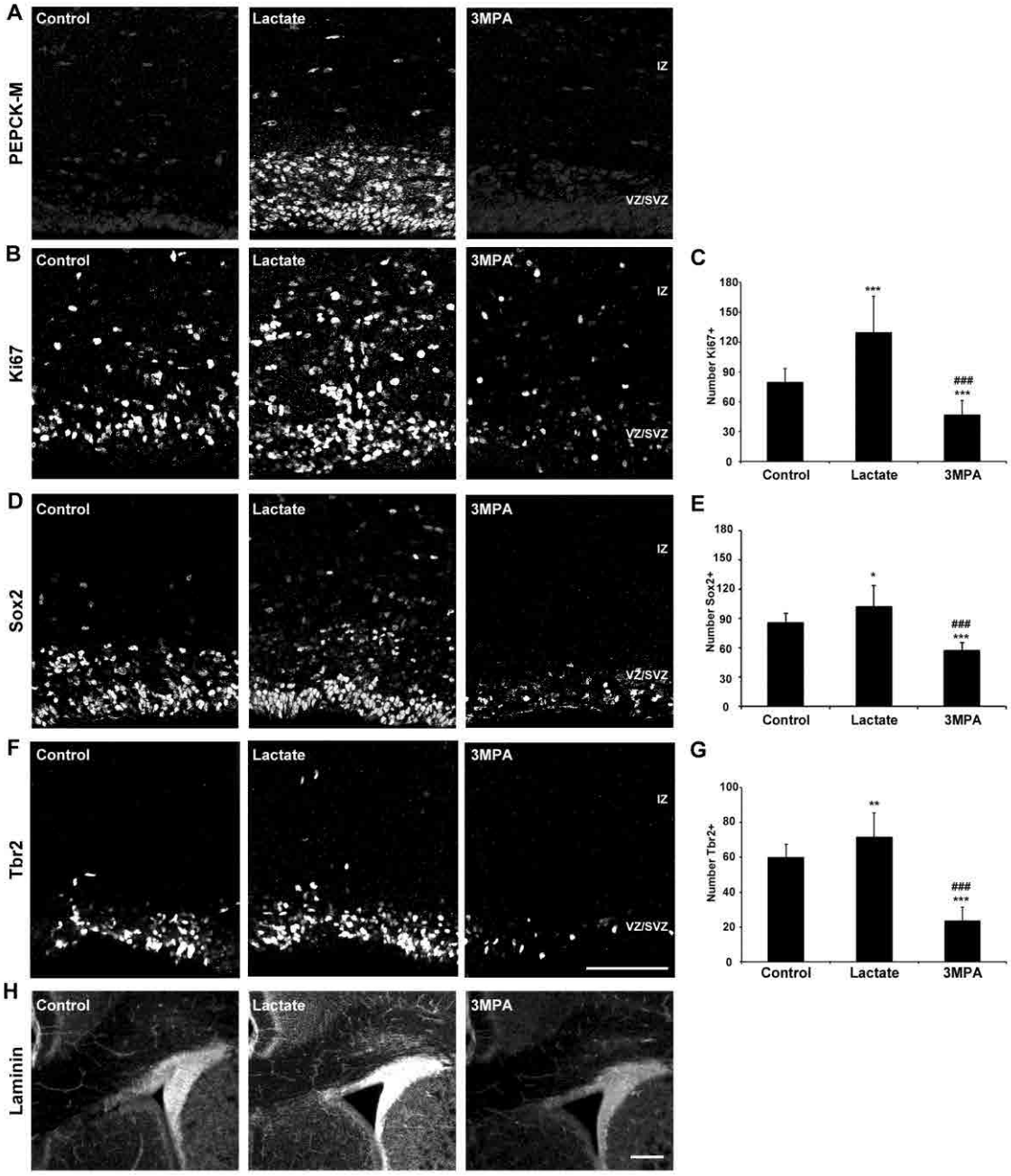

Figure 6: Effect of lactate and 3MPA on cycling cells *in vivo*. (A, B, D, F, and H) Coronal sections of postnatal day 3 (P3) mouse cerebral cortex injected at P0 with vehicle (control), L-lactic acid (lactate), or the PEPCK-M inhibitor 3MPA and stained with **(A)** PEPCK-M, **(B)** Ki67 (proliferative marker), **(D)** Sox2 (NSC/progenitors), **(F)** Tbr2 (neuronal progenitor marker), and (**H)** laminin (basal lamina). Quantification of **(C)** Ki67+ cycling cells, **(E)** Sox2+ NSCs, and **(G)** Tbr2+ neuronal progenitors in the ventricular/subventricular and intermediate zones (VZ/SVZ and IZ) of animals treated

as described in **B**, **D, and F**, respectively**.** Scale bar =100 μm (**A**–**F**), 500 μm (**H**). Values are the average of 8-10 animals. * p<0.05, ** p<0.01, *** p<0.001 compared to the control; ### p<0.001 in a comparison of the treatments, LSD test. Error bars indicate the SD.

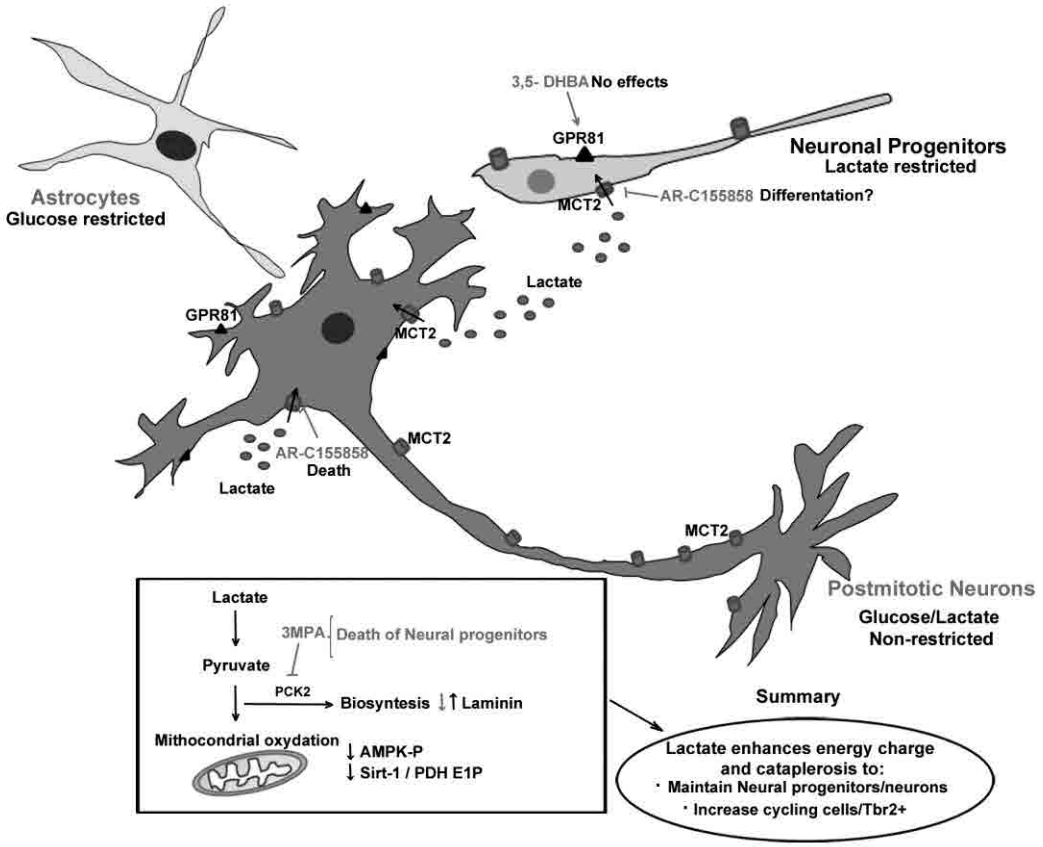

Figure 7. Schematic representation of the proposed effect of lactate in neurons and progenitor cells.

Supplemental information

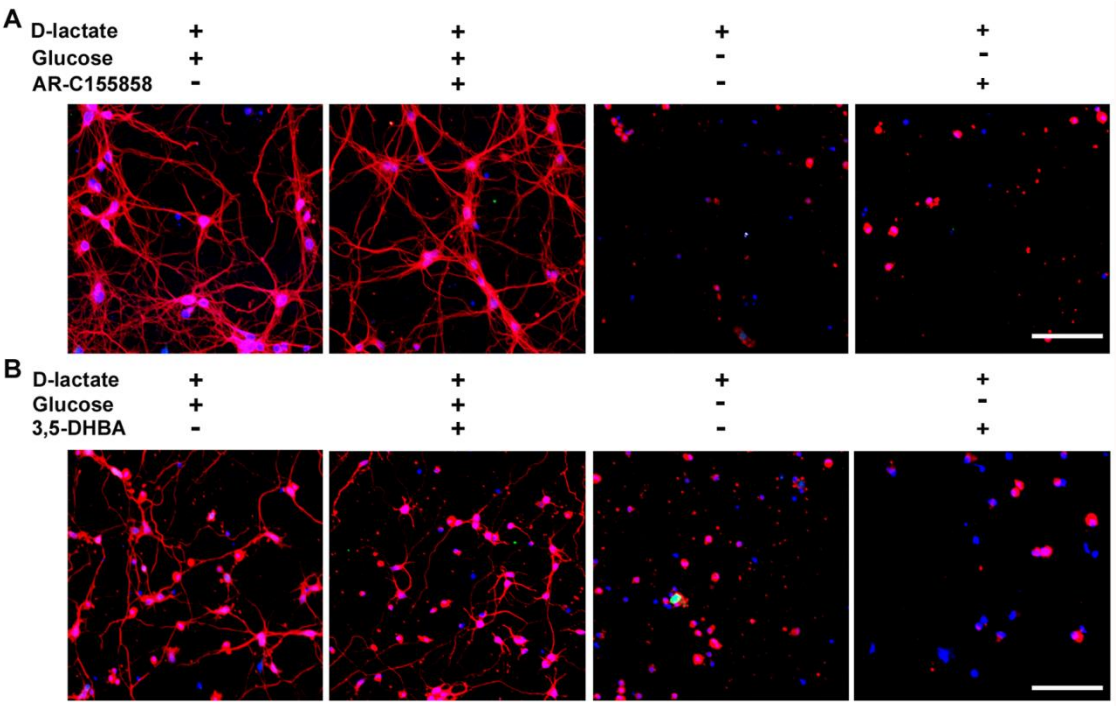

Supplementary figure 1. Inhibitory effect of D-lactate on neuronal progenitor cells *in vitro*. (A) Confocal images of neuronal cell cultures grown in glucose medium supplemented with D-lactic acid (D-lactate) and in D-lactate medium for 5*div* in the presence or absence of AR-C155858, an inhibitor of monocarboxylate transporters 1 and 2. **(B)** Confocal images of neuronal cell cultures grown in glucose medium supplemented with D-lactic acid (D-lactate), and in D-lactate medium for 5*div* in the presence or absence of the lactate receptor agonist 3,5-DHBA. Neurons are stained with Tuj-1 antibody (red), cell nuclei with Topro (blue), and proliferative cells with Ki67 (green). Scale bar =75 μm.

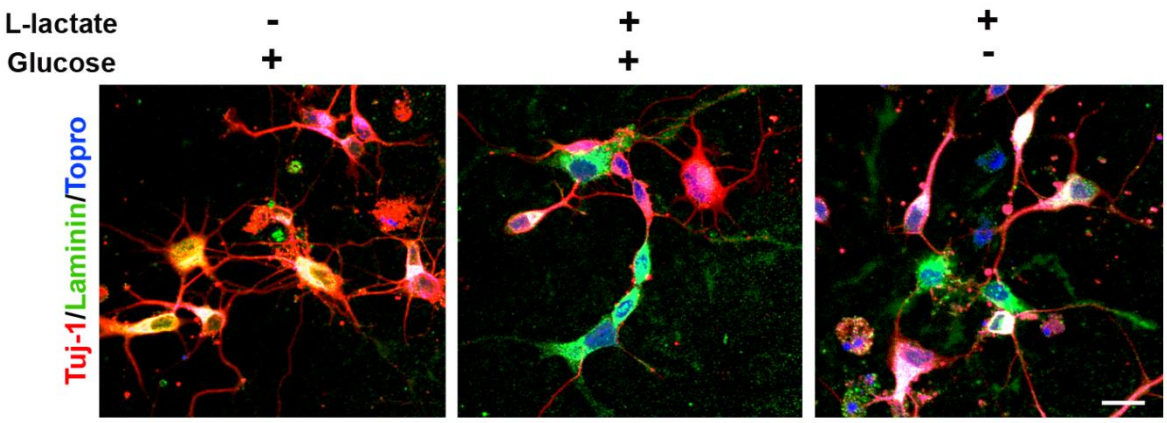

Supplementary figure 2. Laminin expression in neuronal cultures. Confocal images of neuronal cell cultures grown in glucose, glucose + L-lactate, or lactate medium for 5*div and* stained with Tuj-1 (neurons, red), laminin (basal lamina, green), and Topro (nuclei, blue). Scale bar = 10 μm.

Journal of Neuroscience Methods 232 (2014) 93–101

Contents lists available at ScienceDirect

Journal of Neuroscience Methods

journal homepage: www.elsevier.com/locate/jneumeth

Basic Neuroscience

An efficient and reproducible method to culture Bergmann and cortical radial glia using textured PMMA

Zaida Álvarez[a,b], Elena Sena[a], Marta Mattotti[a,c], Elisabeth Engel[b,d,e], Soledad Alcántara[a,*]

[a] Department of Pathology and Experimental Therapeutics, Medical School (Bellvitge Campus), University of Barcelona-UB, Barcelona, Spain
[b] Institute for Bioengineering of Catalonia-IBEC, Barcelona, Spain
[c] Speech and Hearing Research Laboratory, School of Medicine, University of Split, Croatia
[d] Department Material Science and Metallurgical Engineering, Technical University of Catalonia-UPC, Barcelona, Spain
[e] Centro de Investigaciòn Médica en Red, Biomecanica, Biomateriales y Nanotecnologìa-CiberBBN, Barcelona, Spain

HIGHLIGHTS

- Ln2 PMMA scaffold mimics biophysical properties of radial glia stem cell niche.
- Glia grown on ln2 PMMA adopt a BRG/CRG phenotype without added growth factors.
- Ln2 PMMA can be used to easily study the neurogenic potential of radial glia.
- Ln2 PMMA provides an *in vitro* model to study neuron–radial glia interactions.

GRAPHICAL ABSTRACT

ARTICLE INFO

Article history:
Received 13 January 2014
Received in revised form 8 April 2014
Accepted 10 May 2014

Keywords:
Astrocytes
Radial glia
Bergmann glia
Progenitors
Poly-methyl methacrylate (PMMA)
Micro-patterning
Surface topography

ABSTRACT

Background: Radial glia cells comprise the principal population of neural stem cells (NSC) during development. Attempts to develop reproducible radial glia and NSC culture methods have met with variable results, yielding non-adherent cultures or requiring the addition of growth factors. Recent studies demonstrated that a 2-μm patterned poly-methyl methacrylate (ln2 PMMA) grooved scaffold, by mimicking the biophysical and microtopographic properties of the embryonic NSC niche, induces the de-differentiation of glial cells into functional radial glia cells.
New method: Here we describe a method for obtaining cultures of adherent Bergmann radial glia (BRG) and cortical radial glia (CRG). The growth substrate is ln2 PMMA and the addition of growth factors is not required.
Results: Postnatal glia obtained from mouse cerebellum or cerebral cortex and grown on ln2 PMMA adopted a BRG/CRG phenotype characterized by a bipolar shape, the up-regulation of progenitor markers such as nestin and Sox2, and the down-regulation of vimentin and GFAP. Neurons cultured over the BRG/CRG aligned their processes with those of the glial shafts, thus mimicking the behavior of migrating neuronal cells.
Comparison with existing methods: The ln2 PMMA culture method offers an ideal system for analyzing both the biochemical factors controlling the neurogenic potential of BRG/CRG and neuronal migration.

* Corresponding author at: Cell Biology Unit, Department of Experimental Pathology and Therapeutics, School of Medicine (Bellvitge Campus), University of Barcelona, 08907 L'Hospitalet de Llobregat, Barcelona, Spain. Tel.: +34 964024288; fax: +34 964024288.
E-mail address: salcantara@ub.edu (S. Alcántara).

http://dx.doi.org/10.1016/j.jneumeth.2014.05.011

Conclusions: The ln2 PMMA method is a reproducible system to obtain immature BRG/CRG preparations *in vitro*. It can be used to study the properties of CNS progenitor cells as well as the interactions between radial glia and neurons, and supports cultured progenitors for use in different applications.

1. Introduction

Radial glia cells are bipolar, with a long basal process that reaches the outer pial surface and a shorter apical process in contact with the ventricular lumen and serve as a scaffold for neuronal migration (Rakic, 2003). They appear at early stages of central nervous system (CNS) development and comprise the principal population of neural stem cells (NSC), giving rise to the main cellular lineages of the CNS: neurons, astrocytes, oligodendrocytes, ependymocytes and adult NSC (Malatesta et al., 2008). By the time neurogenesis is completed, most radial glia cells have acquired the molecular and cytological features typical of the astroglial lineage whereas others form the NSC that populate adult neurogenic niches. Radial astrocytes persist in the adult brain as Bergmann radial glia (BRG) in the cerebellar cortex and in the eye as Müller cells in the retina. Both cell types retain the characteristics of embryonic radial glia and NSC (Pinto and Gotz, 2007), continuing to express the intermediate filament protein nestin, the L-gutamate/L-aspartate transporter (GLAST), and the transcription factor Sox2, which is involved in stem cell competence, self-renewal and neurosphere formation (Alcock et al., 2007; Reichenbach and Bringmann, 2013; Surzenko et al., 2013).

The ability of radial glia to provide a substrate for neural migration is difficult to study *in vitro* because when cultured in standard serum-containing media the cells rapidly differentiate into astrocytes (Culican et al., 1990). Cultured Bergmann and Müller adult radial glia also lose most of their radial characteristics. Although several *in vitro* approaches have been developed to analyze radial glia functions, they are complicated by the need for fluorescent cell sorting, non-adherent cultures, or require the addition of growth factors such as FGF-2 and EGF [reviewed (Pollard and Conti, 2007)]. Neurosphere generation in the presence of growth factors has been used to analyze the stem cell potential of radial glia, but under these conditions radial glia cells lose their typical elongated shape and are not suitable for neuronal migration studies. A successful approach to study gliophilic neuronal migration is the cortical imprinting assay, which maintains intact radial glia with migrating neurons attached to them (Anton et al., 1997); however, this is a complex and hardly reproducible procedure. Therefore, there is a clear need for an *in vitro* culture system that mimics the radial glia/NSC niche and maintains the shape and function of radial glia cells but does not promote their differentiation.

In this study, we describe an easy and reproducible *in vitro* method to obtain BRG and cortical radial glia (CRG) using line micro-patterned polymethyl methacrylate (PMMA) as the substrate. PMMA is an FDA-approved biocompatible synthetic polymer that is extremely resistant and non-biodegradable. Because of its thermoplastic nature, it can be easily structured by hot embossing (Mills et al., 2007). In previous work we showed that functional CRG can be obtained from the mouse postnatal cerebral cortex by using a 2-μm patterned PMMA (ln2 PMMA) grooved scaffold, without the need for growth factors or extracellular matrix molecules (Mattotti et al., 2012). CRG on ln2 PMMA express the molecular markers of radial glia, including the intermediate filament nestin and the transcription factor Pax6, and support neuronal migration. The embossed substrate thus provides topographical cues that mimic those of the NSC niche, resulting in alterations of both the shape and the differentiation state of the cells (Bettinger et al., 2009; Hoffman-Kim et al., 2010; Keung et al., 2010).

Here we show that ln2 PMMA substrates also support cultures of BRG and likewise obviate the need for the addition of soluble factors. This method confirms the suitability of our *in vitro* system for use in obtaining radial glia from different CNS sources.

2. Materials and methods

2.1. PMMA micropatterning, characterization and sterilization

PMMA sheets (125 μm thick) were supplied by Goodfellow Ltd. (UK). Micropatterns consisting of lines 2-μm-wide and 1 μm deep/tall (ln2) were introduced in the polymer by nanoimprinting lithography (NIL) using an Obducat apparatus (Obducat AB, Sweden) as previously described (Mills et al., 2007). The silicon moulds were provided by AMO GmbH (Aachen, DE) and consisted of 1.5 in. × 1.5 in. silicon squares. Briefly, the mould was positioned on the base of the nanoimprinter with the pattern side face up. The PMMA sheet was placed onto the mould and a sheet of Teflon (125 μm thick) was placed on top of PMMA. The system was heated up to 130 °C, around the transition temperature (T_g) of PMMA, before an imprinting force of 40 bar was applied. After a predetermined embossing time of 600 s, the temperature was gradually reduced while maintaining the applied force. When the temperature reached 80 °C, the pressure was released. The master/polymer was then allowed to slowly cool to room temperature before the two components were carefully separated.

The patterned PMMA films were characterized by white light interferometry (WYKO NT1100) and the software Vision 32 V2.303 (Veeco Instruments, Inc., USA) to confirm replication fidelity and repeatability. Four different PMMA film batches were used. For cell culture, the PMMA films were sterilized with 70% ethanol for 15 min, cut to fit into 60-mm or 20-mm diameter tissue culture dishes (TPP) and used uncoated. Uncoated culture dishes, glass cover slips, and non-patterned PMMA (NP PMMA) served as controls.

2.2. Animals

Cortical or cerebellar glia were obtained from Swiss albino mice at postnatal day 0 (P0) or day 6 (P6), respectively. Cerebellar neurons were obtained from P2 mice. All animal housing and procedures were approved by the Institutional Animal Care and Use Committee in accordance with Spanish and EU regulations.

2.3. Primary cerebellar and cerebral glia cultures

Primary glial cells were prepared essentially as described (Mattotti et al., 2012). Briefly, P0 cerebral cortices and P6 cerebellums were dissected free of the meninges in dissection buffer (0.6% glucose and 0.3% BSA, both from Sigma–Aldrich, USA, in PBS) and digested with trypsin (Biological Industries, Israel) and DNAse I (Sigma) for 10 min at 37 °C. The tissue was dissociated in growing medium (GM), which consisted of Dulbecco's modified Eagle's medium (DMEM, Biological Industries) containing 10% normal horse serum (NHS; Gibco, New Zealand), 1% penicillin-streptomycin (Pen-Strep, Biological Industries) and 2 mM L-glutamine (Biological Industries). The cells were harvested by centrifugation, resuspended in GM, plated and then grown at 37 °C, 5% CO_2 until they reached confluence [25–30 days *in vitro*,

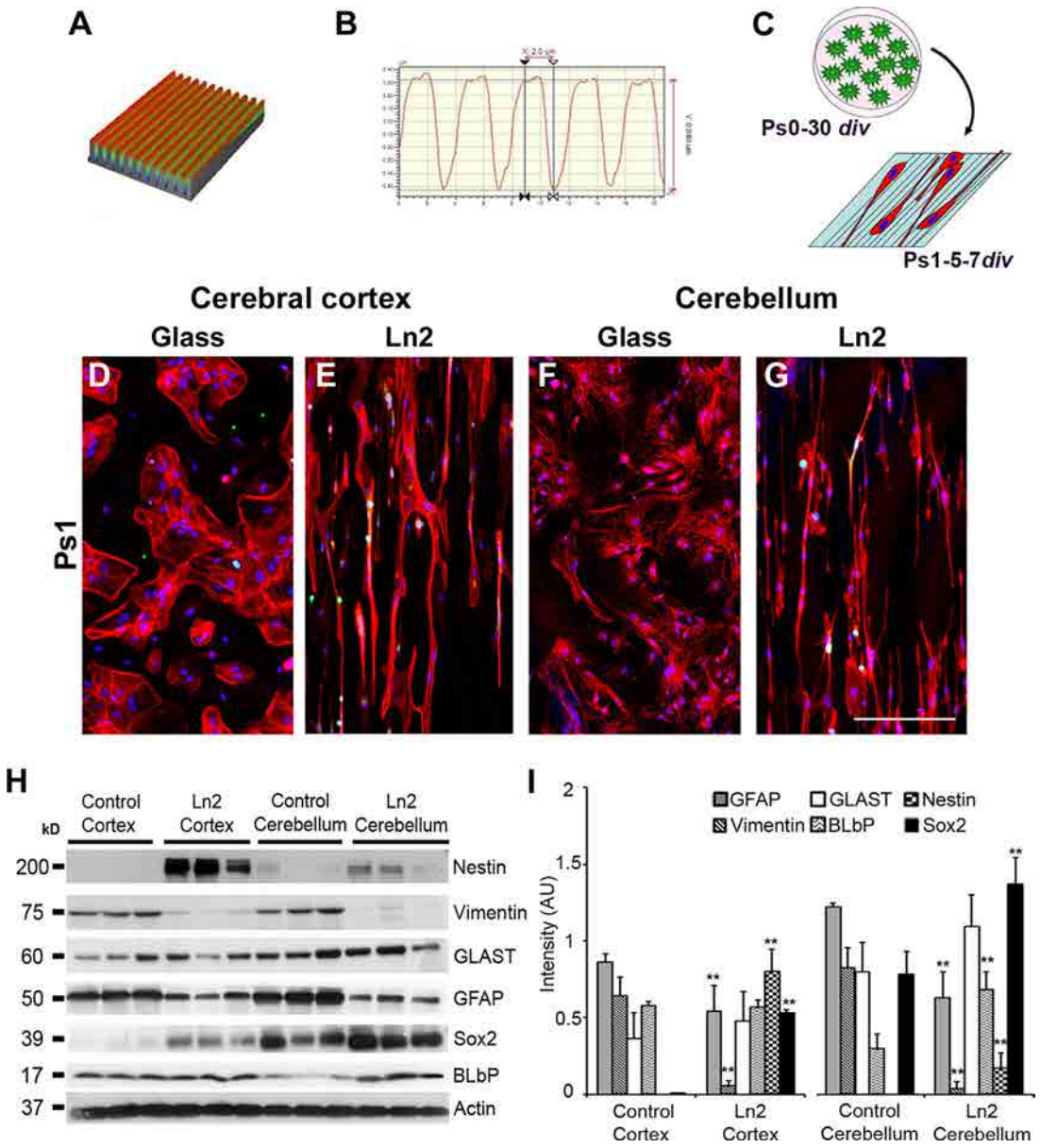

Fig. 1. Characterization of the ln2 PMMA substrate and its effects on the morphology and differentiation of cortical and cerebellar glial cells. (A) White light interferometry 3D image and (B) profile of 2-μm patterned PMMA. (C) Scheme of the culture protocol. (D–G) Confocal images of glial cells stained for actin (phalloidin, red) and Ki67 (cycling cells, green). (H) Western blots showing the expression of progenitor (nestin, Sox2) and glial (vimentin, GLAST, GFAP and BLbP) markers. (I) Quantitative representation of the western blot densitometry (intensity values normalized to actin). Nuclei were stained with TOPRO-3 (blue). Scale bar: 50 μm. $^{**}p < 0.01$: statistical significance compared to the control. (For interpretation of the references to color in this figure legend, the reader is referred to the web version of this article.)

div, passage 0 (Ps0)]. In all experiments, the cells were cultured at a density of 2.5×10^5 cells/cm^2 using glial cells from the first to the third passage (Ps1–Ps3). For successive passages, cells that had reached confluence were trypsinized (Trypsin, Biological Industries) for 10 min at 37 °C and reseeded at the same density. The experiments were performed in triplicate and repeated at least ten times.

For western blotting, the cells were cultured for 5–7 or 15 *div* on 6-well plastic culture plates on either NP PMMA or ln2 PMMA in experimental medium (EM), which consisted of Neurobasal (NB, Biological Industries) medium containing 3% NHS (Gibco), 1% Pen-Strep, and 2 mM L-glutamine. For immunocytochemistry, the cells were plated at the same density on glass cover slips, NP PMMA or ln2 PMMA and placed in 12-well plates. Cell attachment on PMMA was achieved by seeding the cells in a minimal volume of EM in 6- or 12-well plates. After a 5- to 10-min incubation as described above, 2 ml or 1 ml of EM, respectively, was added to the plates.

2.4. Cerebellar neuronal co-cultures

P2 cerebellums were isolated in dissection buffer, digested with trypsin-DNAse I, dissociated and preplated for 30 min in preplating medium [CO_2-equilibrated NB medium supplemented with 5% NHS, 1% Pen-Strep, 0.5 mM L-glutamine and 5.8 ml $NaHCO_3$ 7.5% (Sigma–Aldrich)]. The medium was collected and centrifuged, and the resulting pellet was resuspended in serum-free neuronal culture medium (NB, 1% Pen-Strep, 0.5 mM L-glutamine, 1 × B27, 5.8 ml $NaHCO_3$ 7.5%). P2 cerebellar neurons were plated directly on top of 5 *div* cerebellar glial cells, prepared as described above, at a density

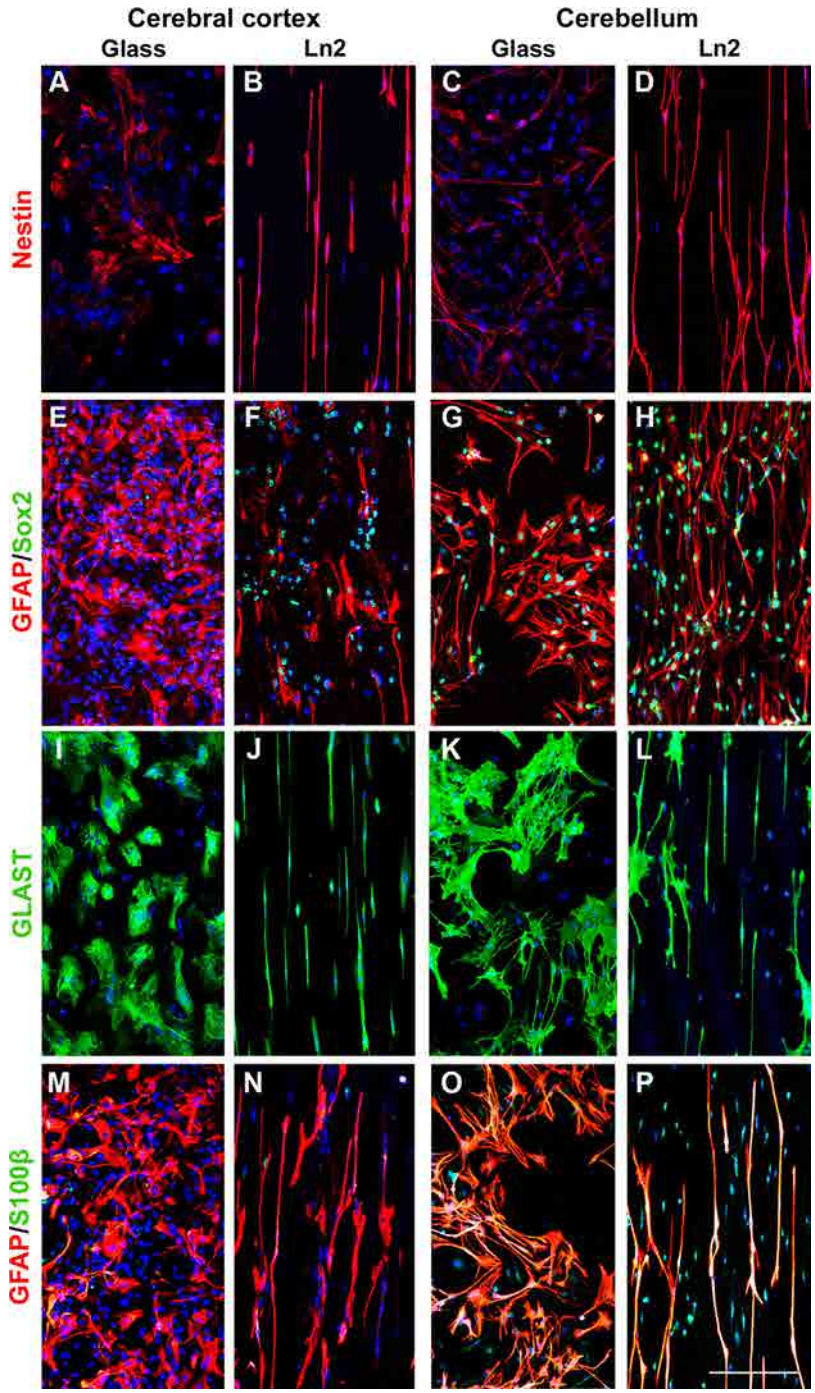

Fig. 2. Immunocytochemical characterization of the cortical and cerebellar glial cell phenotypes obtained on ln2 PMMA. Confocal images of glial cells immunostained for: (A–D) nestin (radial glia, red); (E–H) GFAP (monoclonal, astroglia, red) and Sox2 (NSC/Bergmann glia, green); (I–L) GLAST (astroglia, green); (M–P) GFAP (polyclonal, astroglia, red) and S100β (astroglia, green). Nuclei were stained with TOPRO-3 (blue). Scale bar: 50 μm. (For interpretation of the references to color in this figure legend, the reader is referred to the web version of this article.)

of 2.5×10^5 cells/cm^2 and then cultured for 5 more days in neuronal culture medium.

2.5. Western blot

Total protein extracts were separated by SDS-PAGE and electrotransferred to a nitrocellulose membrane. Then, membranes were blocked in 5% non-fat milk and incubated with primary antibodies (listed below) overnight at 4 °C and then with the corresponding secondary HRP-conjugated antibodies 2 h at room temperature (1:3000, Santa Cruz Biotechnology, San Diego). The protein signal was detected using the ECL chemiluminescence system (Amersham, Buckinghamshire, UK). Densitometry analysis, standardized to actin or AKT as the control for protein loading, was performed using ImageJ software (National Institutes of Health, USA). As similar results were obtained using actin or AKT, the data presented here were quantified based on the actin control. For quantification, triplicate samples were analyzed.

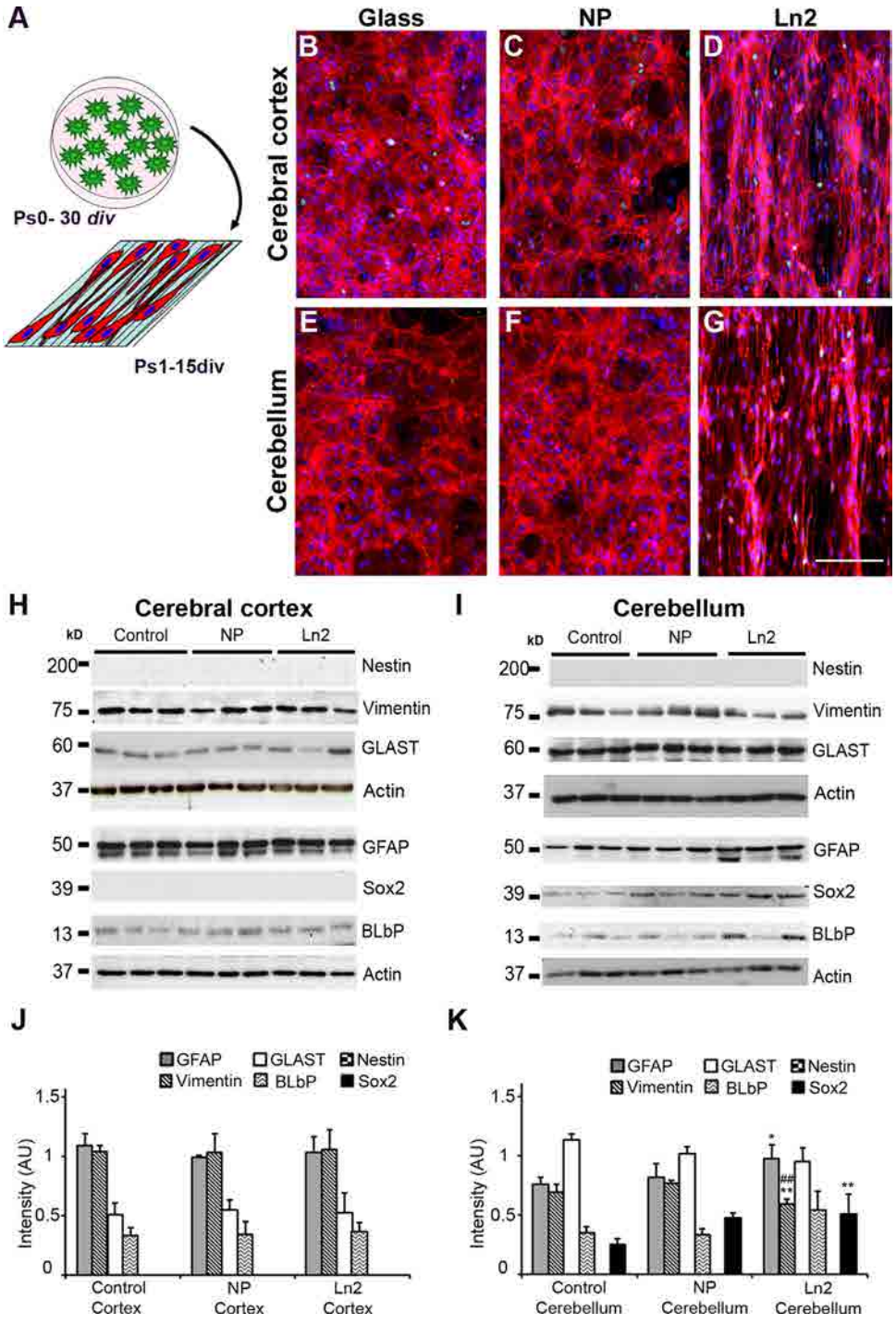

Fig. 3. Characterization of the cortical and cerebellar glial cell phenotypes obtained on In2 PMMA at confluence. (A) Scheme of the culture protocol. (B–G) Confocal images of glial cells stained for actin (phalloidin, red) and Ki67 (cycling cells, green). (H, I) Western blots showing the expression of progenitor (nestin, Sox2) and glial (vimentin, GLAST, GFAP and BLbP) markers. (J, K) Quantitative representation of the western blot densitometry (intensity values normalized to actin). Nuclei were stained with TOPRO-3 (blue). Scale bar: 50 μm. $^{*}p < 0.05$, $^{**}p < 0.01$ compared to the control; $^{\#\#}p < 0.01$ compared to NP PMMA. (For interpretation of the references to color in this figure legend, the reader is referred to the web version of this article.)

2.6. Immunocytochemistry

The cells were fixed for 20 min in 4% paraformaldehyde (PFA) prepared in 0.1 M phosphate buffer (pH 7.3), permeabilized and blocked for 2 h with 0.025% Triton (Sigma–Aldrich) and 1% NHS (Gibco) in PBS and then incubated with primary antibodies (listed below) overnight at 4 °C. The following secondary fluorescent antibodies were then added: anti-rabbit Alexa 488 1:500, anti-mouse Alexa 555 1:500, anti-rabbit Alexa 555 1:500, anti-mouse Alexa 488 1:500, and the nuclear marker TOPRO-3 1:1000 (Molecular Probes, Eugene, Oregon). Phalloidin (1:1000, Sigma–Aldrich) was used to stain F-actin. After 2-h incubation at room temperature, the preparations were washed several times with PBS and mounted with Mowiol (Calbiochem, San Diego, USA) for imaging.

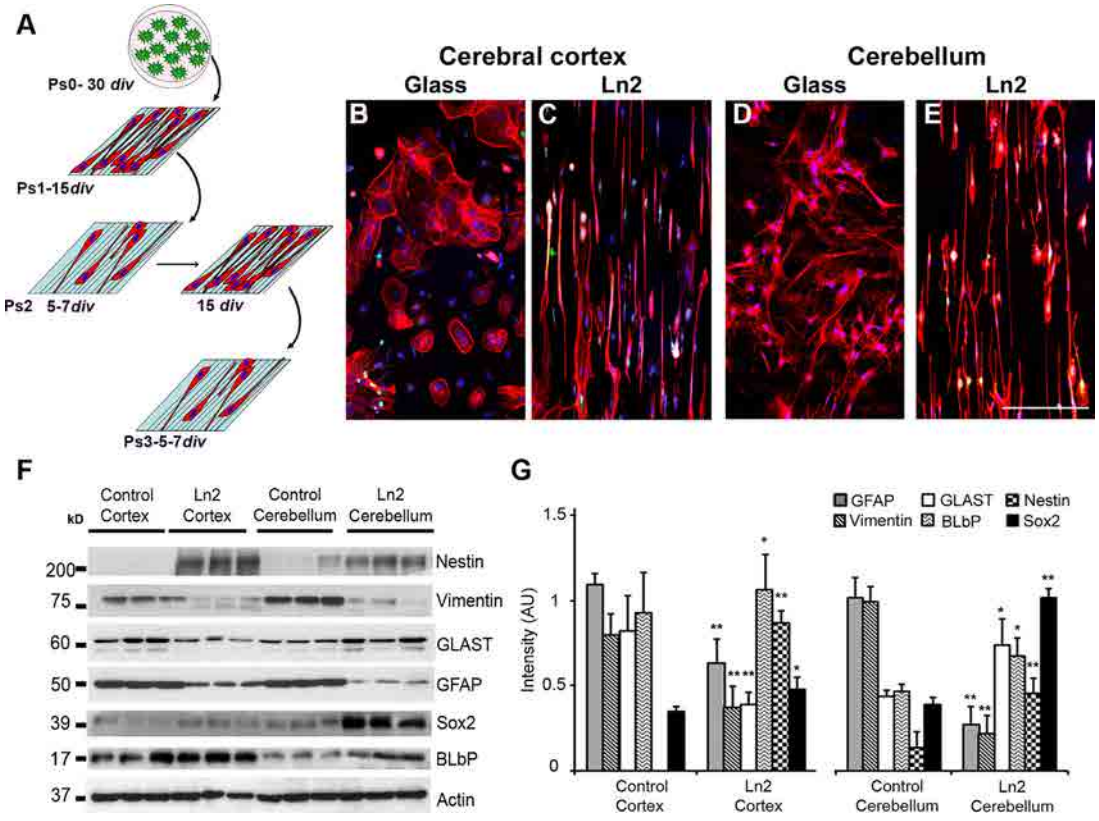

Fig. 4. Radial glia maintenance over successive passages on ln2 PMMA. (A) Scheme of the culture protocol. (B–E) Confocal images of glial cells stained for actin (phalloidin, red) and Ki67 (cycling cells, green). (F) Western blot showing the expression of progenitor (nestin, Sox2) and glial (vimentin, GLAST, GFAP and BLbP) markers. (G) Quantitative representation of the western blot densitometry (intensity values normalized to actin). Nuclei were stained with TOPRO-3 (blue). Scale bar: 50 μm. $^{*}p < 0.05$, $^{**}p < 0.01$ compared to the control. (For interpretation of the references to color in this figure legend, the reader is referred to the web version of this article.)

2.7. Primary antibodies

The following primary antibodies were used (WB/ICC): rabbit polyclonal anti-GFAP (mature astrocyte marker, 1:8000/1:3000, Dako, Denmark), mouse monoclonal anti-GFAP (mature astrocyte marker, –/1:2000, Covance, USA), mouse anti-vimentin (glial cell marker, 1:1000, Santa Cruz Biotechnology), rabbit anti-Sox2 (NSC/Bergmann glial marker, 1:500, Abcam, UK), rabbit anti-GLAST (glial glutamate transporter, 1:1000, Abcam), mouse anti-nestin (radial glia marker, 1:250/1:500, Abnova Corporation), goat anti-actin (loading control, 1:2000/–, Santa Cruz Biotechnology), rabbit anti-Ki67 (proliferation marker, –/1:500, Abcam), mouse anti-S100β (mature astrocyte/Bergmann glia marker, –/1:1000, Millipore, MA, USA), mouse anti-Tuj-1 (neuronal marker, 1:1000/1:3000, Covance), rabbit anti-calbindin (Purkinje and GABAergic interneuron marker, –/1:8000, Swant, Switzerland), rabbit anti-BLbP (radial glia marker, 1:1000/1000, Chemicon, MA, USA), rabbit anti-Olig2 (oligodendrocyte marker, 1:1000/–, Abcam), mouse anti-PDGFRα (oligodendrocyte precursor marker, 1:500/–, Biolegend, USA), and goat anti-AKT (loading control, 1:2000/–, Molecular Probes, USA).

2.8. Imaging and data analysis

Micrographs were captured with a Leica TCS-SL Spectral confocal microscope (Leica Microsystems, Germany). The images were assembled using Adobe Photoshop (v. 7.0), with identical adjustments for contrast, brightness and color balance to obtain optimum visual reproduction of the data. Quantitative image analysis was performed using Image J software (National Institutes of Health, USA).

2.9. Statistical analysis

Statistical analysis was performed using the Statgraphic-plus software. For comparison of the results, a one-way ANOVA and *post hoc* tests were performed using the LSD method; $p < 0.05$ was considered to indicate statistical significance.

3. Results and discussion

During embryonic development, the NSC niche is characterized by the linear topography of radial glia cells. Radial glia shafts of ~1–2 μm form a palisade of radially aligned fibers that serve as migration substrate for neurons. The lipids in radial glia membranes are negatively charged, as they contain high amount of glycoconjugates (Yanagisawa and Yu, 2007). Similarly, PMMA is slightly hydrophobic and negatively charged. With the introduction of a 2-μm linear topography, ln2 PMMA forms a scaffold that mimics the radial glia NSC niche both topographically and with respect to its surface properties (Mattotti et al., 2012). Here we show that this artificial PMMA scaffold can be used to modulate the astrocytic phenotype of glia obtained from the cerebral cortex (Mattotti et al., 2012) or the cerebellum, directing them to immature CRG and BRG phenotypes, respectively.

3.1. Material characterization

The 2-μm line patterns were imprinted on PMMA by NIL as described in Section 2.1. The surface texture was characterized by white light interferometry using a WYKO NT1100 apparatus. The line width of 2.01 ± 0.29 μm and line height of 0.89 ± 0.09 μm ($n = 20$) are within the range obtained in a previous study (Mattotti

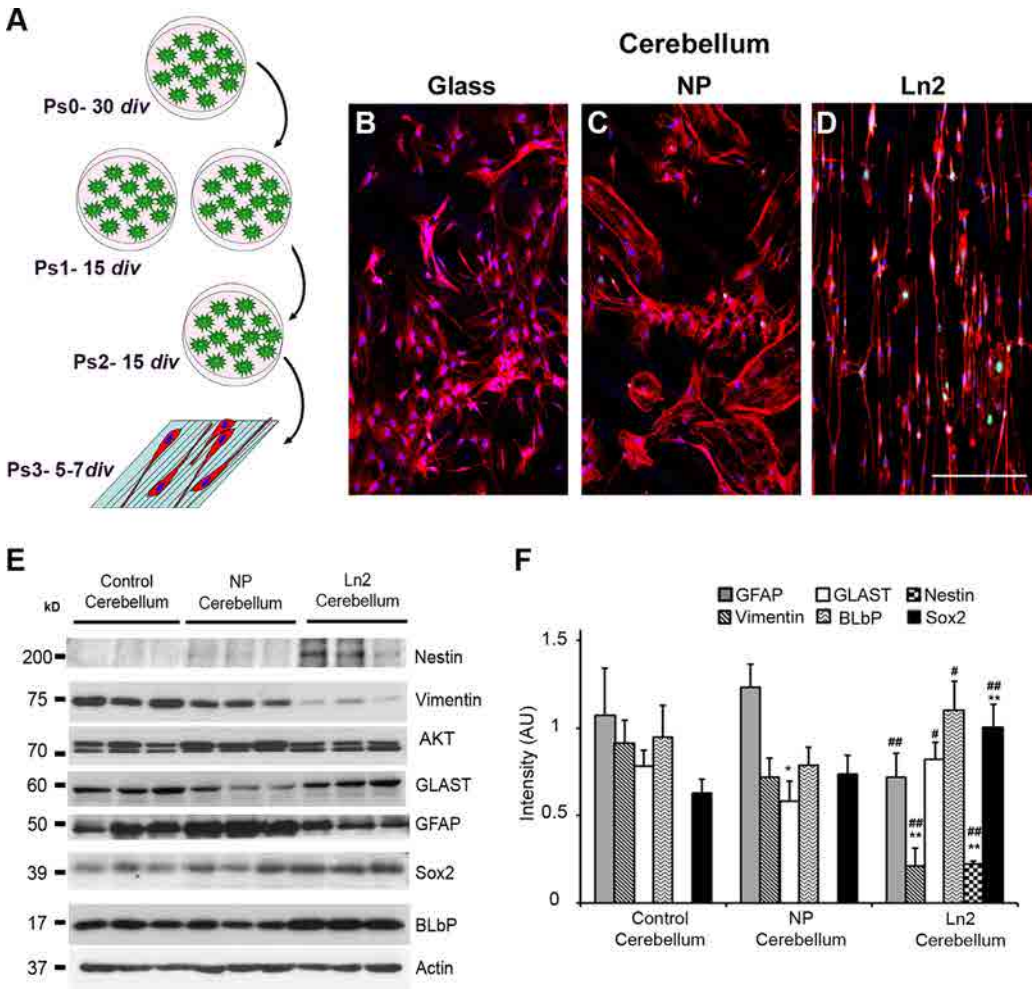

Fig. 5. Radial glia induction on ln2 PMMA after successive passages on tissue culture plates. (A) Scheme of the culture protocol. (B–D) Confocal images of glial cells stained for actin (phalloidin, red) and Ki67 (cycling cells, green). (E) Western blot showing the expression of progenitor (nestin, Sox2) and glial (vimentin, GLAST, GFAP and BLbP) markers. (F) Quantitative representation of the western blot densitometry (intensity values normalized to actin). Nuclei were stained with TOPRO-3 (blue). Scale bar: 50 μm. $^{*}p < 0.05$, $^{**}p < 0.01$ compared to the control; $^{\#}p < 0.05$, $^{\#\#}p < 0.01$ compared to NP PMMA. (For interpretation of the references to color in this figure legend, the reader is referred to the web version of this article.)

et al., 2012), indicating the reproducibility of the embossing technique used to generate the PMMA substrates (Fig. 1A, B).

3.2. Radial glia culture preparation and biochemical characterization

Glial cells were isolated and cultured as described in Section 2.3, becoming confluent after 25–30 days. BRG and CRG differentiation was induced by seeding Ps1 cells at a density of 2.5×10^5 cells/mm^2 on ln2 PMMA in EM. The same procedure was followed for the controls, except that the substrate was either glass/tissue culture plates or NP PMMA.

After 5–7 *div* (Fig. 1C), cell morphology and proliferation were analyzed using phalloidin, an F-actin marker, and Ki67, a marker of cycling cells (Fig. 1D–G, Suppl. Fig. 1A–D). Under the control conditions cortical glia cells exhibited the flattened, spread morphology typical of mature astrocytes (Fig. 1D, Suppl. Fig. 1A, B). The same was observed in control cerebellar glia cultures, although the cells were somewhat elongated (Fig. 1F, Suppl. Fig. 1C, D). In both cases, only a few cells expressed Ki67 (cerebral cortex, glass: $6.2 \pm 3.9\%$; NP PMMA: 5.54 ± 12.3; cerebellum, glass: $6.5 \pm 4.7\%$; NP PMMA: 6.8 ± 3.6). On ln2 PMMA, cortical (Fig. 1E) and cerebellar (Fig. 1G) glial cells were mostly bipolar and aligned in the direction of the imprinted lines. In addition, the number of Ki67$^+$ cycling cells was significantly higher ($13.1 \pm 2.8\%$; $15.4 \pm 3.1\%$, respectively; $p > 0.01$).

Supplementary Figure 1 related to this article can be found, in the online version, at http://dx.doi.org/10.1016/j.jneumeth.2014.05.011.

Western blotting (Fig. 1H, I, Suppl. Fig. 1I, J) and immunocytochemistry (Fig. 2, Suppl. Fig. 1E–H) were then used to analyze the expression of radial glia and glial differentiation markers in cerebral and cerebellar cultures under the same conditions as described above. Nestin, an intermediate filament protein expressed in radial glia (Chen et al., 2009), and the stem cell/Bergmann glia marker Sox2 (Alcock et al., 2007) were used to assess the presence of CRG/BRG. Astrocytic populations were identified based on their expression of glial fibrillary acidic protein (GFAP), vimentin and the calcium-binding protein S100β (Alcock et al., 2007; Cameron and Rakic, 1991; Yamada et al., 2000). Two additional markers, brain lipid-binding protein (BLbP) and glutamate astrocytic transporter (GLAST), are expressed in radial glia cells and adult astrocytes (Yamada and Watanabe, 2002).

Since there were no major differences in cell shape and the expression of glial differentiation markers between cultures grown on glass/tissue culture plastic and NP PMMA (Suppl. Fig. 1), we mainly used the former as reference controls for all ln2 PMMA experiments.

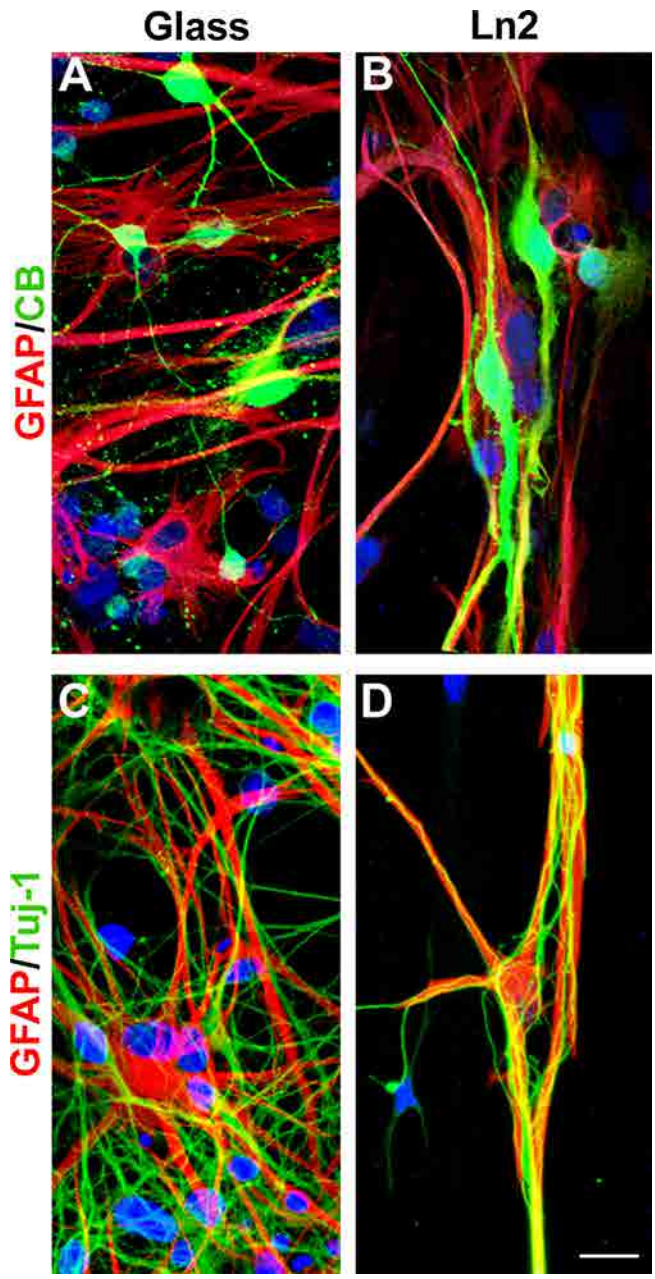

Fig. 6. Effect of ln2-PMMA-induced BRG in cerebellar neurons. Confocal images of glial cells (red) and neurons (green) immunostained for (A, B) GFAP (monoclonal) and calcium-binding protein calbindin (CB) or (C, D) GFAP (polyclonal) and Tuj-1. Scale bar: 10 μm. (For interpretation of the references to color in this figure legend, the reader is referred to the web version of this article.)

Quantitative data obtained by western blotting and densitometry analyses (Fig. 1H, I) showed that expression of the radial glia and stem cell/Bergmann glia markers nestin and Sox2, respectively, was higher and that of the astrocyte markers GFAP and vimentin lower in cortical and cerebellar glia cultured on ln2 PMMA than on the control substrates. In addition, higher levels of BLbP expression were determined in cerebellar glia cultured on ln2 PMMA while GLAST expression remained constant under all conditions. Throughout this study, none of the cells expressed the neuronal marker Tuj-1 or the oligodendroglial markers Olig2 and PDGFR-α, regardless of the substrate used (data not shown). Nestin immunostaining revealed that cells in the cerebral and cerebellar glial cultures grown on ln2 PMMA acquired a similar radial shape (Fig. 2B, D). In cortical cultures, GFAP$^+$ astrocytes were abundant while Sox2- and S100β-expressing cells were scarce and the two markers were rarely co-expressed with GFAP either in control (Fig. 2E, M) or in ln2 PMMA (Fig. 2F, N) cultures. The differences in GFAP staining among the different images can be attributed to the use of monoclonal (Fig. 2E–H) or polyclonal (Fig. 2M–P) GFAP antibodies.

By contrast, cerebellar Bergmann glia co-expressed GFAP with Sox2 and S100β. As expected, double-labeled GFAP$^+$Sox2$^+$ and GFAP$^+$S100β$^+$ cells were abundant in control cerebellar glial cultures (Fig. 2G, O). The intensity of staining indicative of co-localization increased in the ln2 PMMA cultures, while virtually all radial GFAP$^+$ cells co-expressed the other two markers (Fig. 2H, P). GLAST was expressed in Bergmann and cortical glial cells as expected for a general glial marker (Fig. 2I–L). These data indicate that ln2 PMMA induces radial glial cells to differentiate into immature BRG and CRG, with the phenotypes mostly corresponding to those of the late radial glia/early transformation phases in cerebellar cultures (Yamada et al., 2000) and embryonic cortical radial glia (Pinto and Gotz, 2007). Interestingly, in cerebellar cultures ln2 PMMA induced an increase in Sox2 in GFAP$^+$ cells (Fig. 2H), consistent with the increase in the size of the BRG population, while in cortical cultures Sox2 was enriched mostly in GFAP$^-$ cells (Fig. 2F).

After 15 *div* (Fig. 3A) the cells became confluent (Fig. 3B–G) such that there were fewer differences between ln2 PMMA and control cultures. At confluence, markers of astrocyte differentiation were expressed at high levels under all conditions, while the expression of radial glia/NSC markers was low or even absent (Fig. 3H–K). Only in cerebellar cultures were small differences in Sox2 and vimentin expression maintained between ln2 PMMA and control cultures (Fig. 3I, K). These results suggest that a direct interaction between the cells and the substrate is required for BRG/CRG induction, as suggested in recent work showing that cell fate can be directly specified through substrate selection (Goetz et al., 2006) and that effective reproduction of the NSC niche *in vitro* is strongly dependent on cell density (Pierret et al., 2010). One possible explanation is that in the absence of mitogens, the inhibition of cell contact prevails over the inductive effects of the ln2 PMMA substrate in primary non-transformed cells.

3.3. Radial glia maintenance during successive cell passages

To demonstrate that substrate topography signaling is sufficient to induce the radial glia phenotype three successive passages on ln2 PMMA were conducted (Fig. 4A). The cells were seeded at a density of 2.5×10^5 cells/cm^2 on ln2 PMMA and after reaching confluence (15 *div*) they were detached and then reseeded at the same density. The procedure was repeated and the Ps3 cells were analyzed after 5–7 *div* (Fig. 4A). Ps3 cerebral and cerebellar glial cells cultured on ln2 PMMA maintained their radial morphology (Fig. 4B–E) and expressed significantly higher levels of the radial glia markers nestin and BLbP and the NSC/Bergmann glia marker Sox2 (Fig. 4F, G). A similar induction of BRG was obtained when the cerebellar glial culture was allowed to mature *in vitro* and then maintained for several passages on tissue culture plates before being reseeded onto ln2 PMMA (Fig. 5).

Taken together, these results show that our ln2-PMMA-based method is reproducible and can be used to induce and maintain, over several passages, the CRG and BRG morphology and molecular signature.

3.4. BRG support of cerebellar neurons and neuronal processes

Under the culture conditions tested in this work, neurons did not directly adhere either to PMMA or to glass surfaces, but only to glial cells. Early postnatal cerebellar neurons were identified based on their expression of neuronal β-tubulin III (Tuj-1) and the

calcium-binding protein calbindin (Purkinje cells and GABAergic interneurons) (Fig. 6). In control cerebellar glial cultures, cerebellar neurons that had adhered to glial cells for the most part acquired a multipolar and highly ramified shape (Fig. 6A, C), while on ln2 PMMA the cerebellar neurons were bipolar and their processes were in close contact with the BRG, thus resembling migrating neuroblasts (Fig. 6B, D). This result strongly suggests that on ln2 PMMA BRG instruct cerebellar neurons to adopt the morphology of migrating neurons-radial glia complexes, as already described for neurons cultured on ln2-PMMA-induced CRG (Mattotti et al., 2012).

3.5. *Ln2 PMMA as a model system for studying radial glia properties and functions*

With the method described in this work, CRG and BRG can be easily obtained from cerebral cortex and cerebellum by using ln2 micropatterned PMMA as the culture substrate. Unlike other methods, there is no need for previous cell sorting or exogenously added extracellular matrix molecules or growth factors. The robust and reproducible results obtained in this study suggest that our method can also be used for the growth of radial glia from other sources, such as retinal Müller glia or spinal cord. The induced CRG and BRG obtained in this study exhibited a radial glia signature but never generated neurons. This finding provides further support for the use of ln2 PMMA as the substrate in *in vitro* models aimed at studying the effect of epigenetic or environmental factors on the acquisition of neurogenic competence by radial glia. Although additional studies are needed, the biophysical regulation of radial glia by ln2 PMMA, including nestin and Sox2 expression, hints at the possibility of easily growing neural progenitors from different CNS sources and ages, allowing the use of these cells in a wide variety of applications.

Acknowledgements

This study was supported by grants from Spain's Ministerio de Economía y Competitividad (MINECO) [MAT2011-29778-C02-02], co-financed by the European Regional Development Fund, and from Generalitat de Catalunya SGR 2009 719 to S.A., and by fellowship IBEC 10-2009-01 to Z.A. We are grateful to W. Ran for editorial assistance and to B. Torrejón, from the UB's Scientific-Technical Services (Bellvitge Campus), for technical support in confocal microscopy.

References

Alcock J, Scotting P, Sottile V. Bergmann glia as putative stem cells of the mature cerebellum. Med Hypotheses 2007;69:341–5.
Anton ES, Marchionni MA, Lee KF, Rakic P. Role of GGF/neuregulin signaling in interactions between migrating neurons and radial glia in the developing cerebral cortex. Development 1997;124:3501–10.
Bettinger CJ, Langer R, Borenstein JT. Engineering substrate topography at the micro- and nanoscale to control cell function. Angew Chem Int Ed Engl 2009;48:5406–15.
Cameron RS, Rakic P. Glial cell lineage in the cerebral cortex: a review and synthesis. Glia 1991;4:124–37.
Chen J, Kwon CH, Lin L, Li Y, Parada LF. Inducible site-specific recombination in neural stem/progenitor cells. Genesis 2009;47:122–31.
Culican SM, Baumrind NL, Yamamoto M, Pearlman AL. Cortical radial glia: identification in tissue culture and evidence for their transformation to astrocytes. J Neurosci 1990;10:684–92.
Goetz AK, Scheffler B, Chen HX, Wang S, Suslov O, Xiang H, et al. Temporally restricted substrate interactions direct fate and specification of neural precursors derived from embryonic stem cells. Proc Natl Acad Sci U S A 2006;103:11063–8.
Hoffman-Kim D, Mitchel JA, Bellamkonda RV. Topography, cell response, and nerve regeneration. Annu Rev Biomed Eng 2010;12:203–31.
Keung AJ, Kumar S, Schaffer DV. Presentation counts: microenvironmental regulation of stem cells by biophysical and material cues. Annu Rev Cell Dev Biol 2010;26:533–56.
Malatesta P, Appolloni I, Calzolari F. Radial glia and neural stem cells. Cell Tissue Res 2008;331:165–78.
Mattotti M, Alvarez Z, Ortega JA, Planell JA, Engel E, Alcantara S. Inducing functional radial glia-like progenitors from cortical astrocyte cultures using micropatterned PMMA. Biomaterials 2012;33:1759–70.
Mills CA, Fernandez JG, Martinez E, Funes M, Engel E, Errachid A, et al. Directional alignment of MG63 cells on polymer surfaces containing point microstructures. Small 2007;3:871–9.
Pierret C, Morrison JA, Rath P, Zigler RE, Engel LA, Fairchild CL, et al. Developmental cues and persistent neurogenic potential within an in vitro neural niche. BMC Dev Biol 2010;10:5.
Pinto L, Gotz M. Radial glial cell heterogeneity – the source of diverse progeny in the CNS. Prog Neurobiol 2007;83:2–23.
Pollard SM, Conti L. Investigating radial glia in vitro. Prog Neurobiol 2007;83:53–67.
Rakic P. Developmental and evolutionary adaptations of cortical radial glia. Cereb Cortex 2003;13:541–9.
Reichenbach A, Bringmann A. New functions of Muller cells. Glia 2013;61:651–78.
Surzenko N, Crowl T, Bachleda A, Langer L, Pevny L. Sox2 maintains the quiescent progenitor cell state of postnatal retinal Muller glia. Development 2013;140:1445–56.
Yamada K, Fukaya M, Shibata T, Kurihara H, Tanaka K, Inoue Y, et al. Dynamic transformation of Bergmann glial fibers proceeds in correlation with dendritic outgrowth and synapse formation of cerebellar Purkinje cells. J Comp Neurol 2000;418:106–20.
Yamada K, Watanabe M. Cytodifferentiation of Bergmann glia and its relationship with Purkinje cells. Anat Sci Int 2002;77:94–108.
Yanagisawa M, Yu RK. The expression and functions of glycoconjugates in neural stem cells. Glycobiology 2007;17:57R–74R.

Biomaterials 33 (2012) 1759–1770

Contents lists available at SciVerse ScienceDirect

Biomaterials

journal homepage: www.elsevier.com/locate/biomaterials

Inducing functional radial glia-like progenitors from cortical astrocyte cultures using micropatterned PMMA

Marta Mattotti [a,b,d], Zaida Alvarez [b,d], Juan A. Ortega [d], Josep A. Planell [a,b,c], Elisabeth Engel [a,b,c], Soledad Alcántara [d,*]

[a] Dpt. Material Science and Metallurgical Engineering, Technical University of Catalonia-UPC, Barcelona, Spain
[b] Institute for Bioengineering of Catalonia-IBEC, Barcelona, Spain
[c] Centro de Investigación Médica en Red. Biomecanica, Biomateriales y Nanotechnología-CiberBBN, Barcelona, Spain
[d] Dpt. of Pathology and Experimental Therapeutics, Medical School (Bellvitge Campus), University of Barcelona-UB, Barcelona, Spain

ARTICLE INFO

Article history:
Received 9 September 2011
Accepted 10 October 2011
Available online 1 December 2011

Keywords:
Polymethylmethacrylate
Micropatterning
Surface topography
Astrocyte
Nerve guide
Co-culture

ABSTRACT

Radial glia cells (RGC) are multipotent progenitors that generate neurons and glia during CNS development, and which also served as substrate for neuronal migration. After a lesion, reactive glia are the main contributor to CNS regenerative blockage, although some reactive astrocytes are also able to de-differentiate *in situ* into radial glia-like cells (RGLC), providing beneficial effects in terms of CNS recovery. Thus, the identification of substrate properties that potentiate the ability of astrocytes to transform into RGLC in response to a lesion might help in the development of implantable devices that improve endogenous CNS regeneration. Here we demonstrate that functional RGLC can be induced from *in vitro* matured astrocytes by using a precisely-sized micropatterned PMMA grooved scaffold, without added soluble or substrate adsorbed biochemical factors. RGLC were extremely organized and aligned on 2 μm line patterned PMMA and, like their embryonic counterparts, express nestin, the neuron-glial progenitor marker Pax6, and also proliferate, generate different intermediate progenitors and support and direct axonal growth and neuronal migration. Our results suggest that the introduction of line patterns in the size range of the RGC processes in implantable scaffolds might mimic the topography of the embryonic neural stem cell niche, driving endogenous astrocytes into an RGLC phenotype, and thus favoring the regenerative response *in situ*.

1. Introduction

Despite the presence of multipotent neural stem cells (NSC) in the adult central nervous system (CNS), their ability to regenerate after an injury is very limited and there is currently no effective treatment to improve CNS healing. The formation of a glial scar is one of the most important causes of the lack of spontaneous CNS regeneration. Reactive astrocytes, fibroblasts and other glial cells within the scar produce inhibitory molecules for axon growth [1,2]. However, current evidence indicate that astrocytes also play beneficial effects for CNS recovery, as they restart the hemato-encephalic barrier, secrete neurotrophic factors and provide support and guidance for axonal growth [3–5]. Moreover, a pool of early reactive astrocytes changes their phenotype adopting many of the molecular traits of embryonic radial glia and NSC [6,7]. Therefore, a promising strategy can be enhancing the beneficial astrocytic response to obtain a permissive glial environment for neural growth and the re-establishment of functional connections after an injury.

Cell-based approaches to CNS regeneration have had little success, partly because of the limited survival and integration of the implanted cells, which is probably due to the absence of biochemical and topographical cues normally present at the NSC niche. To overcome this problem, the tissue engineering approach aims to provide instructive information to regenerative capable cells through the implantation of intelligent materials that mimic the natural NSC microenvironment. There is increasing evidence that surface topography can modulate the cell response by changing cell morphology and differentiation state. The most

* Corresponding author. Cell Biology Unit, Department of Experimental Pathology and Therapeutics, School of Medicine (Bellvitge Campus), University of Barcelona, 08907 L'Hospitalet de Llobregat, Spain. Tel./fax: +34 954024288.
E-mail address: salcantara@ub.edu (S. Alcántara).

0142-9612/$ – see front matter © 2011 Elsevier Ltd. All rights reserved.
doi:10.1016/j.biomaterials.2011.10.086

recent findings and theories have been elegantly reviewed by Bettinger et al. [8] and Hoffman-Kim [9], the latter focusing specifically on nerve regeneration. Among the results they mention, micropatterned or aligned fibers of poly-caprolactone enhanced the differentiation of retinal progenitor cells into neurons and glia [10] or Schwann cells maturation [11], respectively, while the diameter of electrospun fibers influenced NSC differentiation [12]. Furthermore, mature astrocytes have been shown to de-differentiate *in vitro* under certain specific conditions. For instance, induction of the polycomb transcription factor Bmi1 and exposure to FGF-2 or sulfated hyaluronan can induce stem cell-like features in quiescent astrocytes [13,14]. Astrocytes may also de-differentiate by physical methods, such as freeze-thawing [15] or by mechanical and scratch insults [7]. These findings suggest that differentiated glial cells retain a certain plasticity that might be manipulated to evoke a reparative response to damage by presenting the appropriate signals.

Several recent studies have used micropatterned polymer substrates to direct the growth and differentiation of NSC [16]. However, glial cells and, in particular, astrocytes are the most likely cell types to contact the material after *in vivo* implant. To identify instructive cues that could induce astrocytes to adopt a radial glia-like phenotype permissive for neural growth, we analyzed *in vitro* the differentiation of glial cells in response to linear patterns imprinted on a substrate of poly(methyl methacrylate) (PMMA).

PMMA is a transparent synthetic material that, thank to its thermoplastic nature, can be structured by hot embossing with high resolution [17–19]. It has been used for nerve tissue engineering *in vitro* [20,21] and has recently been successfully employed for rat sciatic nerve regeneration *in vivo* [22]. Here therefore, we used uncoated PMMA films carrying line topographies of different dimensions in order to determine whether the introduction of topographical cues might bias glial differentiation toward a supportive phenotype for neuronal growth.

2. Materials and methods

2.1. PMMA characterization and microstructuring

Characterization of PMMA wettability was achieved via contact angle measurements using an OCA 20 system (Dataphysics, GmbH, Germany). Advancing contact angle measurements were taken using 3 μL Milli-Q water. Four substrates and at least four different measurements were performed on each. Z-potential measurements were carried out using a SurPASS apparatus and VisioLab software (Anton Paar Ltd. - UK). All the measurements were performed four times at the pH of the electrolyte (KCL 1 mM, pH 5.5) after 2h of equilibration using the Adjustable Gap Cell for small samples (20 mm × 10 mm).

Micropatterns were introduced on 125 μm thick PMMA sheets (Goodfellow Ltd., UK) by nano-imprinting lithography (NIL) (Obducat AB, Sweden) and following the protocol described by Mills et al. [17]. Micropatterns consisted of 2 μm and 10 μm wide lines (ln2 and ln10), all 1 μm deep/tall and 1.5″ length. The silicon molds were provided by AMO GmbH (Aachen, DE) and consisted of 1.5″ × 1.5″ silicon squares. For cell culture, PMMA films were sterilized with 70% ethanol for 15 min and cut to fit in 60 mm ø tissue culture dishes. The characterization of patterned PMMA films was achieved by white light interferometry (WYKO NT1100 apparatus and the software Vision 32 V2.303 (Veeco Instruments, Inc, USA)).

2.2. Cell culture

All animal housing and procedures were approved by the Institutional Animal Care and Use Committee in accordance with Spanish and EU regulations. Glial cells were derived from brain cortex of postnatal mice as described elsewhere [23]. Briefly, P0 brain cortices were dissected out free of meninges in dissection buffer (PBS 0.6% glucose (Sigma), 0.3% BSA (Sigma)) and digested with trypsin (Biological Industries) and DNAse I (Sigma) for 10 min at 37 °C. The tissue was dissociated in Dulbecco's Modified Eagle Medium (DMEM, Biological Industries) 10% normal horse serum (NHS, GIBCO), 1% penicillin-streptomycin (Pen-Strep, Biological Industries), and 2 mM L-glutammine (Biological Industries), referred to in this text as growing medium (GM). After centrifugation and resuspension, cells were plated and grown to confluence at 37 °C, 5% CO_2 (approximately 25–30 days *in vitro*, DIV). All the experiments were performed using glial cells from the first passage (Ps1).

To assess the influence of different line topographies on glial cell morphology and differentiation state, Ps1 cells were cultured at a density of 2×10^5 cells/cm^2 for 5 DIV in Neurobasal™ (NB), 3% NHS, 1% Pen-Strep, and 2 mM L-glutamine (experimental medium = EM) on PMMA ln2, ln10 or flat (non patterned = NP). To avoid any confusion caused by the heterogeneity of glia culture types described in the literature, we defined three reference conditions within the *in vitro* system used here to compare biochemical changes of glial cells on PMMA. Control glia were Ps1 glial cells cultured on non-coated culture plastic (for Western blotting) or glass (for ICC) under the same conditions as for PMMA. Reactive/mature glia were obtained by culturing Ps1 glial cells for 8 DIV in EM and with EM supplemented with dibutyril cyclic AMP (dcAMP, 500 mM, SIGMA) during 7 more days [24,25]. Progenitor glia were obtained by culturing Ps1 glial cells for 24h in EM and then in NB supplemented with G5 (GIBCO) for 7 DIV. G5 supplement contains mitogens, such as FGF-2 and EGF, and it is used to maintain neural stem cells in culture; it significantly promotes the proliferation of neuronal precursor cells, radial glial cells and astrocytes *in vitro* [15,26]. The choice of culture conditions for progenitor and reactive glia, and of the EM, was made after numerous preliminary studies using different culture mediums, supplements, serum types and concentrations.

Neurons were obtained from embryonic brains. Brain cortices from E16 mice were isolated in dissection buffer, digested with trypsin-DNAse I, dissociated and preplated for 30 min in preplating medium (CO_2-equilibrated Neurobasal™ supplemented with 5% NHS, 1% Pen-Strep, 0.5 mM L-glutammine, 5.8 μl/ml $NaHCO_3$ (Sigma–Aldrich, Saint Louis, MO)). The supernatant was then collected, centrifuged and resuspended in serum-free neuronal culture medium (NB, 1% Pen-Strep, 0.5 mM L-glutamine, 1x B27, 5.8 μl/ml $NaHCO_3$). Neurons were plated at a density of 2.5×10^5 cells/cm^2, directly on top of 5DIV glial cell cultures, and then cultured for 5 more days in neuronal culture medium.

Explants were obtained from the cerebral cortex of E16 actin-GFAP transgenic mice. Brains were isolated and then cut into 350 μm thick slices with a McIlwain Tissue Chopper (Camden Instruments, UK). Explants of approximately 300 μm diameter were obtained by microdissection, incubated in preplating medium for 1h and seeded on top of glial layers in neuronal culture medium for 2 DIV.

2.3. Western blot

Total extract proteins were separated by SDS-polyacrylamide gel and electrotransferred to a nitrocellulose membrane. Membranes were first blocked in 5% non-fat milk and then incubated with primary antibodies overnight at 4 °C, followed by their corresponding secondary HRP-conjugated antibodies (1:3000, Santa Cruz Biotechnology, San Diego). Protein signal was detected using the ECL chemiluminescent system (Amersham, Buckinghamshire, UK). Densitometric analysis, standardized to actin as a control for protein loading, was performed using ImageJ software (National Institutes of Health, USA).

For quantification, triplicate samples were analyzed.

2.4. Immunocytochemistry and primary antibodies

For immunofluorescence, fixed samples (4% PFA for 1h at RT) were incubated with primary antibodies and appropriate Alexa488 or Alexa555 secondary antibodies (1:500, Molecular Probes, Eugene, Oregon). Phalloidin was used to stain F-actin (1:2000, Sigma–Aldrich, Saint Louis, MO) and To-Pro-3 iodide (1:500, Molecular Probes, Eugene, Oregon) to stain nuclei. Finally, the preparations were coverslipped with Mowiol (Calbiochem, San Diego) for imaging.

The following primary antibodies were used: rabbit anti-GFAP (mature and reactive glia marker, 1:500-1:8000, Dako), mouse anti-Vimentin (reactive glia marker 1:1000, Santa Cruz Biotechnology, INC), rabbit anti-EAAT-2 (mature glia marker 1:500, Cell Signaling) rabbit anti-BLBP (radial glia marker, 1:1000-1:8000, Chemicon), mouse anti-Nestin (progenitor and radial glia marker, 1:250, Abnova Corporation), goat anti-Actin (cytoskeleton Marker, 1:2000, Santa Cruz Biotechnology, INC), mouse anti-Tuj-1 (neuronal marker 1:10000, Covance) and rabbit anti-PH3 (proliferation marker, 1:250, Millipore), goat anti-Pax6 (neurogenic radial glia marker, 1:250, Santa Cruz Biotechnology, INC) and rabbit anti-TBR2 (neurogenic intermediate progenitor cells marker, 1:500, Abcam), rabbit anti-NG2 (oligodendrocytes precursor cells marker, 1:200, Millipore), rabbit anti-Ki67 (proliferation marker, 1:500, Abcam), mouse anti A2B5 (glial precursor cell marker, 1:100, Miltenyi Biotec) and goat anti-Tuj-1 (neuronal marker 1:1000, Covance).

2.5. Flow cytometry analysis

The absolute number of living and dead cells was determined at 1-4 DIV by flow cytometry using a FACScalibur apparatus (Becton Dickinson). For absolute live/dead cell number counts we used propidium iodide (PI, Sigma, 5 μg/mL) to label dead cells and CountBright™ absolute counting beads (Molecular Probes, Invitrogen), according to the protocol suggested by the provider. Ps1 cells were cultured at a density of 2×10^5 cells/cm^2, then trypsinized at 1-4 DIV, and resuspended in 1 ml of PBS. Ten thousand CountBright™ counting beads (Molecular Probes, Invitrogen) were recorded and cell populations were determined based on cell size (FSC) and granularity of the cytoplasm (SSC). The cell suspensions were analyzed after PI incubation. Percentage of positive cells and sample relative fluorescence were

calculated for each window, as determined by the monoparametric analysis. All the samples were measured in triplicates.

2.6. Scanning electron microscopy (SEM)

For SEM imaging, samples were fixed in 2.5% glutaraldehyde in 0.1M PB for 2 h at 4 °C, washed three times, frozen in liquid nitrogen and dehydrated by freeze-drying over 24 h. Then they were gold sputter-coated and observed using a Jeol JSM-6400 scanning electron microscope.

2.7. Video time lapse analysis

For video time lapse analysis, neurons were obtained from the cerebral cortex of E16 actin-GFP transgenic mice and cultured on top of pre-seeded glial cells as described above. After 8 h, the co-cultured cells were placed in the incubation chamber of an Observer.Z1m inverted fluorescent microscope (Carl Zeiss, USA) at 37 °C with 5% CO_2. Cells were imaged in phase contrast and under 488-nm wavelength light. Pictures were taken every 3 min during 3 h. Cell displacement, speed and trajectory were calculated by the aid of the "Manual Tracking" plug-in of the ImageJ software (National Institutes of Health, USA).

2.8. Imaging and analysis of cell orientation and co-localization

Cells were observed using an Axiovert 40 CFL light inverted microscopy (Carl Zeiss, USA). Digital images were taken throughout experimentation using a digital camera controlled by software. Fluorescent preparations were visualized and micrographs were captured with either a Leica TCS-SL Spectral confocal microscope (Leica Microsystems, Mannheim, Germany) or a Nikon Eclipse 800 light microscope (Nikon, Tokyo, Japan). Images were assembled in Adobe Photoshop (v. 7.0), with adjustments for contrast, brightness and color balance to obtain optimum visual reproduction of data. Morphometric and quantitative image analysis was performed using ImageJ software (National Institutes of Health, USA).

Cell alignment was quantified using the FTT-Oval Profile method described previously by Alexander et al. [27]. This method generates plots that represent alignment by a peak at 90° and randomness by a flat line. To this end, astrocytes stained for actin, BLBP and GFAP were considered. Neuron-glia co-localization was quantified using the Intensity Correlation Analysis plug-in on pictures of glial cells stained with BLBP and neurons stained with Tuj-1. Co-localization was represented by Pearson's correlation coefficient (Rr), whose values range between 1 and −1, where 1 represent maximal co-localization and −1 maximal exclusion [28]. Axon alignment from brain explants was analyzed fitting a line along the emitted axons, measuring their angles and plotting their relative frequencies.

The percentage of immunoreactive cells for the distinct differentiation markers was calculated with respect to the total number of cell nuclei stained with TO-PRO-3. Cells were counted manually on a minimum of 10 pictures for each condition.

2.9. Statistical analysis

Statistical analysis was performed using the Statgraphic-plus software. One-way ANOVA and Fisher's least significant difference (LSD) procedure were used to discriminate between the means.

3. Results

3.1. Glial cell orientation and morphology

Besides their distinct composition, glass PMMA and culture plastic (polypropylene) are harder than brain and considered stiff substrates (http://matbase.com; http://goodfellow.com). PMMA and glass were slightly hydrophobic and negatively charged (contact angle: 76°±4 and 73°; Z-potential: −45 ± 5 mV and −80 ± 14 mV respectively), while tissue culture treated polystyrene was slightly hydrophilic and negatively charged [29].

The choice of the pattern type and dimension was taken after an initial screening of different geometries (lines and posts) and width (2, 5, 10 and 20 μm) based on previous studies involving the alignment of osteoblat-like cells [17], and mesenchymal stem cells [19]. Glial cells spread in posts (not shown) and aligned in lines of all sizes. Glial cells on 2 μm lines exhibited better alignment and higher nestin expression than on 10 μm and 20 μm lines, where they behave similarly. Thus, lines of 2 μm and 10 μm were selected for the present study. The replication of micropatterns on PMMA was confirmed by white light interferometry imaging (Fig. 1). Height and width of both 2 μm and 10 μm line patterns were replicated faithfully (ln2: height 0.76 ± 0.3 μm, width 1.92 ± 0.2 μm; ln10: height 0.97 ± 0.02 μm, width 9.9 ± 0.31 μm; $n = 5$).

Using E16 primary neuronal cultures we determined that neurons do not attach to uncoated PMMA films, glass or culture plastic (not shown). By contrast, primary glial cultures from P0 cortices attached and grew on uncoated PMMA, glass and culture plastic. Cells were then stained with phalloidin or actin antibodies for morphometric analysis. Glial cells grown in the control condition (glass and culture plastic) adopted a flattened and well-spread morphology, with the occasional presence of elongated, bipolar or small ramified cells (Fig. 2A). In the presence of dcAMP, the reactive/mature condition, glial cells acquired a stellar morphology with

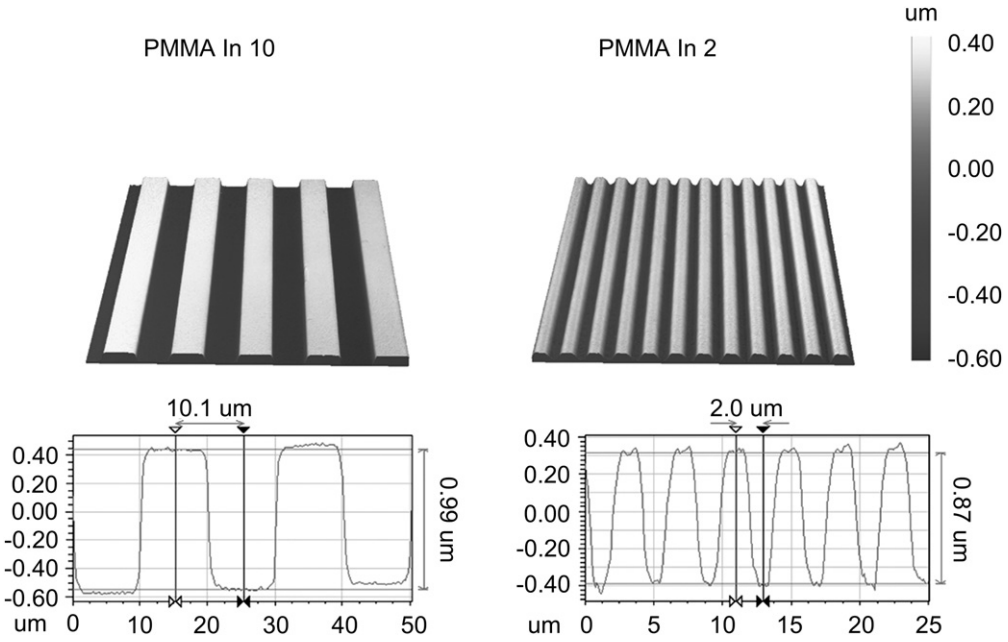

Fig. 1. White light interferometer 3D images and profiles of 10 μm and 2 μm patterned PMMA.

a highly ramified cytoskeleton characteristic of reactive glia (Fig. 2B), while cells grown in the progenitor condition were elongated and bipolar with reduced cytoplasm, a morphology that resembles radial glia and progenitor cells (Fig. 2C). On flat PMMA, as in controls, well-spread astrocytes, small ramified cells and bipolar radial glia-like cells (RGLC) were present (Fig. 2D). However, the branched cytoskeleton arrangements typical of reactive glia were not observed. In the presence of grooved topographies, glial cells adopted elongated shapes resembling RGLC and aligned following the pattern (Fig. 2E–F). FTT-Oval Profile analysis demonstrated that the alignment was better on ln2 than on ln10 (Fig. 2G), which is represented by a higher peak at 90°. SEM images revealed that elongated glial cells extended their processes, with a preference toward the mesa of the topography. They grew on top of the pattern and covered the grooves only in the case of higher cell density (Fig. 2H).

3.2. Biochemical characterization of glial cells

In order to determine whether micropatterns can induce RGLC we characterized glial cultures by immunocytochemistry and Western blot. Glial cultures were immunostained with antibodies against GFAP and BLBP to identify astrocytes, and against nestin to identify progenitors and radial glia-like cells (Fig. 3). Astrocytes expressing GFAP predominated in the reactive, control, NP and ln10 PMMA conditions (78 ± 10%, 75 ± 13%, 89 ± 9%, 81 ± 11% respectively), while they were reduced in progenitor and ln2 PMMA conditions (25 ± 3% and 45 ± 7% respectively). BLBP + astrocytes predominated in the progenitor condition (93 ± 11%), being less abundant in the reactive, control, NP, ln10 and ln2 PMMA (61 ± 17%, 69 ± 13%, 63 ± 21%, 65 ± 6% and 68 ± 4% respectively). Many astrocytes expressed both GFAP and BLBP and when we analyzed their morphology, the number of bipolar cells was significantly increased in the ln2 and ln10 PMMA conditions (43 ± 17% and 27 ± 7% respectively) with respect to NP PMMA and control conditions (17 ± 3% and 16 ± 11% respectively). Nestin + progenitors were scarce in the control and reactive conditions (26 ± 8% and 23 ± 1% respectively), they were abundant in the progenitor condition (81 ± 6%) and intermediate levels were found in NP, ln10 and ln2 PMMA (35 ± 11%, 33 ± 16% and 55 ± 18% respectively).

Western blotting was then used to quantify the relative proportion of the different cell types and their maturation state (Fig. 4A). Densitometry analysis revealed that when glial cells were

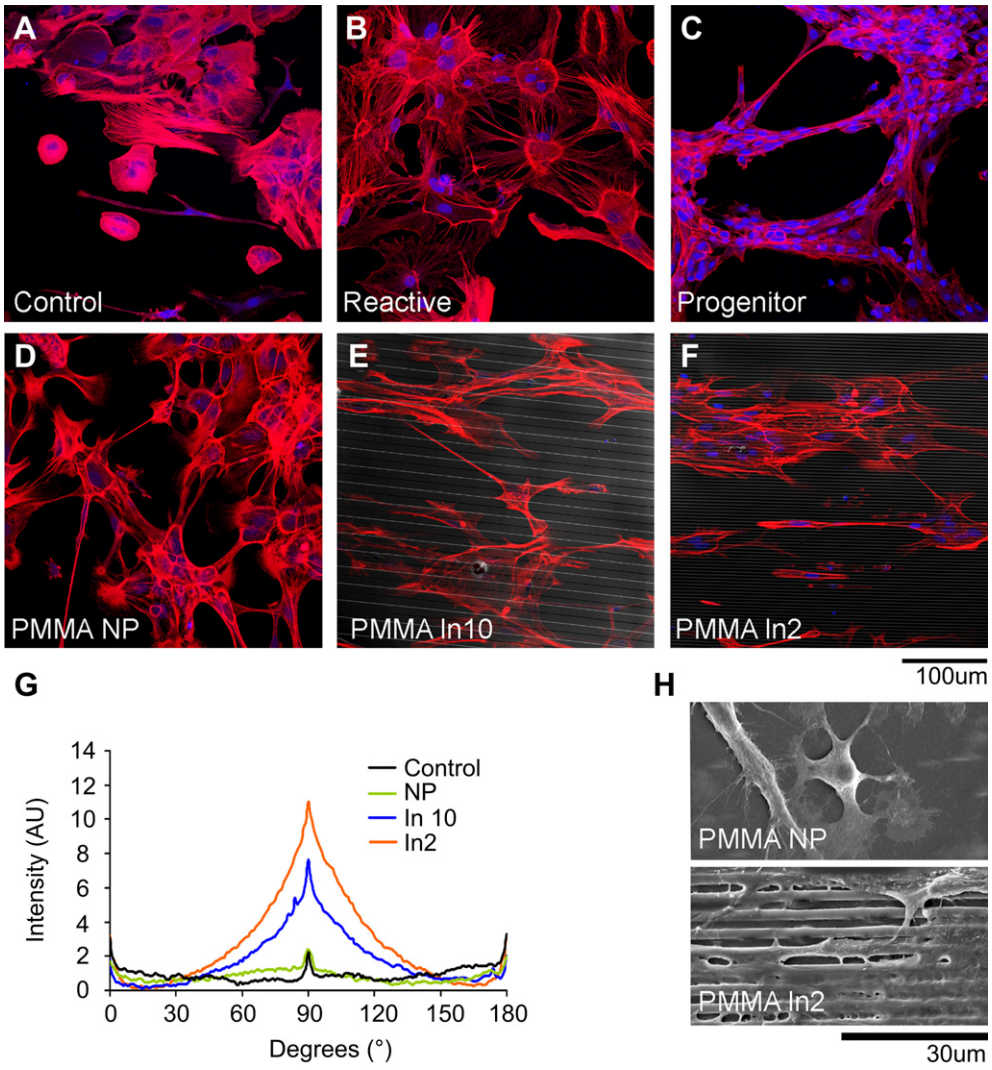

Fig. 2. Effect of PMMA and micropattern on glial cells morphology and orientation. A–F, Confocal images of actin staining (phalloidin, red) and nuclei (TO-PRO-3, blue). G, Graphic representing cell alignment by FTT-Oval profile measurement. Flat line indicates random distribution; peak at 90° indicates alignment parallel to the topography. H, SEM pictures of glial cells on NP and 2 μm lines PMMA. Scale bar A–F = 100 μm; Scale bar H = 30 μm. **Indicates statistical significance respect to control $p \geq 0.001$. (For interpretation of the references to colour in this figure legend, the reader is referred to the web version of this article.)

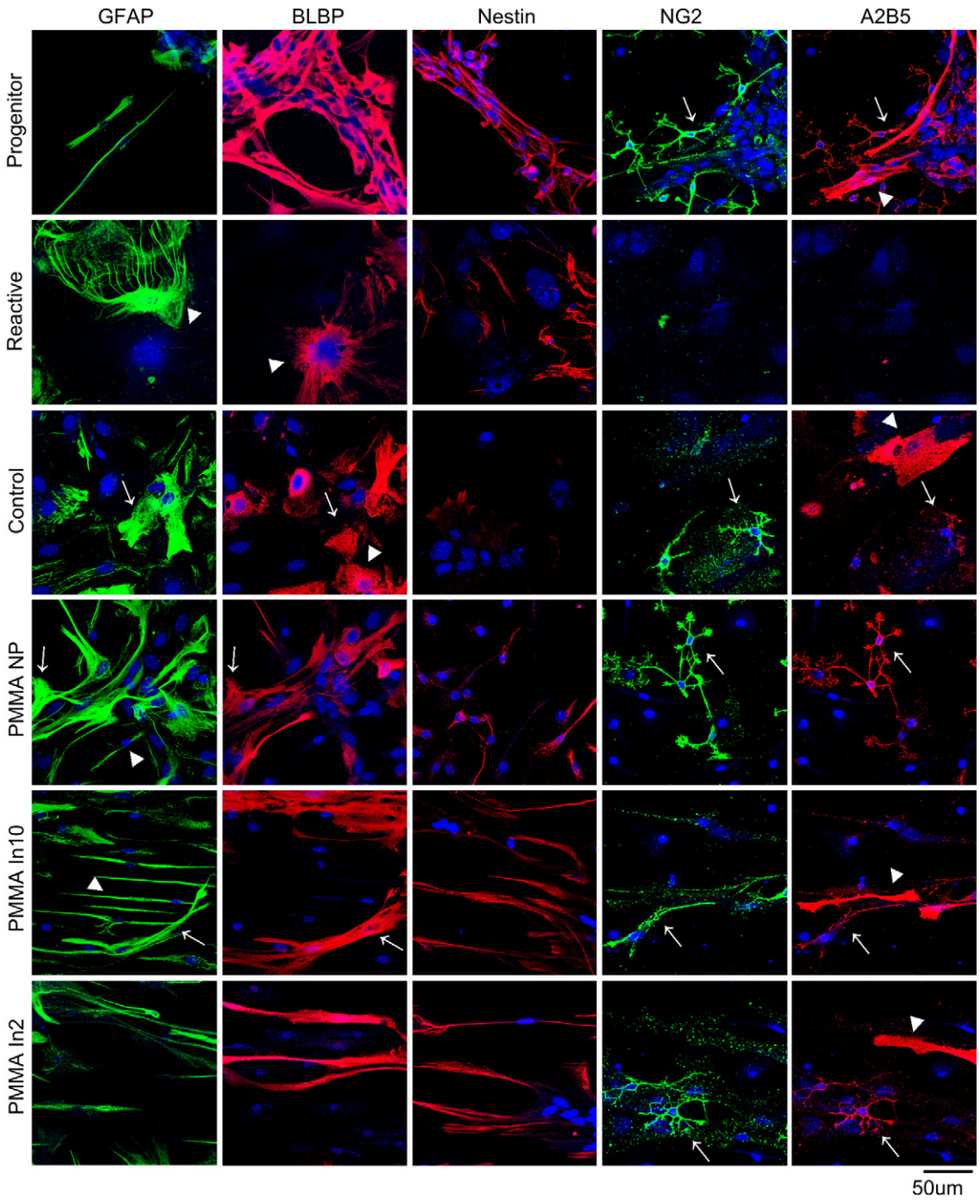

Fig. 3. Cellular composition of glial cultures. Confocal images of glial cells immunostained for different glial and progenitor markers: GFAP and BLBP for astroglia, Nestin for progenitors, and NG2 and A2B5 for different glia-restricted progenitors. Nuclei are stained with TO-PRO-3 (blue). Scale bar = 50 μm. (For interpretation of the references to colour in this figure legend, the reader is referred to the web version of this article.)

grown in the progenitor condition the expression of immaturity markers, such as nestin, and the mitotic marker PH3 dramatically increased with respect to the control, while maturity and reactive markers such as GFAP, vimentin, and the glutamate transporter EAAT-2 were markedly reduced. By contrast, the opposite was observed in the reactive condition where EAAT-2 increased while immature and progenitor markers dramatically decreased with respect to control (Fig. 4B and C). Glial cells grown on PMMA increased the expression of immaturity markers (nestin) while maturation markers decreased (GFAP, EAAT-2). The induction of a progenitor-like phenotype was more dramatic on ln2 PMMA, where proliferation (identified by PH3 expression) was also increased (Fig. 4B and C).

To investigate whether gliogenic or neurogenic progenitors were favored by the micropattern, we analyzed by Western blot the expression of several lineage-specific markers. Pax6 homeodomain transcription factor was used to identify radial glia-like cells that can produce neurons and glia, along with Tbr2, a T-domain transcription factor expressed by intermediate progenitors that produce only neurons, and Tuj-1, a neuronal tubulin expressed by

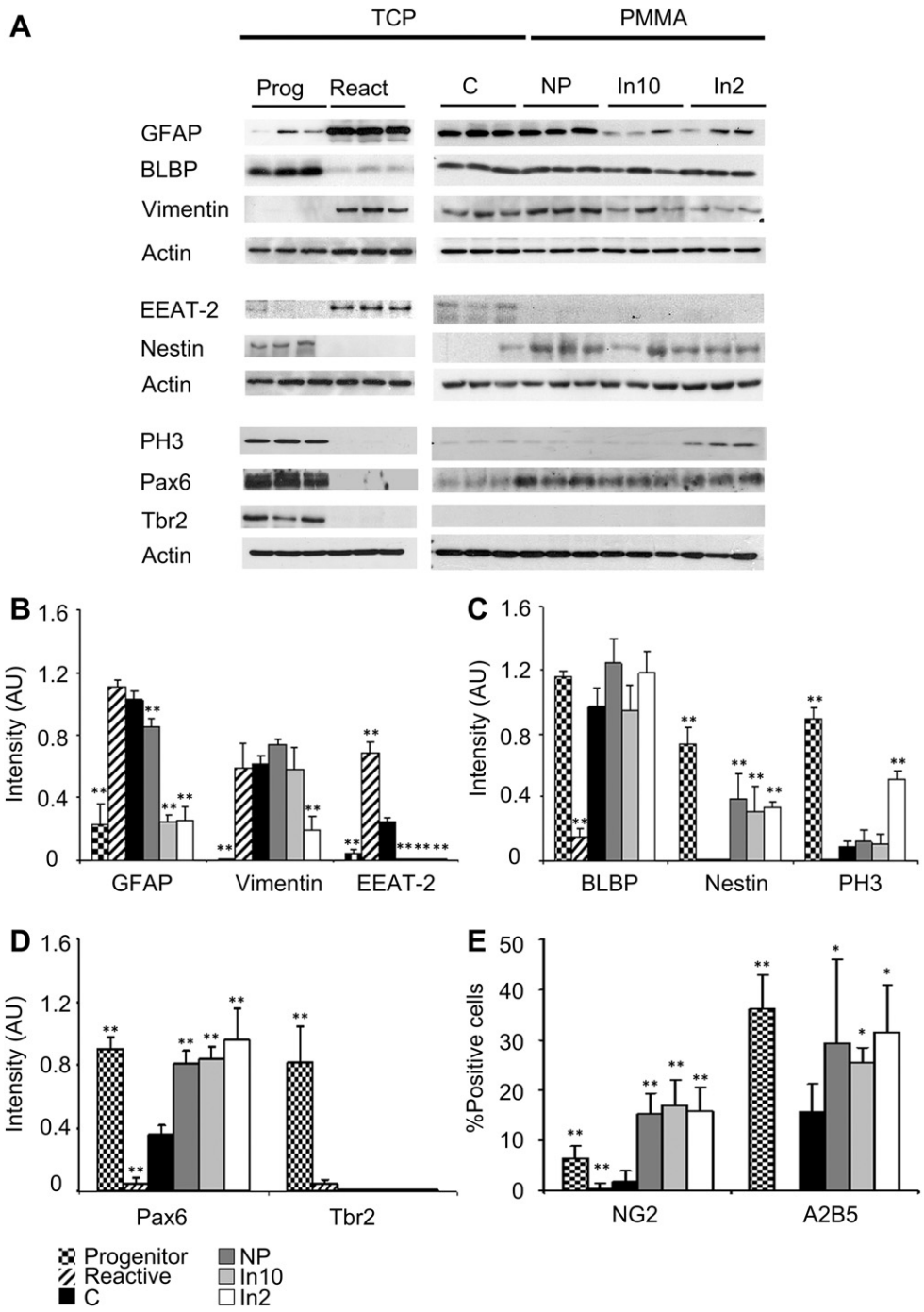

Fig. 4. Biochemical characterization of glial differentiation. A, Western Blots showing the expression of different progenitors and glial differentiation markers. B–D, Quantitative representation of the western blot densitometry (intensity values normalized to actin) grouped by categories: B, mature and reactive glial markers (GFAP, Vimentin and EAAT-2); C, progenitor glial markers (BLBP, Nestin and PH3); and D, neurogenic progenitor markers (Pax6 and Tbr2). E, Graph representing the percentage of immunoreactive cells for glial restricted progenitors markers (NG2 and A2B5) respect the total number of cells by unit area. Prog = progenitor; React = reactive glia; C = control (tissue culture plate); NP = no patterned PMMA; ln10 = 10 μm line patterned PMMA; ln2 = 2 μm line patterned PMMA. **Indicates statistical significance respect to control $p < 0.01$.

postmitotic neurons [30]. Tuj-1 expression was never found in our glial cultures, indicating the absence of differentiated neurons (not shown). Pax6 expression was induced by culture in the progenitor condition and by PMMA whereas Tbr2 expression was only induced by culture in the progenitor condition (Fig. 4A, D).

We then analyzed whether the use of PMMA substrates favored the development of specific sub-populations of glial progenitors. A2B5 ganglioside is a marker of glial restricted progenitors, Olig2 is a helix-loop-helix transcription factor that is early expressed by oligodendrocyte progenitors, while NG2 proteoglycan is expressed by the recently described NG2 glia, a progenitor cell type that can generate oligodendrocytes and protoplasmic astrocytes [31]. Olig2 was not detected by Western blot or ICC in our culture conditions (not shown), while A2B5 and NG2 could only be detected by ICC. A2B5+ glia-restricted progenitors where mostly small bipolar or multipolar cells, although large and elongated flat cells were also occasionally seen. They were abundant in glial cultures grown in the progenitor condition and on ln2 PMMA (36 ± 6.8 and 30.5 ± 5

respectively), less frequently seen in control or on flat and ln10 PMMA (21.4 ± 8.7; 21.3 ± 5.6 and 25.1 ± 6.9 respectively) and absent in the reactive condition (0 ± 0). NG2+ progenitors were small bipolar or mostly multipolar cells, and double labeling studies revealed that most of them were also A2B5 positive. NG2 cells were rare in the control and reactive conditions (1.7 ± 2.2 and 0.5 ± 0.9 respectively), whereas their number increased significantly in the progenitor condition (6.4 ± 2.4) and even greatly on PMMA (flat 15.3 ± 4.1; ln10 17.2 ± 5.1; ln2 15.9 ± 4.6) (Figs. 3 and 4E). Taken together these data suggest that PMMA and more dramatically ln2 PMMA induce RGLC and progenitor phenotypes on glial cultures.

3.3. Glial cell differentiation on patterned PMMA

Ln2 PMMA substrate might induce RGLC trough different mechanisms. RGLC might be: 1) the progeny of RGC that contaminated the initial culture; 2) the result of cell selection trough induced dead of particular cell sub-populations; or 3) the product of the de-differentiation of mature astrocytes. Therefore, we analyzed the level of cell dead and total number of cells in glial cultures grown in control and ln2 PMMA conditions from 1 to 4 div. The total number of cells during the 4 days period analyzed remains almost constant in controls while was slightly reduced at day 4 in ln2 PMMA (Fig. 5A). Only minor differences were found between control and ln2 PMMA substrates at 1 and 4 div. Cell number doubling was not achieved in this 4 days period in neither condition, a result that is concordant with the cell cycle asynchronicity and extremely low proliferation rates observed in our primary culture conditions. The number of dead cells labeled with PI was low and decreased with time, between 9% (control) and 12% (ln2 PMMA, $p < 0.05$) at day 1, and between 2% (control) and 3% (ln2 PMMA) at day 4 (Fig. 5B). These small changes in cell dead and proliferation suggest that the most probable source of RGLC in ln2 PMMA is the de-differentiation of mature astrocytes.

3.4. Neuronal adhesion and migration on topography-modified glial cells

In the developing CNS newborn neurons attach to radial glia which is the main substrate for neuronal migration. Thus, we then analyzed the neuronal supportive behavior of RGLC induced by PMMA substrates. To determine whether oriented RGLC can direct neuronal migration and neurite growth, explants from E16 cerebral cortex were grown on top of aligned (ln 2 PMMA) or random (NP PMMA) glial cells. After 36–48 h axons and some neurons were able to migrate outside the explants. Neuronal outgrowth was radial when grown in random oriented glia with only the 14% of axons aligned (Fig. 6A, C), while on ln2 PMMA they follow the pattern of the aligned glia underneath, with the 80% of axons having an angle less than 20° (Fig. 6B, D). In addition to fibers, neurons also abandoned the explants in some cases, migrating on the aligned glia (Fig. 6E, F).

To corroborate whether topography induced RGLC support and directed neuronal migration we used video time lapse microscopy. Glial cultures from wild type mice were first grown on control (uncoated glass) and ln2 PMMA for 5 DIV, and dissociated E16 neurons from actin-GFP transgenic mice were then seeded on top of them in serum-free neuronal medium. After 8 h, neurons were attached to the subjacent glia and the co-cultures were then placed in the microscope incubation chamber and recorded every 3 min for 3 h. In the control conditions GFP + neurons remained static or exhibited a minimal random movement with an average speed of 14 ± 12 μm/h ($n = 24$), and final displacement of 7 ± 6 μm (Fig. 7A, C, G, supplementary video 1). On ln2 PMMA neurons migrate for relative long distances on RGLC (37 ± 23 μm) with an average speed of 39 ± 11 μm/h ($n = 24$) (Fig. 7B, D, E, supplementary video 2). Neurons moved along the RGLC, and in some cases, they reverted their direction of movement when they reach the end of the RGLC.

Supplementary material associated with this article can be found, in the online version, at doi:10.1016/j.biomaterials.2011.10.086.

To discard the possibility that the neuronal cultures provided RGC that act as substrates for migration, WT glial co-cultures with GFP neurons were left for a further 5 *div*, fixed and stained for BLBP to identify the origin of glial cells (Fig. 7F, G). In both control and ln2 PMMA conditions, neurons were GFP+ and almost all BLBP + glial cells were negative for GFP. This data indicate that embryonic neuronal dissociates does not provide a significant number of glial cells. After 5div, in the control condition BLBP + glial cells were flatted and well-spread and GFP + neurons were well developed and exhibited ramified dendritic branches (Fig. 7F). However, in ln2 PMMA glial cells were elongated and GFP + neurons were mostly bipolar, oriented along the BLBP + RGLC processes and with few or none dendritic branches (Fig. 7G). In both conditions, Z reconstruction showed that neurons grew on the top of glial cells. To quantify the differences in neuron-glia attachment we stained WT co-cultures with Tuj-1 and BLBP. Then we measured the degree of Tuj-1/BLBP co-localization, using the intensity correlation analysis 5 days after the neuronal seeding. The degree of co-localization can be calculated according to the value of Pearson's coefficient (Rr), where Rr equal to 1 indicates maximal co-localization and Rr of −1 indicates maximal exclusion. Glia-neuron co-localization was significantly higher in ln2 PMMA culture (Rr: 0.59 ± 0.11) than in control (Rr: 0.15 ± 0.08) (Fig. 7H–J). Taking together, those results indicate that ln2 PMMA-induced RGLC recapitulates the functions of embryonic RG, providing a good substrate for neural attachment and promoting directional neuronal migration.

4. Discussion

Although glial cells have long been regarded as responsible for the lack of CNS regeneration, due to the formation of the non-

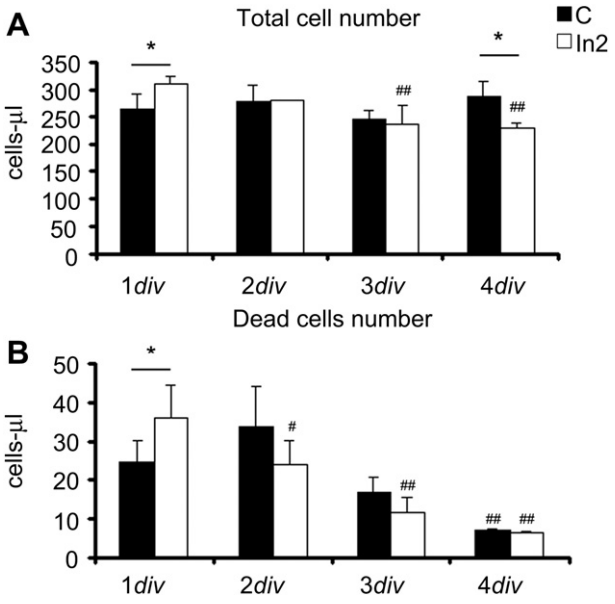

Fig. 5. Graft from flow cytometry analysis showing the evolution of the total cell number and dead cell number on control and PMMA ln2 during 4 days. *Indicates statistical significance between control and PMMA ln2, $p < 0.05$: # indicates statistical significance with respect to 1div in each substrate, #$p < 0.05$, ##$p < 0.01$.

permissive glial scar, it is now clear that they are also beneficial and may play an active role in the induction of neurogenesis from adult neural stem cells [6,32,33]. During embryonic development, radial glia generate directly or indirectly most CNS neurons [34], while at the end of neurogenesis most radial glia transform into parenchymal astrocytes [35], and also originate the adult neural stem cells [36,37]. The direction of differentiation can be partially reverted after a lesion *in vivo*, and some astrocytes can de-

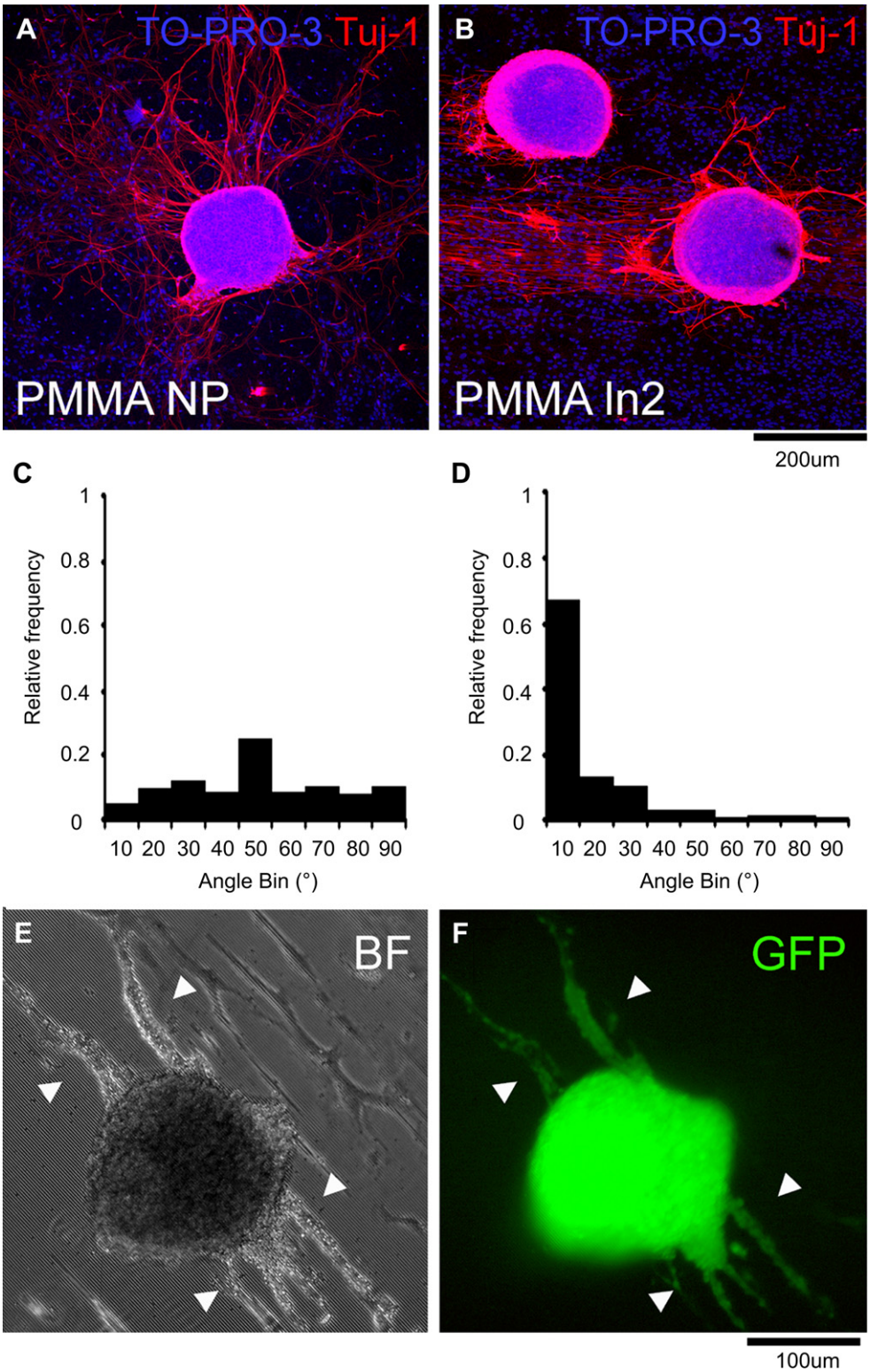

Fig. 6. Effect role of pattern-induced RGLC in neural growth and axonal guidance. A, B, Images showing explants from E16 cerebral cortex cultured on glial cells grown on NP PMMA (A) or Ln2 PMMA (B). Cell nuclei are marked with TO-PRO-3 (blue) and neurons with Tuj-1 antibody (red). Frequency plots representing axonal outgrowth orientation on PMMA NP (C) and PMMA ln2 (D) substrates. E–F, explants from E16 GFP mice cerebral cortex seeded on top of on glia grown on PMMA ln2. E = bright field and F = GFP fluorescence. Neurons exiting from the explants are identified by GFP expression. Scale bars = 200 μm (A, B); 100 μm (E, F). (For interpretation of the references to colour in this figure legend, the reader is referred to the web version of this article.)

differentiate into a radial glia-like phenotype that supports the migration of embryonic transplanted neurons [3]. On this basis, a recent experimental strategy for CNS regeneration is to develop mechanisms that restore the embryonic radial glia neurogenic competence into parenchymal astrocytes [38,39]. Extracellular stimuli, including soluble and adhesive factors *in vivo* and in culture media are important modulators of glial cell phenotype and function [4,40]. However these factors are usually derived from animal sources, they are expensive, and it is difficult to control their optimum concentration and side effects. Recent evidence claims that topographical cues cause changes in cell phenotype [21,41–43]. For instance, Evelyn K.F. Yim et al., promoted hMSC transdifferentiation into neuronal lineages using a collagen coated PDMS carrying line patterns of 350 nm [44], while MR Lee et al. obtained the same from hESC [45]. Thus it can be assumed that by providing appropriate physical stimuli it is possible to bias the response of glial cells to injury, i.e. from the reactive to the radial glia phenotype, the later being more supportive for successful endogenous repair.

The major finding of this study is that *in vitro* matured astrocytes can be reverted to an RGLC phenotype by a precisely-sized micro-patterned PMMA scaffold without added biochemical factors. As do their embryonic counterparts, induced RGLC express the neuron-glial progenitor marker Pax6, and also proliferate, generate intermediate A2B5 and NG2 progenitors, and support and direct neuronal migration and axonal outgrowth.

The composition and physiological status of a primary glial culture is highly heterogeneous and depends on several factors, including the tissue origin and mode of preparation, the selected growth substrate and substrate coating, and the culture medium composition. To overcome this heterogeneity we defined three reference conditions: progenitor, reactive/mature and control (see material and methods for detailed definitions), thus enabling us to compare the physiological changes of cortical glial cells on the different substrates. In these reference conditions, progenitor glia were small bipolar cells characterized by a high proliferation rate and the expression of the progenitor markers (nestin, Pax6, A2B5), whereas reactive/mature glia were large cells with flat or ramified shapes, mostly quiescent, and expressing high levels of maturity markers (GFAP, EAAT-2). Control glia were mostly flat and well-spread, proliferated slowly, and expressed high levels of mature markers, characteristics that define them as cells closer to the reactive/mature condition. When PMMA was used as the substrate, the glial morphology and biochemical marker expression indicate a bias toward a more immature RGLC progenitor phenotype that was dramatically potentiated when PMMA was micropatterned, with grooves no bigger than 2 μm wide/1 μm deep. These results suggest that intrinsic material properties might act synergistically with the micro-topography in the modulation of the astrocytic phenotype. Biophysical and material cues regulate stem cell behavior (reviewed in Keung et al., 2010 [46]). For example, substrate stiffness differentially directs neural stem cells differentiation to neural and glial phenotypes [47–49] and substrate hydrophobicity regulates glial cells adhesion and proliferation [50,51]. PMMA is the most hydrophobic substrate we used here and the study of Biran et al., demonstrated that astrocytes exhibit lower adhesion and increased proliferation with increasing material hydrophobicity [50]. Material chemistry and surface energy affect the adsorption of ECM proteins and thus might regulate cell adhesion and proliferation by modulating integrin signaling [51]. ECM protein adsorption on PMMA is 5–10 times smaller than the amount adsorbed in tissue culture treated polystyrene [52]. Thus, one possibility is that the hydrophobicity and low protein adsorption of PMMA might act synergistically with the micro-topography in the induction of the RGLC phenotype.

After initial seeding, primary glial cultures were grown *in vitro* for 1 month until reach confluence, reflecting the extremely slow proliferation rate in our experimental conditions. One possibility is that the threefold increase in RGLC in Ln2 PMMA was the progeny of RGC that contaminated the initial culture, selected trough induced death of particular cell sub-populations. However, our data strongly argue against this possibility because cell number doubling was not achieved in any substrate in the first 4 days of the study, and the number of dead cells was similar in Ln2 PMMA and control substrates. Therefore, although complementary experiments will be required to fully resolve this question, our results support that the most probably source of RGLC is the de-differentiation of mature astrocytes.

Recent studies have focused on the effect of nano- and micro-topography on cell function (reviewed by Bettinger et al. [8]), and grooved substrates have been tested for neural tissue engineering purposes showing a size-dependent response [9]. For instance, line topographies larger than the cell body (30–200 μm) promote perpendicular alignment, called “cell bridging”, in several cell types such as dorsal root ganglion and Schwann cells [53]. Moreover, mesenchymal stem cell differentiation and cell fate might be directed by changing the groove dimension [44,54]. Cell shape elongation on grooved surfaces is mostly due to oriented mechanical tension created by integrin and focal adhesion rearrangements. The elongation of cytoskeleton and nucleus has been correlated with changes in cell function and differentiation, in part through intracellular calcium regulation [55,56]. Nevertheless the strong proliferative induction of 2 μm grooves that we observed here was rather surprising, as it is reported in the literature that, in general, cells grown on grooved topographies exhibit lower proliferation rates [8,48]. However, in most studies the material surface was modified by adding reactive groups or through coatings with extracellular matrix proteins to improve cell adhesion. It is known that strong cell adhesion to stiff substrates favors the formation of focal contacts and actin-myosin stress fibers [57,58], thus probably limiting cell division. We have observed that RGLC on PMMA or in the progenitor condition gradually lose their adhesion to the substrate, and some of their radial processes detach from them. NSC proliferate when grown as neurospheres, and differentiate when they are forced to adhere to stiff substrates through the addition of adhesive molecules [21,58]. Thus, a loose adherent phenotype might be a requisite to maintain NSC competence and proliferative capacity, and optimizing cell adhesion to the substrate might therefore introduce a bias toward cell differentiation.

Recent evidence strongly supports the idea that in order to maintain or promote proliferation it is also necessary to recreate certain physical characteristics of the specialized progenitor niche [59]. In the embryonic CNS, progenitors and neuroblasts are densely packed in the ventricular areas, with the long processes of radial glia spanning from the ventricular surface to the surrounding pia mater. As the size of radial glia processes is around 2 μm [60], one possibility is that 2 μm grooves mimic the physical structure of the NSC niche during brain development.

Linage tracing experiments suggest that CNS neural progenitors are heterogeneous and mostly arise from sequential differentiation of an early multipotent neuroepithelial progenitor that progressively transforms into radial glia. Radial glia cells, which express Pax6 in the cerebral cortex, can originate neurons and glia, and as development proceeds they also generate different intermediate neuronal restricted (TBR2 positive) or glial restricted (A2B5 positive) amplifying progenitors [30,61]. In our experimental conditions, RGLC and glia-restricted progenitors could be induced by material chemistry and topographical cues, but this was not the case of neuronal restricted progenitors or mature neurons,

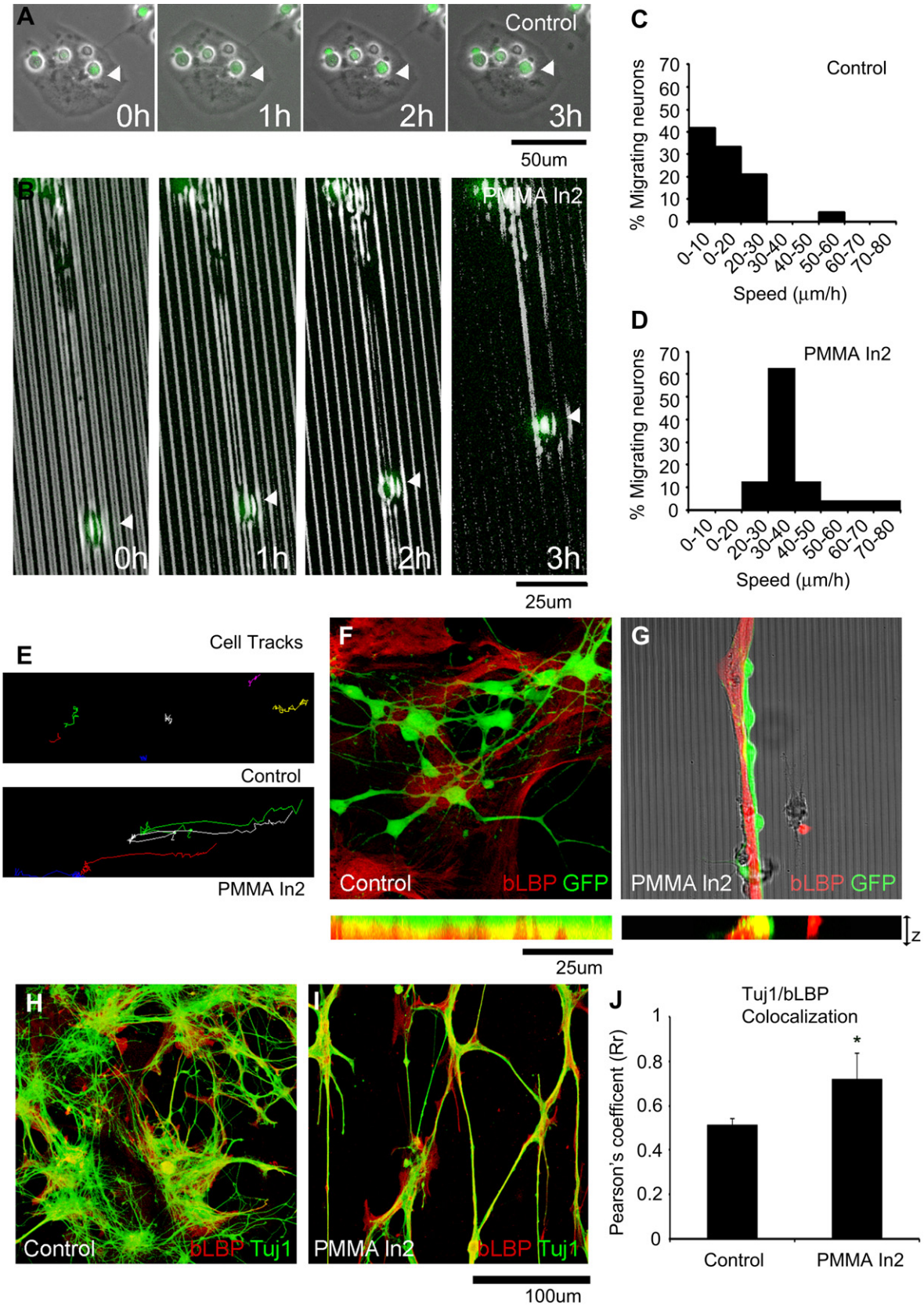

Fig. 7. Role of pattern-induced RGLC in neural migration. Representative time lapse images of E16 GFP neurons (green) seeded on glial cells grown on control (A) and ln2 PMMA (B) of glial cells (bright field). White arrows indicate the position of a representative neuronal body showing its stativity on control condition (A) and its migration on ln2 induced RGLC process (B). C–D, Frequency plot showing the distribution of the speed (μm/h) of migrating neurons ($n = 24$) in control and ln2 PMMA conditions. E, Particle tracks showing neuronal trajectories in control and Ln2 PMMA during a 3h record. F-G, GFP neurons (green) grown on WT glial cells stained with BLBP (red) after 5*div* in control (F) and ln2 PMMA (G) and their Z projections. H–I, neurons labeled with Tuj-1 (green) grown on glial cells labeled with BLBP (red) in control (H) and ln2 PMMA (I) substrates. (J). Graph representing the Pearson's coefficient for neuron/glia co-localization in those cultures. $0 \leq Rr \leq 1$, where 1 = max co-localization and 0 = maximal exclusion. **Indicates statistical significance, $p < 0.01$. Scale bar = 100 μm. Scale bars (A) = 50 μm; (B, F, G) = 25 μm; (E) = 20 μm; (H, I) 100 μm. (For interpretation of the references to colour in this figure legend, the reader is referred to the web version of this article.)

suggesting that the cues which guide progenitor specification to neuronal and glial lineages might be different.

During embryonic development, RGC not only act as NSC but also serve as scaffold for directed neuronal migration [33]. The ability of glial cells to support and orient neural growth has already been studied by other authors. For instance, dorsal root ganglions grew longer neurites on aligned astrocytes and meningeal-coated substrates [62], while neurons grew and oriented on electric field-induced aligned astrocytes [27]. One interesting study reported that neurons could align on top of an astrocyte monolayer even after 3 weeks, and they were able to read the pattern "buried" beneath astrocytes [63]. In our experimental conditions, embryonic cortical neurons adhered to glial cells but not to the substrates themselves; thus, changes in neuronal adhesion directly reflect different glial physiology. RGLC induced by 2 μm grooved PMMA provided better neuronal substrates than did glial cells grown on naive PMMA, glass or culture plastic, and neuronal bodies and neurites align perfectly with the oriented glia. Moreover, neurons migrate relatively long distances using the RGLC as rails, at a speed that is comparable with the embryonic neuronal radial migration [64]. Significant participation of contaminant RGC from neural cultures was also ruled out, as GFP+/BLBP glial cells were rarely observed in our co-cultures. Thus, induced RGLC are functional and reproduce the normal roles of RGC during development, providing a guiding substrate for migrating neurons.

Embryonic neurons are known in turn to direct astrocyte transformation into radial glia through neuregulin secretion and BLBP induction in astrocytes [54]. Here we found that 2 μm patterned PMMA synergizes with embryonic neurons, potentiating astrocyte de-differentiation into RGLC. This effect was manifested by a reduction of the surface covered by glial cells, since they adopted bipolar shapes, and an increase in neuron-glia co-localization compared to control (from 15% to 60%).

The present work report morphological and physiological RGLC progenitor induction from *in vitro* matured astrocytes in response to material composition and topography without the concurrence of biochemical cues. Although PMMA is not the material of choice for *in vivo* implantation after a lesion, our results suggest that substrate-mediated induction of RGLC phenotype in mature astrocytes might improve their ability to sense and respond to other potential regenerative cues, whether provided externally or already present locally.

Although much more work remains to be done, the findings raise the possibility of designing implantable devices that restore *in situ* the embryonic radial glia competence into parenchymal astrocytes. Successful regeneration might then require that implantable materials not only promote neuronal cell growth, but also drive glial physiological responses into a neuron permissive or even a neurogenic phenotype. In this regard, the introduction of line patterns within the size range of RGC processes in implantable scaffolds might mimic the topography of the embryonic neural stem cell niche, and could be a useful tool for driving endogenous astrocytes into a neurogenic RGLC phenotype and a regenerative response *in situ*.

5. Conclusions

This study has demonstrated that in the absence of other biochemical cues, the intrinsic composition and line topography of PMMA is sufficient to drive glial cell de-differentiation into RGLC progenitors. Glial cells, and in particular astrocytes, align and orient in a wide range of line topographies, although, only those in the size range of normal RGC processes (~2 μm) strongly induced astrocyte transformation into RGLC progenitors. These cells reproduce *in vitro* some of the normal functions of radial glia itself, including the generation of different types of intermediate progenitors and the support and orientation of neuronal growth. Our results also suggest that the design of an implantable device to promote CNS regeneration must take in account the glial cell response.

Acknowledgments

This study was supported in part by grants from Spain's Ministerio de Ciencia e Innovación [MAT2008-06887-C03-02/MAT] and [MAT2008-06887-C01/MAT], co-financed by the European Regional Development Fund, to S.A. and J.A.P. respectively; from 2009 SGR 719 to S.A. as well as through the fellowship FPU AP2008-01868 to M.M.

We are grateful to M. Maudsley for editorial assistance and to B. Torrejon and E. Castaño from the Scientific-Technical Services UB (Campus Bellvitge) for technical support in confocal microscopy and cytometry.

References

[1] Yiu G, He Z. Glial inhibition of CNS axon regeneration. Nat Rev Neurosci 2006; 7:617–27.
[2] Fitch MT, Silver J. CNS injury, glial scars, and inflammation: inhibitory extracellular matrices and regeneration failure. Exp Neurol 2008;209:294–301.
[3] Leavitt BR, Hernit-Grant CS, Macklis JD. Mature astrocytes transform into transitional radial glia within adult mouse neocortex that supports directed migration of transplanted immature neurons. Exp Neurol 1999;157:43–57.
[4] White RE, Jakeman LB. Don't fence me in: harnessing the beneficial roles of astrocytes for spinal cord repair. Restor Neurol Neurosci 2008;26:197–214.
[5] Rolls A, Shechter R, Schwartz M. The bright side of the glial scar in CNS repair. Nat Rev Neurosci 2009;10:235–41.
[6] Buffo A, Rolando C, Ceruti S. Astrocytes in the damaged brain: molecular and cellular insights into their reactive response and healing potential. Biochem Pharmacol 2010;79:77–89.
[7] Lang B, Liu HL, Liu R, Feng GD, Jiao XY, Ju G. Astrocytes in injured adult rat spinal cord may acquire the potential of neural stem cells. Neurosci 2004;128: 775–83.
[8] Bettinger CJ, Langer R, Borenstein JT. Engineering substrate topography at the micro- and nanoscale to control cell function. Angew Chem Int Ed Engl 2009; 48:5406–15.
[9] Hoffman-Kim D, Mitchel JA, Bellamkonda RV. Topography, cell response, and nerve regeneration. Annu Rev Biomed Eng 2010;12:203–31.
[10] Steedman M, Tao S, Klassen H, Desai T. Enhanced differentiation of retinal progenitor cells using microfabricated topographical cues. Biomed Microdevices 2010;12:363–9.
[11] Chew SY, Mi R, Hoke A, Leong KW. The effect of the alignment of electrospun fibrous scaffolds on Schwann cell maturation. Biomaterials 2008;29:653–61.
[12] Christopherson GT, Song H, Mao H-Q. The influence of fiber diameter of electrospun substrates on neural stem cell differentiation and proliferation. Biomaterials 2009;30:556.
[13] Moon JH, Yoon BS, Kim B, Park G, Jung HY, Maeng I, et al. Induction of neural stem cell-like cells (NSCLCs) from mouse astrocytes by Bmi1. Biochem Biophys Res Commun 2008;371:267–72.
[14] Yamada T, Sawada R, Tsuchiya T. The effect of sulfated hyaluronan on the morphological transformation and activity of cultured human astrocytes. Biomaterials 2008;29:3503–13.
[15] Tao Y, Guan C, Linyin F. Low temperature induced de-differentiation of astrocytes. J Cell Biochem 2006;99:1096–107.
[16] Recknor JB, Sakaguchi DS, Mallapragada SK. Directed growth and selective differentiation of neural progenitor cells on micropatterned polymer substrates. Biomaterials 2006;27:4098–108.
[17] Mills CA, Fernandez JG, Martinez E, Funes M, Engel E, Errachid A, et al. Directional alignment of MG63 cells on polymer surfaces containing point microstructures. Small 2007;3:871–9.
[18] Engel E, Martinez E, Mills CA, Funes M, Planell JA, Samitier J. Mesenchymal stem cell differentiation on microstructured poly (methyl methacrylate) substrates. Ann Anat 2009;191:136–44.
[19] Martinez E, Engel E, Lopez-Iglesias C, Mills CA, Planell JA, Samitier J. Focused ion beam/scanning electron microscopy characterization of cell behavior on polymer micro-/nanopatterned substrates: a study of cell-substrate interactions. Micron 2008;39:111–6.
[20] Johansson F, Carlberg P, Danielsen N, Montelius L, Kanje M. Axonal outgrowth on nano-imprinted patterns. Biomaterials 2006;27:1251–8.
[21] Martínez-Ramos C, Lainez S, Sancho F, García Esparza MA, Planells-Cases R, García Verdugo JM, et al. Differentiation of postnatal neural stem cells into glia and functional neurons on laminin-coated polymeric substrates. Tissue Eng Part A 2008;14:1365–75.

[22] Merolli A, Rocchi L, Catalano F, Planell J, Engel E, Martinez E, et al. In vivo regeneration of rat sciatic nerve in a double-halved stitch-less guide: a pilot-study. Microsurgery 2009;29:310–8.
[23] Ortega JA, Alcantara S. BDNF/MAPK/ERK-induced BMP7 expression in the developing cerebral cortex induces premature radial glia differentiation and impairs neuronal migration. Cereb Cortex 2010;20:2132–44.
[24] Fedoroff S, McAuley WA, Houle JD, Devon RM. Astrocyte cell lineage. V. Similarity of astrocytes that form in the presence of dBcAMP in cultures to reactive astrocytes in vivo. J Neurosci Res 1984;12:14–27.
[25] Wu VW, Schwartz JP. Cell culture models for reactive gliosis: new perspectives. J Neurosci Res 1998;51:675–81.
[26] Gregg C, Weiss S. Generation of functional radial glial cells by embryonic and adult forebrain neural stem cells. J Neurosci 2003;23:11587–601.
[27] Alexander JK, Fuss B, Colello RJ. Electric field-induced astrocyte alignment directs neurite outgrowth. Neuron Glia Biol 2006;2:93–103.
[28] Comeau JWD, Costantino S, Wiseman PW. A guide to accurate fluorescence microscopy colocalization measurements. Biophys J 2006;91:4611–22.
[29] van Kooten TG, Spijker HT, Busscher HJ. Plasma-treated polystyrene surfaces: model surfaces for studying cell-biomaterial interactions. Biomaterials 2004; 25:1735–47.
[30] Englund C, Fink A, Lau C, Pham D, Daza RA, Bulfone A, et al. Pax6, Tbr2, and Tbr1 are expressed sequentially by radial glia, intermediate progenitor cells, and postmitotic neurons in developing neocortex. J Neurosci 2005;25:247–51.
[31] Zhu X, Bergles DE, Nishiyama A. NG2 cells generate both oligodendrocytes and gray matter astrocytes. Development 2008;135:145–57.
[32] Song H, Stevens CF, Gage FH. Astroglia induce neurogenesis from adult neural stem cells. Nature 2002;417:39–44.
[33] Vaccarino FM, Fagel DM, Ganat Y, Maragnoli ME, Ment LR, Ohkubo Y, et al. Astroglial cells in development, regeneration, and repair. Neuroscientist 2007; 13:173–85.
[34] Kriegstein A, Alvarez-Buylla A. The glial nature of embryonic and adult neural stem cells. Annu Rev Neurosci 2009;32:149–84.
[35] Voigt T. Development of glial cells in the cerebral wall of ferrets: direct tracing of their transformation from radial glia into astrocytes. J Comp Neurol 1989; 289:74–88.
[36] Alvarez-Buylla A, Garcia-Verdugo JM, Tramontin AD. A unified hypothesis on the lineage of neural stem cells. Nat Rev Neurosci 2001;2:287–93.
[37] Chojnacki AK, Mak GK, Weiss S. Identity crisis for adult periventricular neural stem cells: subventricular zone astrocytes, ependymal cells or both? Nat Rev Neurosci 2009;10:153–63.
[38] Berninger B. Making neurons from mature glia: a far-fetched dream? Neuropharmacology 2010;58:894–902.
[39] Costa MR, Gotz M, Berninger B. What determines neurogenic competence in glia? Brain Res Rev 2010;63:47–59.
[40] Discher DE, Janmey P, Wang YL. Tissue cells feel and respond to the stiffness of their substrate. Science 2005;310:1139–43.
[41] Recknor JB, Recknor JC, Sakaguchi DS, Mallapragada SK. Oriented astroglial cell growth on micropatterned polystyrene substrates. Biomaterials 2004;25: 2753–67.
[42] Thompson DM, Buettner HM. Schwann cell response to micropatterned laminin surfaces. Tissue Eng 2001;7:247–65.
[43] Yang IH, Co CC, Ho CC. Spatially controlled co-culture of neurons and glial cells. J Biomed Mater Res A 2005;75:976–84.
[44] Yim EKF, Pang SW, Leong KW. Synthetic nanostructures inducing differentiation of human mesenchymal stem cells into neuronal lineage. Exp Cell Res 2007;313:1820–9.
[45] Lee MR, Kwon KW, Jung H, Kim HN, Suh KY, Kim K, et al. Direct differentiation of human embryonic stem cells into selective neurons on nanoscale ridge/groove pattern arrays. Biomaterials 2010;31:4360–6.
[46] Keung JA, Kumar S, Schaffer DV. Presentation counts: microenviromental regulation of stem cells by biophysical and material cues. Annu Rev Cell Dev Biol 2010;26:533–56.
[47] Hynes SR, Millicent FR, Bertram JP, Lavik EB. A library of tuneable poly(ethylene glycol)/poly(L-lysine) hydrogels to investigate the material cues that influence neural stem cell differentiation. J Biomed Mater Res A 2009;89:499–509.
[48] Saha K, Keung AJ, Irwin EF, Li Y, Little L, Schaffer DV. Substrate modulus directs neural stem cell behaviour. Biophys J 2008;95:4426–38.
[49] Leipzig ND, Shoichet MS. The effect of substrate stiffness on adult neural stem cell behaviour. Biomaterial 2009;30:6867–78.
[50] Biran R, Noble MD, Tresco PA. Characterization of cortical astrocytes on materials of different surface chemistry. J Biomed Mater Res 1999;46: 150–9.
[51] Soria JM, Martínez Ramos C, Bahamonde O, García Cruz DM, Salmerón Sánchez M, García Esparza MA, et al. Influence of the substrate's hydrophilicity on the *in vitro* Schwann cells viability. J Biomed Mater Res A 2007;83: 463–70.
[52] Alaerts JA, De Cupere VM, Moser S, van den Bosh de Aguilar P, Rouxhet PG. Surface characterization of poly(methyl methacrylate) microgrooved for contact guidance of mammalian cells. Biomaterials 2001;22:1635–42.
[53] Goldner JS, Bruder JM, Li G, Gazzola D, Hoffman-Kim D. Neurite bridging across micropatterned grooves. Biomaterials 2006;27:460–72.
[54] Tay CY, Yu H, Pal M, Leong WS, Tan NS, Ng KW, et al. Micropatterned matrix directs differentiation of human mesenchymal stem cells towards myocardial lineage. Exp Cell Res 2010;316:1159–68.
[55] Dalby MJ, Riehle MO, Yarwood SJ, Wilkinson CD, Curtis AS. Nucleus alignment and cell signaling in fibroblasts: response to a micro-grooved topography. Exp Cell Res 2003;284:274–82.
[56] Itano N, Okamoto S, Zhang D, Lipton SA, Ruoslahti E. Cell spreading controls endoplasmic and nuclear calcium: a physical gene regulation pathway from the cell surface to the nucleus. Proc Natl Acad Sci U S A 2003;100:5181–6.
[57] Engler AJ, Sen S, Sweeney HL, Discher DE. Matrix elasticity directs stem cell lineage specification. Cell 2006;126:677–89.
[58] Discher DE, Mooney DJ, Zandstra PW. Growth factors, matrices, and forces combine and control stem cells. Science 2009;324:1673–7.
[59] Keung AJ, Healy KE, Kumar S, Schaffer DV. Biophysics and dynamics of natural and engineered stem cell microenvironments. Rev Syst Biol Med 2010;2: 49–64.
[60] Anton ES, Marchionni MA, Lee KF, Rakic P. Role of GGF/neuregulin signaling in interactions between migrating neurons and radial glia in the developing cerebral cortex. Development 1997;124:3501–10.
[61] Baracskay KL, Kidd GJ, Miller RH, Trapp BD. NG2-positive cells generate A2B5-positive oligodendrocyte precursor cells. Glia 2007;55:1001–10.
[62] Biran R, Noble MD, Tresco PA. Directed nerve outgrowth is enhanced by engineered glial substrates. Exp Neurol 2003;184:141–52.
[63] Sørensen A, Alekseeva T, Katechia K, Robertson M, Riehle MO, Barnett SC. Long-term neurite orientation on astrocyte monolayers aligned by micro-topography. Biomaterials 2007;28:5498.
[64] Youn YH, Pramparo T, Hirotsune S, Wynshaw-Boris A. Distinct dose-dependent cortical neuronal migration and neurite extension defects in Lis1 and Ndel1 mutant mice. J Neurosci 2009;29:15520–30.